JAERI-M
83-075

A STUDY OF GROUP CONSTANT GENERATION METHOD IN FAST REACTOR ANALYSIS

May 1983

Hideki TAKANO

日本原子力研究所
Japan Atomic Energy Research Institute

JAERI-Mレポートは，日本原子力研究所が不定期に公刊している研究報告書です。
入手の問合わせは，日本原子力研究所技術情報部情報資料課（〒319-11茨城県那珂郡東海村）あて，お申しこしください。なお，このほかに財団法人原子力弘済会資料センター（〒319-11 茨城県那珂郡東海村日本原子力研究所内）で複写による実費頒布をおこなっております。

JAERI-M reports are issued irregularly.
Inquiries about availability of the reports should be addressed to Information Section, Division of Technical Information, Japan Atomic Energy Research Institute, Tokai-mura, Naka-gun, Ibaraki-ken 319-11, Japan.

編集兼発行　日本原子力研究所
印　　刷　いばらき印刷㈱

JAERI-M 83-075

A Study of Group Constant Generation Method in Fast Reactor Analysis

Hideki TAKANO

Department of Reactor Engineering,
Tokai Research Establishment, JAERI

(Received April 22, 1983)

Generation methods for group constants have been studied to predict accurately nuclear characteristics for fast reactors. In resonance energy region, the accuracy of the group constants calculated by the approximate weighting spectrum used in the conventional standard group constant set such as the ABBN is investigated. It is shown that the basic assumption of constant collision density for group constant calculations is not always satisfactory for lower energy group below about 1 keV and/or for systems with highly enriched fuel. Furthermore, a multilevel formula is derived without losing the useful characteristics of the Breit-Wigner single-level formula. Using this formula, the interference effects betweeen resonances are examined in the resolved and unresolved resonance regions. In addition, mutual interference between different resonant nuclides is calculated by solving numerically the neutron slowing down equation for infinite homogeneous media, and the effects of the mutual interference on nuclear characteristics are studied.

The cause for a systematic dependence of effective multiplication factors on ^{238}U concentration ratio as seen in the former JAERI-Fast set version 1R is studied by using an adjustment method to important

cross section of ^{235}U, ^{238}U and ^{239}Pu. The cross-section adjustment is performed by using auxiliary equation for simultaneous evaluation. In the unresolved resonance region, the average resonance parameters are searched by an iterative method to fit the adjusted cross sections. Furthermore, Monte Carlo method is applied to generate the ladder of resonance parameters. The resonance shielding factors and infinitely dilute cross sections are produced by ultra-fine group calculations. As a result, the JFS-2 set is generated and the benchmark tests are performed for many physics mock-up cores. It is shown that the prediction of JFS-2 on various nuclear characteristics is more satisfactory than it of ENDF/B-IV or JFS-1R on them.

Moreover, several studies are performed to advance the concept of the group constant set JFS-2 as follows. Accuracy of various interpolation methods for resonance shielding factors is examined and it is shown that the cubic spline interpolation produces the most excellent accuracy with short computing time. The experimental analysis of Doppler effect for structural materials are performed. It is shown that the temperature dependence of capture cross sections should be taken into account for the group constants of these materials. The effect of self-shielding of the iron inelastic scattering cross section on neutron spectra is examined. The effects of the difference between the fission spectra on effective multiplication factor and reaction rate distribution are studied. The effects of the elastic removal cross sections overestimated by using the usual 1/E spectrum on various nuclear characteristics are investigated as compared with them calculated with use of the removal cross sections which are produced by using a fine-group collision density spectrum. It is shown that this effect contributes seriously to the Doppler reactivity.

A new group constant set JFS-3-J2 is generated by considering the results described above, using the recently evaluated nuclear data of JENDL-2B. Also for the JFS-3-J2, the benchmark calculations are performed with the one-and two-dimensional models. It is shown that the JFS-3-J2 predicts various nuclear characteristics very satisfactorily, excepting the overestimate for positive sodium void reactivity. Especially, the average value of effective multiplication factors calculated for fourteen fast critical assemblies with pultonium fuels is 0.9996 and the prediction for k_{eff} is more excellent than it of ENDF/B-IV or JFS-2.

Keywords: Group Constant Set, Fast Reactors, Cross Section Adjustment, Cross Section Evaluation, Neutron Slowing Down Equation, Mutual Interference Effect, Multilevel Formula, Resonance Shielding Factor, Benchmark Tests, Physics Mock-up Assembly, Effective Multiplication Factor, Central Reaction Rate Ratio, Central Sample Worth, Doppler Reactivity Coefficient, Sodium Void Reactivity, Reaction Rate Distribution, Fine-Group Collision Density Specturm, Standard Weighting Specturm, Elastic Removal Cross Section, Fission Spectrum, Structural Materials Doppler Effect, Cubic Spline Interpolation

JAERI－M 83－075

高速炉解析における群定数作成法の研究

日本原子力研究所東海研究所原子炉工学部

高野秀機

（1983年4月22日受理）

高速炉の核特性を精度良く予測するために群定数の作成法について研究した。共鳴エネルギー領域においては，ABBNのような標準群定数セットで使用された近似重みスペクトラムでもって計算した場合の精度を調べ，群定数計算に対する衝突密度一定の基本的な仮定が，1KeV以下のエネルギー群あるいは高濃度の燃料体系においては必ずしも満足ではないことを示した。さらに，ブライト・ウィグナー一準位公式の利点を活かした多準位公式を導出し，分離及び非分離領域での共鳴間の干渉効果を調べた。また，無限均質体系での中性子減速方程式を数値的に解いて，異核種間の干渉効果を計算し，それが核特性へ及ぼす影響を明らかにした。

従来のJAERI－Fast セットJFS－1Rにおいて見られるような実効増倍係数の^{238}U希釈比に対する系統的な依存性の原因を，^{235}U，^{238}Uと^{239}Puの重要な断面積に対して，同時評価のための補助方程式を導入した断面積調整法を用いて明らかにした。非分離共鳴領域においては，調整断面積に良く適合した平均共鳴パラメータを繰り返し法を用いて決定し，さらにモンテカルロ法を用いて共鳴列を作成して，共鳴遮蔽因子と無限希釈断面積を超詳細群計算によってもとめた。このようにして新しく群定数セットJFS－2を作成し，多くの物理的モックアップ炉心に対してベンチマーク計算を実施した。その結果，このセットはENDF／ⅠⅤやJFS－1Rよりも種々の核特性に対して優れた予測精度を示した。

JFS－2セットの群定数の概念を発展さすべく次のような研究を実施した。共鳴遮蔽因子に対する種々の内挿法の精度を調べ，スプライン関数による内挿精度が最も優れていることを示した。構造材核種のドップラー効果の実験解析を行い，群定数セットにこれら核種の捕獲断面積に温度依存性を考慮すべきであることを示した。鉄の非弾性散乱断面積の自己遮蔽効果を計算し，中性子スペクトルへの影響を明らかにした。分裂スペクトラムの核種による相違が実効増倍係数と反応率分布へ与える効果を明らかにした。さらに除去散乱断面積を詳細群での衝突密度スペクトラムを用いて計算し，1／Eスペクトラムを用いることの過大評価が種々の核特性へ与える影響を調べ，特にドップラー効果への影響が重要であることを示した。

上述したいくつかの研究結果を取り入れて，さらに新しい群定数セットJFS－3－J2の作成を，最近の評価済み核データJENDL－2Bを用いて行い，このJFS－3－J2の一，二次元ベンチマーク計算を実施した。その結果，JFS－3－J2セットはナトリウム・ボイド反応度に対する過大評価を除いて，種々の核特性を非常に良く予測することが分った。特に14ケのプルトニウム炉心に対する実効増倍率の平均値は0.9996でありENDF／B－ⅣやJFS－2よりも良い予測精度を示した。

Contents

目　　次

List of Figures

1. Introduction

In reactor calculations, energy-dependent neutron transport and/or diffusion equation is solved on the basis of multigroup theory in which energy variable is not treated as being continous, but the range of interest is divided into a finite number of discrete energy groups. Nuclear design calculations of fast reactors are usually performed using the multigroup diffusion theory. For analysis of fast critical experiments, furthermore, the multigroup transport theory is often used. The multigroup calculations are based on the concept of group constants[1],[2] generated by averaging basic nuclear data over the energy ranges corresponding to the groups, using a weighting spectrum which, in principle, depends on the composition in question. There are two kinds of linear and bilinear weights for the group constant calculations. It is known that the linear weight with real flux is requried for the preservation of reaction rates while the bilinear weight with real and adjoint fluxes is required for the preservation of worths. We will confine our attention to the group constant generated by a linear weighting method which is used for all the group constant sets published extensively. To determine the spectrum in the linear weight, two different methods are used. One is the rigorous method based on a fine group fundamental mode calculation[3]∿[5]. This method, however, has the disadvantage that a costly spectrum calculation must be performed for each different composition. Another is the simple and economic "group constant method" where the composition-dependent cross sections are calculated by interpolating self-shielding facotrs for a given mixture from the pregenerated group constant set. As the typical group constant set, there are the YOM[6], HR[7], ABBN[8], JAERI-Fast I (JFS-1)[9],[10]

CADARACHE-3[11], FD5[12], LIB-IV[13] and KFKINR[14].

The YOM set[6] was generated by using a hard neutron spectrum in a fast reactor of small core size (50 liter core). The dependence of group constants on composition and temperature was not considered. In the HR set[7], the composition-dependent cross sections were considered only for heavy weight resonant nuclides. The calculations of group constants were performed by using a fission spectrum for upper energy group and the spectrum obtained from constant collision density for lower energy groups. In the ABBN set[8], the dependnece of group cross sections on composition was taken into account not only for heavy nuclides, but also light and medium weight ones. Furthermore, temperature dependence of the cross sections was considered. The 25 group structure was provided for the energy range from 0.215 eV to 10.5 MeV. This basic concept of the ABBN set was adopted in the group constant sets[9]-[14] developed after the ABBN. In the JFS-1[9],[10], however, a 70-group structure which the number of group in the ABBN was increased by two or three times was taken to improve the accuracy of elastic removal cross sections of light and medium nuclides[29]. In resonance energy regions, group cross sections of heavy nuclides have been produced by ultrafine group calculations, and the self-shielding factors have been expressed as a function of three variables, composition, temperature and mutual interference parameters[10]. However, the benchmark tests of JFS-1 showed[26] that the discrepancies between the calculated and the measured values were not so small even for the effective multiplication factors and the spectral indices, which were very important integral quantities.

There are not any group constant sets which satisfy well the goal accuracy required from nuclear design study in large fast sodium cooled

reactors.[18),(19)] Accuracy of the group constant depends mainly on the accuracy of the nuclear data and of the weighting spectrum. The accuracy of the nuclear data is not satisfied as compared with those required from nuclear design calculations.[18),(19)] The fast reactor performance parameters are predicted with considerable uncertainty due to lack of accuracy in the nuclear data and also due to errors introduced in the method of calculations, though the source of uncertainties is mainly caused by the nuclear data. To elevate the prediction for the performance parameters, the group constant set generated is often improved on the basis of the reevaluations of the nuclear data, the benchmark tests[(15)-(17)] for many fast critical assemblies or the method of cross section adjustment based on the least square fits.[(11),(12),(20)] The group constant set produced with the cross section adjustment shows naturally satisfactory prediction for the integral data of similary fast criticals to those considered in the adjustment of cross sections. However, the adjusted cross sections are occasionaly widely different from the evaluated values for the differential measured data and hence the validity for the adjusted ones must be assessed as being compared with the differential data. Moreover, when the adjusted cross section set is used for nuclear design study of a large LMFBR, the extrapolation errors for core performance parameters must be studied[(22)] in detail.

Main purpose of the present study is the generation of a group constant set which predicts very satisfactorily the nuclear characteristics important for fast reactors. For this purpose, generation methods for the group constants are studied for both the methods of group constant calculation and nuclear data evaluation. As for the calculation method, there are several problems to be studied. Especially, a serious problem

is that in fast reactors, neutron spectrum is steeply reduced in lower energy region below about 1 keV and hence is very different from the 1/E spectrum which is commonly used for the calculation of group constants. In the present study for this problem, firstly, the accuracies of variously approximate calculation methods for group constant of heavy resonant nuclides are studied by solving numerically neutron slowing down equation. In addition, the overestimate of elastic removal cross sections calculated by using the 1/E spectrum is investigated as being compared with them calculated by using a fine-group collision density spectrum for the core composition of a typical fast reactor. As the other problems, there are the interference effect between resonances, the mutual interference between different resonant nuclides, the Doppler effect of structural materials, the interpolation accuracy of resonance self-shielding factors, the self-shielding effect of inelastic scattering cross section of iron and the effect of different fission spectra on nuclear characteristics. These problems also are studied in detail. As for the evaluation of nuclear data, it is very serious problem that the discrepancies among experimental values of differential cross sections are very large. Hence, though very high accuracy for the measurement of cross sections is required, it will not be satisfied in the near future. In the present study, therefore, the simultaneous evaluation for several important cross sections is studied on the basis of the adjustment method of group cross sections. Moreover, recently evaluated nuclear data is used for calculating the group constants. As the results, two group constant sets are produced and the benchmark tests of these sets are performed for many fast reactors to evaluate the prediction for nuclear characteristics.

In the ABBN set, the self-shielding factors were calculated by

assuming constant collision density. Moreover, the isolated narrow resonance approximation was used in the resolved resonance region, and the approximations called the methods A[23] and B[24] were applied for the unresolved region. The errors introduced by these approximations for effective cross sections have been examined[25] by being compared with those calculated by solving numerically neutron slowing down equation. Chapter 2 is devoted to describe the accuracy of the approximate calculations for group constants. It is shown that the basic assumtion of constnat collision density for group constant calculations is not always satisfactory for lower energy groups below about 1 keV and/or of systems with highly enriched fuel, and that the accuracy of the analytical treatments of methods A[23] and B[24] varies considerably with the energy group, the temperature, and the composition in question. Based on the results studied in this chapter, in the group constant sets of the JFS-type[10],[15],[39],[203], the resonance shielding factors for heavy resonant nuclides are calculated with the use of the accurate method which solves numerically the neutron slowing down equation.

In reactor calculations, most codes for calculating effective cross sections are usually adopted the Breit-Wigner single-level formula, because Doppler broadened cross sections are easily be calculated for both the resolved and unresolved resonance regions using single-level parameters evaluated for many nuclides. However, the single-level formula in which interference effect between resonances is neglected can not exactly represent resonance cross sections. In Chapter 3, a multilevel formula is derived to correct the single-level formula and it is the same as the single-level one except for the inclusion of additional interference parameters (u,v)[40] which represent the contribution of the interference effect. This

derived formula is therefore applicable to reactor calculations without much modifications of the existing codes for calculating the effective cross sections. Using this formula, the multilevel parameters of ^{235}U, ^{233}U and ^{238}U are calculated for typical resolved resonance energy ranges. In the unresolved region, the multilevel parameters are produced with random sampling method using average resonance parameters and level-spacings. The contribution of the interference effect to Doppler effect is examined. These results are mainly used for producing the JFS-2 set.

Several processing codes ETOX[32], MINX[33] and PROF-GROUCH-G[34] were developed to produce economically and conveniently the group constants from the nuclear data files like the ENDF/B-IV[30] or JENDL-1[31]. In these codes, however, the effective cross sections in the resonance regions are calculated by assuming the constant collision density and using the isolated narrow-resonance approximation. In Chapter 4, a processing code TIMS-1[35] in which Doppler broadened cross sections are calculated[69],[116] for ultra-fine group and which the group constants are generated by solving accurately the neutron slowing down equation for infinite homogeneous media including resonance and background nuclei is developed to avoid the errors[25] caused by the approximate calculations. The mutual shielding factors are accurately calculated by using the TIMS-1 code, and the contribution of the mutual shielding effect on nuclear characteristics are examined. Furthermore, the effects of the difference between the calculational methods for the group constants on the several integral quantities are studied by using two group constant sets produced with the TIMS-1 and ETOX. The developed code is used for generating the group constants of the JFS-2[15], JENDL-2B-70[39] and JFS-3-J2[203] sets for fast reactor calculations, and also for

producing the thermal reactor group constants of the SRAC-FASTLIB set.[219]

The original version of the JAERI Fast set (JFS-1)[9),(10)] produced on the basis of an advanced concept of the ABBN[8] has been assessed[26] by the benchmark calculations for the eight fast critical assemblies prescribed by Davey and Hess[16]. The calculational results for the effective multiplication factors (k_{eff}) and the central reaction rate ratios indicated a strong correlation on the concentration of ^{238}U in core, that is, the k_{eff} decreased with increasing the concentration ratio of ^{238}N to ^{239}N or ^{235}N, where N is the atomic number density. The JFS-1 was revised[26] on the basis of the reevaluations of cross sections for ^{235}U, ^{238}U, ^{239}Pu and ^{240}Pu and the revised set was called the JFS-1R. However, the systematic dependence of k_{eff} on the ^{238}U concentration ratio could not be removed even if JFS-1R was used. In Chapter 5, to eliminate this systematic tendency, the adjustment of group cross sections based on the least squares method is performed for the three important cross sections, $^{235}\sigma_f$, $^{238}\sigma_c$ and $^{239}\sigma_f$. These cross sections are adjusted for the energy range from 3.6 keV to 1.4 MeV, and they are reevaluated for the range from 1.4 to 10.5 MeV. Furthermore, the resonance parameters for ^{235}U, ^{238}U, ^{239}Pu and ^{241}Pu[157] are evaluated. In the unresolved resonance region, the average resonance parameters for ^{235}U, ^{238}U and ^{239}Pu are calculated by the least squares fit to the adjusted cross sections. In the resolved region, the interference parameters (u,v) described in Chapter 3 are used. As a result, the JAERI-Fast set version II (JFS-2) is produced by using these evaluated data and the ENDF/B-IV data with use of two processing codes TIMS-1[35] and PROF·GROUCH·G·II.[36] The accurate prediction of JFS-2 for nuclear

characteristics are assessed through the benchmark calculations for many fast critical assemblies. However, it is indicated that the benchmark tests of JFS-2 proposes several problems which the causes are not always clean. Hence, it is requried to study further the group constant generation method and the evaluation of cross sections.

In Chapter 6, the accuracy of the group constants calculated by the conventional standard weighting spectrum of 1/E is investigated by being compared with those produced with a fine-group collision density spectrum for the core composition in a typical fast reactor. The 1/E-spectrum method overestimates the elastic removal cross sections for low energy range below 1 keV, because neutron spectrum is steeply reduced in this energy region in fast reactors. The effect of the overestimate for the elastic removal cross sections on the nuclear characteristics is examined in detail through the benchmark calculations for many fast critical assemblies.

Domestic neutron nuclear data library JENDL-1[31] has been developed in JAERI after the completion of the JFS-2 set. The group constant set of the JFS-type with the 70-group structure has been produced from the JENDL-1 using the processing codes TIMS-1[35] and PROF-GROUCH-GII[36]. Various problems of the JENDL-1 were revealed[37] through the benchmark tests. As a result, the JENDL-2B[38] was produced as an updated file for JENDL-1. Also for the JENDL-2B, the group constant set of the JFS-type has been produced[39] and is called the JENDL-2B-70. The benchmark tests of JENDL-2B-70 showed comparable predictions for nuclear characteristics with the ones of JFS-2, except for the remarkable overestimate of JENDL-2B-70 for sodium void reactivety. In Chapter 7, an advanced set for JENDL-2B-70 is generated by using the code TIMS-PGG[125] on the basis of the studies described in Chapter 6 and Appendix A. The advanced set is called JFS-3-J2[203]

and differs from JENDL-2B-70 in the followings.

(1) The group cross sections are calculated by weighting with a fine-group collision density spectrum, to avoid the overestimate of elastic removal cross sections caused by assuming 1/E-weighting spectrum.(203)

(2) The temperature dependence of capture cross sections for structural materials, iron, chromium and nickel is considered.(44)

(3) The scheme of self-shielding factor tables is corrected to obtain high accuracy of interpolation for the f-table by using natural cubic spline function.(45)

(4) The self-shielding effect of inelastic scattering cross sections is considered for iron.(46)

(5) The neutron group to group transfer matrices of elastic scattering are expanded from P_0 to P_3.

(6) The fission spectrum is calculated for each fissionable isotope.(47)

(7) The JAERI standard group structure established for the intended application to LMFBR, LWR and shielding problems is adopted. The 70 group structure for LMFBR is composed of 69 groups for the energy range from 0.3224 eV the 10 MeV with the lethargy of 0.25 and one thermal group.

The benchmark tests of JFS-3-J2 are performed with the one- and two-dimensional benchmark models. It is shown that the JFS-3-J2 predicts more satisfactorily several nuclear characteristics than the JENDL-2B-70 as a whole. However, several problems which the causes are not clear are proposed also for the JFS-3-J2.

The JFS-3-J2 and JENDL-2B-70 sets are now used for the analyses in JUPITER (Japanese United States Program of Integral Test and Experimental Researches) project, especially JFS-3-J2 for the more realistic reactor calculations where control rod positions are included

in core.

In Appendix A.1, an accuracy of interpolation methods for resonance shielding factors is examined and the cubic spline method is suggested as a very practical means with good accuracy. Furthermore, the effects of the differences among the resonance shielding factors calculated with various interpolations on the nuclear characteristics are studied.

In the group constant sets developed till now, temperature dependence of cross sections of structural materials was neglected, though a strong Doppler effect was reported[42)-(44)] for the structural materials. In Appendix A.2, the Doppler effect of structural materials are studied through the analyses of the sample-Doppler experiments for iron and stainless steel in the FCA assemblies V and VI.

The effect of self-shielding on inelastic scattering cross sections was neglected by assuming a small energy dependence of the cross sections. This assumption is generally valid. An exception is iron for which the energy dependence of both inelastic scattering and total cross sections below about 2 MeV is rapidly. In Appendix A.3, the self-shielding factors of the inelastic scattering cross sections are calculated and the effect of the self-shielding on neutron spectrum is examined.

The fission spectrum of a main fuel isotope in core is commonly used in reactor calculations. However, the fission spectrum depends on fissionable nuclei. In Appendix A.4, the effect of the dependence on the nuclear characteristics is exaimed especially for the mixed fuel cores of uranium and plutonium as seen in FCA assemblies V and VI.

In this thesis, the thirty benchmark cores are used for the benchmark tests of several group constant sets. The one- and/or two-dimensional benchmark models for twelve criticals are described in Appendix B, excepting the eighteen models specified in Refs. (17) and (103).

2. Accuracy of Analytical Treatments for Resonance Absorption in Doppler Resonance Region

2.1 Introduction

In a large fast reactor, a significant contribution to the Doppler reactivity effect and to resonance absorption is provided by the relatively high energy resonance region of heavy elements. This is due to the distinctly harder neutron spectrum of the fast — as compared with thermal — reactors. Hence, an accurate calculation of resonance absorption in this important resonance region is demanded for studies on fast reactor safety and also for accurate estimation of breeding ratio.

There have been proposed in the past a variety of approximate methods[23),(24),(48)~(57)]. Most of these methods, however, have been based on the assumption of "constant collision density", and hence, are valid only when the collision density is weakly energy dependent; that is, when the neutron flux can be assumed to vary as the inverse of total cross section:

$$\phi(E) = \frac{1}{E\ \Sigma_t(E)} \qquad (2\text{-}1)$$

The various methods based on the assumption of Eq.(2-1), can be classified into three categories.

First is the case where individual resonances are experimentally well-known or thought to be theoretically well separated. The generally adopted approximations for this case are those known by the designations narrow-resonance (NR). In the case where the individual resonance are not experimentally well separated, the effective cross section can be obtained statistically by the technique commonly known as Nicholson's Method B under NR approximation[24]. However the assumption of well-separated

resonance is reasonable only in the low energy region, especially, with fissile nuclides. In this low energy region, the assumption expressed by Eq.(2-1) no longer holds, and the collision density is generally not constant, but markedly depressed by resonance absorption. This depression of collision density is particularly strong when the volume ratio of fuel and the concentration of fissile isotopes are high, as in the case of fast reactors. It is very doubtful whether this flux depression could be accurately treated by these conventional methods based on isolated resonance approximation with the assumption of constant collision density within an energy group. Thus, in the low energy region, these methods are likely to introduce considerable error in the calculation of effective cross sections and temperature coefficients.

The second category of approximate method covers cases where the resonances are not separated from each other and strongly overlap on account of the Doppler effect. This means that fluctuation of the cross section is very small. This permits the flux of the assumption of Eq.(2-1) to be evaluated by a series expansion around an average total cross section. This treatment was introduced by Feshbach, Goertzel & Yamauchi[23]. It is considered most useful for treatment of the high energy region, and is generally known as "Method A".

In the keV energy region important for calculating the Doppler effect of reactivity, however, the resonances of fissile nuclei are neither well-separated, nor entirely overlapping. What is more, on the resonances of fissile isotopes are superposed the large resolved resonances of ^{238}U. Therefore, the interaction between neighboring resonances in both same and different nuclear species will vitally affect the Doppler reactivity effect.

The third method covers the case where these interaction effects are taken into account. Various analytical methods have been developed to deal

with this case and the contribution of the interaction to the Doppler effect of reactivity has been discussed by many authors[53)∿57)]. In these methods, however, constant collision density is again assumed and the interference effect between resonance and potential scattering is neglected.

Furthermore, with a sodium cooled fast reactor it should be noted that it contains a large amount of sodium, and that there is a predominant resonance scattering by sodium near 3 keV where the neutron spectrum is strongly depressed. And near this resonance the abnormal energy dependence of the high alpha-value of ^{239}Pu[58)], the ratio of capture to fission, will come to play a very important role relevant to the competition between the absorption due to ^{239}Pu and the slowing down by sodium.

It should therefore be of very pertinent interest to know how much error is incurred by the use of the conventional approximate methods based on the assumption of constant collision density. For the resonances of ^{238}U and of ^{239}Pu, the accuracy of the NR approximation has been scarcely investigated. While for the narrow energy range below 300 eV for ^{239}Pu and 2.5 keV for ^{238}U, this aspect has been studied by Hwang covering the case of an infinite homogeneous medium with a composition typical of a dilute fast reactor, the unresolved region has been examined only by comparisons with the results from an approximate method[59)].

The resonance absorption rate can be accurately obtained by making use of a number of available computer codes[60)∿63)] to solve numerically the slowing down equation, granted that the resonance parameters can be determined experimentally. However, in a large fast reactor, such resolved region is narrower than the Doppler range of interest, and for fissile nuclei in particular the important resonance region definitely belongs to the unresolved region. Thus under the circumstances, the resonance absorption

rate has had to be calculated analytically by statistical treatment based on the statistics of the resolved resonance parameters[23][24][53]～[57]. Now, the resonance parameters and level spacings for the unresolved resonance region can be generated by random sampling method from their statistical distributions, and detailed studies on the mathematical and physical properties and the quantities of interest in fast reactor physics have been made by several authors[64]～[68]. By using these resonance parameter sets, therefore, the resonance absorption rate may be accurately obtained by a computer code prepared for the resolved resonance. The accuracy of conventional methods can thus be examined. A survey of this accuracy should be important for verifying the results obtained for the Doppler reactivity effect by various methods of calculation.

In this Chapter, by using the resonance parameter sets generated successfully in Ref.(68), the accuracy of the basic assumption of Eq.(2-1) for the various conventional methods is examined for the important Doppler resonance region to cover the case of homogeneous medium in fast reactors. The shielding factors and their temperature coefficients obtained by exact calculation of the flux of assumption of Eq.(2-1) are investigated in full detail over many energy groups below 21.5 keV for ^{238}U and below 10 keV for ^{235}U and ^{239}Pu. A similar detailed survey is undertaken also for the case where interaction effects between ^{238}U and ^{239}Pu are taken into account. From the results of studies on several compositions and temperatures, the limits of accuracy for conventional analytical methods will be estimated. In some of the energy groups, the results for several conventional methods are also shown and compared with those of the exact method.

2.2 Calculational Methods of Effective Cross Sections

The effective partial cross section for a process (capture, fission or scattering) is defined by the equation

$$\tilde{\sigma}_x = \frac{\int_{\Delta E} \sigma_x(E)\phi(E)\, dE}{\int_{\Delta E} \phi(E)\, dE} \tag{2-2}$$

where ΔE : Energy interval.

The predominant resonance absorber in a fast reactor is usually ^{238}U, and we may thus logically limit our consideration to the interference effect of a resonance absorber in question with ^{238}U. For the neutron flux $\phi(E)$, we consider the following three cases, and in the next section we shall compare the results obtained.

Case (1) Numerical Calculation

The flux $\phi(E)$ is obtained with precision at ultra fine energy points (about 120,000 points from 20 keV to 100 eV) by solving numerically the neutron slowing down equation. This calculation was performed by the code ERSE[63] using the microscopic cross sections tabulated by the code MCROSS-2[69]. In doing this, the slowing down source by moderators was approximated by those due to a fictitious moderator, i.e.,

$$\sum_j N_j \frac{1}{1-\alpha_j} \int_E^{E/\alpha_j} \sigma_{s_j}(E')\phi(E')\frac{dE'}{E'} \cong \frac{\Sigma_{s_m}}{1-\alpha_{s_m}} \int_E^{E/\alpha_{s_m}} \phi(E')\frac{dE'}{E'} \quad , \tag{2-3}$$

where $$\Sigma_{s_m} = \sum_j N_j \sigma_{s_j} \quad , \tag{2-4}$$

$$\alpha_{s_m} = \left(\frac{\tilde{A}-1}{\tilde{A}+1} \right)^2 \quad , \tag{2-5}$$

and σ_{s_j} is the total cross section of moderator j and assumed to be constant in an energy group. The errors incurred by this approximation using the fictitious moderator has been shown to be very small in the energy region of inferest where the NR approximation may be used for the moderators[70]. The atomic mass number of the moderator used in practical calculations was assumed to be $\tilde{A} = 30$[10].

Case (2) Calculation Based on $1/(E\ \Sigma_t(E))$ Flux

Here, the collision density is taken to be constant throughout each energy interval. This is the basic assumption adopted generally in analytical methods for calculating effective cross sections. In actuality, the collision density is known to depend both on energy and temperature: A large scattering resonance introduces the well-known Placzek oscillation in the collision density, and moreover, in a narrow energy group, strong resonance absorption causes also a gradual depression of the collision density. Therefore, a detailed investigation of the results obtained on this basic assumption, should permit estimation of the limit of accuracy attainable with the analytical methods. For this purpose, the $1/(E\ \Sigma_t(E))$ flux at ultra fine energy points is calculated accurately by superposing the total resonance cross sections of the nuclei under consideration derived with the code MCROSS-2[69].

Case (3) Analytical Calculations

The difficulties of obtaining an exact analytical solution to the neutron slowing down equation have led the development of a number of approximate solutions under the above basic assumption. We shall here take up the two already well established expedients commonly known as Methods A and B.

The Method B deals with cases where the individual resonances are well

separated, that is, where the level spacings of the resonances are greater than Doppler width. For this case, a number of techniques have been devised, which have thoroughly discussed[24][48]∿[52]. The effective cross section of Eq.(2-2) is given by the already familiar expression

$$\tilde{\sigma}_x = \frac{\sum_k \sigma_{0_k} \frac{\Gamma_{x_k}}{E_k} b_k J_k}{\Delta u - \sum_k \frac{\Gamma_k}{E_k} J_k} \quad , \qquad \text{(Method C)} \tag{2-6}$$

where

$$J_k = \frac{1}{2} \int_{-\infty}^{\infty} \frac{\psi_k}{\psi_k + a_k \chi_k + b_k} \, d q_k \quad , \tag{2-7}$$

$$b_k = (\sigma_p + \sigma_m) / \sigma_{0_k} \quad , \tag{2-8}$$

$$a_k = \sigma_{0_{Pk}} / \sigma_{0_k} \quad , \tag{2-9}$$

and Δu is lethargy width, while ψ_k and χ_k respectively represent the usual symmetric and antisymmetric Doppler line shape functions for the k-th resonance.

In Eq.(2-6), the second term of the denominator may be regarded as the correction term for flux depression. This term is often neglected as very small compared with Δu[71]. Then, Eq.(2-6) becomes

$$\tilde{\sigma}_x = \frac{1}{\Delta u} \sum_k \sigma_{0_k} \frac{\Gamma_{x_k}}{E_k} b_k J_k \quad . \qquad \text{(Method B)} \tag{2-10}$$

However, the correction term which we have neglected may not always be small, in particular for fissile isotopes. In highly concentrated systems of fissile isotopes, the difference between the results obtained from Eqs.(2-6) and (2-10) can become very large. The correction term obtained

under the assumption of isolated resonances may be overestimated for fissile isotopes due to narrow level spacings and wider fission widths.

In a case where the resonances are not separated experimentally but only theoretically, the effective cross section is obtained usually by averaging over the statistical distribution functions of each resonance parameter[24]. Then, Eq.(2-6) becomes

$$\langle \tilde{\sigma}_x \rangle_{y_n,y_f} = \frac{\Delta E}{\bar{D}} \frac{\int_0^\infty \int_0^\infty P(y_n)P(y_f)\sigma_0 \frac{\Gamma_x}{E^c} b\ J\ dy_n\ dy_f}{\Delta u - \int_0^\infty \int_0^\infty P(y_n)P(y_f) \frac{\Gamma}{E^c} J\ dy_n\ dy_f} , \qquad (2\text{-}11)$$

where $y_n = \Gamma_n/\bar{\Gamma}_n$, $y_f = \Gamma_f/\bar{\Gamma}_f$.

While $\bar{D}$, is the mean level spacing, $\bar{\Gamma}_n$ and $\bar{\Gamma}_f$ are the average neutron and fission widths, respectively, $P(y_n)$ and $P(y_f)$ are Porter-Thomas distribution functions for the neutron and fission widths, usually assumed to be a chi-squared distribution with 1 and 2 degrees of freedom, respectively, E^c is the mid-value of the energy interval ΔE. Equation (2-11) is usually calculated by the numerical method described by Greebler & Hutching[72]. In the unresolved region, the effective cross section may be also obtained from Eq.(2-6) or (2-10) in place of Eq.(2-11) by using the individual resonance parameters generated statistically[68]. In this case, the resonance parameters are generated in each orbital and total angular momentum, and are arranged in a sequence of resonances over the full energy range of interest. Hence, the sum on k in Eqs.(2-6) and (2-10) is to be extended over all the resonances contained in ΔE. The same meaning is used for the sums on k and k' in the ensuring equations from (2-15) to (2-19).

The Method A covers the case where the resonances are largely washed

out by the Doppler effect and are strongly overlapping. In this energy region the cross sections show only small fluctuations around the average value, that is, there applies everywhere the relation

$$\left| \frac{\sigma_t - \langle \sigma_t \rangle}{\langle \sigma_t \rangle} \right| \ll 1 \quad , \tag{2-12}$$

where $$\langle \sigma_t \rangle = \frac{1}{\Delta E} \int_{\Delta E} \sigma_t(E)\, dE \quad . \tag{2-13}$$

Then, the effective cross section is obtained by[23]

$$\tilde{\sigma}_x = \langle \sigma_x / E\sigma_t \rangle / \langle 1/E\sigma_t \rangle$$

$$= \langle \sigma_x \rangle - \frac{\langle \sigma_x \sigma_{rt} \rangle - \langle \sigma_x \rangle \langle \sigma_{rt} \rangle}{\langle \sigma_t \rangle} \quad , \qquad \text{(Method A)} \tag{2-14}$$

where $$\langle \sigma_x \rangle = \frac{1}{\Delta E} \sum_k \int_{\Delta E} \sigma_{00_k} \frac{\Gamma_{n_k} \Gamma_{x_k}}{\Gamma_k^2} \psi_k \, dE$$

$$= \frac{1}{\Delta E} \frac{\pi}{2} \sum_k \sigma_{00_k} \frac{\Gamma_{n_k} \Gamma_{n_k}}{\Gamma_k} \quad , \tag{2-15}$$

$$\langle \sigma_x \sigma_{rt} \rangle = \frac{1}{\Delta E} \sum_k \sum_{k'} \int_{\Delta E} \sigma_{00_k} \frac{\Gamma_{n_k} \Gamma_{x_k}}{\Gamma_k^2} \psi_k \, \sigma_{00_{k'}} \frac{\Gamma_{n_{k'}}}{\Gamma_{k'}} \psi_{k'} \, dE \quad , \tag{2-16}$$

$$\sigma_{00_k} = 4\pi \lambda\!\!\!^{-2} g_k = 2.6 \times 10^6 \, g_k / E_k \qquad (E_k \text{ in eV}) \quad . \tag{2-17}$$

The integral over two resonances k and k' with different individual total widths Γ_k and $\Gamma_{k'}$ has been derived by Hwang[73], who gave, for $\Gamma_k/\Delta \ll 1$.

$$\int_{-\infty}^{+\infty} \psi_k \psi_{k'} \, dE \cong \left(\frac{\pi}{2}\right)^{3/2} \frac{\Gamma_k \Gamma_{k'}}{2\Delta} \exp\left(-\frac{(E_k - E_{k'})^2}{2\Delta^2}\right) \quad . \tag{2-18}$$

Thus, in this case Eq.(2-16) is decomposed into diagonal and nondiagonal parts:

$$<\sigma_x\sigma_{rt}> = \frac{1}{\Delta E}\left(\frac{\pi}{2}\right)^{3/2}\frac{1}{2\Delta}\left[\sum_k \sigma_{00}^2{}_k \frac{\Gamma_{n_k}^2 \Gamma_{x_k}}{\Gamma_k}\exp\left(-\frac{\Gamma^2}{2\Delta^2}\right)\right.$$

$$\left. + \sum_k \sum_{k\neq k'} \sigma_{00}{}_k \sigma_{00}{}_{k'} \frac{\Gamma_{n_k} \Gamma_{x_k} \Gamma_{n_{k'}}}{\Gamma_k}\exp\left(-\frac{(E_k - E_{k'})^2}{2\Delta^2}\right)\right] \quad . \quad (2\text{-}19)$$

In this high energy region, the indiviudal resonance parameters generated statistically are used for the calculation of Eq.(2-14).

2.3 Comparison between Effective Cross Sections Calculated by Various Methods

In the unresolved resonance region, the individual resonance parameters generated in each (ℓ,J) sequence in Ref.(68) were used for calculating the effective cross sections, where ℓ and J respectively are orbital and total angular momentums. It has been shown that a single sequence of resonances suffices for good representation of the low-resolution pointwise data and statistically satisfy the distribution functions assumed[68]. The p-wave neutron cross sections were adopted for the energy range above 1 keV. Thus, for three cases of the previous section, the effective cross sections were calculated by using the same resonance parameters. The resonance cross sections used in the cases (1) and (2) were obtained by using a multilevel formula based on the Vogt approximation[74]. On the other hand, for the treatments adopted for the analytical calculations, they were assumed to be expressed by the Breit-Wigner single level formula. However, it should be noted that the difference between the multilevel and single level formulas, while important for the resonance cross sections of fissile

nuclei in the lower energy regions[74], it is very small and may be neglected in the high energy region which is of interest here.

Comparison of the results obtained from the foregoing different methods of calculation was made mainly by examining the two quantities

$$E_x = \frac{f_x^{appro.} - f_x^{exact}}{f_x^{exact}} \times 100 \ (\%) \tag{2-20}$$

and

$$\Delta f_x = \frac{f_x\,(T = T_2) - f_x\,(T = T_1)}{T_2 - T_1} \times 10^4 \tag{2-21}$$

where $f_x^{appro.}$ is either the self or the mutual shielding factor obtained from the approximate calculation of the cases (2) and (3), and f_x^{exact} that from the accurate calculation of the case (1), while T represents temperature. These relative errors and temperature coefficients of shielding factor were calculated for three temperatures (300°, 900° and 2,100°K) and for several compositions. In particular, the values of E_x for the basic assumption were examined for ^{235}U, ^{238}U and ^{239}Pu over all the energy groups of practical interest in a large fast reactor. The energy group boundaries and lethargy widths for these cases are given in Table 2.1. The analytical methods were examined in detail for representative energy groups 1, 6 and 13. The results for Eqs.(2-14), (2-10) and (2-6) are shown by symbols A, B and C, respectively, in Figs. 2.1 ~ 3. We here call these three treatments Methods A, B and C, respectively.

Figure 2.1 shows the relative errors for self-shielding factors of ^{235}U in the energy range from group 4 to group 21. When $\sigma_m = 100$ barn, the errors introduced by the basic assumption are small and do not exceed ±2 % for both capture and fission cross section in the groups above 21. However, when the concentration of ^{235}U fuel is higher, the errors can

become very large, as may be seen in the case of $\sigma_m = 10$ barn. In this case, the energy groups in which the errors are below ±5 % are from groups 4 to 12, and the errors caused by the basic assumption show a tendency to become large with decreasing neutron energy. The results for scattering cross section are not shown in this figure, but the errors are smaller than those for capture and fission cross sections.

For $\sigma_m = 100$(b), the errors for the results of the analytical methods are also shown for energy group 13. Methods A and B give comparatively good results, but the error incurred by Method C is very large. The reason for this is overestimation of the correction term for flux depression, because of the very small level spacing of ^{235}U resonances.

Figure 2.2 shows the relative errors of self-shielding factors for ^{238}U in the energy groups from 21.5 keV to 278 eV. From this figure, the errors incurred by adopting the basic assumption are below ±3% for both the capture and scattering cross sections in the energy groups above 598 eV. For these energy groups, therefore, the basic assumption may be considered to provide a very good approximation for ^{238}U. The errors become large for smaller values of σ_m and lower energy groups.

In Fig. 2.2, the results obtained with the analytical calculations also are shown for the three energy groups 1, 6 and 13. In the case of $\sigma_m = 100$ barn, the relative errors with Methods B and C are never much more than ±5 % for these three typical energy groups. When the values of σ_m become small, the errors introduced by Methods B and C become very large. Comparing the relative errors between Methods B and C, it is seen that in the former the effect of the correction term for flux depression is very large. It is however difficult to say which of the two methods is better for the self-shielding factors. The results for Method A are shown for the two groups 1 and 6. Though Method A shows very good results for

the case of $\sigma_m = 100$ barn in group 6, this must be attributed to accidental cancellation of errors, because logically the resonances of ^{238}U must be well separated in group 6.

Figure 2.3 shows the relative errors of ^{239}Pu self-shielding factors in the energy groups from 10 keV to 215 eV. In the case of $\sigma_m = 1,000$ barn, in particular, the results obtained with the basic assumption are very good. The errors introduced by the basic assumption are never much more than ±2.5 % for the case of $\sigma_m = 100$(b) and ±1 % for the case of $\sigma_m = 1,000$(b) in the energy groups above 465 eV for both capture and fission cross sections. The errors for scattering cross sections are not shown, but they are not much different from those of capture and fission cross sections. For ^{239}Pu, it is seen from Fig. 2.3 that the results obtained on the basic assumption are quite similar to those described above for ^{235}U and ^{238}U.

In Fig. 2.3, the results obtained with the analytical treatments also are shown for the two energy groups 6 and 13. The analytical calculations give good results for the case of $\sigma_m = 1,000$(b) in group 6. In this group, Method A provides better values than Methods B and C. When $\sigma_m = 100$(b), the errors are much larger than for $\sigma_m = 1,000$(b).

Figure 2.4 shows the relative errors of shielding factors for ^{239}Pu, which comprises the interaction effect with ^{238}U. In this figure, only the results for the case (2) are shown. Comparing Fig. 2.3 with Fig. 2.4, it is seen that the errors induced by the basic assumption are accentuated by a factor of more than two when the mutual interaction effect are taken into consideration. Except for this important point, the various tendencies seen in the errors are very similar to those for ^{239}Pu shown in Fig. 2.3.

The temperature coefficients for the shielding factors calculated by the various methods are compared. While the temperature variation for the shielding factor may be gusessed from the data given in Figs. 2.3, 3 and 4,

we give explicitly in Tables 2.2 and 3 the temperature coefficients of the self-shielding factor for ^{238}U. Quite naturally, the temperature coefficient is better for the case (2) of the basic assumption than that for any of the analytical methods, that is underestimated a little except for group 1. In group 6, the errors introduced by the analytical Method A are very large, due to non-satisfaction of Eq.(2-12). This method, however, gives comparatively good results in group 1 for $\sigma_m = 100$(b). Methods B and C both incur large errors, though between the two the latter is somewhat better. When σ_m become small, the temperature coefficient becomes large.

Tables 2.4 and 5 show the temperature coefficients of the self-shielding factor for ^{239}Pu. These tables indicate that the analytical methods overestimate the temperature coefficients. Method B gives better results than Method C. The results from the case (2) calculations are very much better than from the analytical treatments.

Table 2.6 provides a comparison of the temperature coefficients for the shielding factor of ^{239}Pu comprising the interaction with ^{238}U, in the two groups 6 and 13. When mutual interaction is put aside, the basic assumption gives compartively good results on the temperature coefficients, but consideration of the mutual interaction effects greatly increases the errors. This is clear from a comparison of the temperature coefficients in group 13. This point is very important for considerations on the Doppler reactivity coefficient and from the practical standpoint of obtaining high α-value for ^{239}Pu.

2.4 Concluding Remarks

The main conclusions that can be drawn from the present study may be summarized as follows:

While the collision density is not constant, and, strictly speaking, depends on energy and temperature, the resonance shielding factors and the temperature coefficients obtained on this assumption for prescribed energy intervals — case (2) treatment — results in good agreement with those from exact numerical treatment — case (1) — for the Doppler resonance region of interest in practical composition of typical large fast reactors. For the resonances of ^{235}U, ^{238}U and ^{239}Pu, when $\sigma_m = 100$ barn, the error of the shielding factors obtained from case (2) treatment is not much above ±3 % for energy groups higher than 14. For lower energy groups and for systems with highly enriched fuel, the basic assumption of constant collision density, represented by Eq.(2-1) is not always satisfactory, and the errors introduced by this assumption have a tendency to become large. Furthermore, the errors introduced in the shielding factors of ^{239}Pu through superposition of the resonances of ^{238}U accentuate the deviations by a factor of more than two.

The best accuracy obtainable with the approximate methods may be represented by the case (2) calculations. We have compared this with the case (3) treatment methods (Methods A, B and C) for typical energy groups and for several compositions and temperatures. It has been found that the accuracy of these methods varies considerably with the energy groups considered, the temperatures in question and the values of σ_m taken up. Except for cases of accidental cancellation of errors, case (3) calculations incur errors several times those of case (2).

The computing costs for the cases (1) and (2) are comparable.

Hence, we conclude that the case (1) should be used for the calculations of effective cross sections.

[NOMENCLATURE]

$\phi(E)$: Neutron flux at energy E

$\Sigma_t(E)$: Macroscopic total cross section ($= \Sigma_a(E) + \Sigma_s(E) + \Sigma_m$)

$\sigma_t(E)$: Microscopic total cross section

$\sigma_a(E)$: Microscopic absorption cross section ($= \sigma_o \frac{\Gamma_\gamma + \Gamma_f}{\Gamma} \psi$)

$\sigma_s(E)$: Microscopic scattering cross section

$$(= \sigma_o \frac{\Gamma_n}{\Gamma} \psi + 2\sigma_{op} \frac{\Gamma_n}{\Gamma} \chi + \sigma_p)$$

σ_m : Sum of total cross sections of all other elements included in medium referred to a single atom of fuel absorber

σ_p : Microscopic potential scattering cross section

σ_{rt} : $\sigma_t - \sigma_m - \sigma_p$

k : Resonance at energy E

$$\psi, \psi_k : \frac{\theta_k}{2\sqrt{\pi}} \int_{-\infty}^{+\infty} \frac{e^{-\frac{\theta_k^2}{4}(q_k - y)^2}}{1 + y^2} dy$$

$$\chi, \chi_k : \frac{\theta_k}{2\sqrt{\pi}} \int_{-\infty}^{+\infty} \frac{y\, e^{-\frac{\theta_k^2}{4}(q_k - y)^2}}{1 + y^2} dy$$

θ_k : Γ_k / Δ

q_k : $2(E - E_k) / \Gamma_k$

Δ : Doppler width ($= \sqrt{\frac{4K\,T\,E_k/M}{M}}$), where K is Bolzman constant, T temperature (°K) and M atomic mass of absorber, respectively

Δu : Lethargy width : $\int_{E_1}^{E_2} \frac{1}{E}\, dE = \ell n(E_2/E_1)$

ΔE : $E_2 - E_1$

Γ_k : Total width of k resonance

Γ_{γ_k} : Radiative width of k resonance

Γ_{n_k} : Neutron width of k resonance

Γ_{f_k} : Fission width of k resonance

σ_o : Peak resonance cross section

σ_{op_k} : $(\sigma_{o_k} \sigma_p q_k \Gamma_{n_k} \Gamma_k)^{1/2}$

g_k : Statistical spin factor

E_1, E_2 : Lower and upper energies, respectively

Table 2.1 Energy group numbers and boundaries used in calculation

Group No.	Lower energy	Upper energy
1	16.6	21.5 (keV)
2	12.9	16.6 (keV)
3	10.0	12.9 (keV)
4	7.73	10.0 (keV)
5	5.98	7.73 (keV)
6	4.65	5.98 (keV)
7	3.60	4.65 (keV)
8	2.78	3.60 (keV)
9	2.15	2.78 (keV)
10	1.66	2.15 (keV)
11	1.29	1.66 (keV)
12	1.0	1.29 (keV)
13	773	1000 (eV)
14	598	773 (eV)
15	465	598 (eV)
16	360	465 (eV)
17	278	360 (eV)
18	215	278 (eV)
19	166	215 (eV)
20	129	166 (eV)
21	100	129 (eV)

Table 2.2 Comparisons of temperature coefficient for self-shielding factors of ^{238}U — σ_m = 10 (b)

Method of calculation	Reaction	Group 1		Group 6		Group 13	
		300° ~ 900°K	300° ~ 2,100°K	300° ~ 900°K	300° ~ 2,100°K	300° ~ 900°K	300° ~ 2,100°K
Method A	Δf_c	0.6433	0.3200	3.065	1.5538		
	Δf_s	0.7100	0.3433				
Method B	Δf_c		0.1655	0.7483	0.4427	0.810	0.5444
	Δf_s		0.1566	0.4716	0.2911	0.2083	0.1661
Method C	Δf_c		0.2238	0.8083	0.6255	1.0433	0.7344
	Δf_s		0.1983	0.6266	0.4027	0.275	0.2239
$1/E\ \Sigma_t$	Δf_c	0.5417	0.2772	1.2116	0.6427	1.0933	0.7472
	Δf_s	0.3383	0.1944	0.7867	0.4516	0.4900	0.3361
Exact	Δf_c	0.5550	0.2694	1.2280	0.6616	1.105	0.7550
	Δf_s	0.3433	0.1956	0.8150	0.4750	0.5167	0.3611

Table 2.3 Comparisons of temperature coefficient for self-shielding factors of ^{238}U — $\sigma_m = 10^2$ (b)

Method of calculation	Reaction	Group 1		Group 6		Group 13	
		300° ~ 900°K	300° ~ 2,100°K	300° ~ 900°K	300° ~ 2,100°K	300° ~ 900°K	300° ~ 2,100°K
Method A	Δf_c	0.1283	0.0650	0.6616	0.3322		
	Δf_s	0.1367	0.0706	0.8416	0.4438		
Method B	Δf_c		0.0617	0.4933	0.2688	1.6133	1.0211
	Δf_s		0.0628	0.4583	0.2650	0.6983	0.4544
Method C	Δf_c			0.5466	0.3016	1.8250	1.1683
	Δf_s			0.500	0.2900	0.7733	0.5983
$1/E\ \Sigma_t$	Δf_c	0.1533	0.0789	0.5833	0.2955	1.6417	1.0183
	Δf_s	0.1400	0.0772	0.5583	0.2955	0.870	0.5583
Exact	Δf_c	0.1500	0.0756	0.5883	0.2988	1.6833	1.0422
	Δf_s	0.1400	0.0772	0.5716	0.3044	0.9067	0.5889

Table 2.4 Comparisons of temperature coefficient for self-shielding factors of ^{239}Pu — $\sigma_m = 10^2$(b)

Method of calculation	Reaction	Group 6		Group 13	
		300° ~ 900°K	300° ~ 2,100°K	300° ~ 900°K	300° ~ 2,100°K
Method A	Δf_c	0.4850	0.2417	2.7133	1.3561
	Δf_f	0.2983	0.1594	1.9100	0.9322
	Δf_s	0.2033	0.0967	1.4917	0.7639
Method B	Δf_c		0.1811	1.1750	0.6483
	Δf_f		0.100	0.7033	0.4150
	Δf_s		0.0689	0.4450	0.2650
Method C	Δf_c		0.2039	1.5200	0.8511
	Δf_f		0.1350	0.9817	0.5822
	Δf_s		0.0772	0.5700	0.3344
$1/E\ \Sigma_t$	Δf_c	0.2783	0.1400	1.2800	0.6767
	Δf_f	0.1783	0.1172	0.7733	0.4589
	Δf_s	0.1167	0.0617	0.5383	0.3106
Exact	Δf_c	0.2733	0.1411	1.2317	0.6517
	Δf_f	0.1750	0.1183	0.7600	0.4589
	Δf_s	0.1167	0.0628	0.5217	0.3033

Table 2.5 Comparisons of temperature coefficient for self-shielding factors of ^{239}Pu — $\sigma_m = 10^3$(b)

Method of calculation	Reaction	Group 6		Group 13	
		300° ~ 900°K	300° ~ 2,100°K	300° ~ 900°K	300° ~ 2,100°K
Method A	Δf_c	0.0533	0.0267	0.3383	0.1689
	Δf_f	0.0317	0.0189	0.2367	0.1150
	Δf_s	0.0350	0.0117	0.1883	0.0961
Method B	Δf_c		0.0233	0.2500	0.1278
	Δf_f		0.0144	0.1700	0.0922
	Δf_s		0.0189	0.1233	0.0661
Method C	Δf_c		0.0267	0.2567	0.1322
	Δf_f		0.0144	0.1767	0.0956
	Δf_s		0.0094	0.1233	0.0656
$1/E\ \Sigma_t$	Δf_c	0.0450	0.0228	0.2383	0.1139
	Δf_f	0.0150	0.0333	0.1733	0.1111
	Δf_s	0.0167	0.0100	0.1300	0.0744
Exact	Δf_c	0.0350	0.0206	0.2367	0.1144
	Δf_f	0.0183	0.0344	0.1733	0.1133
	Δf_s	0.0183	0.0117	0.1250	0.0733

Table 2.6 Comparison of temperature coefficients for shielding factor of ^{239}Pu due to interaction with ^{238}U

Method of calculation	Reaction	σ_m = 100 (b), N_8/N_9 = 5				σ_m = 1000 (b), N_8/N_9 = 50			
		Group 6		Group 13		Group 6		Group 13	
		300° ~ 900°K	300° ~ 2,100°K	300° ~ 900°K	300° ~ 2,100°K	300° ~ 900°K	300° ~ 2,100°K	300° ~ 900°K	300° ~ 2,100°K
$1/E\ \Sigma_t$	f_c	0.2780	0.1435	0.9837	0.4941	0.1209	0.0671	0.0648	0.0235
	f_f	0.1338	0.0975	0.7570	0.4527	0.0122	0.0364	0.2438	0.1698
	f_s	0.1045	0.0619	0.4788	0.2933	0.0348	0.0276	0.1125	0.0938
Exact	f_c	0.2868	0.1526	0.8890	0.4156	0.1306	0.0738	-0.0148	-0.0440
	f_f	0.1267	0.0949	0.6371	0.3873	0.0084	0.0349	0.1225	0.1011
	f_s	0.1146	0.0695	0.4287	0.2600	0.0450	0.0353	0.0737	0.0679

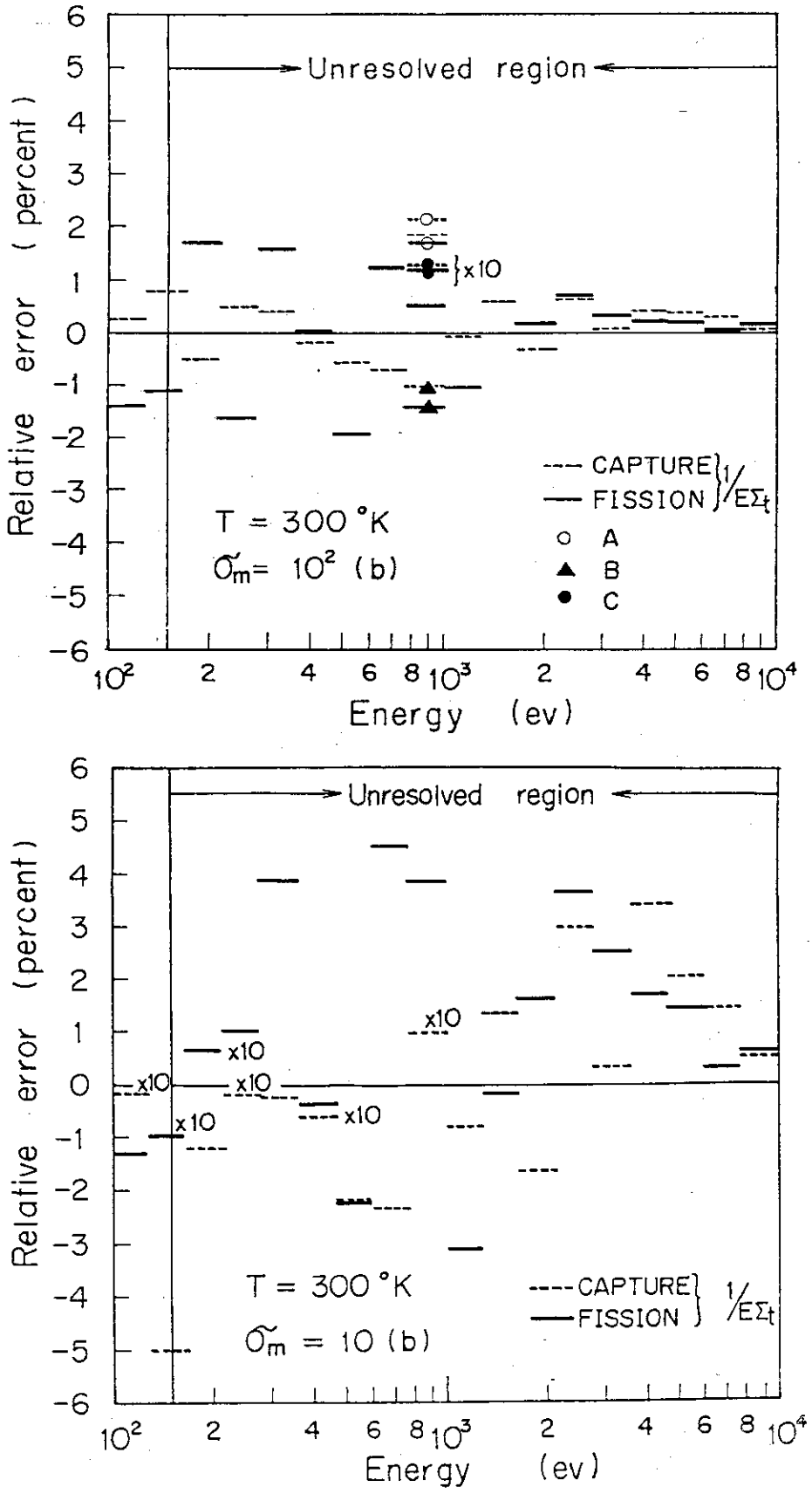

Fig.2.1 Relative errors for ^{235}U self-shielding factors obtained by exact calculation and by several approximate methods of calculation

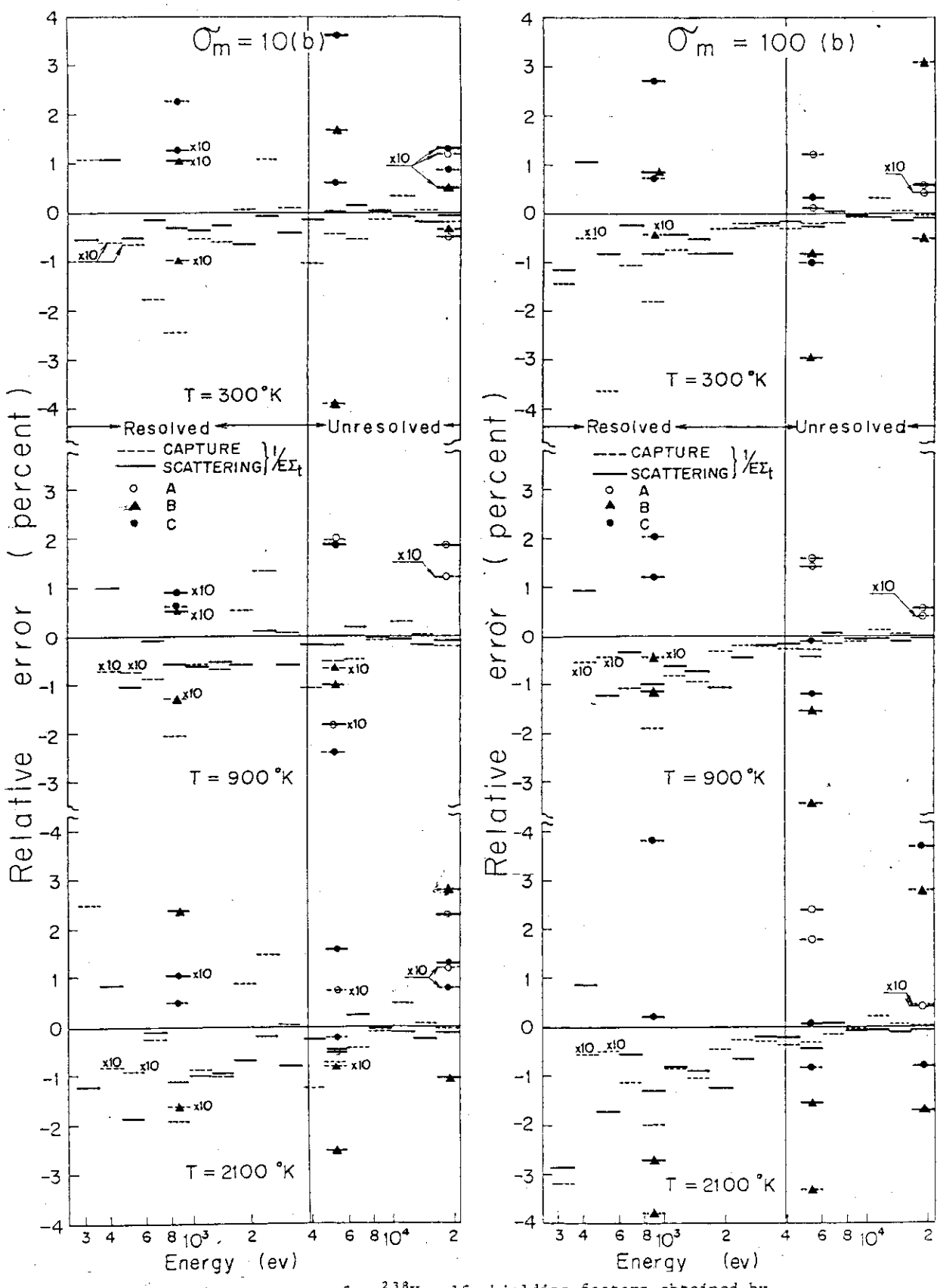

Fig.2.2 Relative errors for ^{238}U self-shielding factors obtained by exact calculation and by several approximate methods of calculation

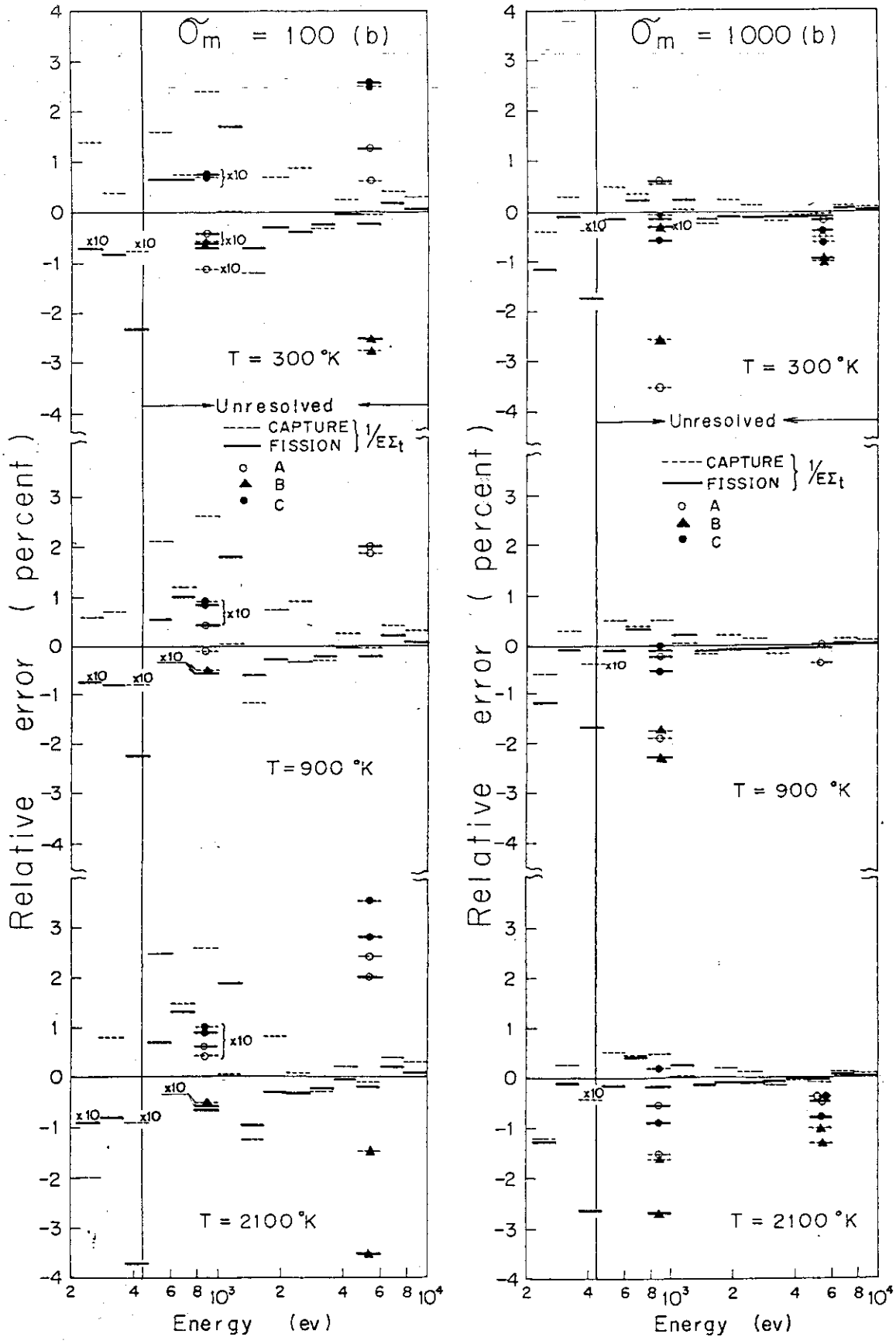

Fig.2.3 Relative errors for ^{239}Pu self-shielding factors obtained by exact calculation and by several approximate methods of calculation

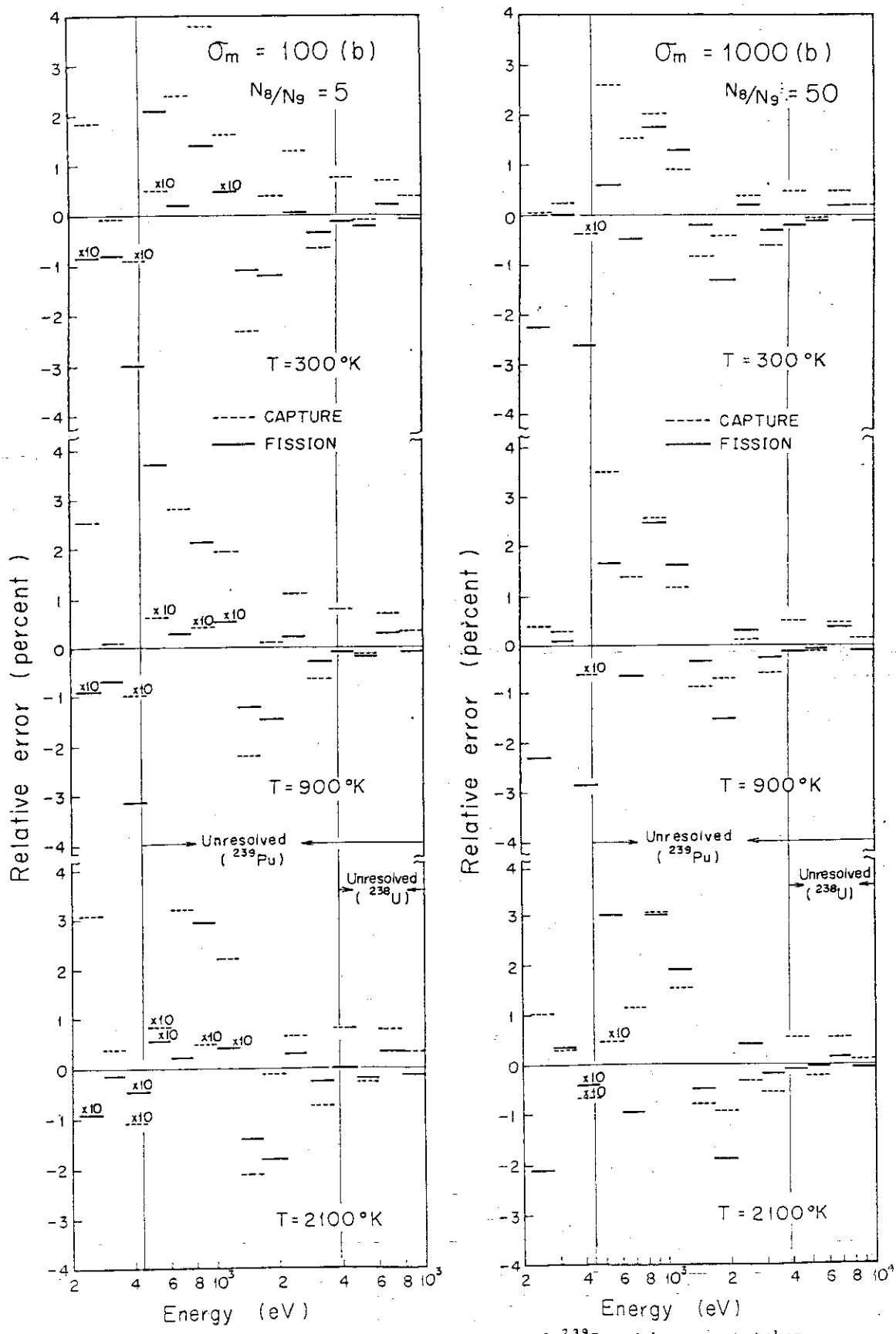

Fig.2.4 Relative errors for shielding factors of ^{239}Pu with account taken of interaction with ^{238}U - obtained from exact calculation and from basic assumption $\phi(E) = 1/(E\ \Sigma_t(E))$.

3. Multi-Level Correction to Breit-Wigner Single-Level Formula

3.1 Introduction

It has been often pointed out that the single-level formula derived by Breit and Wigner[75] can not exactly represent the resonance cross section for fissile nuclei. This is due to an interference effect between resonances[76]. In order to take account of the interference effect, many researchers[61],[76]~[81] have attempted to represent the cross section by using a more general form than the Breit-Wigner formula. The methods developed by Reich-Moore[77] and Vogt[78] were based on the Wigner-Eisenbud resonance theory[79]. None of these methods, however, can easily represent the Doppler broadened cross section. Furthermore, the Vogt formula[78] is too complicated to perform the least squares fit of cross sections for an energy range having many resonances. Adler and Adler[80] introduced the multi-level formula which took these draw-backs away on representing the resonance cross sections. The Adler-Adler formula has therefore been used often for the cross section analysis of fissile nuclei. Furthermore, Brissenden and Durston[16] introduced the multilevel formula in which the interference effect was treated by using the Vogt's parameters. Their expression is devided into two parts of single-level and interference contributions and is very useful for reactor physics purpose.

In reactor physics, most resonance integral codes have usually adopted the Breit-Wigner single-level formula in the following considerations:

1) A large number of the single-level parameters have been already evaluated for many nuclei[82]. 2) The discrepancies between measured and calculated cross sections are generally small, so that the differences can practically be corrected by considering appropriate background cross sections.

3) The Doppler broadened cross sections can easily be calculated.

4) The statistical distribution functions[83][84] are known well for level widths and spacings of resonances. 5) The average cross sections are calculated from the average resonance parameters and the distribution functions[24]. 6) Doppler effect can be calculated for the unresolved resonance region[24].

It will therefore be useful to improve the Breit-Wigner single-level formula so as to include the interference effect between the resonances without losing the useful characteristic. In this Chaper, a multi-level formula is derived on the basis of the formula of Brissenden and Durston[61]. This formula contains a set of new parameters (u,v), to treat the interference effect and to avoid the complication for cross section analysis. In the section 3.3, examples of the least squares fits are shown for the cross sections of ^{235}U, ^{233}U, and ^{238}U in the resolved resonance region. Furthermore, the interference effects are studied for both the energy variations in cross sections and the Doppler effects in the unresolved resonance region.

3.2 Expressions of Reaction Cross Sections

The reaction cross section in generally expressed by the use of the collision matrix $U_{c\bar{c}}$. In the R-matrix theory, the collision matrix is given as follows:[78]

$$U_{c\bar{c}} = \exp[-i(\phi_c + \phi_{\bar{c}})][\delta_{c\bar{c}} + i \sum_{\lambda\bar{\lambda}} \sqrt{\Gamma_{\lambda c}\Gamma_{\bar{\lambda}\bar{c}}}\, A_{\lambda\bar{\lambda}}] \quad , \tag{3-1}$$

where ϕ_c is the hard sphere scattering phase shift, $\delta_{c\bar{c}}$ the Kronecher's delta, λ denotes the resonance level, $\Gamma_{\lambda c}$ is the partial width for decay of the state (λ) through channel c, and A is the level matrix.
The inverse of the level matrix A is given by[78],[85]

$$A^{-1}_{\lambda\bar{\lambda}} = (E_\lambda - E)\delta_{\lambda\bar{\lambda}} - \frac{i}{2}\sum_{\bar{c}} (\Gamma^{1/2}_{\lambda\bar{c}}\ \Gamma^{1/2}_{\bar{\lambda}\bar{c}}) \quad , \tag{3-2}$$

where E_λ is the resonance energy. Practically, the calculation of the cross sections is very difficult when many interacting levels are present. The perturbation approach[61],[80] is therefore useful for the inversion of the level matrix. Adler-Alder used this approach to obtain the relation between the S-matrix[81] and the R-matrix representations. We can derive on approximate level matrix A' by using the method as follows:

$$A = (D+N)^{-1} = D^{-1}(1+ND^{-1})^{-1} \cong D^{-1} - D^{-1}ND^{-1} \quad , \tag{3-3}$$

where D and N are the diagonal and off-diagonal parts for the matrix A^{-1} respectively, and the right hand side of Eq.(3-3) is defined here as an approximate level matrix A':

$$A'_{\lambda\bar{\lambda}} = \frac{\delta_{\lambda\bar{\lambda}}}{Z_\lambda} + \frac{i}{2}(1-\delta_{\lambda\bar{\lambda}})\frac{G_{\lambda\bar{\lambda}}}{Z_\lambda Z_{\bar{\lambda}}} \quad , \tag{3-4}$$

where

$$Z_\lambda = (E_\lambda - E) - \frac{i}{2}\Gamma_\lambda \quad , \tag{3-5}$$

$$\Gamma_\lambda = \sum_c \Gamma_{\lambda c} = \Gamma_{\lambda n} + \Gamma_{\lambda\gamma} + \Gamma_{\lambda f} \quad , \tag{3-6}$$

$$G_{\lambda\bar{\lambda}} = \sum_{\bar{c}} (\Gamma_{\lambda\bar{c}}{}^{1/2}\ \Gamma_{\bar{\lambda}\bar{c}}{}^{1/2}) \tag{3-7}$$

and $\Gamma_{\lambda n}$, $\Gamma_{\lambda\gamma}$ and $\Gamma_{\lambda f}$ represent respectively the neutron, capture and fission width.

The real and imaginary parts of $A'_{\lambda\bar{\lambda}}$ are written as follows:

$$R_e(A'_{\lambda\bar{\lambda}}) = \frac{E_\lambda - E}{|Z_\lambda|^2}\delta_{\lambda\bar{\lambda}} + \frac{1}{2}(1-\delta_{\lambda\bar{\lambda}})G_{\lambda\bar{\lambda}}H^r_{\lambda\bar{\lambda}} \quad , \tag{3-8}$$

$$I_m(A'_{\lambda\lambda'}) = \frac{\Gamma_\lambda}{2|Z_\lambda|^2}\delta_{\lambda\lambda'} + \frac{1}{2}(1-\delta_{\lambda\lambda'})G_{\lambda\lambda'}H^i_{\lambda\lambda'} \tag{3-9}$$

where

$$H^r_{\lambda\lambda'} = \frac{1}{2|Z_\lambda - Z_{\lambda'}|^2}\left[\frac{\Gamma_\lambda(E_\lambda-E_{\lambda'})+(E_\lambda-E)(\Gamma_\lambda-\Gamma_{\lambda'})}{|Z_\lambda|^2} - \frac{\Gamma_{\lambda'}(E_\lambda-E_{\lambda'})+(E_{\lambda'}-E)(\Gamma_\lambda-\Gamma_{\lambda'})}{|Z_{\lambda'}|^2}\right], \tag{3-10}$$

$$H^i_{\lambda\lambda'} = \frac{1}{2|Z_\lambda - Z_{\lambda'}|^2}\left[\frac{\frac{\Gamma_\lambda}{2}(\Gamma_\lambda-\Gamma_{\lambda'})-2(E_\lambda-E)(E_\lambda-E_{\lambda'})}{|Z_\lambda|^2} - \frac{\frac{\Gamma_{\lambda'}}{2}(\Gamma_\lambda-\Gamma_{\lambda'})-2(E_{\lambda'}-E)(E_\lambda-E_{\lambda'})}{|Z_{\lambda'}|^2}\right]. \tag{3-11}$$

Using the representation of the approximate level matrix A', the total cross section is given by the following formula:

$$\begin{aligned}\sigma_t^J &= \frac{2\pi}{k^2} g_J R_e\ (1-U^J_{nn}) \\ &= \frac{2\pi}{k^2} g_J \left[2\sin^2\phi_n + \sum_\lambda \frac{(E_\lambda-E)\Gamma_{\lambda n}\sin 2\phi_n + \frac{\Gamma_\lambda}{2}\Gamma_{\lambda n}\cos 2\phi_n}{(E_\lambda-E)^2+\frac{1}{4}\Gamma_\lambda{}^2}\right. \\ &\quad \left. + \frac{1}{2}\sum_\lambda \sum_{\lambda'\neq\lambda} \sqrt{\Gamma_{\lambda n}\Gamma_{\lambda' n}}\, G_{\lambda\lambda'}\,(H^r_{\lambda\lambda'}\sin 2\phi_n + H^i_{\lambda\lambda'}\cos 2\phi_n)\right], \end{aligned} \tag{3-12}$$

where k is the neutron wave number, g_J the spin statistical factor and J the spin quantum number of the compund nucleus. On the right hand side of Eq.(3-12), the three terms in the brackets represent the contributions from the hard sphere scattering, the resonance reaction and the interference between resonances, respectively. The interference term can be rewritten by using two parameters u_λ and v_λ as follows:

$$\sigma^J_{t,M}(E) = \pi\frac{E}{k^2} g_J \sum_\lambda \frac{1}{\sqrt{E}} \frac{\frac{1}{2}u^t_\lambda\Gamma_\lambda + v^t_\lambda(E_\lambda-E)}{(E_\lambda-E)^2+\frac{1}{4}\Gamma_\lambda{}^2}, \tag{3-13}$$

where the two parameters are given by

$$u_\lambda^t = \sum_{\lambda' \neq \lambda} \frac{\sqrt{\Gamma_{\lambda n}^0 \Gamma_{\lambda' n}^0}\, G_{\lambda\lambda'} \left[2(E_\lambda - E_{\lambda'})\sin 2\phi_n + (\Gamma_\lambda - \Gamma_{\lambda'})\cos 2\phi_n\right]}{(E_\lambda - E_{\lambda'})^2 + \frac{1}{4}(\Gamma_\lambda - \Gamma_{\lambda'})^2} \quad , \tag{3-14}$$

$$v_\lambda^t = \sum_{\lambda' = \lambda} \frac{\sqrt{\Gamma_{\lambda n}^0 \Gamma_{\lambda' n}^0}\, G_{\lambda\lambda'} \left[(\Gamma_{\lambda'} - \Gamma_\lambda)\sin 2\phi_n + 2(E_\lambda - E_{\lambda'})\cos 2\phi_n\right]}{(E_\lambda - E_{\lambda'})^2 + \frac{1}{4}(\Gamma_\lambda - \Gamma_{\lambda'})^2} \quad , \tag{3-15}$$

respectively, and $\Gamma_{\lambda n}^0$ is the reduced neutron width.

Expression for the reaction cross section such as capture and fission cross sections can be written as follows:

$$\sigma_y^J(E) = \sum_{c' \in y} \sigma_{cc'} = \frac{\pi}{k^2} g_J \sum_{c' \in y} \left| \sum_{\lambda,\lambda'} \sqrt{\Gamma_{\lambda c} \Gamma_{\lambda' c}}\, A_{\lambda\lambda'} \right|^2 \quad , \tag{3-16}$$

where y stands for capture or fission reaction.

Using the unitarity of the collision matrix

$$\begin{aligned} \sum_{c'} |U_{cc'}|^2 &= \sum_{c'} \left[\delta_{cc'}^2 - 2\delta_{cc'} \sum_{\lambda\lambda'} \sqrt{\Gamma_{\lambda c} \Gamma_{\lambda' c}}\, I_m(A_{\lambda\lambda'}) + \left| \sum_{\lambda\lambda'} \sqrt{\Gamma_{\lambda c} \Gamma_{\lambda' c}}\, A_{\lambda\lambda'} \right|^2 \right] \\ &= 1 - 2 \sum_{\lambda\lambda'} \sqrt{\Gamma_{\lambda c} \Gamma_{\lambda' c}}\, I_m(A_{\lambda\lambda'}) + \sum_{c'} \left| \sum_{\lambda\lambda'} \sqrt{\Gamma_{\lambda c} \Gamma_{\lambda' c}}\, A_{\lambda\lambda'} \right|^2 \\ &\equiv 1 \quad , \end{aligned} \tag{3-17}$$

the following relation is obtained:

$$\begin{aligned} \sum_{c'} \left| \sum_{\lambda\lambda'} \sqrt{\Gamma_{\lambda c} \Gamma_{\lambda' c}}\, A_{\lambda\lambda'} \right|^2 &\cong 2 \sum_{\lambda\lambda'} \sqrt{\Gamma_{\lambda c} \Gamma_{\lambda' c}}\, I_m(A'_{\lambda\lambda'}) \\ &= \sum_{c'} 2 \sum_{\lambda\lambda'} \sqrt{\Gamma_{\lambda c} \Gamma_{\lambda' c}}\, I_m(A'_{\lambda,\lambda' c}) \quad , \end{aligned} \tag{3-18}$$

where

$$I_m(A'_{\lambda,\bar{\lambda}\bar{c}}) = \frac{\sqrt{\Gamma_{\lambda c}\Gamma_{\bar{\lambda}\bar{c}}}}{2|Z_\lambda|^2}\,\delta_{\lambda\bar{\lambda}} + \frac{1}{2}\,(1-\delta_{\lambda\bar{\lambda}})\,H^i_{\lambda\bar{\lambda}}\sqrt{\Gamma_{\lambda c}\Gamma_{\bar{\lambda}\bar{c}}} \quad . \tag{3-19}$$

Assuming the following relation which is valid for diagonal approximation,

$$\sum_{\bar{c}\in y}\left|\sum_{\lambda\bar{\lambda}}\sqrt{\Gamma_{\lambda c}\Gamma_{\bar{\lambda}\bar{c}}}\,A_{\lambda\bar{\lambda}}\right|^2 \cong \sum_{\bar{c}\in y} 2\left[\sum_{\lambda\bar{\lambda}}\sqrt{\Gamma_{\lambda c}\Gamma_{\bar{\lambda}\bar{c}}}\,I_m(A'_{\lambda,\bar{\lambda}\bar{c}})\right] \quad , \tag{3-20}$$

Eq.(3-16) is rewritten in an approximate form as

$$\sigma^J_y(E) = \frac{\pi}{k^2}\,g_J\sum_\lambda\left[\frac{\Gamma_{\lambda n}\Gamma_{\lambda y}}{(E_\lambda-E)^2+\frac{1}{4}\Gamma_\lambda{}^2} + \sum_{\bar{\lambda}\neq\lambda}\sqrt{\Gamma_{\lambda n}\Gamma_{\bar{\lambda}n}}\,G^y_{\lambda\bar{\lambda}}H^i_{\lambda\bar{\lambda}}\right] \tag{3-21}$$

where

$$G^y_{\lambda\bar{\lambda}} = \sum_{\bar{c}\in y}\sqrt{\Gamma_{\lambda c}\Gamma_{\bar{\lambda}\bar{c}}} \quad . \tag{3-22}$$

In Eq.(3-21), the second term in the brackets shows the interference effect between resonance levels and is written as follows:

$$\sigma^J_{y,M}(E) = \pi\frac{E}{k^2}\,g_J\sum_\lambda\left[\frac{1}{\sqrt{E}}\,\frac{\frac{1}{2}\,u^y_\lambda\Gamma_\lambda + v^y_\lambda(E_\lambda-E)}{(E_\lambda-E)^2+\frac{1}{4}\Gamma_\lambda{}^2}\right] \quad , \tag{3-23}$$

where

$$u^y_\lambda = \sum_{\bar{\lambda}\neq\lambda}\frac{\sqrt{\Gamma^0_{\lambda n}\Gamma^0_{\bar{\lambda}n}}\,G^y_{\lambda\bar{\lambda}}\,(\Gamma_\lambda-\Gamma_{\bar{\lambda}})}{(E_\lambda-E_{\bar{\lambda}})^2+\frac{1}{4}\,(\Gamma_\lambda-\Gamma_{\bar{\lambda}})^2} \quad , \tag{3-24}$$

$$v^y_\lambda = \sum_{\bar{\lambda}\neq\lambda}\frac{-2\sqrt{\Gamma^0_{\lambda n}\Gamma^0_{\bar{\lambda}n}}\,G^y_{\lambda\bar{\lambda}}\,(E_\lambda-E_{\bar{\lambda}})}{(E_\lambda-E_{\bar{\lambda}})^2+\frac{1}{4}\,(\Gamma_\lambda-\Gamma_{\bar{\lambda}})^2} \quad . \tag{3-25}$$

The off-diagonal element for the capture channel is neglected because of

the sign fluctuation for $(\Gamma_{\lambda\gamma})^{1/2}$, that is, $\sum_{\bar{c}\in\gamma} \sqrt{\Gamma_{\lambda c}\Gamma_{\bar{\lambda}\bar{c}}} \cong 0$(78).
Hence, neglecting the second term of Eq.(3-21), the capture cross section is written as follows:

$$\sigma_{\gamma}^{J}(E) = \frac{\pi}{k^2} g_J \sum_{\lambda} \frac{\Gamma_{\lambda n}\Gamma_{\lambda\gamma}}{(E_\lambda - E)^2 + \frac{1}{4}\Gamma_\lambda{}^2} \quad . \tag{3-26}$$

In Eqs.(3-12) and (3-21), each reaction cross section is represented by the summation of a symmetric and an asymmetric function. This expression for the reaction cross section is the same as the Breit-Wigner single-level formula except for the inclusion of the parameters (u_λ, v_λ). Equations (3-12) and (3-21) are very similar to the expressions derived by Brissenden and Durston(61). In the present expressions of Eqs. (3-13) and (3-23), the interference contributions are represented by the parameters (u_λ, v_λ), by which back ground floor cross sections that is difference between experimental cross section and single-level one are represented and temperature dependence of the floor cross sections is considered, to avoid the complication for cross section analysis.
From Eqs.(3-14), (3-15), (3-24) and (3-25), it is seen that the (u_λ, v_λ) parameters decrease with an increase of the distances between the levels λ and $\bar{\lambda}$. Hence the parameters (u_λ, v_λ) can be considered as a kind of parameters that represent the measure of the interference between resonances. These will therefore be called as the interference parameters.
However, these parameters can not generally be calculated from only the single-level parameters, because the signs of $(\Gamma_{\lambda\bar{c}})^{1/2}$ are undertermined, with respect to each channel $\bar{c}$, in the expression of Eq.(3-7) for $G_{\lambda\bar{\lambda}}$.
The calculation of the interference parameters will be performed for both the resolved and unresolved resonance region in the next section.
Also, the contribution of the interference effect to the Doppler coeffi-

cient is evaluated from these parameters.

The expressions described above are derived on the basis of absorber nuclei at rest. In actual fact, however, the absorber nuclei are in thermal motion and hence the influence of the motion on the neutron absorption must be taken into consideration. In the present paper, Maxwellian distribution is assumed for the velocity of the absorber nuclei. Then, using the method developed by Buckler and Pull[86], the Doppler broadened cross sections corresponding to Eqs.(3-12) and (3-21) are easily given as follows:

$$\sigma_t^J(E) = \sigma_p(E) + \frac{4\pi}{k^2}\sqrt{\frac{\alpha}{2m\pi}}\, g_J \sum_\lambda \left[(\Gamma^0_{\lambda n} + \frac{u^t_\lambda}{2})\Phi^r_\lambda \right] + \frac{8\pi R}{k}\frac{\alpha}{2m\pi}\, g_J \sum_\lambda \left[(\Gamma^0_{\lambda n} + \frac{v^t_\lambda}{4kR})\Phi^i_\lambda \right] \quad , \tag{3-27}$$

$$\sigma_y^J(E) = \frac{4\pi}{k^2}\sqrt{\frac{\alpha}{2m\pi}}\, g_J \sum_\lambda \left[(\frac{\Gamma^0_{\lambda n}\Gamma_{\lambda y}}{\Gamma_\lambda} + \frac{u^y_\lambda}{2})\Phi^r_\lambda + \frac{v^y_\lambda}{2}\Phi^i_\lambda \right] \quad , \tag{3-28}$$

where

$$\Phi^r_\lambda = R_e\,(F(w_1) - F(w_2)) \quad , \tag{3-29}$$

$$\Phi^i_\lambda = I_m\,(F(w_1) - F(w_2)) \quad , \tag{3-30}$$

$$F(w) = \int_0^\infty \exp(-x^2)\,\frac{w}{x^2 + w^2}\,dx \quad , \tag{3-31}$$

$$w_1 = \sqrt{\alpha}\,(b + i(a - v_0)) \quad , \tag{3-32}$$

$$w_2 = \sqrt{\alpha}\,(b + i(a + v_0)) \quad , \tag{3-33}$$

$$a - ib = (2E_\lambda - i\Gamma_\lambda)^{1/2} \quad , \tag{3-34}$$

$$\alpha = A_m / 2KT \quad , \tag{3-35}$$

and K, T, V_0, R and σ_p represent the Boltzman constant, absolute temperature, neutron velocity, atomic radius and potential scattering cross section, respectively.

The resonance scattering cross section is now given by

$$\sigma_n^J(E) = \sigma_t^J(E) - \sigma_p(E) - \sum_y \sigma_y^J(E)$$

$$= \frac{4\pi}{k^2}\sqrt{\frac{\alpha}{2m\pi}}\, g_J \sum_\lambda \left[\left(\frac{\Gamma^0_{\lambda n}\Gamma_{\lambda n}}{\Gamma_\lambda} + \frac{u^n_\lambda}{2}\right)\Phi_\lambda \right]$$

$$+ \frac{8\pi R}{k}\sqrt{\frac{\alpha}{2m\pi}}\, g_J \sum_\lambda \left[\left(\Gamma^0_{\lambda n} + \frac{v^n_\lambda}{4kR}\right)\Phi^i_\lambda \right] \quad , \tag{3-36}$$

where

$$u^n_\lambda = u^t_\lambda - \sum_y u^y_\lambda \quad , \tag{3-37}$$

$$v^n_\lambda = v^t_\lambda - \sum_y v^y_\lambda \quad . \tag{3-38}$$

When $\sqrt{E_\lambda/E}$ is nearly equal to unity and $\frac{1}{2}\Gamma_\lambda/E_\lambda \ll 1$, the functions Φ^r_λ and Φ^i_λ are reduced to the usual Doppler line shape functions $\psi_\lambda(\theta,x)$ and $X_\lambda(\theta,x)$, respectively. The assumptions will approximately hold near resonance energy in the relatively high energy region, and Eqs.(3-27), (3-38) and (3-36) can be written as follows:

$$\sigma_t^J(E) = \sigma_p(E) + \sum_\lambda \left[\sigma_{0\lambda}(1+u_{\lambda t})\psi_\lambda(\theta,x) + \sigma_{0p\lambda}\left(1+\frac{\sigma_{0\lambda}}{\sigma_{0p\lambda}} v_{\lambda t}\right)X_\lambda(\theta,x) \right] , \tag{3-39}$$

$$\sigma_y^J(E) = \sum_\lambda \sigma_{0\lambda} \left[\left(\frac{\Gamma_{\lambda y}}{\Gamma_\lambda} + u_{\lambda y}\right)\psi_\lambda(\theta,x) + v_{\lambda y}\, X_\lambda(\theta,x) \right] \quad , \tag{3-40}$$

$$\sigma_n^J(E) = \sum_\lambda \left[\sigma_{0\lambda}\left(\frac{\Gamma_{\lambda n}}{\Gamma_\lambda} + u_{\lambda n}\right)\psi_\lambda(\theta,x) + \sigma_{0p\lambda}\left(1+\frac{\sigma_{0\lambda}}{\sigma_{0p\lambda}} v_{\lambda n}\right)X_\lambda(\theta,x) \right] , \tag{3-41}$$

where

$$\sigma_{0\lambda} = \frac{4\pi}{k^2} g_J \frac{\Gamma_{\lambda n}}{\Gamma_\lambda} \quad , \tag{3-42}$$

$$\sigma_{0p\lambda} = 2\sqrt{\sigma_{0\lambda}\sigma_p g_J \Gamma_{\lambda n}/\Gamma_\lambda} \quad , \quad \sigma_p = 4\pi R^2 \quad , \tag{3-43}$$

$$u_{\lambda t} = u_\lambda^t / 2\Gamma_{\lambda n}^0 \quad , \quad v_{\lambda t} = v_\lambda^t / 2\Gamma_{\lambda n}^0 \quad , \tag{3-44}$$

$$u_{\lambda y} = u_\lambda^y / 2\Gamma_{\lambda n}^0 \quad , \quad v_{\lambda y} = v_\lambda^y / 2\Gamma_{\lambda n}^0 \quad , \tag{3-45}$$

$$u_{\lambda n} = u_\lambda^n / 2\Gamma_{\lambda n}^0 \quad , \quad v_{\lambda n} = v_\lambda^n / 2\Gamma_{\lambda n}^0 \quad . \tag{3-46}$$

Equations (3-39), (3-40) and (3-41) are similar to the Alder-Alder expression[80] for reaction y given by

$$\sigma_y^J(E) = \frac{C}{\sqrt{E}} \sum_\lambda \frac{g_J}{\nu_\lambda} [G_\lambda^y \psi(\xi_\lambda, x_\lambda) + H_\lambda^y X(\xi_\lambda, x_\lambda)] \quad ,$$

$$x = (E - E_\lambda)/\nu_\lambda \quad ,$$

$$C = 6.52 \times 10^5 \quad (\text{b eV}) \quad ,$$

$$\xi_\lambda = \left(\frac{A\nu_\lambda^2}{kTE} \right)^{\frac{1}{2}} \quad ,$$

and ν_λ, G_λ^y and H_λ^y are the fitted parameters for reaction y. There are eight fitted parameters (E_λ, ν_λ, G_λ^γ, G_λ^f, G_λ^n, G_λ^n, H_λ^γ, H_λ^f and H_λ^n) in their expression, and on the other hand the present ones have ten fitted parameters (E_λ, Γ_γ, Γ_n, Γ_f, u_λ^γ, u_λ^f, u_λ^n, v_λ^γ, v_λ^f and v_λ^n). Hence, generally, the Adler-Adler formula is more convinient than the present one for cross section analysis. However, the multilevel formula is mainly necessary to describe properly the cross sections for fissile nuclides in which the single-level formula is good expression for capture and elastic scattering cross sections. Then, the ten parameters in the present formula are reduced to the six ones (E_λ, Γ_γ, Γ_n, Γ_f, u_λ^f and v_λ^f) by making use of the single-level parameters for other four parameters. Furthermore, it should be noticed that the statistical distributions for the fitted

parameters Γ_γ, Γ_n and Γ_f are well known, though they for u_λ and v_λ are unknown such as the Adler-Adler parameters. The cross section analysis will be performed by using the present formula in the next section.

3.3 Interference Parameters and Interference Effects

3.3.1 Resolved Resonance Energy Region

In the resolved resonance region, the many single-level parameters have been analysed and evaluated[82] on the basis of the Breit-Wigner single-level formula. The Breit-Wigner formula has been extensively used for the calculation of the reactor characteristics, because of the reasons described in the introduction. However, it is well known[76] that the reaction cross section of fissile nuclei can not adequately be represented by this single-level formula, because of the interference effect between the resonances levels. The interference effect may be accepted as the difference between the experimental cross section and the single-level cross section calculated by the Breit-Wigner single-level formula using the available single-level parameters. The interference effect will be represented by the formula derived in the previous section. Therefore, the parameters u_λ and v_λ can be calculated[87] to minimize the quantity:

$$Q = \sum_i w_i \left| \sigma_{y,exp}(E_i) - (\sigma_{y,B}(E_i) + \sigma_{y,M}(E_i)) \right|^2 , \qquad (3\text{-}47)$$

where $\sigma_{y,exp}(E_i)$ is the measured cross section, $\sigma_{y,B}(E_i)$ is the Breit-Wigner single-level cross section, $\sigma_{y,M}(E_i)$ is the trial function for the term of the interference effect represented in Eqs.(3-27), (3-28) and (3-36), and w_i is the statistical weights of experimental errors for cross sections.

The least squares fits were performed for the ^{235}U and ^{233}U fission cross sections and for the ^{238}U total cross section. The obtained results are as follows:

^{235}U: The fission cross sections for the energy range below 12.54 eV were studied by using the experimental data of Michauden[88] (12.54 - 0.3788 eV) and of Shore and Sailor[76](0.37 - 0.1 eV). The single-level parameters (E_λ,$\Gamma_{\lambda n}$,$\Gamma_{\lambda\gamma}$,$\Gamma_{\lambda f}$) used for the calculation of the cross section $\sigma_{y,B}$ are shown in Table 3.1[76][88]. These single-level parameters were analysed from the resonance experiments by Michauden and by Shore and Sailor. The least squares fits were performed for 576 data points with the 19 levels below 11.66 eV to determine the parameters u_λ^f and v_λ^f. The obtained parameters u_λ^f and v_λ^f are shown in columns 6 and 7 in Table 3.1, respectively. Figure 3.1 shows the comparison between the measured values ($\sigma_{y,exp}$), the single-level cross sections ($\sigma_{y,B}$) and the modified cross sections ($\sigma_{y,B}+\sigma_{y,M}$). This figure shows that Eq.(3-28) can nicely reproduce the measured fission cross section in the lower energy region.

The integral quantities were also compared with the experimental values. The averaged cross sections $<\sigma_{y,exp}>$, $<\sigma_{y,B}>$ and $<\sigma_{y,B}+\sigma_{y,M}>$ and the resonance integrals $RI_{y,exp}$, $RI_{y,B}$ and $RI_{y,B}+RI_{y,M}$ were calculated. The deviations of $<\sigma_{y,B}>$ and $<\sigma_{y,B}+\sigma_{y,M}>$ from $<\sigma_{y,exp}>$ were -11.5% and -1.7%, respectively, and those of $RI_{y,B}$ and $RI_{y,B}+RI_{y,M}$ from $RI_{y,exp}$ were -14.7% and -0.246%, respectively. The single-level cross section considerably underpredicts the integral quantities but the present least squares fit extremely improves the situation though somewhat in underprediction.

^{233}U: The experimental data of the fission cross sections were obtained for the energy range of 45 ~ 20 eV from the data table given in Ref.(89). The data of 495 points with 44 resonance levels were analysed by using the least squares fit with the trial function of Eq.(3-28). The single-level parameters used for the present calculation are given in Table 3.2[90], together with the obtained parameters u_λ^f, and v_λ^f.

Table 3.2[90], together with the obtained parameters u_λ^f and v_λ^f. The results calculated by using these parameters u_λ^f and v_λ^f and the single-level parameters are compared with the experimental values in Fig.3.2. As seen from Fig.3.2, both the Breit-Wigner single-level formula and the expression derived in this article well reproduce the measured cross sections. In the comparison of the integral quantities, however, the deviations of $< \sigma_{y,B} >$ and $< \sigma_{y,B} + \sigma_{y,M} >$ from $< \sigma_{y,exp} >$ were -2.95% and 0.094%, respectively, and those of $RI_{y,B}$ and $RI_{y,B} + RI_{y,M}$ from $RI_{y,exp}$ were -3.15% and 0.127%, respectively. This result also shows that the present formula gives an improvement to the Breit-Wigner single-level formula.

^{238}U: It is well-known that the Breit-Wigner single-level formula gives a very good representation for the cross section of the non-fissile nuclide with a large level spacing such as ^{238}U. However, we experience the case where the total or scattering cross sections given by the single-level formula become negative at the lower energy side of the resonance which interferes strongly with the potential scattering. Because, the single-level parameter is determined for only one resonance in question without considering the contribution from other resonances to the resonance. It is seen easily that this negative cross section appears only for the case of $\lambda > 2$ in Eq. (3-27) or (3-36). Hence, this negative cross sections may be corrected by considering the iterference effect between resonance levels through the parameters (u_λ, v_λ) of Eq. (3-27) or (3-39).

For example, the ^{238}U total cross section calculated by using the single-level parameters shown in Table 2.3 takes a large negative value (-5 harns) at energy of 1961 eV. But the experimental data of Garg et al.[91] show about 4 barns near 1961 eV. Using Eq.(3-27) the total cross sections were analysed by the least squares fit for the energy range

from 2020 to 1920 eV. The parameters (u_λ, v_λ) thus obtained are shown for two resonances of 1974.65 and 9168.66 eV in Table 3.3. The total cross sections calculated by using the single-level parameters and the parameters (u_λ, v_λ) are compared with the experimental data in Fig.3.3. This figure shows that the present formula of Eq.(3-27) can reproduce the reasonable curve of the total cross section of ^{238}U also in the case where the resonance interferes strongly with the potential scattering.
In addition, it is seen from Table 3.3 that for the two resonances, the contribution from the u_λ-interference term to the total cross section is very small as compared with the single-level symmetry terms. On the other hand, the v_λ-interference terms give the influence of -16% and -7% on the single-level asymmetry terms, as shown at the last column in Table 3.3.

From the results described above, it can be said that the interference parameters (u_λ, v_λ) introduced for an improvement of the single-level formula play a very significant role in the analyses of the measured cross sections. The calculation of the parameters can easily be performed from the least squares fitting to the measured data.

For fertile materials, it should be noticed that the parameters (u_λ, v_λ) can be calculated from single-level parameters by considering only the entrance channel for neutron channel, that is, $G_{\lambda\lambda'} = \sqrt{\Gamma_{\lambda n}\Gamma_{\lambda' n}}$.
And then we could reproduce a similar total cross section curve to the fitted cross sections in Fig.3.3. Furthermore, we have already proved also for the unresolved resonance regions that the present multi-level formula could correct[92] such the failure of the single-level formula as ^{238}U total cross sections became negative values in the case where resonance generated by random sampling method interfers strongly with the potential scattering.

3.3.2 Unresolved Resonance Energy Region

Several techniques[64]~[68] have been developed for the generation of resonance parameters by random sampling from the distribution functions of the resolved resonance parameters and level spacing. Starting with some initial energy, resonance parameters are generated over the complete energy range of interest. The merits of generating resonance parameters are that both the effects of the self-interference between resonances in one nuclide and of the mutual resonance-interactions between different nuclei can accurately be taken into account for the calculation of effective cross sections[25]. In the unresolved resonance region, the interference parameters (u_λ, v_λ) can be calculated by using the generated resonance parameters and energies, where according to the Vogt's definition[78] the off-diagonal elements of the level matrix are defined as follows:

$$G_{\lambda\bar{\lambda}} = \sqrt{\Gamma_{\lambda n}\Gamma_{\bar{\lambda} n}} + (\Gamma_{\lambda f})^{1/2} (\Gamma_{\bar{\lambda} f})^{1/2} \cos\theta_{\lambda\bar{\lambda}} \quad , \qquad \lambda \neq \bar{\lambda} \quad , \qquad (3\text{-}48)$$

in which the capture channel is neglected[78] because of the sign fluctuation for $(\Gamma_{\lambda\gamma})^{1/2}$. For the neutron channels, only the entrance channel is taken into consideration. The off-diagonal terms for the fission channel is defined[78] by the scalar product of two vectors whose components are equal to $(\Gamma_{\lambda f})^{1/2}$. For the fissile nuclei, especially, the value of the neutron width is always sufficiently small compared to that of the total width and hence the neutron channel can be neglected. The main contribution to the off-diagonal elements comes from the fission channels.

In the calculation of the interference parameters (u_λ, v_λ), the assumption $|N/D| \ll 1$ used in the expansion for the level matrix must be examined for the unresolved resonance region. This assumption is generally

valid because $|E_\lambda - E|$ is larger than the total width except for the case of $E_\lambda \cong E$. For $E \cong E_\lambda$, however, the diagonal element is the main contributor to the cross section, and $N \ll D$ is satisfied for the other elements ($\lambda \neq \bar{\lambda}$). The acceptance of this assumption will therefore be reasonable in the calculation of the resonance cross sections. This fact can be ascertained also from numerical experiments.

In order to assess the validity of the perturbation approach of Eq.(3-3), the R-matrix parameters for ^{235}U were generated for the energy range from 1 to 2 keV using the ARCFIT-3 code[93]. The average resonance parameters used were $< \Gamma_f >_{J=3} = 0.353$ eV, $< \Gamma_f >_{J=4} = 0.152$ eV, $< \Gamma_n^0 > = 0.000132\ (\text{eV})^{1/2}$ and $< \Gamma_\gamma > = 0.0479$ eV, and the average level spacing was 1.16 eV. The fission channel number used was 3 and the χ^2-distribution with the degree of freedom one was assumed for each fission channel. The examination of the validity of the perturbation approach becomes cumbersome when a sizable number of levels and energy points are considered. The interference effects of a level (λ) with the neighboring levels are main contributors to off-diagonal elements in the vicinity energy E_λ. Hence, many studies have been done for two-level interference effects[8][94][95]. In the case of two levels, the direct inversion for the level matrix A^{-1} is given by

$$A = D^{-1}(1 + ND^{-1})^{-1} = \begin{pmatrix} D_{11}^{-1} & 0 \\ 0 & D_{22}^{-1} \end{pmatrix} \begin{pmatrix} \frac{1}{|B|} & \frac{-N_{12}}{D_{22}|B|} \\ \frac{-N_{21}}{D_{11}|B|} & \frac{1}{|B|} \end{pmatrix} \quad (3\text{-}49)$$

where

$$|B| = 1 - N_{12}N_{21}/D_{11}D_{22} \ . \quad (3\text{-}50)$$

If the approximation, $|B| \cong 1$, is satisfied, hence, $A \cong D^{-1}(1-ND^{-1})$, the perturbation approach is valid. Therefore, the validity of the perturbation approach can be examined by calculating the values of $\left|N_{\lambda\bar{\lambda}}N_{\bar{\lambda}\lambda}/D_{\lambda\lambda}D_{\bar{\lambda}\bar{\lambda}}\right|_{\lambda\neq\bar{\lambda}}$ for neighboring levels λ and $\bar{\lambda}$ in the vicinity of the resonance energy E_λ. The values were calculated for 180 levels over the range of 1712 to 1800 eV. Figure 3.4 shows the values of $\left|N_{\lambda\bar{\lambda}}N_{\bar{\lambda}\lambda}/D_{\lambda\lambda}D_{\bar{\lambda}\bar{\lambda}}\right|_{\lambda\neq\bar{\lambda}}$ for the three cases of $E = E_\lambda$, $E = E_\lambda \pm 0.1$ eV and $E = E_\lambda \pm 0.2$ eV. It is seen from this figure that the perturbation approach is generally valid. Though the values show the largest values in the case of $E = E_\lambda$, fortunately, asymmetric term of Eq.(3-23) becomes zero and, furthermore, u_λ is generally smaller than $2\Gamma^0_{\lambda n}\Gamma_{\lambda y}/\Gamma_\lambda$ because $(E_\lambda - E_{\bar{\lambda}})^2$ in the denominator of Eq.(3-24) is normally larger than the total width. Therefore, the perturbation approach is valid also for $E = E_\lambda$ in the calculation of the resonance cross sections.

The calculations of the cross sections of ^{235}U and ^{239}Pu were performed by considering many level interference effects for the energy range from 1 to 2 keV. Figures 3.5 and 3.6 show two examples of the calculated fission cross sections for ^{235}U and ^{239}Pu at the temperature 300°K. There are considerable discrepancies between the energy variations of the fission cross sections calculated by the Breit-Wigner single-level formula and the present formula. Such discrepancies due to the interference effect between resonances are especially important when their contributions to the Doppler reactivity effect is to be evaluated for a nuclear reactor. In order to estimate the contribution, the resonance shielding factors of ^{235}U and ^{239}Pu were calculated for the temperatures 300 and 900°K using the MCROSS-2 code[69]. The energy range considered in the calculation were 2 - 1.5 and 1.5 - 1.0 keV. Table 3.4 shows comparisons of the results calculated by the two different formulas. The differences

in the Doppler effect between the two calculated results are 5 ~ 7% for ^{235}U and smaller for ^{239}Pu. These differences are exactly due to the interference effect between the resonances, because the infinitely dilute cross sections given by the two formulas are almost equal to each other. This can easily be examined by performing the x-integration of Eq.(3-40) as follows:

$$\sum_{\lambda} \int_{-\infty}^{\infty} \sigma_{0\lambda} v_{\lambda y} \chi_{\lambda}(\theta,x)dx = 0 \quad , \tag{3-51}$$

$$\sum_{\lambda} \int_{-\infty}^{\infty} \sigma_{0\lambda} u_{\lambda y} \psi_{\lambda}(\theta,x)dx = \frac{\pi}{2} \sum_{\lambda} \sigma_{0\lambda} \Gamma_{\lambda} u_{\lambda y} \quad . \tag{3-52}$$

Eq.(3-52) becomes zero for $\lambda > 1$, because of $\sum_{\lambda} \sum_{\lambda' \neq \lambda} (\Gamma_{\lambda} - \Gamma_{\lambda'}) = 0$, $\lambda > 1$. Therefore, the infinitely dilute cross sections for a sufficiently wide energy range are the same for these two formulas. In other words, the present formula can represent the same experimental data as those evaluated by using the single-level formula for the unresolved resonance region.

3.4 Concluding Remarks

Without losing the useful characteristics of the Breit-Wigner single-level formula, we have proposed a simple way to take into account the interference effect between resonances. The improved formula contains the interference parameters $(u_{\lambda}, v_{\lambda})$ which represent the interference effect, in addition to the usual single-level parameters. This representation of $(u_{\lambda}, v_{\lambda})$ is more convenient than the Brissenden's one with the Vogt parameters which are somewhat complicated for the purpose of analyzing neutron cross section data. Furthermore, the statistical distributions for the parameters (Γ_{γ}, Γ_{n} and Γ_{f}) fitted by the present formula are well

known, though they for (u_λ, v_λ) are unknown such the Adler-Adler parameters.

In the resolved resonance region, the present formula can well represent the measured cross sections, which can not sufficiently be analyzed by the single-level formula. The interference parameters (u_λ, v_λ) were calculated for typical resonance regions of ^{235}U, ^{233}U and of ^{238}U by using the least squares fit.

In the unresolved resonance region, the interference parameters (u_λ, v_λ) can be reproduced with random sampling method using the single-level average resonance parameters and spacings. Infinitely dilute cross sections calculated by the Breit-Wigner single-level formula are substantially identical to those by the present formula. Therefore, the present expression reproduces the same experimental data as obtained from the single-level formula in the unresolved resonance region. The contribution of the interference effect to the Doppler effect has been examined from a comparison of the resonance shielding factors given by the two formulas. The differences in the Doppler effects caused by these two approaches are 5 ~ 7% for ^{235}U and smaller for ^{239}Pu.

Table 3.1 Single-level parameters of ^{235}U used for the present calculation and the obtained interference parameters

E_λ (ev)	g_J	$\Gamma^\circ_{\lambda n}$ ($\times 10^{-1}$ (mev))	$\Gamma_{\lambda r}$ (mev)	$\Gamma_{\lambda f}$ (mev)	u^f_λ ($(ev)^{1/2} \times 10^{-6}$)	v^f_λ ($(ev)^{1/2} \times 10^{-6}$)
-0.95	0.5	13.56	27.6	169.4	-656.4	76.30
0.29	0.5	0.05942	35.0	100.0	-0.03863	1.211
1.135	0.5	0.1446	42.0	115.0	-0.6671	-3.469
2.03	0.5	0.05475	38.0	10.0	0.01979	0.1301
2.84	0.5	0.01958	47.9	157.0	-0.3339	2.206
3.14	0.5	0.1580	51.0	116.0	-2.406	0.07634
3.61	0.5	0.2526	46.0	47.0	0.9298	-2.445
4.84	0.5	0.2727	37.0	3.8	-0.08677	0.1226
5.435	0.5	0.01458	86.6	134.0	4.453	-1.249
5.732	0.5	0.04887	49.0	443.0	7.758	9.209
6.19	0.5	0.1407	40.0	40.0	2.743	-0.2739
6.38	0.5	1.029	33.0	12.0	-5.656	1.026
7.07	0.5	0.4739	36.0	28.0	-1.536	1.157
8.78	0.5	3.982	50.0	82.0	-5.805	16.31
9.28	0.5	0.6565	65.0	95.0	1.030	-4.390
9.74	0.5	0.08331	40.0	500.0	38.17	-11.86
10.18	0.5	0.2006	37.0	58.0	0.5826	3.668
10.80	0.5	0.04869	40.0	733.0	20.77	14.30
11.6	0.5	1.728	36.0	3.5	3.470	-0.4448

Single-level parameters E_λ, $\Gamma^\circ_{\lambda n}$, $\Gamma_{\lambda r}$ and $\Gamma_{\lambda f}$ were analysed by Mi chauden[15], and Shore and Sailor[2].

Table 3.2 Single-level parameters of ^{233}U used for the present calculation and the obtained interference parameters

E_λ (ev)	g_J	$\Gamma^\circ_{\lambda n}$ (mev)	$\Gamma_{\lambda\gamma}$ (mev)	$\Gamma_{\lambda f}$ (mev)	u^f_λ $((ev)^{1/2}\times10^{-5})$	v^f_λ $((ev)^{1/2}\times10^{-5})$
20.58	0.5	0.38	45.0	360.	-3.887	-3.712
21.88	0.5	0.53	45.0	200.	-2.827	-8.432
22.36	0.5	1.51	45.0	350.	5.049	-12.21
22.96	0.5	0.18	45.0	450.	5.418	0.2439
23.78	0.5	0.22	45.0	390.	1.054	-4.380
24.26	0.5	0.105	45.0	530.	4.572	-1.985
24.64	0.5	0.01	45.0	200.	1.167	0.05183
25.27	0.5	0.30	45.0	260.	0.6183	-2.007
25.75	0.5	0.10	45.0	340.	2.228	-3.083
26.08	0.5	0.05	45.0	200.	3.274	-0.3374
26.30	0.5	0.035	45.0	100.	0.3842	1.460
26.65	0.5	0.17	45.0	300.	0.3982	-1.178
27.05	0.5	0.015	45.0	200.	0.8950	-0.00672
27.74	0.5	0.135	45.0	800.	6.927	-2.879
28.00	0.5	0.007	45.0	130.	0.8424	1.241
28.32	0.5	0.105	45.0	250.	0.2539	0.8499
28.85	0.5	0.135	45.0	320.	4.719	1.038
29.12	0.5	0.338	45.0	290.	-3.293	1.749
29.59	0.5	0.073	45.0	150.	-0.6360	-0.8894
30.30	0.5	0.02	45.0	130.	0.01171	-0.2715
30.73	0.5	0.215	45.0	260.	0.3682	-2.855
31.35	0.5	0.10	45.0	230.	1.964	-2.553
31.66	0.5	0.075	45.0	200.	2.100	1.811
32.04	0.5	0.30	45.0	170.	0.3869	-2.150
33.11	0.5	0.27	45.0	750.	2.688	-11.33
33.67	0.5	0.11	45.0	500.	10.49	-7.340
34.06	0.5	0.155	45.0	480.	12.56	6.245
34.55	0.5	0.37	45.0	550.	3.916	7.150
35.27	0.5	0.114	45.0	450.	9.915	2.809
35.62	0.5	0.024	45.0	300.	4.907	7.433
35.96	0.5	0.14	45.0	750.	-15.33	15.58
36.59	0.5	0.20	45.0	110.	-2.882	-2.083
37.51	0.5	0.21	45.0	380.	-1.816	-1.786
39.08	0.5	0.055	45.0	200.	-0.4270	-4.609
39.32	0.5	0.056	45.0	250.	8.326	-2.941
39.56	0.5	0.055	45.0	250.	4.916	4.989
39.89	0.5	0.145	45.0	600.	-2.399	13.31
40.49	0.5	0.175	45.0	650.	-8.463	3.521
41.06	0.5	0.091	45.0	190.	-2.129	-1.903
41.75	0.5	0.009	45.0	150.	0.06860	0.7762
42.16	0.5	0.035	45.0	350.	-2.433	2.707
42.66	0.5	0.19	45.0	140.	-2.976	-3.207
43.53	0.5	0.093	45.0	240.	-0.8844	-1.856
44.58	0.5	0.086	45.0	660.	0.4863	-2.261

Single-level parameters E_λ, $\Gamma^\circ_{\lambda n}$, $\Gamma_{\lambda\gamma}$ and $\Gamma_{\lambda f}$ were analyzed by Bergen[17]

Table 3.3 Single-level parameters of ^{238}U used for the present calculation and the obtained interference parameters

E_λ (ev)	g_j	$\Gamma^\circ_{\lambda n}$ (mev)	$\Gamma_{\lambda\gamma}$ (mev)	u^t_λ $((ev)^{1/2}\times10^{-4})$	v^t_λ $((ev)^{1/2}\times10^{-4})$	$u^t_\lambda/2\Gamma^\circ_{\lambda n}$	$\sigma_{o\lambda}v^t_\lambda/2\sigma_{op\lambda}\Gamma^\circ_{\lambda n}$
1808.26	1.0	0.4000	13.6				
1845.6	1.0	0.3101	11.8				
1902.27	1.0	0.4801	12.1				
1917.1	1.0	0.4999	24.64				
1968.66	1.0	13.00	24.64	0.5085	-7.8861	0.0021	-0.16
1974.65	1.0	10.50	24.64	1.3545	-2.9279	0.0065	-0.07
2023.58	1.0	4,500	24.64				
2031.26	1.0	1.1	24.64				
2088.63	1.0	0.2998	24.64				
2096.49	1.0	0.2201	24.64				

Single-level parameters E_λ and $\Gamma^\circ_{\lambda n}$ were analysed by Garg[18].

Table 3.4 Comparison of infinitely dilute fission cross sections $\sigma_f(\infty)$ and self-shielding factors f calculated by the Breit-Wigner single-level and the present formula.

Material	Energy Range	Breit-Wigner results			Present results		
		$\sigma_f(\infty)$	f (300°K)	Δ f(900-300°K)	$\sigma_f(\infty)$	f (300°K)	Δ f (900-300°K)
^{235}U	2.0 - 1.5 KeV	6.295	0.8882	0.0373	6.294	0.8862	0.0390
	1.5 - 1.0 KeV	7.586	0.8713	0.0351	7.591	0.8663	0.0378
^{239}Pu	2.0 - 1.5 KeV	3.918	0.7014	0.0648	3.918	0.6960	0.0651
	1.5 - 1.0 KeV	6.014	0.7090	0.0752	6.022	0.7044	0.0739

$\Delta f = f(900°K) - f(300°K)$

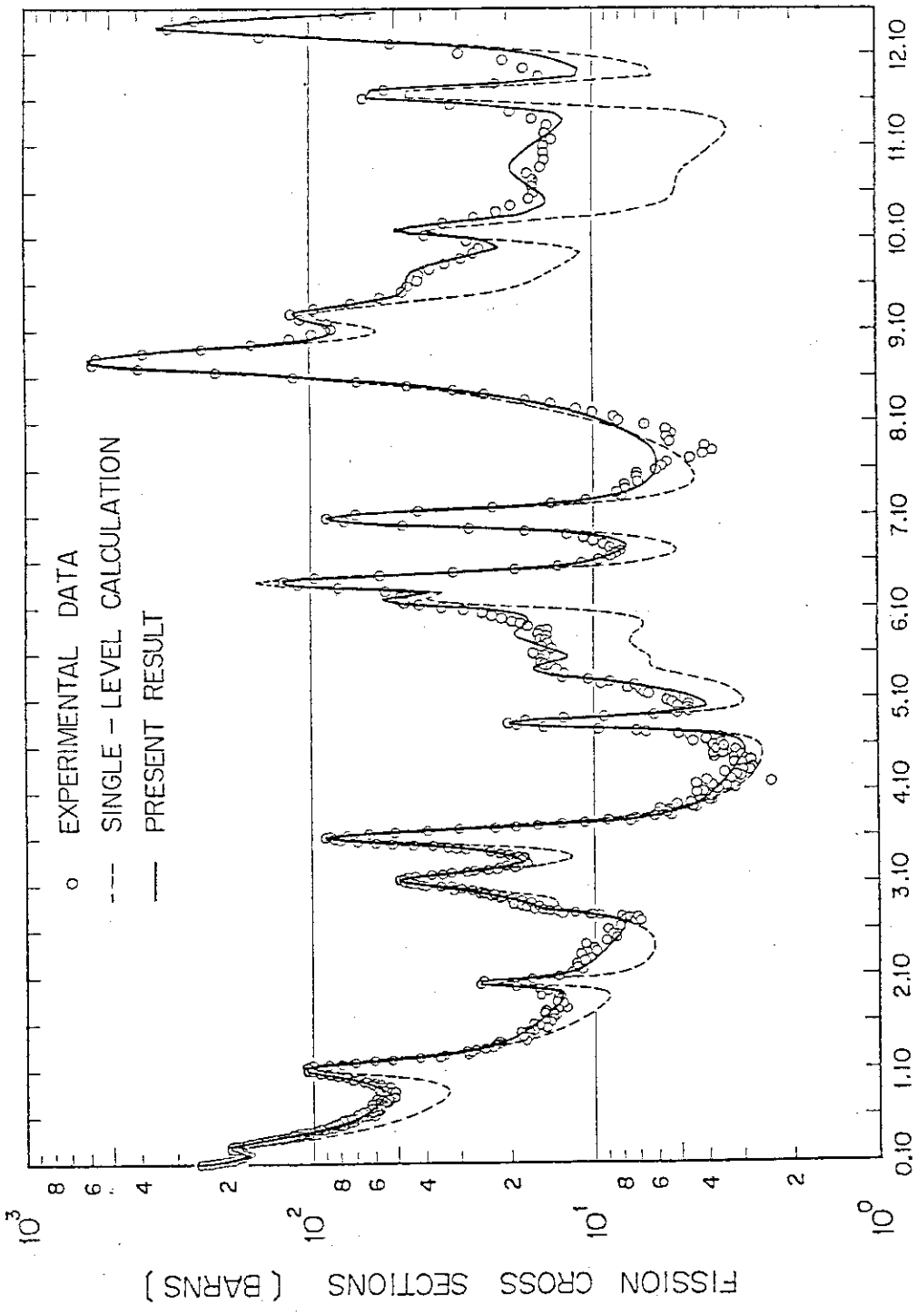

Fig.3.1 Comparison of ^{235}U fission cross sections from 12.4 to 0.1 eV. The circles are experimental data of Michauden[88] (12.54-0.3788eV) and of Shore and Sailor[76] (0.37-0.1 eV). The dotted line is the cross sections calculated by using the single-level parameters in Table 3.1. The solid line is the present least squares fit.

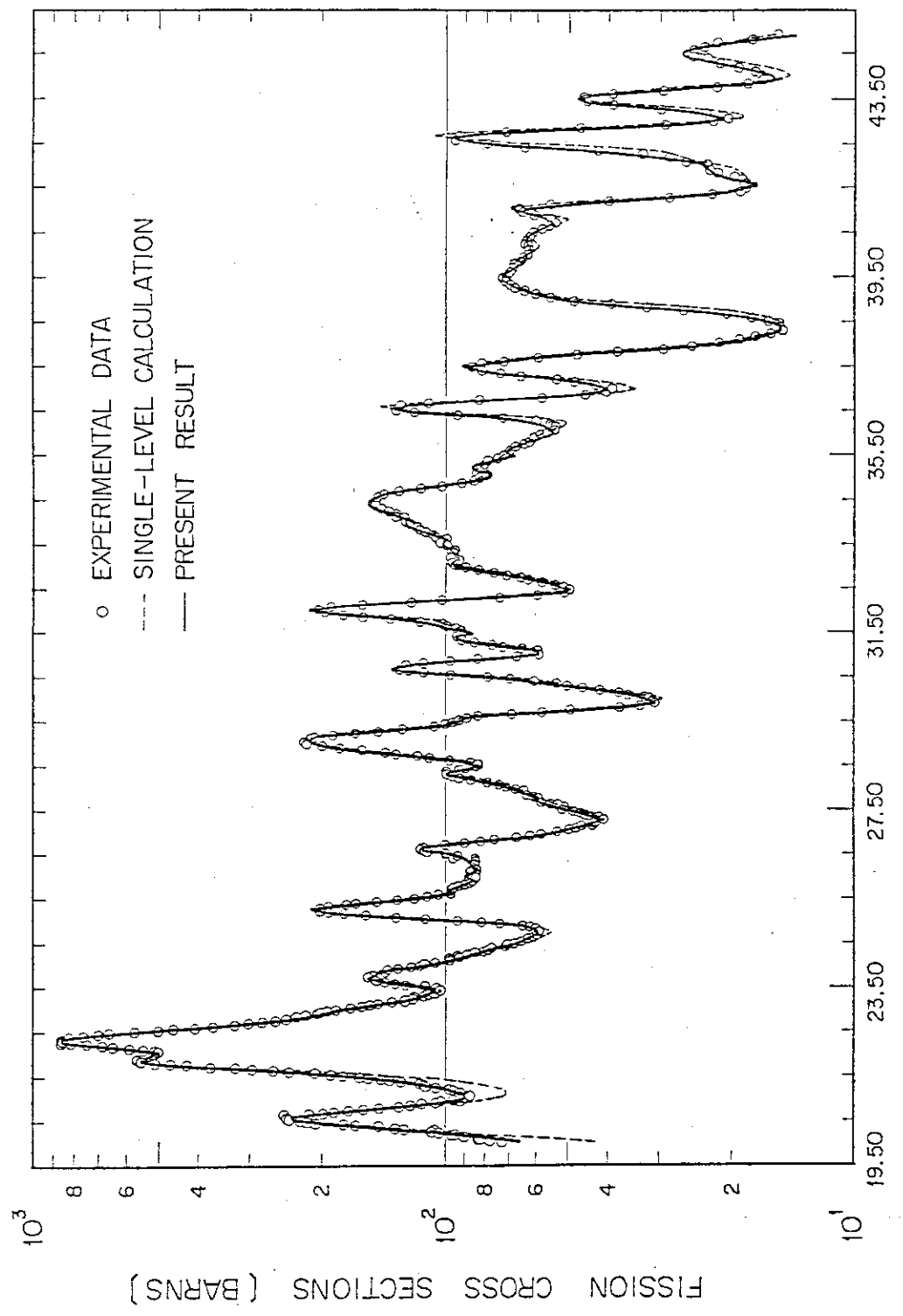

Fig.3.2 Comparison of ^{233}U fission cross sections from 45.5 to 20,0 eV.
The circules are the experimental data from Petrel bomb explosion[89].
The dotted line is the cross sections calculated by using the single-level parameters in Table 3.2. The solid line is the present least squares fit.

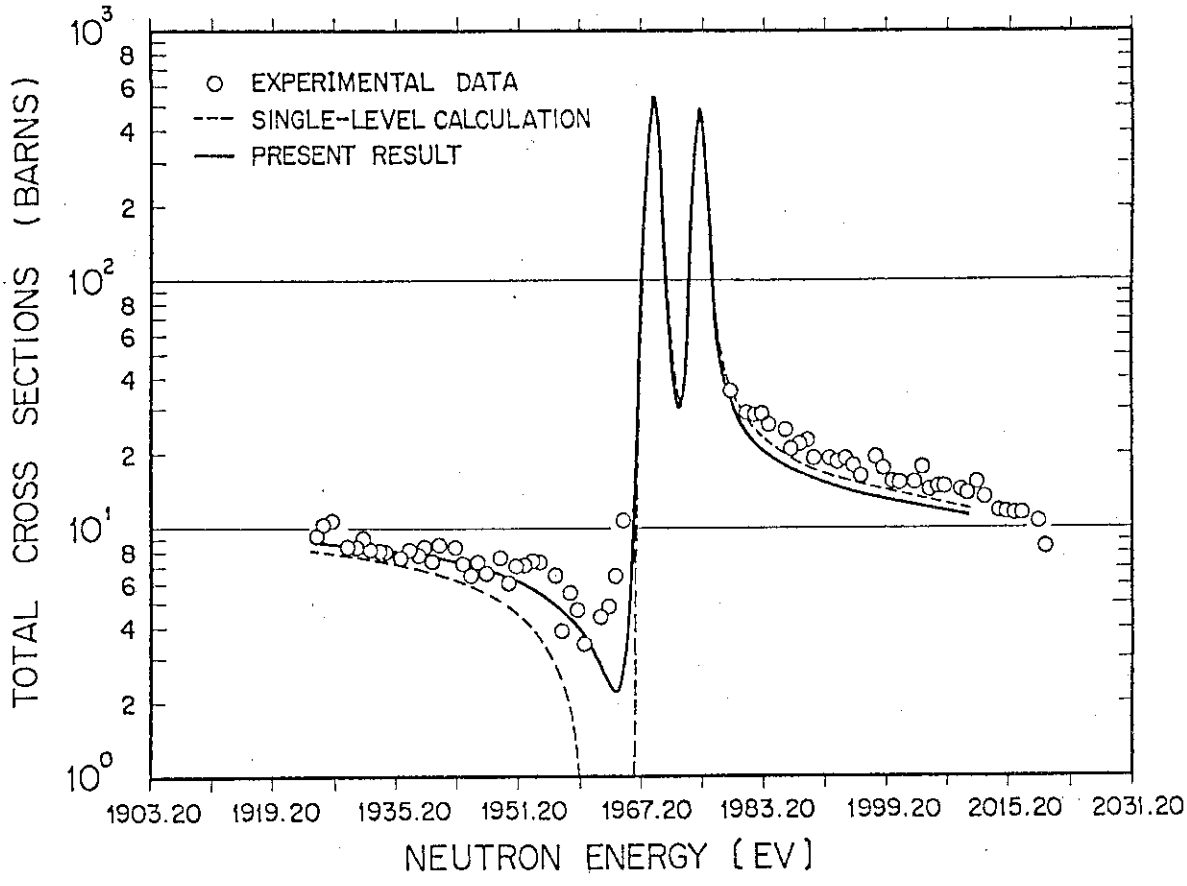

Fig.3.3 Comparison of ^{238}U total cross sections from 2020 to 1920 eV. The circles are the experimental data of Garg et al.[91] The dotted line is the cross sections calculated by using the potential scattering cross section of 10.6 barns and the single-level parameters in Table 3.3. The solid line is the present least squares fit.

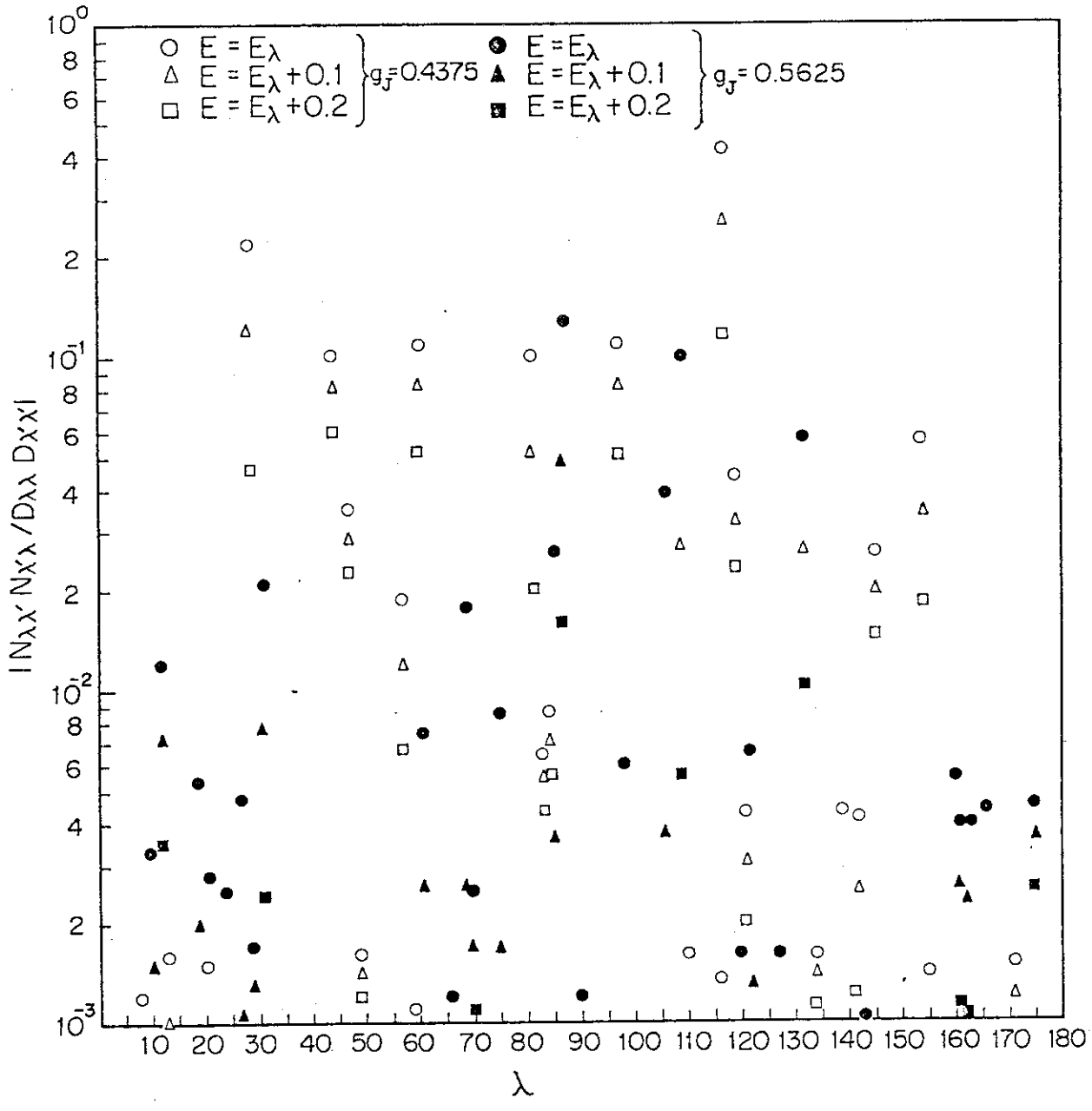

Fig.3.4 The values of $|N_{\lambda\lambda'}N_{\lambda'\lambda}/D_{\lambda\lambda}D_{\lambda'\lambda'}|$ calculated for 180 resonance levels of ^{235}U by using the ARCFIT-3 code in the energy range of 1800 to 1712 eV. The values for some levels were smaller than 10^{-3}, so that these were not presented in this figure.

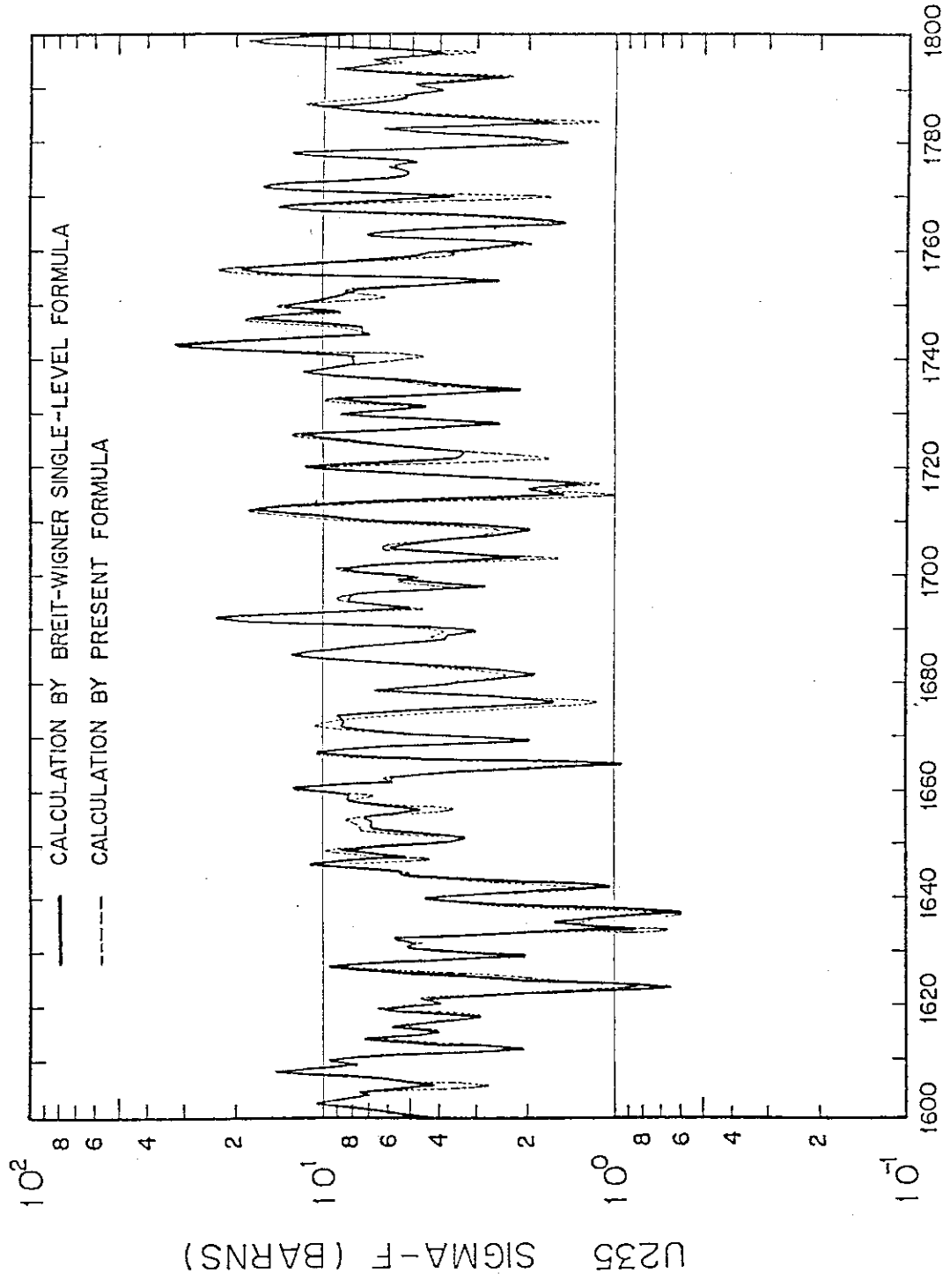

Fig.3.5 Comparison of the energy variations of the fission cross sections of ^{235}U calculated by the Breit-Wigner single-level and the present formulas.

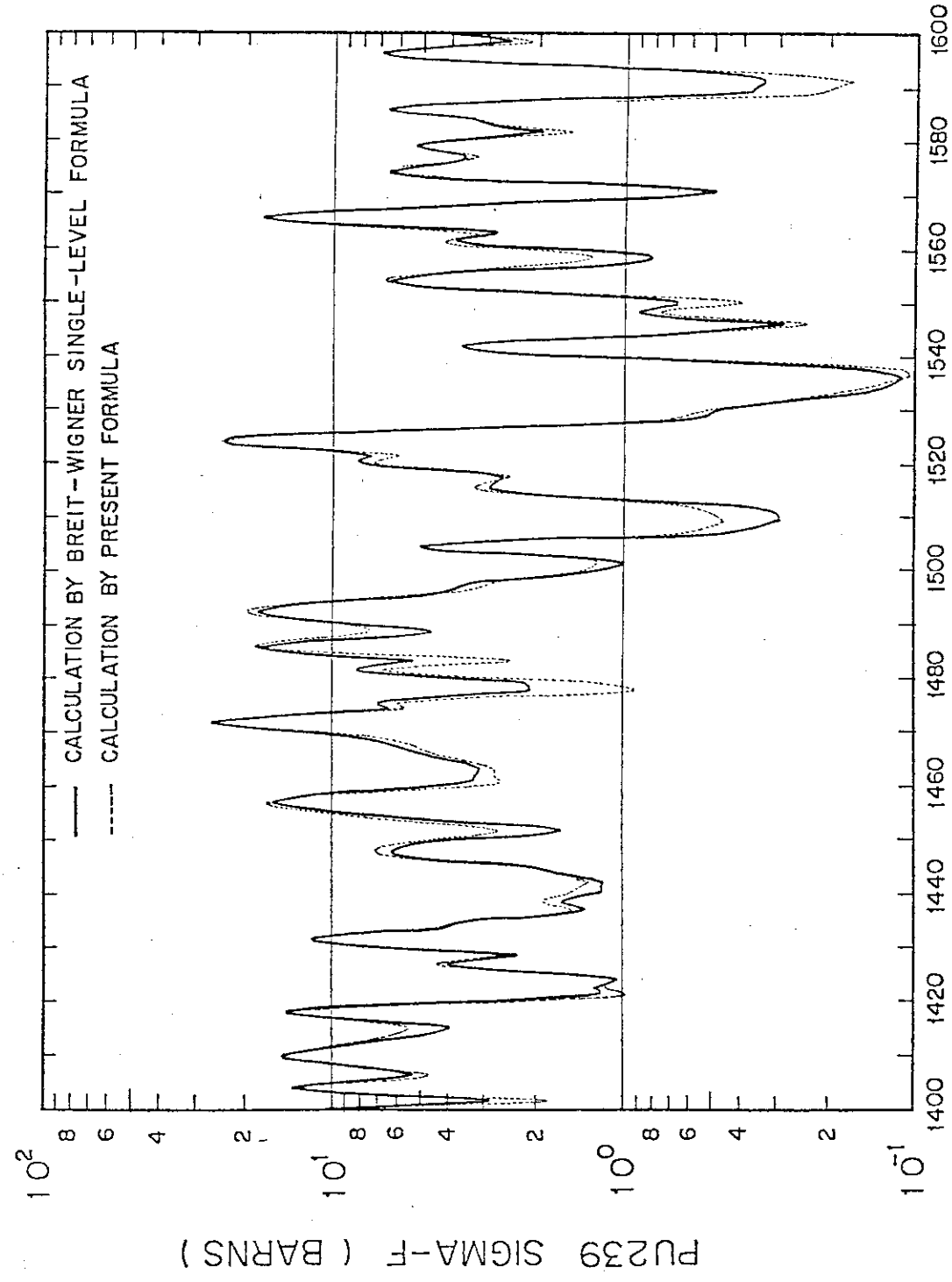

Fig.3.6 Comparison of the energy variations of the fission cross sections of ^{239}Pu calculated by the Breit-Wigner single-level and the present formulas.

4. Calculational Method of Group Constants of Heavy Resonant Nuclei

4.1 Introduction

The multigroup transport or diffusion calculations are often based on the concent of multigroup constants set such as the ABBN[8] or JAERI Fast set[9],[10]. The principal advantage of the multigroup constant method is that reactor calculation can be made by using the same group constant set for various reactors with different compositions and sizes. Consequently, some processing codes such as ETOX[22], MINX[23] and PROF-GROUCH-G[34] were developed to calculate economically and conveniently, the group constants using an updated data file. However, the calculational method of group constants used in these codes are different. Especially, the effective cross sections in resonance energy region are calculated by using various methods.

Though the ETOX and MINX codes can take into account for both the composition and temperature dependence of group cross sections the effective group cross sections are calculated by assuming the constancy of collision density. Moreover, the isolated narrow-resonance approximation is used for unresolved resonance region. Therefore, the mutal interference between resonances of different nucli and the self-overlapping effects are ignored. Furthermore, the self-shieldig of elastic removal cross section is assumed to be neglected.

A processing code TIMS-1 which calculates the effective cross sections by solving numerically the neutron slowing down equation using the recurrence formula[62] for slowing down source has been developed, in order to avoid the errors caused from the approximations used in the ETOX and MINX codes, as described in Chapter 2. In this Chapter, the calculational methods of group constant used with the TIMS-1 code

are described. Furthermore, the mutual interference between different heavy resonant nuclei is studied using this code. The group constants calculated with TIMS-1 and ETOX are compared and the effects of the difference between two cross sections on nuclear characteristics are also studied.

4.2 Average Cross Sections in the Unresolved Resonance Region

The average cross sections are defined by

$$\langle\sigma_x\rangle = \frac{1}{\Delta E}\int_{\Delta E}\sigma_x(E)dE \tag{4-1}$$

where x stands for the capture, fission, elastic and inelastic scattering reactions and ΔE the energy interval. Eq.(4-1) is expressed by using the Breit-Wigner single-level formula[96]

$$\langle\sigma_x\rangle_{\Delta E} = \frac{2\pi}{k^2}\sum_{\ell J} g_J \left\langle\frac{\Gamma_n\Gamma_\gamma}{\Gamma}\right\rangle_{\ell,J}/\bar{D}_{\ell,J} \quad , \tag{4-2}$$

$$\langle\sigma_f\rangle_{\Delta E} = \frac{2\pi}{k^2}\sum_{\ell J} g_J \left\langle\frac{\Gamma_n\Gamma_f}{\Gamma}\right\rangle_{\ell,J}/\bar{D}_{\ell,J} \quad , \tag{4-3}$$

$$\langle\sigma_{in}\rangle_{\Delta E} = \frac{2\pi}{k^2}\sum_{\ell J} g_J \left\langle\frac{\Gamma_n\Gamma_{in}}{\Gamma}\right\rangle_{\ell,J}/\bar{D}_{\ell,J} \quad , \tag{4-4}$$

$$\langle\sigma_n\rangle_{\Delta E} = \frac{4\pi}{k^2}\sum_{\ell J} g_J (2\ell+1)\sin^2\phi_\ell + \frac{2\pi^2}{k^2}\sum_{\ell J}\frac{g_J}{\bar{D}_\ell}\left[\left\langle\frac{\Gamma_n\Gamma_n}{\Gamma}\right\rangle_{\ell,J} - 2\bar{\Gamma}_{n,\ell,J}\sin^2\phi_\ell\right] , \tag{4-5}$$

$$\langle\sigma_t\rangle_{\Delta E} = \langle\sigma_c\rangle_{\Delta E} + \langle\sigma_f\rangle_{\Delta E} + \langle\sigma_n\rangle_{\Delta E} + \langle\sigma_{in}\rangle_{\Delta E} \quad , \tag{4-6}$$

where the brackets mean the statistical average over the χ-square distribution with a designated degree of freedom. The integrations for

the statistical average are written by using average resonance parameters:

$$\left\langle \frac{\Gamma_n \Gamma_\gamma}{\Gamma} \right\rangle = \bar{\Gamma}_\gamma \left\langle \frac{u}{1+u+v+w} \right\rangle = \bar{\Gamma}_n \int_0^\infty\int_0^\infty\int_0^\infty \frac{uP_\nu(u)P_\eta(v)P_\zeta(w)}{1+au+bv+cw}\,dudvdw \quad , \tag{4-7}$$

$$\left\langle \frac{\Gamma_n \Gamma_f}{\Gamma} \right\rangle = \bar{\Gamma}_\gamma \left\langle \frac{uv}{1+u+v+w} \right\rangle = \bar{\Gamma}_n\, b\int_0^\infty\int_0^\infty\int_0^\infty \frac{uP_\nu(u)vP_\eta(v)P_\zeta(w)}{1+au+bv+cw}\,dudvdw, \tag{4-8}$$

$$\left\langle \frac{\Gamma_n \Gamma_n}{\Gamma} \right\rangle = \bar{\Gamma}_\gamma \left\langle \frac{u^2}{1+u+v+w} \right\rangle = \bar{\Gamma}_n\, a\int_0^\infty\int_0^\infty\int_0^\infty \frac{u^2P_\nu(u)P_\eta(v)P_\zeta(w)}{1+au+bv+cw}\,dudvdw, \tag{4-9}$$

$$\left\langle \frac{\Gamma_n \Gamma_{in}}{\Gamma} \right\rangle = \bar{\Gamma}_\gamma \left\langle \frac{uw}{1+u+v+w} \right\rangle = \bar{\Gamma}_n\, c\int_0^\infty\int_0^\infty\int_0^\infty \frac{uP_\nu(u)P_\eta(v)wP_\zeta(w)}{1+au+bv+cw}\,dudvdw, \tag{4-10}$$

where $u = \Gamma_n/\bar{\Gamma}_\gamma$, $v = \Gamma_f/\bar{\Gamma}_\gamma$, $w = \Gamma_{in}/\bar{\Gamma}_\gamma$, $a = \Gamma_n/\bar{\Gamma}_\gamma$, $b = \bar{\Gamma}_f/\bar{\Gamma}_\gamma$, $c = \bar{\Gamma}_{in}/\bar{\Gamma}_\gamma$ and ν, η and ζ are the numbers of degree of freedom for neutron, fission and inelastic scattering widths, respectively. The function $P(u)$ is the χ-square distribution function given by

$$P_n(x)dx = \frac{n}{2\Gamma(n/2)} \left(\frac{nx}{2\bar{x}}\right)^{\frac{n}{2}-1} \exp\left(-\frac{nx}{2\bar{x}}\right) \frac{dx}{x} \quad , \tag{4-11}$$

where $\bar{x}$ is the mean value of x, n the degree of freedom and $\Gamma(n/2)$ the Γ-function. Each integration is numerically performed by using the Gauss-Laguerre formula with fifteen points.

The average neutron widths for ℓth-wave neutrons and spin J-states are defined as

$$\bar{\Gamma}_{n\ell J} = \Gamma^0_{n\ell J} \sqrt{E}\, \mu_\ell\, \nu_{n\ell J} \quad . \tag{4-12}$$

where

$$\mu_\ell \begin{cases} 1 & \text{for } \ell = 0 \quad (4\text{-}13) \\ (k\hat{R})^2/(1 + (k\hat{R})^2) & \text{for } \ell = 1 \quad (4\text{-}14) \\ (k\hat{R})^4/(9 + 3(k\hat{R})^2 + (k\hat{R})^4) & \text{for } \ell = 2 \quad , \quad (4\text{-}15) \end{cases}$$

where $\hat{R}$ is the nuclear radius (in units of 10^{-12}cm).

4.3 Generation of Resonance Parameters by Monte Carlo Method

Resonance widths and level spacing are distributed round their mean values according to the χ^2- and Wignear distributions, respectively. The χ^2-distribution of Eq.(4-11) is known as the distribution that a statistical variable

$$x = X_1^2 + X_2^2 + \text{---------} + X_n^2 \tag{4-16}$$

follows, where the n samples X_1, X_2, -----, X_n distribute normally

$$P(x)dx = \frac{1}{\sqrt{2\pi}} \exp(-x^2/2)dx \quad , \tag{4-17}$$

Hence, the statistical variables distributed according to the χ^2-distribution are produced by generating the samples which ditribute nomally.

Now, let ξ_1 and ξ_2 are independent samples distributed uniformally in the range from 0 to 1, then, the variables x_1 and x_2 defined by

$$x_1 = (-2\ell n\xi_1)^{1/2} \sin 2\pi \xi_2 \tag{4-18}$$

$$x_2 = (-2\ell n\xi_1)^{1/2} \cos 2\pi \xi_2 \tag{4-19}$$

are distributed normally. That is, the Jacobian is

$$\frac{\partial(\xi_1,\xi_2)}{\partial(X_1,X_2)} = \frac{1}{2\pi} \exp\left(- \frac{x_1^2 + x_2^2}{2} \right) \tag{4-20}$$

or

$$d\xi_1 \, d\xi_2 = P(x_1)dx_1 \cdot P(x_2)dx_2 \ . \tag{4-21}$$

The wigner distribution needed for level spacing is obtained from the χ^2-distribution with 2 degrees of freedom.

$$P_2(x)dx = e^{-x}dx \tag{4-22}$$

be the variable inversion

$$y = 2\sqrt{x/\pi} \quad , \tag{4-23}$$

that is,

$$P_2(x)dx = \frac{\pi}{2} y \exp(-\pi y^2/4)dy \quad . \tag{4-24}$$

In the unresolved region, hence, the resonance parameters and the level spacings are generated by using Monte Carlo method from the Porter-Thomas and Wigner distributions, respectively. The ladders of resonance parameters are repeatedly generated until a ladder satisfies the following conditions:

$$\left| \frac{\langle\sigma_x\rangle - \bar{\sigma}_x}{\langle\sigma_x\rangle} \right| \Delta E_n \leq \varepsilon_\sigma \quad , \tag{4-25}$$

$$\left| \frac{\langle\Gamma_x\rangle - \bar{\Gamma}_x}{\langle\Gamma_x\rangle} \right| \Delta E_n \leq \varepsilon_\Gamma \quad , \tag{4-26}$$

$$\Delta En = \frac{1}{2}(E_{n-1} + E_n) - \frac{1}{2}(E_n + E_{n+1}) \tag{4-27}$$

where $\langle\sigma_x\rangle$ is the evaluated average cross section of Eq.(4-1), $\bar{\sigma}_x$ and $\bar{\Gamma}_x$ mean the values of the cross section and partial width averaged over a generated ladder of resonance parameters, respectively, and ε_σ and ε_Γ are the assumed errors for the average cross sections and partial width in the energy range ΔE_n, respectively.

The generated ladder of resonance parameters and the resolved resonance parameters are connected finally and a set of resonance parameters is supplied in the energy range from the unresolved to the resolved regions.

4.4 Doppler-broadened Cross Sections

The calculations for s-wave neutron cross section are performed by the use of either the Breit-Wigner single-level formula or the multilevel formula as described in Chapter 3. On the other hand, the reaction cross sections for p- and d-wave neutrons are assumed to be expressed by the single-level formula as follows:

$$\sigma_t(E) = \frac{4}{k^2}\sqrt{\frac{\alpha}{2m\pi}}\ \frac{(\mu_\ell)}{E}\ g_J \sum_\lambda \Gamma^0_{\lambda n\ell}\ (E_\lambda \Phi^r_\lambda(w) + \frac{1}{2}\Gamma_\lambda \Phi^i_\lambda(w)) \quad , \qquad (4\text{-}28)$$

$$\sigma_x(E) = \frac{4}{k}\sqrt{\frac{\alpha}{2m\pi}}\ \frac{(\mu_\ell)}{E}\ g_J \sum_\lambda \frac{\Gamma^0_{\lambda n\ell}\Gamma_{\lambda x}}{\Gamma_\lambda}\ (E_\lambda \Phi^r_\lambda(w) + \frac{1}{2}\Gamma_\lambda \Phi^i_\lambda(w)) \ , \qquad (4\text{-}29)$$

The cross section at an energy E is expressed by summing up the contribution from each individual resonance (λ).

$$\sigma_x(E) = \sum_{\lambda \in \ell, J} \sigma_{x,\lambda}(E) \quad . \qquad (4\text{-}30)$$

Strictly speaking the summation shoud be made over an infinite number of resonances but, in practice, the contributions from very far resonance can be neglected. Thus a practical limit is set for the number of resonances λ to be considered, such quantity as to be necessary and sufficient for obtaining reliable cross section curves. For this purpose we introduce the following three conditions:

(1) For evaluating the cross section for a given energy E, the reasonances nearest to the energy of interest should be taken into acount.

(2) The cross section curve obtained should be smooth enough as to have no discontinuity introduced by the neglect of contributions

from the remote levels.

(3) The average cross sections over some energy range should not depend on λ which are larger than the practical λ value to be uniquely determined. The energy range should be wide enough to contain many resonance levels.

The cross section were calcualted numerically by taking account of condition (1), and the values of λ that satisfy the conditions (2) and (3) have been explored for ^{235}U, ^{238}U and ^{239}Pu over several energy ranges. It was found that the practical values of λ depend significantly on level spacings, on interference between potential and resonance scattering, and on the effect of Doppler broadening.

Figures 4.1 and 4.2 show the variation in the s-wave (i.e. $\ell = 0$) cross section curves of ^{235}U for several values of λ and temperature, respectively. From Fig. 4.1, it is seen that the cross section curve for $\lambda = 16$ is quite smooth at 300 °K. For $\lambda = 8$ and 4, however the curves seem to be very curious. This might possibly be due among some factors to the neglected resonance tails and to the very narrow level spacing and wide fission widths adopted. At 10 keV, the Doppler width for ^{235}U is about 2.1 eV for 300 °K where the mean level spacing are 1.143 eV for J = 3 and 0.889 eV for J = 4. In the energy region shown in Figs. 4.1 and 4.2 there are 81 resonances having unequal, random level spacings. The energy range to be considered for a fixed λ value should vary from one energy point to another because of the condition (1). And it should also be noted that the sums of resonances broadened by Doppler effect often behave like a gross pseudo resonance. Therefore the peaks of the cross section curves in Figs. 4.1 and 4.2 do not always correspond to one particular resonance.

At temperature above 300 °K, the resoance peaks are strongly flattened out by the Doppler effect, so that their tails extend their influence into far-off energy points. At 10 keV, the Doppler widths are about 3.63 eV for 900 °K and 5.55 eV for 2100 °K. The Doppler effect may be observed from Fig. 4.2. The λ = 16 gives a resonable cross section curve for T = 300 °K, but unreasonable results for T = 900 °K and 2,100 °K. This indicates that obviously the integrated values of cross sections are not conserved when temperature change. This means that, to obtain meaningful results, the practical values of λ depend considerably on temperature when dealing with a nucleus with narrow level spacing such as ^{235}U.

For ^{238}U, whose level spacing are very much wider than with ^{235}U, it is not necessary to consider changing with temperature the number of resonances λ for practical purposes. However, in this case the large effect of the interference scattering become important. This is illustrated in Fig. 4.3, which shows the variations in the total cross section of ^{238}U in the neighborhood of 1 keV. The cross section curve for λ = 9 is quite smooth, while that for λ = 6 has two discontinuities at approximately 983.5 and 948.5 eV. The 983.5 eV discontinuity comes from neglecting the positive effect of interference scattering due to the 936.5 eV level, and that around 948.5 eV from neglecting the negative interference effect of the 991.8 eV level. This latter effect in particular influences the cross section within a range of about 90 eV above and below the resonacne energy.

The level spacing of ^{239}Pu are comparatively wide, so that, as compared with ^{235}U, the practically adopted number of resonances λ is not as sensitive to temperature variations. Moreover, the resonance width are often very wide, and the interference scattering effect is

small. All this makes the treatment of the ^{239}Pu resonances fairely easy.

In Figs. 4.4(a) ∿ (c), the variations in the average cross sections of ^{235}U are plotted for three energy ranges and temperatures. It is seen that in the case of T = 300 °K the value of λ = 16 satisfies the condition (2), but not the condition (3). From Fig. 4.4(a), it could be said that a value of about 20 should be chosen to satisfy condition (3). But in this case of room temperature, the difference in the average cross section between λ = 16 and λ = 20 is small. The non-conservation of the integrated cross section caused by the temperature variation is evident from these three figures. To meet the conditions (1) ∿ (3), 20, 30 and 40 may be adopted as practical values of λ, for T = 300 °K, 900 °K and 2,100 °K respectively, judging from Figs. 4.1, 4.4 (a) ∿ (c). These λ values can be used in common for the three energy regions and reactions.

Figures 4.5(a), (b) show the average cross sections of ^{238}U in two energy ranges. From these figures, it is seen that the average cross sections of ^{238}U do not depend strongly on temperature by virtue of the very wide level spacings. In Fig. 4.5(b), the difference in average total cross section between T = 300 °K and T = 2,100 °K comes from the Doppler effect of the comparatively large scattering resonance near 21.3 keV. This large interference makes that the average total cross sections vary non-uniformly with λ. Neverthless the variations in average totla cross section are small for $\lambda \geqq 9$, so that for practical purposes the values of λ = 9 may be chosen as satisfying the condition (3).

Figure 4.6(a), (b) are the average cross sections for ^{239}Pu. In these figures the conditions (3) is satisfied by adopting λ = 7, 8

and 11 for T = 300°, 900°and 2,100 °K respectively.

Table 4.2 shows the numebr of resonances λ that should satisfy all three conditions, and cover several energy ranges. By using these λ values the s-wave cross section curves of ^{235}U, ^{238}U and ^{239}Pu can be determined with good accuracy for the energy ranges considered here. The error to be expected with these λ values when applied to other energy regions sholud further be quite small. For practical purposes, cross section curves for energies below 35 keV for ^{238}U and below 10 keV for ^{235}U and ^{239}Pu can be quite reliable when drawn using these λ values. For instance, Fig. 4.7 shows the total cross sections of ^{238}U for T = 300 °K in the energy range from 0.315 eV to 30 keV. Figure 4.8 shows the temperature dependent cross section of ^{239}Pu in the energy range from 9.96 to 27.8 eV. Infinitely diluted cross sections in many energy groups have been calculated by using the λ values of Tbale 4.2 and compared with analytical results from resonance parameters. Good agreement has been generally obtained.

4.5 Calculation of Neutron Spectrum

Neutron balance equation in an infinite homogeneous system can be expressed as

$$\Sigma_t(u)\phi(u) = \sum_i \frac{1}{1-\alpha_i} \int_{u-\varepsilon_i}^{u} e^{u'-u}\Sigma_{si}(u')\phi(u')du' \qquad (4\text{-}31)$$

$$\varepsilon_i = -\ell n\ \alpha_i \qquad (4\text{-}32)$$

where Σ_{si} is the scattering cross section of the i-th scatterer and $\phi(u)$ the neutron spctrum at the lethargy u.

By with $\psi(u) = \phi(u)e^{u}$, Eq.(4-31) is written by

$$\Sigma_t(u)\psi(u) = \sum_i \frac{1}{1-\alpha_i} \int_{u-\varepsilon_i}^{u} \Sigma_{si}(u')\psi(u')du' \quad . \tag{4-33}$$

This equation is more simple than Eq.(4-31). In the PEACO[97] code, Eq.(4-33) is used in place of Eq.(4-31), because the factor exp(u) multiplied to $\phi(u)$ may serve to reduce round errors appeared in the recurrence formula introduced later for the numerical calculation of neutron slowing-down source.

$$\psi^m = \int_{u_0}^{u_+} \psi(u)du = \int_{u_0}^{u_+} \phi(u)e^{u}du \quad , \tag{4-34}$$

$$F_i^m = \int_{u_0}^{u_+} \Sigma_{si}(u)\psi(u)du = \Sigma_{si}^m \psi^m \tag{4-35}$$

where u_+ and u_0 are the upper and lower lethargy boundaries of the ultrafine group m, respectively. Then, the slowing down source is shown to be written as

$$\begin{aligned} S_i^m &= \int_{u_0}^{u_+} S_i(u)du = \frac{1}{1-\alpha_i} \int_{u_0}^{u_+} du \int_{u-\varepsilon_i}^{u} \Sigma_{si}(u')\psi(u')du' \\ &\cong \frac{\Delta u_m}{1-\alpha_i} \int_{u_0-\varepsilon_i}^{u_0} F_i(u)du = S_i^{m-1} + \frac{\Delta u_m}{1-\alpha_i} [F^m - F^{m-L_i^m}] \end{aligned} \tag{4-36}$$

where Δu_m is the lethargy width of ultrafine group m and L_i^m is the maximum number of groups which corresponds to the maximum lethargy gain by elastic collision. In the derivation of Eq.(4-36), the self-scatter term was neglected because the effect of self-scatter was shown to be quite insignificant[97]. In the PEACO-7 code, the scattering rate $F_i^{m-L_i^m}$ is

approximately calculated by using the intermediate-group method of Kier[62]. The accuracy of this approximation was also studied and shown to be quite satisfactory[97]. Assuming the asymptotic flux distribution above the lethargy range under consideration, the neutron spectra can be calculated recussively by using Eq.(4-36) for the slowing down source.

In Eq.(4-33), two resonant materials and a fictitious moderator, which the admixture potential scattering cross section is σ_0, are considered for calculating the group constants of the JFS type. It was found[10] that the mass of fictitious moderator should be determined as follows: The logarithmic energy loss ξ of the fictitious mass is equal to the average $\overline{\xi}$ of the moderators of interest in the present calculation. The fictitious mass A = 30[10] was recommended for producing the group constants for fast reactor calculation. In the TIMS-1 code, A = 30 is beforehand ready as the default value of the moderator mass. Using the microscopic cross sections of ^{238}U shown in Fig.4.7, the neutron spectrum calculated for the case of $\sigma_0 = 1.0$ and A = 30 is shown in Fig.4.9 as an example.

The effective group cross section for reaction x is calculated by using the neutron spectra on the ultrafine lethargy meshes as follows:

$$\tilde{\sigma}_x(\sigma_0,T,R) = \sum_{m\in\Delta E} \sigma_x^m(T)\ \phi^m(\sigma_0,T,R) \ /\ \sum_{m\in\Delta E} \phi^m(\sigma_0,T,R) \quad , \qquad (4\text{-}37)$$

where ϕ^m is the neutron spectrum at the ultrafine lethargy group (m), σ_x^m the energy-dependent cross section at temperature T(°K), σ_0 the admixture background potential scattering cross section of the Bondarenko type and R the atomic density ratio of the resonant element (2) to the resonant element (1) of interest. Furthermore, a current weight total cross section is defined as

$$\tilde{\sigma}_{t,1}(\sigma_0,T,R) = \frac{\sum_{m\in\Delta E} \phi^m(\sigma_0,T,R)}{\sum_{m\in\Delta E} \frac{\phi^m(\sigma_0,T,R)}{(\sigma^m_{t,1}(T) + R\sigma^m_{t,2}(T) + \sigma_0)}} - \frac{\sum_{m\in\Delta E} \phi^m(\sigma_0,T,R)}{\sum_{m\in\Delta E} \frac{\phi^m(\sigma_0,T,R)}{(R\sigma_{t,2}(T) + \sigma_0)}} \quad , \tag{4-38}$$

where $\sigma_{t,1}$ is the total cross section of the resonant element (1) of interest and $\sigma_{t,2}$ that of the other resonant element (2). This special total cross section thus defined is used to calculate the effective diffusion coefficient.

When R becomes zero, Eq.(4-38) is written by

$$\tilde{\sigma}_{t,1}(\sigma_0,T) = \frac{\sum_{m\in\Delta E} \phi^m(\sigma_0,T)}{\sum_{m\in\Delta E} \frac{\phi^m(\sigma_0,T)}{(\sigma^m_{t,1}(T) + \sigma_0)}} - \sigma_0 \quad . \tag{4-39}$$

This express the total cross section of Bondarenko type. In the TIMS-1, to avoid round errors Eqs.(4-38) and (4-39) are rewritten by respectively,

$$\tilde{\sigma}_{t,1}(\sigma_0,T,R) = \frac{\left(\sum_{m\in\Delta E} \frac{\sigma^m_{t,1}(T)\phi^m(\sigma_0,T,R)}{(\sigma^m_{t,1}(T) + R\sigma^m_{t,2}(T) + \sigma_0)}\right)}{\left(\sum_{m\in\Delta E} \frac{\phi^m(\sigma_0,t,R)}{\sigma^m_{t,1}(T) + R\sigma^m_{t,2}(T) + \sigma_0}\right)} \quad , \tag{4-40}$$

$$\tilde{\sigma}_{t,1}(\sigma_0,T) = \frac{\sum_{m\in\Delta E} \frac{\sigma^m_{t,1}(T)\phi^m(\sigma_0,T)}{\sigma^m_{t,1}(T) + \sigma_0}}{\sum_{m\in\Delta E} \frac{\phi^m(\sigma_0,T)}{\sigma^m_{t,1}(T) + \sigma_0}} \quad . \tag{4-41}$$

These equations are shown to approach to the commonly defined total cross section of Eq.(4-37), when σ_0-value becomes infinite.

The elastic removal cross section is given by

$$\tilde{\sigma}_{er}(\sigma_0,T,R) = \frac{\sum_{m\in\Delta E'} \sigma_n^m(T)\phi^m(\sigma_0,T,R)\,\frac{E_L-\alpha E_m}{(1-\alpha)E_m}}{\sum_{m\in\Delta E} \phi^m(\sigma_0,T,R)} \quad , \tag{4-42}$$

$$\Delta E' = E_L / \alpha - E_L \quad , \tag{4-43}$$

$$\alpha = (A_1 - 1)^2 / (A_1 + 1)^2 \quad , \tag{4-44}$$

where E_L is the lower energy boundary of integration interval ΔE, $\sigma_n^m(T)$ the elastic scatttering cross section and A_1 the atomic mass for the resonant element (1) of interest.

The resonance self-shielding factors, i.e., the f-factors are defined by

$$f_x(\sigma_0,T,R) = \frac{\tilde{\sigma}_x(\sigma_0,T,R)}{\tilde{\sigma}_x(\infty,300,0)} \quad . \tag{4-45}$$

4.6 Fluctuation of Self-shielding Factors by Random Sampling

In the unresolved resonance region, the group constants are calculated by using a ladder of resonance parameters generated with Monte Carlo method. Therefore, the generated group constants depend on random numbers. If the random number dependence is remarkable, the resonance parameters should be generated so many times, and the calculated group constants should be averaged. If this averaging process is required,

however, the computing costs will be very expensive. In the TIMS-1 code, a ladder of resonance parameters is selected as satisfying the conditions of Eqs.(4-25) and (4-26). The errors of 5 and 15% for ε_σ and ε_Γ are assumed respectively in this study. The six ladders satisfying the conditions were sellected for ^{235}U and ^{238}U by using the nuclear data of ENDF/B-IV, and the self-shielding factors were calculated for $\sigma_0 = 100$ and $A = 30$. The magnitude of the fluctuation among the calculated self-shielding factors are shown in Tables 4.3 and 4.4. These tables show very small fluctuation for each reaction and energy group. Thus, we can conclude that the group constants may be calculated by using only one ladder satisfying the conditions of Eqs.(4-25) and (4-26) under the assumed errors.

4.7 Mutual Interference Between Different Heavy Resonant Nuclei

The effect of resonance overlap on Doppler coefficients in fast reactors has been studied by using analytical methods[55),(56)]. To estimate accurately the overlap effect, however, the numerical calculations are demanded. The calculations have been performed and the results showed that the analytical methods caused non-negligible errors for the effective cross sections in the resonance region below about 1 keV[10),(25)]. The mutual resonances overlap effect between two different isotopes on effective multiplication factor (k_{eff}) and Doppler coefficient has been studied by Kamei and Mizuta[98] for a composition of prototype fast reactor, and they showed that the effect was negligibly small. Their studies were performed by using a detailed calculational method, but assuming the group energy independent background total cross section.

In this Section, the effects of mutual resonance overlap on effective

multiplication factors, reaction rates and Doppler effects are studied. The effects are calculated by using the "table look-up" method, in order to consider the group energy dependence of background total cross section.

4.7.1 Mutual Shielding Factors

Mutual shielding factors for ^{235}U, ^{238}U, ^{239}Pu and ^{240}Pu were exactly calculated with the use of the TIMS-1 code[35] which solves numerically neutron slowing down equation by using a recurrence formula for neutron slowing down source. The nuclear data of ENDF/B-IV[30] were used in the present calculations. In the unresolved resonance region, a set of resonance parameters were generated by using a random sampling method[35]. The mutual shielding factors were calculated for eight σ_o-values (0, 0.1, 1.0, 10, 10^2, 10^3, 10^4, 10^5 and 10^6 barns), four temperatures (T = 300, 800, 2100 and 4500 °K) and six concentration ratios between two different resonant isotopes (R = 0, 0.1, 1.0, 10, 10^3 and 10^6).

The parameters σ_0 and R are defined as follows:

$$\sigma_b = \sigma_0 + \sigma_R \quad , \tag{4-1}$$

$$\sigma_0 = \frac{1}{N_j} \sum_{i \neq j,k} N_i \sigma_{t,i} \quad , \tag{4-2}$$

$$\sigma_R = R_j \sigma_{t,k} \quad , \tag{4-3}$$

$$R_j = N_k / N_j \quad , \tag{4-4}$$

where N_j is the atomic number density of resonant material (j) considered for the calculation of resonance shielding factor, N_k the atomic number density of background resonant material (k) and σ_t the total cross section. When, $R_j = 0$, hence, σ_b equals to σ_0 of Bondarenko's scheme[8]. In the present calculations, the four cases of ratio $^{240}R = {}^{238}N/{}^{240}N$, $^{239}R = {}^{238}N/{}^{239}N$, $^{238}R = {}^{239}N/{}^{238}N$ and $^{235}R = {}^{238}N/{}^{235}N$ are considered and the mutual

interference effects are studied.

The dependence of resonance shielding factors for ^{238}U, ^{239}Pu and ^{240}Pu on σ_0 and R are shown for several energy groups in Figs.4.10～4.15. It is seen from these figures that the resonance shielding factors depend considerably on the competition between σ_0 and R-values. In Figs.4.10～4.13, the mutual shielding for capture of $^{240}Pu(^{240}f_c)$ are shown as the function of σ_0 and $^{240}R = {}^{238}N/{}^{240}N$. It is seen from Fig.4.10 that $^{240}f_c$ approach to about 0.6 even for the case of $\sigma_0 = 10^5$ with the increase of ^{240}R-values. This is because of an accidental overlapping between two resonances at 66.62 eV of ^{240}Pu and 66.15 eV of ^{238}U over the energy range from 59.8 to 77.3 eV. Inversely, Fig.4.13 shows an example approaching to larger shielding factor than unit, because of widely different neutron spectrum from 1/E-shape due to the background resonance 189.6 eV of ^{238}U. Of course, when ^{240}R values are smaller than 10^3, $^{240}f_c$ approaches to unity with increasing σ_0-values as seen in Figs.4.11 and 4.13.

The mutual shielding for ^{239}Pu and ^{238}U calculated for the energy range of 77.3～59.8 eV are shown respectively in Figs.4.14 and 4.15. The mutual interference effects by overlapping between the resonances at 66.15 eV of ^{238}U and 65.7 eV of ^{239}Pu are seen also from these figures.

The mutual shielding effect becomes conspeciously with increasing R, that is, when the concentration of the resonant material in interest is very lower than that of the background resonant materials, the shielding factors do not always converge at unity even for a large $\sigma_0 = 10^6$. The mutual shielding factors of ^{235}U, ^{238}U, ^{239}Pu and ^{240}Pu calculated for $R = 10^6$ and $\sigma_0 = 10^6$ are shown in Table 4.5. As seen from this table, the mutual shielding factors are remarkably different from unity in several energy groups below 1 keV, where some large resonances of ^{238}U exist mostly. This may appeal to a notice for analysing integral

measurements for material of very small quantity such as reaction rate or small sample reactivity worth for ^{240}Pu measured in core and/or blanket region of fast critical assembly.

4.7.2 Contribution of Mutual Interference Effect on Integral Quantities in Fast Reactors

Reactor calculations were performed with one-dimensional diffusion and first order perturbation approximations[99], using the group constants library of JAERI-Fast set type produced from the ENDF/B-4 file.
The dependence of the resonance shielding factors on R-parameters is comparatively similary to that on σ_0-parameters. In the "table look-up" method, hence, the interpolation for R-parameter was made by using the same method as the σ_0-interpolation, i.e., using the cubic spline function which interpolates accurately the resonance shielding factors as the function of σ_0, R and temperature[45].

Effective Multiplication Factors (k_{eff})

The effects of resonance interference on the effective multiplication factors were calculated for the 14 benchmark cores with pultonium fuels which are 11 assemblies selected by Hardie et al.[17], two MOZART cores of MZA and MZB, and the FCA-V-2 assembly. The main characteristics for 14 benchmark cores are shown in Table 4.6. The deviations of the effective multiplication factors calculated with the mutual shielding effect from those without it are shown in Table 4.7. It is seen from this table that the mutual shielding effects are very small and never more than 0.16 percent on the effective multiplication factors.

Radial Reaction Rates

In analyses of reaction rates, it is wellknown that the disagreement between experiment and calculation are commonly observed in the vicinity of the boundary between core and blanket, and in the blanket region especially. Here, the effects of the mutual interference on the reaction rates are studied. In the calculation of the fission reaction rate of ^{239}Pu, for instance, the fission cross sections for infinite dilution are used in the blanket region, because ^{239}Pu is not contained in the region. However, really the reaction rate is measured by using foil or counter in which ^{239}Pu is contained. Hence, effective cross sections of ^{239}Pu for very large σ_0 and ^{239}R-values may be used in place of the infinitely dilute cross sections, considering the mutual shielding effect of ^{238}U.

For the Japanese prototype fast reactor "MONJU" mock-up assembly MZB, the radial reaction rates were calculated with one-dimensional diffusion theory. In the blanket region, the contribution of the fission reaction rate of ^{239}Pu below 1 keV accounts for considerable rate as seen from Fig.4.16. Hence, the mutual shielding effect may be seen on the reaction rates of ^{239}Pu and ^{235}U in the blanket region. The atomic number density for ^{239}Pu, 10^{-9}($\times 10^{22}$ atom/cc) was assumed in the blanket. Figure 4.17 shows the deviations of the radial reaction rates calculated with considering the mutual shielding effect from those without it. The mutual shielding effects were never more than 3.5% for the capture reaction rate of ^{239}Pu in the blanket region. The effect becomes larger for the reaction rates in the outer blanket region, because of a softer neutron spectrum.

Doppler Reactivity Coefficient

The Doppler reactivities were calculated with and without the mutual shielding effect for the isothermal Doppler experimental reactor

SEFOR[100]. The calculations were performed by using one-dimensional spherical model specified in Ref.(100). The results calculated for the temperature change from 677 to 1365 °K are shown in Table 4.8. The mutual shielding effect produces larger Doppler reactivities for both the fission and capture components. As the result, for the total Doppler reactivity, the effect cancels out and becomes negligibly small. Figure 4.18 shows the groupwise contribution of Doppler reactivity which is the difference of the reactivities calculated with the mutual shielding effect from that without it. From this figure, though the mutual shielding effect are remarkably seen in the energy range from 100 eV to 2 keV, the total reactivity of fission and capture parts becomes small due to the cancellation between positive and negative reactivities.

The concluding remarks are as follows. The mutual shielding effects between ^{239}Pu and ^{238}U on the radial reaction rates of ^{239}Pu are not more than a few percent in the blanket region for a typical fast reactor. Furthermore, the mutual shielding effects on the effective multiplication factors and Doppler reactivity were negligibly small due to the cancellation between the variations of positive and negative reactivities caused by fission and capture cross sections.

4.8 Comparison Between Group Constants Produced by Processing Codes TIMS-1 and ETOX

In this section, we study the influence of two different group cross sections sets on some integral quantities: One was produced by using the processing codes PROF-GROUH-G-II[36] and ETOX[32], and another was produced by PROF-GROUCH-G-II and TIMS-1[35]. The evaluated nuclear data of JENDL-1 were used in both calculations. The codes ETOX and TIMS-1 calculate the group cross sections of heavy resonant nuclides in the resonance energy regions. In the two sets, the group constants of light and medium nuclei and of heavy nuclei in smooth region above resonance energy have been calculated by the PROF-GROUCH-G-II code. Thus, the effects of different methods between TIMS-1 and ETOX on integral quantities can be studied by performing the neutronics calculation using two group constants sets.

The self-shielding factors calculated with two codes TIMS-1 and ETOX are compared. Some integral quantities, such as effective multiplication factors and Doppler reactivity worths were calculated by using these different group constants sets, and compared with the experimental results.

4.8.1 Comparison of Self-Shielding Factors

The self-shielding factors calculated with the TIMS-1 and ETOX codes are compared for some typical energy groups in Figs.4.19 and 4.20. In these figures, the quantity σ_0 expresses the admixture background scattering cross section of Bondarenko's type.

In Fig.4.19, the self-shielding factors for capture cross sections of ^{238}U are compared for several energy groups. The discrepancies between the self-shielding factors depend on the compositions, i.e. σ_0-values. Here, a small σ_0-value corresponds to the σ_0-value for high enriched fuel

systems, where the 1/E neutron spectrum assumed in the ETOX code differ considerably from the accurate spectrum calculated by the TIMS-1 code. Hence, the discrepancies between the self-shielding factors may be mostly attributed to the difference in the neutron spectra assumed for the calculation.

Fig.4.20 shows the self-shielding factors for fission cross sections of ^{239}Pu for several energy groups. The results compared between the self-shielding factors can be similarly summarised to those observed for ^{238}U as mentioned above.

In the next section, thus, we study the effects of the differences between the self-shielding factors on the integral quantities in fast reactor systems.

4.8.2 Integral Quantities Calculated by Using Two Different Cross Section Sets

The differences between the two cross-section sets produced by the TIMS-1 and ETOX codes exist only in the effective cross sections of heavy nuclides in the resonance energy regions. As integral quantities to be studied, we selected the effective multiplication factor (k_{eff}), Doppler reactivity effect and sodium void reactivity effect. The neutronics calculation were performed with the use of diffusion theory code.

Main characteristics of fast reactor critical assemblies used for the neutronics calculations are summarized in Table 4.9. Assembly FCA-VI-1 is the physics mockup core of JOYO (Experimental Fast Reactor). The SEFOR assembly is the testing core for both static power reactivity and rapid super-prompt-critical reactivity measurements. The benchmark sepecification model[100] was used in the present calculation. The assemblies ZPPR-2 and ZPR-6-7 are the demonstration fast reactor

benchmark core to provide physics data necessary for LMFBR design.

Effective Multiplication Factor

The effective multiplication factors calculated with the two-dimensional R-Z homogeneous model are shown in Table 4.10. The differences between the effective multiplication factors calculated by using the two sets are negligibly small for FCA-VI-1 and SEFOR, but are about 0.1 percent for the other ones. These results are small, compared with the value 0.2% that is the accuracy[18] of goal requested from design study for a large fast breeder reactor.

Sodium Void Reactivity Effect

The experimental results of sodium void reactivity effect in ZPPR assembly 2 have been analyzed with one-dimensional spherical homogeneous model. The sodium-voided zone consists of 93 matrix positions with all voided 12 inches each half core. In the present analysis, some corrections such as two-dimensional, cell-heterogeneity and neutron streaming effects were not considered, because the present aim lies only in studying the influence of two different calculational methods for group constants on sodium void reactivity worth.

Table 4.11 shows the comparison of the sodium void reactivity separated in each component term. The difference between the two different sets is -3% for the total reactivity, 0.0075 ($\Delta k/k$), though the differences by 6.5% and 11% are observed for "$\Sigma_{i\to j}$" and "$\nu\Sigma_f$" components, respectively.

Doppler Reactivity Effect

The experiment in ZPPR assembly 2 was the sample Doppler reactivity measurement for the natural UO_2 (NUO_2), and in SEFOR assembly was the measurement of the isothermal Doppler coefficient for the full core.

The results analysed for the NUO_2 sample Doppler experiment in ZPPR-2 are shown in Table 4.12. The calculation was performed with the one-dimensional first-order perturbation theory. Both the results calculated for the two-sets overestimate the experimental values by 10-14%, though the results for TIMS-1 are smaller than the ones for ETOX. The comparison of the groupwise Doppler reactivity worth in Fig.4.21 indicates remarkable discrepancies between the calculated results. It is observed that the results of ETOX are larger than ones of TIMS-1 in the unresolved resonance region and reversely small in the resolved region. This tendency produces an accidental cancellation between the results of ETOX and TIMS-1 for the total Doppler reactivity and the results give nothing but good agreement.

The results analysed for the Doppler reactivity measurement of full core in SEFOR assembly are compared in Table 4.13. This analysis was performed with the first-order perturbation theory using two-dimensional R-Z benchmark model. In both the results of ETOX and TIMS-1, the positive Doppler reactivity by fission component term is more than 30% of the negative one by capture. The differences in the group-wise fission component terms between TIMS-1 and ETOX is remarkable as seen from Fig.4.22, and the result of TIMS-1 is larger than the one of ETOX, especially in the unresolved region. The differences between the capture components in Fig.4.23 show a similar tendency also as the results of the NUO_2 sample Doppler analysis indicated in Fig.4.21. The different tendencies for the fission and capture terms between the results of TIMS-1 and ETOX can be estimated simply from the fact that the temperature dependence of the self-shielding factors differs between the results of TIMS-1 and ETOX, depending on the σ_0-values. The discrepancy between TIMS-1 and ETOX for the total Doppler reactivity worth is -4% while the goal accuracy[18] for Doppler effect is ±7%.

The temperature and composition dependence of effective group cross

sections calculated with the processing code ETOX differ considerably from those calculated with the TIMS-1 code. Particularly as for the Doppler effect of the shielding factors, the difference between the results of TIMS-1 and ETOX depends strongly on the energy groups and the compositions. The effects of these differences on the effective multiplication factor, Na-void effect and Doppler effect were studied and were no more than 0.15%, -3% and -4% respectively. These values are comparable with the goal accuracies requested from design study in a large fast breeder reactor.

4.9 Concluding Remarks

The very severe accuracies of goal for important nuclear characteristics are required from the design study on a large fast breeder reactor. In order to satisfy the goal accuracies, there are many problems to be studied in detail. It is one of them that errors caused by the conventional approximations should not be included in the group constants used for reactor calculations. For this purpose, the TIMS-1 code which calculates the group average cross sections by solving numerically the neutron slowing down equation were developed. This code prepares also a very useful tool to calculate the mutual shielding factors.

The analyses for several fast critical assemblies were performed by the use of the group constants generated by TIMS-1 and ETOX. It was concluded from the computational results that the accurate calculations for the group constants was needed for the reactor calculations. Especially, it will be so for reaction rate calculation because of a softer neutron spectrum at blanket region in a large fast reactor.

Although the accurate calculations of TIMS-1 consume about ten times as compared with those of ETOX, the tables of resonance shielding factors are generated only once. The reactor calculations for various compositions and temperatures can be always performed by using the same tables.

Table 4.1 Ultrafine and fine group structures used in the MCROSS-2 code

Group no.	Energy boundary (eV)	No. of fine group	No. of ultra-fine group	Lethargy width
1	100000 - 46500	766	7660	0.0001
2	46500 - 21500	772	7720	0.0001
3	21500 - 10000	766	7660	0.0001
4	10000 - 4650	766	7660	0.0001
5	4650 - 1000	768	7680	0.0002
6	1000 - 465	383	3830	0.0002
7	465 - 100	615	6150	0.00025
8	100 - 46.5	307	3070	0.00025
9	46.5 - 10	308	3080	0.0005
10	10 - 4.65	153	1530	0.0005
11	4.65 - 0.2	630	6300	0.0005

Table 4.2 Number of resonances to be taken into account for obtaining practically reliable s-wave (ℓ = 0) cross section curves

T(°K)	^{235}U	^{238}U	^{239}Pu
300	20	9	7
900	30	9	8
2,100	40	9	11

Table 4.3 Fluctuation of self-shielding factors of ^{238}U;

$$\chi_f = \sqrt{\frac{1}{N}\sum_{i=1}^{N}(f_i - \bar{f})^2/\bar{f}} \quad (\%)$$

Energy (keV)	χ_{fc}	χ_{fn}	χ_{ft}	χ_{fer}
46.5 - 36.0	0.008	0.007	0.016	0.118
36.0 - 27.8	0.008	0.014	0.027	0.0273
27.8 - 21.5	0.006	0.019	0.037	0.124
21.5 - 16.6	0.019	0.024	0.046	0.203
16.6 - 12.9	0.027	0.031	0.058	0.089
12.9 - 10.0	0.038	0.132	0.248	0.127
10.0 - 7.73	0.027	0.043	0.075	0.449
7.73 - 5.98	0.024	0.076	0.142	1.107
5.98 - 4.65	0.064	0.059	0.110	0.106
4.65 - 3.60	0.066	0.052	0.091	0.021

Table 4.4 Fluctuation of self-shielding factors of ^{235}U;

$$\chi_f = \sqrt{\frac{1}{N}\sum_{i=1}^{N}(f_i - \bar{f})^2/\bar{f}} \quad (\%)$$

Energy (keV)	χ_{ff}	χ_{fc}	χ_{fn}	χ_{ft}	χ_{fer}
4.65 - 3.60	0.01	0.13	0.03	0.08	0.31
3.60 - 2.78	0.06	0.25	0.06	0.10	0.35
2.78 - 2.15	0.09	0.48	0.07	0.05	0.09
2.15 - 1.66	0.42	0.10	0.10	0.02	0.10
1.66 - 1.29	0.19	0.26	0.08	0.37	0.43
1.29 - 1.00	0.18	0.12	0.30	0.20	1.01
1.00 - 0.773	0.50	0.74	0.35	0.90	0.79
0.773 - 0.598	0.14	0.23	0.06	0.04	2.33
0.598 - 0.465	0.50	0.70	0.30	0.77	1.90

Table 4.5 Infinitely dilute cross sections and mutual shielding factors of ^{235}U, ^{238}U, ^{239}Pu and ^{240}Pu calculated with $\sigma_0 = 10^6$ barns and $R = 10^6$

Upper energy limit (eV)	^{235}U				^{239}Pu				^{238}U		^{240}Pu	
	$\sigma_f(\infty)$ (b)	f_f	$\sigma_c(\infty)$ (b)	f_c	$\sigma_f(\infty)$ (b)	f_f	$\sigma_c(\infty)$ (b)	f_c	$\sigma_c(\infty)$ (b)	f_c	$\sigma_c(\infty)$ (b)	f_c
10000	2.94	1.00	1.35	0.99	2.00	0.99	1.19	0.98	0.74	0.97	1.27	1.01
7730	3.39	1.00	1.40	1.01	1.93	0.98	1.42	0.99	0.83	0.98	1.40	0.97
5980	3.64	1.01	1.41	1.00	2.30	1.00	1.85	0.99	0.80	1.01	1.61	1.01
4650	4.73	1.00	1.52	0.98	2.73	0.96	2.22	0.99	1.10	0.99	1.82	1.02
3600	4.67	1.00	1.63	1.00	3.62	0.97	2.45	0.94	1.18	0.96	1.88	0.98
2780	5.00	0.99	1.90	1.05	3.34	0.98	3.13	0.94	1.49	1.01	2.57	1.08
2150	6.01	1.01	2.50	0.98	3.55	0.91	4.05	1.14	1.58	0.94	2.71	0.96
1660	7.30	1.07	2.75	1.03	4.20	0.99	2.71	1.00	1.56	1.03	3.19	0.98
1290	8.23	1.01	3.82	0.94	6.65	0.96	3.99	0.94	2.28	1.05	3.79	1.00
1000	7.77	0.96	4.63	0.99	6.43	1.14	5.23	1.08	3.25	1.24	5.92	0.95
773	10.0	1.02	4.69	1.02	3.17	1.05	5.83	1.01	2.88	1.21	4.40	0.94
598	14.8	1.01	4.87	1.04	16.4	0.96	9.11	0.97	3.86	1.20	6.20	1.01
465	12.0	1.01	4.87	1.03	6.03	1.01	5.02	0.96	2.69	1.33	7.32	0.98
360	14.6	1.01	6.59	1.10	11.7	1.00	15.9	1.03	4.51	1.32	11.29	1.13
278	21.5	0.91	11.5	0.99	17.5	1.01	20.5	1.03	6.51	1.12	6.06	0.99
215	20.4	1.03	9.82	1.05	17.3	0.95	10.1	1.02	15.5	1.66	11.72	1.67
166	23.7	1.00	10.5	1.02	17.9	1.01	18.3	0.96	2.46	0.74	21.83	1.03
129	29.2	1.06	15.8	0.78	20.3	0.93	22.7	0.88	44.4	0.65	41.70	0.78
100	23.7	0.65	12.7	1.04	42.6	1.09	24.8	1.15	4.89	1.05	23.87	1.18
77.3	24.9	1.02	9.28	1.03	64.0	0.97	32.0	0.80	44.3	0.24	100.1	0.61
59.8	57.2	1.16	25.8	1.00	61.4	1.02	54.3	1.02	0.13	0.94	0.26	0.99
46.5	30.3	1.01	15.6	1.08	10.8	1.31	56.8	1.36	163.0	1.58	197.4	0.73
36.0	57.4	1.03	36.1	0.93	3.73	1.04	3.51	0.73	1.76	0.90	0.44	0.88
27.8	40.0	0.85	19.4	0.94	51.1	0.75	40.2	0.84	2.19	0.65	0.42	0.71
16.6	70.5	1.11	44.8	0.73	35.8	1.45	34.2	1.48	237.0	1.51	76.31	0.19
12.9	34.5	0.92	17.3	1.05	103.0	1.01	73.9	1.00	0.35	0.99	0.24	1.00
10.0	46.1	0.99	70.3	1.10	174.0	0.99	91.6	1.04	0.55	1.14	0.27	0.98
7.73	98.7	1.08	34.9	1.04	75.1	0.69	64.3	0.68	1.16	0.69	0.43	0.97
5.98	31.4	1.05	54.5	0.52	18.6	1.98	12.0	2.41	505.0	1.24	0.76	0.92
4.65	11.7	0.69	20.9	1.13	7.85	1.00	0.81	0.98	2.95	1.03	1.43	1.03

Table 4.6 Characteristics of benchmark critical assemblies

Assembly Name	Concentration ratio					Core Volume (ℓ)	Remarks
	Inner Core				Blanket		
	^{238}R	^{239}R	^{235}R	^{240}R	^{235}R		
ZEBRA-3	0.11	9.2	140.0	176.6	137.6	60	Hard spectrum (80% above 100 keV)
SNEAK-7B	0.12	8.1	55.0	91.3	250.0	310	
NZB	0.15	6.6	138.0	32.4	139.0	1800	
ZPR-6-7	0.15	6.6	460.0	58.0	500.0	3100	L/D = 0.9
FCA-5-2	0.18	5.6	4.0	62.5	138.0	200	Pu/EU = 1/3
ZPR-3-48	0.22	4.5	463.0	74.0	500.0	410	Soft spectrum due to added C
ZPR-3-49	0.22	4.5	463.0	74.0	500.0	450	Remove Na for ZPR-3-48
ZPR-3-50	0.22	4.5	463.0	74.0	500.0	340	additional C for ZPR-3-48
ZPR-3-56B	0.22	4.6	443.0	34.4	——	610	Ni reflector
ZPPR-2	0.15	6.5	451.0	50.0	463.0	2400	Equal volume 2 zone core L/D = 0.5
MZA	0.25	3.9	137.0	16.6	138.6	570	
SNEAK-7A	0.33	3.0	135.0	34.0	250.0	110	
ZPR-3-53	0.64	1.6	433.0	26.0	500.0	220	U reflector
ZPR-3-54	0.64	1.6	433.0	26.0	——	190	Iron reflector

Tabl 4.7 Deviations of the multiplication factors calculated with the mutual shielding effect from those without it in 14 fast critical assemblies

Assembly	%Δk	Assembly	%Δk
ZEBRA-3	0.03	ZPR-3-50	0.16
SNEAK-7B	0.05	ZPR-3-56B	0.12
MZB	0.10	ZPPR-2	0.10
ZPR-6-7	0.12	MZA	0.08
FCA-5-2	0.02	SNEAK-7A	0.07
ZPR-3-48	0.10	ZPR-3-53	0.07
ZPR-3-49	0.08	ZPR-3-54	0.07

Table 4.8 Doppler reactivities calculated with and without the mutual shielding effect in the SEFOR assembly

	Doppler effect		$\Delta k_M - \Delta k_N$
	Δk_M	Δk_N	
Fission	2.23×10^{-3}	2.04×10^{-3}	0.19×10^{-3}
Capture	-7.37×10^{-3}	-7.24×10^{-3}	-0.13×10^{-3}
Total	-5.14×10^{-3}	-5.20×10^{-3}	0.06×10^{-3}

Δk_M : With mutual shielding effect

Δk_N : Without mutual shielding effect

Table 4.9 Main Characteristics of Fast Reactor Critical Assemblies

Assembly	Fuel	R = Fertile/Fissile		Core volume (ℓ)
		Inner core	Outer core	
FCA-VI-1	Pu U	4.3	3.0	473
SEFOR	Pu	4,3		558
ZPPR-2	Pu	6.5	4.0	2400
ZPR-6-7	Pu	6.5	6.5	2920
LMFBR*	Pu	8.7	6.6	9950

* Large sodium-cooled fast breeder reactor for an international comparison calculation

Table 4.10 Effective Multiplication Factors Calculated with the Code 2-Dimensional R-Z Diffusion

Assembly \ Set	TIMS-1	ETOX	TIMS/ETOX
FCA-VI-1	0.99797	0.99819	0.9998
ZPPR-2	0.99135	0.99275	0.9986
ZPR-6-7 (H 240*)	0.99022	0.99134	0.9989
LMFBR** (Na-in)	1.02372	1.02494	0.9988
SEFOR	1.02327	1.02332	0.9999

* high enriched Pu core

** NEACRP international benchmark core

Table 4.11 Central Na-void Reactivity by 70-Group 1-Dimensional 1st Order Perturbation Calculation in ZPPR-2 Assembly

Component \ Set	TIMS-1	ETOX	Difference between TIMS-1 and ETOX
Δk by $\nu\Sigma_f$	-3.632 - 5	-3.281 - 5	-3.51 - 6
Δk by $\Sigma_{i\to j}$	3.556 - 3	3.340 - 3	2.16 - 4
Δk by Σ_a	1.134 - 3	1.112 - 3	2.20 - 5
Δk by Σ_{in}	3.340 - 3	3.326 - 3	1.40 - 5
Δk by D	-4.884 - 4	-4.826 - 4	-5.80 - 6
Total reactivity ($\Delta k/k$)	7.505 - 3	7.262 - 3	2.43 - 4

Table 4.12 Comparison of Doppler Reactivity Effects Calculated with One-dimensional First Order Perturbation Code using Two Different Cross Section Sets in ZPPR-2

T (°K)	Exp. ($\times 10^{-6}\Delta k/k$)	Calculation ($\times 10^{-6}\Delta k/k$)	
		TIMS-1	ETOX
300 - 500	-2.41	-2.656 (1.10)	-2.690 (1.12)
300 - 800	-4.93	-5.497 (1.12)	-5.547 (1.13)
300 - 1100	-6.76	-7.540 (1.12)	-7.589 (1.14)

The C/E-values are shown in the parentheses

Table 4.13 Comaprison between Reactivity Components Calculated with Two-Dimensional First Order Perturbation Code in SEFOR Assembly

	Exp. ($\times 10^{-3}\Delta k/k$)	Calculation ($\times 10^{-3}\Delta k/k$)		
		TIMS-1	ETOX	ETOX/TIMS-1
$\nu\Sigma_f$		3.817	3.388	0.89
Σ_c		-10.19	-9.983	0.98
Total		- 6.326	-6.537	1.03
T $\frac{\Delta k}{k}$	-8.10	- 9.610 (1.19)	-9.981 (1.23)	1.04

The C/E-values are shown in the parentheses

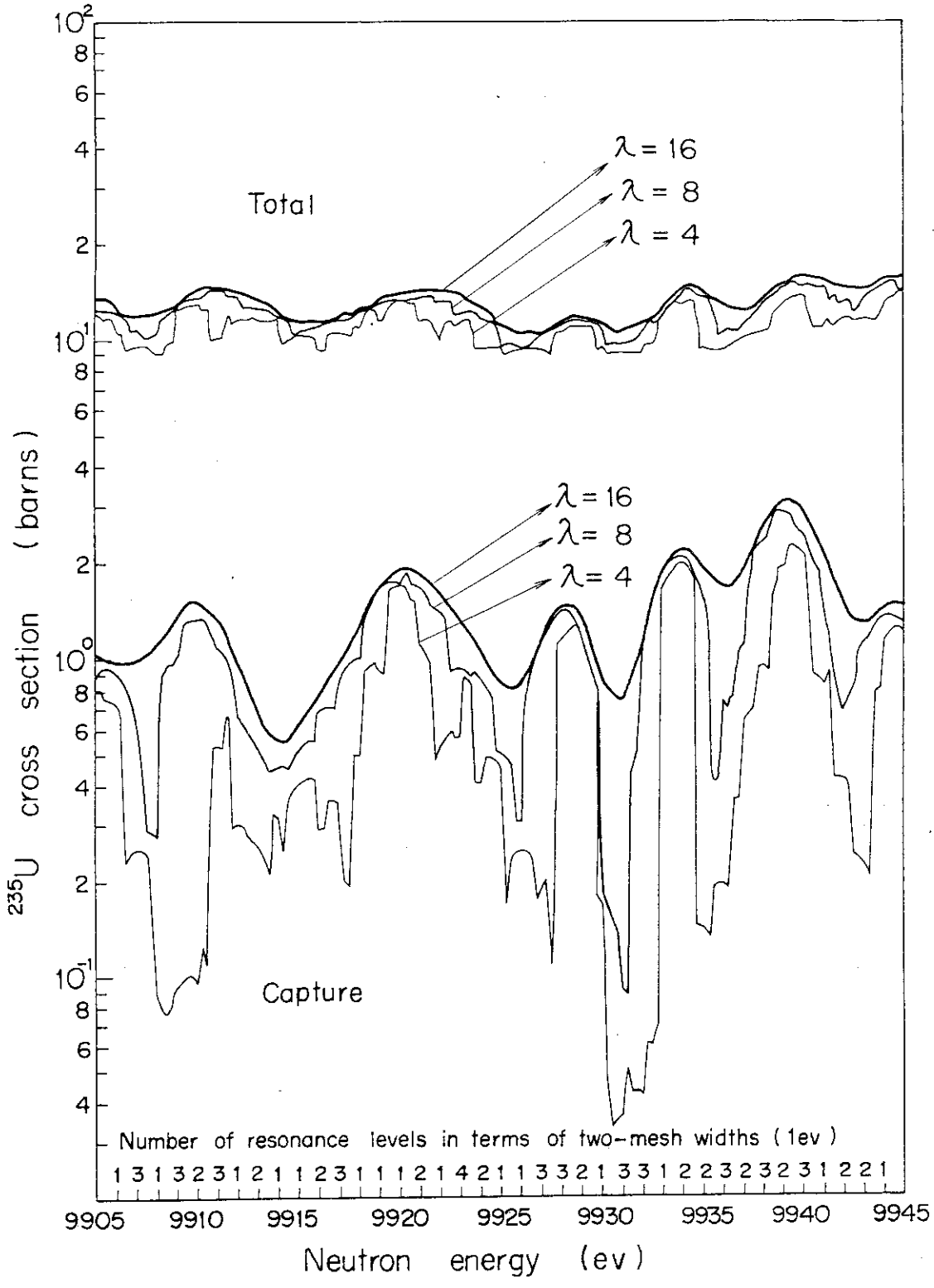

Fig. 4.1 Variation in ^{235}U cross section curves for several value of λ (Mesh width : 0.5 eV)

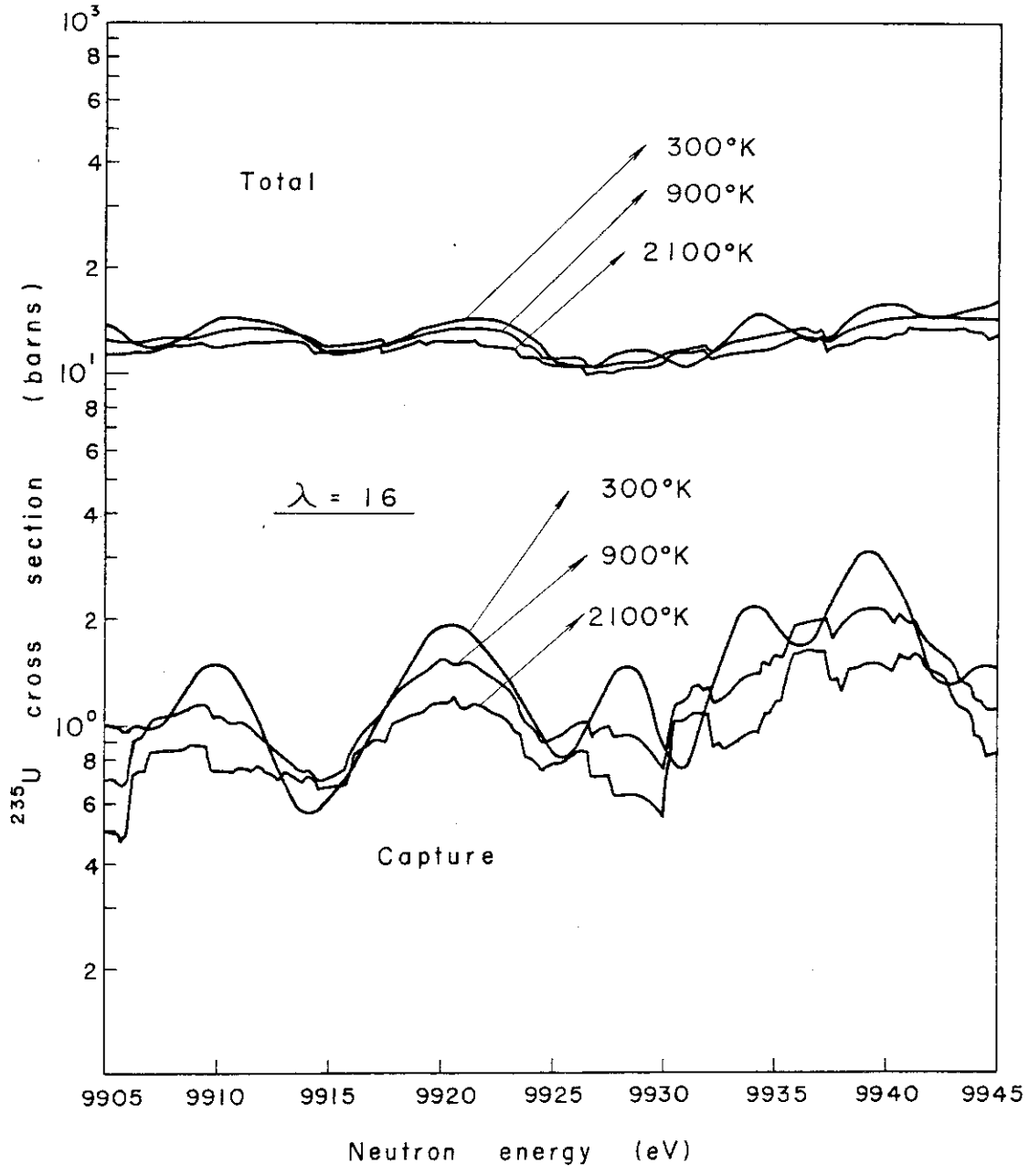

Fig. 4.2 Temperature dependence of ^{235}U cross section curves for λ = 16 (Mesh width : 0.5 eV)

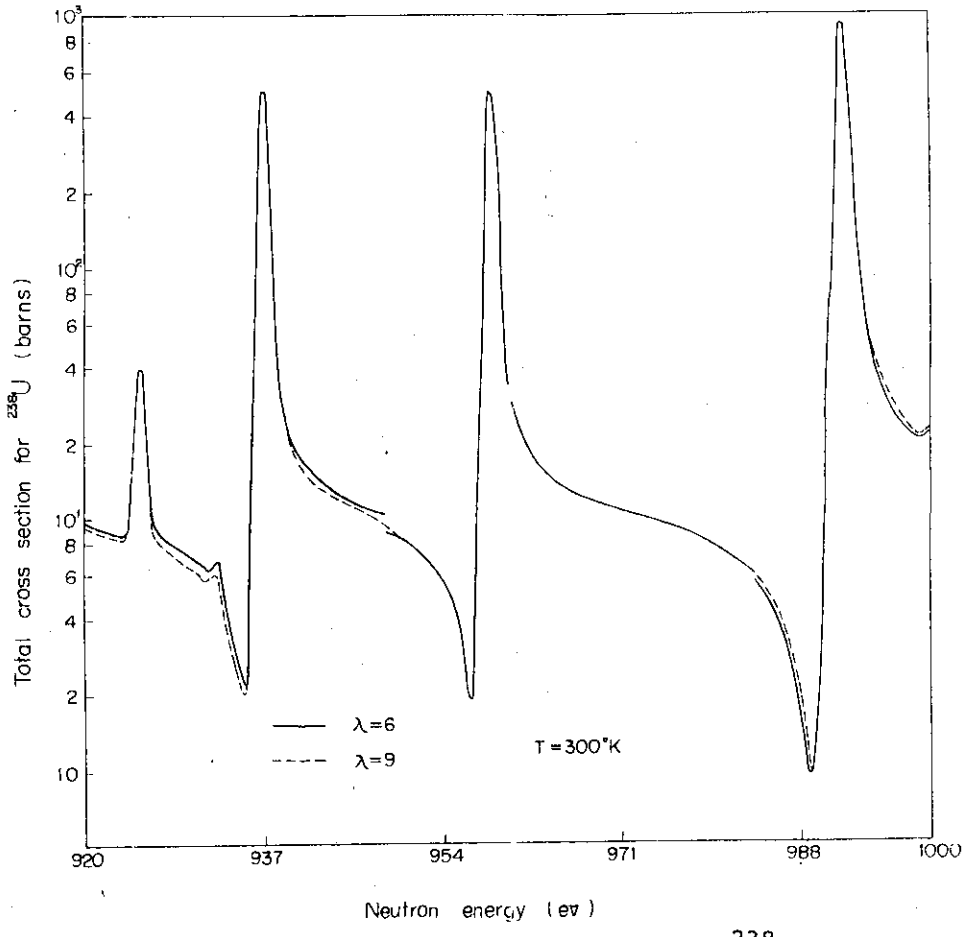

Fig. 4.3 Interference scattering effect of ^{238}U resonance

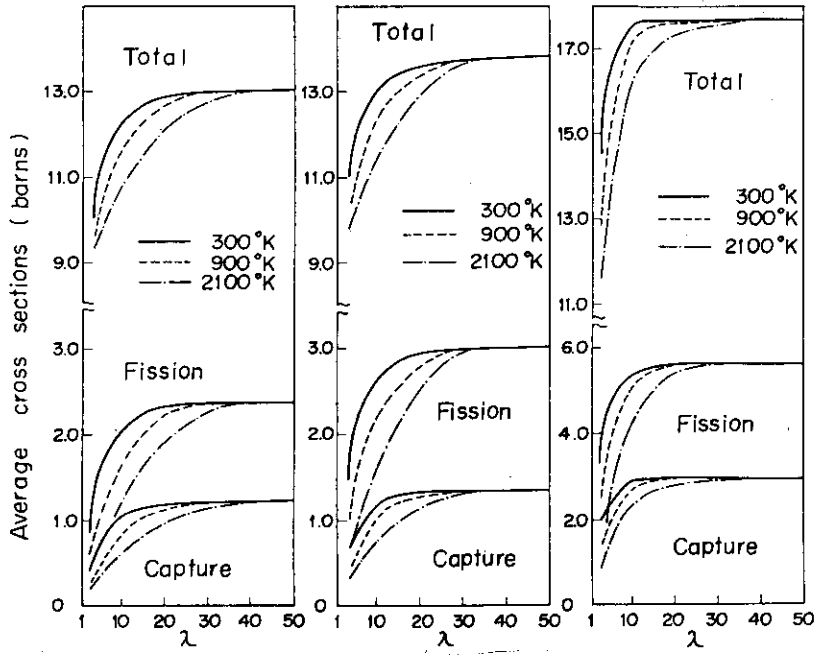

(a) 10.0 ∿ 9.9 keV (b) 5.98 ∿ 5.88 keV (c) 1.0 ∿ 0.97 keV

(Mesh width : 0.5 eV) (Mesh width : 0.25 eV) (Mesh width : 0.05 eV)

Fig.4.4 Variation in ^{235}U average cross sections

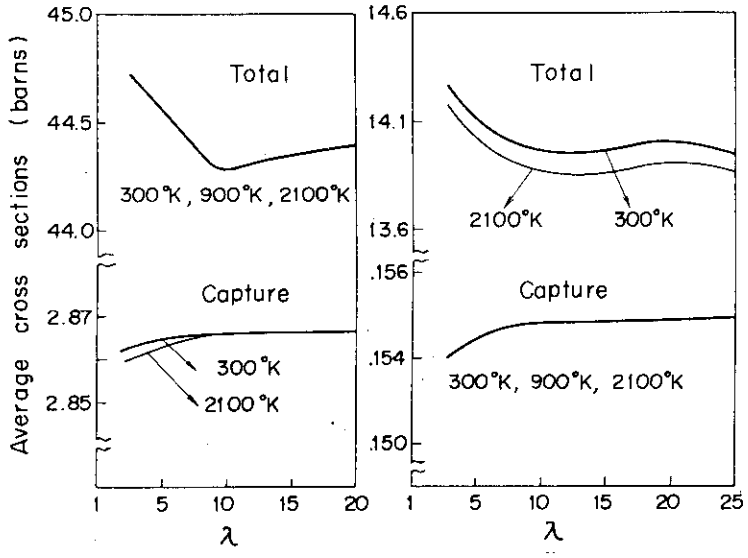

(a) 1.0 ∿ 0.92 keV (Mesh width : 0.05 eV)　　(b) 21.3 ∿ 21.0 keV (Mesh width : 0.5 eV)

Fig.4.5 Variation in ^{238}U average cross sections

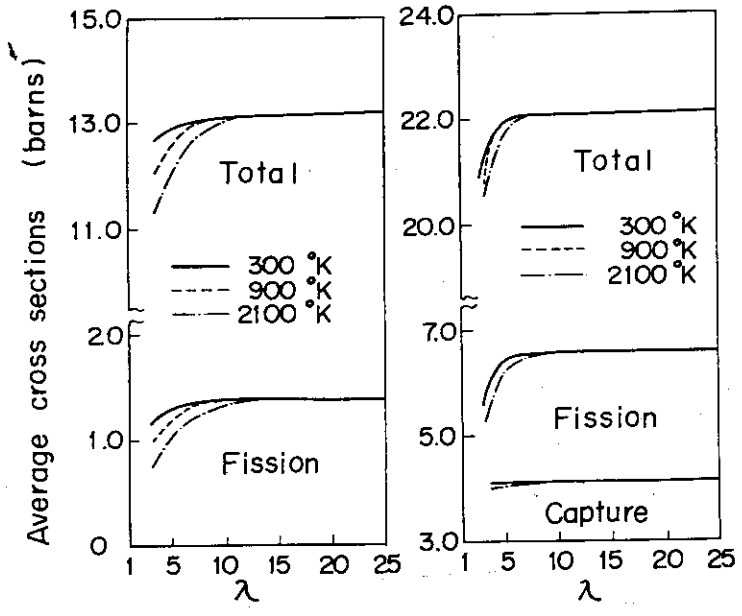

(a) 10.0 ∿ 9.9 keV (Mesh Width : 0.5 eV)　　(b) 1.0 ∿ 0.9 keV (Mesh width : 0.05 eV)

Fig.4.6 Variation in ^{239}Pu average cross sections

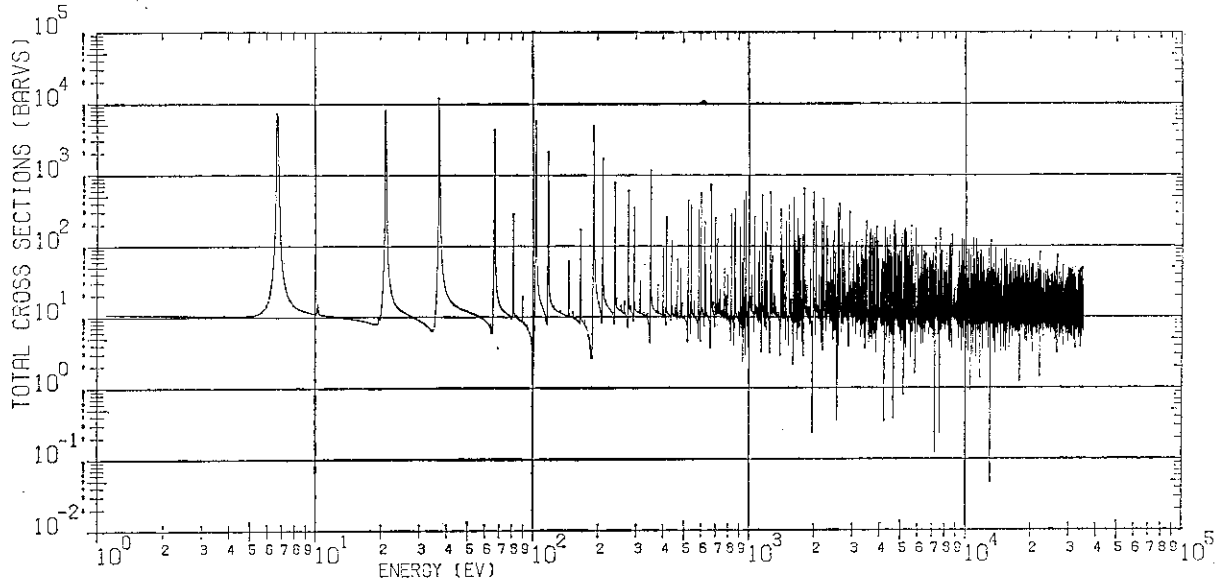

Fig. 4.7 Doppler Broadened cross section of ^{238}U in the energy range from 1.0 eV to 35 KeV.

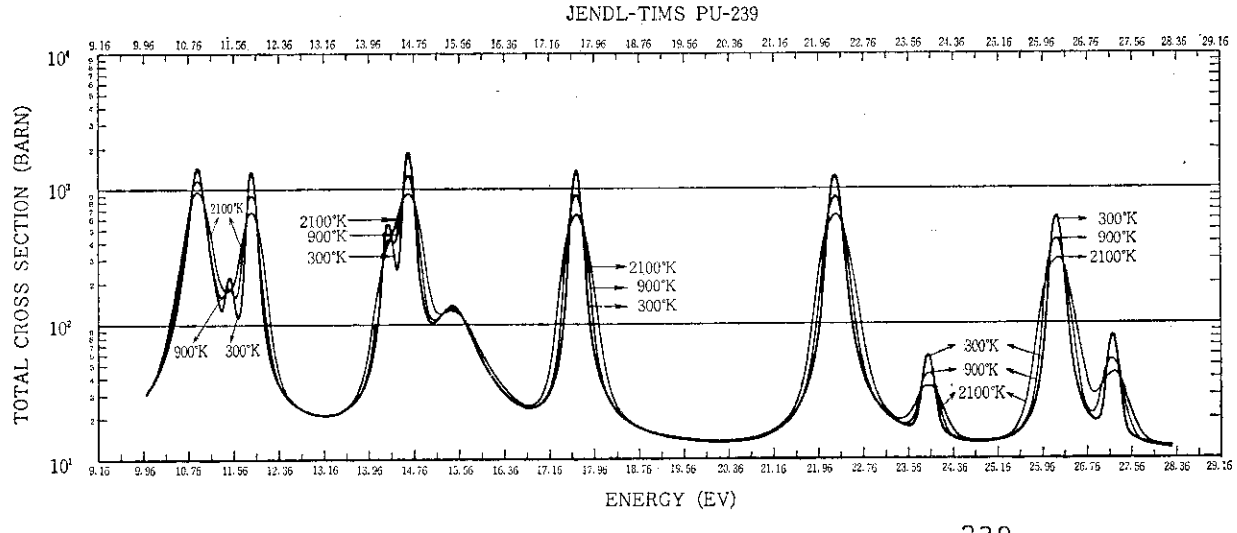

Fig. 4.8 Temperature dependent cross sections of ^{239}Pu in the energy range from 9.96 to 27.8 eV drawed with XSPLOT.

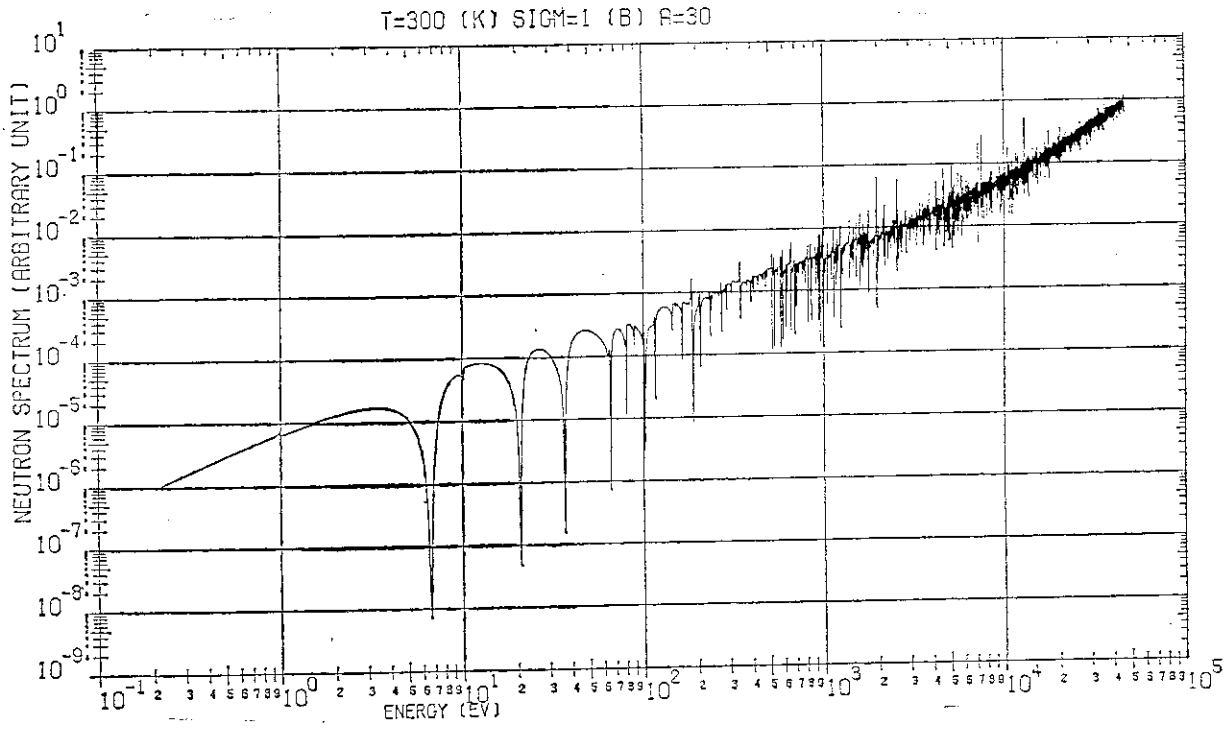

Fig.4.9 Neutron spectrum calculated for T = 300°K, σ_0 = 1.0 and average moderator mass A = 30 using TIMS-1.

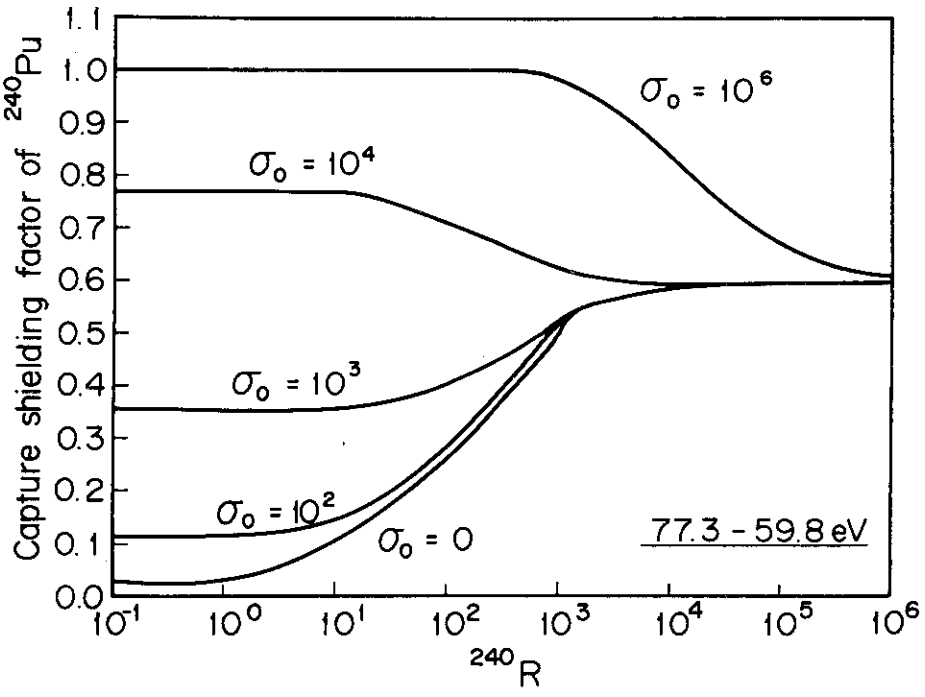

Fig. 4.10 Dependence of resonance capture shielding factors for ^{240}Pu on ^{240}R values in the energy range from 59.8 to 77.3 eV.

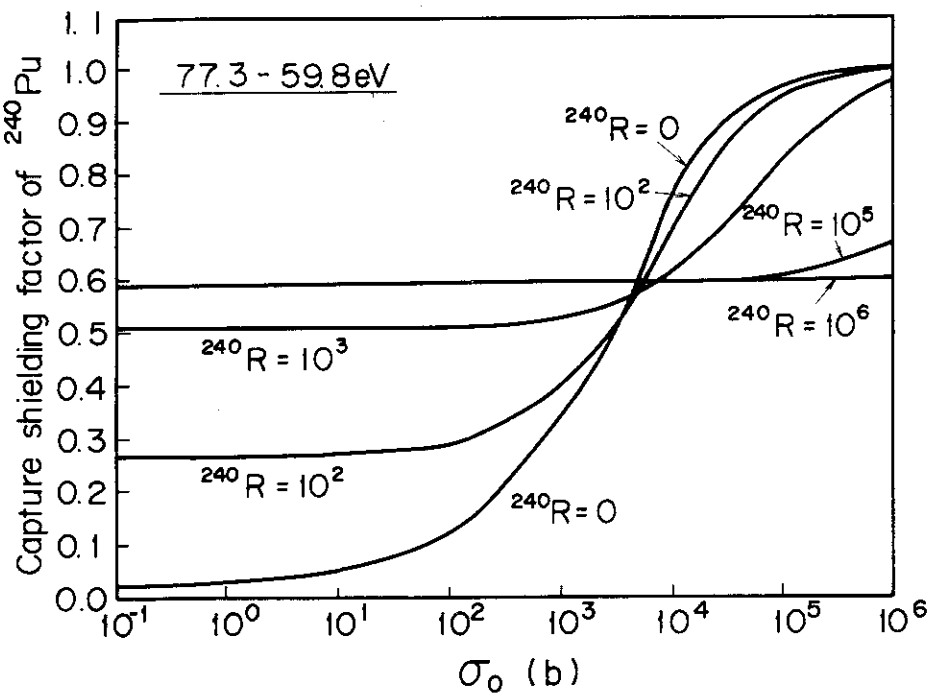

Fig. 4.11 Dependence of resonance capture sheilding factors for ^{240}Pu on $^{\sigma}0$ values in the energy range from 59.8 to 77.3 eV.

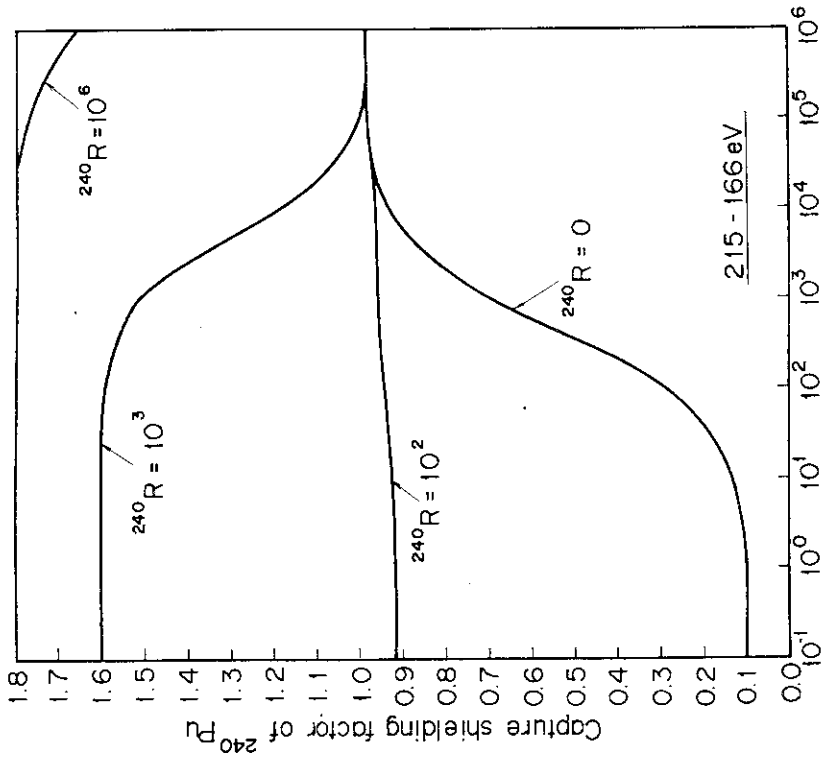

Fig. 4.13 Dependence of resonance capture shielding factors for ^{240}Pu on σ_0 values in the energy range from 166 to 215 eV.

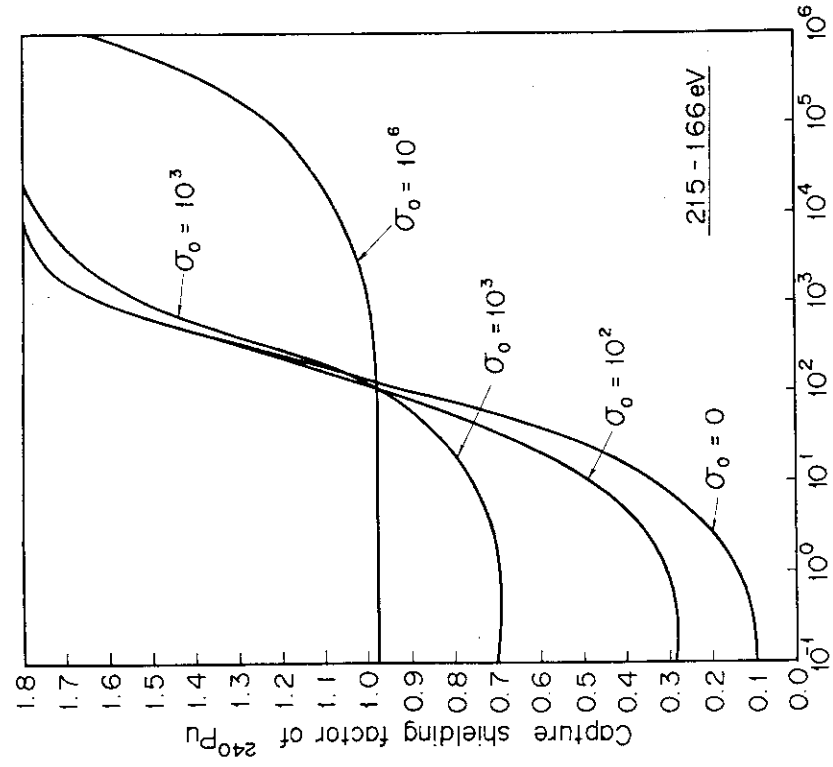

Fig. 4.12 Dependence of resonance capture shielding factors for ^{240}Pu on ^{240}R values in the energy range from 166 to 215 eV.

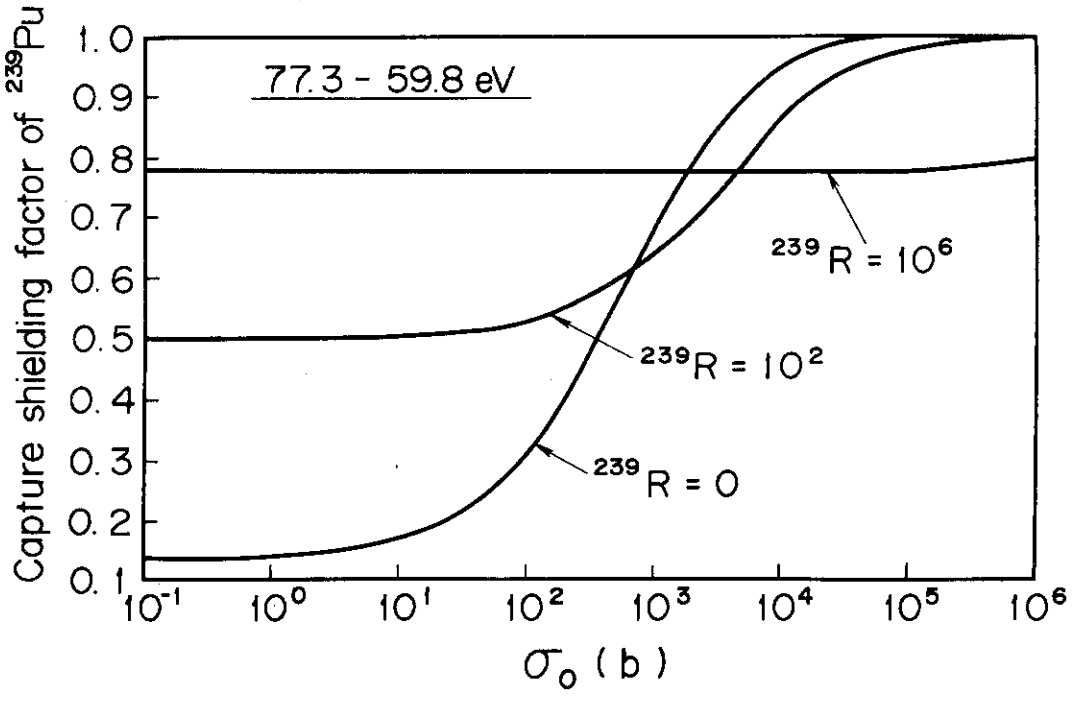

Fig. 4.14 Resonance shielding factor of ^{239}Pu calculated with the resonance overlap effect between ^{239}Pu and ^{238}U in the energy range fron 59.8 to 77.3 eV.

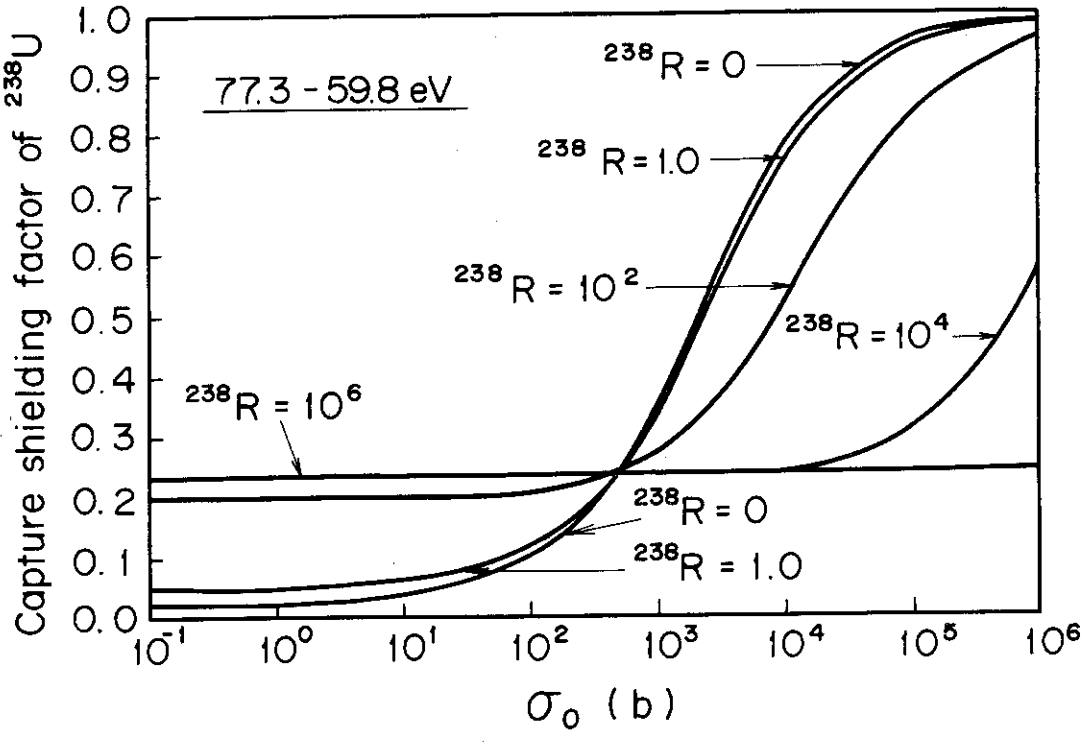

Fig.4.15 Resonance shielding factor of ^{238}U calculated with the resonance overlap effect between ^{239}Pu and ^{238}U in the energy range from 59.8 to 77.3 eV.

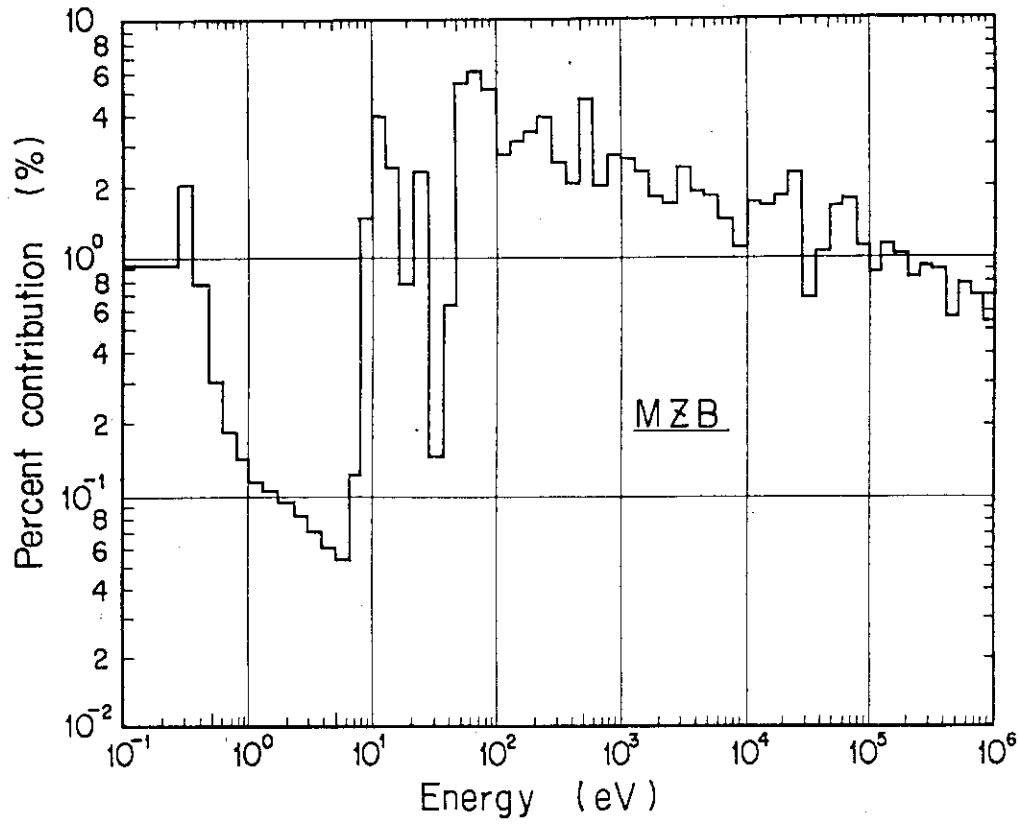

Fig. 4.16 Groupwise contribution of ^{239}Pu fission reaction rate in the blanket region of MZB.

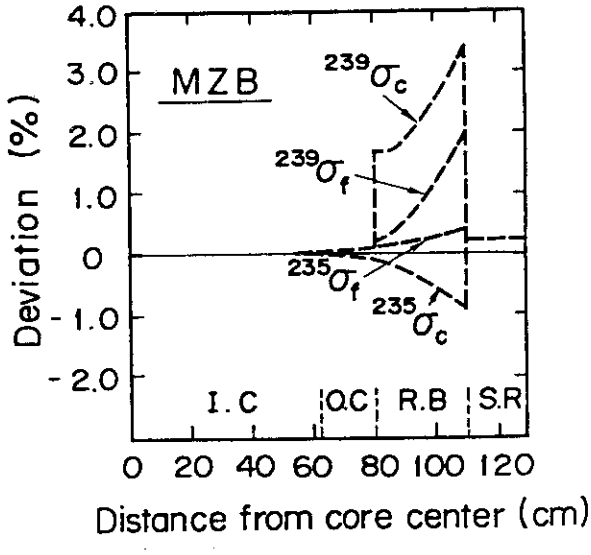

Fig. 4.17 Deviations of the radial reaction rates calculated with considering the mutual shielding effect from those without it.

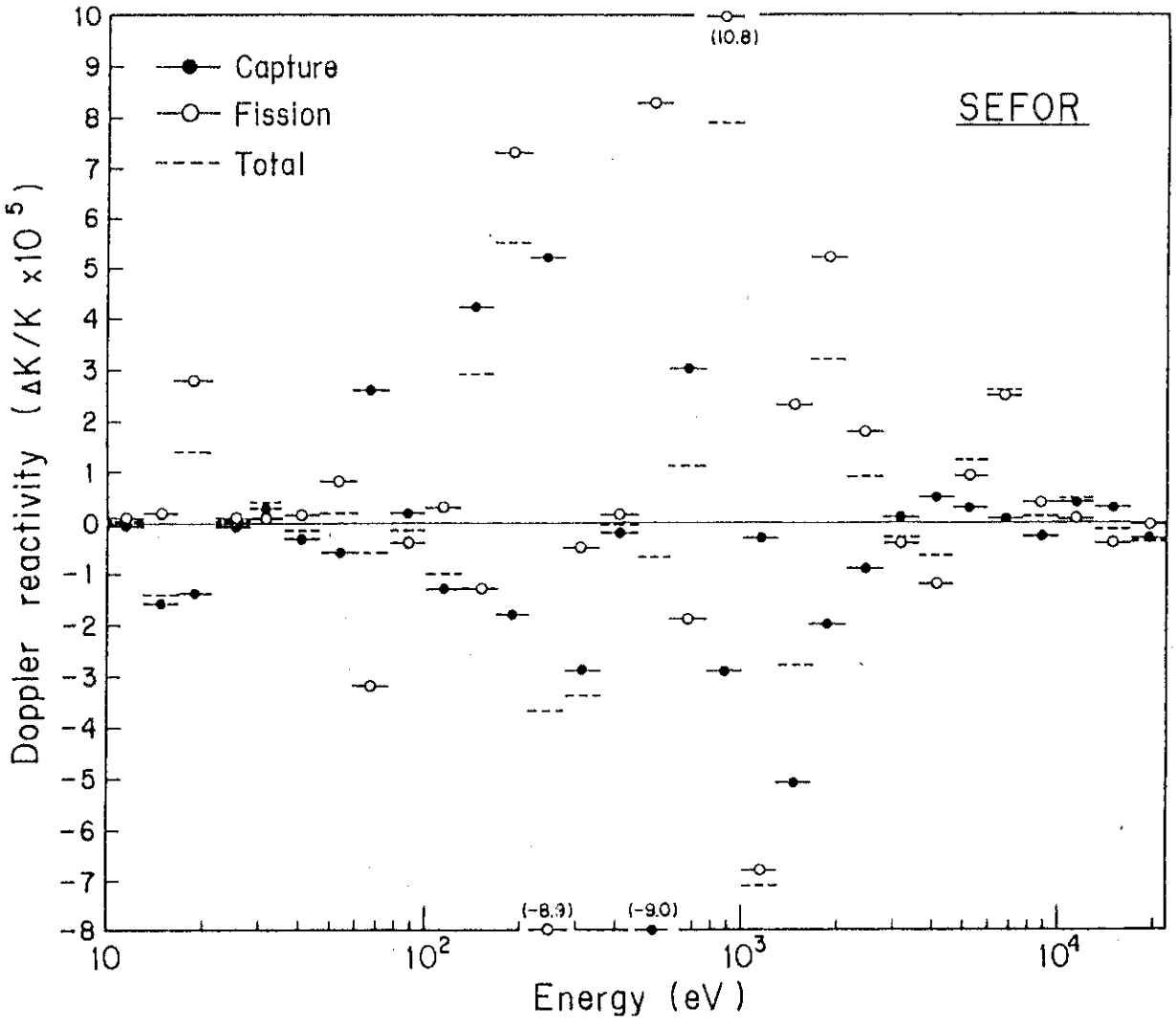

Fig. 4.18 Groupwise contribution of Doppler reactivity which is the diffirence of the reactities calculated with the mutual shielding effect from those without it.

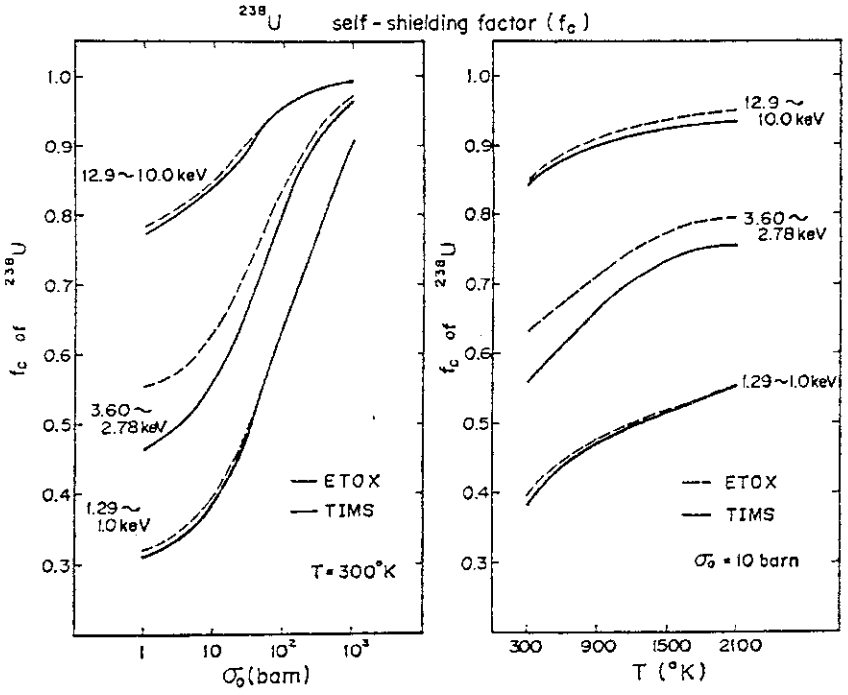

Fig.4.19 Comparison of capture self-shielding factors of ^{238}U calculated with the TIMS-1 and ETOX codes

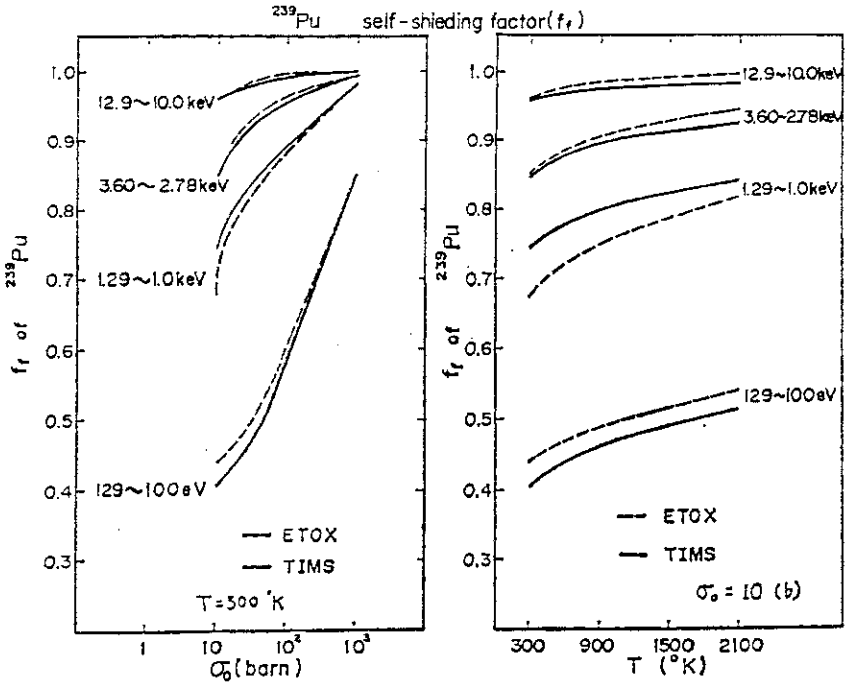

Fig.4.20 Comparison of fission self-shielding factors of ^{239}Pu calculated with the TIMS-1 and ETOX codes

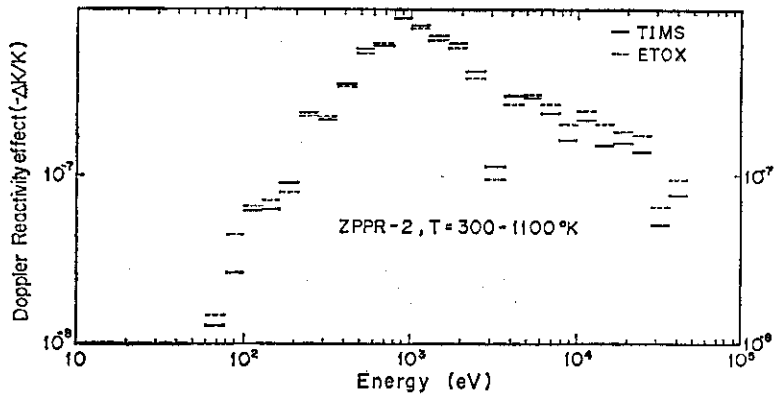

Fig.4.21 Energy group-wise contribution of Doppler reactivity effect calculated by one-dimensional first order perturbation code in ZPPR assembly 2.

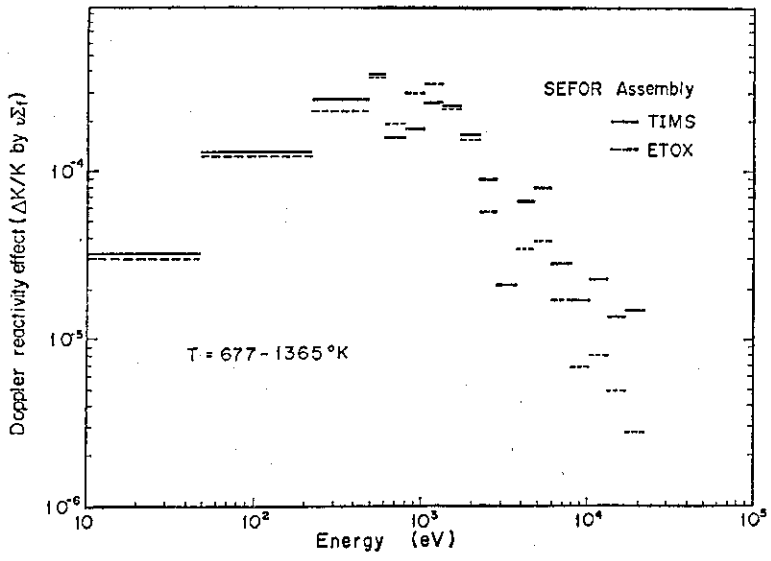

Fig.4.22 Energy group-wise contribution of fiission Doppler reactivity effect calculated by two-dimensional first order perturbation code in SEFOR assembly

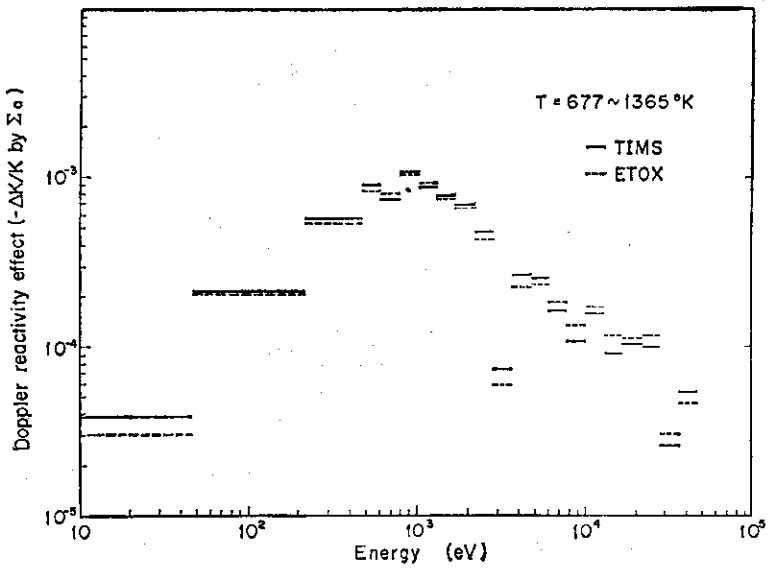

Fig.4.23 Energy group-wise contribution of capture Doppler reactivity effect calculated by two-dimensional first order perturbation code in SEFOR assembly

5. Production of JAERI-Fast Group Constants Set, Version II

5.1 Introduction

The benchmark tests of the JAERI-Fast set (JFS-1)[9],[10] were performed[26] using the calculational models prescribed by Davey and Hess[16]. The results of this benchmark tests have proposed various informations required for the corrections to be made in the group constants of JFS-1. The discrepancies between the calculated and the experimental values were not so small even for the effective multiplication factors (k_{eff}) and spectral indices, which were very important integral quantities. Especially, there existed clearly a systematic tendency of k_{eff} dependence on ^{238}U concentration, that is, the calculated k_{eff} decreased with increasing ^{238}U concentration ratio of ^{238}N to ^{235}N or ^{239}N, where N is the atomic number density. Based on the primary assessment of JFS-1, the cross sections of ^{238}U, ^{235}U, ^{239}Pu and ^{240}Pu were reevaluated. This revised version of JFS-1 was called the JFS-1R. The discrepancies between the calculated and measured values for k_{eff} and spectral indices became smaller for this version. However, the systematic dependence of k_{eff} on the ^{238}U concentration ratio could not be eliminated even if JFS-1R was used, as seen in Figs.5.1 and 5.2. Such systematic tendency was also reported by several researchers[26],[102] who calculated the benchmark models of Davey and Hess using the ENDF/B-II and III data.

In order to eliminate the systematic tendency of k_{eff} depending on the ^{238}U concentration ratio, in the present study, the revision work for JFS-1R is mainly performed by the adjustment of cross section based on the method of the least squares. The capture cross section of ^{238}U and the fission cross sections of ^{235}U and ^{239}Pu are adjusted in the energy range

from 3.6 keV to 1.4 MeV. For the energy range from 1.4 to 10 MeV, these cross sections are reevaluated. The other nuclei except for ^{235}U, ^{238}U, ^{239}Pu, ^{240}Pu, ^{241}Pu and ^{10}B are mainly adopted from the ENDF/B-IV nuclear data, because they are newer and more accurate evaluation data than those adopted in JFS-1. In Sections 5.2 ~ 5.4, the cross section adjustment and evaluations for the heavy nuclei are mainly described. To examine the applicability of JFS-2 thus developed, furthermore the benchmark test are performed for many fast critical assemblies[103]. Various integral quantities, such as effective multiplication factors, spectral indices, sample worths and Doppler reactivity effects are calculated and compared with the experimental results. These results are given in Section 5.5.

5.2 Adjustment for Cross Sections of ^{235}U, ^{238}U and ^{239}Pu by the Method of Least Squares

Although there are many measurements of the important cross sections for the design of fast reactors, the measured values do not generally agree with each other and are generally scattered over a fairly wide range. The uncertainties in these cross sections are supposed to be 5 ~ 30%[104],[105] for the important energy region for large fast reactors. These large uncertainties can not be permitted even for the prediction of the critical mass. In order to remove the uncertainty in the cross sections, it will be requested that the differential cross sections are measured with sufficiently high accuracy. However, it can not reasonably be expected that this request is satisfied in the near future.

To overcome this circumstance, the method of adjustment of group cross sections is often used. This is the method of least squares in which the cross sections under consideration are adjusted so as to fit the integral

data obtained from neutronic calculations to the corresponding measured values. The resulting group cross sections can therefore be considered as fitting parameters. This method of least squares provides a very useful feedback information from the integral data to evaluate the differential cross sections, as long as there exist larger uncertainties in the integral data due to nuclear data uncertainties, compared with the accuracy required from design study for large fast reactors[105]. This approach has extensively been studied by many researchers[20],[106]~[115]. The practical application of the adjustment method has firstly been made by Rowland *et al.*[109] and the adjusted cross section sets, FGL-series[12], were produced. On the other hand, the theoritical studies have extensively been made by Mitani and Kuroi[114]. Furthermore, they practically applied their theory to produce the adjusted cross section set AGLI[113]. In the present study, the cross section adjustment is performed by introducing newly auxiliary equation and sensitivity coefficients.

In this section, the systematic dependence of k_{eff} on the ^{238}U concentration ratio is eliminated by using the method of least squares. For this purpose, the three important reaction cross sections, $^{235}\sigma_f$, $^{238}\sigma_c$ and $^{239}\sigma_f$ are adjusted by this method for the energy range of 3.6 keV to 1.4 MeV. These cross sections and the energy range were selected from the following reasons: The sensitivity of these cross sections to k_{eff} is very large in this energy range. Many measurements for these cross sections have been performed so that the uncertainties (standard deviations) of these measured cross sections can be estimated accurately by using these experimental data.

Method of Least Squares

In fast reactors, the calculations of the integral quantities are made generally with use of multigroup energy model and hence these quanti-

ties can be considered as a complicated function of the group cross sections. Then, a set of observation equations for the method of least squares can be written for each of critical assemblies as follows:

$$k_\ell + \varepsilon_\ell = f_\ell(\sigma_{jm}) \quad , \tag{5-1}$$

where σ_{jm} is the true value of group cross section for reaction (j) and energy group (m), k_ℓ the measured multiplication factor and ε_ℓ the experimental error for critical assembly (ℓ). When σ^r_{jm} is the reference cross section to be adjusted, Eq.(5-1) can be rewritten by means of Taylor's expansion in the following form:

$$\sum_{j,m} S_{\ell jm}(\sigma_{jm} - \sigma^r_{jm}) / \sigma^r_{jm} = k_\ell - k^r_\ell + \varepsilon_\ell \quad , \tag{5-2}$$

where k^r_ℓ and $S_{\ell jm}$ stand for respectively the calculated k_{eff} and the sensitivity coefficient defined by $(\partial f_\ell / \partial \sigma^r_{jm})\sigma^r_{jm}$.

The number of group cross sections to be adjusted is generally much larger than that of the considered integral data. In order to obtain a unique solution by the method of least squares, various auxiliary equations[106)~(114)] are introduced. The auxiliary equations considered here are as follows:

$$\sigma_{jm} = \sigma^r_{jm} - \varepsilon_{jm} \quad , \tag{5-3}$$

$$\gamma_{ijm} = \gamma^r_{ijm} - \varepsilon_{ijm} \quad , \tag{5-4}$$

where ε_{jm} is the true error of group cross section, and γ_{ijm}, γ^r_{ijm} and ε_{ijm} are the true, reference and error values for the relative ratio of group cross sections for reactions i and j, respectively. When the experimental errors ε_ℓ, ε_{jm} and ε_{ijm} can be assumed to be normally distributed about zero with the standard deviations Δk_ℓ, $\Delta\sigma_{jm}$ and $\Delta\gamma_{ijm}$, the method of least squares leads to minimize the following quadratic form:

$$Q = \sum_{\ell} W_{\ell}\{u_{\ell} - \sum_{j,m} \bar{S}_{\ell jm}(\sigma_{jm} - \sigma^{r}_{jm})\}^{2} + \sum_{j,m} W_{jm}(\sigma_{jm} - \sigma^{r}_{jm})^{2}$$

$$+ \sum_{i,j,m} W_{ijm}(\gamma_{ijm} - \gamma^{r}_{ijm})^{2} \quad , \tag{5-5}$$

$$u_{\ell} = k_{\ell} - k^{r}_{\ell} + \varepsilon_{\ell} \quad , \qquad \bar{S}_{\ell jm} = S_{\ell jm} / \sigma^{r}_{jm} \quad ,$$

where W_{ℓ}, W_{jm} and W_{ijm} are the statistical weights which are the reciprocal of variance of u_{ℓ}, σ_{jm} and γ_{ijm}, respectively. Then, the estimator σ_{jm} of group cross section can be obtained by minimizing the quadratic form of Eq.(5-5), i.e.,

$$\sigma_{jm} = \sigma^{r}_{jm} + x_{jm} / W_{jm} \quad , \tag{5-6}$$

where x_{jm} is found by solving the following simultaneous equations which are derived by setting the derivatives of Q equal to zero,

$$(1 + \sum_{i} C_{ijm}(1-Z_{im}))x_{jm} + \sum_{\ell} W_{\ell}\bar{S}_{\ell jm} \sum_{j'm'} \bar{S}_{\ell j'm'} x_{j'm'} W^{-1}_{j'm'}$$

$$= \sum_{\ell} W_{\ell}\bar{S}_{\ell jm}u_{\ell} + W_{jm}\varepsilon_{jm} + \sum_{i} C_{ijm}W_{jm}\sigma^{r}_{jm}Z_{im} + \sum_{i} C_{ijm}W_{jm}\sigma^{r}_{jm}\varepsilon_{ijm}, \tag{5-7}$$

where

$$Z_{im} = (\sigma_{im} - \sigma^{r}_{im}) / \sigma_{im} \quad ,$$

$$C_{ijm} = W_{ijm}W_{jm}(1 - Z_{im})(\sigma^{r}_{im})^{-2} \quad . \tag{5-8}$$

For Eq.(5-7), the set of 72 simultaneous equations for 3 nuclides and 24 group cross sections as shown in Table 3 is solved. Firstly the solution $x^{(1)}_{jm}$ by assuming $Z_{im} = 0$ are obtained. Secondly, $x^{(2)}_{jm}$ is obtained by using $x^{(1)}_{jm}$. This process is repeated until $|Q^{n} - Q^{n+1}| \leq \varepsilon$ and $|k_{\ell} - k^{r}_{\ell}| \leq \varepsilon_{\ell}$ are achieved.

Sensitivity Coefficient

The sensitivities for the capture cross section of ^{238}U and the fission cross sections of ^{235}U and ^{239}Pu are calculated by the 10% change for these cross sections in the energy range from 1.0 keV to 10.0 MeV. The groupwise sensitivity coefficients for fission and capture cross sections are defined by using the formula of perturbation cross section[102] as follows:

$$S_{\ell jmf} = \frac{\frac{1}{k^r_\ell}\nu_{jm}\sigma^r_{jmf}\phi_m \sum_i \chi_i\phi^*_i - \sigma^r_{jmf}\phi_m\phi^*_m}{\frac{1}{k^r_\ell}\sum_m \nu_{jm}\sigma^r_{jmf}\phi_m \sum_i \chi_i\phi^*_i - \sum_m \sigma^r_{jmf}\phi_m\phi^*_m} \cdot \frac{\delta k^r_{\ell jf}}{10}, \quad \text{for fission,} \tag{5-9}$$

and

$$S_{\ell jmc} = \frac{-\sigma^r_{jmc}\phi_m\phi^*_m}{\sum_m \sigma^r_{jmc}\phi_m\phi^*_m} \cdot \frac{\delta k^r_{\ell jc}}{10}, \quad \text{for capture,} \tag{5-10}$$

where δk^r_ℓ is the deviation of k^r_ℓ due to the 10% cross section change and the other notations are conventional.

It has been assumed that the integral quantity depends linearly on the sensitivity coefficients and the variation of cross sections adjusted. The accuracy of the assumption was tested for the adjusted cross sections. These adjusted cross sections were generated by changing $^{235}\sigma_f$, $^{238}\sigma_c$ and $^{239}\sigma_f$ by 1 ~ 20% in the energy range from 3.6 keV to 1.4 MeV. *Table* 5.1 shows the comparison of k_{eff} calculated by using the sensitivity coefficients with that obtained directly with the diffusion code EXPANDA-70D for eight critical assemblies of which main characteristics are shown in *Table* 5.2. The calculated results show a good linearlity on the sensitivity coefficients.

Standard Deviation of Measured Data

The group cross sections adjusted by the method of least squares depend strongly on the standard deviations assumed for the integral data and the original group cross sections. Therefore, these standard deviations should carefully be determined.

In the present study, only the effective multiplication factor is adopted as the integral data because of its better measurement accuracy than for reaction rate ratio or material worth. The main aim of the study is to eliminate the systematic dependence of k_{eff} on the ^{238}U concentration ratio by using the adjustment method of least squares. The experimental errors of k_{eff} indicated by Davey and Hess[102] are 0.3 ~ 0.4% for the eight assemblies considered. However, as the adjustment is made here only for the cross sections of $^{238}\sigma_c$, $^{235}\sigma_f$ and $^{239}\sigma_f$ in the energy range from 3.6 keV to 1.4 MeV, the contribution of uncertainties in the unadjusted cross sections to the criticality must be considered. Furthermore, the present analysis is based on the diffusion theory with homogenized cross sections under the assumption that the transport correction factor and heterogeneity effect are independent on multigroup cross section sets. By considering this background, the standard deviation of 1.5% for k_{eff} was assumed for all cores.

In Eq.(5-5), we assume the normal distribution around σ_{jm} with standard deviation $\Delta\sigma_{jm}$. Since the standard deviations for group cross sections have not generally been assigned, even in evaluated nuclear data file, the standard deviations of $^{235}\sigma_f$, $^{238}\sigma_c$ and $^{239}\sigma_f$ have been calculated by a statistical analysis[104] using many experimental data in NUEDADA file[117]. The mean values of cross sections and the standard deviations were calculated for the 25 ABBN group structure in the energy range above 1 keV. The results of the statistical analysis indicated

that many experimental data is normally distributed in each energy group. *Table* 5.3 shows the standard deviations used for the adjustment of cross sections based on the least squares method.

For the relative ratios of cross sections, the statistical analysis was not performed because of lack of sufficient measured data. The standard deviations for the relative ratios were assumed to be 3% for $^{239}\sigma_f/^{235}\sigma_f$ and 6% for $^{238}\sigma_c/^{235}\sigma_f$, from the experimental errors known for the relative measurements.

Cross Sections Estimated by the Method of Least Squares

The estimations of the group cross sections for $^{235}\sigma_f$, $^{238}\sigma_c$ and $^{239}\sigma_f$ have been performed by solving Eq.(5-7) under the following considerations: The data of Pfletschinger *et al.*[118] for $^{239}\sigma_f/^{235}\sigma_f$ and of Davey's[119] evaluation for $^{238}\sigma_c/^{235}\sigma_f$ were selected for the reference relative values of differential cross sections. The statistical mean values shown in *Table* 5.4 were selected as the reference cross sections of $^{235}\sigma_f$. Then, the reference cross sections for $^{238}\sigma_c$ and $^{239}\sigma_f$ can be calculated from the mean values of $^{235}\sigma_f$ and the relative ratios. The contribution of these cross sections changed from the original data of JFS-1R to k_ℓ^r was calculated by using the sensitivity coefficients. Furthermore, the assembly ZPR-3-6F was removed in the calculation of cross section adjustment, because the adjusted amounts of cross sections exceeded considerably the standard deviations given in *Table* 5.3, that is, the values adjusted were not adopted in comparison with the differential data. This removal of ZPR-3-6F was also supported by χ-square test of Kuroi *et al.*[115]

The unadjusted and adjusted effective multiplication factors are compared in *Fig.*5.3. It is seen from this figure that the k_{eff} dependence

on ^{238}U concentration is considerably reduced for the adjusted k_{eff}. In this figure, the contribution of the adjustments to k_{ℓ}^{r} is indicated for $^{235}\sigma_f$, $^{238}\sigma_c$ and $^{239}\sigma_f$. It is seen that the systematic dependence of k_{eff} on the ^{238}U concentration is removed mainly by the adjustment of $^{238}\sigma_c$.

Figure 5.4 shows the spectral indices calculated by using the adjusted cross section set. The spectral indices of $<\sigma_f^{239}/\sigma_f^{235}>$, $<\sigma_c^{238}/\sigma_f^{235}>$ and $<\sigma_f^{240}/\sigma_f^{235}>$ are in a good agreement with the experiments. The extent of discrepancy in the reaction rate ratios of $^{238}\sigma_f$ depends still on the ^{238}U concentration. The reason for it may be attributed to the use of the unadjusted $^{238}\sigma_f$.

The adjusted cross sections for $^{235}\sigma_f$, $^{238}\sigma_c$ and $^{239}\sigma_f$ are compared with the experimental data or the evaluated data in *Figs.*5.5～5.7, respectively. The adjusted fission cross section of ^{235}U are similar to the data of Leroy[120] below 500 keV, and to those of Smirekin *et al.*[121] in the energy range from 500 to 1400 keV. The adjusted capture cross sections of ^{238}U are in a good agreement with the experimental data of Moxon[122] below 100 keV, and are close of the data of Fricke *et al.*[123] for the energy range of 100 to 800 keV. Those of ^{239}Pu are much more close to the data of Szabo[124] and Szabo *et al.*[125] than Prince's evaluation[126]. *Figures* 5.8 and 5.9 show comparisons of the adjusted relative values $^{239}\sigma_f/^{235}\sigma_f$ and $^{238}\sigma_c/^{235}\sigma_f$ with the experimental data, respectively. The adjusted values of $^{239}\sigma_f/^{235}\sigma_f$ are higher by about 2～4% than the data of Pfletschinger *et al.*[119] above 50 keV. On the other hand, those of $^{238}\sigma_c/^{235}\sigma_f$ become somewhat lower than the data evaluated by Davey and those of Poenitz[127]. The discrepancies between the adjusted values and data of Davey increase with a decrease of energy. However, the experimental data are very scanty in energy range below

100 keV. In this energy region, the low absolute data of $^{238}\sigma_c$ measured by Moxon were recently adopted[128),(129)]. The relative measurement for $^{238}\sigma_c/^{235}\sigma_f$ should positively be performed for this energy range.

Figure 5.10 shows the deviation of the adjusted values of $^{239}\sigma_f/^{235}\sigma_f$ from the experimental values of Pfletschinger *et al.*[118] In this figure, case (B) or (A) is meant whether Eq.(5-5) contains Eq.(5-4) or not. It is seen from this figure that case (B) produces better results than case (A) in comparison of the values adjusted with the differential data. Use of the case (B) can considerably preserve the relative ratios of the cross sections adjusted. It should be noticed that the spectral indices of $<\sigma_f^{239}/\sigma_f^{235}>$ and $<\sigma_c^{238}/\sigma_f^{235}>$ are in a good agreement with the experimental values.

The energy range considered in the present adjustment includes the unresolved resonance region. Therefore, the average resonance parameters should be evaluated so as to be consistent with these adjusted cross sections. This evaluation will be described in Section 5.3.

5.3 Evaluation of Resonance Parameters for ^{235}U, ^{238}U, ^{239}Pu and ^{241}Pu

5.3.1 Unresolved Resonance Region

In Section 5.2, the cross sections of ^{235}U, ^{238}U and ^{239}Pu were adjusted by the method of least squares. The energy range considered for the adjustment included the unresolved resonance region for these nuclides. In the unresolved region, therefore, the average resonance parameters should be evaluated so as to fit the adjusted ones. The evaluation was performed by the least squares fit to the adjusted cross sections. The calculation of the fitting was made by using the ARCFIT-2 code[103] in which the resonance parameters are searched by an iterative method.

The average resonance parameters obtained for ^{238}U are shown in *Table* 5.5. The atomic radius and scattering radius are assumed to be 8.6(fm) and 9.21(fm) respectively. The resonance parameters adopted for ^{238}U in JFS-1 were $D_0 = 36.6$ eV, $S_{\ell=0} = 1.03 \times 10^{-4}$, $S_{\ell=1} = 2.0 \times 10^{-4}$ and $<\Gamma_\gamma> = 19.1$ MeV, respectively, where the level-spacing of compound nucleus of spin J can be derived from the conventional expression $D_J = D_0/(2J+1)$. Especially, the lower value of Glass[130] has been adopted for the capture width. In recent measurements, however, this value has not been recommended. The present result obtained by the least squares fit was $D_0 = 41.6$ eV, $S_{\ell=0} = 0.928 \times 10^{-4}$, $S_{\ell=1} = 1.4 \times 10^{-4}$, $S_{\ell=2} = 0.83 \times 10^{-4}$ and $<\Gamma_\gamma> = 23.0$ MeV. The capture width $<\Gamma_\gamma> = 23.0$ MeV is slightly smaller than 23.7 ± 1.1 of Asghar *et al.*[131], 23.5 of Pitterle[129] and 23.55 of Rahn[132]. The strength function of s-wave neutrons $S_{\ell=0} = 0.928 \times 10^{-4}$ is slightly larger than $(0.9 \pm 0.11) \times 10^{-4}$ of Abagyan *et al.*[133], 0.9×10^{-4} of Pitterle and $(0.9 \pm 0.1) \times 10^{-4}$ of Seth[134], and smaller than $(1.02 \pm 0.1) \times 10^{-4}$ of Rahn[132]. The p-wave neutron strength function $S_{\ell=1} = 1.4 \times 10^{-4}$ is the same as the value of Rahn and is smaller than $(1.7 \pm 0.3) \times 10^{-4}$ of BNL-325-3d[135]. *Figures* 5.11 and 5.12 show the comparison of the calculated cross section curves for capture and total reactions, respectively, with the measured or evaluated data.

The average resonance parameters for ^{235}U obtained from the least squares fit are shown in *Tables* 5.5 and 5.6, where use is made of the atomic radius of 8.3(fm) and the scattering radius of 9.13(fm). In the calculation of the least squares fit, the same resonance parameters and fission channel schem (see *Table* 5.7) as those adopted for JFS-1 were used and only the strength functions for s-wave and p-wave neutrons were fitted. The obtained strength function $S_{\ell=0} = 1.057 \times 10^{-4}$ is nearly equal $(1.05 \pm 0.15) \times 10^{-4}$ of Hughes[136]. The calculated cross section curve

for fission is compared with the experimental data in *Fig.*5.13.

In the evaluation of the resonance parameters for ^{239}Pu, $D_0 = 8.8$ eV and fission channel level scheme of JFS-1 and $<\Gamma_\gamma> = 41.6$ MeV of ENDF/B-IV were used for the cross section fit, and the strength functions of $S_{\ell=0} = 0.95 \times 10^{-4}$ and $S_{\ell=1} = 3.038 \times 10^{-4}$ were obtained for s- and p-wave neutrons, respectively. The atomic radius and the scattering radius are respectively 8.9(fm) and 8.38(fm). The evaluated resonance parameters are shown in *Tables* 5.5 and 5.8. The calculated cross section curve is compared with the measured values in *Fig.*5.14.

The temperature dependence of cross sections of ^{241}Pu was not considered in the resonance energy region of the JFS-1 set. Therefore, the resonance parameters of ^{241}Pu were evaluated as follows.

For the resonances of ^{241}Pu in the resolved energy range, several sets of resonance parameters based on single-or multi-level fits are available.[137) ~ (142)] But the resolved range is limited to a very low energy domain —— below 50 eV even with the most extensive analysis by Pattenden[137]. In this case, the resolved resonance parameters as given by BNL-325[143] (below 35 eV) and by Pattenden (36.3 to 50.4 eV) have been adopted.

In the Doppler energy range of interest for a large fast reactor, the resonances of ^{241}Pu are not resolved, but average resonance parameters can be obtained from the analysis of low resolution data for this unresolved region. For the average capture width, $<\Gamma_\gamma> = 40$ MeV was adopted, which is the result of multi-level fits[139)~(142)] and recommended also by Doherty and Hennies.[144),(145)]

For the strength function of the s-wave neutrons, there are several values that have been recommended: $S_0 = 1.31 \times 10^{-4}$ (Prince[146]), $(1.26 \pm 0.27) \times 10^{-4}$ (Doherty[144]), $(1.3 \pm 0.3) \times 10^{-4}$ (Uttely[147]),

$(1.3 \pm 0.75) \times 10^{-4}$ (Yiftah[148]) and 1.9×10^{-4} (Craig[138]). The large value of Craig, has been supported by Kikuchi from analyses of Petrel[149] data using a double-humped fission potential[150]. On the other hand, while the strength function of the p-wave neutron is one of the principal unknowns, fortunately, its contribution to cross sections below 10 keV is very small.

The fission width can be calculated as a function of energy from fission channel theory[151] using the fission channel scheme recommended by Lynn[152]. This calculation can be done by means of the code ARCFIT-2[103] which calculates the average cross sections by single level formula for resonance shape. In this case, the main fitting parameters are the s- and p-wave strength functions and the fission barrier positions.

Measured data are available for fission and total cross sections, but not for capture. In *Fig.*5.15, the experimental and evaluated values of fission cross sections are shown for the energy range from 10 eV to 100 keV. Many experimental data are plotted below 2 keV. For the high energy range, there exist data by Simpson *et al.*[149] and by Perkin *et al.*[153], and, in the present fitting of cross sections, the emphasis was put on these data. The atomic radius and potential scattering cross section used for this calculation were 8.30 in Fermi units and 8.7 barns, respectively.

For each fission channel of the compound states, a chi-square distribution with one degree of freedom was assumed. The results fitted for fission, capture and total cross sections are shown by the curves in *Figs.*5.15, 5.16 and 5.17, respectively. The s-wave strength function obtained, $S = 1.31 \times 10^{-4}$, and it is in good agreement with the ones on the small side mentioned above. In the present evaluation, the p-wave neutron cross sections for both capture and fission below 10 keV are very small.

In *Table* 5.9 are given the average resonance parameters thus obtained. *Table* 5.10 and 5.8 summarise the calculated fission widths and barrier positions for those.

For the purpose of considering the energy variation in the fission cross sections of Petrel for the low energy range, using the average resonance parameters in Tables 5.9 and 5.10, the ladders of resonance parameters for an energy range from 10 keV to 50.4 eV were generated. The method used was the same as the procedure described in Chapter 4. The cross sections thus derived are also shown in *Figs*.5.15, 5.16 and 5.17. The average for the generated resonance parameters are shown in *Table* 5.11, and these are in good agreement with the values in *Table* 5.9.

For comparing the results with the experimental data, one of the most important quantities is the total resonance integral. For fission, there are the two values measured by Hardy *et al.*[154], i.e., 565 ± 33 and 581 ± 33 barns for above 0.5 eV. The value of 566 barns for the energy range 0.5 eV to 10 keV, can be obtained from the calculations based on the cross sections derived here. For energies above 10 keV, the corresponding value is 18 barns from JFS-1, and 16 barns from ABBN group constant sets. Hence, the present reevaluated value is in very resonable agreement with the experimental data of Hardy et al..
For the capture resonance integral, the value calculated for the energy range from 0.5 eV to 10 keV was 167 barns, but unfortunatedly no corresponding measured data are available for comparison.

In the resonance region, the uncertainties of fission and capture cross sections for ^{241}Pu are very large, those for σ_f being known to be ±20%, and ±30% for σ_c[145]. For the unresolved region, in particular, measured capture cross section data are extremely scanty. From the results and discussions mentioned above, therefore, the present recommended

cross section values and average resonance parameters of ^{241}Pu for the unresolved region should prove most useful.

5.3.2 Resolved Resonance Region

In the resolved resonance region the resonance parameters were changed from the data used in JFS-1 to the ones listed in *Table* 5.12. For ^{235}U and ^{238}U, the multilevel parameters calculated in Chapter 3 were used. Furthermore, the multilevel parameters for ^{239}Pu were calculated using the formula described in Chapter 3, to fit the experimental data of Cote *et al.*[159] The results are compared with the fission cross sections calculated by the single-level formula in Fig.5.18. The resonance parameters of ^{235}U, ^{238}U, ^{239}Pu and ^{241}Pu adopted in JFS-2 are shown in *Tables* 5.13 ~ 5.17. The multilevel correction parameters (u,v)[40] which represent the interference effect between resonances are also given for ^{235}U, ^{238}U and ^{239}Pu in these tables.

5.4 Evaluation of Cross Sections for Heavy Nuclei in High Energy Region

In order to remove the discrepancy in the spectral index $<\sigma_f^{238}/\sigma_f^{235}>$ depending on the ^{238}U concentration in the JFS-1, the cross sections for heavy nuclei are reevaluated in high energy region above 1.4 MeV where the cross section adjustment was not carried out.

$^{235}\sigma_f$: The fission cross sections of ^{235}U used in JFS-1 are compared with the several experimental and/or evaluated data in *Fig.*5.19. The values of JFS-1 are in relatively good agreement with the experimental data of Czirr *et al.*[160] The data of JFS-1 are closer to the results evaluated by Nakagawa *et al.*[128] for the JENDL-1 than those by Sowerby *et al.*[161] Hence, $^{235}\sigma_f$ was not adjusted in the present evaluation for

the energy range above 1.4 MeV.

$^{238}\sigma_f$: *Figures* 5.20 and 5.21 show the values of the ratio $^{238}\sigma_f/^{235}\sigma_f$. The values of JFS-1 and ENDF/B-IV are larger than the measured data and Sowerby's evaluation in the energy range from 1.4 to 5.1 MeV. The data of Meadows[162] and Grundl[163] were taken into account for our evaluation for this energy range. The resulting evaluated values became smaller than those adopted in JFS-1 by about 2%. However, the benchmark test using JFS-1R indicated that the ratios of the calculated spectral indices of $<\sigma_f^{238}/\sigma_f^{235}>$ to the measured ones become generally smaller than unity with an increase of the ^{238}U concentration ratio as shown in *Fig.*5.2. Therefore, this tendency may result from another cause attributable to the other cross sections than $^{238}\sigma_f$. The present evaluated $^{238}\sigma_f$ is compared with the experimental data in *Fig.*5.22. The evaluated cross sections adopted in JFS-2 are larger than the experimental data and are comparable with the evaluation of Nakagawa *et al.*[128]

$^{239}\sigma_f$: A comparison of the fission cross section ratio $^{239}\sigma_f/^{235}\sigma_f$ is given in Fig.5.23. It is seen from this figure that the uncertainty in $^{239}\sigma_f/^{235}\sigma_f$ is considerably large for the energy range from 1 to 6 MeV. The values of JFS-1 show a tendency to take higher values in this energy range. In the present evaluation, we have selected the data of Sowerby obtained from fitting of experimental data[161]. Thus, $^{239}\sigma_f$ are obtained from the values of $^{235}\sigma_f$ and $^{239}\sigma_f/^{235}\sigma_f$. The calculated values of JFS-2 are compared with the experimental data of Hansen *et al.*[164] in *Fig.*5.24. These values are larger than those of ENDF/B-IV, but are within the error bars of the data of Hansen et al.

The ratios $^{238}\sigma_f/^{239}\sigma_f$ calculated from the presently evaluated ^{238}U and ^{239}Pu for the range from 1.4 to 6.1 MeV are compared with the data of Hansen *et al.* in *Fig.*5.25. The values of JFS-2 are smaller than those of ENDF/B-IV.

5.5 Benchmark Tests of the JFS-2 Set

Group constants for JFS-2 were calculated by using the present evaluated nuclear data and the ENDF/B-IV[179)-(190)] data with use of two processing codes TIMS-1[35] and PROF GROUCH·G·II[36]. The TIMS-1 calculates infinitely dilute cross sections and self-shielding factors for heavy resonant nuclei on the basis of the method described in Chapter 4. On the other hand, the PROF·GROUCH·G·II which is an advanced code on the SUPERTOG code[165] calculates infinitely dilute cross sections, group to group transfer matrices for elastic, inelastic and (n,2n) scattering cross sections, and self-shielding factors based on the assumption of the constant collision density. This code is used for the calculations for light and intermediate weight nuclei and smooth cross sections of heavy nuclei. The nuclides adopted in JFS-2 are listed in *Table* 5.18. The code numbers used in the standard neutronic codes in JAERI are also shown in this table. Tables 5.19 and 5.20 show the standard 70 and 25 group structures of JFS-2 and the fission spectra for ^{235}U and ^{239}Pu, respectively. The group constants for 27 nuclides were tabulated in Ref.(15).

Benchmark tests of JFS-2 have been performed for 21 assemblies with use of one-dimensional diffusion and first order perturbation approximations. We adopted 18 benchmark assemblies selected Hardie *et al.*[17], and added JOYO mock-up core (FCA-V-2) and MOZART cores (MZA and MZB). The characteristics for the 14 Pu-cores were shown in *Table* 4.6. In *Table* 5.21, the main characteristics of a Pu core (VERA-11A) and 6 the U-cores are shown. These assemblies have very wide varieties from 12 to 4000 liters in core size, from no fertile materials to fertile-to-fissile ratio of 8 in core, and Pu-fueled and U-fueled cores and so on.

In this study, the benchmark calculations are based on one-dimensional diffusion and homogeneous models. Hence, several correction factors such as heterogeneity, transport effects etc. are needed. The correction factors to the effective multiplication factors are shown in *Table* 5.22. These correction factors were taken from Ref.(17) for the 18 assemblies, from Ref.(166) for MZA and MZB, and were calculated for FCA-V-2 on the basis of the detailed analysis.

The benchmark calculations were made with both the 70 and 25 group structures of JFS-2, and with the group constant set of JFS type produced from the ENDF/B-IV nuclear data. The calculated results are compared with the form of C/E values.

Effective Multiplication Factors: Table 5.23

The average value for k_{eff} calculated with the JFS-2-70 gives $\overline{k_{eff}} = 0.9983$ with the standard deviation of 1.2%. The results for ENDF/B-IV are less reactivity and especially $\overline{k_{eff}}$ for the Pu-cores is 0.9858*. The discrepancies between the Pu cores and U cores are 0.7%, 1.0% and 0.3% for JFS-2-70, ENDF/B-4-70 and JFS-2-25 respectively. The reason of this discrepancy is not clear, because the present evaluated relative ratios, $^{239}\sigma_f/^{235}\sigma_f$ approach to upper limit of experimental data as seen in *Fig.*5.8. The k_{eff} calculated for ZPR-3-54 is abnormally under-estimated. Hence, when ZPR/3-54 is omitted from the statistical average, $\overline{k_{eff}}$ for the Pu cores are 0.9993 for JFS-2-70, 0.9885 for ENDF/B-4-70 and 1.0029 for JFS-2-25, respectively. Then, the discrepancy between the Pu cores and U cores becomes 0.4% for JFS-2-70 and the standard deviation is

* The present value is about 1.0% less than one calculated by Hardie et al.(17). This disagreement seems to be too large to be caused by the different method of group constants production and/or one-dimensional diffusion code. However, the recent results calculated by Lesage and Mcknight(167) agree with the present results.

reduced from 1.2% to 0.4%. The ZPR-3 assembly 54 has the same core composition as ZPR-3-53, but the assembly 53 has a U reflector while the assembly 54 has an iron reflector. However, the k_{eff} calculated for ZPR-3-53 shows very good value of 0.998 for JFS-2-70. Hence, the reason of less reactivity for ZPR-3-54 may be due to the iron cross section data adopted in ENDF/B-IV or the calculational method of group constants. In the present calculation, diffusion coefficient was calculated by using total cross section defined in Eq.(4-39). The diffusion coefficient may be overestimated especially for the window resonance region of iron in a pure iron system. The transport calculation for ZPR-3-54 showed quite well result of $k_{eff} = 0.99$. Therefore, the definition for the current weight total cross section should be studied in more detail.

The discrepancy between the results for JFS-2-70 and JFS-2-25 is very small as for $\overline{k}_{eff}$, though the discrepancies are about 1% for SNEAK-7A, ZPR-3-54 and ZPR-3-50. The discrepancies are mainly caused by the difference of elastic removal cross sections between 70 and 25 group structures.

JFS-2 is more preferable than ENDF/B-4-70 which underestimates significantly for the LMFBR mockup cores ZPR-6-7, ZPPR-2 and MZB.

Central Reaction Rate Ratios: Tables 5.24 ~ 5.28

The ratios of ^{238}U, ^{239}Pu and ^{240}Pu fission to ^{235}U fission, and of ^{238}U capture to ^{235}U and ^{239}Pu fission were calculated with one-dimensional diffusion model. The results calculated for three sets of JFS-2-70, ENDF/B-4-70 and JFS-2-25 are compared in *Tables* 5.24 ~ 5.28.

Ratio of ^{238}U fission to ^{235}U fission: Table 5.24

For three sets, the ratios of ^{238}U fission to ^{235}U fission are overestimated on an average. The results of JFS-2-25 are larger than those of JFS-2-70. The fission cross sections of ^{238}U is a threshold reaction.

Hence the reaction rate is very sensitive to high energy spectrum above 1 MeV. Therefore, the core spectrum calculated by JFS-2-25 is harder than the one by JFS-2-70, because of the difference of elastic removal cross sections between two sets.

Ratio of ^{239}Pu fission to ^{235}U fission: Table 5.25

The ratio of ^{239}Pu fission to ^{235}U fission is underestimated by ~3% for Pu core and overestimated by ~1% for U core on an average. This discrepancy between Pu and U core is hard to understand due to the same reason described for k_{eff}. The discrepancies between three sets are very small.

Ratio of ^{240}Pu fission to ^{235}U fission: Table 5.25

The results calculated for three sets are overestimated and the agreements between calculation and experiment are very poor. Furthermore the standard deviation for the Pu cores shows large value of about 12%. Hence a reevaluation may be suggested for the fission cross section of ^{240}Pu.

Ratio of ^{238}U capture to ^{239}Pu fission: Table 5.26

The ratio of ^{238}U capture to ^{239}Pu fission is overestimated for the Pu cores and underestimated by 3% for the U cores. Especially, the overestimate for ZPR-6-7 and MZB which are the mockup cores of LMFBR is very significant, because the ratio of ^{238}U capture to ^{239}Pu fission is an index for breeding ratio in a fast reactor.

Ratio of ^{238}U capture to ^{235}U fission: Table 5.27

The discrepancy between Pu and U cores is very small on an average, though the results calculated for FCA-5-2 are considerably low C/E values. The average value of C/E is 0.993 for JFS-2-70 when FCA-V-2 is omitted from the statistical average.

Central Sample Worths: Tables 5.29 ~ 5.32

The central sample worths were calculated with the first order perturbation theory. The conversion factors from inhour/kg to %Δk/k and the correction factors from one-dimensional to two-dimensional calculation were taken from the values of Hardie *et al.*[17].

Table 5.29 shows the comparison of the worths of ^{239}Pu calculated by using the JFS-2-70 and ENDF/B-4-70 sets. Through the results of two sets are in very good agreement with each other, they are overestimated considerably for the Pu cores, and for U cores are in good agreement with the experiments except for VERA-1B. The discrepancy between the Pu and U cores is very large. This reason may be due to some systematic errors in the present benchmark calculation, some of which might be caused by the conversion factors because of large uncertainty in delayed neutron data. Hence, to avoid this scaling problem, both the calculated and measured sample worths were normalized to those of ^{239}Pu, respectively.

Table 5.30 shows the comparison of the sample worths of ^{235}U and ^{238}U normalized to those of ^{239}Pu. The average value of C/E is about unity for three sets, therefore the balance among ^{239}Pu, ^{235}U and ^{238}U is very satisfactory.

The normalized worths of ^{10}B and Mo are shown in *Table* 5.31. The worths of ^{10}B lie systematically samller than unity except for several cores, and the average of C/E is about 0.9. The ^{10}B has a typical 1/v cross section regarded as a standard cross section. Hence, the worth of ^{10}B is very sensitive to the neutron spectrum from medium to low energy region. The dicrepancies among three sets must be thus mainly caused by the differences of the neutron spectra.

The worths of Mo are systematically overestimated and the standard deviation is small. The worth is also sensitive to the neutron spectrum

in low energy region such as the case of ^{10}B, because Mo is a resonance material. Hence, the main inconsistency between the C/E-values of the ^{10}B and Mo worths may be due to the capture cross section of Mo adopted in three sets, that is, the resonance self-shielding factors were not calculated for the unresolved resonance region above 1 keV.

Table 5.32 shows the comparison of the sample worths of scattering materials, sodium and iron. As for the worth of iron, the statistical averages of C/E are 1.05 for JFS-2-70 and 1.10 for ENDF/B-4-70, and the standard deviations are 16 and 17% respectively. In this case, no systematic error is found. On the other hand, as for the sodium worth, the agreements between the calculations and experiments are very poor. The discrepancies between the results of three sets are also large as seen for ZEBRA-2 and ZPR-3-49. It may be the main reasons that the absolute value of central reactivity worth is small and it is very sensitive to the adjoint spectrum.

5.6 Analysis of Doppler Reactivity Coefficients

In this section, the temperature dependence of the group cross sections in the JAERI-Fast Set Version II is tested from the analyses of Doppler experiments performed with two different methods. One is the Doppler reactivity measurement for the whole core of SEFOR assembly[100][101]. Another is the sample Doppler reactivity measurements performed for the natural UO_2 (NUO_2) in FCA assemblies V-1, VI-1 and VI-2[168],[169], and ZPR-6 assembly 7[170],[171], and ZPPR assemblies 2[172] and 3. The main characteristics of these assemblies are summarized in *Table* 5.33. The Doppler measurement methods used at JAERI and ANL are the sample oscillation-reactivity difference technique. In this technique, a Doppler

sample and a reference sample are periodically exchanged at the point in a reactor where the Doppler effect is to be measured. The Doppler samples are 2.5 cm in diameter and 15 cm long at FCA assemblies, and 2.54 cm in diameter and 30.48 cm long at ZPR and ZPPR assemblies. The measurements in FCA assemblies have been performed at the core center in the reactor. In ZPR-6 assembly 7, the Doppler experiments were conducted in both the reference and high-Pu-240 inner cores. In ZPPR assembly 2, the Doppler effects were measured in the normal and Na-voided inner cores. Furthermore, in the normal plate inner core of ZPPR-2 the Doppler effects were measured at different axial positions. The Doppler effects in ZPPR-3 were measured at three positions adjacent to B_4C control rod (CR), Na follower channel rod (CRP) and midway between CR and CRP. In these measurements, the samples are electrically heated from room temperature (~300°K) up to ~1100°K.

The fast critical assemblies in which these sample Doppler measurements have been made are constructed from small plates of fertile, fissile and diluent materials arranged in stainless steel drawers. An example of the configuration is shown for FCA-V assembly 1 in *Fig.*5.26. Because of this arrangement, unavoidable heterogeneities occur significantly in the environment of the small Doppler sample. These heterogeneities affect the gross real and adjoint flux in the vicinity of the sample. In the present calculation, the resonance heterogeneity effect is considered by the usual equivalent relation $\sigma_e = \alpha(1-C)/(N\ell)$, where N and ℓ stand for the atomic number density of resonance material and the mean chord length of the sample, and the factor $\alpha(1-C)$ is assumed to be 1.35. The environments of the sample was homogenized with the stainless steel drawer and vacuum. The atomic compositions for the Doppler sample and the stainless steel environment (buffer) are shown in *Table* 5.34. The plate heterogeneity

effect was calculated by using the integral transport code SLAROM[173]. The plate cell models and the regional atomic compositions are shown in *Figs.*5.31～5.33 for FCA and ZPR assemblies, respectively.

The calculations of Doppler effect were performed with the use of three codes of EXPANDA-70D[99], CITATION[174] and CIPER[175]. The two-dimensional R-Z diffusion calculations were performed on the FCA assemblies, ZPR-6 assembly 7, ZPPR assembly 2 and SEFOR assembly, with 25 energy groups collapsed from 70 groups with use of the one-dimensional diffusion spectrum. The 25 and 70 group structures are shown in *Table* 5.35. The three-dimensional diffusion first order perturbation calculation was made also for the analysis of Doppler effect in ZPPR assembly 3. The results calculated with the use of these methods are compared with the experimental values for each assembly in *Tables* 5.36～5.42. In these tables, "Homo" and "Hetero" mean the homogeneous and heterogeneous calculations for the core plate cell, respectively.

Table 5.36 shows the comparison of the Doppler reactivity effects and multiplication factors (k_{eff}) calculated by using JFS-2 with the experimental values for FCA assemblies. The calculated results are in a very good agreement with the experimental values. The heterogeneous calculation reproduces the experimental values better than the homogeneous calculation.

Table 5.37 shows the comparisons between Doppler reactivity effects calculated and measured for two kinds of cores in ZPR-6 assembly 7. The reference core are composed of comparatively clean plutonium, while the H240 core contains comparatively dirty plutonium. The Doppler measurements were made at the center position of the cores. Also *Table* 5.37 indicates that the heterogeneous calculations can predict much better results than the homogeneous ones. The conspicuous difference between Doppler effects calculated by the homogeneous and heterogeneous models comes from the

remarked differences in the core spectra as shown in *Fig.*5.30. The multiplication factors for the reference core are 0.9946 and 1.00511 for the homogeneous and heterogeneous calculations, respectively, and for the H240 core 0.99502 and 1.0122, respectively.

The Doppler effects of NUO_2 in ZPPR assembly 2 were measured in two cases with and without sodium in the inner core. The measurements were performed on two configurations with "heterogeneous" plate fuel and with "homogeneous" rod fuel in order to test the heterogeneity effect for LMFBR design[172]. *Table* 5.38 shows the comparison between the calculated and measured Doppler effects in the normal inner core of ZPPR assembly 2. The Doppler effects measured in the homogeneous rod cell (or heterogeneous plate fuel) are compared with the results calculated with the homogeneous (or heterogeneous) model. Both the calculated values for "Homo" and "Hetero" agree quite well with the experimental values of rod and plate, respectively. Furthermore, the calculated plate heterogeneity effects are in a very good agreement with the experiments. The comparison between Doppler effects calculated and measured in the Na-voided inner core is given in *Table* 5.39. The ratios of the calculated to experimental results are nearly equal to 1.00 for the heterogeneous results. In the sample temperature of 1100°K, the discrepancy between the calculation and experiment for the heterogeneity effect is 12%. However, only for the temperature 1100°K, the ratio of "rod" to "plate" value exceeds 1.00 in the measurement.

The analysis of the spatially dependent Doppler reactivity worth is performed hereafter. In ZPPR assemblies 2 and 3, the Doppler effects have been measured at the positions traversed axially or radially from the core center. *Table* 5.40 shows the comparison between the Doppler effects calculated and measured at three different axial positions; at the core

center $z = 0$, at $z = 12$ and at $z = 24$ inches from the center of the normal core of ZPPR-2. The calculated results are in a comparatively good agreement with the measured values except for the case of the temperature 500°K at $z = 24$ inches. The Doppler reactivity worths at $z = 24$ inches are small and hence the experimental errors are large. The experimental values of Doppler reactivity worth at $z = 24$ inches indicates a curious temperature dependence compared with those for the other calculated and measured Doppler effects.

In ZPPR assembly 3, the 19 control rods are loaded in the inner core and the core interface. The Doppler effects are measured at three drawer positions adjacent to the B_4C control rod (CR), Na follower channel rod (CRP) and midway between CR and CRP. In the Doppler sample regions, the flux are thought to change spatially strongly. Hence, the three-dimensional diffusion calculation is really needed to take account of the spatial change. The calculation was performed with the use of 18 energy groups collapsed from 25 groups with the two-dimensional R-Z diffusion spectrum. The calculated results are shown in *Table* 5.41, where the models 1 and 2 mean the following calculational models: For the model 1 the three dimensional diffusion calculation is performed by replacing the Doppler region by the core compositions, that is, the flux-depression due to the Doppler sample is not considered in the reference real and adjoint fluxes used for the first order perturbation theory. In the model 2, on the other hand, the flux-depression for the reference real and adjoint fluxes were considered by using the average cross sections calculated with the SLAROM code for the cylindrical model shown in *Fig* 5.31. The exact calculation of the model 2 was performed only for the position 1. The Doppler reactivity effects at the positions 2 and 3 were calculated only for the model 1. The values in the parentheses are obtained by

multiplying the results of the model 1 by the ratios of the results for the model 2 to model 1 at the position 1. The results for the model 2 are in a good agreement with the experimental data.

In SEFOR assembly, the Doppler measurements were performed by measuring the reactivity change due to the power increase from zero to 20 MW, while holding the coolant temperature constant[100]. This experimental isothermal Doppler coefficient was $T\frac{dk}{dT} = -0.0081 \pm 0.001$ and the experimental uncertainty is ±12%. However, it should be noted that the experimental value may increase by about 10% when a recent value[176] of β_{eff} is taken into consideration.

In the benchmark specification, three models are recommended, i.e., the first order perturbation theory calculations in one-dimensional spherical and/or slab and two-dimensional R-Z geometry. The present calculations are performed with the spherical and R-Z models for the case where the fuel temperature in the reactor core rises from 677 to 1365°K.
The reactivity changes due to the temperature rise were calculated with 70-group structure of JFS-2 for the spherical model and with 25-group structure collapsed by the resulting spectrum for the R-Z model.
The comparison of the calculated results with the measured values is given in *Table* 5.42. In this table, the correction factors for the calculated multiplication factor and the Doppler coefficient are taken from the values recommended in Ref.(100). The calculated multiplication factor in the R-Z model is practically equal to 1.00. The Doppler coefficient is in a very good agreement with the experimental value obtained with a recent value of β_{eff}.

Table 5.43 shows the comparison of ^{238}U Doppler effects calculated with the use of JFS-1R and JFS-2. The differences between the results calculated with these two sets lie in the range from 6 to 18%.

The differences become dominant for the FCA-V assembly 1 with a harder spectrum core and the ZPPR assembly 2 with the sodium-voided core. One reason for the differences is that the core spectrum calculated with JFS-2 is softer than that calculated with JFS-1R. Another reason is due to the differences between the resonance parameters used in JFS-1R and 2. The results calculated with JFS-2 exhibit a preferable tendency to agree generally better with the experimental values than the results of JFS-1R.

The statistical average of the C/E-values for the Doppler reactivities shown in *Tables* 5.36 ~ 5.41 is 0.98 and the standard deviation is about 4.4% for the cases considering the resonance and plate heterogeneity effects. We conclude thus that the JAERI-Fast Set Version-II gives the C/E-values which are always near to unity for the analyses of the whole core and NUO_2 sample Doppler experiments.

5.7 Concluding Remarks

The JAERI-Fast set version II (JFS-2) has been mainly developed on the basis of the cross section adjustment and the evaluations of nuclear data. The applicability and assessment of JFS-2 has been made through the benchmark tests for many fast critical assemblies. As a result, the JFS-2 predicts accurately effective multiplication factor, reaction rate ratios and Doppler reactivity coefficients as follows:

1) A systematic dependence of k_{eff} on concentration of ^{238}U in core was removed, though it was seen in the original JAERI Fast set.
2) The mean value and standard deviation for C/E values of k_{eff} was 0.9993 and 0.4% for 14 Pu cores excepting ZPR-3-54, and 0.9983 and 1.2% for all the 21 cores, respectively. The JFS-2 predicts better k_{eff} than the ENDF/B-IV which underestimates by 1% as a whole.

3) The mean values of C/E for the central reaction rate ratios were 0.997 for ^{238}U capture to ^{239}Pu fission, 0.980 for ^{238}U capture to ^{235}U fission, 0.980 for ^{239}Pu fission to ^{235}U fission and 1.03 for ^{238}U fission to ^{235}U fission, respectively.

4) The Doppler reactivity coefficients were accurately predicted with the mean C/E-value of 0.98 and the standard deviation of 4.4%.

As main reactor physics parameters except for those described above, there are sodium void reactivity, reaction rate distribution and control rod worth. Applicability of JFS-2 to these physics parameters has been studied in detail by several researchers[27)-(29),(177),(178)]. As the results, it was shown that the sodium void coefficients were well predicted except for such restricted regions as adjoinning to control rod positions[(27)]. The reaction rate distributions were predicted within an error of ±3% in the core regions and ±5% for the radial blanket[(177)]. The central control rod worths were satisfactory predicted except for the result for ZPPR-3 phase 3, and the systematic tendency of the C/E values on the ^{10}B concentration was not seen[(178)]. Hence, the JFS-2 is concluded to be sufficiently adequate for the technological study of fast reactors in the present status.

However, there exist several problems on the JFS-2 as seen from the benchmark tests: the inconsitent dicrepancies for k_{eff} and the ratio of ^{239}Pu fission to ^{235}U fission between the Pu and U cores, the overestimate for the ratios of ^{238}U and ^{240}Pu fission to ^{235}U fission and for the sample worths of Cr and Mo, the underestimate of the ^{10}B worth, and the overestimate for the ratio of ^{238}U capture to ^{239}Pu fission in the LMFBR mockup cores ZPR-6-7 and MZB. The reasons for these problems are not always clean. It will be required to study further the group constant generation method and the evaluation of neutron cross sections on the

basis of the differential data measured with higher accuracy.

Table 5.1 Accuracy of the use of sensitivity coefficients (comparison of effective multiplication factors)

Assembly No.	S-Method	D-Method	S－D＝δk_ℓ
2	1.001	1.000	＋0.001
3	1.004	1.005	－0.001
4	0.984	0.985	－0.001
6	1.006	1.005	＋0.001
7	1.014	1.013	＋0.001
8	0.990	0.991	－0.001
9	1.006	1.007	－0.001
10	0.986	0.988	－0.002

S-Method: $k_\ell = k_\ell^r + \sum_{im} S_{\ell im}(\sigma_{im}^t - \sigma_{im}^r)$

D-Method: k_ℓ is calculated with EXPANDA-70D using estimated σ_{im}^t value.

Table 5.2 Main characteristics of benchmark test core assemblies

No.	Assembly	Ratio of concentration $^8N/(^6N$ or $^9N)$	Main composition of core and blanket ($\times 10^{22}$/cm^3)					Core radius (cm)	Blanket thickness (cm)
			Core			Blanket			
			^{235}U	^{238}U	^{239}Pu	^{235}U	^{238}U		
2	VERA-11A	0.05	0.0	0.0	0.7213	0.025	3.44	13.985	43.0
3	ZPR-3-48	4.5	0.0016	0.7405	0.1645	0.0083	3.998	46.46	30.0
4	ZEBRA-3	8.6	0.0228	3.156	0.3465	0.0301	4.099	23.67	30.5
6	VERA-1B	0.07	0.7349	0.0469		0.0250	3.440	19.138	39.45
7	ZPR-3-6F	1.1	0.6727	0.7576		0.0089	4.0026	22.985	30.50
8	ZPR-3-11	7.5	0.4567	3.439		0.0089	4.0026	31.61	30.0
9	ZPR-3-12	3.8	0.4516	1.694		0.0089	4.0026	28.76	30.5
10	ZEBRA-2	6.2	0.2523	1.555		0.0301	4.099	45.593	31.7
11	FCA-V-2	2.3	0.1470	0.5836	0.1046	0.02891	3.989	36.232	30.0
12	ZPPR-2	5.5	0.00124	0.5569	0.08469	0.001937	0.8955	61.91	40.0
			0.00116	0.5218	0.12796				

Table 5.3 Standard deviation for differential cross sections $^{235}\sigma_f$, $^{238}\sigma_c$ and $^{239}\sigma_f$

Group No.	Energy boundary	Standard deviation (%)		
		$^{235}\sigma_f$	$^{238}\sigma_c$	$^{239}\sigma_f$
1	1.4 – 1.1 (MeV)	4.0	17.9	3.75
2	1.1 – 0.8 ,,	4.0	17.0	3.75
3	0.8 – 0.63 ,,	4.0	17.0	4.0
4	0.63– 0.5 ,,	4.0	17.0	4.0
5	0.5 – 0.4 ,,	4.0	17.0	4.0
6	0.4 – 0.31 ,,	4.0	11.0	5.68
7	0.31– 0.25 ,,	4.0	11.0	5.68
8	0.25– 0.2 ,,	4.0	11.0	5.68
9	0.2 – 0.15 ,,	4.0	13.0	5.5
10	0.15– 0.12 ,,	4.0	13.0	5.5
11	0.12– 0.1 ,,	4.0	13.0	5.5
12	100.0 –77.3 (keV)	6.0	15.0	9.1
13	77.3 –59.8 ,,	6.1	15.0	9.1
14	59.8 –46.5 ,,	6.1	15.0	9.1
15	46.5 –36.0 ,,	8.0	16.0	12.0
16	36.0 –27.8 ,,	10.3	16.0	16.0
17	27.8 –21.5 ,,	10.3	16.0	16.0
18	21.5 –16.6 ,,	11.1	16.0	25.0
19	16.6 –12.9 ,,	11.1	16.0	25.0
20	12.9 –10.0 ,,	11.1	16.0	25.0
21	10.0 – 7.73 ,,	13.0	16.0	30.0
22	7.73– 5.98 ,,	13.0	16.0	30.0
23	5.98– 4.65 ,,	13.0	16.0	30.0
24	4.65– 3.60 ,,	13.0	17.0	30.0

Table 5.4 Reference values for $^{235}\sigma_f$, $^{238}\sigma_c/^{235}\sigma_f$ and $^{239}\sigma_f/^{235}\sigma_f$ used for adjustment of group cross sections

Energy group	$^{235}\sigma_f^r$ (barns)	$^{239}\sigma_f^r/^{235}\sigma_f^r$	$^{238}\sigma_c^r/^{235}\sigma_f^r$
1.4 – 1.1 (MeV)	1.27	1.40	0.100
1.1 – 0.8 ,,	1.20	1.38	0.123
0.8 – 0.63 ,,	1.14	1.39	0.123
0.63– 0.50 ,,	1.16	1.36	0.115
0.5 – 0.4 ,,	1.19	1.28	0.107
0.4 – 0.31 ,,	1.25	1.20	0.106
0.31– 0.25 ,,	1.30	1.14	0.108
0.25– 0.2 ,,	1.35	1.09	0.112
0.2 – 0.15 ,,	1.42	1.03	0.115
0.15– 0.12 ,,	1.51	0.99	0.117
0.12– 0.1 ,,	1.54	0.96	0.121
100 –77.3 (keV)	1.60	0.93	0.128
77.3 –59.8 ,,	1.73	0.88	0.150
59.8 –46.5 ,,	1.80	0.83	0.180
46.5 –36.0 ,,	1.82	0.79	0.200
36.0 –27.8 ,,	1.95	0.79	0.208
27.8 –21.5 ,,	2.10	0.74	0.218
21.5 –16.6 ,,	2.20	0.71	0.225
16.6 –12.9 ,,	2.30	0.68	0.234
12.9 –10.0 ,,	2.50	0.66	0.238
10.0 – 7.73 ,,	2.70	0.65	0.245
7.73– 5.98 ,,	3.0	0.64	0.248
5.98– 4.65 ,,	3.40	0.62	0.255
4.65– 3.60 ,,	3.70	0.61	0.260

Table 5.5 Average resonance parameters of ^{238}U, ^{235}U and ^{239}Pu obtained by the least squares fit of adjusted cross sections

Isotope	(ℓ, J)	$\langle D_{\ell J}\rangle$ (eV)	$\langle \Gamma^{0}_{n\ell J}\rangle \times 10^{3}$ (eV)	$\langle \Gamma_{\gamma}\rangle$ (eV)
^{238}U	(0,0.5)	20.8	1.930	0.023
	(1,0.5)	20.8	2.912	0.023
	(1,1.5)	10.4	1.456	0.023
	(2,1.5)	10.4	1.718*	0.023
	(2,2.5)	6.93	1.145*	0.023
^{235}U	(0,3)	1.143	0.121	0.0479
	(0,4)	0.8889	0.0940	0.0479
	(1,2)	1.60	0.2576	0.0479
	(1,3)	1.143	0.3680*	0.0479
	(1,4)	0.8889	0.2862*	0.0479
	(1,5)	0.7273	0.1171	0.0479
^{239}Pu	(0,0)	8.8	0.836	0.0416
	(0,1)	2.933	0.2787	0.0416
	(1,0)	8.8	2.673*	0.0146
	(1,1)	2.933	0.8911	0.0416
	(1,2)	1.76	0.5347	0.0416

* The χ^2 distribution with the degree of freedom 2 was assumed.

Table 5.6 Average fission widths of ^{235}U obtained from the ARCFIT-2 code

Energy	ℓ	J	Γ_f (eV)	Γ_{f1}	Γ_{f2}	Γ_{f3}
150 eV ～ 3500 eV	0	3	0.376	0.181	0.181	0.014
	0	4	0.152	0.141	0.011	
	1	2	0.705	0.254	0.252	0.199
	1	3	0.322	0.180	0.142	
	1	4	0.392	0.141	0.140	0.110
	1	5	0.205	0.115	0.090	
3.5 keV ～ 10.0 keV	0	3	0.375	0.180	0.180	0.015
	0	4	0.151	0.140	0.011	
	1	2	0.702	0.252	0.250	0.200
	1	3	0.321	0.179	0.143	
	1	4	0.390	0.140	0.139	0.111
	1	5	0.205	0.114	0.091	
10.0 keV ～ 50 keV	0	3	0.369	0.176	0.176	0.017
	0	4	0.149	0.136	0.013	
	1	2	0.691	0.245	0.244	0.202
	1	3	0.319	0.174	0.145	
	1	4	0.384	0.136	0.135	0.112
	1	5	0.203	0.111	0.092	
50 keV ～ 100 keV	0	3	0.352	0.163	0.163	0.026
	0	4	0.147	0.127	0.02	
	1	2	0.659	0.228	0.228	0.204
	1	3	0.308	0.163	0.145	
	1	4	0.366	0.127	0.126	0.113
	1	5	0.196	0.103	0.093	

Table 5.7 Average fission widths of ^{239}Pu obtained from the ARCFIT-2 code

Energy	ℓ	J	Γ_f (eV)	Γ_{f1}	Γ_{f2}	Γ_{f3}
	0	0	1.712	1.395	0.317	
150 eV	0	1	0.036	0.036		
～	1	0	0			
5 keV	1	1	0.939	0.465	0.463	0.011
	1	2	0.558	0.279	0.273	0.006
	0	0	1.713	1.385	0.328	
5 keV	0	1	0.037	0.037		
～	1	0	0			
10 keV	1	1	0.933	0.462	0.46	0.0113
	1	2	0.555	0.277	0.271	0.007
	0	0	1.718	1.368	0.349	
10 keV	0	1	0.04	0.04		
～	1	0	0			
25 keV	1	1	0.923	0.456	0.455	0.0123
	1	2	0.546	0.271	0.267	0.008
	0	0	1.736	1.312	0.424	
25 keV	0	1	0.052	0.052		
～	1	0	0			
50 keV	1	1	0.89	0.437	0.436	0.0163
	1	2	0.531	0.262	0.259	0.01
	0	0	1.763	1.256	0.506	
50 keV	0	1	0.07	0.07		
～	1	0	0			
100 keV	1	1	0.859	0.419	0.48	0.0217
	1	2	0.513	0.251	0.249	0.013

Table 5.8 Barrier positions for fission (Barrier height hw=0.5 MeV)

(Units: MeV)

Isotope	(ℓ, J^π)	1	2	3
^{235}U	$(0,3^-)$	−0.8	−0.5	0.2
	$(0,4^-)$	−0.5	0.2	
	$(1,2^+)$	−1.1	−0.4	−0.1
	$(1,3^+)$	−0.4	−0.1	
	$(1,4^+)$	−1.1	−0.4	−0.1
	$(1,5^+)$	−0.4	−0.1	
^{239}Pu	$(0,0^+)$	−1.5	0.1	
	$(0,1^+)$	0.2		
	$(1,1^-)$	−0.9	−0.45	0.3
	$(1,2^-)$	−0.5	−0.3	0.3
^{241}Pu	$(0,2^+)$	−0.5	0.1	0.6
	$(0,3^+)$	−0.2	0.5	
	$(1,1^-)$	−0.6	−0.2	0.6
	$(1,2^-)$	−0.2	0.1	0.6
	$(1,3^-)$	−0.6	−0.3	0.1
	$(1,4^-)$	−0.2	0.1	0.6

Table 5.9 Average resonance parameters used for constructing ladders

(ℓ, J)	$D_{\ell, J}$ (eV)	$\Gamma^{\circ}_{n\ell J}$ (eV)	Γ_f (eV)	Γ_r (eV)
(0, 2)	2.333	3.057×10^{-4}	0.473 ≀ 0.454	0.04
(0, 3)	1.667	2.183×10^{-4}	0.222 ≀ 0.247	0.04
(1, 1)	3.90	15.21×10^{-4}	1.04 ≀ 1.19	0.04
(1, 2)	2.333	9.099×10^{-4}	0.466 ≀ 0.427	0.04
(1. 3)	1.667	6.499×10^{-4}	0.562 ≀ 0.585	0.04
(1, 4)	1.30	5.070×10^{-4}	0.259 ≀ 0.237	0.04

Table 5.10 Fission widths and numbers of fission channels used for constructing ladders (energy range below 100 keV)

(ℓ, J)	No. of channels	Γ_{fi} (eV)			Γ_f(eV) = $\sum_{i=1}^{3} \Gamma_{fi}$ (eV)
		1	2	3	
(0, 2)	3	0.315 ∿ 0.372	0.158 ∿ 0.083	0.0006 ∿ 0.0002	0.473 ∿ 0.454
(0, 3)	2	0.220 ∿ 0.246	0.0015 ∿ 0.001		0.222 ∿ 0.247
(1, 1)	3	0.525 ∿ 0.620	0.514 ∿ 0.574	0.001 ∿ 0.0003	1.04 ∿ 1.19
(1, 2)	3	0.308 ∿ 0.345	0.158 ∿ 0.083	0.0006 ∿ 0.0002	0.466 ∿ 0.427
(1, 3)	3	0.225 ∿ 0.266	0.224 ∿ 0.260	0.113 ∿ 0.059	0.562 ∿ 0.585
(1, 4)	3	0.171 ∿ 0.191	0.088 ∿ 0.046	0.0003 ∿ 0.0001	0.259 ∿ 0.237

Table 5.11 Average values for the constructed resonance parameters

(ℓ, J)	D (eV)	Γ_n° (eV)	Γ_f (eV)
(0, 2)	2.305	2.963×10^{-4}	0.445
(0, 3)	1.651	2.219×10^{-4}	0.2464
(1, 1)	3.868	1.507×10^{-3}	1.179
(1, 2)	2.305	9.145×10^{-4}	0.4255
(1, 3)	1.647	6.377×10^{-4}	0.5822
(1, 4)	1.286	5.025×10^{-4}	0.2359

Table 5.12 List of references for resonance parameters adopted in JFS-2

Nuclide	Energy range(eV)	References	Remarks
^{235}U	147.33 ～ 63.13 62.44 ～ 12.85 11.66 ～ -0.95	Schmidt[155] Drawbauch & Gibson[156] Takano & Ishiguro[157]	 Multilevel Correction
^{238}U	3953.9 ～ 6.67 1974.65～1968.66	ENDF/B-4 Takano & Ishiguro[157]	Modified = 0.023eV Multilevel Correction
^{239}Pu	658.0 ～ 14.31 11.9 ～ -1.2	BNL-325 3d.[135] Takano	 Multilevel Correction
^{241}Pu	50.4 ～ -0.16	Pattenden[158]	

Table 5.13 Single- and multi-level resonance parameters of ^{235}U

ENERGY (EV)	COMPOUND NUCLEUS SPIN	REDUCED NEUTRON WIDTH	CAPTURE WIDTH	FISSION WIDTH	U PARAMETER	V PARAMETER
147.330	0.5000	0.4200E-03	0.0479	0.0469	0.0	0.0
145.600	0.5000	0.6000E-03	0.0479	0.0499	0.0	0.0
143.120	0.5000	0.1003E-04	0.0479	0.0452	0.0	0.0
142.050	0.5000	0.4700E-03	0.0479	0.0409	0.0	0.0
141.800	0.5000	0.4997E-04	0.0479	0.0594	0.0	0.0
140.240	0.4380	0.1100E-03	0.0479	0.0570	0.0	0.0
139.170	0.5000	0.4001E-04	0.0479	0.0647	0.0	0.0
137.510	0.5000	0.2600E-03	0.0479	0.0292	0.0	0.0
136.290	0.5000	0.2700E-03	0.0479	0.0357	0.0	0.0
135.470	0.5000	0.3400E-03	0.0479	0.0484	0.0	0.0
132.150	0.5000	0.3400E-03	0.0479	0.0922	0.0	0.0
133.620	0.5000	0.3800E-03	0.0479	0.0402	0.0	0.0
133.040	0.5000	0.9996E-04	0.0479	0.0630	0.0	0.0
132.680	0.5000	0.1000E-03	0.0479	0.0409	0.0	0.0
132.110	0.5000	0.1900E-03	0.0479	0.0786	0.0	0.0
131.640	0.5000	0.9003E-04	0.0479	0.2175	0.0	0.0
131.230	0.5000	0.1900E-03	0.0479	0.2080	0.0	0.0
129.920	0.5000	0.1500E-03	0.0479	0.0515	0.0	0.0
128.140	0.5000	0.1300E-03	0.0479	0.0515	0.0	0.0
127.740	0.5000	0.5698E-04	0.0479	0.0812	0.0	0.0
126.450	0.5000	0.3500E-03	0.0479	0.0371	0.0	0.0
126.010	0.5000	0.1800E-03	0.0479	0.0383	0.0	0.0
125.620	0.5000	0.3700E-03	0.0479	0.0352	0.0	0.0
124.750	0.5000	0.1950E-03	0.0479	0.0855	0.0	0.0
123.960	0.5000	0.9970E-05	0.0479	0.1226	0.0	0.0
123.590	0.5000	0.3598E-04	0.0479	0.0886	0.0	0.0
122.890	0.5000	0.5403E-04	0.0479	0.0666	0.0	0.0
121.900	0.5000	0.5100E-03	0.0479	0.0647	0.0	0.0
118.620	0.5000	0.2800E-03	0.0479	0.0592	0.0	0.0
118.300	0.5000	0.1400E-03	0.0479	0.0998	0.0	0.0
115.920	0.5000	0.2660E-03	0.0479	0.0675	0.0	0.0
115.080	0.5000	0.4102E-04	0.0479	0.1710	0.0	0.0
113.540	0.5000	0.1350E-03	0.0479	0.0440	0.0	0.0
111.660	0.5000	0.1070E-03	0.0478	0.0291	0.0	0.0
111.130	0.5000	0.4601E-04	0.0591	0.0434	0.0	0.0
110.180	0.5000	0.5497E-04	0.0479	0.0134	0.0	0.0
109.820	0.5000	0.2020E-03	0.0737	0.0242	0.0	0.0
108.860	0.5000	0.1210E-03	0.0646	0.0311	0.0	0.0
108.060	0.5000	0.4204E-04	0.0479	0.0095	0.0	0.0
107.610	0.5000	0.3970E-03	0.0507	0.0222	0.0	0.0
106.720	0.5000	0.1074E-04	0.0479	0.0726	0.0	0.0
106.090	0.5000	0.1130E-03	0.0479	0.0577	0.0	0.0
105.550	0.5000	0.2998E-04	0.0479	0.0383	0.0	0.0
105.180	0.5000	0.2340E-03	0.0479	0.0737	0.0	0.0
104.160	0.5000	0.2597E-04	0.0479	0.0335	0.0	0.0
103.500	0.5000	0.2030E-03	0.0479	0.0960	0.0	0.0
102.940	0.5000	0.2480E-03	0.0479	0.0371	0.0	0.0
101.850	0.5000	0.3597E-04	0.0553	0.0513	0.0	0.0
100.980	0.5000	0.9902E-04	0.0465	0.0445	0.0	0.0
100.290	0.5000	0.6600E-04	0.0465	0.0878	0.0	0.0
99.530	0.5000	0.6205E-04	0.0479	0.1065	0.0	0.0
98.100	0.5000	0.2810E-03	0.0479	0.0812	0.0	0.0
96.410	0.5000	0.1050E-03	0.0479	0.1112	0.0	0.0
95.560	0.5000	0.1620E-03	0.0479	0.1040	0.0	0.0
94.340	0.5000	0.7197E-04	0.0479	0.0070	0.0	0.0
94.080	0.5000	0.4100E-03	0.0564	0.0146	0.0	0.0
93.240	0.5000	0.3397E-04	0.0777	0.0850	0.0	0.0
92.580	0.5000	0.2630E-03	0.0543	0.0412	0.0	0.0
92.060	0.5000	0.7504E-04	0.0421	0.0922	0.0	0.0
91.260	0.5000	0.3100E-03	0.0479	0.0599	0.0	0.0
90.340	0.5000	0.5100E-03	0.0438	0.0144	0.0	0.0
89.800	0.5000	0.6996E-04	0.0397	0.0976	0.0	0.0
89.100	0.5000	0.1896E-04	0.0479	0.0922	0.0	0.0
88.780	0.5000	0.3500E-03	0.0479	0.0967	0.0	0.0
87.600	0.5000	0.7896E-04	0.0479	0.1022	0.0	0.0
86.790	0.5000	0.7696E-04	0.0479	0.0922	0.0	0.0
86.250	0.5000	0.5384E-05	0.0479	0.1112	0.0	0.0
85.630	0.5000	0.6495E-04	0.0479	0.0886	0.0	0.0
85.000	0.5000	0.1100E-03	0.0479	0.0621	0.0	0.0
84.280	0.5000	0.2070E-03	0.0479	0.0812	0.0	0.0
84.050	0.5000	0.1641E-03	0.0479	0.0656	0.0	0.0
83.610	0.5000	0.1280E-03	0.0447	0.0721	0.0	0.0
82.640	0.5000	0.2420E-03	0.0479	0.0148	0.0	0.0
82.100	0.5000	0.5518E-05	0.0479	0.1294	0.0	0.0
81.420	0.5000	0.9897E-04	0.0390	0.0700	0.0	0.0
80.340	0.5000	0.8200E-04	0.0560	0.1130	0.0	0.0
79.670	0.5000	0.7697E-04	0.0450	0.0750	0.0	0.0
78.470	0.5000	0.1501E-04	0.0479	0.0383	0.0	0.0
78.100	0.5000	0.1150E-03	0.0400	0.0990	0.0	0.0
77.500	0.5000	0.1160E-03	0.0650	0.0550	0.0	0.0
76.770	0.5000	0.7761E-05	0.0290	0.0459	0.0	0.0
75.530	0.5000	0.1420E-03	0.0479	0.0371	0.0	0.0
75.180	0.5000	0.1500E-03	0.0479	0.0666	0.0	0.0
74.540	0.5000	0.3430E-03	0.0540	0.0610	0.0	0.0
72.910	0.5000	0.2998E-04	0.0479	0.1228	0.0	0.0
72.370	0.5000	0.3760E-03	0.0520	0.0750	0.0	0.0
71.520	0.5000	0.5498E-04	0.0479	0.1710	0.0	0.0
70.750	0.5000	0.2670E-03	0.0479	0.0800	0.0	0.0
70.430	0.5000	0.3460E-03	0.0479	0.0726	0.0	0.0
69.290	0.5000	0.8902E-04	0.0479	0.0888	0.0	0.0
68.510	0.5000	0.1595E-04	0.0479	0.0469	0.0	0.0
67.220	0.5000	0.1098E-04	0.0771	0.0658	0.0	0.0
66.400	0.5000	0.4504E-04	0.0390	0.0280	0.0	0.0
65.780	0.5000	0.3798E-04	0.0300	0.0300	0.0	0.0
64.290	0.5000	0.1560E-03	0.0430	0.0160	0.0	0.0
64.280	0.5000	0.1560E-03	0.0430	0.0160	0.0	0.0
63.630	0.5000	0.1580E-03	0.0479	0.0422	0.0	0.0
62.443	0.5000	0.7606E-04	0.1240	0.7220	0.0	0.0
61.081	0.5000	0.1030E-03	0.1210	0.2810	0.0	0.0
60.815	0.5000	0.1988E-04	0.0410	0.1010	0.0	0.0
60.205	0.5000	0.1436E-03	0.0581	0.2050	0.0	0.0
59.792	0.5000	0.1267E-04	0.0473	0.1420	0.0	0.0
58.689	0.5000	0.1583E-03	0.0439	0.0899	0.0	0.0
58.092	0.5000	0.1446E-03	0.0126	0.0123	0.0	0.0
57.869	0.5000	0.1066E-03	0.0390	0.0937	0.0	0.0
56.532	0.5000	0.4668E-03	0.0040	0.0075	0.0	0.0
56.245	0.5000	0.7614E-03	0.0415	0.9350	0.0	0.0
55.870	0.5000	0.2023E-03	0.0742	0.1260	0.0	0.0
55.112	0.5000	0.2996E-03	0.0048	0.0051	0.0	0.0
54.140	0.5000	0.3778E-04	0.0741	0.2620	0.0	0.0
53.455	0.5000	0.7085E-04	0.0403	0.0826	0.0	0.0
52.243	0.5000	0.3771E-03	0.0721	0.3560	0.0	0.0
51.653	0.5000	0.4536E-04	0.0145	0.0345	0.0	0.0
51.295	0.5000	0.4806E-03	0.0560	0.1150	0.0	0.0
50.482	0.5000	0.1710E-03	0.0519	0.0753	0.0	0.0
50.123	0.5000	0.3333E-04	0.0186	0.0124	0.0	0.0
49.448	0.5000	0.1362E-03	0.0636	0.0256	0.0	0.0
48.788	0.5000	0.1529E-03	0.1040	0.1410	0.0	0.0
48.319	0.5000	0.1728E-03	0.0817	0.2660	0.0	0.0
47.980	0.5000	0.1096E-03	0.0496	0.0453	0.0	0.0
47.020	0.5000	0.1502E-03	0.0585	0.1210	0.0	0.0
46.808	0.5000	0.9442E-04	0.0415	0.1050	0.0	0.0
45.800	0.5000	0.2896E-04	0.0590	0.0924	0.0	0.0
44.948	0.5000	0.1454E-03	0.0879	0.5520	0.0	0.0
44.619	0.5000	0.1186E-03	0.0546	0.1170	0.0	0.0
43.962	0.5000	0.1029E-03	0.0637	0.1290	0.0	0.0
43.407	0.5000	0.1028E-03	0.0602	0.0354	0.0	0.0
42.723	0.5000	0.5064E-04	0.0718	0.0299	0.0	0.0
42.240	0.5000	0.7524E-04	0.0780	0.1310	0.0	0.0
41.887	0.5000	0.1899E-03	0.0497	0.0223	0.0	0.0
41.611	0.5000	0.1380E-04	0.0008	0.0009	0.0	0.0
41.398	0.5000	0.1201E-03	0.0770	0.3990	0.0	0.0
40.562	0.5000	0.6485E-04	0.0538	0.2170	0.0	0.0
39.911	0.5000	0.4923E-04	0.0223	0.1530	0.0	0.0
39.420	0.5000	0.3912E-03	0.0413	0.0614	0.0	0.0
38.288	0.5000	0.9082E-04	0.0836	0.4710	0.0	0.0
35.205	0.5000	0.7663E-03	0.0519	0.1050	0.0	0.0
34.866	0.5000	0.2110E-03	0.0408	0.1160	0.0	0.0
34.379	0.5000	0.3713E-03	0.0478	0.0479	0.0	0.0
33.540	0.5000	0.3151E-03	0.0440	0.0328	0.0	0.0
32.086	0.5000	0.3303E-03	0.0461	0.0659	0.0	0.0
30.891	0.5000	0.8888E-04	0.0367	0.0200	0.0	0.0
30.627	0.5000	0.4680E-04	0.0672	0.1310	0.0	0.0
29.668	0.5000	0.3486E-04	0.0524	0.0395	0.0	0.0
28.756	0.5000	0.5594E-03	0.0231	0.0727	0.0	0.0
28.371	0.5000	0.5482E-04	0.0817	0.2070	0.0	0.0
27.823	0.5000	0.1356E-03	0.0506	0.0873	0.0	0.0
27.182	0.5000	0.1017E-04	0.0006	0.0005	0.0	0.0
26.822	0.5000	0.4595E-04	0.0055	0.1260	0.0	0.0
26.482	0.5000	0.1018E-03	0.0489	0.1610	0.0	0.0
25.757	0.5000	0.1931E-04	0.0455	0.1310	0.0	0.0
25.590	0.5000	0.5756E-04	0.0104	0.2530	0.0	0.0
25.473	0.5000	0.8656E-04	0.0218	0.4380	0.0	0.0
25.239	0.5000	0.1931E-04	0.0071	0.1920	0.0	0.0
25.067	0.5000	0.2417E-04	0.0343	0.2520	0.0	0.0
24.735	0.5000	0.8474E-04	0.0069	0.7800	0.0	0.0
24.350	0.5000	0.3607E-04	0.0491	0.0772	0.0	0.0
24.231	0.5000	0.4063E-04	0.0301	0.0189	0.0	0.0
23.605	0.5000	0.2180E-03	0.0862	0.2100	0.0	0.0
23.408	0.5000	0.1197E-03	0.0218	0.0044	0.0	0.0
22.933	0.5000	0.8958E-04	0.0410	0.0468	0.0	0.0
21.064	0.5000	0.3377E-03	0.0408	0.0328	0.0	0.0
20.628	0.5000	0.3677E-04	0.0396	0.0418	0.0	0.0
20.132	0.5000	0.3521E-04	0.0966	0.2670	0.0	0.0
19.295	0.5000	0.7408E-03	0.0396	0.0590	0.0	0.0
18.969	0.5000	0.1975E-04	0.0126	0.0368	0.0	0.0
18.051	0.5000	0.9462E-04	0.0495	0.1340	0.0	0.0
16.664	0.5000	0.7006E-04	0.0436	0.1079	0.0	0.0
16.086	0.5000	0.9050E-04	0.0339	0.0208	0.0	0.0
15.407	0.5000	0.5987E-04	0.0382	0.0445	0.0	0.0
14.541	0.5000	0.2596E-04	0.0351	0.0177	0.0	0.0
13.986	0.5000	0.1736E-03	0.0841	0.4950	0.0	0.0
13.695	0.5000	0.2702E-05	0.0007	0.0044	0.0	0.0
13.270	0.5000	0.8235E-05	0.0433	0.0767	0.0	0.0
12.860	0.5000	0.1422E-04	0.0522	0.0604	0.0	0.0
12.395	0.5000	0.3621E-03	0.0366	0.0288	0.0	0.0
11.660	0.5000	0.1728E-03	0.0360	0.0035	0.34696E-05	-0.44482E-06
10.800	0.5000	0.4869E-05	0.0400	0.7330	0.20787E-04	0.14304E-04
10.180	0.5000	0.2006E-04	0.0370	0.0580	0.58257E-06	0.36676E-05
9.740	0.5000	0.8331E-05	0.0400	0.5000	0.38174E-04	-0.11864E-04
9.280	0.5000	0.6565E-04	0.0650	0.0950	0.10297E-05	-0.43898E-05
8.780	0.5000	0.3982E-03	0.0500	0.0820	-0.58052E-05	0.16307E-04
7.070	0.5000	0.4739E-04	0.0360	0.0280	-0.15363E-05	0.11566E-05
6.380	0.5000	0.1029E-03	0.0330	0.0120	-0.56558E-05	0.10255E-05
6.190	0.5000	0.1407E-04	0.0400	0.0400	0.27432E-05	-0.27386E-06
5.732	0.5000	0.4887E-05	0.0490	0.4430	0.77584E-05	0.92087E-05
5.435	0.5000	0.1458E-03	0.0866	0.1340	0.44530E-05	-0.12486E-05
4.840	0.5000	0.2727E-04	0.0370	0.0038	-0.86770E-07	0.12258E-06
3.610	0.5000	0.4526E-04	0.0460	0.0470	0.92978E-06	-0.24446E-05
3.140	0.5000	0.1580E-04	0.0510	0.1160	-0.24060E-05	0.76336E-07
2.840	0.5000	0.1958E-05	0.0479	0.1570	-0.33394E-06	0.22062E-05
2.030	0.5000	0.5475E-05	0.0380	0.0100	0.19794E-07	0.13011E-06
1.135	0.5000	0.1446E-04	0.0420	0.1150	-0.66706E-06	-0.34687E-05
0.290	0.5000	0.5942E-05	0.0350	0.1000	-0.38630E-07	0.12106E-05
-0.950	0.5000	0.1356E-02	0.0276	0.1694	-0.65639E-03	0.76299E-04

Table 5.14 Single- and multi-level resonance parameters of s-wave neutrons for ^{238}U

ENERGY (EV)	COMPOUND NUCLEUS SPIN	REDUCED NEUTRON WIDTH	CAPTURE WIDTH	FISSION WIDTH
3953.900	1.0000	0.1733E-02	0.0230	0.0
3939.000	1.0000	0.2071E-02	0.0230	0.0
3913.400	1.0000	0.1439E-02	0.0230	0.0
3901.300	1.0000	0.4323E-02	0.0230	0.0
3872.100	1.0000	0.2732E-02	0.0230	0.0
3856.400	1.0000	0.7971E-02	0.0230	0.0
3830.300	1.0000	0.1777E-03	0.0230	0.0
3780.800	1.0000	0.5692E-02	0.0230	0.0
3763.600	1.0000	0.1174E-02	0.0230	0.0
3737.200	1.0000	0.3190E-02	0.0230	0.0
3715.500	1.0000	0.1312E-02	0.0230	0.0
3692.000	1.0000	0.5266E-02	0.0230	0.0
3671.800	1.0000	0.1304E-03	0.0230	0.0
3628.300	1.0000	0.6973E-02	0.0230	0.0
3621.800	1.0000	0.3323E-03	0.0230	0.0
3593.300	1.0000	0.6673E-03	0.0230	0.0
3572.700	1.0000	0.5521E-02	0.0230	0.0
3560.500	1.0000	0.3687E-02	0.0230	0.0
3526.400	1.0000	0.8420E-04	0.0230	0.0
3493.300	1.0000	0.1590E-03	0.0230	0.0
3484.300	1.0000	0.1779E-02	0.0230	0.0
3456.300	1.0000	0.8505E-02	0.0230	0.0
3435.300	1.0000	0.5972E-02	0.0230	0.0
3417.700	1.0000	0.7013E-04	0.0230	0.0
3407.900	1.0000	0.3255E-02	0.0230	0.0
3388.300	1.0000	0.2491E-03	0.0230	0.0
3354.000	1.0000	0.1865E-02	0.0230	0.0
3332.900	1.0000	0.1213E-02	0.0230	0.0
3320.200	1.0000	0.1788E-02	0.0230	0.0
3310.300	1.0000	0.2138E-02	0.0230	0.0
3295.200	1.0000	0.1394E-03	0.0230	0.0
3278.200	1.0000	0.4104E-02	0.0230	0.0
3272.000	1.0000	0.1399E-03	0.0230	0.0
3248.100	1.0000	0.4913E-03	0.0230	0.0
3224.900	1.0000	0.5811E-03	0.0230	0.0
3217.000	1.0000	0.1410E-03	0.0230	0.0
3204.900	1.0000	0.1289E-02	0.0230	0.0
3188.100	1.0000	0.1417E-02	0.0230	0.0
3177.800	1.0000	0.1313E-02	0.0230	0.0
3168.500	1.0000	0.2132E-03	0.0230	0.0
3148.100	1.0000	0.1337E-02	0.0230	0.0
3132.600	1.0000	0.1429E-03	0.0230	0.0
3108.800	1.0000	0.3408E-02	0.0230	0.0
3058.100	1.0000	0.5787E-03	0.0230	0.0
3042.500	1.0000	0.6345E-04	0.0230	0.0
3027.800	1.0000	0.2272E-02	0.0230	0.0
3015.100	1.0000	0.3005E-04	0.0230	0.0
3002.400	1.0000	0.2135E-02	0.0230	0.0
2986.300	1.0000	0.1006E-03	0.0230	0.0
2965.800	1.0000	0.6060E-04	0.0230	0.0
2955.700	1.0000	0.3863E-03	0.0230	0.0
2933.000	1.0000	0.5724E-03	0.0230	0.0
2896.300	1.0000	0.2787E-03	0.0230	0.0
2882.000	1.0000	0.1025E-01	0.0230	0.0
2864.100	1.0000	0.3270E-02	0.0230	0.0
2828.000	1.0000	0.3291E-03	0.0230	0.0
2805.400	1.0000	0.1510E-03	0.0230	0.0
2786.000	1.0000	0.2292E-03	0.0230	0.0
2761.600	1.0000	0.4396E-03	0.0230	0.0
2749.700	1.0000	0.8582E-03	0.0230	0.0
2732.400	1.0000	0.3444E-04	0.0230	0.0
2716.500	1.0000	0.2782E-02	0.0230	0.0
2695.600	1.0000	0.3660E-03	0.0230	0.0
2671.300	1.0000	0.4644E-02	0.0230	0.0
2631.700	1.0000	0.6823E-04	0.0230	0.0
2619.100	1.0000	0.8793E-03	0.0230	0.0
2596.500	1.0000	0.1315E-01	0.0230	0.0
2579.900	1.0000	0.6497E-02	0.0230	0.0
2558.500	1.0000	0.4547E-02	0.0230	0.0
2547.200	1.0000	0.1090E-01	0.0230	0.0
2520.700	1.0000	0.2788E-03	0.0230	0.0
2488.400	1.0000	0.1764E-02	0.0230	0.0
2454.800	1.0000	0.3835E-03	0.0230	0.0
2445.500	1.0000	0.3943E-02	0.0230	0.0
2425.700	1.0000	0.2741E-02	0.0230	0.0
2410.800	1.0000	0.9369E-04	0.0230	0.0
2391.400	1.0000	0.5317E-03	0.0230	0.0
2355.300	1.0000	0.1257E-02	0.0230	0.0
2352.800	1.0000	0.9690E-03	0.0230	0.0
2339.000	1.0000	0.1964E-03	0.0230	0.0
2315.500	1.0000	0.4364E-03	0.0230	0.0
2281.700	1.0000	0.2826E-02	0.0230	0.0
2267.000	1.0000	0.4411E-02	0.0230	0.0
2258.800	1.0000	0.1810E-02	0.0230	0.0
2241.000	1.0000	0.3169E-04	0.0230	0.0
2217.000	1.0000	0.8495E-04	0.0230	0.0
2200.600	1.0000	0.2558E-02	0.0230	0.0
2186.000	1.0000	0.1326E-01	0.0230	0.0
2152.200	1.0000	0.5173E-02	0.0230	0.0
2144.600	1.0000	0.1339E-02	0.0230	0.0
2123.800	1.0000	0.6944E-04	0.0230	0.0
2095.900	1.0000	0.5024E-03	0.0230	0.0
2088.100	1.0000	0.5909E-03	0.0230	0.0
2070.900	1.0000	0.6592E-04	0.0230	0.0
2029.800	1.0000	0.1354E-02	0.0230	0.0
2022.800	1.0000	0.4780E-02	0.0230	0.0
1974.650	1.0000	0.1050E-01	0.0246	0.0
1968.660	1.0000	0.1300E-01	0.0246	0.0
1953.400	1.0000	0.8372E-04	0.0230	0.0
1916.500	1.0000	0.5688E-03	0.0230	0.0
1902.400	1.0000	0.6878E-03	0.0230	0.0
1870.000	1.0000	0.6244E-04	0.0230	0.0
1868.000	1.0000	0.6247E-04	0.0230	0.0
1845.500	1.0000	0.3026E-03	0.0230	0.0
1807.900	1.0000	0.3410E-03	0.0230	0.0
1795.500	1.0000	0.7080E-04	0.0230	0.0
1782.100	1.0000	0.1587E-01	0.0230	0.0
1755.200	1.0000	0.2506E-02	0.0270	0.0
1722.200	1.0000	0.3615E-03	0.0230	0.0
1709.000	1.0000	0.2032E-02	0.0280	0.0
1688.300	1.0000	0.2239E-02	0.0230	0.0
1661.300	1.0000	0.4171E-02	0.0230	0.0
1637.400	1.0000	0.1236E-02	0.0230	0.0
1622.000	1.0000	0.1738E-02	0.0230	0.0
1597.500	1.0000	0.8682E-02	0.0230	0.0
1566.000	1.0000	0.1365E-03	0.0230	0.0
1546.500	1.0000	0.1017E-03	0.0230	0.0
1533.000	1.0000	0.1022E-04	0.0230	0.0
1522.300	1.0000	0.6151E-02	0.0230	0.0
1473.400	1.0000	0.3256E-02	0.0230	0.0
1443.500	1.0000	0.4738E-03	0.0230	0.0
1427.400	1.0000	0.7702E-03	0.0260	0.0
1419.200	1.0000	0.2389E-03	0.0230	0.0
1405.200	1.0000	0.1867E-02	0.0230	0.0
1393.200	1.0000	0.4876E-02	0.0230	0.0
1332.700	1.0000	0.4383E-04	0.0230	0.0
1316.300	1.0000	0.1103E-03	0.0230	0.0
1298.100	1.0000	0.1249E-03	0.0230	0.0
1272.700	1.0000	0.7568E-03	0.0230	0.0
1266.800	1.0000	0.6209E-03	0.0210	0.0
1244.900	1.0000	0.7936E-02	0.0230	0.0
1211.100	1.0000	0.2586E-03	0.0230	0.0001
1194.500	1.0000	0.2575E-02	0.0230	0.0
1176.600	1.0000	0.1749E-02	0.0230	0.0
1167.500	1.0000	0.2488E-03	0.0230	0.0
1140.400	1.0000	0.6515E-02	0.0230	0.0
1131.100	1.0000	0.8920E-04	0.0230	0.0
1108.900	1.0000	0.8108E-03	0.0230	0.0
1099.000	1.0000	0.5128E-03	0.0220	0.0
1054.800	1.0000	0.2740E-02	0.0230	0.0
1029.400	1.0000	0.7792E-04	0.0230	0.0
1022.900	1.0000	0.2595E-03	0.0230	0.0
1011.600	1.0000	0.4999E-04	0.0230	0.0
991.400	1.0000	0.1239E-01	0.0300	0.0
958.000	1.0000	0.6152E-02	0.0230	0.0
936.600	1.0000	0.4463E-02	0.0230	0.0
924.500	1.0000	0.4572E-03	0.0230	0.0
904.500	1.0000	0.1729E-02	0.0268	0.0
866.000	1.0000	0.1937E-03	0.0230	0.0
856.100	1.0000	0.2826E-02	0.0230	0.0
850.600	1.0000	0.1889E-02	0.0230	0.0
821.500	1.0000	0.2303E-02	0.0230	0.0
790.700	1.0000	0.2322E-03	0.0230	0.0
779.300	1.0000	0.7164E-04	0.0230	0.0
765.000	1.0000	0.2755E-03	0.0230	0.0
732.500	1.0000	0.9237E-04	0.0230	0.0
721.400	1.0000	0.4468E-04	0.0230	0.0003
708.000	1.0000	0.7892E-03	0.0260	0.0
692.900	1.0000	0.1664E-02	0.0230	0.0
661.100	1.0000	0.5274E-02	0.0251	0.0
628.500	1.0000	0.2673E-03	0.0230	0.0
619.800	1.0000	0.1326E-02	0.0230	0.0
594.800	1.0000	0.3489E-02	0.0230	0.0
579.900	1.0000	0.1831E-02	0.0230	0.0
555.900	1.0000	0.3393E-04	0.0230	0.0
535.200	1.0000	0.2032E-02	0.0230	0.0
518.300	1.0000	0.2267E-02	0.0230	0.0
478.300	1.0000	0.1738E-03	0.0230	0.0
462.800	1.0000	0.2557E-03	0.0230	0.0
454.100	1.0000	0.2159E-04	0.0230	0.0
433.700	1.0000	0.4792E-03	0.0230	0.0
410.200	1.0000	0.1017E-02	0.0230	0.0
397.400	1.0000	0.3210E-03	0.0252	0.0
376.800	1.0000	0.6491E-04	0.0230	0.0
347.700	1.0000	0.4483E-02	0.0230	0.0
311.200	1.0000	0.6236E-04	0.0230	0.0
291.000	1.0000	0.9954E-03	0.0230	0.0
273.600	1.0000	0.1632E-02	0.0230	0.0
237.200	1.0000	0.1890E-02	0.0230	0.0
208.400	1.0000	0.3816E-02	0.0230	0.0
189.600	1.0000	0.1227E-01	0.0247	0.0
165.200	1.0000	0.2645E-03	0.0230	0.0
145.600	1.0000	0.7376E-04	0.0230	0.0
116.800	1.0000	0.2616E-02	0.0230	0.0
102.500	1.0000	0.7013E-02	0.0260	0.0
80.740	1.0000	0.2226E-03	0.0230	0.0
66.150	1.0000	0.3111E-02	0.0230	0.0
36.800	1.0000	0.5127E-02	0.0260	0.0
20.900	1.0000	0.1925E-02	0.0268	0.0
6.670	1.0000	0.5808E-03	0.0256	0.0
-18.000	1.0000	0.1130E-02	0.0250	0.0

U PARAMETER: 0.13545E-03−0.29279E-03
V PARAMETER: 0.50850E-04−0.78861E-03

Table 5.15 Single-level resonance parameters of p-wave neutrons for ^{238}U

ENERGY (EV)	COMPOUND NUCLEUS SPIN	REDUCED NEUTRON WIDTH	CAPTURE WIDTH	FISSION WIDTH
1289.000	1.0000	0.1597E-02	0.0230	0.0
1285.000	1.0000	0.2140E-02	0.0230	0.0
1275.000	1.0000	0.6495E-02	0.0230	0.0
1263.000	1.0000	0.1647E-02	0.0230	0.0
1260.000	1.0000	0.1102E-02	0.0230	0.0
1251.000	1.0000	0.5012E-02	0.0230	0.0
1233.000	1.0000	0.3414E-02	0.0230	0.0
1230.000	1.0000	0.2856E-02	0.0230	0.0
1220.000	1.0000	0.3469E-02	0.0230	0.0
1201.000	1.0000	0.2663E-02	0.0230	0.0
1185.000	1.0000	0.1208E-02	0.0230	0.0
1159.000	1.0000	0.4994E-02	0.0230	0.0
1155.000	1.0000	0.5020E-02	0.0230	0.0
1150.000	1.0000	0.1453E-02	0.0230	0.0
1119.000	1.0000	0.4605E-02	0.0230	0.0
1103.000	1.0000	0.1277E-01	0.0230	0.0
1094.000	1.0000	0.6846E-02	0.0230	0.0
1081.000	1.0000	0.6928E-02	0.0230	0.0
1074.000	1.0000	0.4897E-02	0.0230	0.0
1071.000	1.0000	0.1405E-02	0.0230	0.0
1068.000	1.0000	0.7054E-02	0.0230	0.0
1062.000	1.0000	0.6403E-02	0.0230	0.0
1047.000	1.0000	0.3633E-02	0.0230	0.0
1031.000	1.0000	0.5949E-02	0.0230	0.0
1004.000	1.0000	0.1625E-02	0.0230	0.0
985.600	1.0000	0.2386E-02	0.0230	0.0
976.800	1.0000	0.6449E-02	0.0230	0.0
964.900	1.0000	0.4106E-02	0.0230	0.0
962.300	1.0000	0.1649E-02	0.0230	0.0
940.100	1.0000	0.4269E-02	0.0230	0.0
932.300	1.0000	0.1729E-02	0.0230	0.0
909.500	1.0000	0.1076E-01	0.0230	0.0
890.600	1.0000	0.6757E-02	0.0230	0.0
871.600	1.0000	0.9560E-03	0.0230	0.0
860.000	1.0000	0.1463E-02	0.0230	0.0
846.900	1.0000	0.7984E-02	0.0230	0.0
832.400	1.0000	0.1639E-02	0.0230	0.0
828.800	1.0000	0.3093E-02	0.0230	0.0
808.200	1.0000	0.4282E-02	0.0230	0.0
787.400	1.0000	0.4229E-02	0.0230	0.0
756.000	1.0000	0.5323E-02	0.0230	0.0
743.200	1.0000	0.3641E-02	0.0230	0.0
739.800	1.0000	0.1222E-02	0.0230	0.0
734.800	1.0000	0.1852E-02	0.0230	0.0
729.400	1.0000	0.1248E-01	0.0230	0.0
713.900	1.0000	0.3222E-02	0.0230	0.0
712.500	1.0000	0.7756E-02	0.0230	0.0
697.500	1.0000	0.3203E-02	0.0230	0.0
688.200	1.0000	0.1225E-02	0.0230	0.0
681.100	1.0000	0.8298E-03	0.0230	0.0
677.500	1.0000	0.1115E-01	0.0230	0.0
667.800	1.0000	0.3276E-02	0.0230	0.0
632.500	1.0000	0.2781E-02	0.0230	0.0
624.800	1.0000	0.1259E-01	0.0230	0.0
614.700	1.0000	0.2256E-02	0.0230	0.0
606.100	1.0000	0.4447E-02	0.0230	0.0
584.700	1.0000	0.2086E-02	0.0230	0.0
550.500	1.0000	0.1712E-02	0.0230	0.0
542.300	1.0000	0.3113E-02	0.0230	0.0
523.200	1.0000	0.5543E-02	0.0230	0.0
498.900	1.0000	0.2645E-02	0.0230	0.0
488.200	1.0000	0.1412E-01	0.0230	0.0
484.000	1.0000	0.2768E-02	0.0230	0.0
466.800	1.0000	0.2435E-02	0.0230	0.0
448.400	1.0000	0.1552E-02	0.0230	0.0
439.700	1.0000	0.8257E-02	0.0230	0.0
415.500	1.0000	0.7248E-03	0.0230	0.0
413.500	1.0000	0.1460E-02	0.0230	0.0
407.600	1.0000	0.2984E-02	0.0230	0.0
400.500	1.0000	0.1225E-02	0.0230	0.0
395.500	1.0000	0.1873E-02	0.0230	0.0
373.700	1.0000	0.1359E-02	0.0230	0.0
366.400	1.0000	0.8401E-03	0.0230	0.0
354.700	1.0000	0.1103E-02	0.0230	0.0
351.800	1.0000	0.7441E-02	0.0230	0.0
337.000	1.0000	0.4365E-02	0.0230	0.0
331.300	1.0000	0.2035E-02	0.0230	0.0
322.800	1.0000	0.1905E-02	0.0230	0.0
306.300	1.0000	0.9157E-03	0.0230	0.0
295.000	1.0000	0.2422E-02	0.0230	0.0
282.300	1.0000	0.5692E-02	0.0230	0.0
275.800	1.0000	0.7502E-02	0.0230	0.0
263.900	1.0000	0.1317E-01	0.0230	0.0
257.600	1.0000	0.1484E-02	0.0230	0.0
253.900	1.0000	0.6066E-02	0.0230	0.0
242.600	1.0000	0.1013E-01	0.0230	0.0
239.900	1.0000	0.3302E-02	0.0230	0.0
218.800	1.0000	0.2274E-02	0.0230	0.0
215.000	1.0000	0.3191E-02	0.0230	0.0
203.000	1.0000	0.1697E-02	0.0230	0.0
200.500	1.0000	0.3457E-02	0.0230	0.0
196.400	1.0000	0.2674E-02	0.0230	0.0
173.100	1.0000	0.3231E-02	0.0230	0.0
158.900	1.0000	0.1470E-02	0.0230	0.0
152.400	1.0000	0.4824E-02	0.0230	0.0
133.300	1.0000	0.2072E-02	0.0230	0.0
124.300	1.0000	0.2832E-02	0.0230	0.0
121.600	1.0000	0.1097E-02	0.0230	0.0
111.400	1.0000	0.2086E-02	0.0230	0.0
98.200	1.0000	0.2016E-02	0.0230	0.0
93.300	1.0000	0.1361E-02	0.0230	0.0
91.000	1.0000	0.1695E-02	0.0230	0.0
89.190	1.0000	0.2620E-01	0.0230	0.0
83.570	1.0000	0.2022E-02	0.0230	0.0
63.540	1.0000	0.2663E-02	0.0230	0.0
49.500	1.0000	0.4224E-03	0.0230	0.0
45.190	1.0000	0.8071E-03	0.0230	0.0
19.500	1.0000	0.2847E-02	0.0230	0.0
10.220	1.0000	0.1171E-01	0.0230	0.0

Table 5.16 Single- and multi-level reseonance parameters of ^{239}Pu

ENERGY (EV)	COMPOUND NUCLEUS SPIN	REDUCED NEUTRON WIDTH	CAPTURE WIDTH	FISSION WIDTH
658.290	0.7500	0.3170E-02	0.0400	0.0190
646.650	0.5000	0.5899E-04	0.0387	0.0
644.940	0.7500	0.2310E-03	0.0400	0.0030
641.420	0.5000	0.2764E-04	0.0400	0.0
639.280	0.7500	0.3665E-03	0.0400	0.0060
636.470	0.5000	0.3171E-03	0.0400	0.0160
632.970	0.5000	0.1351E-02	0.0400	3.8000
628.210	0.5000	0.8777E-04	0.0400	0.0090
625.170	0.7500	0.3146E-03	0.0400	0.0075
622.390	0.7500	0.3928E-03	0.0400	0.0098
620.240	0.7500	0.4765E-03	0.0400	0.0054
612.820	0.5000	0.3555E-03	0.0400	0.0140
609.290	0.7500	0.6374E-03	0.0400	0.0066
607.640	0.7500	0.3949E-03	0.0400	0.0077
604.010	0.7500	0.1020E-02	0.0400	0.0035
598.040	0.5000	0.8833E-03	0.0400	5.9150
597.350	0.7500	0.3519E-03	0.0400	0.0050
593.520	0.5000	0.1314E-03	0.0400	0.0040
589.940	0.5000	0.2059E-04	0.0400	0.0
588.090	0.7500	0.4646E-03	0.0400	0.0100
584.810	0.5000	0.2895E-04	0.0400	0.0
579.040	0.7500	0.2854E-03	0.0400	0.0070
578.000	0.5000	0.1040E-03	0.0400	0.0360
575.770	0.7500	0.1659E-02	0.0400	0.0080
574.000	0.5000	0.3318E-02	0.0400	0.2200
571.110	0.7500	0.3599E-03	0.0400	0.0330
565.810	0.5000	0.5970E-03	0.0387	0.0050
564.030	0.5000	0.4126E-03	0.0387	0.0020
562.840	0.5000	0.2259E-02	0.0387	0.0
559.160	0.7500	0.1150E-02	0.0400	0.0210
555.720	0.5000	0.2079E-03	0.0387	0.0
554.130	0.5000	0.2218E-02	0.0400	1.1400
553.500	0.7500	0.4817E-03	0.0400	0.0030
549.670	0.7500	0.5033E-03	0.0400	0.0070
547.140	0.5000	0.7695E-04	0.0387	0.0
545.850	0.5000	0.7490E-03	0.0400	1.1200
543.080	0.7500	0.5035E-03	0.0400	0.0050
541.550	0.5000	0.3438E-03	0.0387	0.0
540.710	0.5000	0.1720E-03	0.0387	0.0
539.170	0.7500	0.4910E-03	0.0400	0.0024
530.520	0.5000	0.2770E-02	0.0400	0.0750
527.380	0.5000	0.6532E-04	0.0387	0.0160
526.000	0.5000	0.6540E-04	0.0387	0.0510
525.400	0.5000	0.5279E-02	0.0400	10.5000
524.210	0.7500	0.1336E-02	0.0400	0.0200
520.220	0.7500	0.6547E-03	0.0400	0.0430
517.980	0.5000	0.3076E-04	0.0387	0.0
516.570	0.5000	0.1320E-04	0.0387	0.0
515.160	0.5000	0.4406E-04	0.0387	0.0
511.520	0.5000	0.5704E-03	0.0400	3.3000
509.740	0.7500	0.2309E-02	0.0400	0.1670
508.220	0.5000	0.3105E-04	0.0387	0.0
505.780	0.5000	0.4002E-04	0.0387	0.0
502.860	0.7500	0.5292E-03	0.0400	0.0320
500.500	0.7500	0.1520E-03	0.0400	0.0320
495.630	0.5000	0.5390E-04	0.0387	0.0
494.100	0.7500	0.2069E-03	0.0400	0.0700
490.650	0.5000	0.9029E-03	0.0387	2.2200
487.810	0.5000	0.2354E-03	0.0387	0.0
487.290	0.5000	0.1495E-03	0.0387	0.0
484.150	0.5000	0.1772E-03	0.0387	0.0
479.240	0.5000	0.9136E-05	0.0387	0.0
476.900	0.5000	0.1236E-03	0.0400	1.9500
475.310	0.5000	0.2614E-03	0.0400	0.5350
473.100	0.7500	0.1900E-03	0.0400	0.0100
470.000	0.5000	0.6919E-03	0.0400	5.0300
468.200	0.5000	0.3004E-03	0.0400	2.0450
462.640	0.5000	0.3719E-04	0.0387	0.0860
461.260	0.5000	0.1630E-03	0.0387	0.0524
458.800	0.7500	0.2148E-03	0.0400	0.0330
457.330	0.5000	0.5190E-03	0.0387	0.1180
455.730	0.5000	0.1860E-02	0.0400	0.4950
454.450	0.5000	0.3284E-04	0.0387	0.0
451.350	0.7500	0.6621E-03	0.0387	0.0037
449.750	0.5000	0.9431E-04	0.0387	0.0
442.410	0.5000	0.4992E-03	0.0387	0.3370
440.070	0.5000	0.2002E-04	0.0387	0.0
438.720	0.7500	0.1388E-03	0.0387	0.0030
437.760	0.7500	0.1287E-03	0.0387	0.0100
432.730	0.5000	0.7403E-04	0.0387	0.0
431.290	0.5000	0.3515E-03	0.0387	3.4430
429.640	0.5000	0.2731E-03	0.0387	0.7270
426.370	0.5000	0.7168E-03	0.0387	6.9130
425.670	0.5000	0.1939E-04	0.0387	0.0
419.850	0.7500	0.2964E-03	0.0387	0.0740
417.600	0.5000	0.1174E-03	0.0387	0.1780
415.660	0.5000	0.2399E-03	0.0387	0.0180

ENERGY (EV)	COMPOUND NUCLEUS SPIN	REDUCED NEUTRON WIDTH	CAPTURE WIDTH	FISSION WIDTH
412.310	0.7500	0.4403E-03	0.0387	0.0700
408.710	0.5000	0.9596E-04	0.0387	0.0580
406.950	0.5000	0.7237E-04	0.0387	0.3020
406.030	0.5000	0.1355E-03	0.0387	0.0
404.240	0.7500	0.1154E-02	0.0387	0.0760
401.560	0.7500	0.9681E-03	0.0387	0.1540
396.910	0.5000	0.1591E-03	0.0387	0.0610
394.430	0.7500	0.3283E-03	0.0387	0.0520
391.520	0.5000	0.9552E-04	0.0387	0.0680
389.510	0.5000	0.1059E-03	0.0387	0.0210
385.900	0.5000	0.7127E-04	0.0387	0.9550
384.260	5.2500	0.4154E-04	0.0387	0.0750
382.430	0.5000	0.3222E-04	0.0387	0.0850
378.040	0.5000	0.9669E-04	0.0387	0.0
377.100	0.5000	0.1535E-03	0.0387	0.0390
375.020	0.5000	0.2066E-03	0.0387	0.0060
371.720	0.5000	0.5965E-03	0.0387	3.3350
370.310	0.5000	0.2027E-03	0.0387	0.0230
368.330	0.5000	0.3126E-04	0.0387	0.0
366.000	0.5000	0.2823E-03	0.0387	4.9470
361.280	0.5000	0.1736E-04	0.0387	0.0
359.990	0.5000	0.8749E-04	0.0387	0.0800
357.870	0.5000	0.2379E-03	0.0387	5.9490
354.890	0.5000	0.3185E-04	0.0387	0.0
352.820	0.7500	0.2073E-03	0.0387	0.0170
350.300	0.7500	0.1149E-02	0.0387	0.0350
346.560	0.5000	0.2793E-03	0.0387	1.1480
343.180	0.7500	0.8525E-03	0.0387	0.0180
339.240	0.5000	0.2671E-03	0.0387	0.0330
337.950	0.7500	0.4384E-03	0.0387	0.0110
335.930	0.7500	0.9675E-03	0.0387	0.0180
333.910	0.7500	0.3006E-03	0.0387	0.0100
329.650	0.5000	0.3084E-03	0.0387	1.9470
325.300	0.7500	0.4731E-03	0.0387	0.0460
323.360	0.5000	0.1679E-02	0.0387	0.0470
321.750	0.5000	0.1115E-04	0.0387	0.0
316.660	0.7500	0.2903E-03	0.0387	0.0250
313.620	0.7500	0.7680E-03	0.0387	0.0100
311.120	0.5000	0.4139E-04	0.0387	0.0
309.010	0.7500	0.8002E-03	0.0387	0.0240
308.200	0.5000	0.2506E-03	0.0387	0.0980
301.810	0.7500	0.1048E-02	0.0387	0.0480
298.590	0.7500	0.6096E-03	0.0387	0.0200
296.460	0.7500	0.1859E-03	0.0387	0.0300
292.330	0.5000	0.3474E-03	0.0387	0.0720
288.300	0.5000	0.4712E-05	0.0387	0.0
288.000	0.5000	0.8839E-03	0.0387	6.0280
285.730	0.5000	0.5916E-05	0.0387	0.0
282.920	0.7500	0.1474E-02	0.0387	0.0110
279.590	0.5000	0.6579E-03	0.0387	0.0560
277.230	0.5000	0.5405E-03	0.0387	5.2600
275.570	0.7500	0.1470E-02	0.0387	0.0720
274.800	0.5000	0.8445E-03	0.0387	0.7300
272.620	0.7500	0.1627E-02	0.0387	0.0310
269.540	0.7500	0.2518E-03	0.0387	0.0280
269.110	0.5000	0.1280E-03	0.0387	0.0830
264.230	0.5000	0.1538E-04	0.0387	0.0
262.740	0.5000	0.2246E-03	0.0387	0.0100
262.370	0.5000	0.2840E-02	0.0387	6.1480
259.000	0.7500	0.1657E-04	0.0387	0.0
256.110	0.7500	0.3749E-03	0.0387	0.0320
254.580	0.7500	0.1671E-03	0.0387	0.0250
251.230	0.7500	0.1682E-02	0.0400	0.0160
248.860	0.7500	0.9352E-03	0.0420	0.0050
247.500	0.5000	0.8835E-04	0.0387	0.2270
242.880	0.7500	0.4021E-03	0.0350	0.0560
240.600	0.5000	0.3223E-05	0.0387	0.0
239.040	0.7500	0.3406E-03	0.0520	0.0160
234.320	0.7500	0.6533E-03	0.0490	0.0150
232.630	0.5000	0.4327E-04	0.0387	0.0
231.400	0.7500	0.7582E-03	0.0390	0.0050
227.890	0.7500	0.1122E-03	0.0330	0.0320
227.770	0.5000	0.1126E-02	0.0400	7.9260
224.890	0.5000	0.1707E-03	0.0387	0.0250
223.160	0.7500	0.2231E-03	0.0387	0.0090
220.220	0.7500	0.5211E-03	0.0330	0.0110
219.490	0.7500	0.2412E-03	0.0400	0.0260
216.530	0.7500	0.4304E-03	0.0390	0.0110
213.280	0.5000	0.4793E-04	0.0387	0.1630
212.020	0.5000	0.8241E-04	0.0387	1.4560
211.090	0.5000	0.1101E-03	0.0387	0.7450
207.370	0.7500	0.4861E-03	0.0436	0.0060
203.930	0.5000	0.1898E-02	0.0400	0.3160
203.460	0.5000	0.4206E-03	0.0387	0.0

ENERGY (EV)	COMPOUND NUCLEUS SPIN	REDUCED NEUTRON WIDTH	CAPTURE WIDTH	FISSION WIDTH	V PARAMETER
199.390	0.7500	0.6610E-03	0.0410	0.0830	0.0
196.690	0.7500	0.3437E-03	0.0460	0.0610	0.0
195.360	0.5000	0.2039E-02	0.0360	0.3350	0.0
190.640	0.5000	0.1818E-03	0.0510	0.0110	0.0
188.270	0.5000	0.5685E-04	0.0410	0.0100	0.0
184.870	0.5000	0.5884E-03	0.0400	2.0280	0.0
183.640	0.5000	0.1771E-03	0.0387	0.0280	0.0
178.900	0.7500	0.9121E-04	0.0430	0.0140	0.0
177.220	0.7500	0.2684E-03	0.0410	0.0060	0.0
175.980	0.5000	0.2367E-03	0.0410	0.0310	0.0
174.560	0.5000	0.3784E-05	0.0387	0.0	0.0
171.080	0.5000	0.6804E-04	0.0400	0.9000	0.0
170.490	0.5000	0.6586E-04	0.0400	0.1170	0.0
167.100	0.7500	0.4477E-03	0.0320	0.0720	0.0
164.540	0.7500	0.2131E-02	0.0427	0.0080	0.0
161.960	0.5000	0.1650E-04	0.0400	0.1100	0.0
160.800	0.5000	0.1577E-04	0.0387	0.0	0.0
157.080	0.5000	0.1372E-02	0.0400	0.6260	0.0
149.420	0.7500	0.1363E-03	0.0470	0.0520	0.0
148.210	0.5000	0.5750E-04	0.0387	0.1020	0.0
147.440	0.5000	0.1318E-03	0.0387	0.9560	0.0
146.250	0.5000	0.8931E-03	0.0400	0.0120	0.0
143.470	0.7500	0.3506E-03	0.0420	0.0370	0.0
142.920	0.7500	0.2788E-03	0.0540	0.0800	0.0
139.280	0.5000	0.1525E-04	0.0387	0.0	0.0
136.750	0.5000	0.4378E-03	0.0320	0.0840	0.0
133.780	0.7500	0.4830E-03	0.0440	0.0060	0.0
131.750	0.5000	0.1568E-02	0.0400	3.7240	0.0
127.510	0.7500	0.4723E-04	0.0387	0.0250	0.0
126.200	0.5000	0.2635E-03	0.0387	0.0200	0.0
123.440	0.7500	0.4500E-04	0.0387	0.0390	0.0
120.990	0.5000	0.3427E-03	0.0350	0.0390	0.0
118.830	0.7500	0.1585E-02	0.0420	0.0430	0.0
116.030	0.5000	0.5022E-03	0.0300	0.2050	0.0
115.100	0.7500	0.1988E-04	0.0400	0.1600	0.0
114.440	0.5000	0.7478E-04	0.0387	1.4560	0.0
110.380	0.7500	0.4188E-04	0.0387	0.0130	0.0
106.670	0.7500	0.8391E-03	0.0400	0.0260	0.0
105.300	0.7500	0.4678E-03	0.0370	0.0060	0.0
102.990	0.7500	0.1590E-03	0.0350	0.0110	0.0
100.250	0.5000	0.5593E-03	0.0387	5.9470	0.0
96.490	0.5000	0.6800E-03	0.0387	1.6450	0.0
95.360	0.7500	0.2150E-03	0.0387	0.0330	0.0
92.970	0.7500	0.7260E-04	0.0470	0.0090	0.0
90.750	0.7500	0.1291E-02	0.0390	0.0090	0.0
85.480	0.5000	0.1276E-02	0.0410	0.0170	0.0
85.320	0.5000	0.3031E-02	0.0387	2.1000	0.0
83.520	0.5000	0.1313E-03	0.0387	1.7060	0.0
82.680	0.5000	0.8248E-04	0.0400	0.0490	0.0
81.760	0.5000	0.6636E-03	0.0387	1.9960	0.0
78.950	0.5000	0.6753E-05	0.0400	0.1400	0.0
74.950	0.7500	0.2657E-02	0.0400	0.0890	0.0
74.050	0.7500	0.3680E-03	0.0360	0.0320	0.0
65.710	0.7500	0.1497E-02	0.0480	0.0700	0.0
65.360	0.5000	0.6679E-04	0.0387	0.0	0.0
63.080	0.7500	0.1007E-03	0.0387	0.1110	0.0
60.940	0.5000	0.1409E-02	0.0387	6.7360	0.0
59.220	0.7500	0.7450E-03	0.0440	0.1400	0.0
58.840	0.5000	0.5866E-03	0.0420	0.8490	0.0
57.440	0.5000	0.9500E-03	0.0560	0.4590	0.0
55.630	0.7500	0.1966E-03	0.0356	0.0230	0.0
52.600	0.7500	0.1443E-02	0.0430	0.0080	0.0
50.080	0.7500	0.4192E-03	0.0420	0.0130	0.0
49.600	0.5000	0.2840E-03	0.0387	0.7460	0.0
47.600	0.5000	0.4276E-03	0.0440	0.2300	0.0
44.480	0.7500	0.9096E-03	0.0440	0.0050	0.0
41.660	0.5000	0.3563E-03	0.0540	0.0500	0.0
41.420	0.7500	0.6422E-03	0.0440	0.0040	0.0
35.500	0.7500	0.5035E-04	0.0400	0.0050	0.0
34.600	0.5000	0.3400E-05	0.0387	0.0	0.0
32.310	0.5000	0.7389E-04	0.0430	0.1100	0.0
27.240	0.5000	0.3832E-04	0.0390	0.0040	0.0
26.240	0.7500	0.2902E-03	0.0370	0.0430	0.0
23.900	0.7500	0.1773E-04	0.0320	0.0410	0.0
22.290	0.7500	0.5366E-03	0.0440	0.0650	0.0
17.660	0.7500	0.4252E-03	0.0430	0.0380	0.0
15.460	0.5000	0.2391E-03	0.0370	0.6620	0.0
14.680	0.7500	0.4872E-03	0.0380	0.0330	0.0
14.310	0.7500	0.1568E-03	0.0370	0.0650	0.0
11.890	0.7500	0.2939E-03	0.0420	0.0240	0.0
11.480	0.7500	0.7674E-04	0.0387	0.0000	-0.13442E-03
10.930	0.7500	0.5544E-03	0.0460	0.1380	0.71302E-04
7.820	0.7500	0.2932E-03	0.0400	0.0470	-0.69812E-05
0.296	0.7500	0.1348E-03	0.0390	0.0600	-0.15061E-04
-1.200	0.7500	0.7038E-03	0.0390	0.2010	0.73758E-04

Table 5.17 Single-level resonance parameters of ^{241}Pu

Energy (eV)	Compound nucleus spin	Reduced neutron width	Capture width	Fission width
0.50400E 02	0.50000E 00	0.79994E-04	0.40000E-01	0.54400E-01
0.48200E 02	0.50000E 00	0.89995E-03	0.40000E-01	0.58370E 00
0.46700E 02	0.50000E 00	0.21994E-03	0.40000E-01	0.21000E 00
0.43200E 02	0.50000E 00	0.30003E-04	0.40000E-01	0.40000E-01
0.42700E 02	0.50000E 00	0.17997E-04	0.40000E-01	0.70000E-01
0.41700E 02	0.50000E 00	0.26001E-03	0.40000E-01	0.18000E 00
0.40800E 02	0.50000E 00	0.13000E-03	0.40000E-01	0.26000E 00
0.40000E 02	0.50000E 00	0.32998E-03	0.40000E-01	0.20000E 00
0.39300E 02	0.50000E 00	0.21997E-03	0.40000E-01	0.15000E 00
0.38200E 02	0.50000E 00	0.18008E-03	0.40000E-01	0.13000E 00
0.36300E 02	0.50000E 00	0.40000E-04	0.40000E-01	0.16000E 00
0.35000E 02	0.50000E 00	0.35006E-03	0.40000E-01	0.70000E 00
0.33700E 02	0.50000E 00	0.19999E-03	0.40000E-01	0.46000E 00
0.33000E 02	0.50000E 00	0.69997E-04	0.40000E-01	0.36000E 00
0.30900E 02	0.50000E 00	0.52008E-03	0.40000E-01	0.31000E 00
0.29400E 02	0.50000E 00	0.13000E-03	0.50000E-01	0.40000E-01
0.28800E 02	0.50000E 00	0.90002E-03	0.40000E-01	0.66000E 00
0.28000E 02	0.50000E 00	0.19994E-04	0.40000E-01	0.11000E 00
0.26400E 02	0.50000E 00	0.86005E-03	0.40000E-01	0.26000E 00
0.24700E 02	0.50000E 00	0.90002E-05	0.40000E-01	0.20000E-01
0.24000E 02	0.50000E 00	0.32007E-03	0.40000E-01	0.18000E 00
0.23700E 02	0.50000E 00	0.58994E-04	0.40000E-01	0.14000E 00
0.23000E 02	0.50000E 00	0.25022E-03	0.40000E-01	0.32000E 00
0.21900E 02	0.50000E 00	0.32010E-04	0.40000E-01	0.59850E-01
0.20700E 02	0.50000E 00	0.74994E-04	0.40000E-01	0.50000E-01
0.20500E 02	0.50000E 00	0.39998E-04	0.30000E-01	0.98200E-02
0.18200E 02	0.50000E 00	0.37012E-04	0.40000E-01	0.26840E-01
0.17830E 02	0.50000E 00	0.75997E-03	0.33000E-01	0.23000E-01
0.16690E 02	0.50000E 00	0.30010E-03	0.40000E-01	0.18000E 00
0.15980E 02	0.50000E 00	0.37999E-03	0.40000E-01	0.46500E 00
0.14750E 02	0.50000E 00	0.16000E-02	0.28000E-01	0.12000E 00
0.13400E 02	0.50000E 00	0.59990E-03	0.30000E-01	0.39000E-01
0.12780E 02	0.50000E 00	0.22001E-03	0.40000E-01	0.23500E 00
0.10100E 02	0.50000E 00	0.47010E-03	0.40000E-01	0.90000E 00
0.95000E 01	0.50000E 00	0.59989E-04	0.40000E-01	0.12000E 00
0.86000E 01	0.50000E 00	0.33002E-03	0.30000E-01	0.80000E-01
0.69300E 01	0.50000E 00	0.27001E-03	0.40000E-01	0.95000E-01
0.59200E 01	0.50000E 00	0.99996E-03	0.40000E-01	0.13500E 01
0.45800E 01	0.50000E 00	0.19999E-03	0.40000E-01	0.16000E 00
0.43000E 01	0.50000E 00	0.32002E-03	0.38000E-01	0.32000E-01
0.26000E 00	0.50000E 00	0.10000E-03	0.35000E-01	0.75000E-01
−0.16000E 00	0.50000E 00	0.72500E-04	0.40000E-01	0.60000E-01

Table 5.18 Dictionary of Nuclides in JFS-2

Nuclide	Code number	Mass	Original data
Be	4	9.0	ENDF/B-IV
^{10}B	105	10.0	UK-70
^{11}B	115	11.0	ENDF/B-IV
C	6	12.0	ENDF/B-IV
O	8	16.0	↓
Na	11	23.0	
Al	13	27.0	
Si	14	28.1	
Cr	24	52.0	
Mn	25	54.9	
Fe	26	55.8	
Ni	28	58.7	
Cu	29	63.5	
Mo	42	96.0	
^{232}Th	902	232.0	
^{233}U	923	233.0	
^{234}U	924	234.0	
^{235}U	925	235.1	JFS-2
^{236}U	926	236.0	ENDF/B-IV
^{238}U	928	238.1	JFS-2
^{239}Pu	949	239.1	↓
^{240}Pu	940	240.1	
^{241}Pu	941	241.1	
^{242}Pu	942	242.1	ENDF/B-IV
^{241}Am	951	241.0	ENDF/B-IV
FP(^{239}Pu)	999	237.0	JENDL-1
FP(^{235}Pu)	995	233.0	JENDL-1

Table 5.19 70-group structure and fission neutron spectrum

Group	Upper energy		Lower energy	DU	Pu-239 CHI (I)	U-235 CHI (I)
1	10.5	(MeV)	8.3	0.2351	0.005900	0.004550
2	8.3	(MeV)	6.5	0.2445	0.017473	0.014450
3	6.5	(MeV)	5.1	0.2426	0.037086	0.032430
4	5.1	(MeV)	4.0	0.2429	0.062499	0.057118
5	4.0	(MeV)	3.1	0.2549	0.091977	0.087111
6	3.1	(MeV)	2.5	0.2151	0.092750	0.090206
7	2.5	(MeV)	1.9	0.2744	0.126361	0.125610
8	1.9	(MeV)	1.4	0.3054	0.135103	0.136994
9	1.4	(MeV)	1.1	0.2412	0.093987	0.096682
10	1.1	(MeV)	0.8	0.3185	0.101534	0.105592
11	0.8	(MeV)	0.63	0.2389	0.059144	0.062034
12	0.63	(MeV)	0.50	0.2311	0.044785	0.047231
13	0.50	(MeV)	0.40	0.2231	0.033398	0.035370
14	0.40	(MeV)	0.31	0.2549	0.028577	0.030370
15	0.31	(MeV)	0.25	0.2151	0.017864	0.019036
16	0.25	(MeV)	0.20	0.2231	0.013882	0.014823
17	0.20	(MeV)	0.15	0.2877	0.012686	0.013570
18	0.15	(MeV)	0.12	0.2231	0.006884	0.007375
19	0.12	(MeV)	0.10	0.1823	0.004219	0.004524
20	100	(KeV)	77.3	0.2575	0.004363	0.004682
21	77.3	(keV)	59.8	0.2567	0.003001	0.003223
22	59.8	(keV)	46.5	0.2516	0.002031	0.002182
23	46.5	(keV)	36.0	0.2559	0.001425	0.001531
24	36.0	(keV)	27.8	0.2585	0.000985	0.001059
25	27.8	(keV)	21.5	0.2570	0.000669	0.000719
26	21.5	(keV)	16.6	0.2587	0.000459	0.000494
27	16.6	(keV)	12.9	0.2522	0.000306	0.000329
28	12.9	(keV)	10.0	0.2546	0.000212	0.000228
29	10.0	(keV)	7.73	0.2575	0.000146	0.000157
30	7.73	(keV)	5.98	0.2567	0.000099	0.000107
31	5.98	(keV)	4.65	0.2516	0.000066	0.000072
32	4.65	(keV)	3.60	0.2559	0.000046	0.000050
33	3.60	(keV)	2.78	0.2585	0.000032	0.000034
34	2.78	(keV)	2.15	0.2570	0.000021	0.000023
35	2.15	(keV)	1.66	0.2587	0.000015	0.000016
36	1.66	(keV)	1.29	0.2522	0.000010	0.000011
37	1.29	(keV)	1.00	0.2546	0.000007	0.000007
38	1000	(ev)	773	0.2575		
39	773	(ev)	598	0.2567		
40	598	(ev)	465	0.2516		
41	465	(ev)	360	0.2559		
42	360	(ev)	278	0.2585		
43	278	(ev)	215	0.2570		
44	215	(ev)	166	0.2587		
45	166	(ev)	129	0.2522		
46	129	(ev)	100	0.2546		
47	100	(ev)	77.3	0.2575		
48	77.3	(ev)	59.8	0.2567		
49	59.8	(ev)	46.5	0.2516		
50	46.5	(ev)	36.0	0.2559		
51	36.0	(ev)	27.8	0.2585		

Table 5.19 (Continued)

52	27.8 (ev)	21.5	0.2570
53	21.5 (ev)	16.6	0.2587
54	16.6 (ev)	12.9	0.2522
55	12.9 (ev)	10.0	0.2546
56	10.0 (ev)	7.73	0.2575
57	7.73 (ev)	5.98	0.2567
58	5.98 (ev)	4.65	0.2516
59	4.65 (ev)	3.60	0.2559
60	3.60 (ev)	2.78	0.2585
61	2.78 (ev)	2.15	0.2570
62	2.15 (ev)	1.66	0.2587
63	1.66 (ev)	1.29	0.2522
64	1.29 (ev)	1.0	0.2546
65	1.00 (ev)	0.773	0.2575
66	0.773 (ev)	0.598	0.2567
67	0.598 (ev)	0.465	0.2516
68	0.465 (ev)	0.360	0.2559
69	0.360 (ev)	0.278	0.2585
70	0.278 (ev)	0.215	0.2570

Table 5.20 25-group structure and fission neutron spectrum

Group	Upper energy	Lower energy	DU	Pu-239 CHI (I)	U-235 CHI (I)
1	10.5 (MeV)	6.5 (MeV)	0.4800	0.023372	0.019000
2	6.5 (MeV)	4.0 (MeV)	0.4800	0.099585	0.089549
3	4.0 (MeV)	2.5 (MeV)	0.4800	0.184727	0.177317
4	2.5 (MeV)	1.4 (MeV)	0.5700	0.261464	0.262604
5	1.4 (MeV)	0.8 (MeV)	0.5700	0.195521	0.202274
6	0.8 (MeV)	0.4 (MeV)	0.6900	0.137327	0.144635
7	0.4 (MeV)	0.2 (MeV)	0.6900	0.060323	0.064229
8	0.2 (MeV)	100 (keV)	0.6900	0.023788	0.025468
9	100 (keV)	46.5 (keV)	0.7700	0.009395	0.010087
10	46.5 (keV)	21.5 (keV)	0.7700	0.003078	0.003310
11	21.5 (keV)	10.0 (keV)	0.7700	0.000977	0.001051
12	10.0 (keV)	4.65 (keV)	0.7700	0.000312	0.000336
13	4.65 (keV)	2.15 (keV)	0.7700	0.000100	0.000107
14	2.15 (keV)	1000 (ev)	0.7700	0.000031	0.000034
15	1000 (ev)	465 (ev)	0.7700		
16	465 (ev)	215 (ev)	0.7700		
17	215 (ev)	100 (ev)	0.7700		
18	100 (ev)	46.5 (ev)	0.7700		
19	46.5 (ev)	21.5 (ev)	0.7700		
20	21.5 (ev)	10.0 (ev)	0.7700		
21	10.0 (ev)	4.65 (ev)	0.7700		
22	4.65 (ev)	2.15 (ev)	0.7700		
23	2.15 (ev)	1.0 (ev)	0.7700		
24	1.0 (ev)	0.465 (ev)	0.7700		
25	0.465 (ev)	0.215 (ev)	0.7700		

Table 5.21 Characteristics of benchmark assemblies

Assembly Name	Fissile Fuel	Fertile to Fissile Ratio	Core Volume(ℓ)	Remarks
VERA-11A	Pu	0.05	12	Pu + C, NoU in core
VERA-1B	U	0.07	30	90% EU + C
ZPR-3-6F	U	1.1	50	
ZPR-3-12	U	3.8	100	U + C
ZPR-3-11	U	7.5	140	
ZEBRA-2	U	6.2	430	U + C
ZPR-6-6A	U	5.0	4,000	L/D = 0.8

Table 5.22 Correction factors to k_{eff} calculated with homogeneous one-dimensional difusion model

	1 to dim.	S_n	Heterogeneous
1 VERA-11A	0.0035	0.0472	0.0*
2 VERA-1B	0.0038	0.0237	0.0*
3 ZPR-3-6F	-0.0028	0.0192	0.0*
4 ZEBRA-3	-0.0006	0.0126	0.0*
5 ZPR-3-12	-0.0009	0.0099	0.0*
6 SNEAK-7A	0.0061	0.0120	-0.0045**
7 ZPR-3-11	0.0001	0.0060	0.0*
8 ZPR-3-54	-0.0164	0.0144	0.0230
9 ZPR-3-53	-0.0150	0.0087	0.0230
10 SNEAK-7B	0.0042	0.0047	-0.0021**
11 ZPR-3-50	-0.0133	0.0056	0.0220
12 ZPR-3-48	-0.0009	0.0064	0.0183
13 ZEBRA-2	-0.0007	0.0033	0.0*
14 ZPR-3-49	-0.0139	0.0068	0.0158
15 ZPR-3-56B	-0.0166	0.0065	0.0102
16 ZPR-6-7	-0.0020	0.0016	0.0166
17 ZPR-6-6A	-0.0013	0.0013	0.0073
18 ZPPR-2	0.0003	0.0024	0.0175
19 MZA	-0.0196	0.0075	0.0140
20 MZB	-0.0186	0.0036	0.0123
21 FCA-V-2	-0.0150	0.0098	0.0024

* The atomic densities and/or sizes were adjusted to account for heterogeneities.

** Includes corrections for cylindricalization, actual control rod position, and heterogeneity.

Table 5.23 Comparison of effective multiplication factors

* Plutonium fuel

No.	Assembly	Experimental	Calculation/Experiment		
			JFS-2-70	ENDF/B-4-70	JFS-2-25
1	VERA-11A	1.00000	0.99234	0.98500 (-0.736)	0.99472 (0.239)
4	ZEBRA-3	1.00000	0.99826	0.99192 (-0.637)	1.00018 (0.192)
6	SNEAK-7A	1.00000	1.00342	0.99344 (-0.993)	1.01155 (1.155)
8	ZPR-3-54	1.00000	0.95477	0.94836 (-0.671)	0.94257 (-1.279)
9	ZPR-3-53	1.00000	0.99838	0.99051 (-0.789)	1.00256 (0.418)
10	SNEAK-7B	1.00000	1.00117	0.99025 (-1.09)	1.00703 (0.585)
11	ZPR-3-50	1.00000	0.99894	0.98952 (-0.943)	1.00903 (1.010)
12	ZPR-3-48	1.00000	1.00345	0.99210 (-1.13)	1.00925 (0.578)
14	ZPR-3-49	1.00000	1.00453	0.99403 (-1.05)	1.01298 (0.836)
15	ZPR3-56B	1.00000	0.99390	0.98199 (-1.12)	0.99190 (-0.201)
16	ZPR-6-7	1.00000	1.00035	0.98545 (-1.51)	0.99952 (-0.082)
18	ZPPR-2	1.00000	1.00568	0.99151 (-1.41)	1.00458 (-0.109)
19	MZA	1.01080	0.99906	0.98596 (-1.31)	1.00184 (0.178)
20	MZB	1.00400	0.99848	0.98373 (-1.48)	0.99813 (-0.035)
21	FCA-5-2	1.00000	0.99276	0.98404 (-0.878)	0.99748 (0.475)
* Average of C/E			0.99637	0.98585 (-1.06)	0.99889 (0.252)
* Stnd. dev. of C/E			0.01179	0.01070	0.01619

Table 5.23 (continued)

* Uranium fuel

No.	Assembly	Experimental	Calculation/Experiment		
			JFS-2-70	ENDF/B-4-70	JFS-2-25
2	VERA-1B	1.00000	1.00360	0.99418 (-0.94)	1.00268 (-0.09)
3	ZPR-3-6F	1.00000	1.01660	1.00831 (-0.82)	1.01719 (0.06)
5	ZPR-3-12	1.00000	1.00697	0.99873 (-0.82)	1.00434 (-0.26)
7	ZPR-3-11	1.00000	1.00800	1.00504 (-0.29)	1.00060 (-0.73)
13	ZEBRA-2	1.00000	0.98523	0.97814 (-0.72)	0.98458 (-0.07)
17	ZPR-6-6A	1.00000	1.00191	0.98946 (-1.2)	0.99946 (-0.24)
* Average of C/E			1.00327	0.99564 (-0.76)	1.00147 (-0.18)
* Stnd. dev. of C/E			0.01002	0.01004	0.00955
Summary of all assemblies					
* Average of C/E			0.99834	0.98865 (-0.97)	0.99963 (0.13)
* Stnd. dev. of C/E			0.01159	0.01141	0.01465

The parentheses show the percent deviations of k_{eff} for ENDF/B-4-70 and JFS-2-25 from JFS-2-70.

Table 5.24 Comparison of C/E of central reaction rate ratio —— σ_f(U-238)/σ_f(U-235)

* Plutonium fuel

No.	Assembly	Experiment	JFS-2-70	ENDF/B-4-70	JFS-2-25
1	VERA-11A	0.07700	1.09495	1.08422	1.11722
4	ZEBRA-3	0.04610	0.98528	0.98668	0.99941
6	SNEAK-7A	0.04480	0.92563	0.92982	0.95416
8	ZPR-3-54	0.02540	1.19479	1.19580	1.29822
9	ZPR-3-53	0.02540	1.14623	1.14877	1.23032
10	SNEAK-7B	0.03300	0.98425	0.99606	1.00225
11	ZPR-3-50	0.02510	1.13434	1.14065	1.19880
12	ZPR-3-48	0.03260	1.01759	1.02168	1.05580
14	ZPR-3-49	0.03450	1.04717	1.05382	1.08488
15	ZPR-3-56	0.03080	0.94983	0.95487	0.97388
16	ZPR-6-7	0.02300	0.91811	0.92602	0.94407
18	ZPPR-2	0.02010	1.05380	1.06233	1.08526
19	MZA	0.03366	0.95778	0.96207	0.97960
20	MZB	0.02256	0.98072	0.98860	1.01134
21	FCA-5-2	0.03960	1.09665	1.10694	1.12023
* Average of C/E			1.03248	1.03722	1.07036
* Stnd. dev. of C/E			0.08275	0.08143	0.10311

* Uranium fuel

No.	Assembly	Experiment	JFS-2-70	ENDF/B-4-70	JFS-2-25
2	VERA-1B	0.06600	1.1502	1.1837	1.1970
3	ZPR-3-6F	0.07800	0.95528	0.98592	0.96396
5	ZPR-3-12	0.04700	1.02970	1.0506	1.0578
7	ZPR-3-11	0.03800	1.02804	1.041927	1.04865
13	ZEBRA-2	0.03200	1.0322	1.04376	1.0727
17	ZPR-6-6A	0.02450	0.92570	0.93025	0.95701
* Average of C/E			1.02019	1.03935	1.0495
* Stnd. dev. of C/E			0.07112	0.0771	0.0798

Table 5.25 Comparison of C/E of central reaction rate ratio —— σ_f(Pu-239)/σ_f(U-235)

*Plutonium fuel

No.	Assembly	Experiment	JFS-2-70	ENDF/B-4-70	JFS-2-25
1	VERA-11A	1.07000	1.07328	1.06678	1.06992
4	ZEBRA-3	1.19000	0.98046	0.98133	0.97416
6	SNEAK-7A	1.01600	0.95284	0.95624	0.95387
8	ZPR-3-54	0.92800	0.94207	0.94565	0.94511
9	ZPR-3-53	0.92800	0.93459	0.93848	0.93489
10	SNEAK-7B	1.01200	0.97507	0.98360	0.97344
11	ZPR-3-50	0.90300	0.97940	0.98426	0.98422
12	ZPR-3-48	0.97600	0.98171	0.98370	0.98307
14	ZPR-3-49	0.98600	0.99460	1.00025	0.99855
15	ZPR-3-56	1.02800	0.93588	0.93982	0.92943
16	ZPR-6-7	0.95300	0.95251	0.95600	0.94862
18	ZPPR-2	0.93700	0.96954	0.97310	0.96590
19	MZA	1.01338	0.96880	0.97221	0.96083
20	MZB	0.94877	0.97039	0.97425	0.96657
21	FCA-5-2	1.10400	0.96256	0.96603	0.95630
* Average of C/E			0.97158	0.97478	0.96966
* Stnd. dev. of C/E			0.03209	0.03008	0.03237

* Uranium fuel

No.	Assembly	Experiment	JFS-2-70	ENDF/B-4-70	JFS-2-25
2	VERA-1B	1.07000	1.05874	1.06557	1.07359
3	ZPR-3-6F	1.22000	1.01433	1.01795	1.00855
5	ZPR-3-12	1.12000	0.98667	0.99356	0.99414
7	ZPR-3-11	1.19000	0.97593	0.98092	0.97295
13	ZEBRA-2	0.98700	0.9986	1.00670	1.02137
17	ZPR-6-6A	——	——	——	——
* Average of C/E			1.00686	1.01292	1.01412
* Stnd. dev. of C/E			0.02891	0.02913	0.03380

Table 5.26 Comparison of C/E of central reaction rate ratio —— σ_c(U-238)/σ_f(Pu-239)

* Plutonium fuel

No.	Assembly	Experiment	JFS-2-70	ENDF/B-4-70	JFS-2-25
1	VERA-11A	——	——	——	——
4	ZEBRA-3	——	——	——	——
6	SNEAK-7A	0.13500	1.01149	1.02853	0.99623
8	ZPR-3-54	——	——	——	——
9	ZPR-3-53	——	——	——	——
10	SNEAK-7B	0.12900	1.03107	1.05126	1.02007
11	ZPR-3-50	——	——	——	——
12	ZPR-3-48	0.14100	0.97129	0.98499	0.96249
14	ZPR-3-49	——	——	——	——
15	ZPR-3-56	——	——	——	——
16	ZPR-6-7	0.14300	1.06177	1.07992	1.06461
18	ZPPR-2	——	——	——	——
19	MZA	0.12970	1.04606	1.06306	1.05885
20	MZB	0.14240	1.04639	1.06437	1.05072
21	FCA-5-2	0.12680	0.94026	0.95403	0.95285
* Average of C/E			1.01547	1.03231	1.01512
* Stnd. dev. of C/E			0.04124	0.04306	0.04252

* Uranium fuel

No.	Assembly	Experiment	JFS-2-70	ENDF/B-4-70	JFS-2-25
2	VERA-1B	0.12200	0.91153	0.91573	0.90249
3	ZPR-3-6F	0.08500	0.97616	0.94308	0.99583
5	ZPR-3-12	0.11000	0.98646	0.99091	0.97469
7	ZPR-3-11	0.09400	1.02183	1.00653	1.03388
13	ZEBRA-2	0.13800	0.96522	0.97995	0.93023
17	ZPR-6-6A	——	——	——	——
* Average of C/E			0.97224	0.96724	0.96742
* Stnd. dev. of C/E			0.03581	0.03317	0.04660

Table 5.27 Comparison of C/E of central reaction rate ratio —— σ_c(U-238)/σ_f(U-235)

*Plutonium fuel

No.	Assembly	Experiment	JFS-2-70	ENDF/B-4-70	JFS-2-25
1	VERA-11A	——	——	——	——
4	ZEBRA-3	——	——	——	——
6	SNEAK-7A	0.13760	0.96070	0.98037	0.94723
8	ZPR-3-54	——	——	——	——
9	ZPR-3-53	——	——	——	——
10	SNEAK-7B	0.13100	1.00189	1.03045	0.98956
11	ZPR-3-50	——	——	——	——
12	ZPR-3-48	0.13800	0.95087	0.96623	0.94355
14	ZPR-3-49	——	——	——	——
15	ZPR-3-56	——	——	——	——
16	ZPR-6-7	0.13600	1.01342	1.03453	1.01198
18	ZPPR-2	——	——	——	——
19	MZA	0.13143	1.01343	1.03352	1.01738
20	MZB	0.13510	1.01541	1.03697	1.01560
21	FCA-5-2	0.14000	0.90497	0.92154	0.91113
* Average of C/E			0.98010	1.00051	0.97663
* Stnd. dev. of C/E			0.03931	0.04190	0.03936

* Uranium fuel

No.	Assembly	Experiment	JFS-2-70	ENDF/B-4-70	JFS-2-25
2	VERA-1B	0.13100	0.96169	0.9685	0.9617
3	ZPR-3-6F	0.10400	0.9873	0.9550	0.9991
5	ZPR-3-12	0.12300	0.97489	0.98364	0.96808
7	ZPR-3-11	0.11200	0.99599	0.98452	1.0031
13	ZEBRA-2	0.13600	0.96533	0.98574	0.94934
17	ZPR-6-6A	0.13900	0.99856	1.0214	1.0004
* Average of C/E			0.98063	0.9831	0.98029
* Stnd. dev. of C/E			0.01430	0.0203	0.02130

Table 5.28 Comparison of C/E of central reaction rate ratio —— σ_f(Pu-240)/σ_f(U-235)

* Plutonium fuel

No.	Assembly	Experiment	JFS-2-70	ENDF/B-4-70	JFS-2-25
1	VERA-11A	0.47500	1.03237	1.03091	1.03507
4	ZEBRA-3	0.37300	1.01187	0.99521	1.02084
6	SNEAK-7A	——	——	——	——
8	ZPR-3-54	0.17400	1.18133	1.16361	1.23633
9	ZPR-3-53	0.17400	1.14028	1.12306	1.18185
10	SNEAK-7B	——	——	——	——
11	ZPR-3-50	0.15900	1.30269	1.26498	1.35072
12	ZPR-3-48	0.24300	1.04624	1.01263	1.07214
14	ZPR-3-49	——	——	——	——
15	ZPR-3-56	0.28200	0.85060	0.81448	0.84532
16	ZPR-6-7	——	——	——	——
18	ZPPR-2	0.17000	1.11126	1.04369	1.11046
19	MZA	0.25993	0.99723	0.96307	0.99162
20	MZB	0.19193	1.02836	0.96965	1.03041
21	FCA-5-2	——	——	——	——
* Average of C/E			1.07022	1.03813	1.08748
* Stnd. dev. of C/E			0.11563	0.11719	0.13394

* Uranium fuel

No.	Assembly	Experiment	JFS-2-70	ENDF/B-4-70	JFS-2-25
2	VERA-1B	0.39900	1.1470	1.1899	1.1666
3	ZPR-3-6F	0.53000	0.9618	0.99852	0.95608
5	ZPR-3-12	——	——	——	——
7	ZPR-3-11	0.34000	1.0395	1.0323	1.0572
13	ZEBRA-2	0.23700	1.0955	1.0606	1.1349
17	ZPR-6-6A	——	——	——	——
* Average of C/E			1.0610	1.0703	1.0787
* Stnd. dev. of C/E			0.0687	0.0724	0.0812

Table 5.29 Comparison of central sample worth of ^{239}Pu

Assembly	Fuel	Experiment (Inhour/kg)	Inhour/kg / %Δk/k	C/E	
				JFS-2-70	ENDF/B-4-70
VERA-1B	U	674	376.9	0.877	0.88
ZPR-3-6F	U	452	407.2	0.983	0.99
ZEBRA-3	Pu	1,144	837.9	1.18	1.18
ZPR-3-12	U	436	427.6	0.957	0.97
SNEAK-7A	Pu	1,023	911.8	1.04	1.05
ZPR-3-11	U	411	462.6	0.989	0.99
ZPR-3-54	Pu	738	968.8	1.44	1.48
ZPR-3-53	Pu	681	950.3	1.20	1.22
SNEAK-7B	Pu	584	843.7	1.05	1.06
ZPR-3-50	Pu	564	930.1	1.14	1.15
ZPR-3-48	Pu	445	932.5	1.17	1.18
ZEBRA-2	U	195	442.3	1.08	1.08
ZPR-3-49	Pu	415	934.4	1.10	1.11
ZPR-3-56	Pu	372	975.6	1.27	1.30
ZPR-6-7	Pu	158	972.5	1.21	1.23
ZPR-6-6A	U	57	431.9	1.05	1.04
Average of C/E				1.11	1.12
Stand. dev. of C/E				0.13	0.14

Table 5.30 Comparison of C/E for sample worths of ^{235}U and ^{238}U normalized to those of ^{239}Pu

Assembly	U-235			U-238		
	JFS-2-70	ENDF/B-4-70	JFS-2-25	JFS-2-70	ENDF/B-4-70	JFS-2-25
VERA-1B	1.0059	0.9866	1.0054	1.6340	1.7660	1.6676
ZPR-3-6F	0.8341	0.8280	0.8346	——	——	——
ZEBRA-3	1.0141	1.0209	1.0196	0.9749	0.9575	0.9804
ZPR-3-12	1.0064	1.0075	1.0027	0.9736	0.9694	0.9482
SNEAK-7A	0.9853	1.0048	0.9755	1.0928	1.0986	1.0701
ZPR-3-11	1.0521	1.0562	1.0555	1.0232	1.0144	1.0316
ZPR-3-54	0.9705	1.0212	0.9618	0.7583	0.7823	0.6763
ZPR-3-53	0.9720	1.0289	0.9633	0.8909	0.9161	0.8333
SNEAK-7B	1.0198	1.0267	1.0157	1.0865	1.0854	1.0877
ZPR-3-50	0.9676	1.0005	0.9540	0.8781	0.8869	0.8363
ZPR-3-48	0.9977	1.0186	0.9896	0.9068	0.9013	0.8898
ZEBRA-2	1.0146	1.0224	1.0001	0.9027	0.9421	0.8658
ZPR-3-49	1.0727	1.0875	1.0612	0.9998	0.9974	0.9792
ZPR-3-56	0.9558	0.9725	0.9568	1.0120	1.0039	1.0127
ZPR-6-7	0.9735	0.9945	0.9717	0.8590	0.8497	0.8628
ZPR-6-6A	1.0227	1.0370	1.0190	1.0161	1.0773	1.0107
Average of C/E	0.992	1.007	0.987	1.0006	1.0165	0.9835
Stand. dev. of C/E	0.0572	0.0588	0.0572	0.1904	0.2178	0.2109

Table 5.31 Comparison of C/E for sample worths of ^{10}B and Mo normalized to those of ^{239}Pu

Assembly	B-10			Mo		
	JFS-2-70	ENDF/B-4-70	JFS-2-25	JFS-2-70	ENDF/B-4-70	JFS-2-25
VERA-1B	1.0640	1.0485	1.0414	——	——	——
ZPR-3-6F	0.9866	0.9595	1.0434	1.2766	1.3045	1.3494
ZEBRA-3	0.8840	0.8743	0.9053	——	——	——
ZPR-3-12	——	——	——	1.2060	1.2329	1.2290
SNEAK-7A	1.0100	0.9552	1.0313	——	——	——
ZPR-3-11	0.9521	0.9312	0.9723	1.2046	1.2358	1.2248
ZPR-3-54	0.6679	0.6454	0.6335	——	——	——
ZPR-3-53	0.7243	0.6999	0.6994	——	——	——
SNEAK-7B	1.0093	0.9582	1.0535	——	——	——
ZPR-3-50	0.8852	0.8464	0.8657	——	——	——
ZPR-3-48	0.9058	0.8585	0.9140	1.2669	1.2656	1.2654
ZEBRA-2	0.7490	0.7500	0.7370	——	——	——
ZPR-3-49	0.9555	0.9064	0.9628	——	——	——
ZPR-3-56	0.8705	0.8187	0.9090	——	——	——
ZPR-6-7	1.0049	0.9443	1.0445	1.2796	1.2692	1.3021
ZPR-6-6A	0.8973	0.9120	0.9133	——	——	——
Average of C/E	0.9044	0.8739	0.915	1.246	1.26	1.274
Stand. dev. of C/E	0.1090	0.1021	0.1271	0.0505	0.0536	0.0607

Table 5.32 Comparison of C/E for sample worths of sodium and iron normalized to those of ^{239}Pu

Assembly	Na			Fe		
	JFS-2-70	ENDF/B-4-70	JFS-2-25	JFS-2-70	ENDF/B-4-70	JFS-2-25
VERA-1B	4.0428	3.9778	3.8569	——	——	——
ZPR-3-6F	0.4178	0.3539	0.3619	1.1324	1.3170	0.7896
ZEBRA-3	0.9575	1.0551	1.1181	——	——	——
ZPR-3-12	——	——	——	1.2501	1.3297	1.2556
SNEAK-7A	——	——	——	0.7762	0.8207	0.7938
ZPR-3-11	1.4293	1.7061	1.6563	1.2451	1.3430	1.2389
ZPR-3-54	——	——	——	——	——	——
ZPR-3-53	1.4401	1.0442	0.5253	1.1704	1.1111	1.4540
SNEAK-7B	——	——	——	1.0180	1.0503	1.0321
ZPR-3-50	0.4258	0.2435	-0.0087	1.1266	1.1435	1.2182
ZPR-3-48	1.6351	1.8660	1.6352	1.0187	1.0587	1.0532
ZEBRA-2	2.5311	3.6555	-0.6232	1.2409	1.2514	1.3728
ZPR-3-49	0.7194	-0.6642	-0.9092	0.9239	0.9561	0.9391
ZPR-3-56	1.7200	1.8920	1.6515	0.8148	0.8513	0.8235
ZPR-6-7	0.9638	0.9969	0.9346	0.9269	0.9509	0.9649
ZPR-6-6A	-2.0457	0.2637	-2.0355	——	——	——
Average of C/E	1.188	1.3682	0.678	1.054	1.099	1.078
Stand. dev. of C/E	1.31	1.26	1.39	0.155	0.171	0.210

Table 5.33 Main characteristics of critical assemblies used for analysis of Doppler reactivity effect

Assembly	Fuel	$R=\frac{\text{Fertile N}}{\text{Fissile N}}$	Core volume (l)	Doppler sample	
				Material	Size (cm)
FAC-V-1	Pu, U	2.6	145	NUO_2	2.5ϕ, 15L
FAC-VI-1	Pu, U	$R_1=4.3$, $R_0=3.0$	223	NUO_2	2.5ϕ, 15L
FCA-VI-2	Pu, U	$R_1=6.9$, $R_0=2.5$	246	NUO_2	2.5ϕ, 15L
SEFOR	Pu	4.3	558	All core on power	
ZPPR-2 (L. 90)	Pu	$R_1=6.5$, $R_0=4.0$	2400	NUO_2	2.54ϕ, 30.48L
ZPPR-3 (Phase. 3)	Pu	$R_1=4.9$, $R_0=3.3$	2400	NUO_2	2.54ϕ, 30.48L
ZPR-6-7	Pu	$R_1=6.5$, $R_0=6.5$	3120	NUO_2	2.54ϕ, 30.48L

R_1 and R_0 mean the atomic density ratio of fertile materials to fissile materials in the inner and outer cores, respectively.

Table 5.34 Atomic compositions of Doppler sample NUO_2 and sample buffer

(10^{24} atoms/cc)

	JAERI		ANL	
	NUO_2	Buffer	NUO_2	Buffer
U-235	1.503 –4		1.0 –4	
U-238	2.0632–2		1.56–2	
O	4.156 –2		3.14–2	
Cr		6.15 –3		1.2385–2
Fe		2.239–2		4.7278–2
Ni		2.681–3		6.71 –3
Al				7.58 –4

Table 5.35 Group structures of 25 and 70 energy groups used for Doppler effect calculations

25 group	70 group	Lower energy	
1	10	800	(keV)
2	16	200	(keV)
3	22	46.5	(keV)
4	23	36.0	(keV)
5	24	27.8	(keV)
6	25	21.5	(keV)
7	26	16.6	(keV)
8	27	12.9	(keV)
9	28	10.0	(keV)
10	29	7.73	(keV)
11	30	5.98	(keV)
12	31	4.65	(keV)
13	32	3.6	(keV)
14	33	2.78	(keV)
15	34	2.15	(keV)
16	35	1.66	(keV)
17	36	1.29	(keV)
18	37	1.0	(keV)
19	38	773	(eV)
20	39	598	(eV)
21	40	465	(eV)
22	43	215	(eV)
23	49	46.5	(eV)
24	55	10.0	(eV)
25	70	0.215	(eV)

Table 5.36 Doppler effects of NUO_2 obtained by 2-dimensional R-Z first order perturbation calculation in FCA assemblies V-1, VI-1 and VI-2

Assembly		Doppler effect, $-\Delta k/k \times 10^6$		
		Exp.	Homo	Hetero
FCA-V-1	k_{eff}	1.00	0.99852	1.00182
	300– 600°k	4.66	3.78 (0.81)	4.08 (0.88)
	300– 850°k	7.12	5.98 (0.84)	6.42 (0.90)
	300–1100°k	9.18	7.54 (0.82)	8.07 (0.88)
FCA-VI-1	k_{eff}	1.00	0.9917	0.99839
	300– 650°k	5.19	5.09 (0.98)	5.29 (1.02)
	300– 850°k	7.51	7.21 (0.96)	7.50 (1.00)
	300–1100°k	9.38	9.26 (0.99)	9.64 (1.03)
FCA-VI-2	k_{eff}	1.00	0.99849	1.00634
	300– 850°k	6.83	6.47 (0.95)	6.87 (1.01)
	300–1100°k	8.78	8.35 (0.95)	8.89 (1.01)

The C/E values are presented in the parentheses.

Table 5.37 Doppler effects of NUO_2 obtained by 2-dimensional R-Z first order perturbation calculation in ZPR-6-7

	T(°K)	Doppler effect, $-\Delta k/k \times 10^6$ Exp.	Homo	Hetero
Ref. core	494	3.154	2.66	3.24
			(0.85)	(1.03)
	771	6.393	5.25	6.46
			(0.82)	(1.01)
	1075	9.158	7.28	9.02
			(0.79)	(0.99)
H240 core	507	3.416	2.78	3.30
			(0.81)	(0.97)
	792	6.80	5.42	6.49
			(0.80)	(0.95)
	1054	9.413	7.18	8.66
			(0.76)	(0.92)

C/E values are presented in the parentheses; $\%\Delta k/k = 1033$ lh for Ref. core and 1027 lh for H240 core.

Table 5.38 Comparison of NUO_2 Doppler effects in the normal inner core plate of ZPPR assembly 2 (2-dimensional R-Z first order perturbation calculation)

Temperature (°K)	Doppler effect, $\Delta k/k \times 10^6$ Experiment			Calculation					
				Homo		Hetero		Homo/Hetero	
	rod	plate	rod/plate	cal.	cal/rod	cal.	cal/plate	cal	C/E
Cold worth	-71.9 ± 0.1	-72.62 ± 0.22	0.990	−78.61	1.09	−82.79	1.18	0.950	0.96
300– 500	-2.11 ± 0.1	-2.41 ± 0.09	0.876	−2.03	0.96	−2.24	0.93	0.906	1.03
300– 800	-4.55 ± 0.1	-4.93 ± 0.1	0.923	−4.18	0.92	−4.62	0.94	0.906	0.982
300–1100	-6.00 ± 0.1	-6.76 ± 0.1	0.888	−5.73	0.95	−6.36	0.94	0.901	1.01

$\%\ \Delta k/k = 998.49$ lh

Table 5.39 Comparison of NUO_2 Doppler effects in the Na-voided inner core plate of ZPPR assembly 2
(2-dimensional R-Z first order perturbation calculation)

Temperature (°K)	Doppler effect, $\Delta k/k \times 10^6$								
	Experiment			Calculation					
				Homo		Hetero		Homo/Hetero	
	rod	plate	rod/plate	cal.	cal/rod	cal.	cal/plate	cal.	C/E
Cold worth	−64.52	−70.1±0.22	0.920	−69.65	1.08	−70.98	1.01	0.981	1.07
300– 500	−1.546±0.12	−1.632±0.10	0.947	−1.456	0.94	−1.626	0.99	0.895	0.95
300– 800	−3.121±0.12	−3.296±0.13	0.947	−2.961	0.95	−3.335	1.01	0.888	0.94
300–1100	−4.536±0.12	−4.514±0.12	1.005	−4.022	0.89	−4.559	1.01	0.882	0.88

Table 5.40 Comparison of NUO_2 Doppler effect at different axial positions in the normal plate core of ZPPR assembly 2
(2-dimensional R-Z first order perturbation calculation)

Temperature (°K)	Doppler effect, $\Delta k/k \times 10^5$								
	$Z=0$			$Z=12$ inch up			$Z=24$ inch up		
	Exp.	cal.	C/E	Exp.	cal.	C/E	Exp.	cal.	C/E
300– 500	−2.41±0.1	−2.24	0.93	−1.52±0.1	−1.36	0.89	−0.348±0.1	−0.199	0.57
300– 800	−4.93±0.1	−4.62	0.94	−3.39±0.1	−2.81	0.83	−0.424±0.1	−0.411	0.97
300–1100	−6.76±0.1	−6.36	0.94	−4.60±0.1	−3.88	0.84	−0.635±0.1	−0.557	0.88

Table 5.41 Comparison of NUO_2 Doppler effect in the normal configuration of ZPPR assembly 3 phase 3. Three dimensional perturbation calculation of 18 energy groups

Temperature (°C)	Doppler effect ($\Delta k/k \times 10^6$)				
	Experiment	Calculation		Cal./Exp.	
		model 1	model 2	model 1	model 2
Position 1					
500	−1.004 ± 0.032	−0.894	−1.009	0.89	1.00
650	−1.545 ± 0.033	−1.40	−1.587	0.91	1.03
800	−1.928 ± 0.033	−1.82	−2.065	0.94	1.07
950	−2.327 ± 0.033	−2.18	−2.469	0.94	1.06
1100	−2.662 ± 0.032	−2.48	−2.814	0.93	1.06
Position 2					
500	−1.690 ± 0.033	−1.352	(−1.526)	0.80	(0.90)
650	−2.633 ± 0.033	−2.138	(−2.424)	0.81	(0.92)
800	−3.485 ± 0.034	−2.786	(−3.161)	0.80	(0.91)
950	−4.157 ± 0.034	−3.341	(−3.784)	0.80	(0.91)
1100	−4.653 ± 0.034	−3.817	(−4.331)	0.82	(0.93)
Position 3					
500	−1.913 ± 0.032	−1.620	(−1.828)	0.85	(0.96)
650	−2.922 ± 0.034	−2.559	(−2.900)	0.88	(1.00)
800	−3.760 ± 0.034	−3.344	(−3.794)	0.89	(1.01)
950	−4.472 ± 0.035	−4.018	(−4.551)	0.90	(1.02)
1100	−5.097 ± 0.034	−4.595	(−5.214)	0.90	(1.02)

Positions are: 1) adjacent to CR, 3) adjacent to CRP and 2) midway between CR and CRP.

Parentheses show the values estimated from the results of the model 1 and model 2 at position-1.

% $\Delta k/k$ = 1051.6 Ih

Table 5.42 Analysis of full core isothermal Doppler effect in SEFOR assembly

		Spherical model	R-Z model
k_{eff}	Calculation	1.02643	1.00211
	Correction	-0.00149	-0.00149
	Corrected	1.02494	1.00061
$T\frac{dk}{dT}$	Experiment	-0.0081 (-0.00891)* ±0.001	-0.0081 (-0.00891)* ±0.001
	Calculation	-0.00784	-0.00844
	Correction	-0.00065	-0.00065
	Corrected	-0.00849	-0.00909
	C/E	1.05 (0.953)*	1.12 (1.02)*

* Recent results obtained with the modified β_{eff} (176)

Table 5.43 Comparison of NUO_2 Doppler effects calculated with JFS-1R, 2 and ENDF/B-IV (1-dimensional spherical diffusion, first order perturbation calculation)

Assembly	T (°K)	Exp.	Doppler effect, $\Delta K/K \times 10^6$						JFS-2/JFS-1R
			JFS-1R		JFS-2		ENDF/B-4-70		
			Cal.	C/E	Cal.	C/E	Cal.	C/E	
FCA-V-1	300- 600	-4.66±0.1	-3.18	0.68	-3.76	0.81	-4.14	0.89	1.18
	300- 850	-7.12±0.1	-5.03	0.71	-5.92	0.83	-6.57	0.92	1.18
	300-1100	-9.18±0.2	-6.35	0.69	-7.44	0.81	-8.31	0.91	1.17
FCA-VI-1	300- 650	-5.19±0.34	-4.47	0.86	-4.96	0.96	-4.82	0.93	1.11
	300- 850	-7.51±0.33	-6.36	0.85	-7.02	0.93	-6.86	0.91	1.10
	300-1100	-9.38±0.4	-8.20	0.87	-9.01	0.96	-8.82	0.94	1.10
FCA-VI-2	300- 850	-6.83±0.1	-5.83	0.85	-6.20	0.91	-5.90	0.86	1.06
	300-1100	-8.78±0.1	-7.58	0.86	-8.02	0.91	-7.65	0.87	1.06
ZPPR-2	300- 500	-2.11±0.1	-2.11	1.00	-2.28	1.08	-2.23	0.93	1.08
(Normal)	300- 800	-4.55±0.1	-4.37	0.96	-4.65	1.02	-4.61	0.94	1.06
	300-1100	-6.00±0.1	-6.00	1.00	-6.37	1.06	-6.31	0.93	1.06
ZPPR-2	300- 500	-1.55±0.1	-1.13	0.73	-1.33	0.85	-1.33	0.82	1.18
(Na-void)	300- 800	-3.12±0.12	-1.27	0.73	-2.66	0.85	-2.69	0.82	1.17
	300-1100	-4.54±0.12	-3.04	0.67	-3.58	0.79	-3.63	0.80	1.17

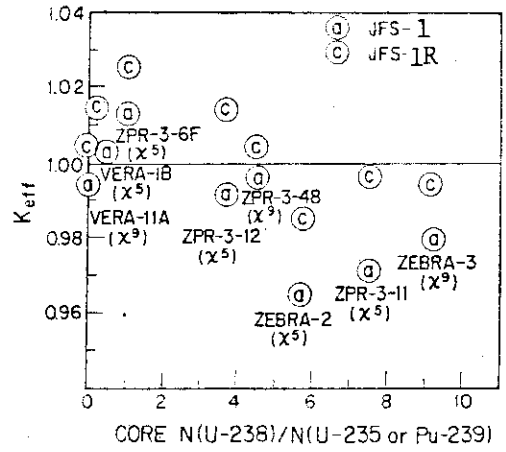

Fig.5.1 Comparison of effective multiplication factors. The symbols ⓐ and ⓒ indicate the results calculated by using JFS-1 and JFS-1R, respectively (χ^5 and χ^9 stand for the fission spectrum of ^{235}U and ^{239}Pu, respectively).

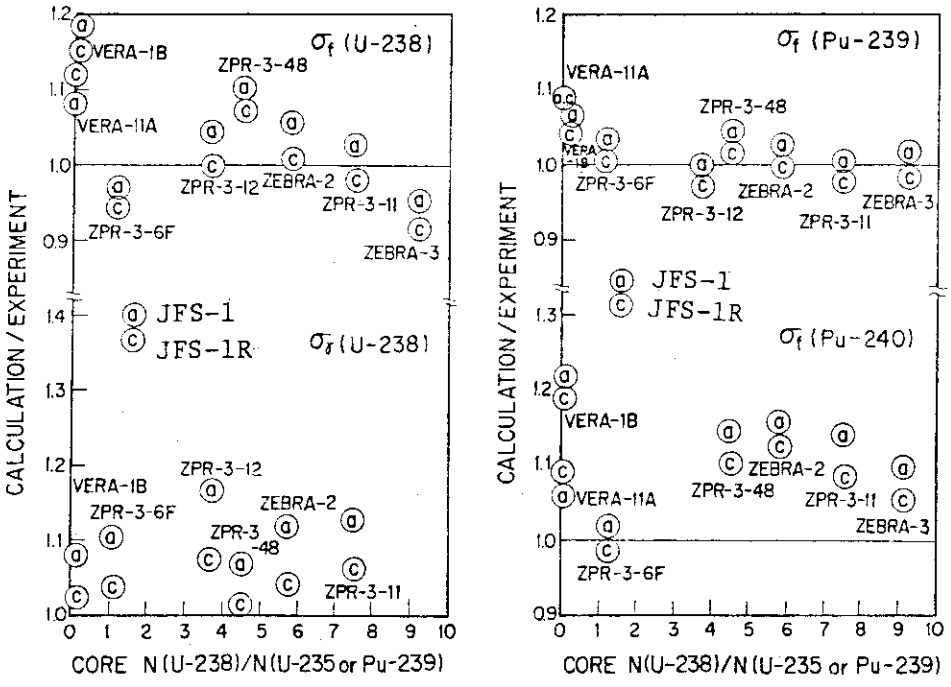

Fig.5.2 Comparison of spectral indices. The symbol ⓐ and ⓒ indicate the results calculated by using JFS-1 and JFS-1R, respectively.

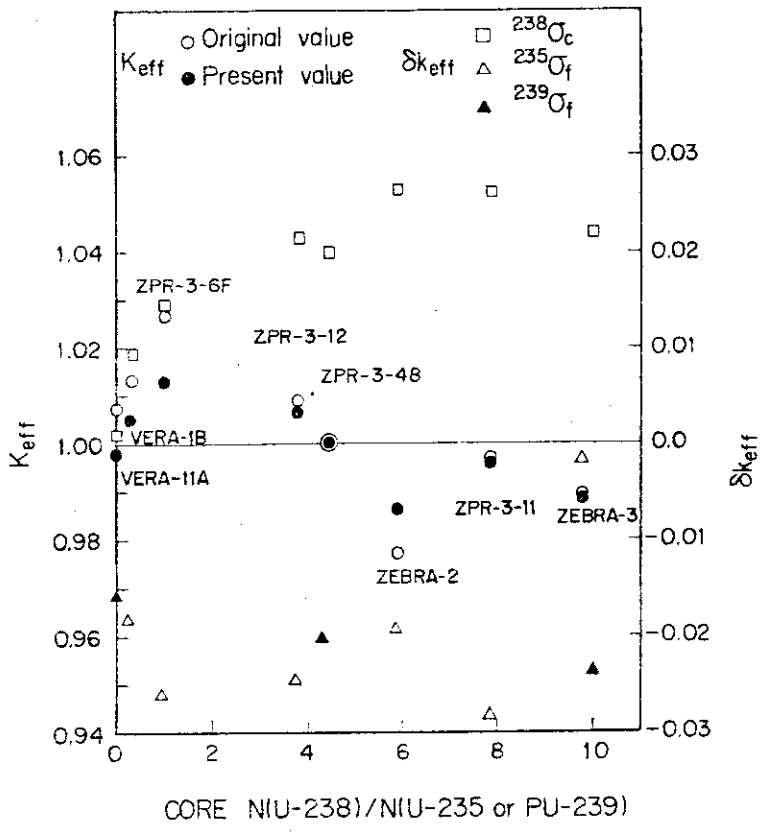

Fig.5.3 Adjusted effective multiplication factors and the contribution from the adjusted cross sections to k_{eff}.

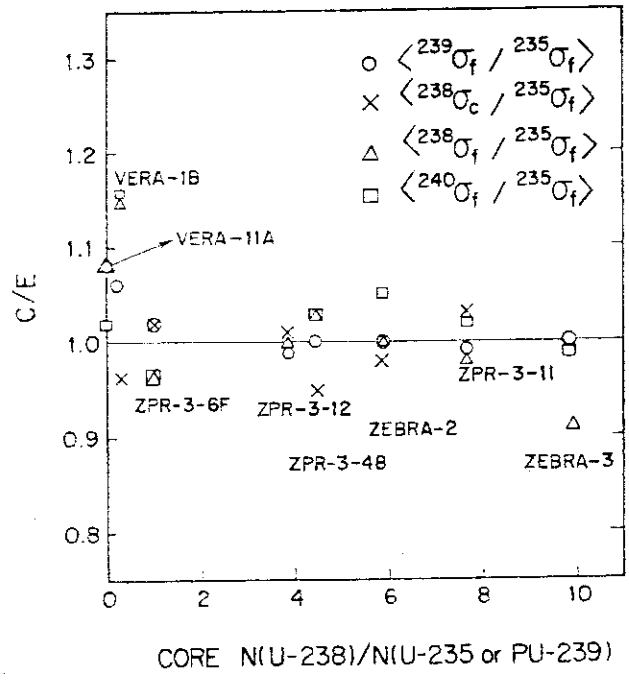

Fig.5.4 Spectral indices calculated from the adjusted cross sections.

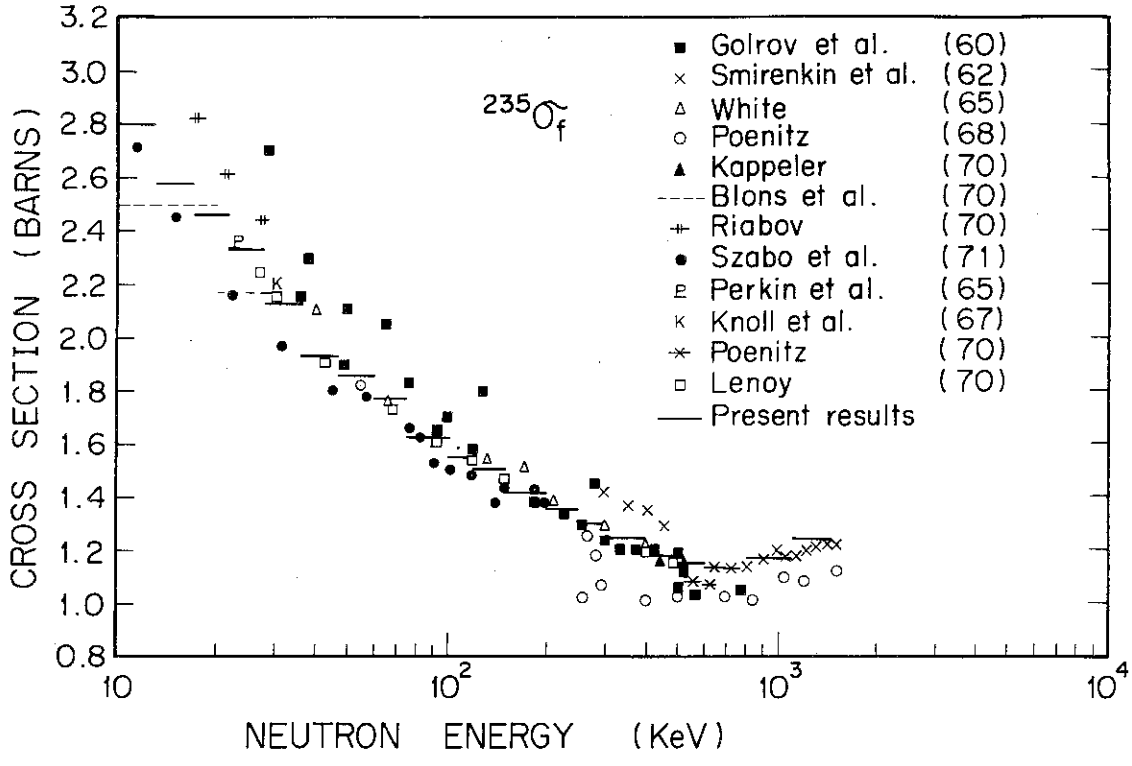

Fig. 5.5 Comparison of fission cross sections for ^{235}U.

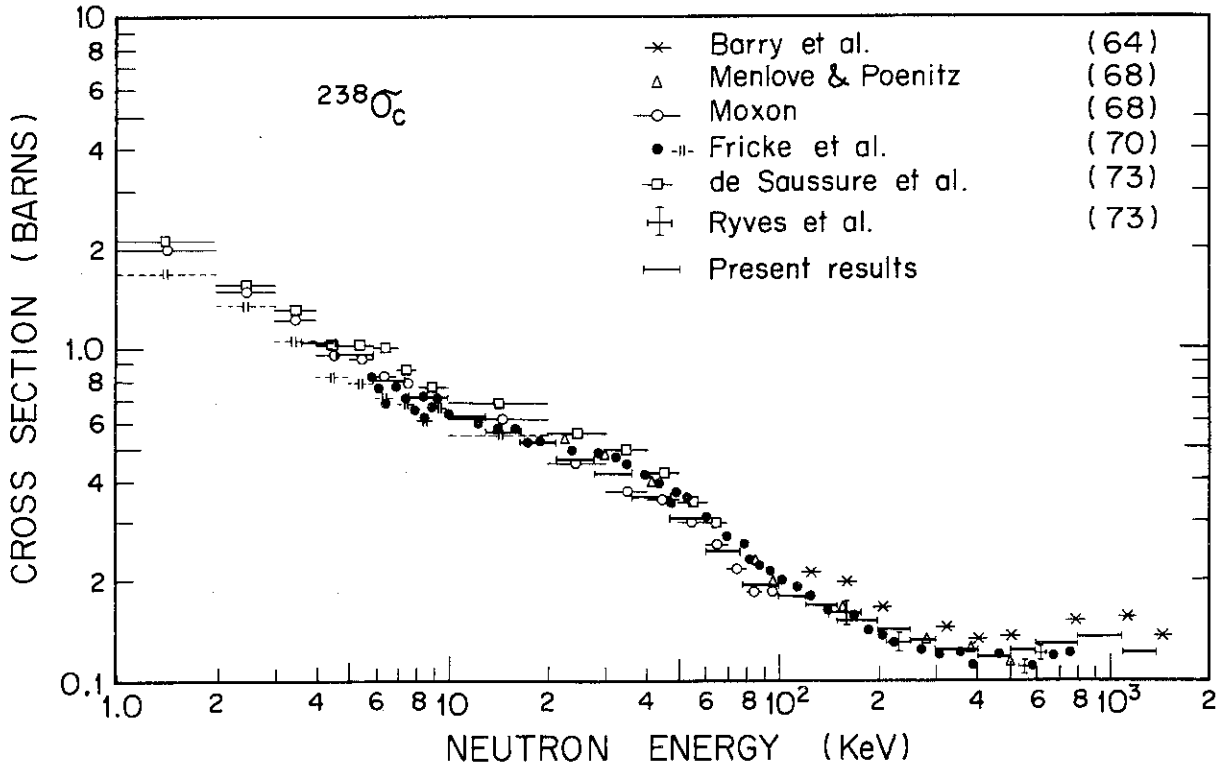

Fig. 5.6 Comparison of capture cross sections for ^{238}U.

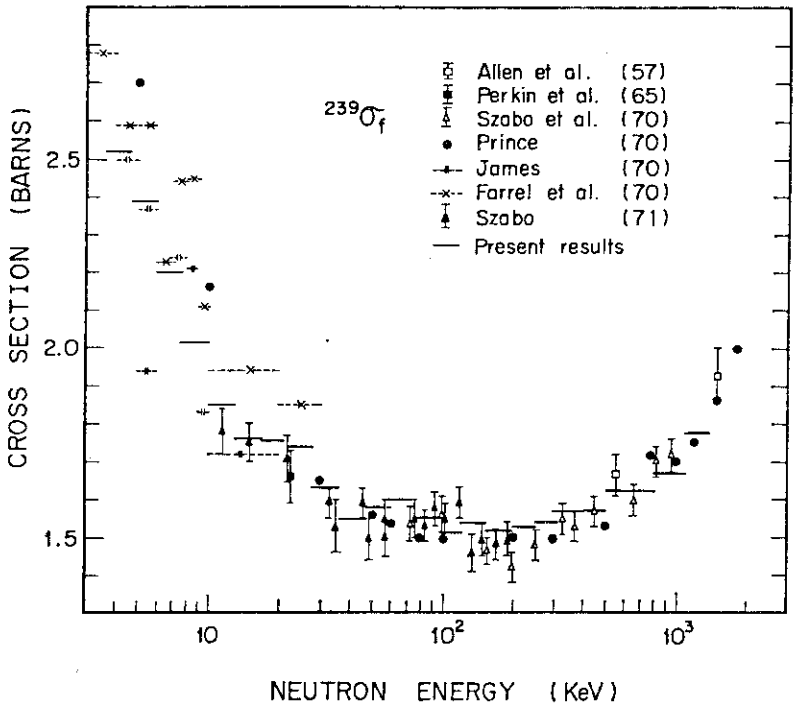

Fig.5.7 Comparison fission cross sections for ^{239}Pu.

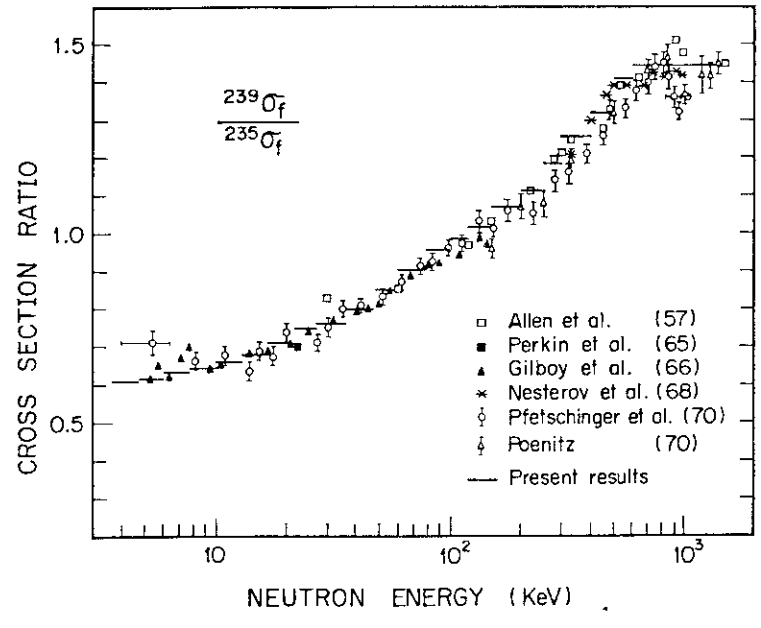

Fig.5.8 Comparison of relative ratios, $^{239}\sigma_f/^{235}\sigma_f$.

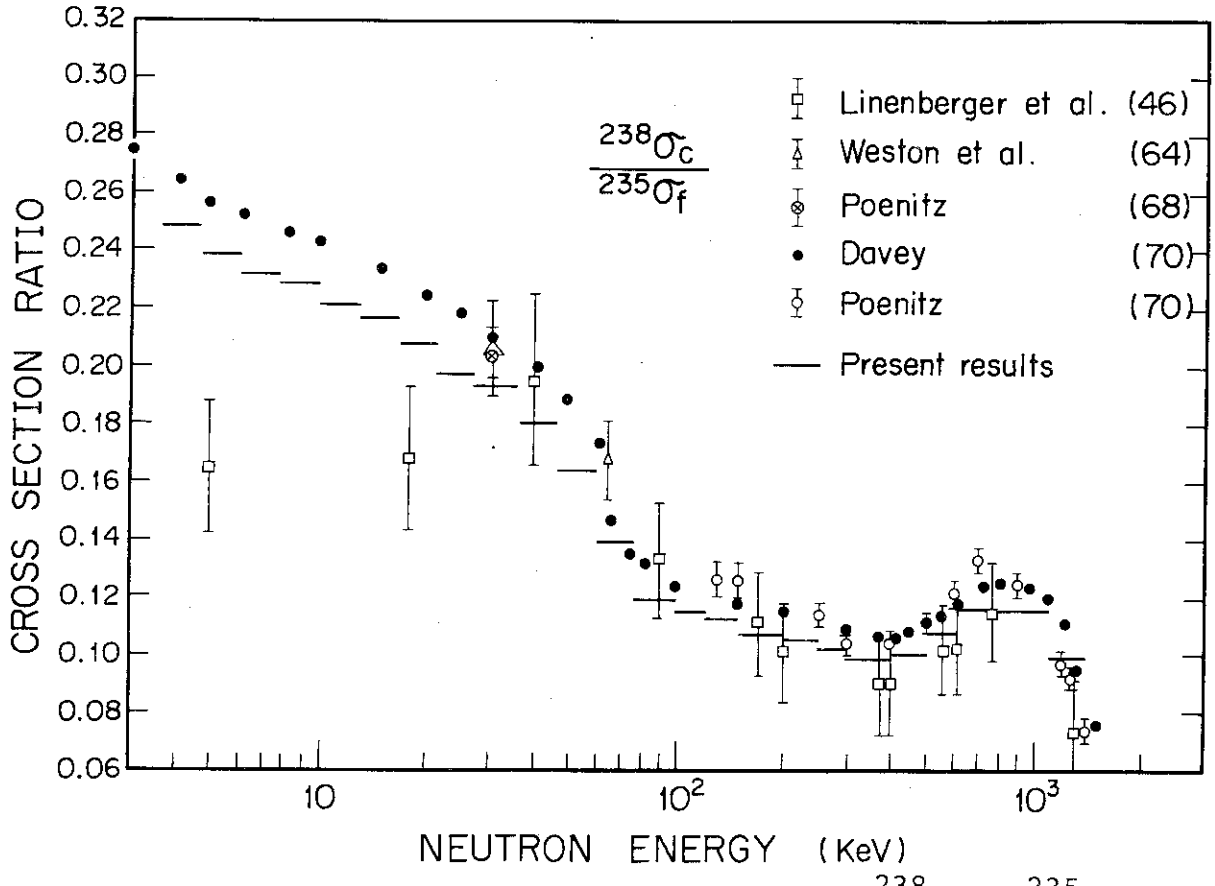

Fig. 5.9 Comparison of relative ratios, $^{238}\sigma_c$ / $^{235}\sigma_f$.

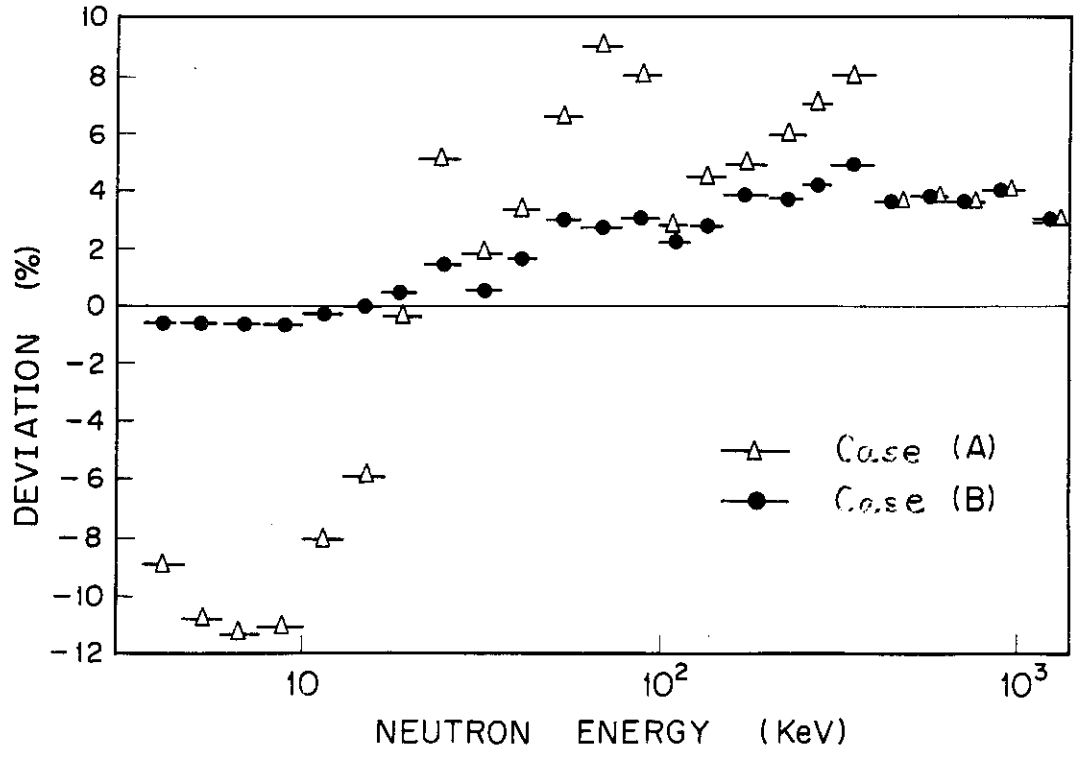

Fig. 5.10 Deviation of adjusted $^{239}\sigma_f$ / $^{235}\sigma_f$ from measured reference values.

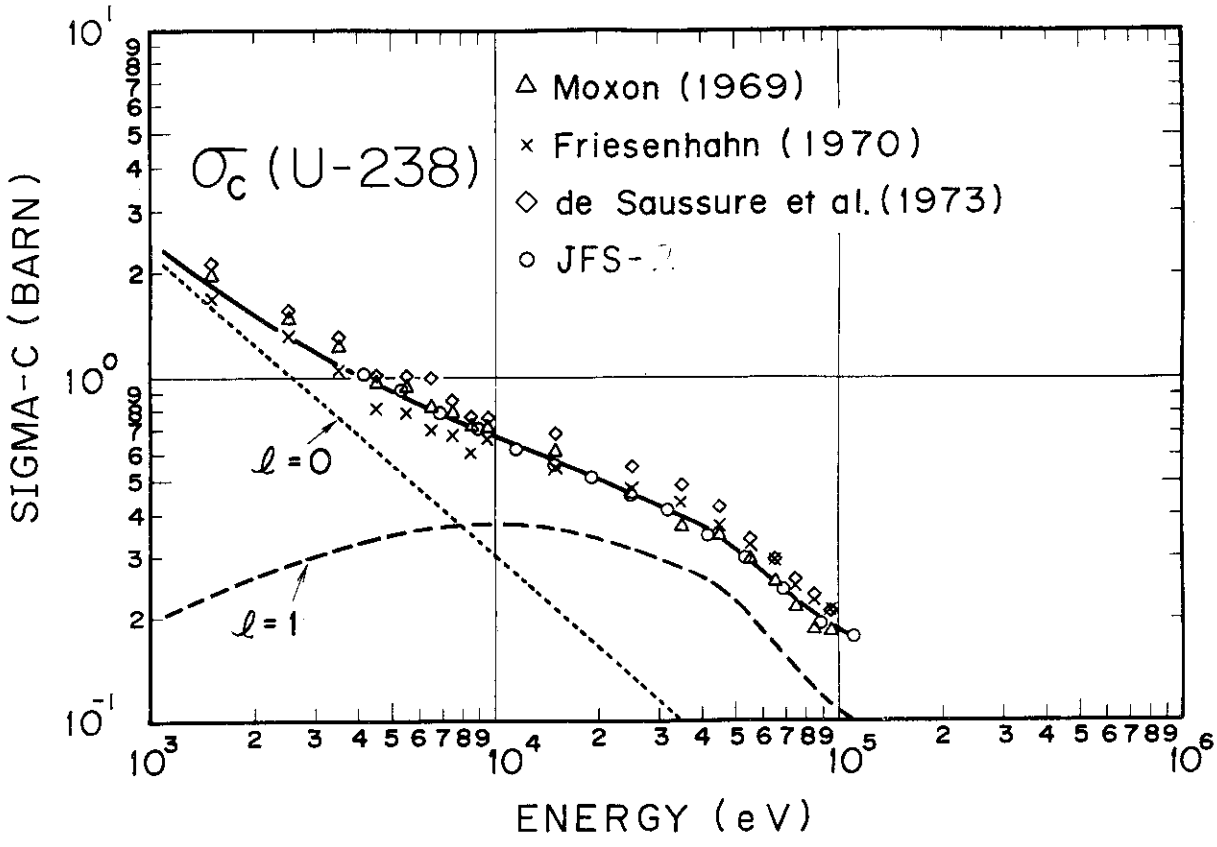

Fig. 5.11 Capture cross sections of ^{238}U fitted by using the ARCFIT-2 code.

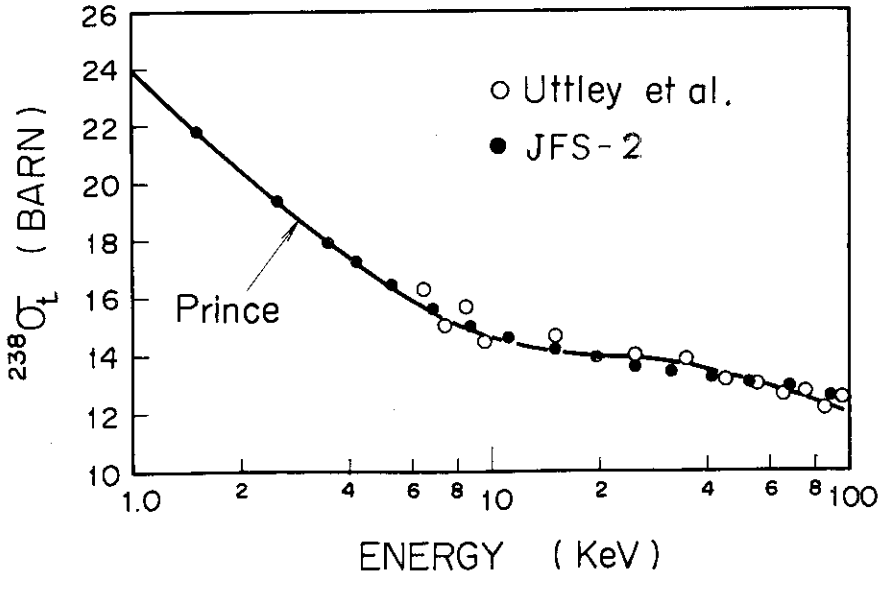

Fig. 5. 12 Total cross sections of ^{238}U fitted by using the ARCFIT-2 code.

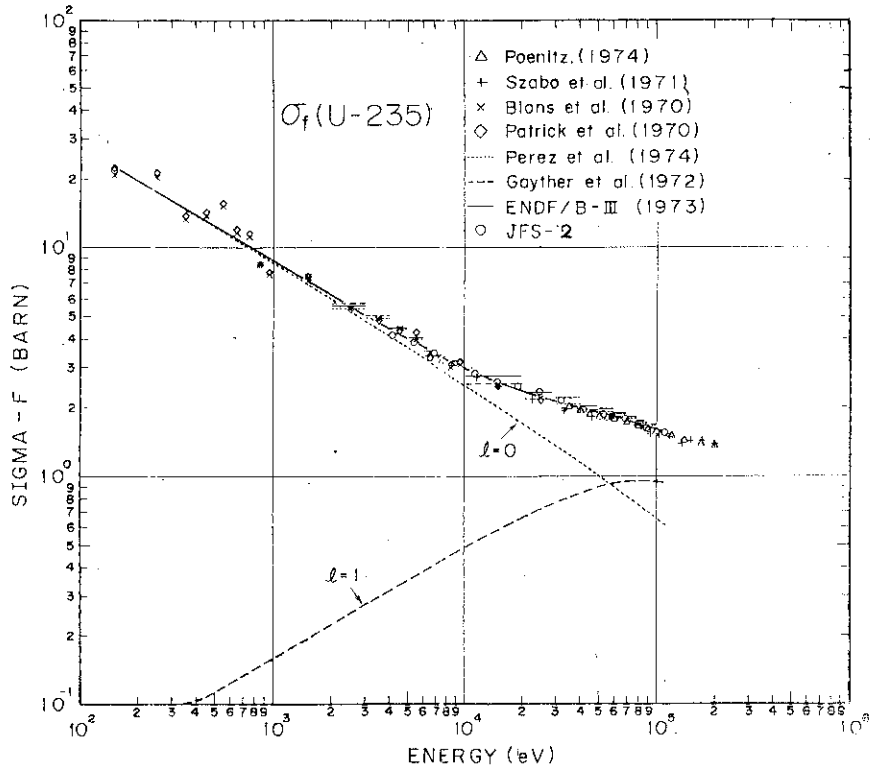

Fig. 5.13 Fission cross sections of ^{235}U fitted by using the ARCFIT-2 code.

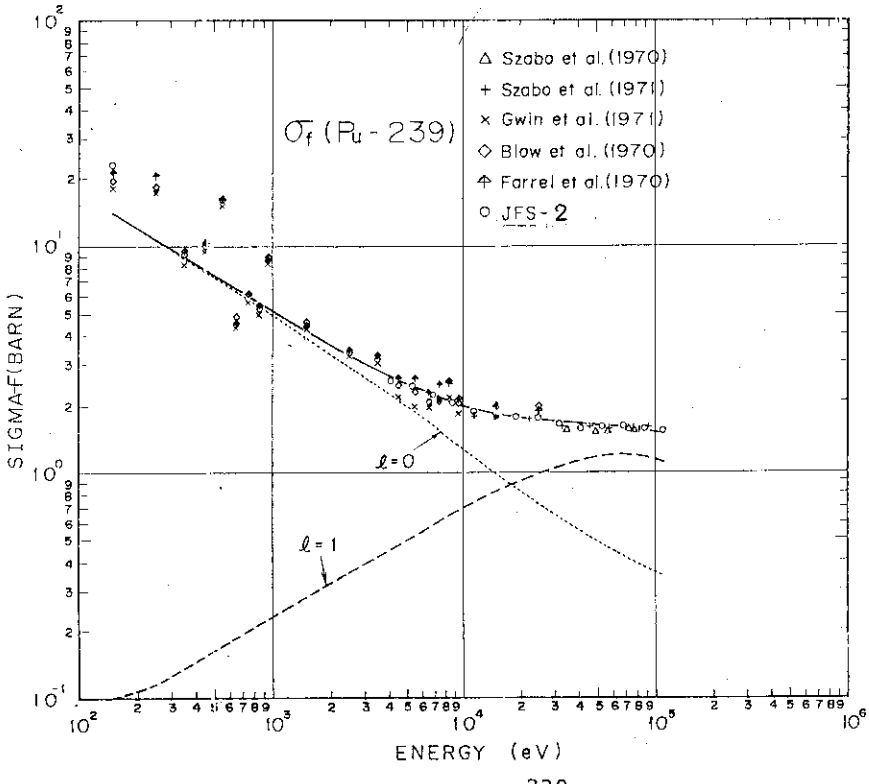

Fig. 5.14 Fission cross sections of ^{239}Pu fitted by using the ARCFIT-2 code.

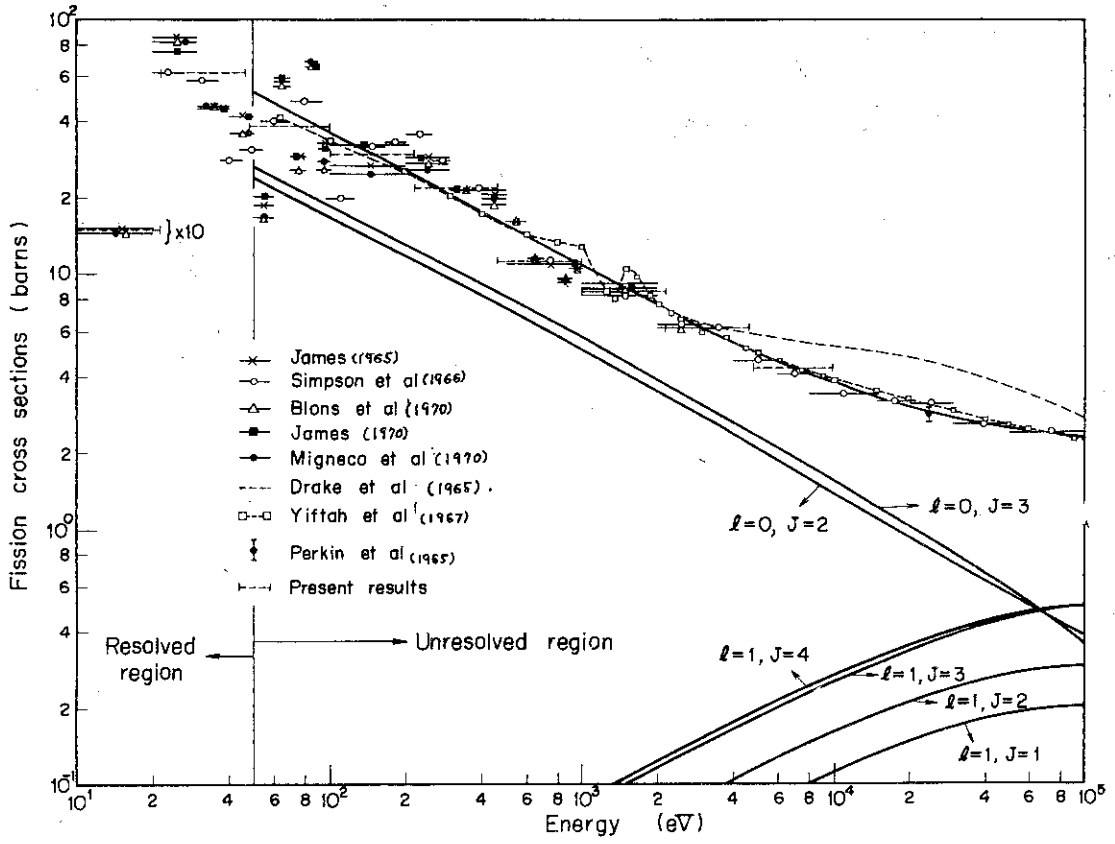

Fig. 5.15 Comparison of fission cross sections for evaluations and experiments (The curves show the results by the ARCFIT-2 code).

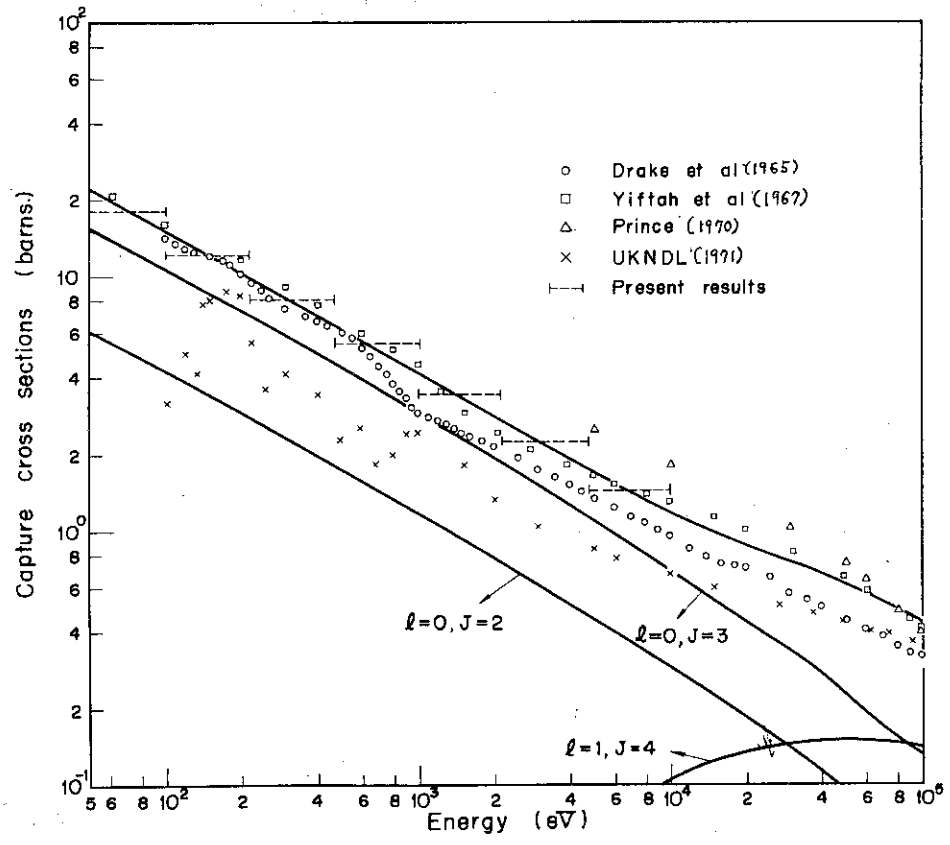

Fig. 5.16 Comparison of capture cross sections for evaluations (The curves show the results by the ARCFIT-2 code)

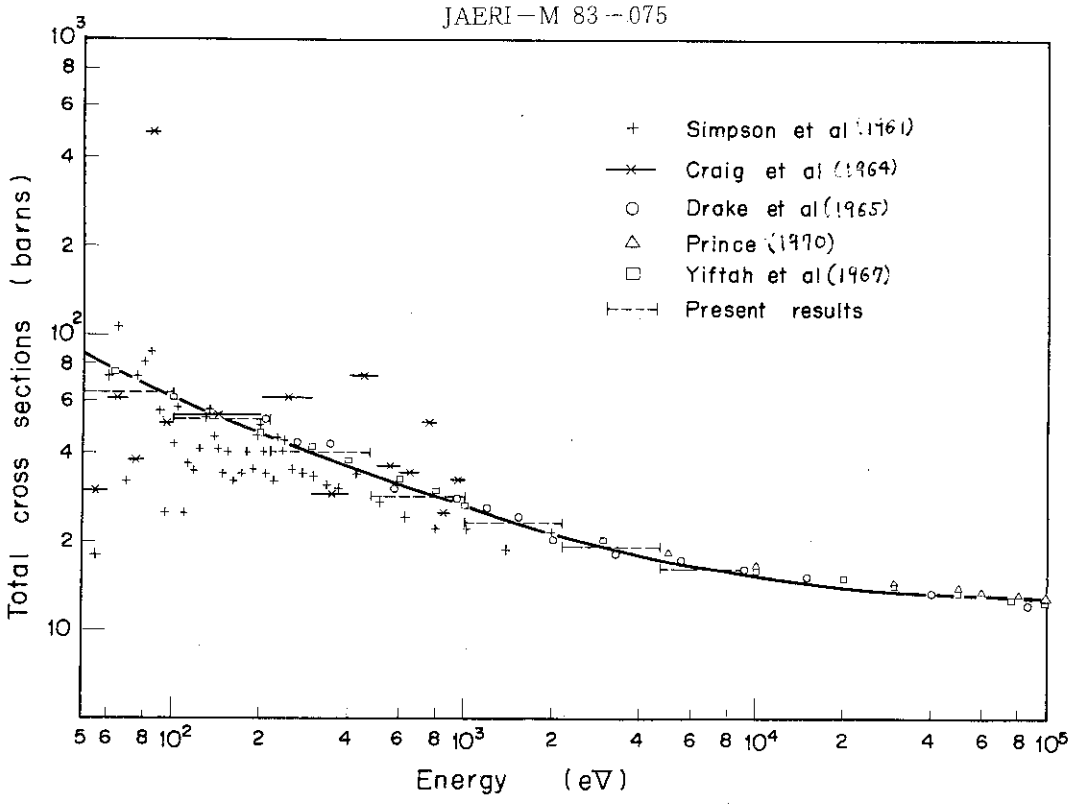

Fig. 5.17 Comparison of total cross sections for evaluations and experiments (The curves show the results by the ARCFIT-2 code).

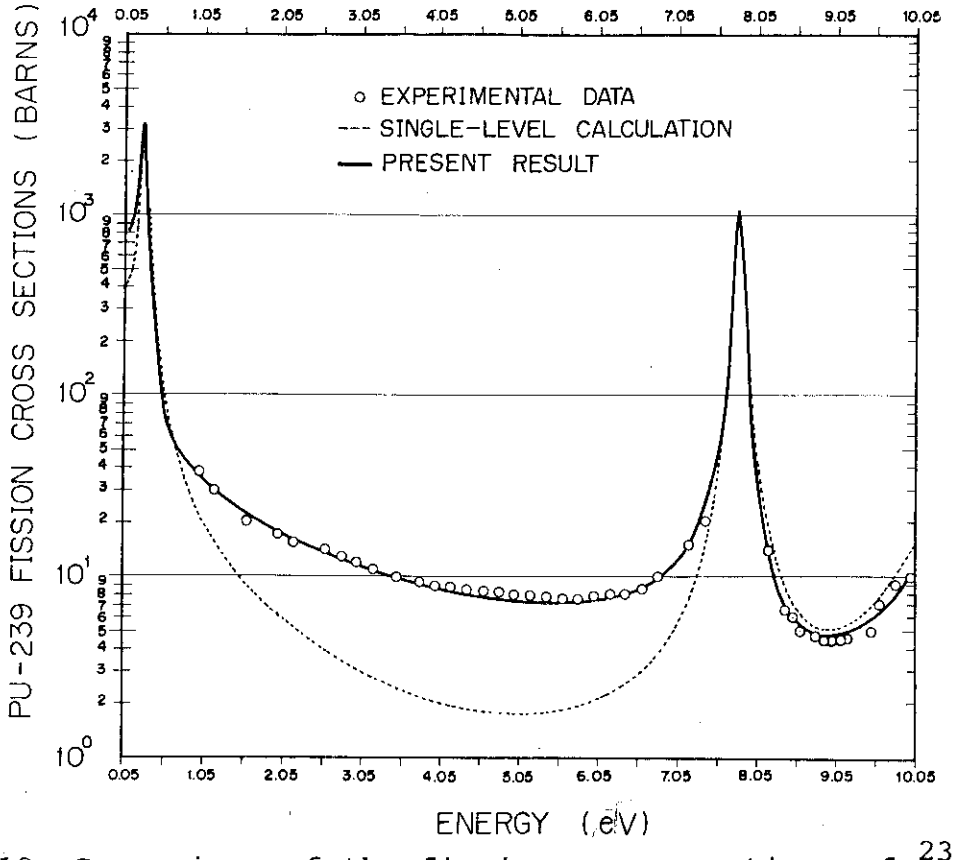

Fig. 5.18 Comparison of the fission cross sections of ^{239}Pu calculated by the single-level and multilevel formulas with the experimental data of Cote et al.[159].

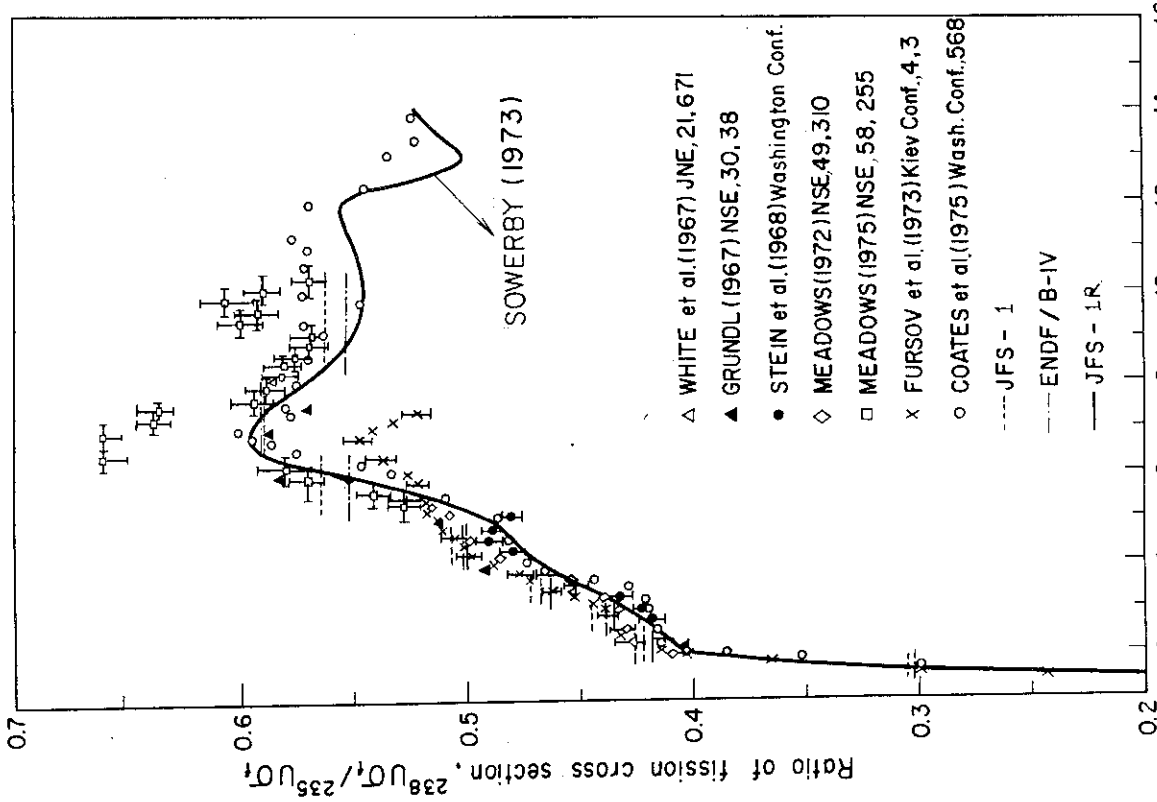

Fig. 5.20 Comparison of ratios of fission cross sections, $^{238}\sigma_f$ / $^{235}\sigma_f$.

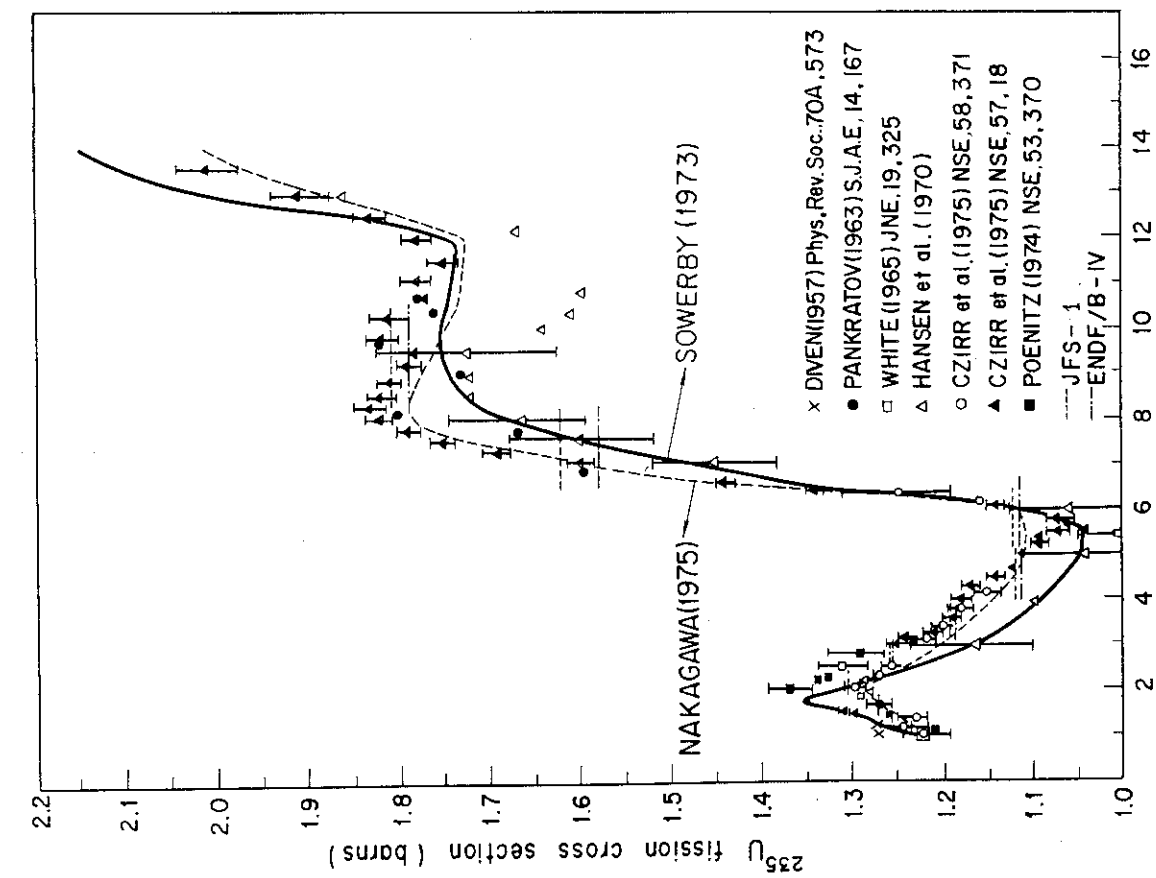

Fig. 5.19 Comparison of fission cross sections of ^{235}U.

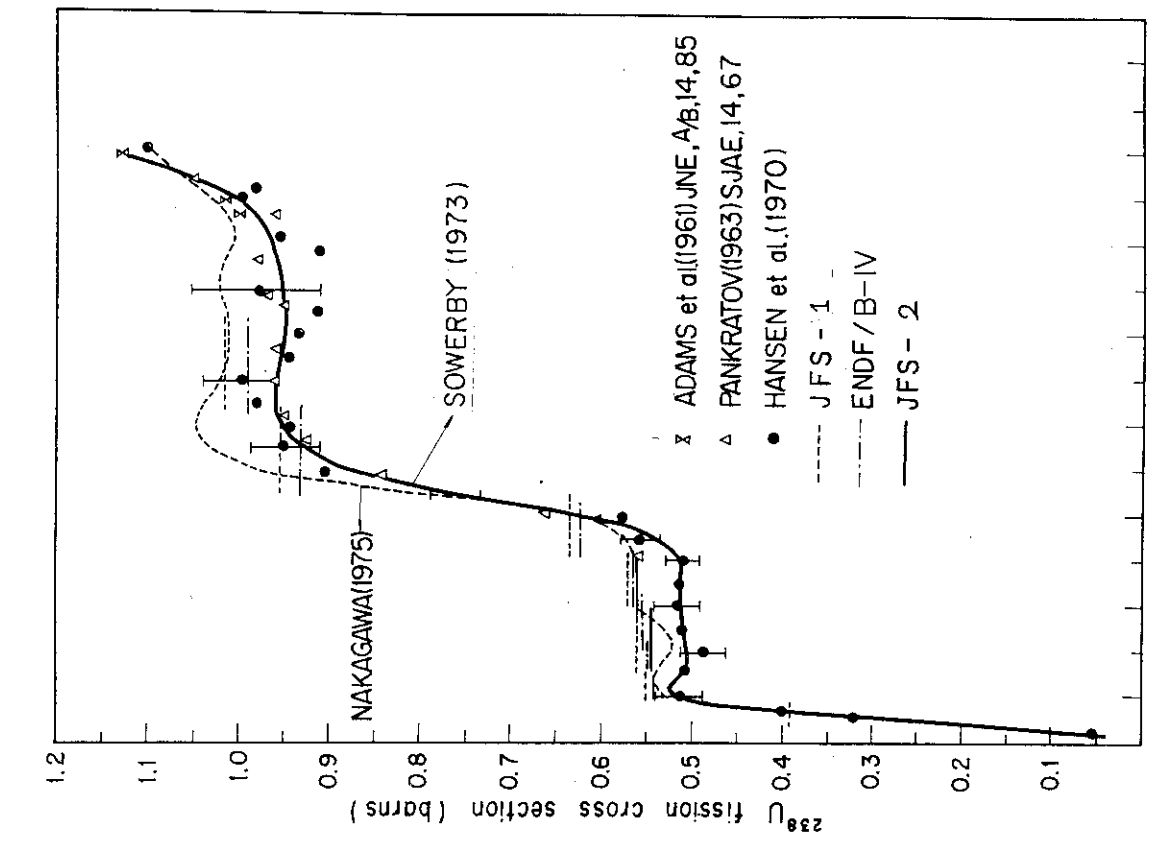

Fig. 5.22 Comparison of fission cross sections of ^{238}U.

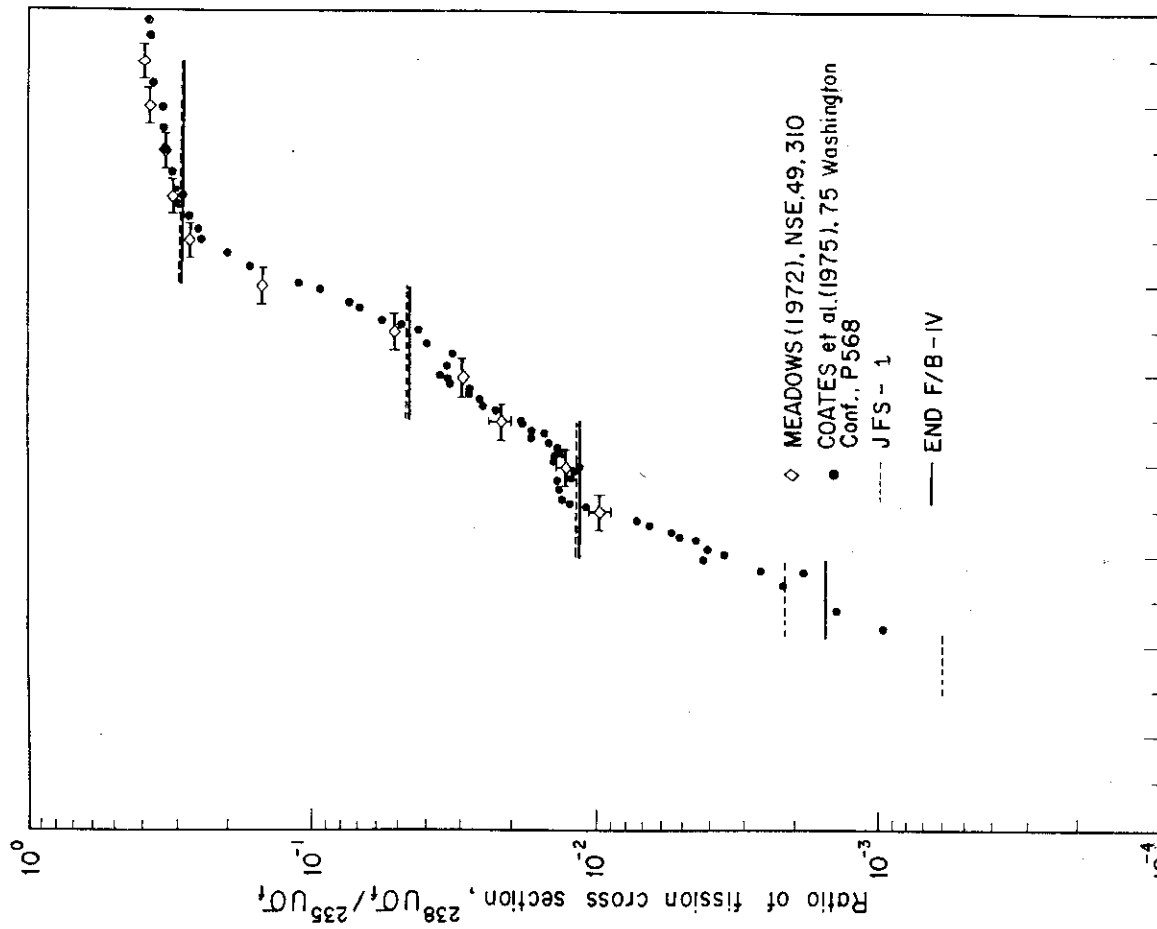

Fig. 5.21 Comparison of ratios of fission cross sections, $^{238}\sigma_f$ / $^{235}\sigma_f$.

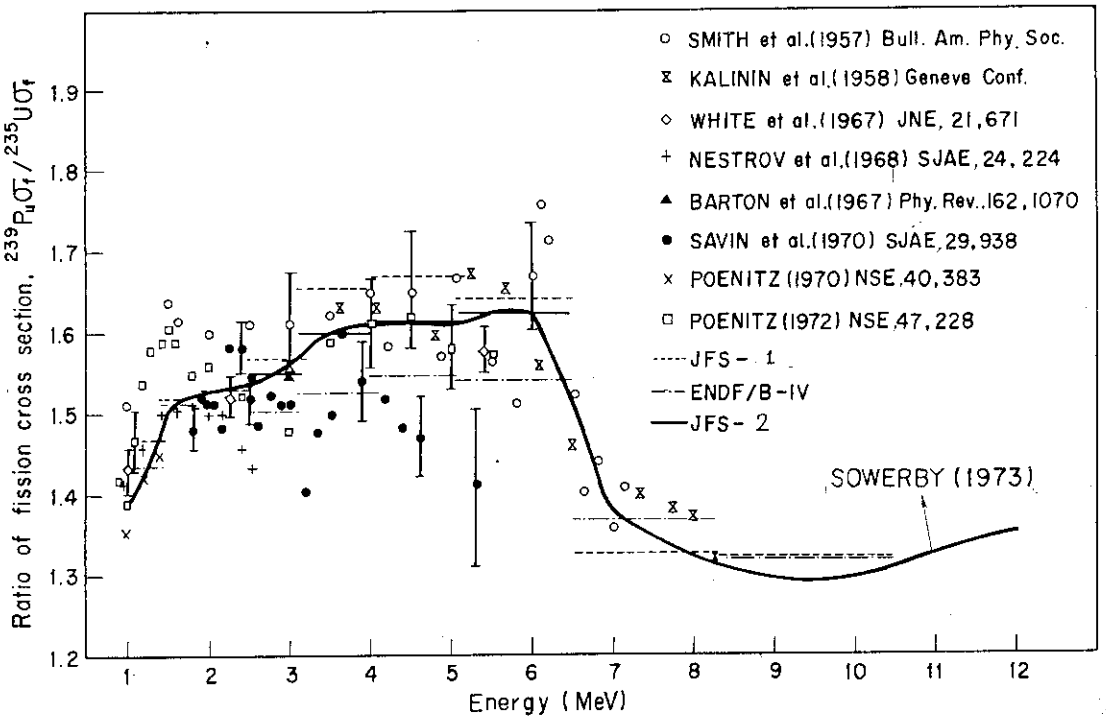

Fig. 5.23 Comparison of ratios of fission cross sections, $^{239}\sigma_f$ / $^{235}\sigma_f$.

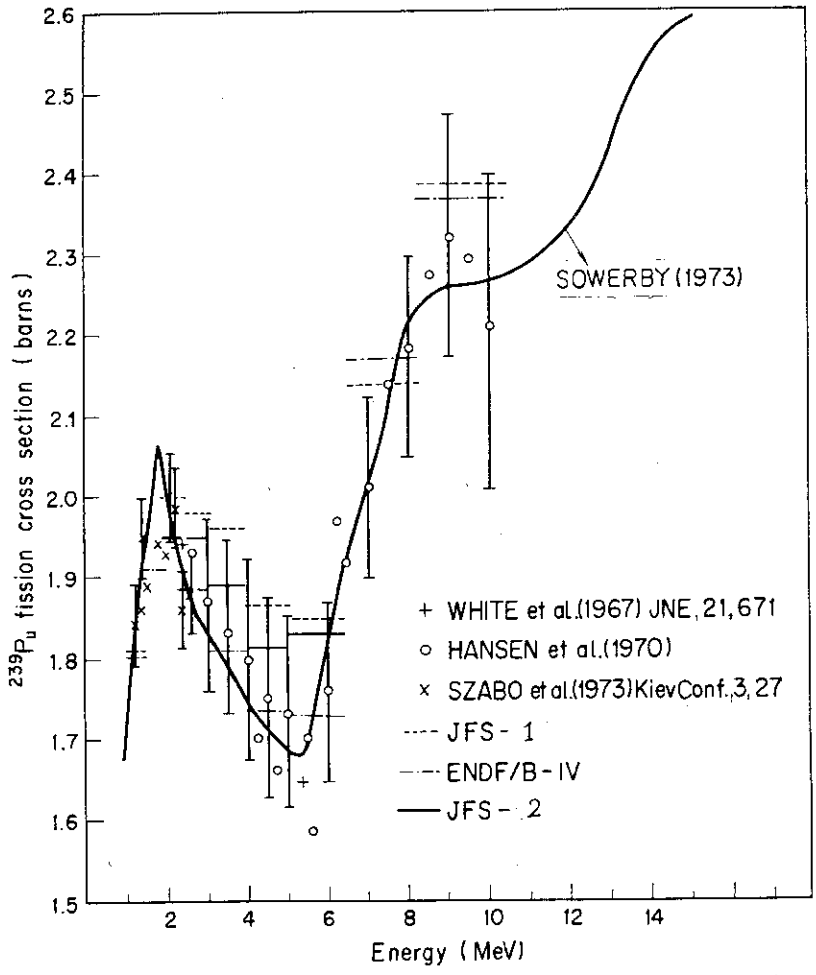

Fig. 5.24 Comparison of fission cross sections of ^{239}Pu.

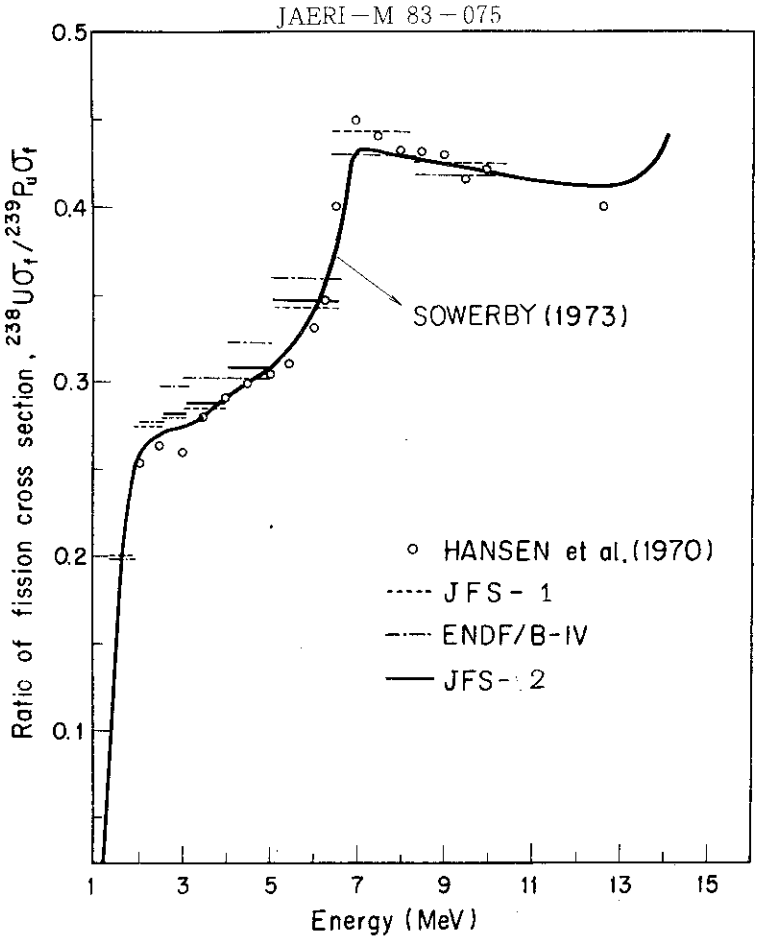

Fig. 5.25 Comparison of ratios of fission cross sections, $^{238}\sigma_f$ / $^{239}\sigma_f$.

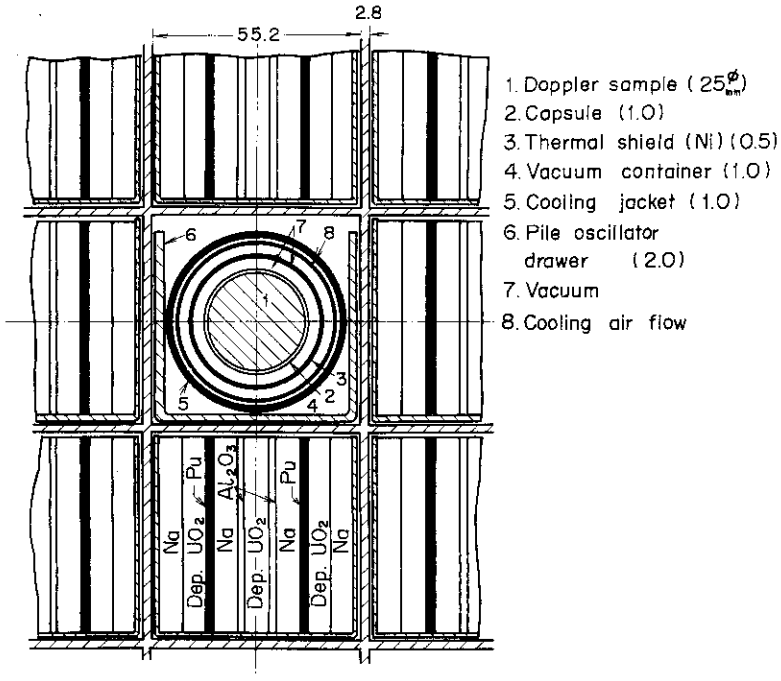

Fig. 5.26 Cross-section view of Doppler sample and fuel drawers in FCA-V assembly 1.

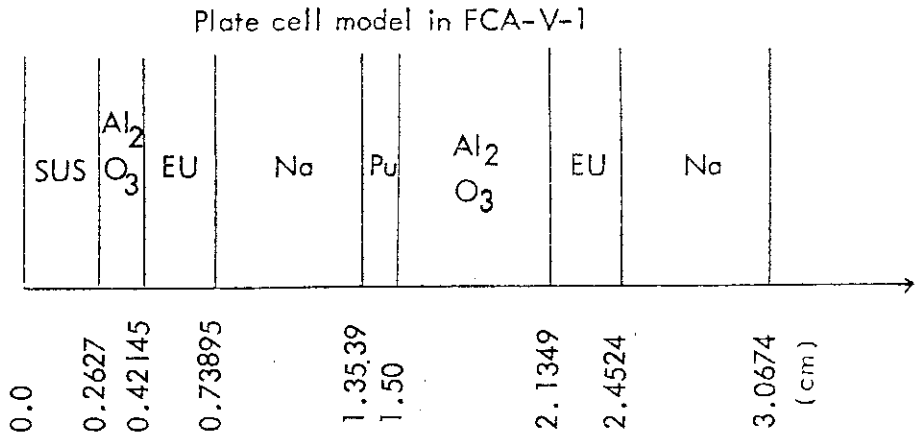

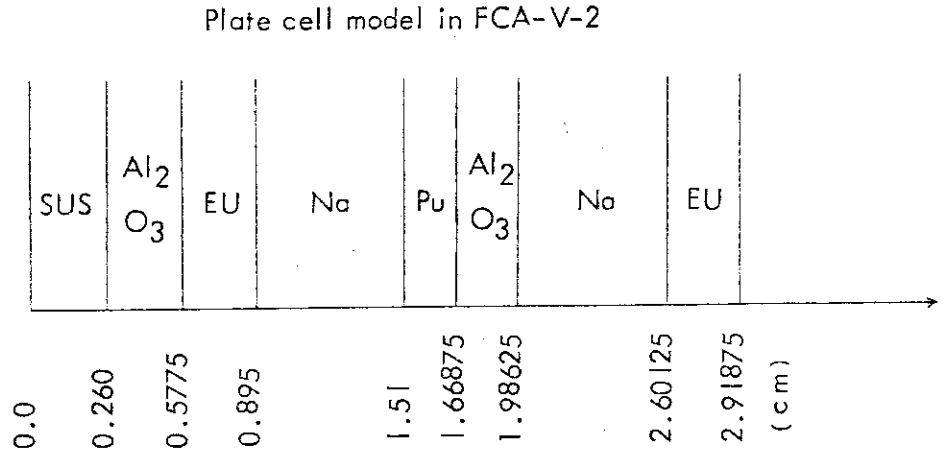

Region	SUS	Al_2O_3	EU	Na	Pu
Nuclide					
Pu-239					1.9963
Pu-240					0.17823
U-235			0.85194		
U-238			3.3821		
O		5.7292			
Na				1.808	
Al		3.8476			
Cr	1.1219	0.08507	0.08507	0.3645	0.6173
Fe	3.8934	0.2952	0.2952	1.3385	2.2662
Ni	0.40889	0.03101	0.03101	0.2198	0.25839

Fig. 5.27 Plate cell models and regionwise nuclide densities in FCA-V assemblies 1 and 2.

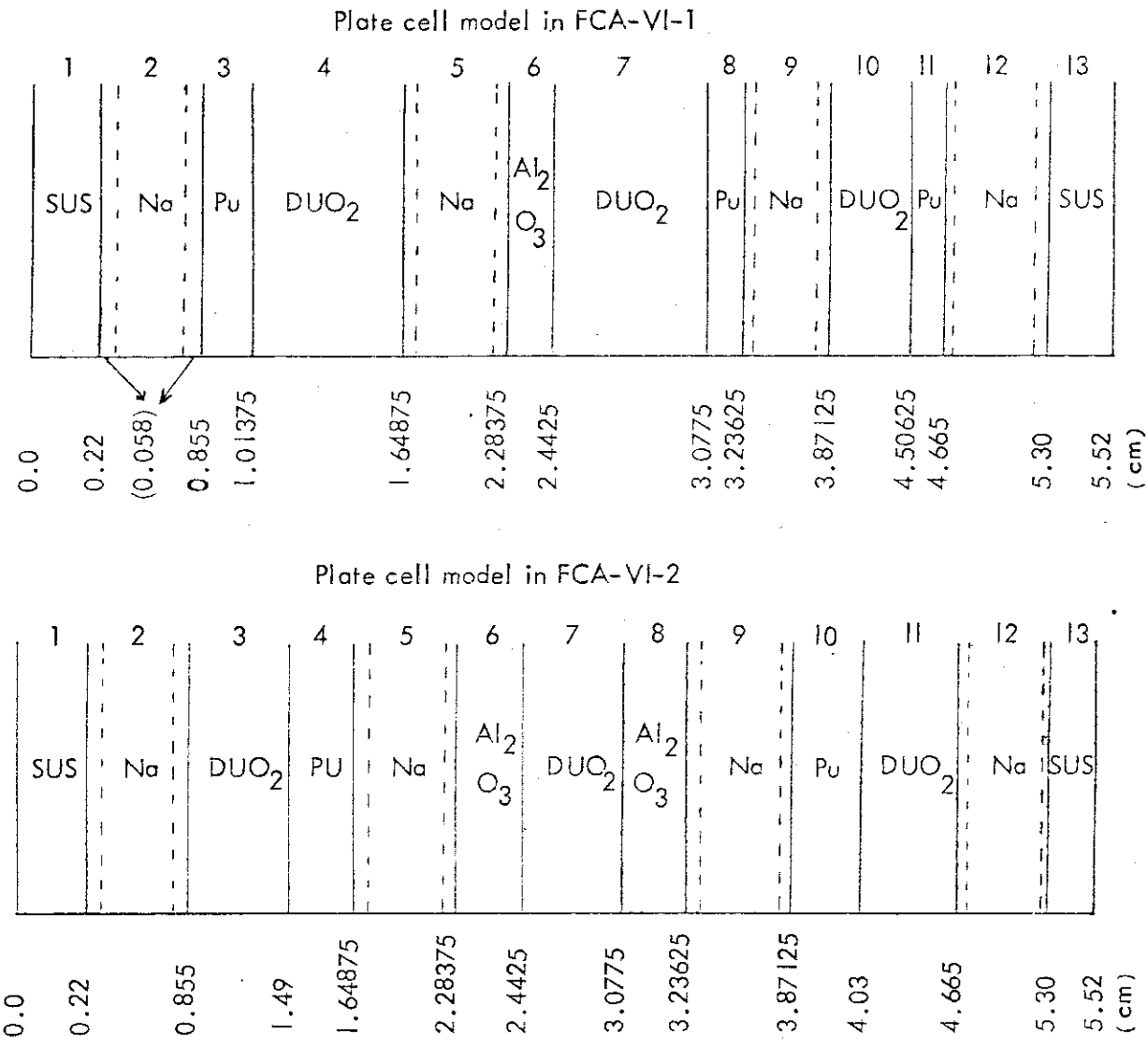

	SUS	Na-sample cover	Na	Na－cover	DUO_2	Pu (92)**	Pu (75)**	Al_2O_3
*	0.22	0.058	0.519	0.635	0.635	0.15875	0.15875	0.15875
Pu-239						1.81666	1.65734	
Pu-240						0.16017	0.58775	
Pu-241						0.01515	0.19703	
U-235					0.00413			
U-238					2.00322			
O					4.01470			5.86815
Na			2.0358	1.66391				
Al						0.26073	0.31940	3.91210
Cr	1.36670	1.43808	0.12675	0.3663	0.18223	0.56773	0.59999	0.08223
Fe	4.97584	5.33149	0.46462	1.35368	0.29937	2.10128	2.22099	0.29937
Ni	0.59577	0.68273	0.05709	0.17138	0.03584	0.26748	0.28287	0.03584

* Thickness in units of cm, ** Two compositions for Pu region

Fig. 5.28 Plate cell models and regionwise nuclide densities in FVA-VI assemblies 1 and 2.

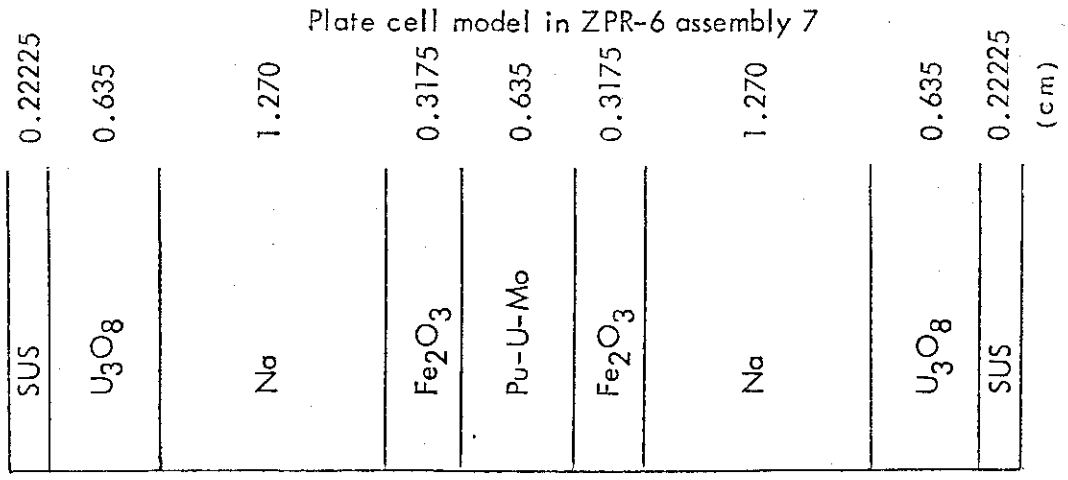

	*	Inner core				Outer core	
				(UPPER MATRIX)			
	25	8.75	E-4	9.927	E-4	8.75	E-4
	24	1.0303	E-2	1.33711	E-2	1.0303	E-2
SUS	28	4.51	E-3	5.8269	E-3	4.51	E-3
	26	3.5911	E-2	4.90428	E-2	3.5911	E-2
	42	8.6	E-5	5.52	E-5	8.6	E-5
	8	4.17591	E-2			4.17591	E-2
U_3O_8	925	3.33	E-5			3.33	E-5
	926	8.0	E-7			8.0	E-7
	928	1.563	E-2			1.563	E-2
	25	9.93	E-5			1.031	E-4
	24	1.3308	E-3			1.327	E-3
Na	28	6.822	E-4			6.277	E-4
	11	2.19957	E-2			4.7011	E-3
	26	4.6853	E-3			2.17341	E-2
Fe_2O_3	26	3.16387	E-2			3.6951	E-2
	8	4.74709	E-2			5.54375	E-2
		(Ref.)		(H240)			
	25	2.325	E-4	3.177	E-4	2.263	E-4
	24	2.7236	E-3	2.6479	E-3	2.6519	E-3
	28	1.3641	E-3	1.3168	E-3	1.3288	E-3
	26	9.4969	E-3	8.9288	E-3	9.2461	E-3
	42	2.1296	E-3	2.0728	E-3	2.1449	E-3
Pu-U-Mo	949	8.3978	E-3	7.9251	E-3	8.4099	E-3
	940	1.142	E-3	3.1047	E-3	1.1437	E-3
	941	1.256	E-4	5.615	E-4	1.433	E-4
	942	1.34	E-5	1.65	E-5	1.67	E-5
	925	5.26	E-5	4.89	E-5	5.3	E-5
	926	1.20	E-6	1.1	E-6	1.2	E-6
	928	2.35161	E-2	2.16982	E-2	2.37198	E-2

* Material code number shown in Table A-1

Fig. 5.29 Plate cell model and regionwise nuclide densities in ZPR-6 assembly 7.

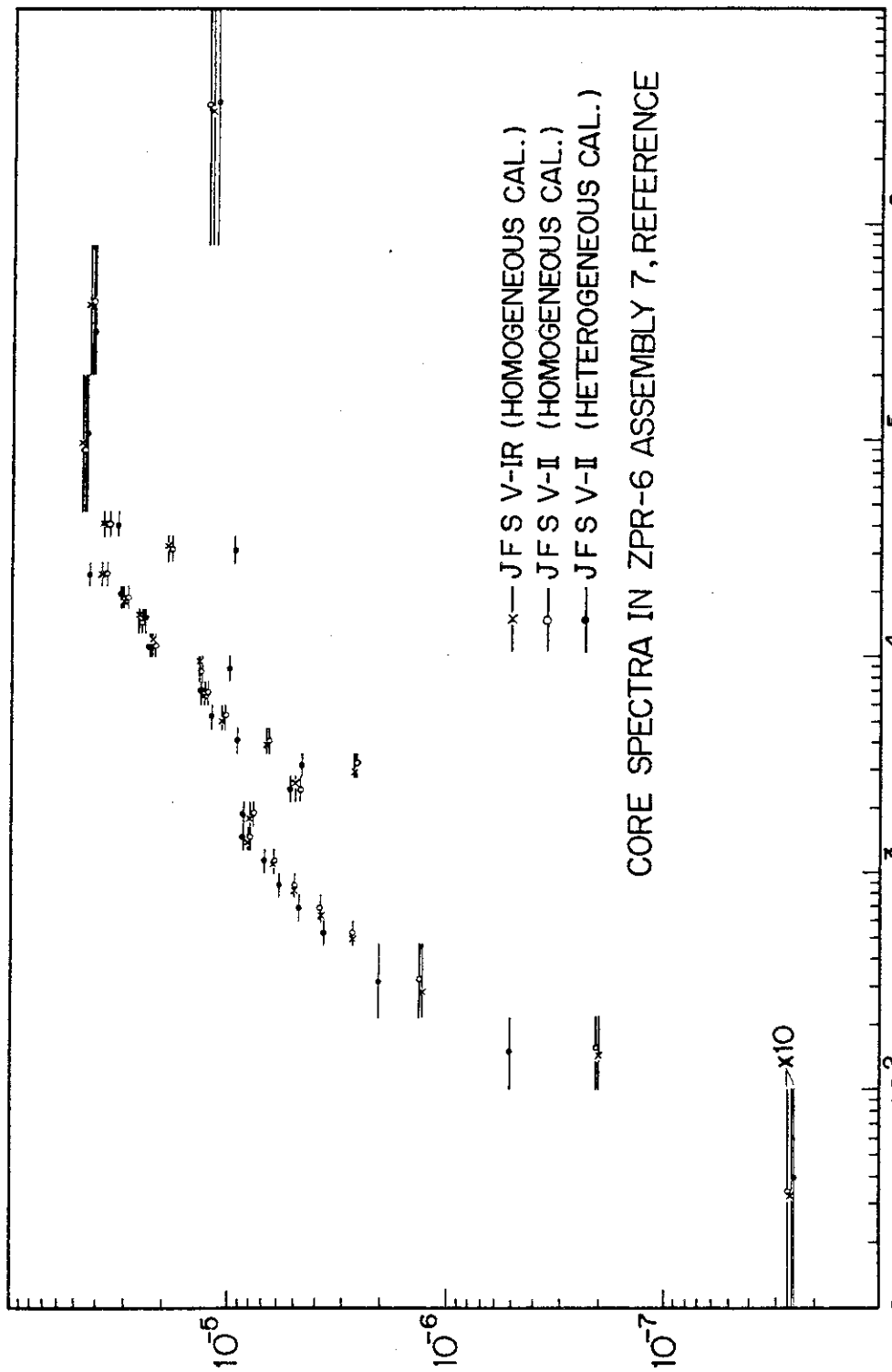

Fig. 5.30 Comparison of core spectra in ZPR-6-7, reference core

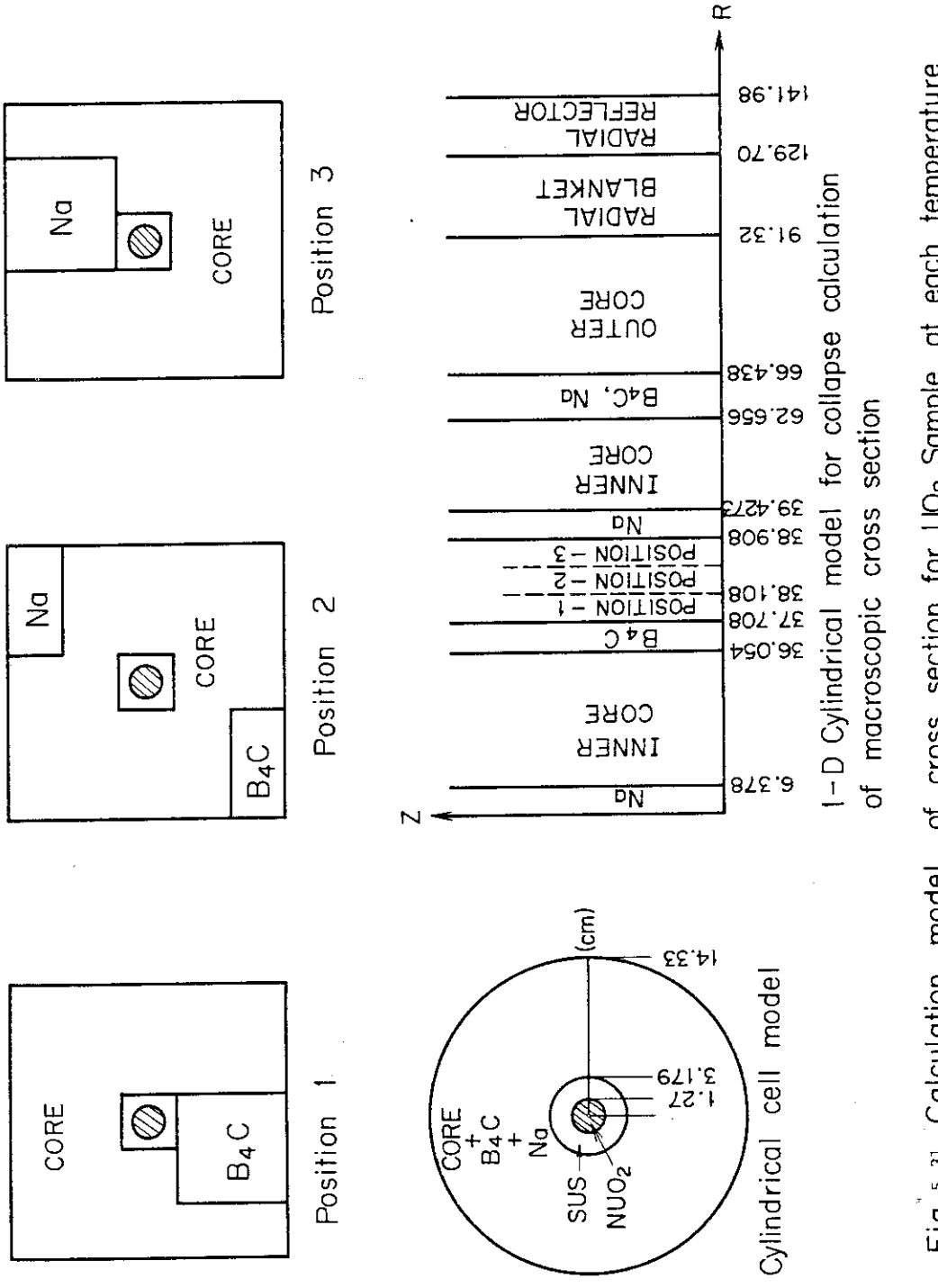

Fig.5.31 Calculation model of cross section for UO_2 Sample at each temperature

6. Group Constants Produced by Using Fine-Group Collision Density Spectrum

6.1 Introduction

One of the serious inadequacies of multigroup constant method used widely is concerned with the treatment of elastic removal cross section for light and medium weight nuclei[209)-(211)]. In the method, "1/E-spectrum" is usually assumed for broad energy behaviour of neutron spectrum. In fast reactor, neutron spectra are steeply reduced in the low energy groups below 10 keV. Hence, the assumption of "1/E-spectrum" overestimates the elastic removal cross sections. The overestimate brings an inaccuracy in the calculation of the neutron flux. In order to correct the overestimate, the method called "REMO-correction"[212] is useful, that is, in place of 1/E-spectrum, the group cross sections are weighted by using a fine-group collision density spectrum. The adequacy for the "REMO-correction" method has been studied[213], and it was pronounced[214] that the multiplication factor and Doppler reactivity coefficient calculated by the "REMO-correction" method were in very good agreement with the results calculated with a fine group fundamental mode calculation code ESELEM-4[5].

In KFK, the REMO-correction is considered by modifying the removal cross sections of the KFK INR set in which group constants are produced by assuming 1/E spectrum with the 25 group structure of ABBN. The modification is performed for each different composition using the 208-group collision density spectra obtained with one-dimensional calculation for the core compositions of interest. Hence, such calculations for the REMO-correction require very timeconsuming and troublesome procedures. In this case, furthermore, the REMO-correction is

restricted to the energy region above 1 keV which may be not completely adequate for calculation of Doppler effect.

In the present study, the group cross sections are calculated by using a fine-group collision density spectrum for the core composition in a typical fast reactor, that is, the group constant set consists of the cross sections made the REMO-correction. Hence, it is very advantage that this set is the same scheme as convensional set, because neutronic calculation codes available for convensional set are able to be used without any modifications. However, the independence of fine-group collision density spectrum on the core compositions is assumed in this calculation. In fast reactor, the assumption may be reasonably accepted as compared with the one of 1/E spectrum, because neutron spectra for core and blankets are steeply reduced in the low energy region below 10 keV.

In this Chapter, the two sets of group constants are generated by weighting two different spectra of "collision density" and "1/E" using the basic nuclear data of the JENDL-2 compilation[14]. In order to assess the effects of "REMO-correction" on nuclear characteristics (effective multiplication factors, central reaction rate ratios, central reaction rate ratios, central sample worths, Doppler reactivity coefficients, sodium void reactivity coefficient and control rod reactivity worth), the benchmark calculations are performed by using the two sets for 18 fast critical assemblies selected by Hardie et al.[17], SEFOR, MZA, MZB, some FCA assemblies and NEACRP benchmark core LMFBR, and the results calculated with the two sets are compared with each other.

6.2 Comparison of Group Cross Sections Calculated by Using 1/E and Collision Density Spectra.

The group-averaged cross sections are defined by

$$\bar{\sigma}^{i}_{x,g}(\sigma_0,T) = \frac{\int_{\Delta Eg} \sigma^{i}_{x}(E,T)\phi^{i}(E,T,\sigma_0)dE}{\int_{\Delta Eg} \phi^{i}(E,T,\sigma_0)dE} \quad , \tag{6-1}$$

where σ^{i}_{x} is the cross section of reaction type x and of isotope i at temperature T, ΔEg the energy interval for group g, ϕ^{i} the weighting function and σ_0 the background total cross section per atom of the isotope i. As for the weighting function, the following form is assumed:

$$\phi^{i}(E,\sigma_0,T) = \frac{\phi_0(E)}{\sigma^{i}_{t}(E,T) + \sigma_0} \quad , \tag{6-2}$$

where $\phi_0(E)$ represents the broad energy behavior of the neutron spectrum and σ^{i}_{t} the total cross section of isotope i.

Standard Spectrum Weighting Method (SDE)

In many codes[32)-(34)] for production of group-averaged cross sections, $\phi_0(E)$ in Eq.(2) is assumed by

$$\phi_0(E) = \begin{cases} \dfrac{1}{E} & (< 1 \text{ MeV}) \quad , \qquad (6\text{-}3) \\ \chi(E) & (\geq 1 \text{ MeV}) \quad , \qquad (6\text{-}4) \end{cases}$$

where $\chi(E)$ is the fission spectrum.

The assumption of the constant collision density in the neutron slowing down energy region below 1 MeV is based on the narrow resonance

approximation. However, this assumption is not valid in the neighbouring energy region of large scattering resonances of light and intermediate weight nucled and in the low energy region below 1 keV where the flux is abruptly depressed. Especially, the assumption results in the over-estimates of elastic removal scattering cross section in the lower energy range.

Collision Density Spectrum Weighting Method (CDR)

The collision density spectrum F(E) for the inner core composition of a prototype fast reactor MONJU was calculated by using the ESELEM-4 code[5] in order to obtain the fine-group weighting spectrum. The collision density spectrum calculated is shown in Fig. 6.1, and by using the spectrum F(E), the elastic removal scattering cross section is calculated by

$$\bar{\sigma}^{i}_{er,g}(\sigma_0,T) = \frac{\int_{E_g}^{E_g/\alpha} \sigma^{i}_{s}(E,T)\phi^{i}(E,T,\sigma_0)\,\frac{E_g-\alpha E}{(1-\alpha)E}\,dE}{\int_{E_g}^{E_{g-1}} \phi^{i}(E,T,\sigma_0)\,dE} \quad , \qquad (6\text{-}5)$$

$$\phi^{i}(E,T,\sigma_0) = \frac{F(E)}{\sigma^{i}_{t}(E,T) + \sigma_0} \quad . \qquad (6\text{-}6)$$

The advantage of the weighting spectrum of Eq. (6-6) is that the group constants depending on compositions σ_0 and temperatures T are generated for using the collision density spectrum of a typical fast reactor in place of 1/E spectrum. Hence, the broad energy behavior of neutron spectrum in fast reactor can be considered for the group constant set using Eq. (6-6).

The calculations of group-averaged cross sections were performed with the TIMS-PGG[215] code system by using the nuclear data of the JENDL-2 compilation. The group constants of 27 nuclides that are necessary for usual reactor calculations were produced with the SDE- and CDR-methods, and these compilations are called the SDS and CDS sets(*), respectively.

The elastic removal cross sections calculated with the SDS- and CDS-methods are compared for four typical nuclei in Figs. 7.2-5. It is seen from these figures that the SDS-calculation overestimate evidently the elastic removal cross section in most energy groups, especially low energy region where the scattering cross sections for scattering materials are constant.

6.3 Comparison of Nuclear Characteristics

The nuclear characteristics in fast reactors are calculated by using the two cross-section sets, i.e., the SDS- and CDS-sets, and the results are discussed in this section.

The effective multiplication factors, central reaction rate ratios and central sample worths were calculated for 21 fast critical assemblies, which were often used in benchmark test to cross-section set. Doppler effects, radial reaction rates, sodium void reactivity and control rod worth were calculated for some fast reactors. There calculations were performed by using one- and two-dimensional diffusion theories.

---

*) The group constants for heavy resonant nuclei in the resolved and unresolved resonance regions were calculated with the TIMS-1 code[35]. Hence, these group constants are the same for both the SDS- and CDS-sets.

Effective Multiplication Factor

The calculations for effective multiplication factors (k_{eff}) were performed and the percent deviations of k_{eff}'s calculated with the CSD-set from those calculated with the SDS-set are shown in Fig. 6.6. The deviations are never more than 0.35 percent. The CDS-set gives larger values of k_{eff} for the plutonium-fueled cores and smaller ones for the uranium-fueled cores, except for several assemblies, because $\eta(=\nu\sigma_f/\sigma_a)$ of ^{235}U is smaller than the one of ^{239}Pu in high energy region and the neutron spectra calculated with the SDS-set become softer due to the overestimate of the elastic removal cross sections. Figure 6.7 shows the comparison of the neutron spectra at the core center in MZB calculated with the CDS- and SDS-sets. The spectrum calculated with the SDS-set is overestimated especially in the low energy range below 1 keV. This fact can be pronounced also for the other assembly.

Central Reaction Rate Ratio

The ratios of the calculations to the experiments for the central reaction rate ratios are shown as the function of the core volume in Figs. 6.8-12. From these figures, we concluded as follows.

$^{239}\sigma_f\phi/^{235}\sigma_f\phi$ (Fig. 6.8): The C/E-values calculated with the CDS-set become larger by about one percent and come slightly near the unity than the SDS-results underestimated for the assemblies with large core volume, while the dependence of the C/E-values on the core volume is seen for both the CDS- and SDS-results.

$^{238}\sigma_\gamma\phi/^{235}\sigma_f\phi$ and $^{238}\sigma_\gamma\phi/^{239}\sigma_f\phi$ (Figs. 6.9 and 10): The differences between the results calculated with the two sets are about one percent. As for $^{238}\sigma_\gamma\phi/^{239}\sigma_f\phi$, the SDS-results become larger than

the CDS-results, because of the softer spectrum as seen in Fig. 6.7. In these figures, the dependences of the C/E-values on the core volume are obviously seen, that is, the C/E-values increase with the core volume. In these figures, the results calculated with the JAERI-Fast Set Version 2 (JFS-2)[5] are also shown, and the results also depend on the core volume, though the dependence is reduced. We do not have the resonable answer to the cause for this dependence, yet.

$^{238}\sigma_f\phi/^{235}\sigma_f\phi$ and $^{240}\sigma_f\phi/^{235}\sigma_f\phi$ (Figs. 6.11 and 12): The differences between the SDS and CDS-results are smaller than one percent. The calculated results are overestimated, though the dependence of C/E-values on the core volume is not observed.

Central Sample Worth

In order to avoid the scaling problem which is attributed to be caused by the errors in the kinematic parameters, the calculated and measured sample worths were normalized to those of ^{239}Pu respectively. The C/E-values of the normalized sample worths calculated with the SDS and CDS sets are shown as the function of the core volume in Figs. 6.13-15.

Figure 11.13 shows the C/E-values of the normalized sample worths of ^{235}U. The calculated results show a tendency of overestimate with increase of the core volume, though the CDS-results are corrected slightly.

The sample worths of ^{10}B are compared in Fig. 6.14. This nuclide has a standard $\frac{1}{v}$ absorption cross sections. The worth is sensitive to the variation of neutron spectrum in the low energy region. The CDS-results calculated with a hardened spectrum increase the tendency of underestimate for the SDS-results, and also for the dependence of the C/E-values

on the core volume. The dependence shows the existence of an inconsistency in the neutron spectrum at the core, when we reconsider the dependence of $^{238}\sigma_{\gamma}\phi/^{239}\sigma_{f}\Phi$ on the core volume. That is, the results shown in Fig. 7.10 request that core spectrum should be hardened with the increase of the core volume, and on the other hand, the results for ^{10}B worth suggest soften spectrum. The cause of this inconsistency is not clear. In Fig. 6.14, the C/E-values of ^{10}B worths calculated with JFS-2[15] are also shown, and it should be noticed that their dependence on the core volume is not seen. The differences between the results for JFS-2 and JENDL-2 may be caused from the discrepancies between the other cross sections except for ^{10}B, because ^{10}B is a typical "$\frac{1}{v}$ cross section" and has a well-assigned value.

Figure 6.15 shows the C/E-values of the normalized worths of iron. The differences between the results calculated with the CDS and SDS-sets are small excepting the result for SNEAK-7A. Also for the scattering materials such as Na, Cr, Ni and Al etc., the differences were small.

Figure 6.16 shows the C/E-values of the normalized worths of Mo. The differences between the results for the CDS and SDS-sets depend on the core volume, and for ZPR-6-7 the difference is about 8%. The sample worth of Mo is sensitive to the variation of neutron spectrum in the low energy region, because Mo is resonance absorber. The resonance self-shielding factors were calculated for the energy region below 30 keV in the two sets.

Doppler Reactivity Coefficients

Doppler coefficients are very sensitive to the shape of neutron spectrum at the core. The neutron spectra calculated with the CDS-set are hardened as shown in Fig. 6.7. Hence, the Dopller coefficients calculated with the CDS-set are reduced. The calculations of Doppler coefficients were performed by using one-dimensional perturbation theory for a whole core Doppler experiment in SEFOR and small sample Doppler experiments in FCA-V-1, V-2, V1-1, V1-2, ZPR-3-47 and ZPPR-2. The calculated results are shown in Table 6.1. From this table, it is seen that the SDS-results underestimate the experimental values, and furthermore, the CDS-results underestimate considerably by 8 ∿ 14 % than the SDS-results. These results (C/E-values) were calculated with the homogeneous core model. Hence, the core heterogeneity effects should be considered as described in Ref.(15). Hence, the C/E-values corrected by using the heterogeneity effects in Ref.(15) are presented in the parentheses in Table 6.1. The corrected results become larger, but the CDS-results still underestimate the experimental data. This underestimate for the Doppler coefficients suggests that the calculated core spectra are too hard and/or resonance capture cross sections of ^{238}U are small. However, this conclusion is inconsistent with the fact described as to the reaction rate ratios, $^{238}\sigma_{\gamma}\phi/^{239}\sigma_{f}\phi$, but consistent with the results suggested from ^{10}B sample worth calculations.

Radial Reaction Rates

The calculations of radial reaction rates were performed by using one-dimensional diffusion code in the fast critical assemblies ZPPR-2,

MZB and FCA-V1-2. The results calculated were normalized to 1.0 at the core center. The differences between the reaction rates calculated with the CDS- and SDS-sets are shown in the form of the deviations of the SDS-results from the CDS-results for ZPPR-2 and FCA-V1-2 in Figs. 6.17 and 18, respectively. The results calculated for MZB were very similar to those for ZPPR-2. The deviations are very small in the inner core (I.C) region, and they become negative in the outer core (O.C) region for both ZPPR-2 and FCA-V1-2. That is, the SDS-results become smaller than the CDS-results in the outer core region. In the radial blanket (R.B) region, however, the deviations become larger, and moreover, the tendencies for the deviations in ZPPR-2 and FCA-V1-2 are entirely different. This difference is caused by the existence of the radial reflector (R.R). This reason is explained as follows. Fast neutrons entered from the blanket to the reflector zone are reflected and/or moderated. Then, the calculation by the SDS-set produces more slowed down neutrons than that by the CDS-set, because of larger elastic-removal cross sections. Hence, the neutron spectrum calculated with the SDS-set become considerably soft in the reflector. In the FCA-6-2 assembly without the reflector, on the other hand, the leakage of fast neutrons for the CDS-set become larger than that for the SDS-set. On the relative comparison for the neutron spectrum at the core center, hence, in the blanket region the spectra calculated by the CDS-set are softer than those for the SDS-set.

Control Rod Reactivity Worth

The central boron control rod worth was calculated with two-dimensional diffusion theory for the NEACRP LMFBR international comparison

calculational model. The boron control rod and Na-filled zones with the radius of 7.2 cm are located at the core center. The calculated results are shown in Table 6.2. The rod worth calculated with the CDS set becomes larger than the SDS-result, though the difference between the two results is small and ∿2 %.

Sodium-Void Reactivity

The sodium void effect was calculated for the cylindrical voided zone of 30.5 cm at the core center in the ZPPR-2 assembly. The calculated results are given in Table 6.3. The sodium void reactivity calculated with the CDS-set becomes more positive than that calculated with the SDS-set, though the difference between the total reactivities calculated is very small, because of cancellation for the reactivity-difference between Δk's by the scattering and the absorption terms.

6.4 Concluding Remarks

The elastic removal cross sections overestimated by using "1/E-spectrum" caused very softened neutron spectrum, especially for low energy range below 1 keV. Hence, the integral quantities such as Doppler reactivity coefficients, reaction rates in blanket region and central sample worths of ^{10}B and Mo which were very sensitive to the neutron flux shape in the low energy region were considerably affected by the softened spectrum. The softened spectrum caused the overestimates of ∿10 % for the Doppler reactivity and ∿5 % for the central sample worths of ^{10}B and Mo. The effect of it on the effective multiplication factors was never more than 0.35 % and on the control rod reactivity ∿2 % for central region of a NEACRP benchmark core. The effect was very small

for the central reaction rate ratios and sodium void coefficient. For the radial reaction rates, non-negligible effects are seen in the blanket region.

In comparison of the calculations with the experiments, however, the CDS-results were not able to remove several problems as seen in the results calculated with the SDS-set, that is, the systematic dependence of C/E values on the core volume as for the central reaction rate ratios of ^{238}U capture to ^{235}U fission or ^{239}Pu fission, and the overestimates for ^{238}U fission to ^{235}U fission. Furthermore, the Doppler effects calculated with the CDS set underestimate the experimental values, though they for the SDS set overestimate the experiments for several assemblies. These problems can not always explain the cause, and hence the evaluations of cross sections and the calculational methods for the group constants and/or the nuclear characteristics should be studied, though the used cross sections may be a main cause. In addition, the accuracy of the use of a typical collision density spectrum in the present study may be examined, especially for the neutron spectrum in the blanket and/or reflector.

Table 6.1 Doppler reactivity coefficients (C/E-values) calculated with the CDS and SDS-sets using one-dimensional diffusion code

Assembly	Temperature (°K)	C/E-value		SDS/CDS
		SDS	CDS	
SEFOR*	677 ~ 1365	1.05	0.97	1.08
FCA-V-1**	300 ~ 573	0.97 (1.06)	0.86 (0.94)	1.13
	300 ~ 823	0.99 (1.06)	0.87 (0.93)	1.14
	300 ~ 1073	0.96 (1.03)	0.85 (0.91)	1.13
FCA-V-2**	300 ~ 1073	0.82	0.72	1.14
FCA-VI-1**	300 ~ 623	0.99 (1.03)	0.88 (0.92)	1.13
	300 ~ 823	0.95 (0.99)	0.84 (0.87)	1.13
	300 ~ 1073	0.97 (1.01)	0.86 (0.89)	1.13
FCA-VI-2**	300 ~ 823	0.91 (0.96)	0.81 (0.86)	1.12
	300 ~ 1073	0.90 (0.95)	0.81 (0.86)	1.11
ZPR-3-47**	300 ~ 500	0.98	0.90	1.09
	300 ~ 800	0.95	0.86	1.10
	300 ~ 1100	0.94	0.86	1.09
ZPPR-2** (normal1)	300 ~ 500	1.00 (1.11)	0.90 (1.00)	1.11
	300 ~ 800	0.97 (1.08)	0.87 (0.97)	1.11
	300 ~ 1100	0.95 (1.05)	0.85 (0.94)	1.12
ZPPR-2** (Na-voided)	300 ~ 500	0.84 (0.94)	0.76 (0.85)	1.11
	300 ~ 800	0.81 (0.92)	0.73 (0.82)	1.11
	300 ~ 1100	0.79 (0.89)	0.71 (0.80)	1.11

* Whole core Doppler experiment

** Small sample Doppler experiments for natural UO_2

The results corrected by the heterogeneity effect taken from Ref.(15) are presented in the parentheses.

Table 6.2 Comparison of Boron control rod reactivities calculated with the CDS and SDS-sets in LMFBR

	Cross sections set	
	SDS	CDS
$k_{Na\text{-}filled}$	1.01463	1.01660
k_{rod}	1.01212	1.01403
$\frac{k_{rod} - k_{Na\text{-}filled}}{k_{Na\text{-}filled}}$	-0.00247	-0.00253

Table 6.3 Comparison of sodium void effects calculated with the CDS and SDS-sets using one-dimensional diffusion and exact perturbation theories in ZPPR-2

Component \ Set	SDS	CDS	Difference
Δk by $\nu\Sigma_f$	-0.000237	-0.000213	-0.000026
Δk by $\Sigma_{i\to j}$	0.00446	0.00497	-0.00051
Δk by Σ_a	0.00231	0.00209	0.00022
Δk by Σ_{in}	0.00385	0.00385	0.0
Δk by D	-0.00073	-0.00073	0.0
Total reactivity ($\Delta k/k$)	0.00966	0.00996	-0.0003

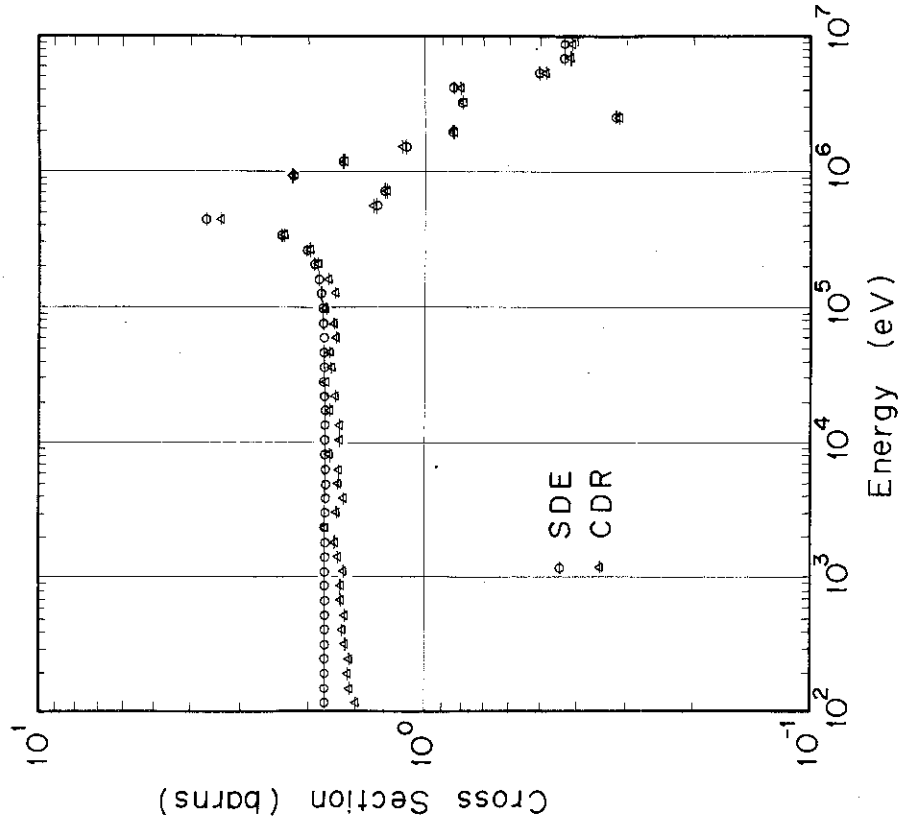

Fig. 6.2 Comparison of oxigen elastic removal cross sections calculated with the SDE and CDR-methods.

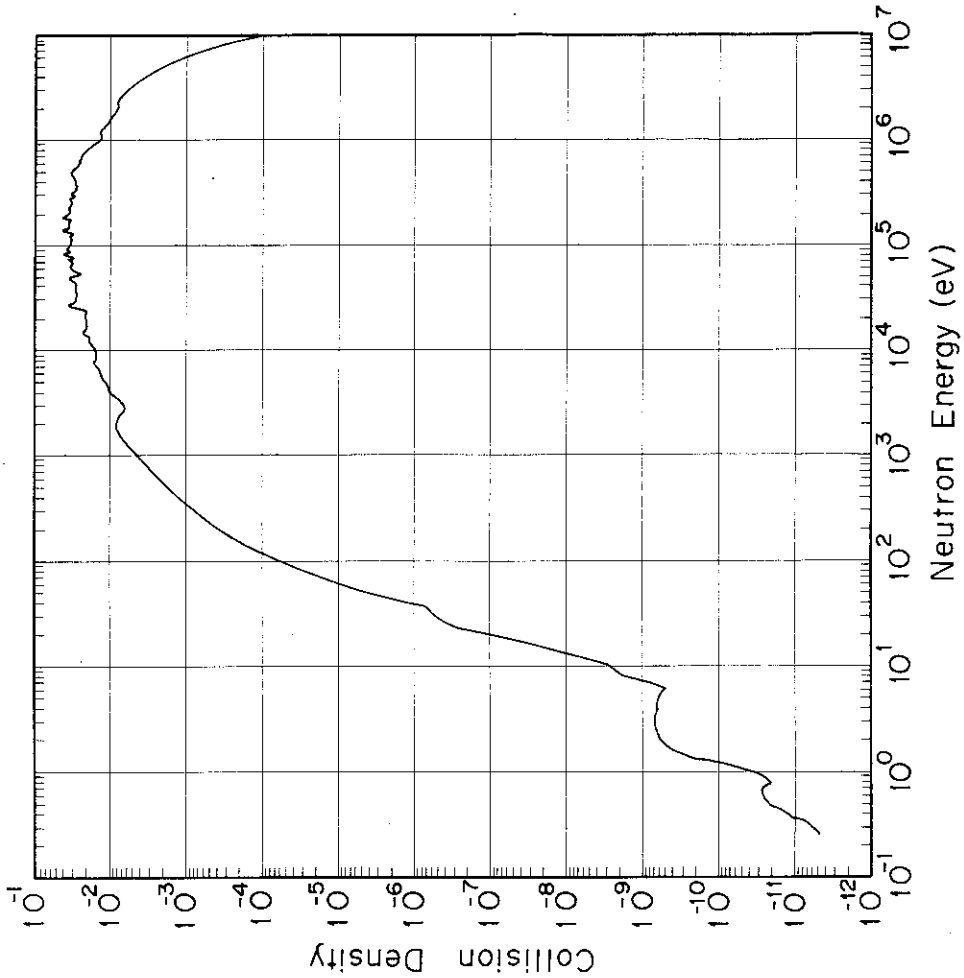

Fig. 6.1 Collision density spectrum calculated for the inner core composition of a prototype fast reactor MONJU using the fine neutron spectrum calculation code ESELEM-4.

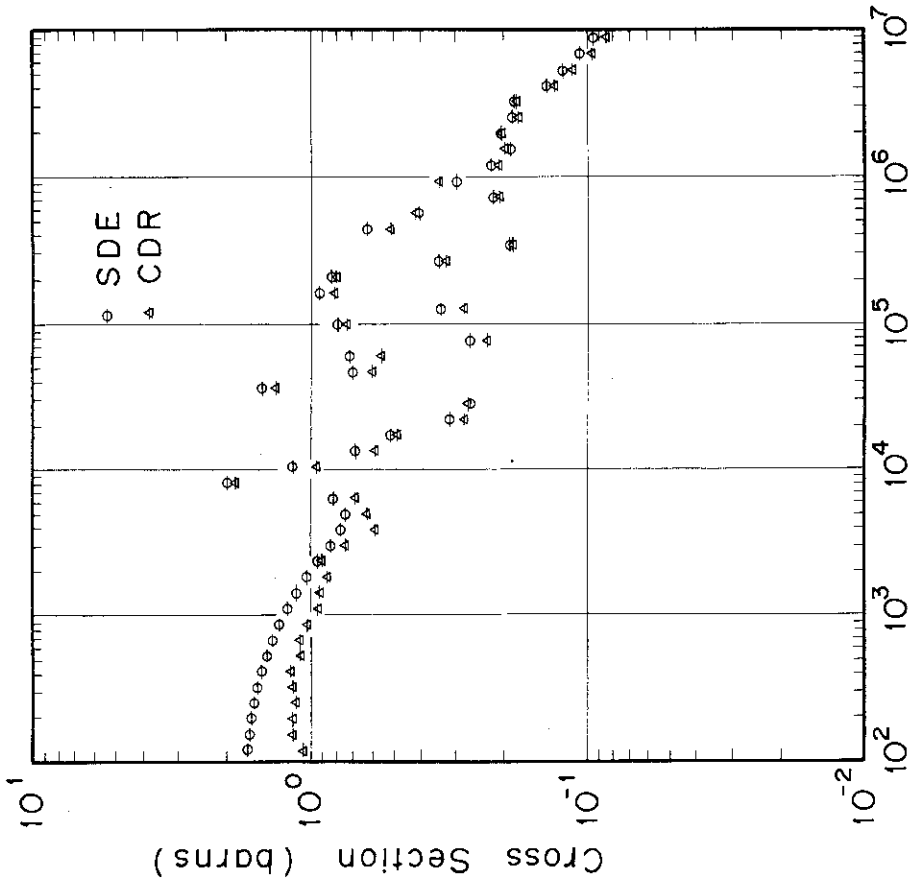

Fig. 6.4 Comparison of iron elastic removal cross sections calculated with the SDE- and CDR-methods.

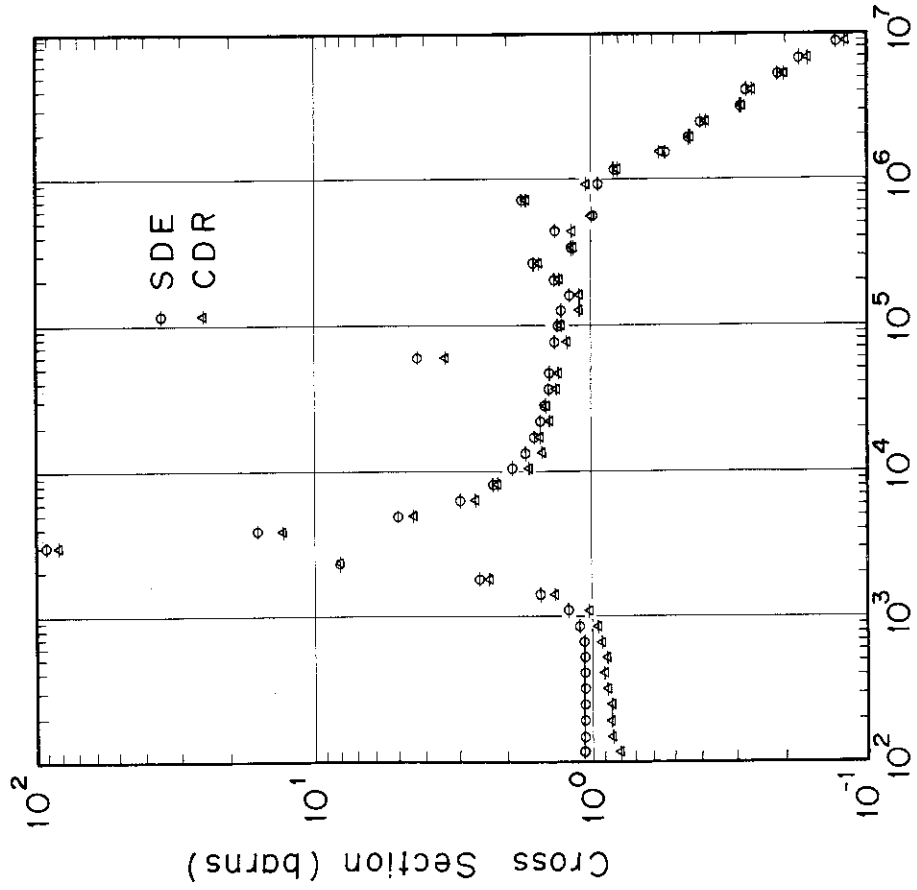

Fig. 6.3 Comparison of sodium elastic removal cross sections calculated with the SDE- and CDR-methods.

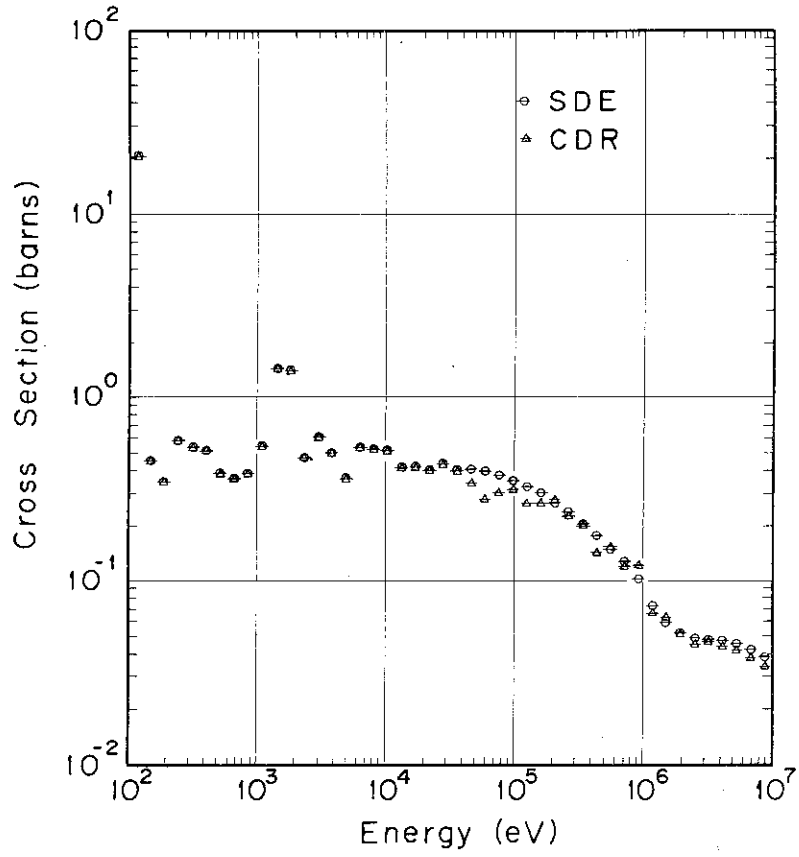

Fig. 6.5 Comparison of ^{238}U elastic removal cross sections calculated with the SDE- and CDR-methods in the energy region from 31.8 keV to 10 MeV. For the energy groups below 31.8 keV the only results calculated with the TFMS-1 code are shown.

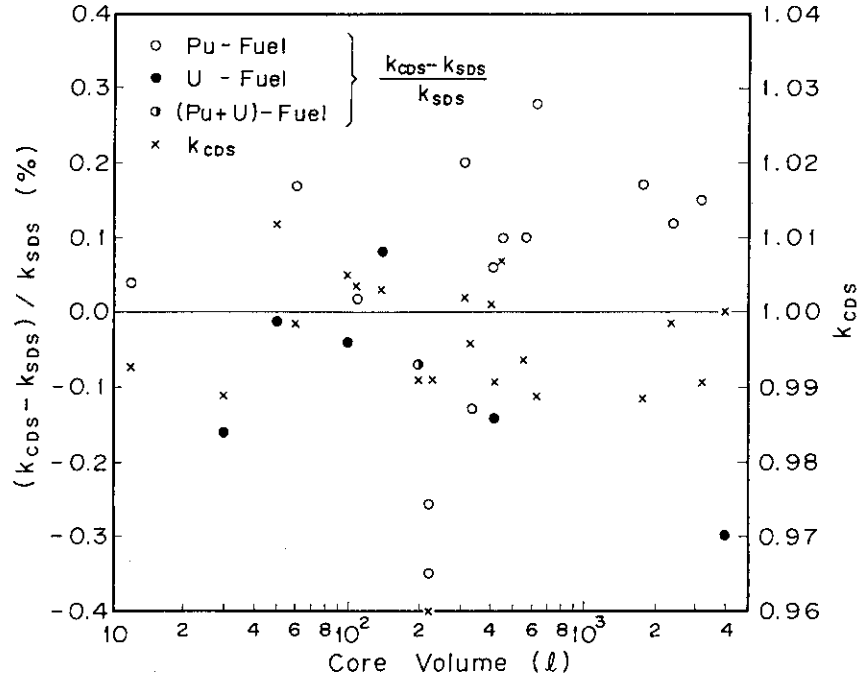

Fig.6.6 The effective multiplication factors (k_{CDS}) calculated with the CDS-sets and the deviations of k_{CDS} from those calculated with the SDS-set.

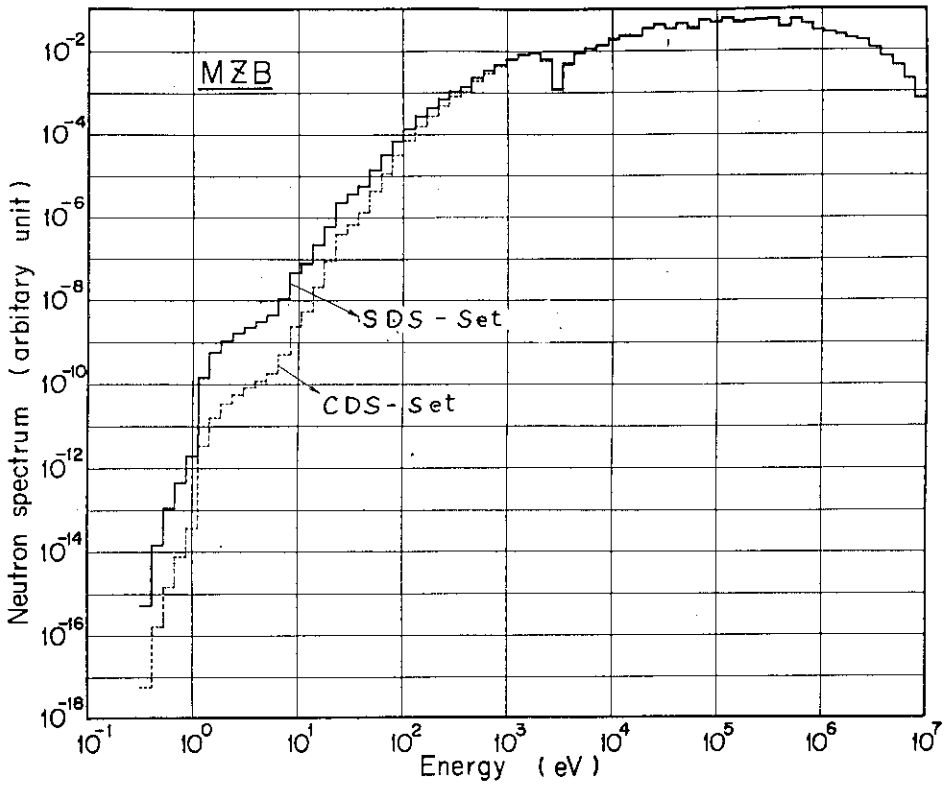

Fig.6.7 Comparison of the neutron spectra calculated with the SDS- and CDS-sets at the core center in the MZB assemblies.

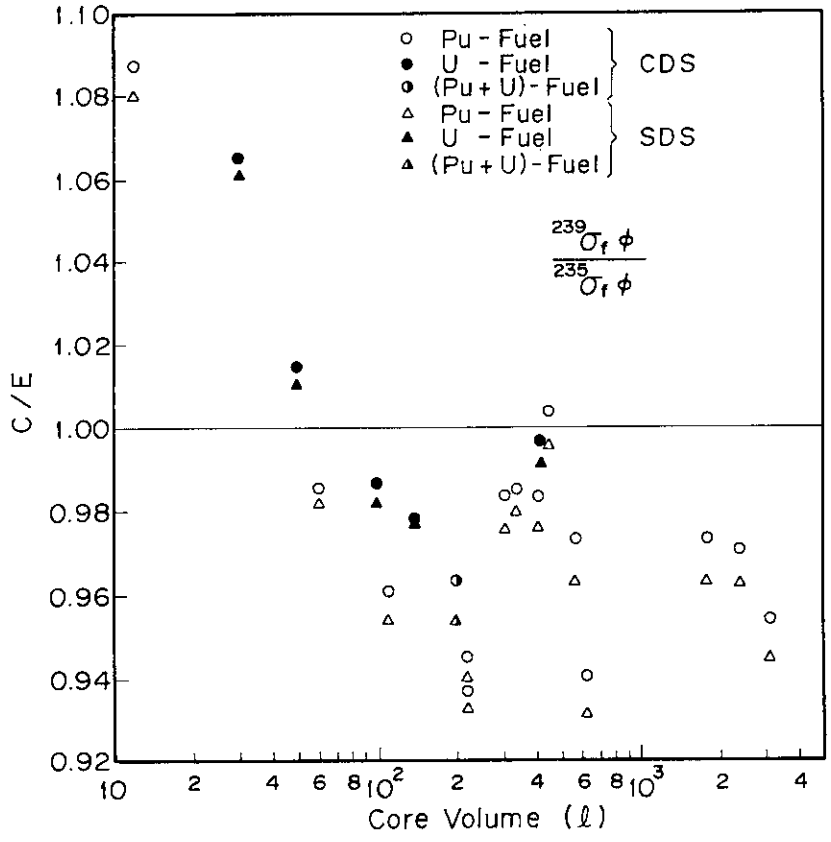

Fig.6.8 Comparison of the C/E-values for the central reaction rate ratios, $^{239}\sigma_f\phi/^{235}\sigma_f\phi$, calculated with the SDS- and CDS-sets.

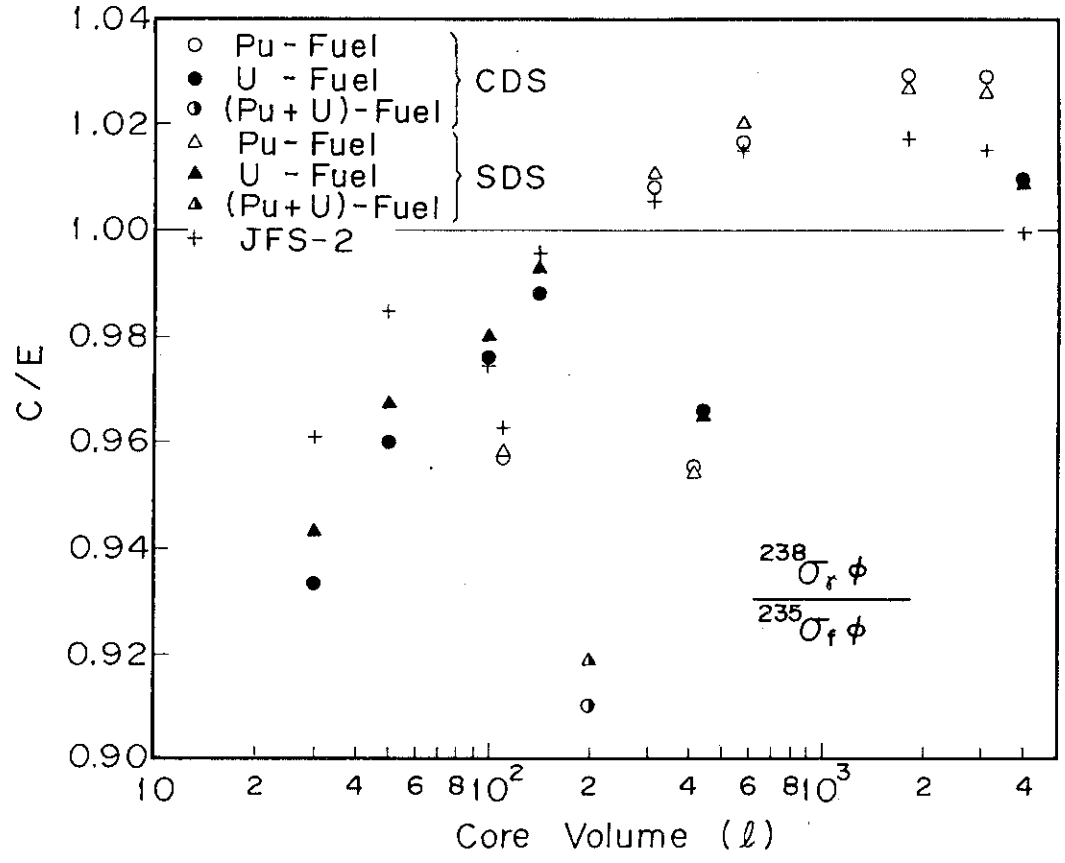

Fig.6.9 Comparison of the C/E-values for the central reaction rate ratios, $^{238}\sigma_\gamma\phi/^{235}\sigma_f\phi$, calculated with the SDS- and CDS-sets.

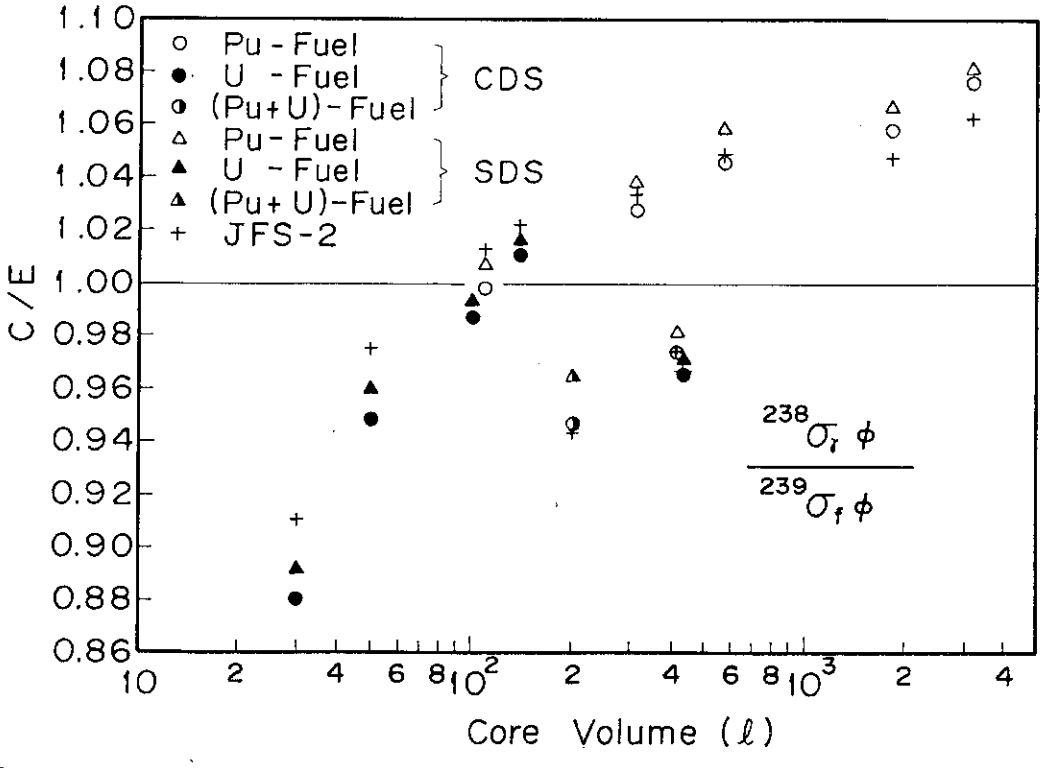

Fig.6.10 Comparison of the C/E-values for the central reaction rate ratios, $^{238}\sigma_\gamma\phi/^{239}\sigma_f\phi$, calculated with the SDS- and CDS-sets.

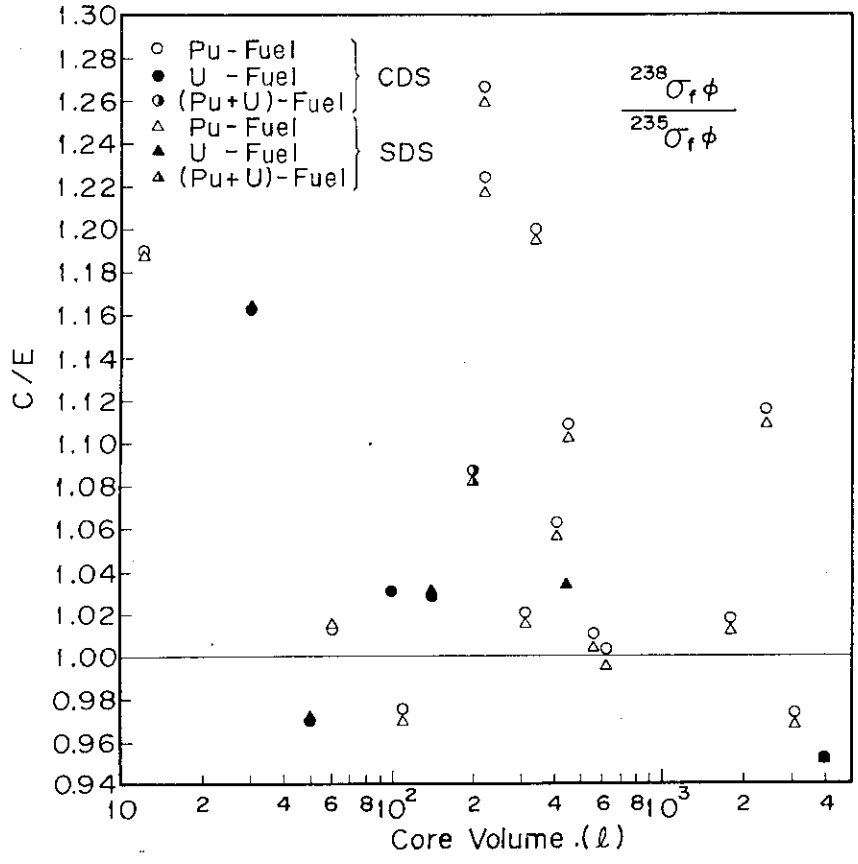

Fig.6.11 Comparison of the C/E-values for the central reaction rate ratios, $^{238}\sigma_f\phi/^{235}\sigma_f\phi$, calculated with the SDS- and CDS-sets.

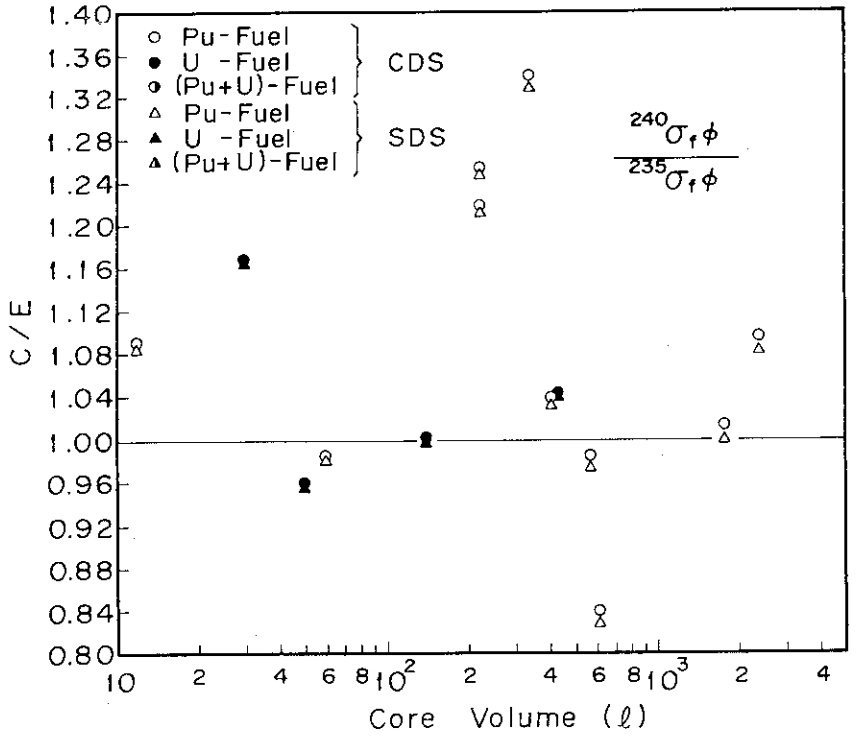

Fig.6.12 Comparison of the C/E-values for the central reaction rate ratios, $^{240}\sigma_f\phi/^{235}\sigma_f\phi$, calculated with the SDS- and CDS-sets.

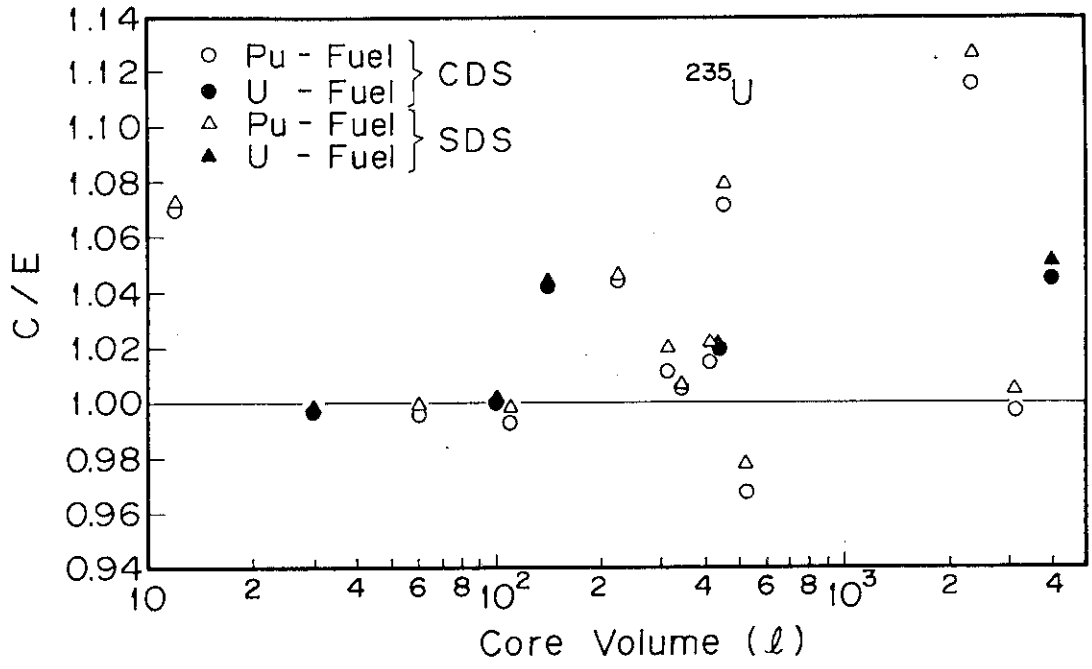

Fig.6.13 Comaprison of the C/E-values for the central sample worth of ^{235}U calculated with the SDS- and CDS-sets.

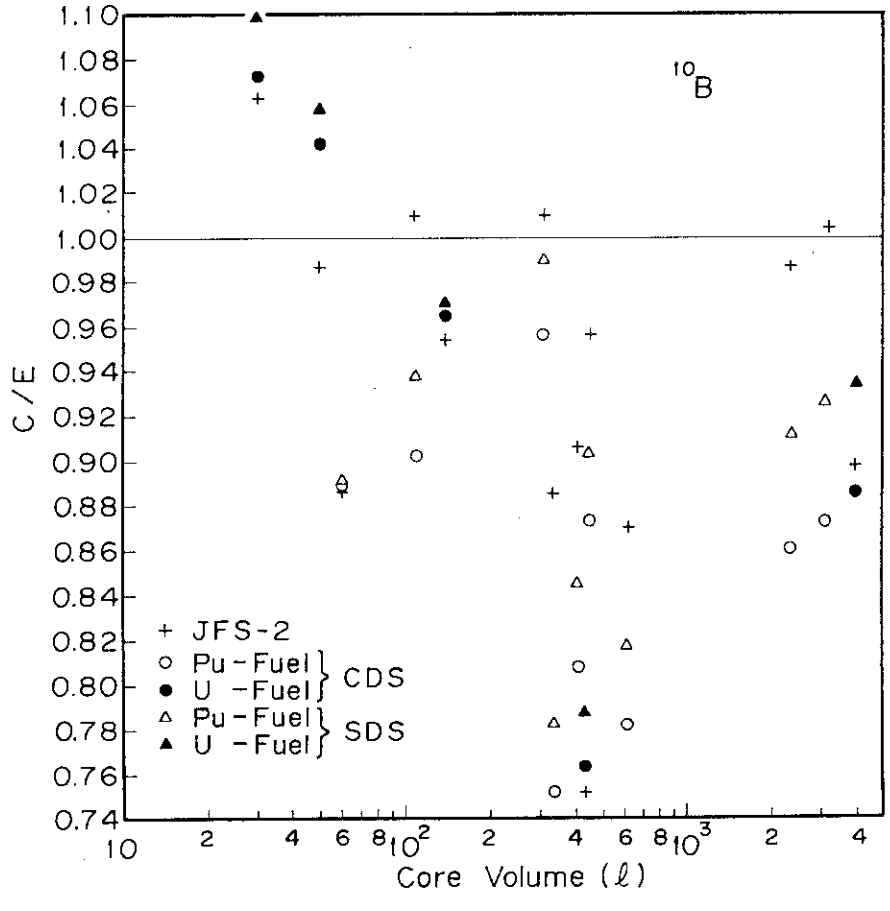

Fig.6.14 Comparison of the C/E-values for the central sample worth of ^{10}B calculated with the SDS- and CDS-sets.

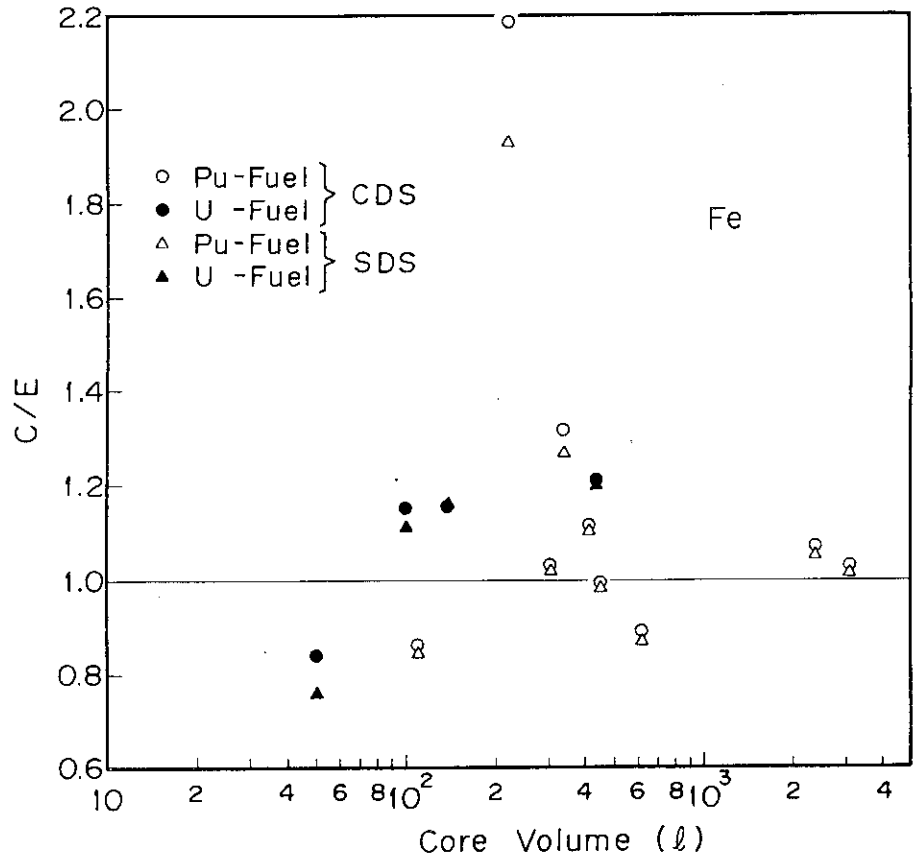

Fig.6.15 Comparison of the C/E-values for the central sample worth of iron calculated with the SDS- and CDS-sets.

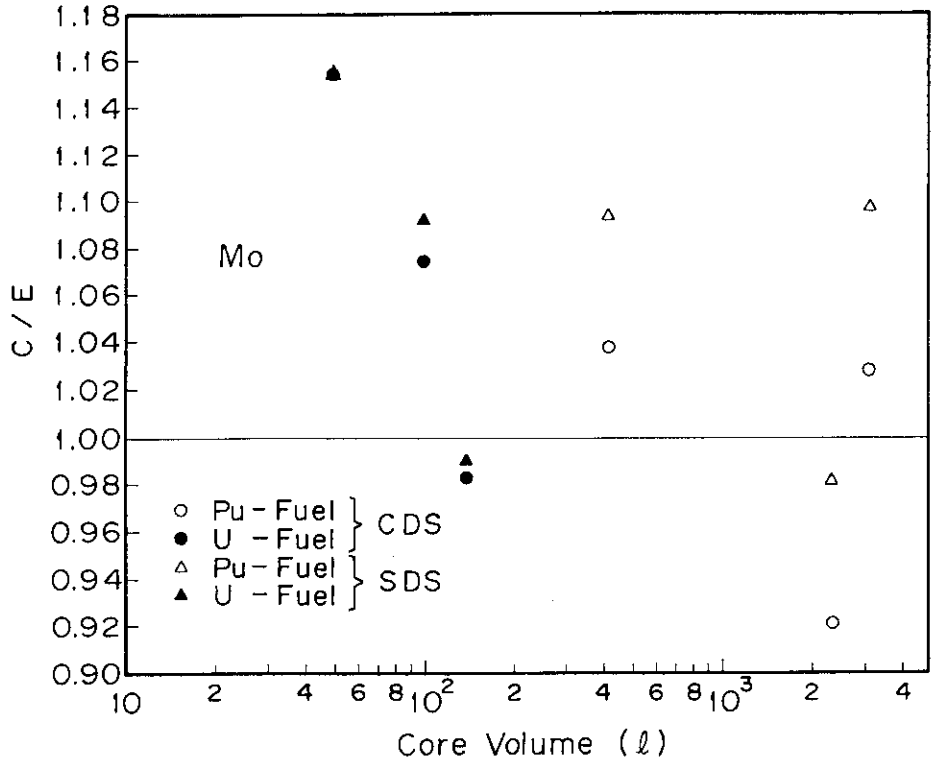

Fig.6.16 Comparison of the C/E-values for the central sample worth of Mo calculated with the SDS- and CDS-sets.

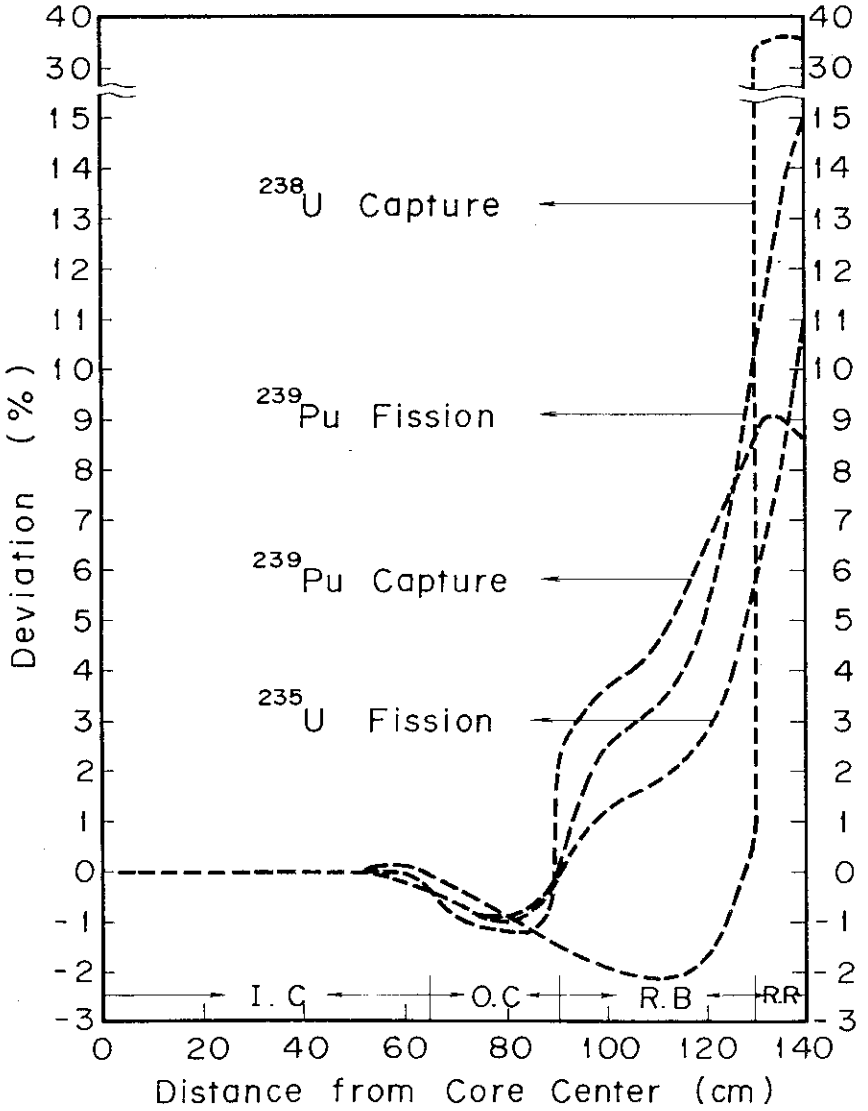

Fig.6.17 Deviation of the reaction rates calculated with the SDS-set from those calculated with the CDS-set in ZPPR-2.

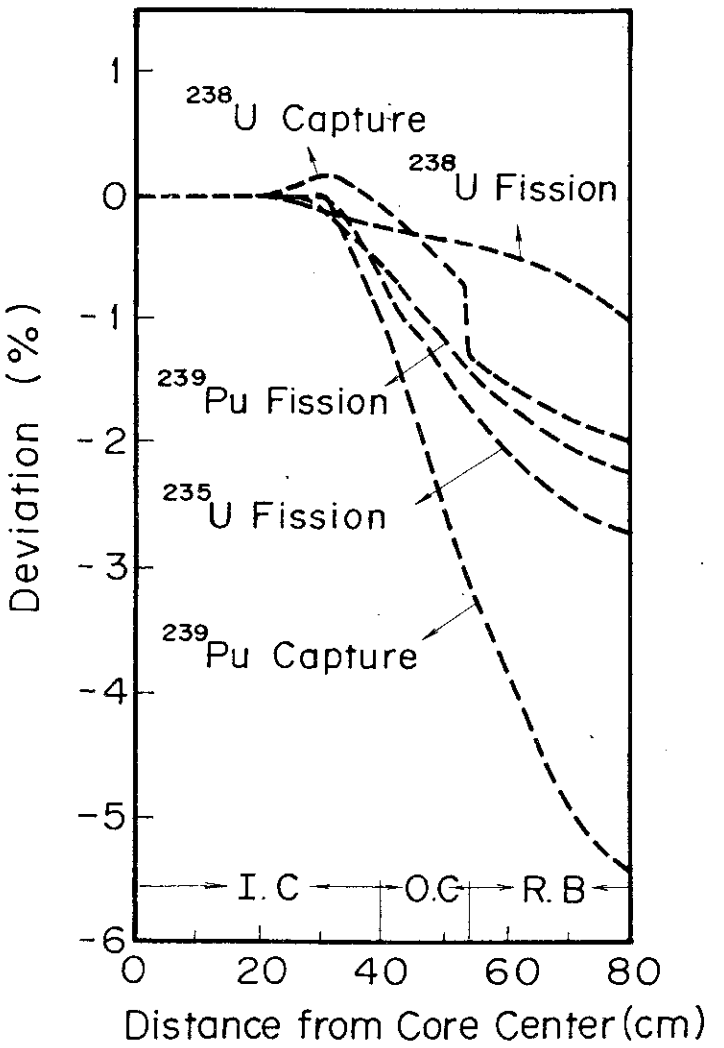

Fig.6.18 Deviation of the reaction rates calculated with the SDS-set from those calculated with the CDS-set in FCA-6-2.

7. Benchmark Tests of the Fast Reactor Group Constant Set JFS-3-J2

7.1 Introduction

Domestic neutron nuclear data library JENDL-1[31] has been developed in JAERI in cooperation with Japanese Nuclear Data Committe (JNDC). after the completion of the JAERI-Fast set version II. Using the JENDL-1, the group constant set of the JFS type with 70 group structure was produced[37] by using the TIMS-1 and PROF-GROUCH-G II codes. Various problems of JENDL-1 were revealed through the benchmark tests and the reevaluation works for neutron cross sections of several nuclides were requested. As the results, the JENDL-2B file was produced as the updated file of JENDL-1. Also for JENDL-2B, the group constant set of JFS type was generated and is called JENDL-2B-70. The benchmark tests of JENDL-2B-70 showed[39] comparable results with ones of JFS-2 described in Chapter 5, except for the overestimate of ∿30 % for the sodium void reactivity. This set is now used for the analyses in JUPITER (Japanese United States Program of Integral Tests and Experimental Researches) project. Furthermore, an advanced set for JENDL-2B-70 has been produced on the basis of the results studied mainly in Chapter 6 and Appendix A. The advanced set is called JFS-3-J2 and differs from JENDL-2B-70 in the followings.

(1) The group cross sections are generated by weighting with a fine-group collision density spectrum calculated for the inner core composition of a prototype fast reactor MONJU, to avoid the overestimate of elastic removal cross sections caused by assuming 1/E-weighting spectrum as described in Chapter 6.

(2) An accuracy of interpolation methods for resonance self-shielding factors has been studied[45] and as the results, the cubic spline method has been recommended as described in Appendix A.1. In JFS-3-J2, the scheme of the shielding factors is corrected to obtain high accracy of interpolation and are tabulated for 8 admixture background cross sections σ_0 = 0, 1, 10, 10^2, 10^3, 10^4, 10^5 and 10^6 barns, 4 temperatures 300, 800, 2100 and 4500 °K and 4 mutual shielding parameters for important heavy resonant materials, respectively.

(3) In JENDL-2B-70, the cross sections were calculated for a temperature 0 °K, excepting the importance heavy resonant elements ^{235}U, ^{238}U, ^{239}Pu, ^{240}Pu and ^{241}Pu processed with the TIMS-1[35] code. However, a strong Doppler effect has been often reported[42]-[44] for structural materials as described in Appendix A.2. Hence, the temperature dependence of capture cross sections for iron, chromium and nickel is considered in the JFS-3-J2 set.

(4) The effect of self-shielding on inelastic scattering cross sections was neglected by assuming a small energy dependence of the cross sections. This assumption is generally valid. An exception[46] is iron for which the energy dependence of both inelastic scatteirng and total cross sections below ∿2 MeV is rapidly as seen in Appendix A.3. Hence, the self-shielding factors of inelastic scattering cross sections are tabulated in JFS-3-J2.

(5) In more accurate calculations of transport theory, Legendre higher order terms of scatteing are required. The neutron group to group transfer matrics of elastic scattering are expanded from P_0 to P_3.

(6) The fission spectrum depends on fissionable materials. In the reactor calculations for thorium, uranium or pulutonium fuel core,

the fission spectrum for a main fuel isotope may be used. For mixed fuels of uarnium and plutonium as seen in FCA V and V1 assemblies, an averaged fission spectrum[47] may be defined to produce an accurate spectrum, as described in Appendix A.4. In the present group constant library, hence, the fission spectrum for each fissionable element is included.

(7) The JAERI standard group structure established for the intended application to LMFBR, LWR and shielding problems is adopted. The 70 group structure for LMFBR is composed of 69 groups for the energy range from 0.3224 eV the 10 MeV with the lethargy of 0.25 and one thermal group, as shown in Table 7.1.

The production of JFS-3-J2 has been performed by using a code system TIMS-PGG[215] which has been developed by connecting functionaly the TIMS-1, RESENDD[216], PROF-GROUCH-GIIR[217] and several utility codes. The flow chart is shown in Fig. 7.1. In this figure, the standard neutronic codes in JAERI which are available for JFS-3-J2 are also shown. In the present status, the group constants for the 30 nuclides are generated by using the TIMS-PGG code system. The selected nuclides and the code numbers used in the standard neutronic codes are shown in Table 7.2. The tables of the group constants for the fifteen important nuclides in fast reactor calculations are shown in Ref.(215).

In the next section, the benchmark tests of JFS-3-J2 are performed and the results are discussed by being compared with those calculated with the JENDL-2B-70 set. In Section 7.3, furthermore, the detailed analyses for several integral experiments (sodium void reactivity and

reaction rate distribution) are performed and the applicability of JFS-3-J2 is discussed.

7.2 Comparison between Benchmark Tests for the JFS-3-J2 and JENDL-2B-70 Sets

Benchmark calculations were performed for 21 fast critical assemblies with the one-dimensional models used in the benchmark tests of JFS-2. The 21 assemblies consist of 18 assemblies selected by Hardie et al., the MOZART cores (MZA, MZB) and FCA-V assembly 2. Te results calculated with JFS-3-J2 and JENDL-2B-70 were compared in the form of C/E values.

Effective Multiplication Factors: Table 7.3

The average of C/E-values calculated with JFS-3-J2 is 0.9988 as a whole and it is better than 0.9948 of JENDL-2B-70. The standard deviation for JFS-3-J2 is nearly equal to that of JENDL-2B-70 for both the plutonium and uranium fuel cores. The average values for the plutonum cores are 0.9966 for JFS-3-J2 and 0.9933 for JENDL-2B-70. The value averaged by omitting ZPR-3-54 is 0.9996 for JFS-3-J2 and hence the applicability to k_{eff} is very satisfactory.

Central Reaction Rate Ratios

a) σ_f(U-238)/σ_f(U-235): Tables 7.4 and 5

In the plutonium cores, the calculated values are overestimated by 7 % for JFS-3-J2 and 10 % for JENDL-2B-70 on the average, respectively, though the overestimates are smaller for the uranium cores.

Though the overestimates of JENDL-2B-70 are reduced by ∿2 % in the results of JFS-3-J2, there are seen the discrepancies between the Pu and U cores which was very small for JFS-2 as described in Chapter 5.

b) σ_f(Pu-239)/σ_f(U-235): Table 7.6

The values calculated with JFS-3-J2 are underestimated by ∿3 % for the plutonium cores, though they are in good agreement with the experimental values for the U-cores. The results of JENDL-2B-70 becomes large by ∿0.6 % on the average for the Pu cores.

c) σ_c(U-238)/σ_f(Pu-239): Table 7.7

The resuls of JFS-3-J2 become smaller than those of JENDL-2B-70, and the average of C/E values is nearly equal to unity. However, for ZPR-6-7, MZA and MZB there exist the same overestimates as the result for JFS-2 in Chapter 5.

Central Sample Worths: Tables 7.8 and 9

In order to avoid the scaling problem, both the calculated and measured sample worths were normalized to those of ^{239}Pu, respectively. The C/E values are compared in Tables 7.8 and 9.

For the sample worths of ^{235}U and ^{238}U, the discrepancies between JFS-3-J2 and JENDL-2B-70 are small and both results are in very good agreement with the experiments on the average. The worths of ^{10}B calculated with JFS-3-J2 become about 3 % smaller than those of JENDL-2B-70, and the calculated value is underestimated by ∿13 % on the average. The averaged worths of carbon are overestimated by ∿30 % for both JFS-3-J2 and JENDL-2B-70. As for the sodium worths, the differences between

the calculated and measured values are very large and the sign is negative for some cases. The averaged worths of iron calculated with JFS-3-J2 becomes 15 % larger than that of JENDL-2B-70.

7.3 Benchmark Calculations with Two-dimensional Model

The applicability of JFS-3-J2 was tested to sodium void reactivities and reaction rate distributions in the FCA-V1-2 and ZPPR-9 assemblies. Especially, ZPPR-9 is a clean physics benchmark with a core volume of 4600 liters to study the effects of two-core zones with a more realistic LMFBR height and oxide blanket, and is the first assembly of the JUPITER program. The calculations are based on the two-dimensional model and the perturbation theory. The cell heterogeneity effect was calculated with the use of the integral transport code SLAROM. Also for the JFS-2 and JFS-3-B4 sets, the calculations were performed and the results were compared with those of JFS-3-J2. The JFS-3-B4 set was produced by using the TIMS-PGG code system from the ENDF/B-IV nuclear data file.

7.3.1 Sodium Void Reactivity: Table 7.10

The correction factors of the heterogeneity to homogeneous, the exact to the first-order perturbation and the transport to diffusion were calculated by using the JFS-3-J2 set. The heterogeneity effect contains the streaming effect considered by introducing anisotoropic diffusion coefficients. The independence of the correction factors on different group constant sets was assumed and the same correction factors were used for the JFS-3-B4 and JFS-2.

The results calculated with the JFS-3-J2 are considerably overestimated by 31 ∿ 55 % for FCA-V1-2 and 10 ∿ 55 % for ZPPR-9 with

the increase of voided regions. The results for JFS-3-B4 are also overestimated, though they are smaller by ∿5 % than those of JFS-3-J2. On the other hand, the JFS-2 shows better prediction than those for JFS-3-J2 and JFS-3-B4, though the JFS-2 underestimates for small voided regions and overestimates for large ones. The results for JFS-2 are very satisfactory for the target accuracy of ±20 %[19] requested from the prediction of fast breeder characteristics.

In the sodium void reactivity, the scattering component provides about 80 ∿ 90 percents of the total reactivity. The scattering term is very sensitive to the change of adjoint flux, because the reactivity of scattering term changes as a factor of $(\phi^*_{i+1} - \phi^*_i)$ where ϕ^*_i is the adjoint flux at the energy group (i). Figure 7.2 shows the comparison of the groupwise contributions of the scattering terms calculated with the three different sets for the sodium voided region of 7×7×8 packs in FCA-V1-2. From this figure, the positive reactivities are seen for the energy region above 20 keV and there are large positive contributions in the vicinity of 60 keV and 2 MeV. Furthermore, for the JFS-3-J2 the positive reactivity contributions are seen in the neighhood of 3 keV, i.e., the sodium resonance, while the JFS-2 show the negative reactivitives in the same region. As a whole, the results of JFS-2 show lower reactivities than those of JFS-3-J2 and JFS-3-B4, because the dependence of the adjoint spectrum for JFS-2 on the energy is gentler slope than the other ones as seen in Fig. 7.3. The discrepancies in the vicinity of the sodium resonance should be noticed especially.

Though the total reactivities for JFS-3-J2 and JFS-3-B4 are the same about, the tendency for the group contributions is very different. The JFS-3-J2 has larger reactivities in the vicinity of 4 keV and 5 MeV,

and smaller ones in the range from 5 to 100 keV in comparison with the result of JFS-3-B4. These differences are mainly caused by both the discrepancies in the perturbed macroscopic cross sections and the adjoint spectra as seen in Fig. 7.3.

The group constants for JFS-2 and JFS-3-B4 have been produced by using the nuclear data of ENDF/B-1V, except for ^{235}U, ^{238}U, ^{239}Pu, ^{240}Pu, ^{241}Pu and ^{10}B. Hence, the discrepancy between the sodium void reactivities calculated with the two sets is due to the difference in the adjoint spectra caused by these different cross sections, especially, by ^{238}U and ^{239}Pu.

7.3.2 Reaction Rate Distribution

The analyses of the reaction rate distributions in the FCA-V1-2 and ZPPR-9 assemblies have been performed with the two-dimensional models. The heterogeneity effect was calculated by using the integral transport code SLAROM and the S_n transport calculations were performed by the TWOTRAN-II code.

FCA-V1-2: Figs. 7.4 ∿ 7.8

The radial and axial reaction rate traverses are shown in Figs. 7.4 ∿ 7.8, respectively, as the form of the distribution normalized to unity at the core center and of the C/E value. In these figures, the results calculated with the JFS-3-J2, JFS-3-B4 and JFS-2 are compared. The calculations for radial traverses of ^{239}Pu, ^{235}U and ^{238}U fission rate are overestimated in the region from the driver to the middle of blanket, and underestimated steeply in the edge of blanket. The tendencies of C/E values for the three sets are similary to each other, though the results for JFS-3-B4 are more overestimated.

Especially, the overesitmates for ^{238}U fission rates are very remarkable in the driver region, and the distribution calculated is not smooth as compared with the experiment. On the other hand, the axial distributions of ^{235}U and ^{238}U fission rates are in very good agreement with the experiments in the test region. In the edge of blanket, however, the calculation is considerably underestimated in the same as the case of the radial traverse.

ZPPR-9: Figs. 7.9 and 7.20

In ZPPR-9, the fission reaction rate distributions for many nuclides, ^{239}Pu, ^{235}U, ^{238}U, ^{233}U, ^{234}U, ^{236}U and ^{240}Pu, and the capture reaction rate for ^{238}U were measured. The results calculated with the three sets are compared with the experiments in Figs. 7.9 ∿ 7.19. The calculational and experimental values were normalized to unity at the next position from the core center, respectively.

^{239}Pu fission rate: Figs. 7.9 and 7.10

The calculated radial distributions are overestimated in the region from the outer side of inner core to the outer core. The result of JFS-2 shows the smallest overestimate. The axial distribution was measured only for the inner core region. The calculations are underestimated in the outer reigon of inner core, though the result of JFS-2 shows the smallest underestimate of 1.3 %.

^{238}U fission rate: Figs. 7.11 and 7.12

The radial and axial distributions are compared in Figs. 7.11

and 7.12 respectively. The radial distributions are overestimated in the radial blanket and axial distributions are considerably underestimated in the axial blanket. The cause of the large discrepancy between the radial and axial distributions is not alway clear.

^{238}U capture rate: Figs. 7.13 and 7.14

The agreement between the calculations and experiments is very satisfactory for the radial and axial distributions in the blankets, as compared with the results of the ^{238}U fission reaction rates, though the overestimate for the radial distributions and the underestimate for the axial ones are seen. The results for JFS-2 are more satisfactory than those for JFS-3-J2 and JFS-3-B4.

^{235}U fission rate: Figs. 7.15 and 7.16

The calculational values for JFS-2 are in good agreement with the experimental values. The results of JFS-3-B4 show the largest overestimate for the radial distribution in the outer core and the largest underestimate for the axial distribution in the axial blanket.

^{233}U, ^{234}U, ^{236}U and ^{240}Pu fission rates: Figs. 7.17 ∿ 7.20

The radial fission rates for these nuclides are overestimated in the outer core region and underestimated in the blanket. Especially, the fission rates of ^{234}U and ^{236}U are remarkably underestimated in the blanket. The discrepancy between these underestimates and the overestimate for ^{238}U fission rate as seen in Fig. 7.11 is not clear, because the fission cross sections for these nuclides are the threshold reaction.

7.4 Concluding Remarks

The one-dimensional bechmark calculations have been performed for the two sets of JFS-3-J2 and JENDL-2B-70. The average value for the C/E-values of k_{eff} was 0.9988 for all the twenty-one cores, and 0.9996 for the fourteen pultonium fuel cores excepting the ZPR-3-54 assembly. These results were more satisfactory than those of JENDL-2B-70, ENDF/B-IV and JFS-2. The predictions of JFS-3-J2 to various central reaction rate ratios were better than them of JENDL-2B-70, and comparable with them of JFS-2. However, also the advanced set JFS-3-J2 for JENDL-2B-70 were not able to remove the underestimate for the central reaction rate ratio of ^{239}Pu fission to ^{235}U fission and the overestimate for the sodium void reactivity. To remove these problems, the evaluation method for cross sections based on the adjustment method as used for the production of JFS-2 may be studies in detail.

The sodium void reactivities and reaction rate distributions have been analysed in detail with the two-dimensional models for the FCA-VI-2 and ZPPR-9 assemblies. The calculations have been performed by using three sets of JFS-3-J2, JFS-3-B4 and JFS-2. The sodium void reactivities calculated for JFS-3-J2 and JFS-3-B4 were remarkably overestimated with the increase of the sodium voided region, while the results of JFS-2 were satisfactory.

The radial reaction rate distributions have been overestimated in the region from outer core (or driver) to the middle of blanket and underestimated in outer side of the blanket, though an exception is the overestimate for ^{238}U fission rate in the blanket region of ZPPR-9. The axial reaction rate traverses have been underestimated with the progress of the region from the core to the blanket. Especially, the axial traverse of ^{238}U fission rate in ZPPR-9 was

remarkably underestimated in the blanket.

In the present study, the JFS-3-J2 set was generated on the basis of the advanced concept for JENDL-2B-70 which is the group constants of the JFS-2 type and, moreover, using the recently evaluated nuclear data of JENDL-2. However, the benchmark tests of JFS-3-J2 showed that the prediction for nuclear characteristics was not always satisfactory in comparison with the results calculated with the JFS-2 set as a whole. This may propose a limitation of the prediction for nuclear characteristics calculated by using the nuclear data compilations which are produced only by conventional evaluation works. In the present accuracy of the nuclear data, hence, to elevate the prediction for JFS-3-J2, the reevaluations of nuclear data should be examined on the basis of the sensitivity and/or the adjustment studies for group cross sections.

Table 7.1 Seventy group structure of JFS-3-J2 library

Group	Upper energy		Lower energy		Lethargy width
1	10.0	(MeV)	7.7880	(MeV)	0.250
2	7.7880		6.0653		0.250
3	6.0653		4.7237		0.250
4	4.7237		3.6788		0.250
5	3.6788		2.8650		0.250
6	2.8650		2.2313		0.250
7	2.2313		1.7377		0.250
8	1.7377		1.3534		0.250
9	1.3534		1.0540		0.250
10	1.0540		0.82085		0.250
11	0.82085		0.63928		0.250
12	0.63928		0.49787		0.250
13	0.49787		0.38774		0.250
14	0.38774		0.30197		0.250
15	0.30197		0.23518		0.250
16	0.23518		0.18316		0.250
17	0.18316		0.14264		0.250
18	0.14264		0.11109		0.250
19	0.11109	(MeV)	0.086517	(MeV)	0.250
20	86.517	(keV)	67.379	(keV)	0.250
21	67.379		52.475		0.250
22	52.475		40.868		0.250
23	40.868		31.828		0.250
24	31.828		24.788		0.250
25	24.788		19.305		0.250
26	19.305		15.034		0.250
27	15.034		11.709		0.250
28	11.709		9.1188		0.250
29	9.1188		7.1017		0.250
30	7.1017		5.5308		0.250
31	5.5308		4.3074		0.250
32	4.3074		3.3546		0.250
33	3.3546		2.6126		0.250
34	2.6126		2.0347		0.250
35	2.0347	(keV)	1.5846	(keV)	0.250

Table 7.1 (Continued)

Group	Upper energy	Lower energy	Lethargy width
36	1.5846	1.2341	0.250
37	1.2341 (keV)	0.96112 (keV)	0.250
38	961.12 (eV)	748.52 (eV)	0.250
39	748.52	582.95	0.250
40	582.95	454.00	0.250
41	454.00	353.58	0.250
42	353.58	275.36	0.250
43	275.36	214.45	0.250
44	214.45	167.02	0.250
45	167.02	130.07	0.250
46	130.07	101.30	0.250
47	101.30	78.893	0.250
48	78.893	61.442	0.250
49	61.442	47.851	0.250
50	47.851	37.267	0.250
51	37.267	29.023	0.250
52	29.023	22.603	0.250
53	22.603	17.603	0.250
54	17.603	13.710	0.250
55	13.710	10.677	0.250
56	10.677	8.3153	0.250
57	8.3153	6.4760	0.250
58	6.4760	5.0435	0.250
59	5.0435	3.9279	0.250
60	3.9279	3.0590	0.250
61	3.0590	2.3824	0.250
62	2.3824	1.8554	0.250
63	1.8554	1.4450	0.250
64	1.4450	1.1254	0.250
65	1.1254	0.87642	0.250
66	0.87642	0.68256	0.250
67	0.68256	0.53158	0.250
68	0.53158	0.41399	0.250
69	0.41399	0.32242	0.250
70	0.32242 (eV)	10^{-5} (eV)	10.650

Table 7.2 Nuclides contained in JFS-3-J2 and nuclear data file used for the production

No.	Nuclide	Nuclear data file	MATNO	Code No.	No. of σ_0	No. of T
1	U-235	JENDL-2	9235	925	8	4
2	U-238	JENDL-2	9238	928	8	4
3	Pu-239	JENDL-2	9439	949	8	4
4	Pu-240	JENDL-2	9440	940	8	4
5	Pu-241	JENDL-2	9441	941	8	4
6	U-234	JENDL-1	1921	924	8	4
7	Th-232	JENDL-1	1901	902	8	4
8	Am-241	JENDL-1	1951	951	8	1
9	Ni	JENDL-2	2800	28	8	4
10	Cr	JENDL-2	2400	24	8	4
11	Fe	JENDL-2	2600	26	8	4
12	Mo	JENDL-1	1420	42	8	1
13	Cu	JENDL-1	1290	29	8	1
14	Mn	JENDL-1	1251	25	8	1
15	Si	JENDL-1	1140	14	8	1
16	Aℓ	JENDL-1	1131	13	8	1
17	Na	JENDL-1	1111	11	8	1
18	C	JENDL-1	1061	6	8	1
19	B-10	JENDL-1	1051	105	8	1
20	H-1	JENDL-1	1011	1	8	1
21	U-233	ENDF/B-IV	1260	923	8	4
22	U-236	ENDF/B-IV	1163	926	8	4
23	Pu-242	ENDF/B-IV	1161	942	8	4
24	Be	ENDF/B-IV	1289	4	8	1
25	B-11	ENDF/B-IV	1160	115	8	1
26	O	ENDF/B-IV	1276	8	8	1
27	Ta-181	JENDL-1	1731	731	8	4
28	Np-237	ENDF/B-1V	1236	937	8	4
29	Eu-151	ENDF/B-1V	1240	631	8	4
30	Eu-153	JENDL-1	1631	633	8	4

Table 7.3 Comparison of effective multiplication factors calculated with one-dimensional diffusion model

* PLUTONIUM FUEL ASSEMBLY	JFS-3-J2	JENDL-2B-70	* URANIUM FUEL ASSEMBLY	JFS-3-J2	JENDL-2B-70
VERA-11A	0.99487	0.99236	VERA-1B	0.99990	0.99537
ZEBRA-3	1.00153	0.99825	ZPR-3-6F	1.01377	1.01225
SNEAK-7A	1.00667	1.00135	ZPR-3-12	1.00717	1.00114
ZPR-3-54	0.95412	0.95443	ZPR-3-11	1.00475	1.00211
ZPR-3-53	0.99284	0.99116	ZEBRA-2	0.99411	0.98314
SNEAK-7B	1.00602	0.99852	ZPR-6-6A	1.00549	0.99384
ZPR-3-50	1.00134	0.99709	* AVERAGE OF C/E	1.00420	0.99881
ZPR-3-48	1.00482	1.00049	* AVERAGE (C/E)-1.0	0.00420	-0.00119
ZPR-3-49	1.01048	1.00546			
ZPR-3-56B	0.99220	0.98885	* AVERAGE OF ABS(1.0-C/E)	0.00619	0.00636
ZPR-6-7	0.99607	0.99368			
ZPPR-2	1.00302	1.00037	* STND. DEV. OF C/E	0.00609	0.00870
MZA	0.99869	0.99449			
MZB(1)	0.99537	0.99113			
FCA-5-2	0.99052	0.99118	SUMMARY OF ALL ASSEMBLIES		
* AVERAGE OF C/E	0.99657 (0.9996)	0.99325 (0.99603)	* AVERAGE OF C/E	0.99875	0.99484
* AVERAGE (C/E)-1.0	-0.00343	-0.00675	* AVERAGE (C/E)-1.0	-0.00125	-0.00516
* AVERAGE OF ABS(1.0-C/E)	0.00795	1.00777	* AVERAGE OF ABS(1.0-C/E)	0.00745	0.00737
* STUND, DEV. OF C/E	0.01271	0.01134	* STND. DEV. OF C/E	0.01174	0.01094

The values averaged by omitting ZPR-3-54 are presented in the parentheses.

Table 7.4 Comparison of central reaction rate ratios, ^{238}U fission/^{235}U fission in the plutonium cores

* C/E OF CENTRAL REACTION RATE RATIO

* PLUTONIUM FUEL

NO.	ASSEMBLY	EXPERIMENT	JFS-3-J2	JENDL-2B-70
1	VERA-11A	.0.07700	1.18920	1.19512
4	ZEBRA-3	0.04610	0.99966	1.01831
6	SNEAK-7A	0.04480	0.96597	0.98531
8	ZPR-3-54	0.02540	1.25663	1.28831
9	ZPR-3-53	0.02540	1.21043	1.24520
10	SNEAK-7B	0.03300	1.01234	1.03589
11	ZPR-3-50	0.02510	1.17903	1.21640
12	ZPR-3-48	0.03260	1.04852	1.07510
14	ZPR-3-49	0.03450	1.09399	1.11971
15	ZPR-3-56	0.03080	0.98962	1.00845
16	ZPR-6-7	0.02300	0.95751	0.97974
18	ZPPR-2	0.02010	1.09709	1.12270
19	MZA	0.03366	0.99901	1.02070
20	MZB	0.02256	1.02141	1.04750
21	FCA-5-2	0.03960	1.05781	1.12503
* AVERAGE OF C/E			1.07188	1.0989
* AVERAGE(C/E)-1.0			0.07188	0.0989
* AVERAGE OF ABS(1.0-C/E)			0.08364	0.10356
* STND.DEV.OF C/E			0.09242	0.09560

Table 7.5 Comparison of central reaction rate ratios, ^{238}U fission/^{235}U fission in the uranium cores

* C/E CENTRAL REATION RATE RATIO ---

* URANIUM FUEL

No.	ASSEMBLY	EXPERIMENT	JFS-3-J2	JENDL-2B-70
2	VERA-1B	0.06600	1.15981	1.17348
3	ZPR-3-6F	0.07800	0.94354	0.95136
5	ZPR-3-12	0.04700	1.01969	1.03974
7	ZPR-3-11	0.03800	1.01329	1.03310
13	ZEBRA-2	0.02300	1.02035	1.04898
17	ZPR-6-6A	0.02450	0.94392	0.96096
* AVERAGE OF C/E			1.01677	1.03460
* AVERAGE(C/E)- 1.0			0.01677	0.0346
* AVERAGE OF ABS(1.0 - C/E)			0.05428	0.06383
* STND. DEV. OF C/E			0.07207	0.07289

SUMMARY OF ALL ASSEMBLIES

* AVERAGE OF C/E	1.05613	1.08053
* AVERAGE (C/E) - 1.0	0.05613	0.08053
* AVERAGE OF ABS (1.0 - C/E)	0.07526	0.09221
* STND. DEV. OF C/E	0.09058	0.09429

Table 7.6 Comparison of central reaction rate ratios, ^{239}Pu fission/^{235}U fission

* C/E OF CENTRAL REACTION RATE RATIO

* PLUTONIUM FUEL

NO.	ASSEMBLY	EXPERIMENT	JFS-3-J2	JENDL-2B-70
1	VERA-11A	1.07000	1.08517	1.08303
4	ZEBRA-3	1.19000	0.98387	0.98184
6	SNEAK-7A	1.01600	0.95831	0.96457
8	ZPR-3-54	0.92800	0.93915	0.95418
9	ZPR-3-53	0.92800	0.93138	0.94739
10	SNEAK-7B	1.01200	0.98205	0.98437
11	ZPR-3-50	0.90300	0.97884	0.99314
12	ZPR-3-48	0.97600	0.97971	0.98711
14	ZPR-3-49	0.98600	1.00067	1.00565
15	ZPR-3-56	1.02800	0.93658	0.94125
16	ZPR-6-7	0.95300	0.94911	0.95607
18	ZPPR-2	0.93700	0.96593	0.97497
19	MZA	1.01338	0.96971	0.97484
20	MZB	0.94877	0.96786	0.97629
21	FCA-5-2	1.10400	0.96164	0.96401
* AVERAGE OF C/E			0.97267	0.97938
* AVERAGE (C/E)-1.0			-0.02733	-0.02062
* AVERAGE OF ABS (1.0-C/E)			0.03878	0.03244
* STND. DEV. OF C/E			0.03543	0.03244

* URANIUM FUEL

No.	ASSEMBLY	EXPERIMENT	JFS-3-J2	JENDL-2B-70
2	VERA-1B	1.07000	1.06529	1.06721
3	ZPR-3-6F	1.22000	1.01435	1.01138
5	ZPR-3-12	1.12000	0.98564	0.98572
7	ZPR-3-11	1.19000	0.97803	0.97617
13	ZEBRA-2	0.98700	0.99606	1.00285
17	ZPR-6-6A	---	---	
* AVERAGE OF C/E			1.00788	1.00867
* AVERAGE (C/E)-1.0			0.00788	0.00867
* AVERAGE OF ABS (1.0-C/E)			0.02398	0.02391
* STND. DEV. OF C/E			0.03118	0.03178

SUMMARY OF ALL ASSEMBLIES

* AVERAGE OF C/E	0.98147	0.9867
* AVERAGE (C/E)-1.0	-0.01853	-0.0133
* AVERAGE OF ABS (1.0-C/E)	0.03508	0.03031
* STND. DEV. OF C/E	0.03765	0.03468

Table 7.7 Comparison of central reaction rate ratios, ^{238}U capture/ ^{239}Pu fission

* C/E OF CENTRAL REACTION RATE RATIO

* PLUTONIUM FUEL

N.	ASSEMBLY	EXPERIMENT	JFS-3-J2	JENDL-2B-70
2	VERA-11A	---	---	---
4	ZEBRA-3	---	---	---
6	SNEAK-7A	0.13500	0.98358	1.00745
8	ZPR-3-54	---	---	---
9	ZPR3-53	---	---	---
10	SNEAK-7B	0.12900	1.01625	1.0413
11	ZPR-3-50	---	---	---
12	ZPR-3-48	0.14100	0.95773	0.97744
14	ZPR-3-49	---	---	---
15	ZPR-3-56	---	---	---
16	ZPR-6-7	0.14300	1.05865	1.07245
18	ZPPR-2	---	---	---
19	MZA	0.12970	1.03271	1.0514
20	MZB	0.1424	1.04216	1.05666
21	FCA-5-2	0.12680	0.93925	0.95332
* AVERAGE OF C/E			1.00433	1.02286
* AVERAGE(C/E) - 1.0			0.00433	0.02286
* AVERAGE OF ABS(1.0 - C/E)			0.03846	0.04264
* STND. DEV. OF C/E			0.04169	0.04122

Table 7.8 Comparison of sample worths of ^{235}U, ^{238}U and ^{240}Pu.

No.	ASSEMBLY	U-235		U-238		PU-240	
		JFS-3-J2	JENDL-2B-70	JES-3-J2	JENDL-2B-70	JFS-3-J2	JENDL-2B-70
1	VERA-11A	1.0699	1.0703	---		---	
2	VERA-1B	0.9972	0.9985	1.9674	1.915	---	
3	ZPR-3-6F	0.8216	0.8236	---		---	
4	ZEBRA-3	0.9967	0.9996	0.9557	0.976	---	
5	ZPR-3-12	0.9996	1.0025	1.0155	1.03	---	
6	SNEAK-7A	0.9929	0.9828	1.0063	1.04	0.7573	0.7528
7	ZPR-3-11	1.0438	1.0465	1.0011	1.02	---	
8	ZPR-3-54	1.0464	1.0236	0.6427	0.676	---	
9	ZPR-3-53	1.0561	1.0316	0.7569	0.787	---	
10	SNEAK-7B	1.0122	1.0096	1.0787	1.095	0.8283	0.8353
11	ZPR-3-50	1.0060	0.9862	0.8142	0.838	---	
12	ZPR-3-48	1.0169	1.0051	0.8657	0.889	---	
13	ZEBRA-2	1.0190	1.0163	0.9538	0.954	0.5878	0.5894
14	ZPR-3-49	1.0729	1.0646	0.9597	0.984	---	
15	ZPR-3-56	0.9692	0.961	0.9724	1.0094	---	
16	ZPR-6-7	0.9990	0.9852	0.8225	0.849	---	
17	ZPR-6-6A	1.0421	1.0368	1.0802	1.09	---	
18	ZPPR-2	1.1193	1.1039	---		---	
19	MZA	---		---		---	
20	MZB	---		---		---	
AV.OF C/E		1.0156	1.0082	0.9928	1.01	0.7244	0.7251
AV.ABS(1 - C/E)		0.0405	0.0374	0.1604	0.149	0.2756	0.2749
STAND. DEV		0.0590	0.0565	0.2858	0.267	0.1009	0.1015
RMS.FROM1.0		0.0610	0.0571	0.2859	0.267	0.2934	0.2930

Table 7.9 Comparison of sample worths of ^{10}B, C, Na and Fe

Assembly	^{10}B		C		Na		Fe	
	JFS-3-J2	JENDL-2B-70	JFS-3-J2	JENDL-2B-70	JFS-3-J2	JENDL-2B-70	JFS-3-J2	JENDL-2B-70
VERA-1B	1.076	1.09	1.08	1.04	4.77	4.13	—	—
ZPR-3-6F	1.045	1.05	0.838	0.821	0.499	0.414	0.877	0.828
ZEBRA-3	0.895	0.892	0.820	0.920	1.18	1.29	—	—
ZPR-3-12	—	—	0.461	0.344	—	—	1.15	1.02
SNEAK-7A	0.922	0.953	—	—	—	—	0.86	0.76
ZPR-3-11	0.975	0.970	0.885	1.18	1.51	1.67	1.13	1.10
ZPR-3-54	0.566	0.594	—	—	—	—	—	—
ZPR-3-53	0.610	0.637	—	—	0.185	0.092	2.15	1.37
SNEAK-7B	0.973	0.99	—	—	—	—	1.02	0.956
ZPR-3-50	0.780	0.813	—	—	-0.145	-0.170	1.30	1.12
ZPR-3-48	0.833	0.864	5.00	4.84	3.01	2.83	1.11	1.00
ZEBRA-2	0.776	0.775	0.607	0.435	2.43	2.25	1.22	1.02
ZPR-3-49	0.892	0.922	—	—	-2.56	-2.96	0.983	0.907
ZPR-3-56	0.802	0.835	1.54	1.53	2.36	2.27	0.877	0.80
ZPR-6-7	0.907	0.957	1.36	1.32	1.28	1.21	1.02	0.91
ZPR-6-6A	0.912	0.939	0.608	0.463	-1.39	-1.89	—	—
ZPPR-2	0.893	0.942	1.13	1.09	1.29	1.22	1.05	0.937
AV. OF C/E	0.866	0.889	1.30	1.27	1.11	0.951	1.13	0.979
AV. ABS(1-C/E)	0.149	0.129	0.63	0.64	1.40	1.42	0.195	0.118
STAND. DEV.	0.134	0.131	1.21	1.18	1.82	1.83	0.320	0.154
RMS. FROM 1.0	0.189	0.171	1.25	1.21	1.82	1.83	0.346	0.156

Table 7.10 Comparison of sodium void reactivities calculated with the JFS-3-J2, JFS-3-B4 and JFS-2 sets

Assembly name	Voided region	Experiment ($\Delta k/k \times 10^{-4}$)	Correction factor			C/E		
			Het	Ep	Tra	JFS-3-J2	JFS-3-B4	JFS-2
FCA-VI-2	3x3x4 packs	2.13±0.05	0.821	1.039	1.00	1.312	1.269	0.915
	5x5x4 packs	5.51±0.08	0.813	1.082	1.00	1.372	1.332	0.957
	5x5x6 packs	7.65±0.08	0.804	1.092	1.00	1.398	1.359	0.966
	7x7x6 packs	12.53±0.11	0.788	1.094	1.00	1.490	1.455	1.024
	7x7x8 packs	14.65±0.11	0.774	1.103	1.00	1.547	1.515	1.046
ZPPR-9	9 drawers	1.041±0.017	0.845	1.038	1.018	1.097	1.057	0.856
	37 drawers	3.972±0.014	0.844	1.044	1.00	1.161	1.119	0.906
	97 drawers	10.098±0.007	0.839	1.059	0.968	1.157	1.117	0.902
	97 drawers	12.803±0.003	0.781	1.072	0.984	1.251	1.209	0.944
	97 drawers	10.885±0.007	0.720	1.101	0.990	1.362	1.320	0.996
	97 drawers	8.398±0.01	0.645	1.112	1.002	1.551	1.509	1.104

Het : Ratio of heterogeneity to homogeneous calculations

Ep : Ratio of exact to first-order perturbation calculations

Tra : Ratio of transport to diffusion calculations. For FCA-VI-2, Tra = 1.0 was assumed and for ZPPR-9 were taken from Ref. (218).

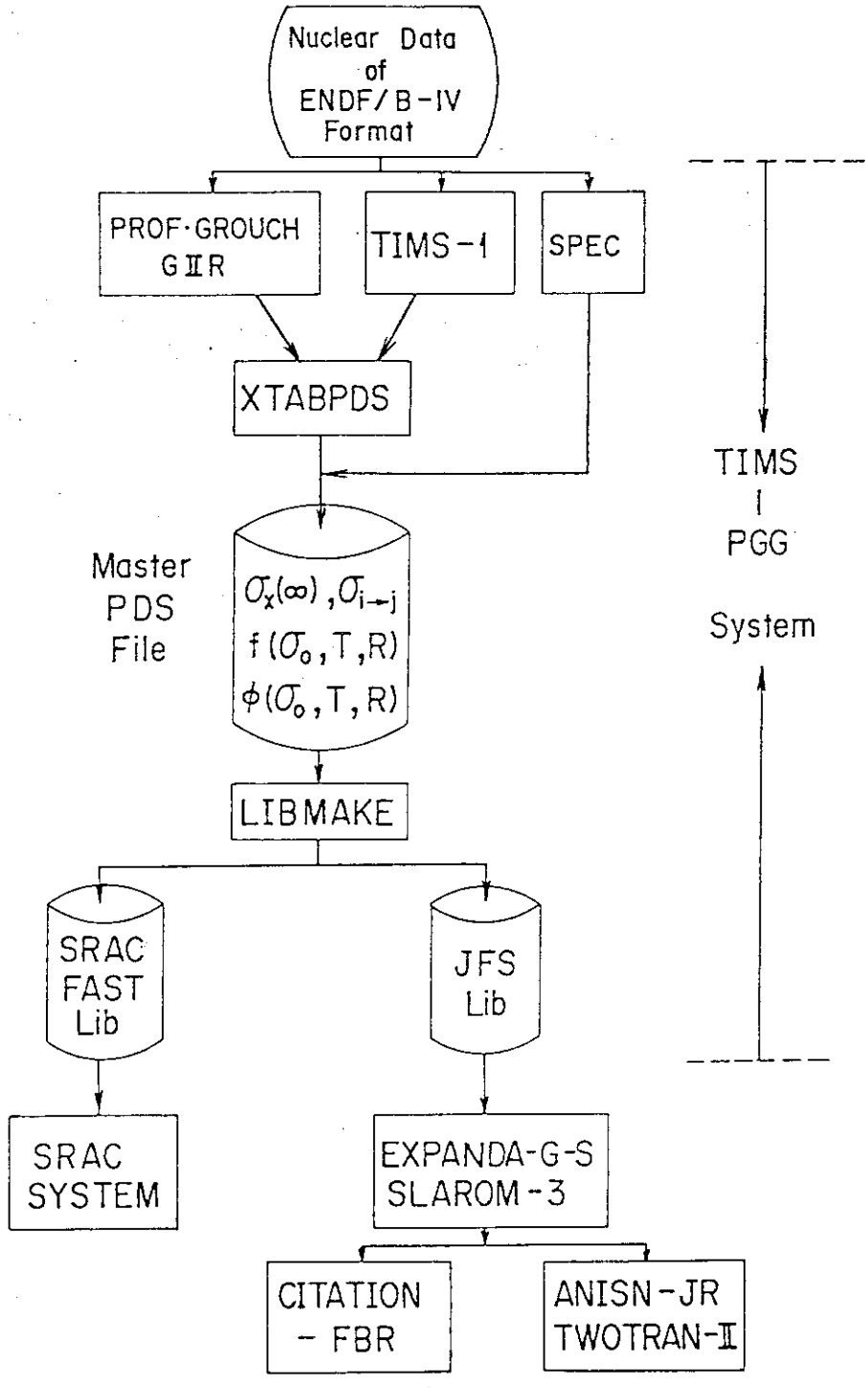

Fig.7.1 Flowchart of the TIMS-PGG code system

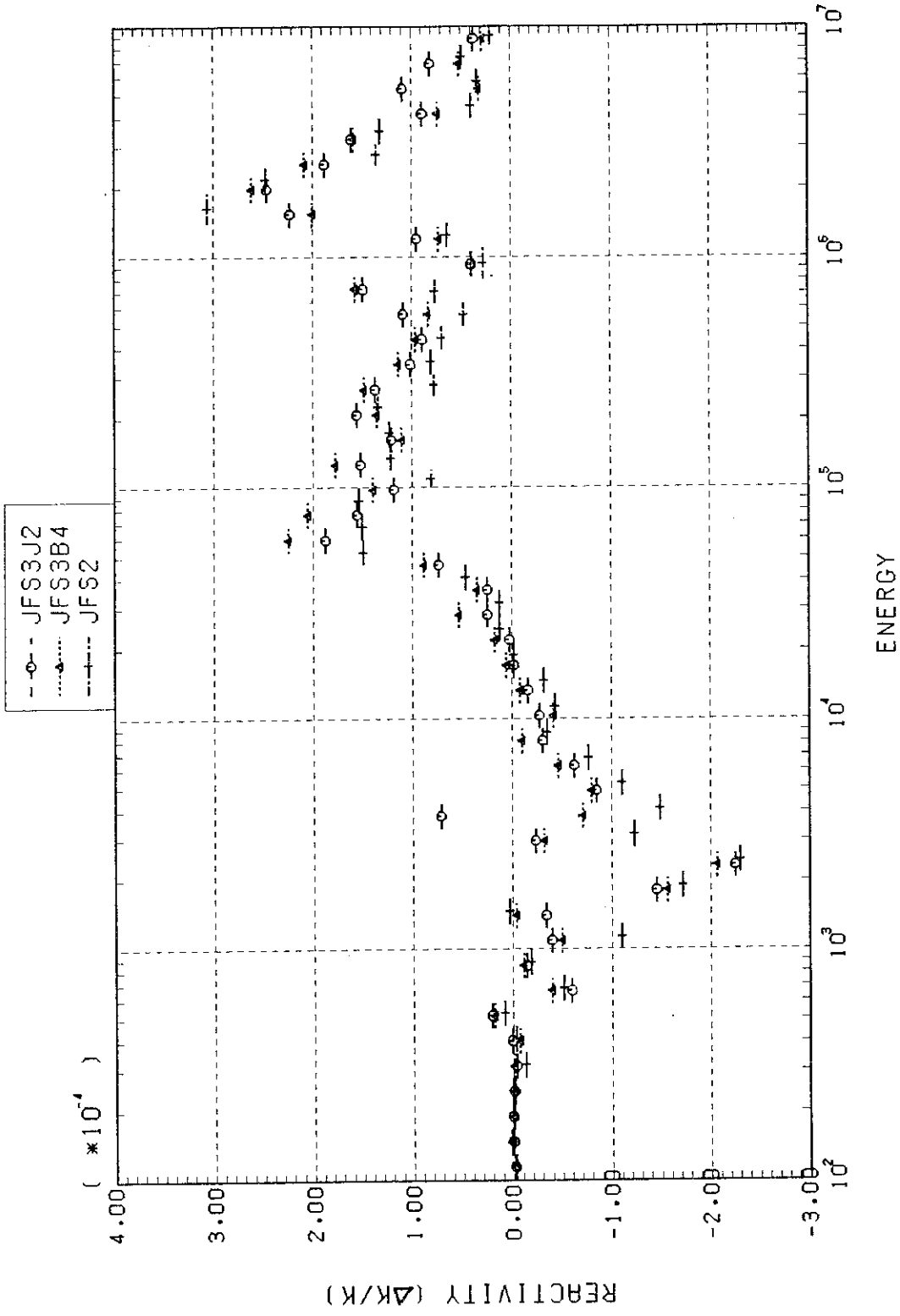

Fig.7.2 Comparison of groupwise contributions for the scattering term of sodium void reactivity calculated for the voided region of 7 x 7 x 8 packs in FCA-VI-2 assembly.

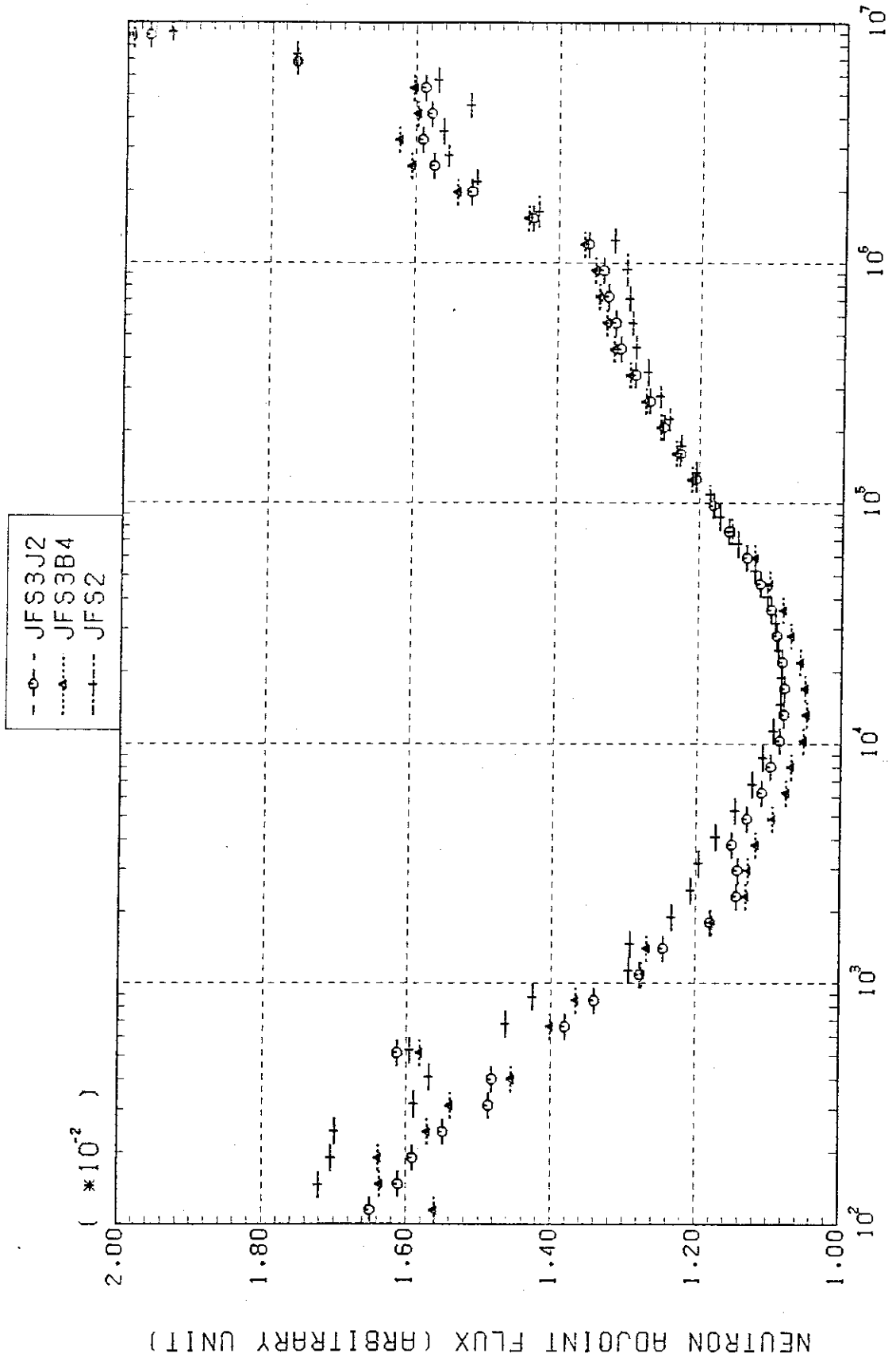

Fig.7.3 Comparison of adjoint fluxes calculated with the JFS-3-J2, JFS-3-B4 and JFS-2 sets for FCA-VI-2 assembly.

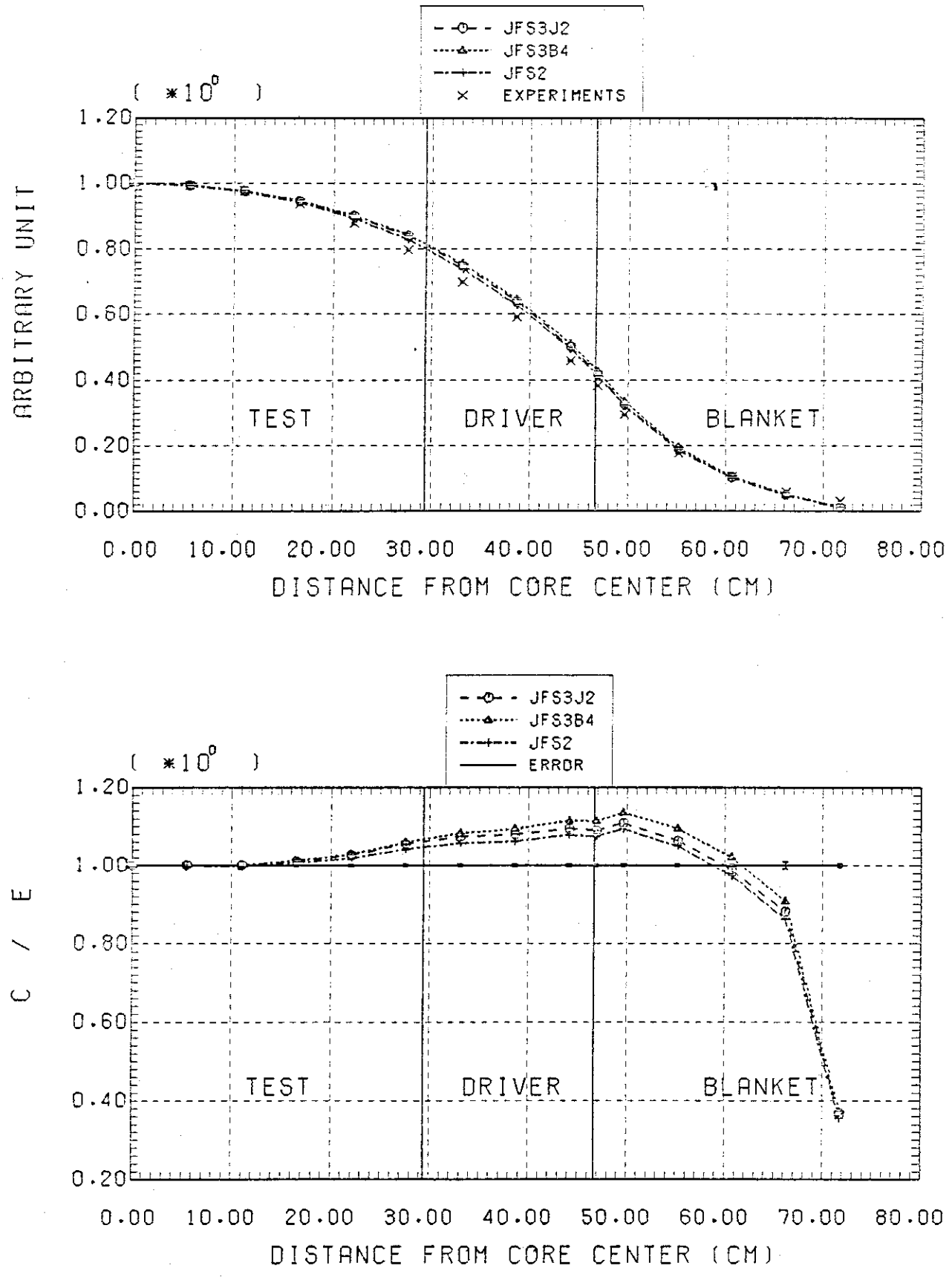

Fig.7.4 Comparison between the calculational and experimental radial distributions of ^{239}Pu fission rate in FCA-VI-2.

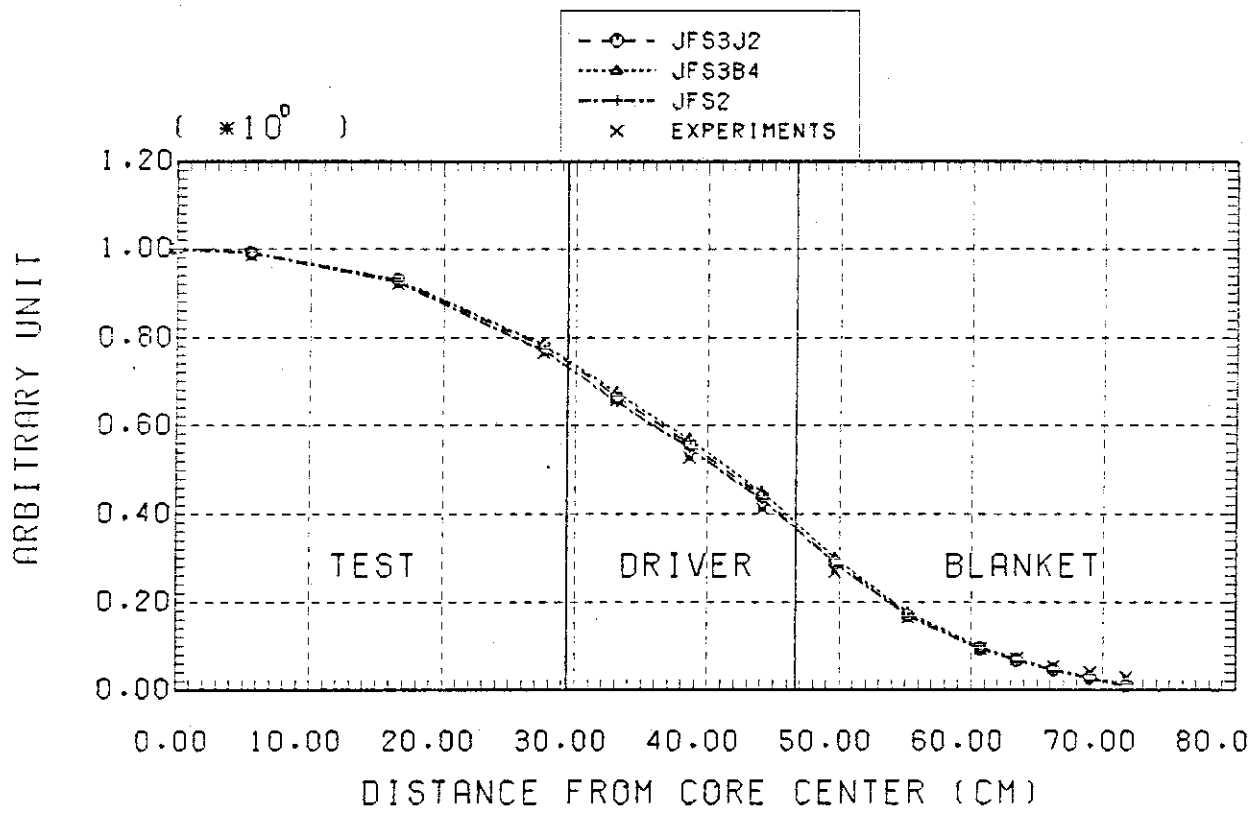

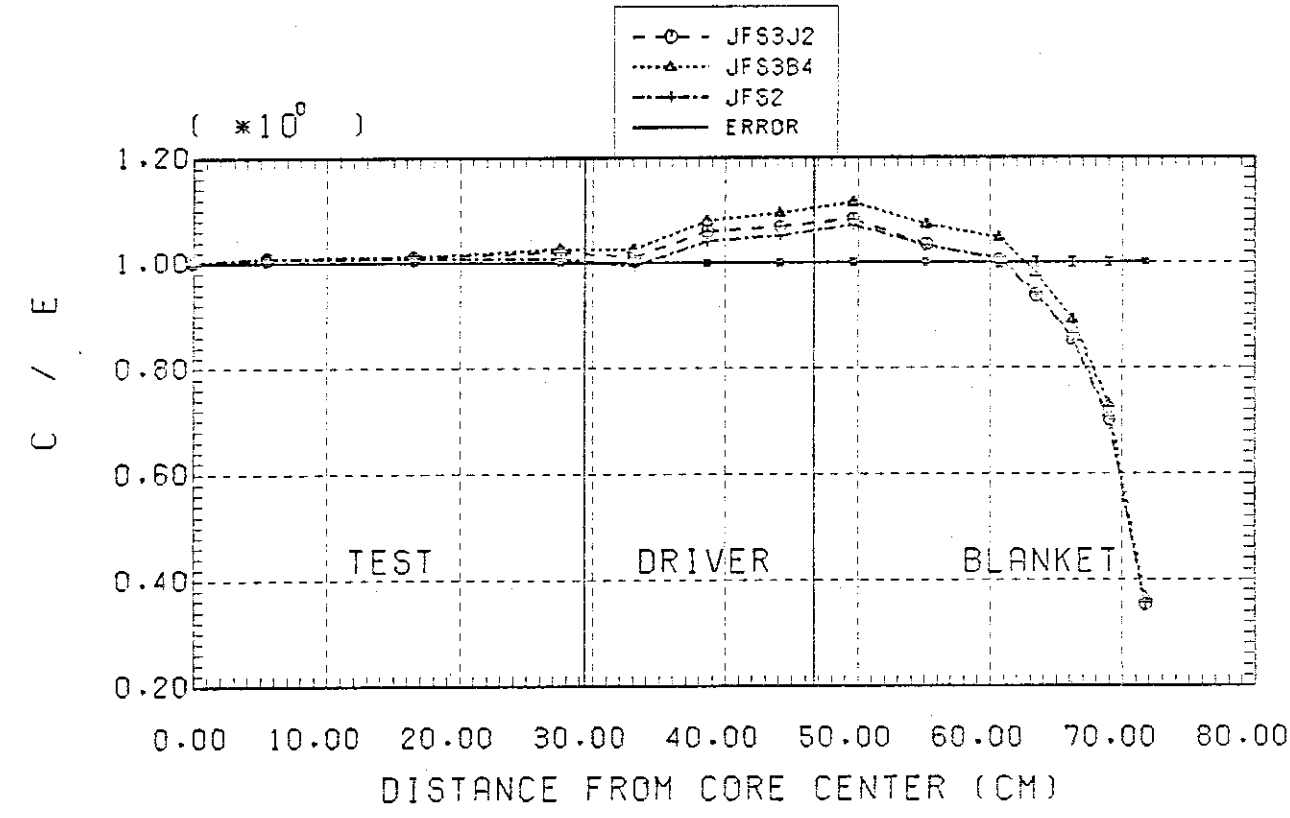

Fig.7.5 Comparison between the calculational and experimental radial distributions of ^{235}U fission rate in FCA-VI-2.

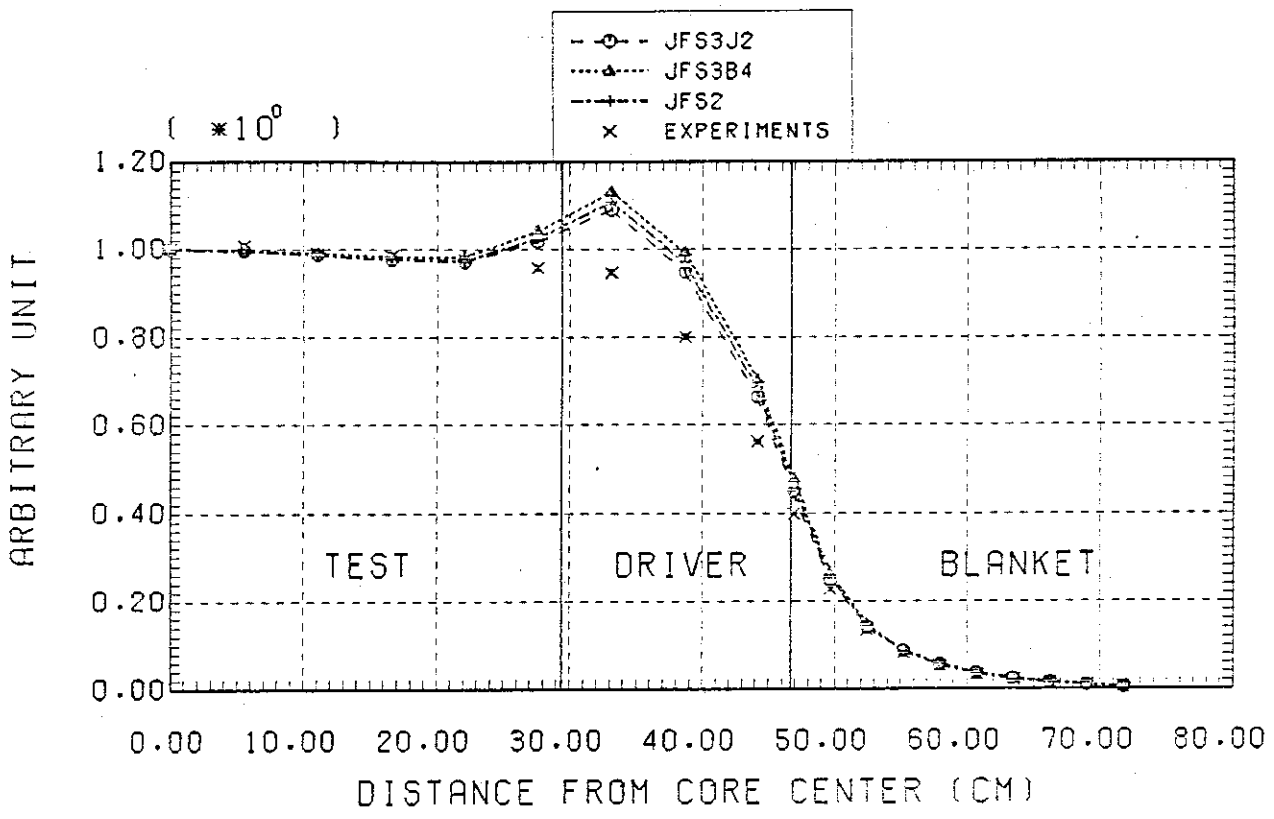

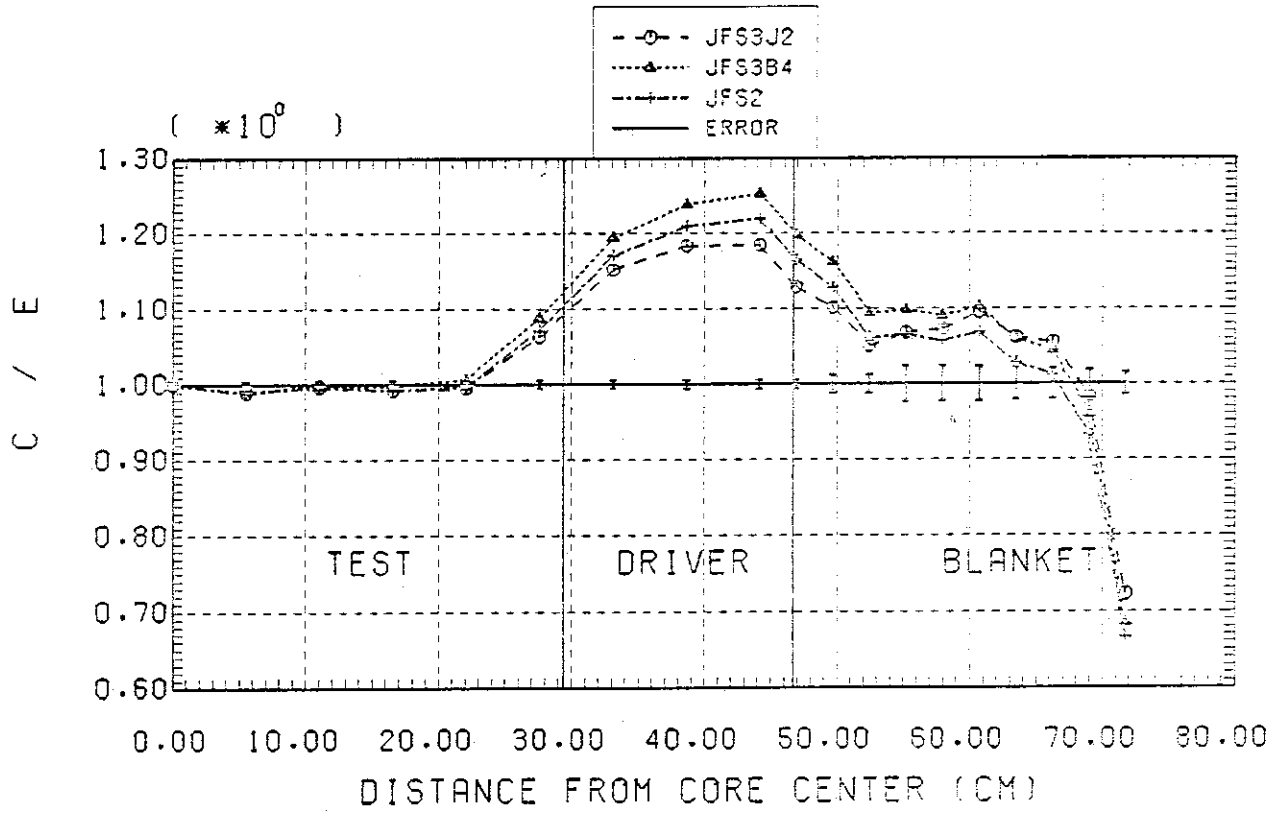

Fig. 7.6 Comparison between the calculational and experimental radial distributions of ^{238}U fission rate in FCA-VI-2.

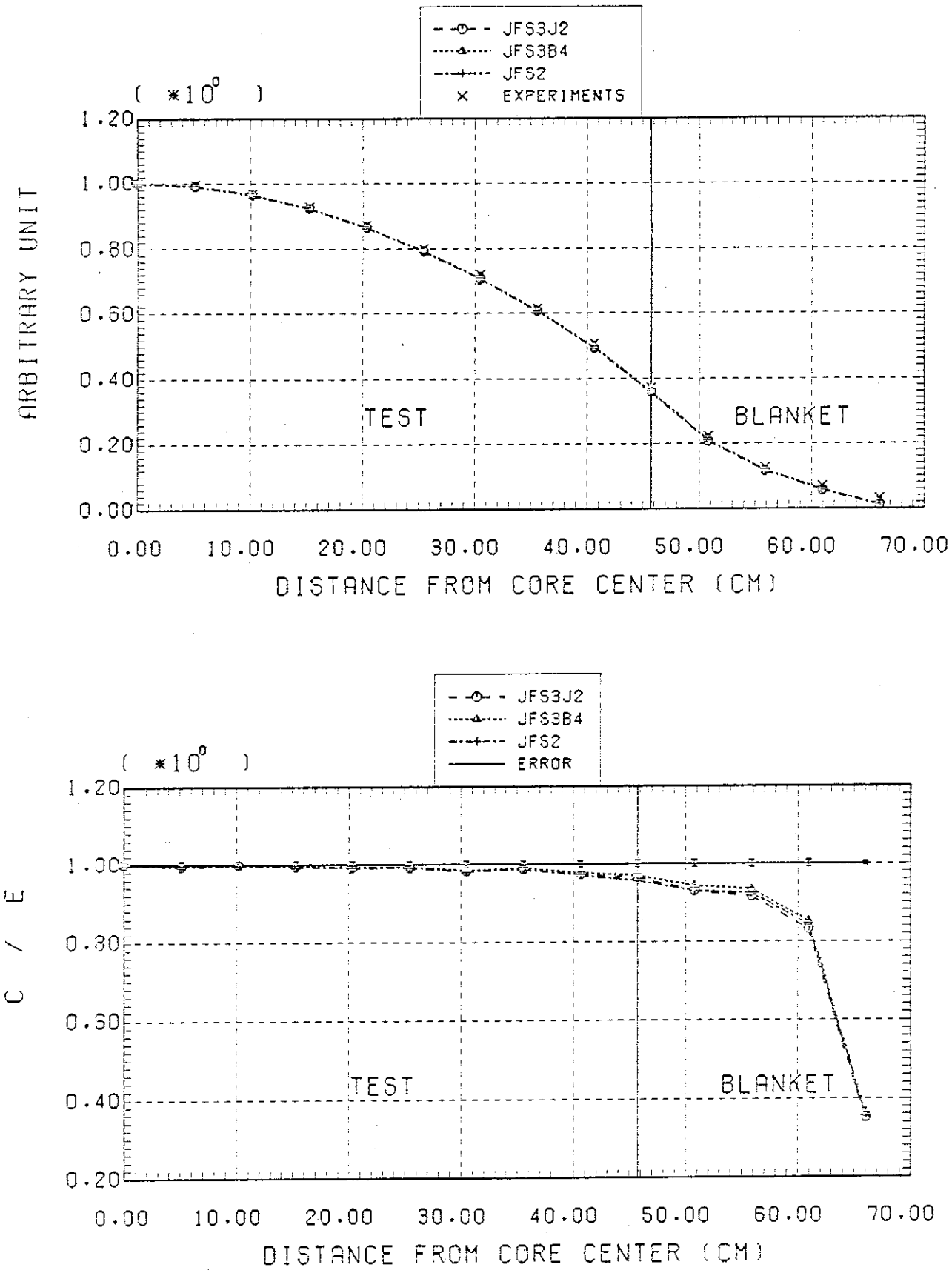

Fig.7.7 Comparison between the calculational and experimental axial distributions of ^{235}U fission rate in FCA-VI-2.

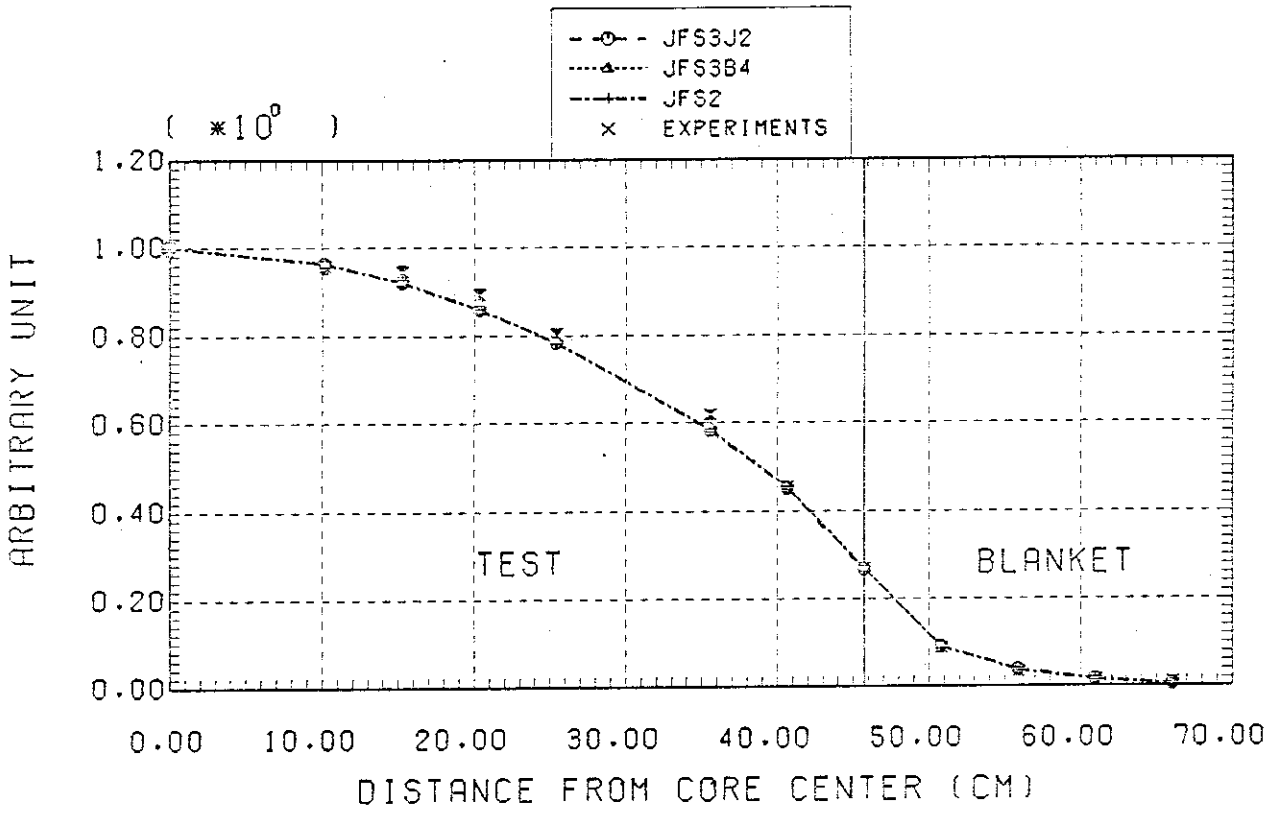

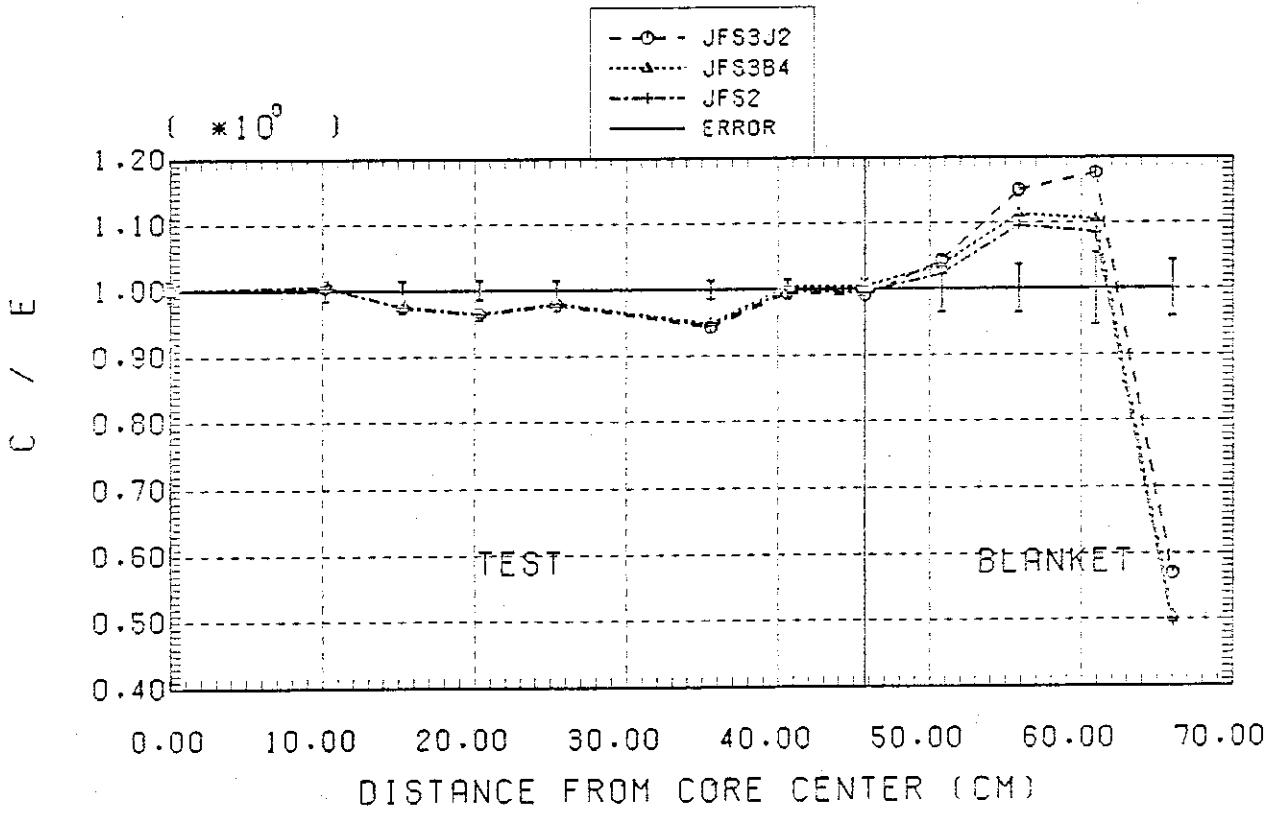

Fig.7.8 Comparison between the calculational and experimental axial distribution of ^{238}U fission rate in FCA-VI-2.

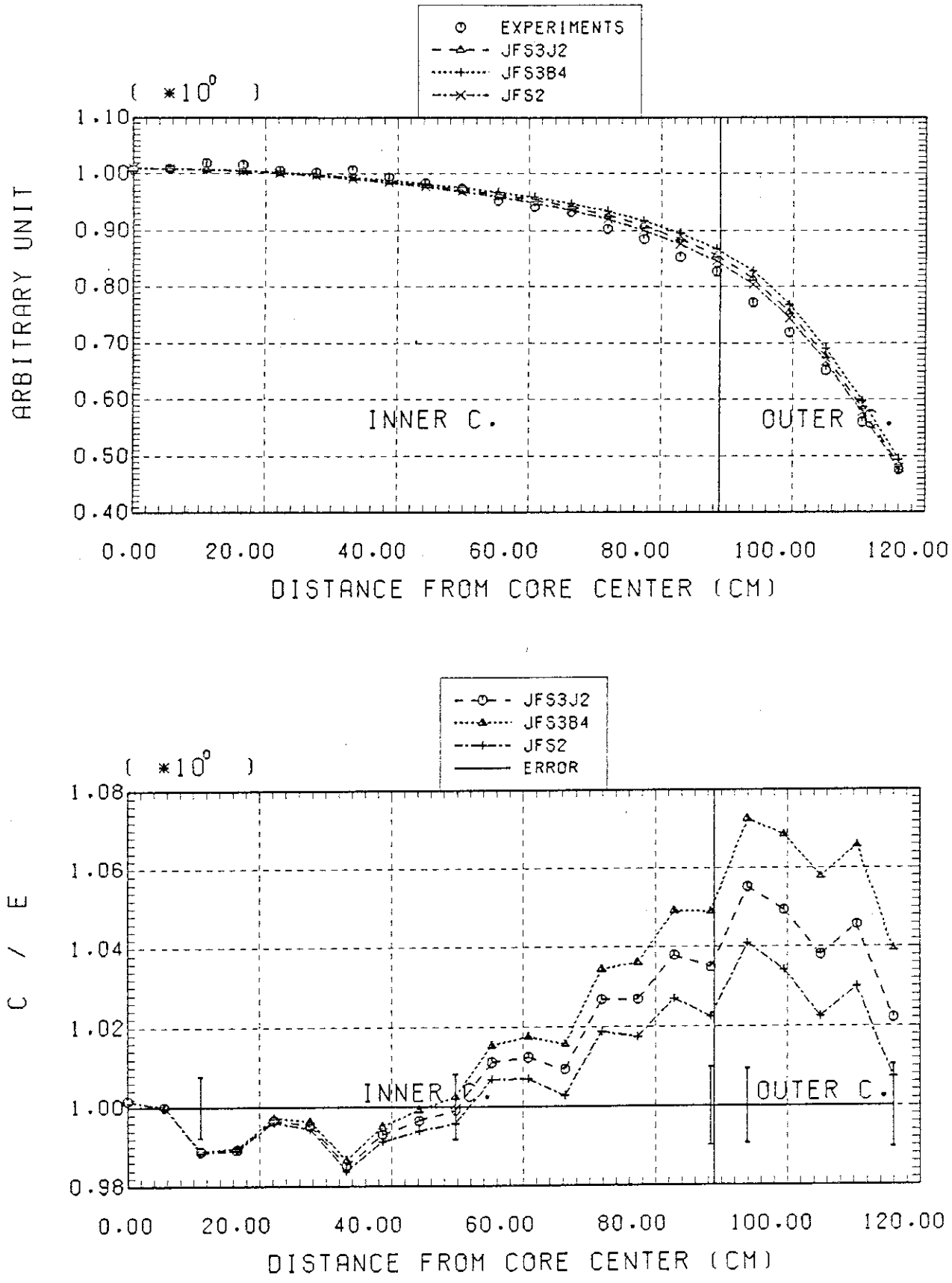

Fig. 7.9 Comparison between the calculational and experimental radial distributions of ^{239}Pu fission rate in ZPPR-9.

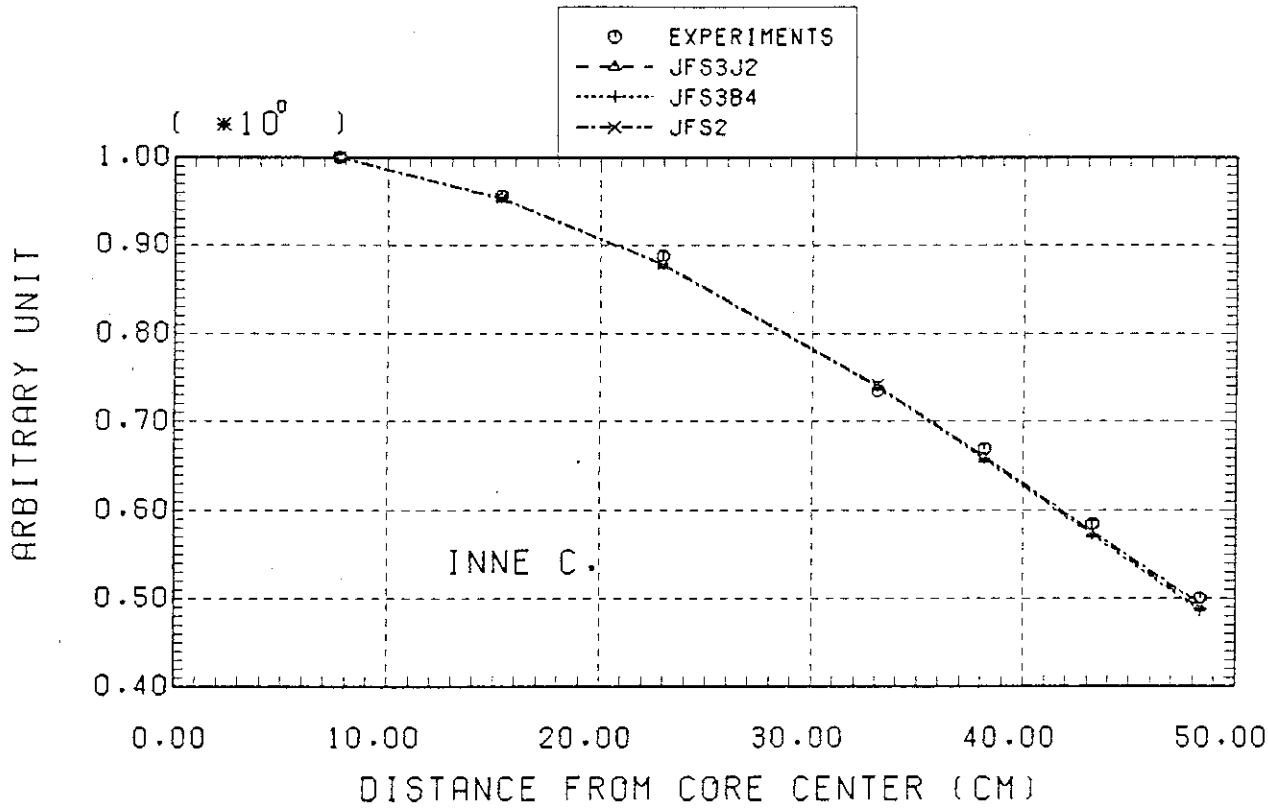

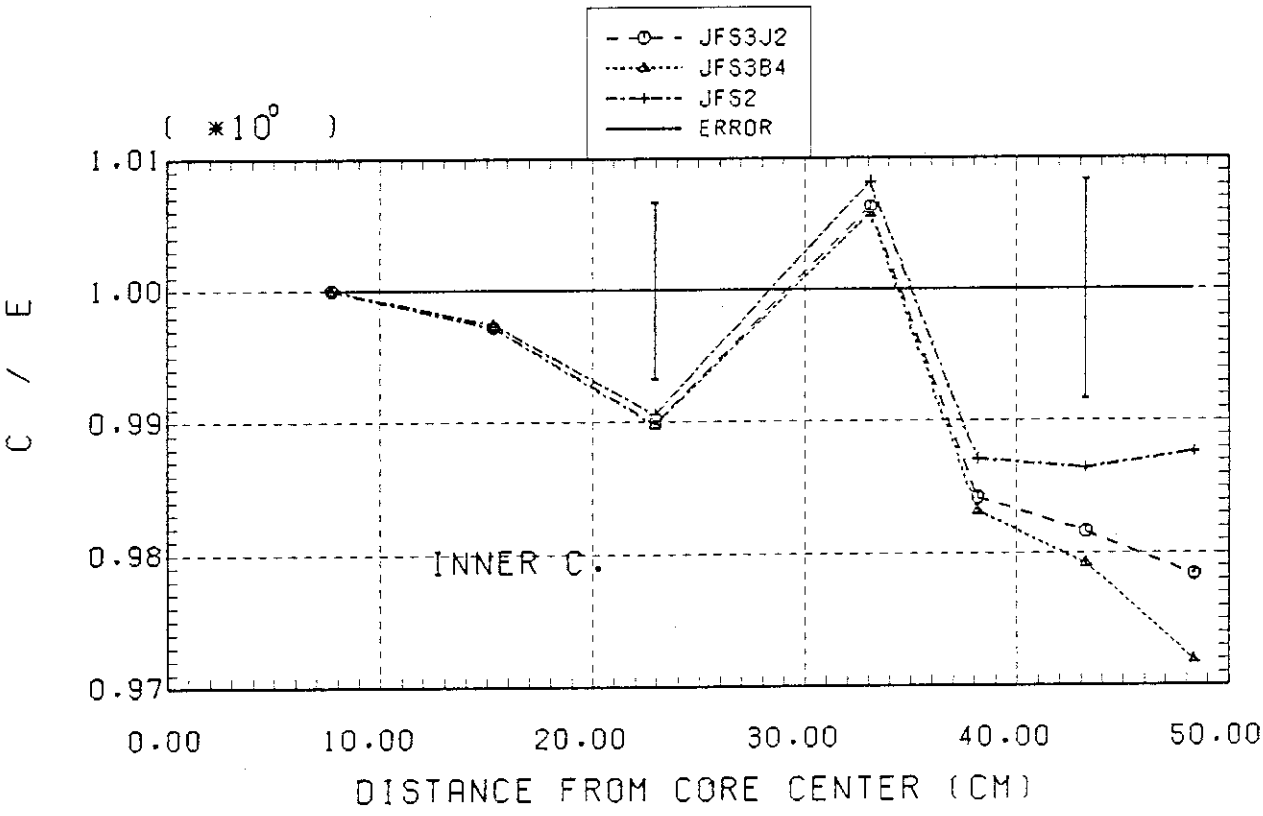

Fig.7.10 Comparison between the calculational and experimental axial distributions of ^{239}Pu fission rate in ZPPR-9.

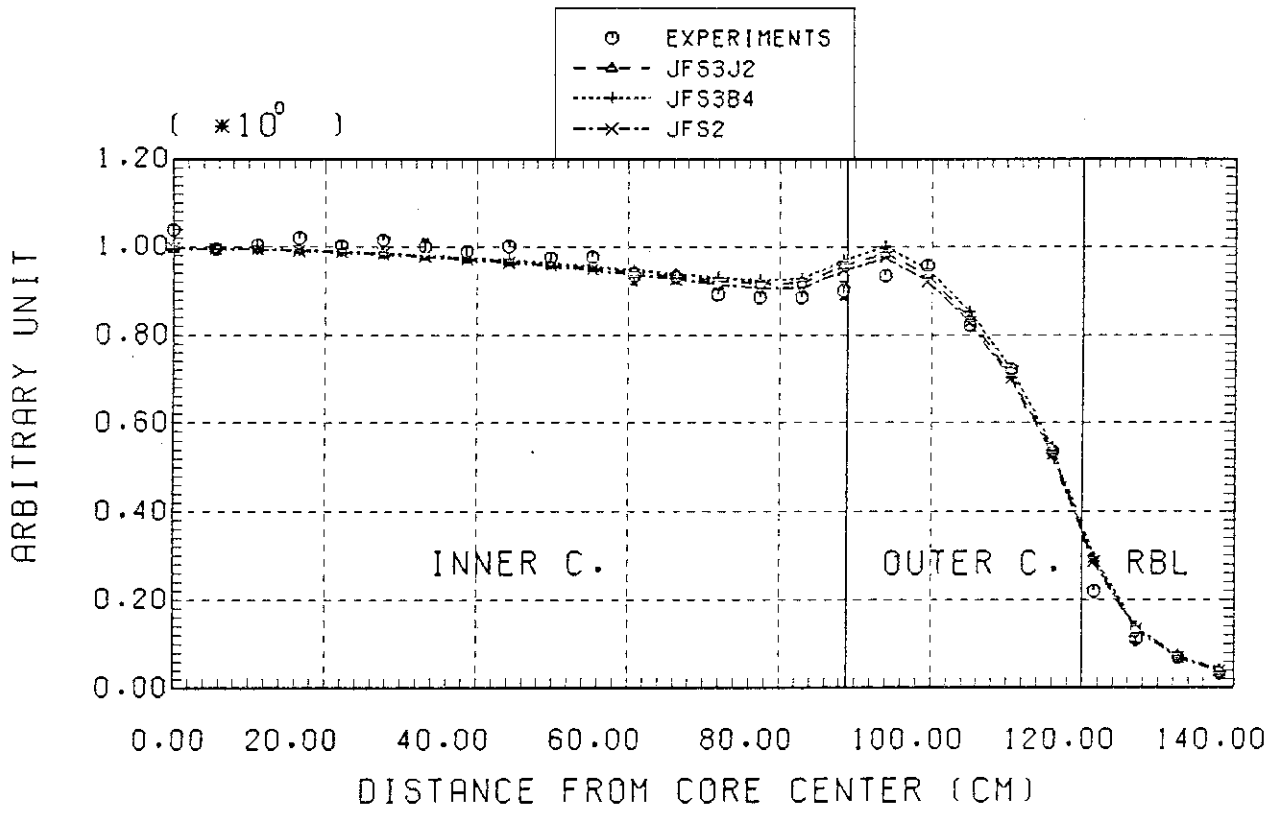

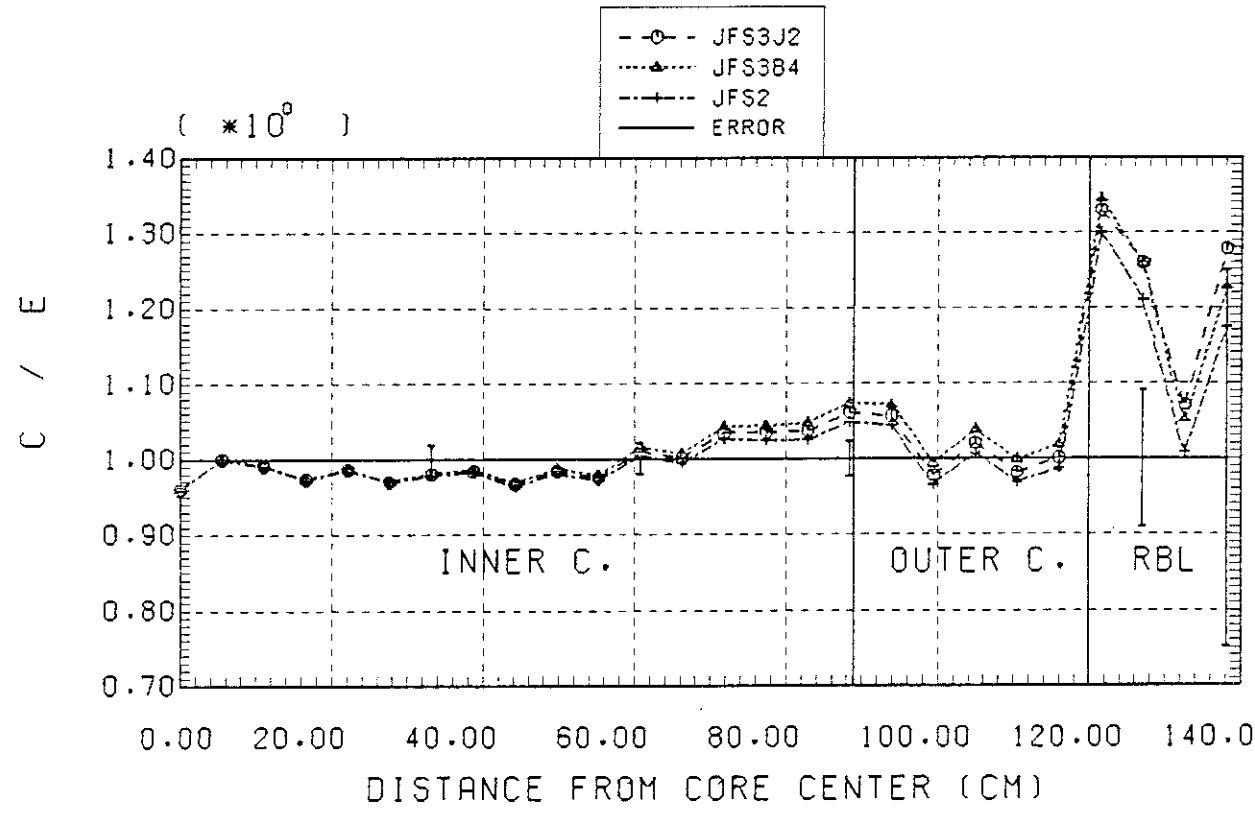

Fig.7.11 Comparison between the calculational and experimental radial distributions of ^{238}U fission rate in ZPPR-9.

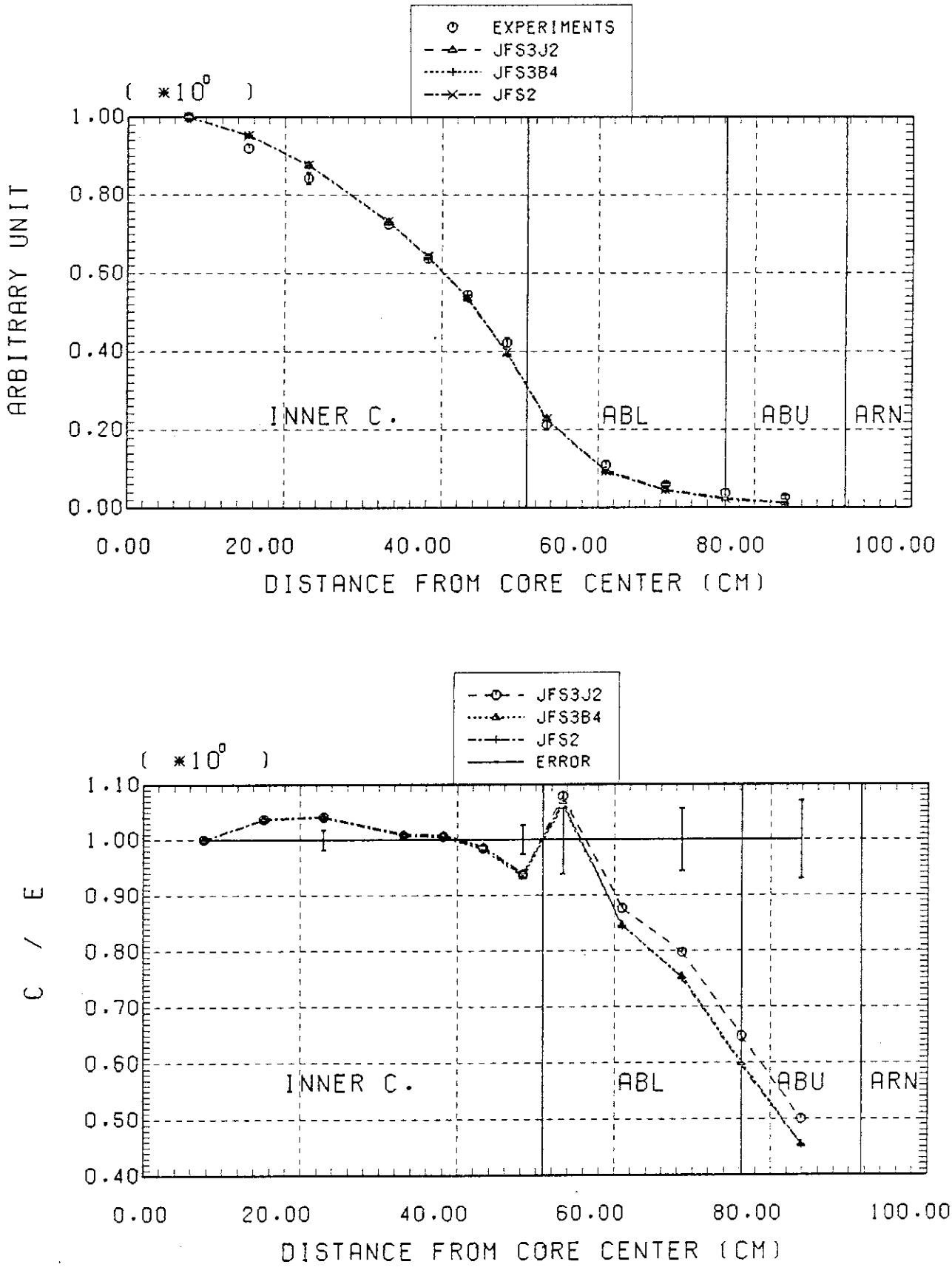

Fig.7.12 Comparison between the calculational and experimental axial distributions of ^{238}U fission rate in ZPPR-9.

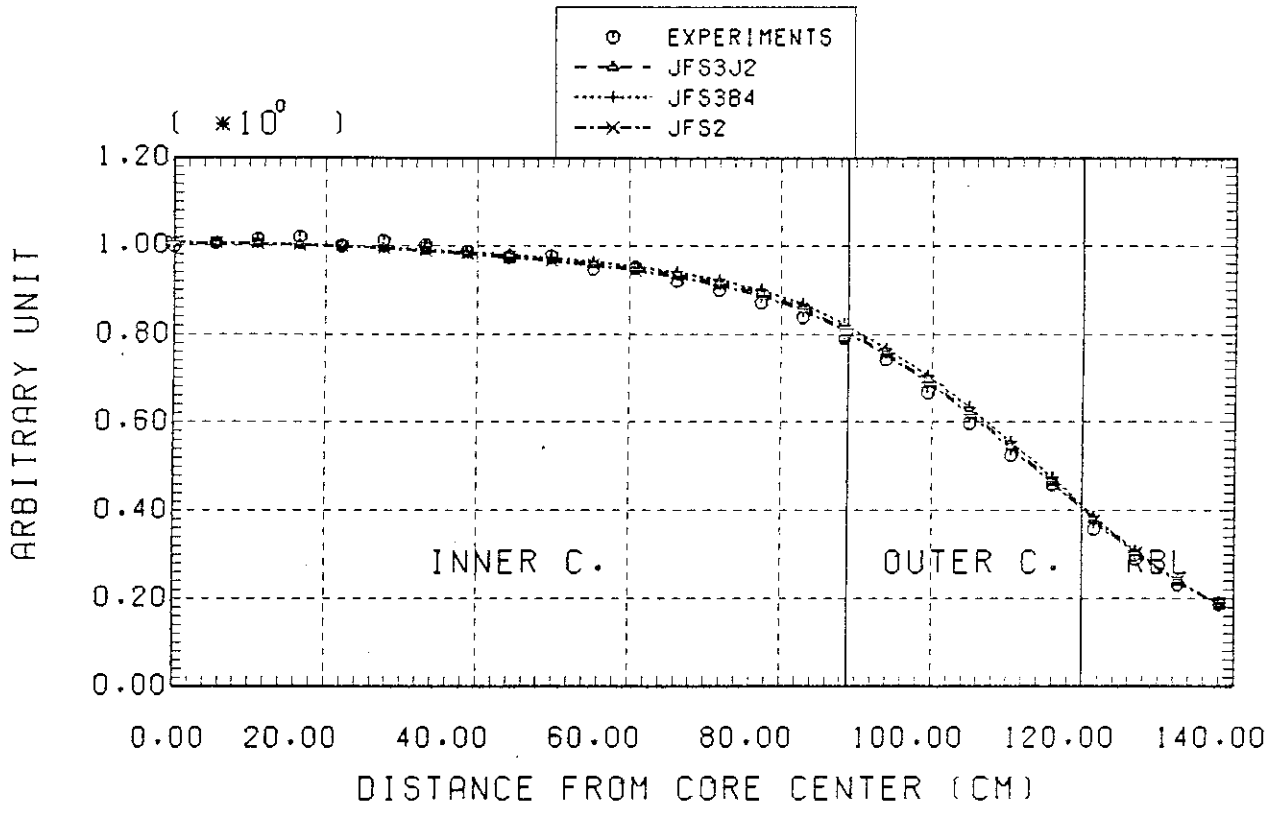

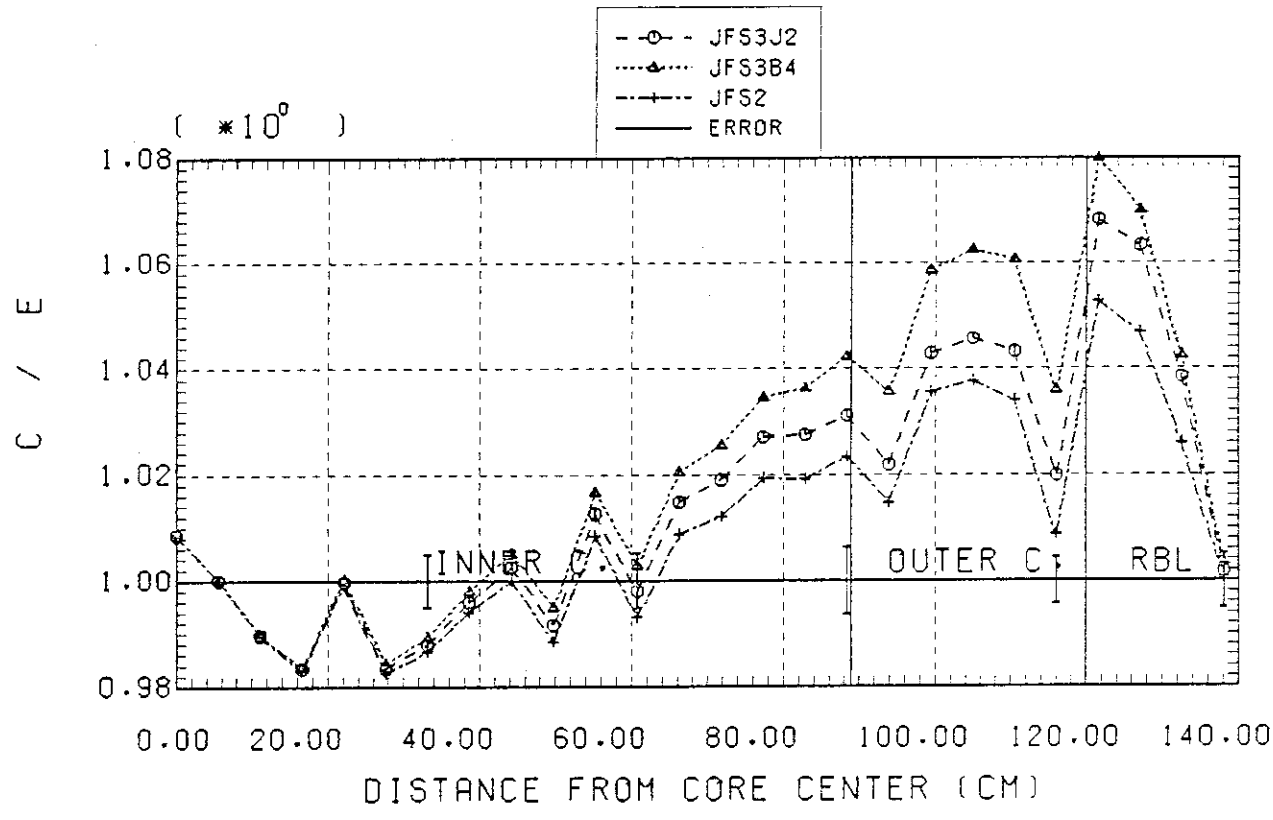

Fig.7.13 Comparison between the calculational and experimental radial distributions of ^{238}U capture rate in ZPPR-9.

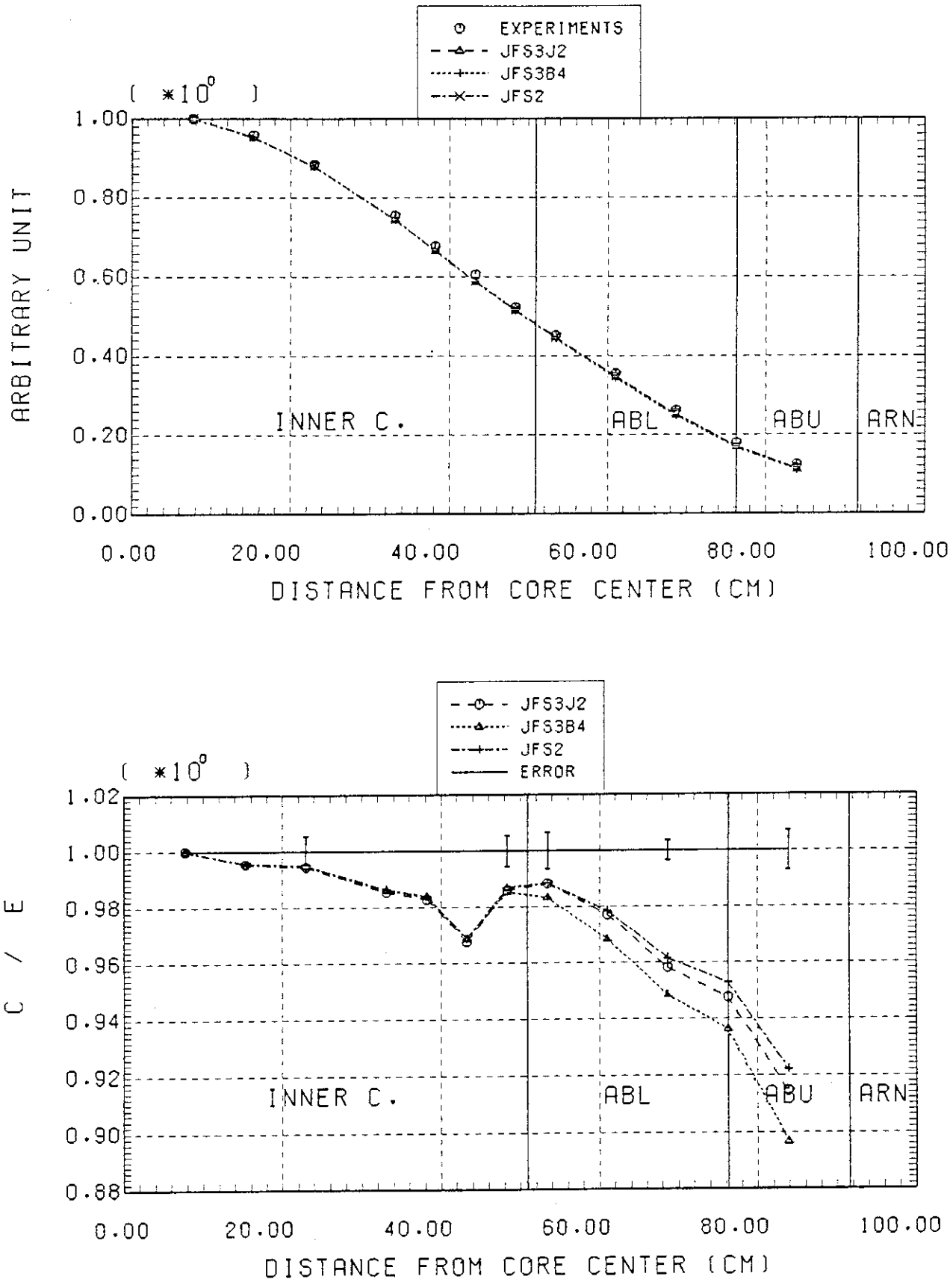

Fig.7.14 Comparison between the calculational and experimental axial distributions of ^{238}U capture rate in ZPPR-9.

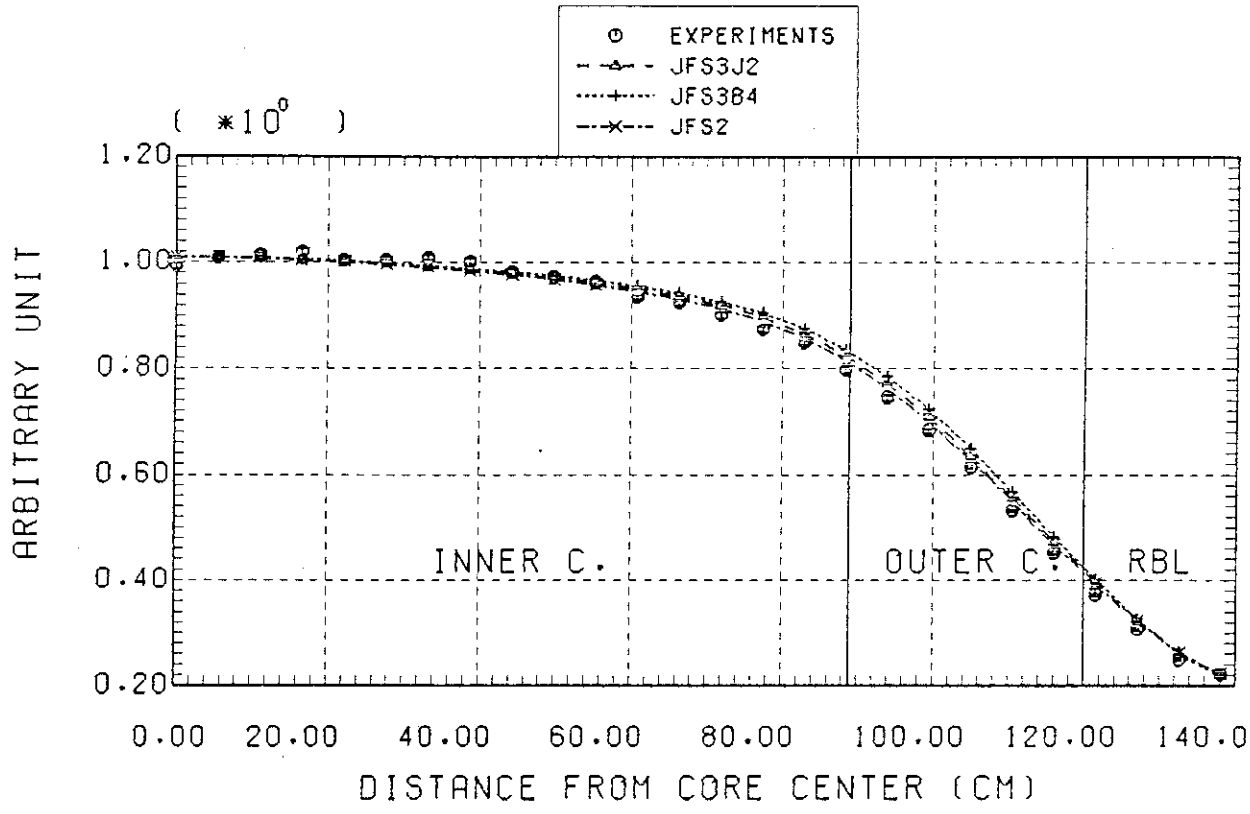

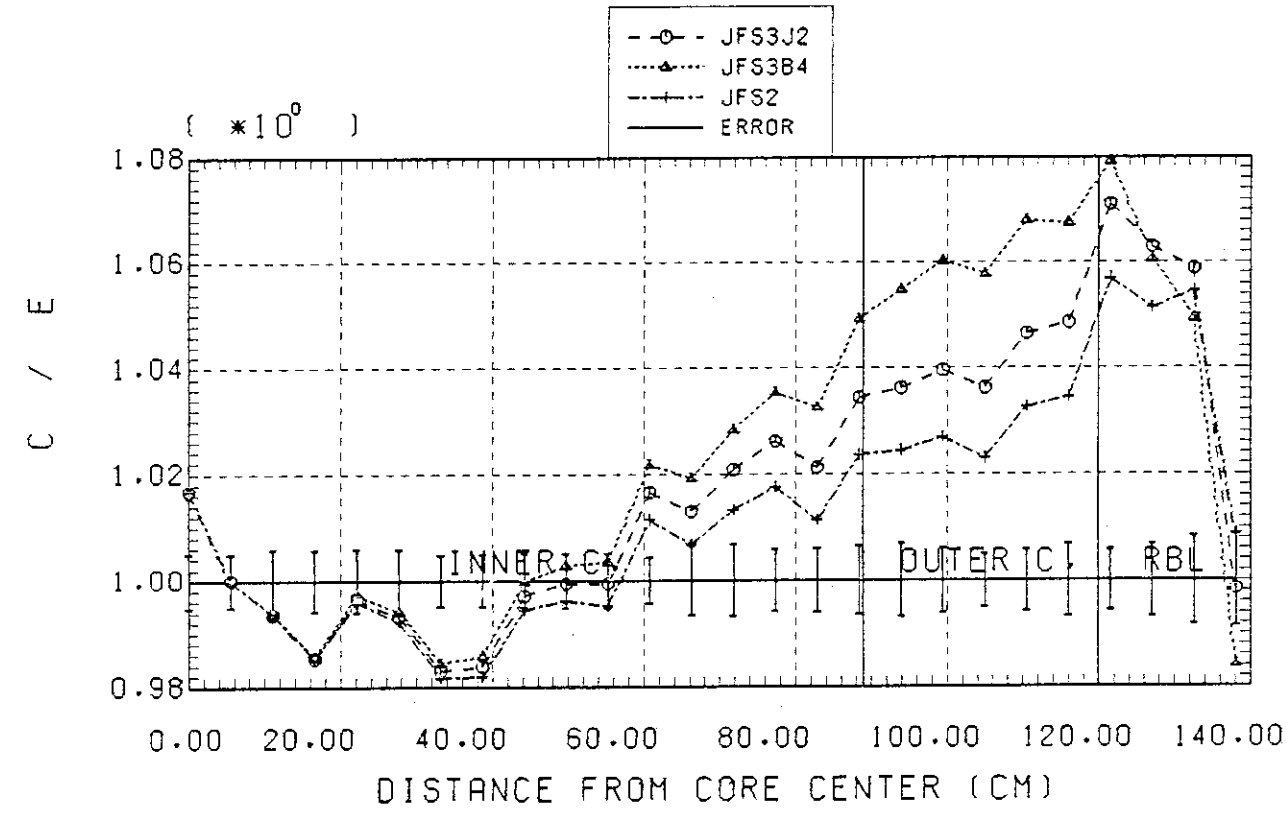

Fig.7.15 Comparison between the calculational and experimental radial distributions of ^{235}U fission rate in ZPPR-9.

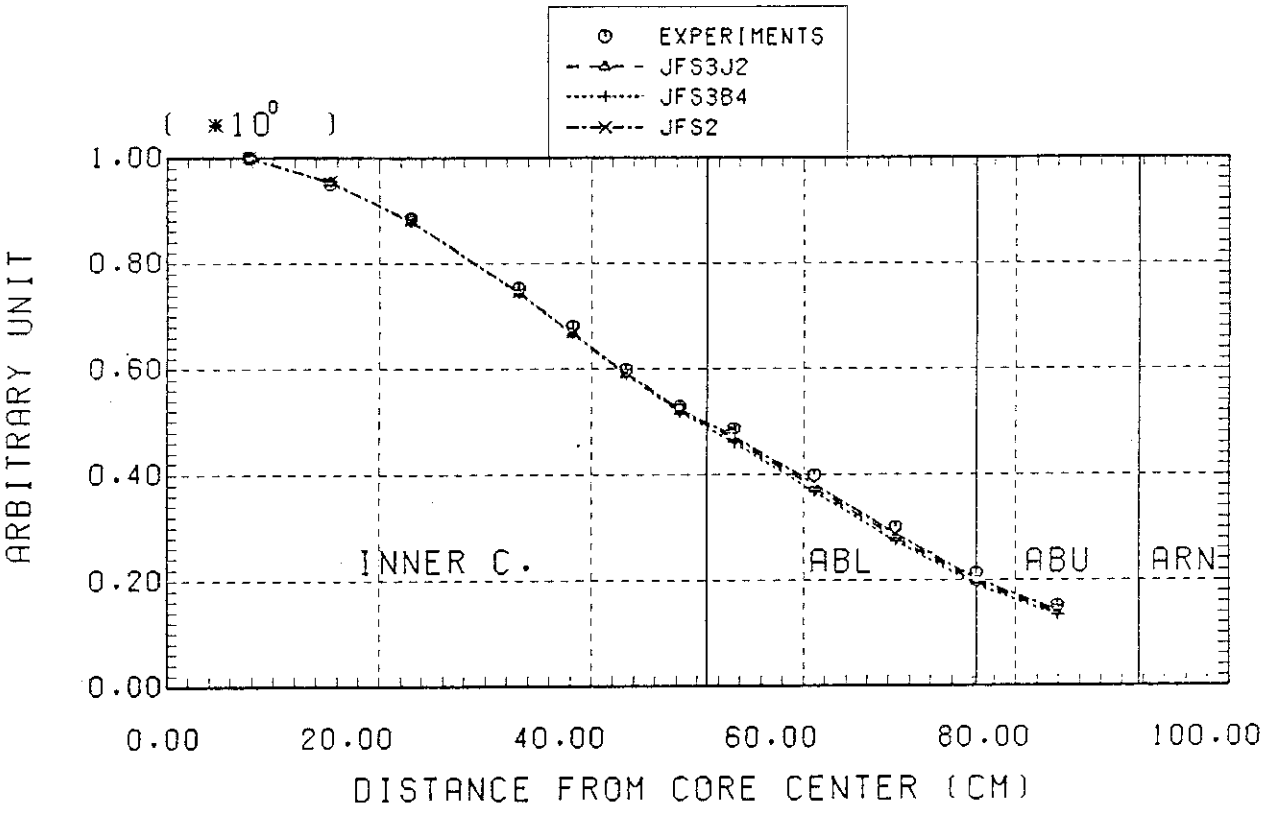

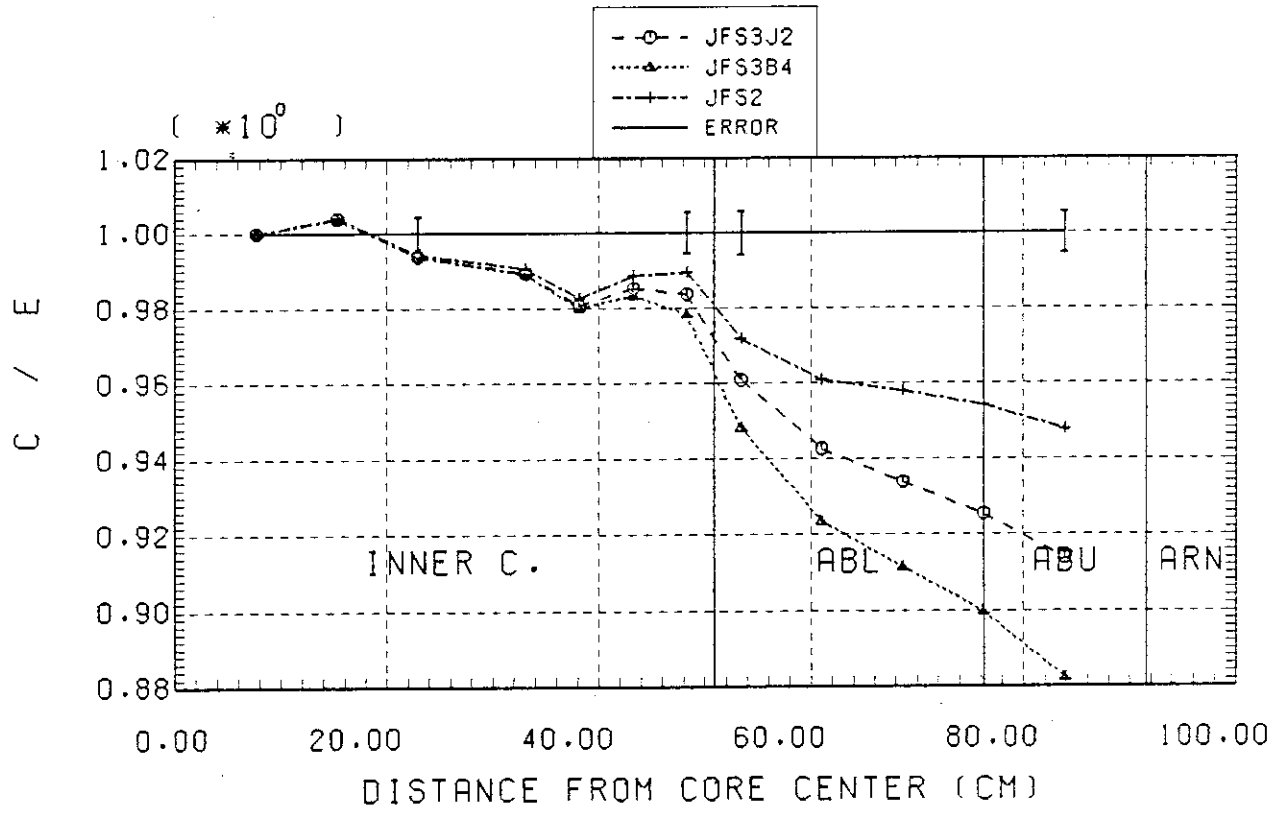

Fig.7.16 Comparison between the calculational and experimental axial distributions of ^{235}U fission rate in ZPPR-9.

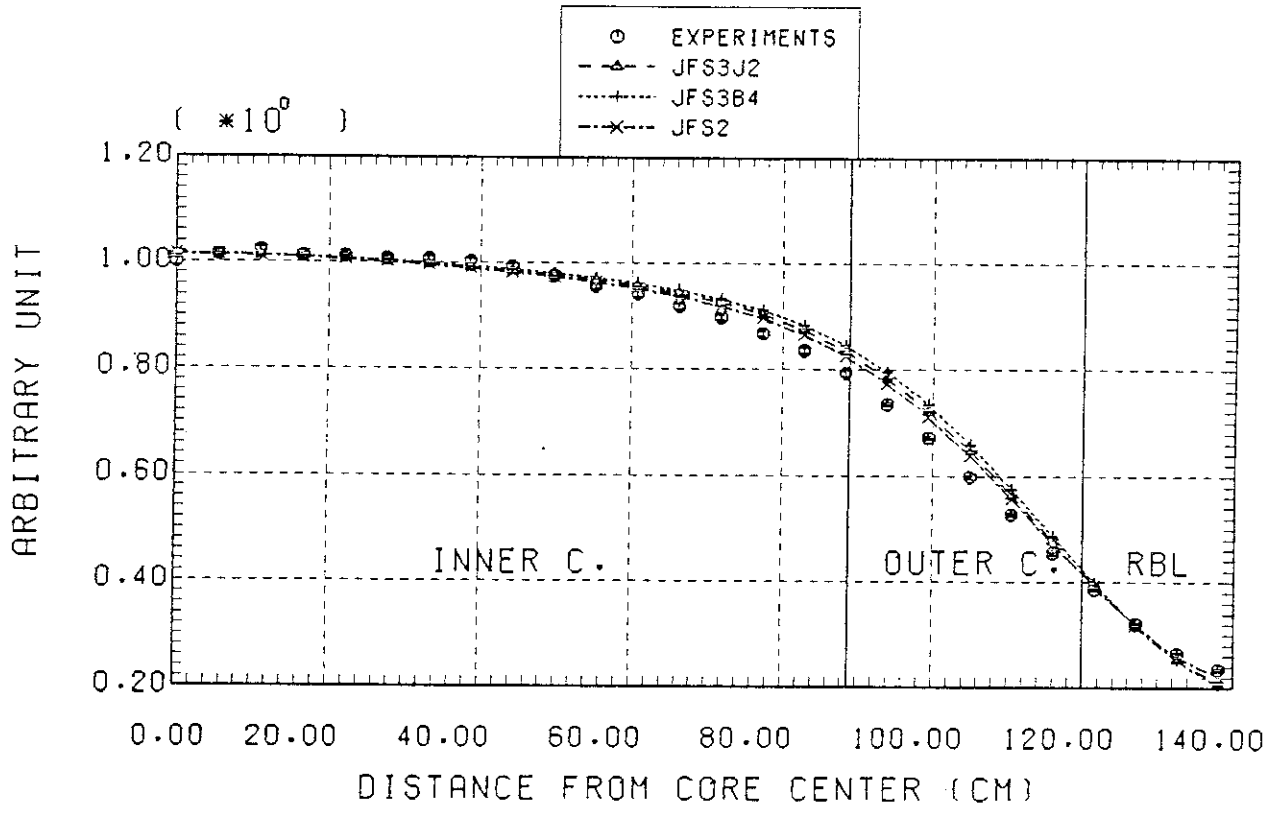

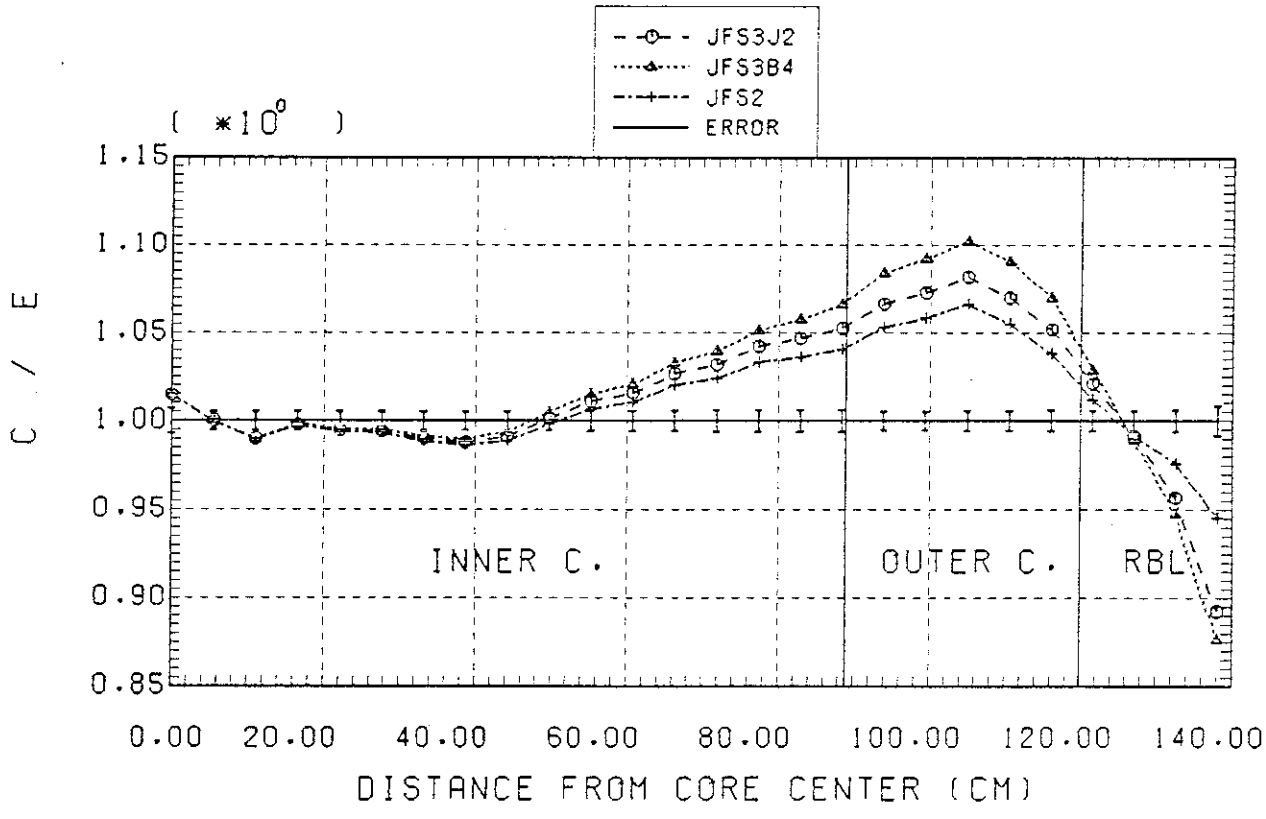

Fig.7.17 Comparison between the calculational and experimental radial distributions of ^{233}U fission rate in ZPPR-9.

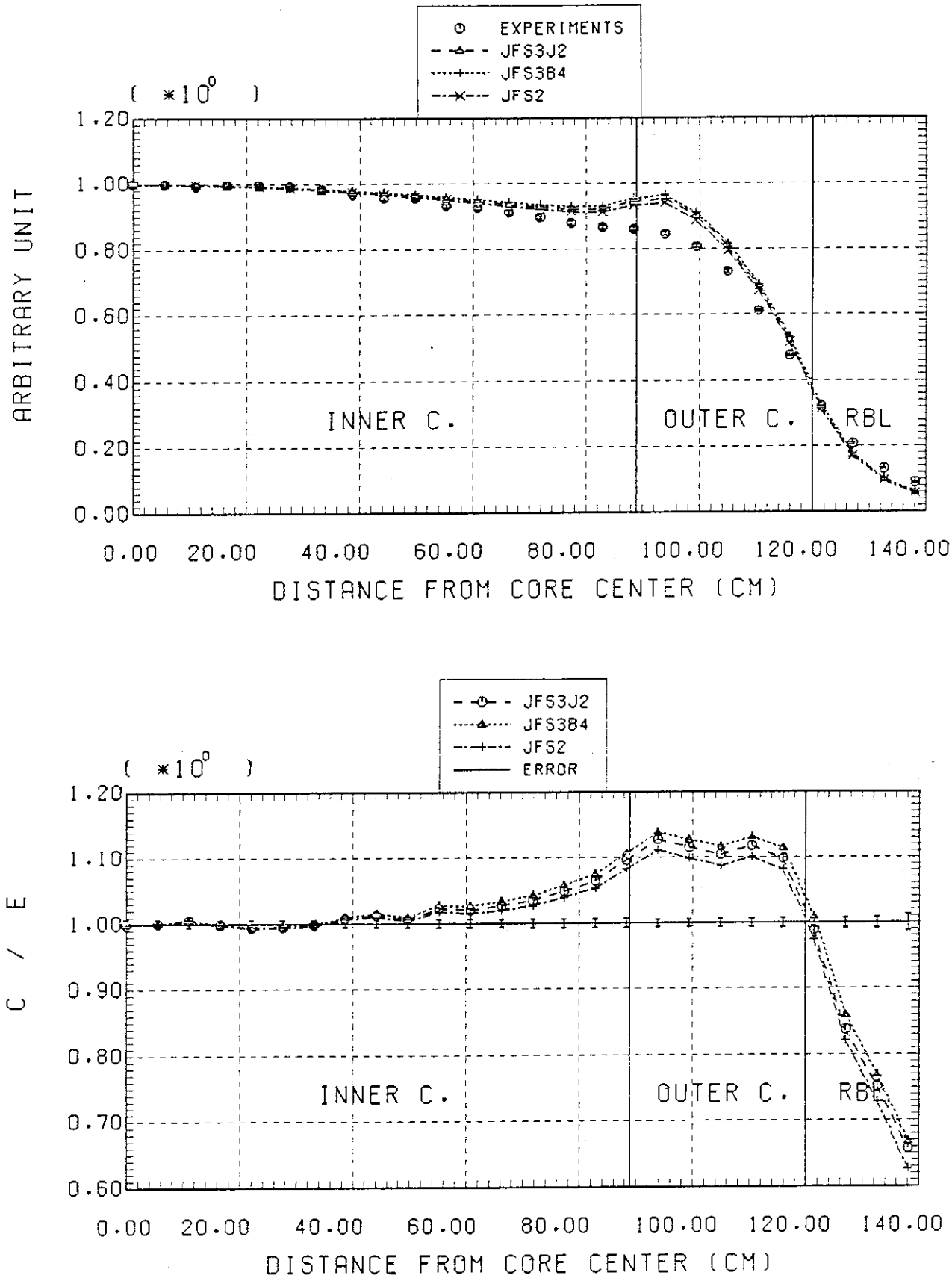

Fig.7.18 Comparison between the calculational and experimental radial distributions of ^{234}U fission rate in ZPPR-9.

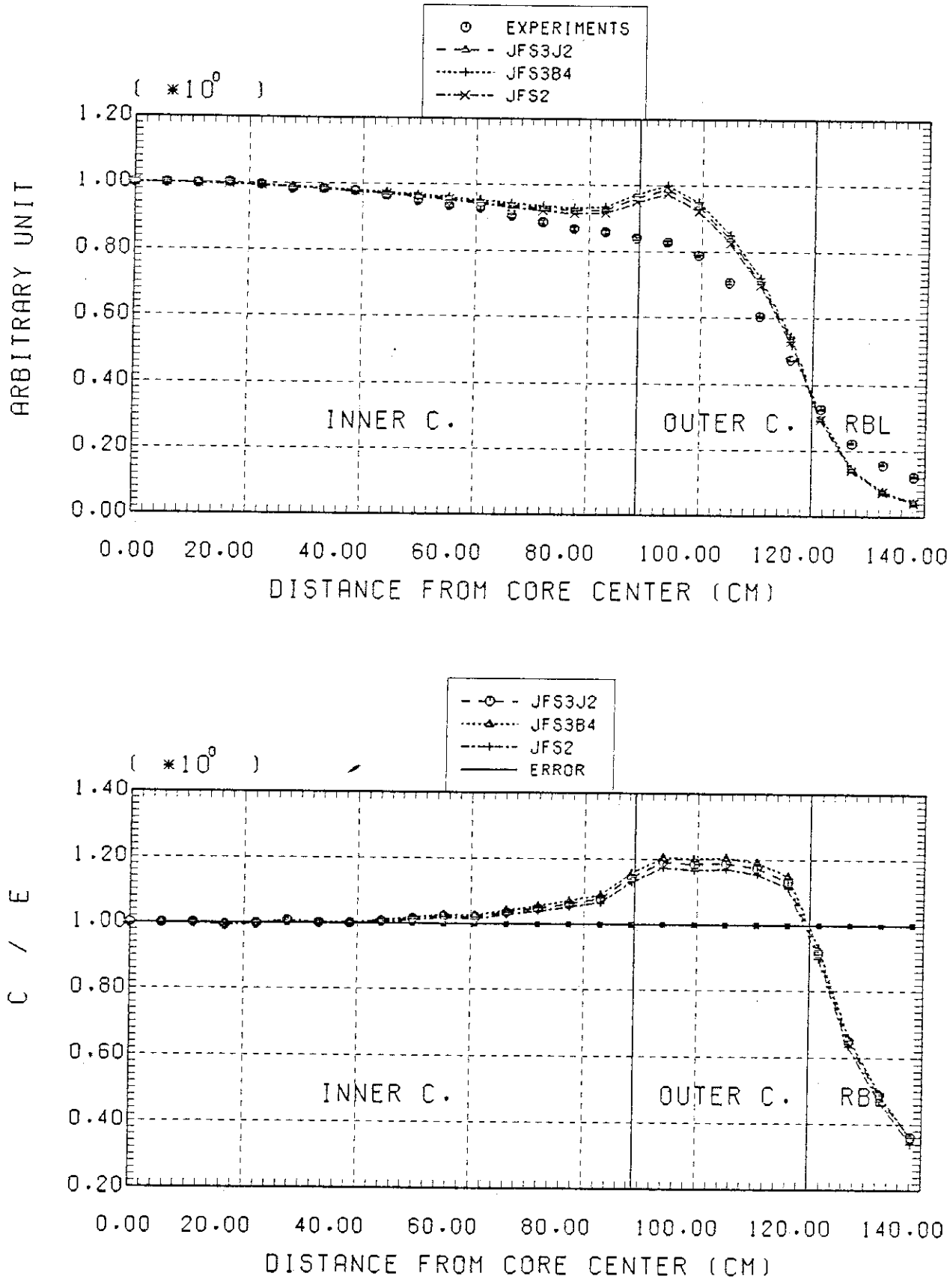

Fig. 7.19 Comparison between the calculational and experimental radial distributions of ^{236}U fission rate in ZPPR-9.

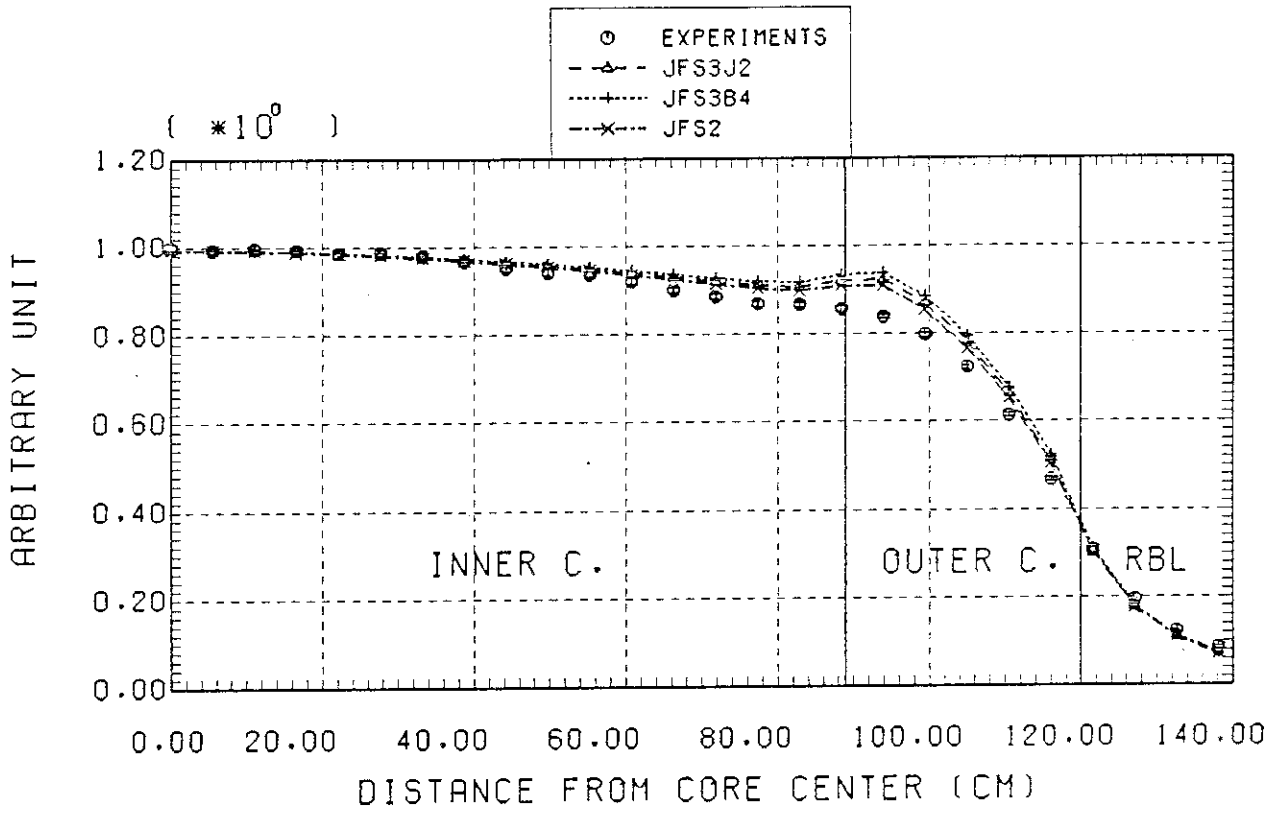

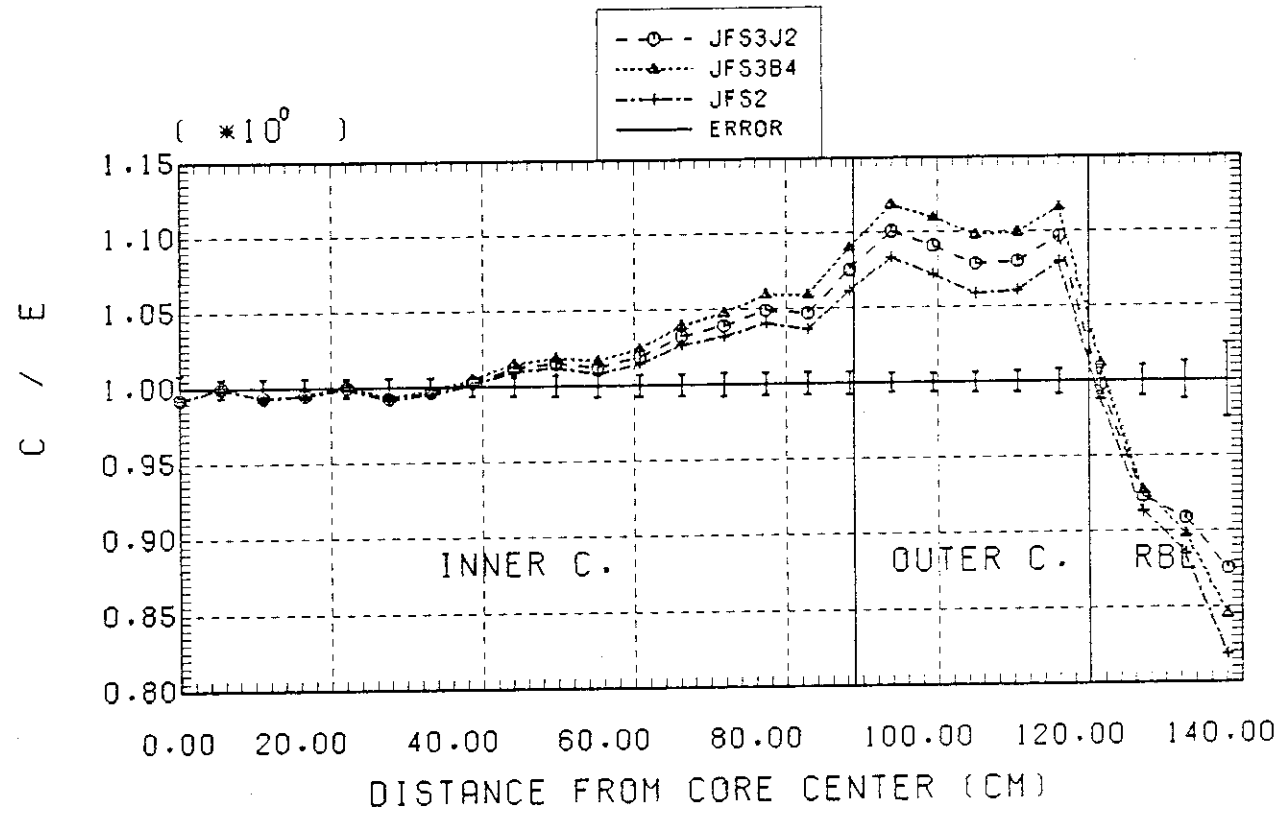

Fig.7.20 Comparison between the calculational and experimental radial distributions of ^{240}Pu fission rate in ZPPR-9.

8. Conclusions

The main purpose of the present work is to produce the group constant set to predict accurately important neutronics parameters for fast reactors. For this purpose, the generation methods for the group constants have been mainly studied for both the methods for calculating the group constants and evaluating nuclear data of heavy resonant nuclides. The accuracy of the group constants calculated by the approximate weighting spectra used in the conventional standard group constant set such as the ABBN has been examined by solving numerically neutron slowing down equation. Furthermore, the interference effects between resonances have been studied by deriving a multilevel formula in the resolved and unresolved resonance regions. In addition, the effects of mutual interference between different resonant nuclides on nuclear characteristics have been investigated. To eliminate a systematic dependence of effective multiplication factors on ^{238}U concentration ratio as seen in the JFS-1R set, a simultaneous evaluation for several important cross sections has been studied on the basis of the adjustment method of group cross section. Based on these studies, the JAERI Fast set version II(JFS-2) has been generated and the benchmark calculations for many fast critical assemblies have been performed. The result of the benchmark tests showed that the prediction of JFS-2 on various nuclear characteristics was more satisfactory than it of ENDF/B-Ⅳ or JFS-1R on them.

Moreover, several studies have been examined to advance the concept of the group constant set of JFS-2 as follows. The effects of the elastic removal cross sections overestimated by using the usual 1/E spectrum on various nuclear characteristics have been investigated as compared with them calculated with use of the removal cross sections

which are produced by using a fine-group collision density spectrum for the core composition of a prototype fast reactor MONJU. It was shown that the effect contributed seriously to the Doppler reactivity, the sample worths of ^{10}B and M_0 and the effective multiplication factors. Moreover, the accuracy of various methods for interpolating the resonance shielding factors has been examined and it was concluded that the natural cubic spline function produced the most excellent accuracy with short computing time. In addition, it was shown that the temperature dependence of capture cross sections for structural materials should be considered for the group constants, through the experimental analysis of the structural materials Doppler effects. The effect of self-shielding of the iron inelastic scattering cross section on neutron spectrum has been studied. Furthermore, the effects of the difference between the fission spectra on nuclear characteristics have been examined. Based on these studies, a new JFS-3-J2 set has been produced as an advanced set for JFS-2 using the recently evaluated nuclear data library JENDL-2B. The applicability of JFS-3-J2 to the nuclear characteristics has been also examined by performing the benchmark calculations. It was shown that the JFS-3-J2 predicted various nuclear characteristics very satisfactorily, excepting the overestimate for positive sodium soid reactivity. Especially, the prediction for effective multiplication factors was more excellent than it of ENDF/B-IV or JFS-2.

The main results obtained in each Chapter are summarized as follows. In Chapter 2, the accuracy of the approximate calculation methods for the group constants of heavy resonant nuclei in the resolved and unresolved resonance regions has been examined. The resonance shielding factors and the temperature coefficients calculated on the basic assumption of the constant collision density has not been satisfactory

for lower energy groups below about 1 keV and/or for system with highly enriched fuel, while they have resulted in good agreement with those from accurately numerical calculation for higher energy groups than 1 keV and for practical composition on typical large fast reactors. Furthermore, the accuracy of the analytical treatment methods (Methods A and B) used for the generation of the conventional group constant set such as ABBN has varied considerably with the energy group considered, the temperature in question and the composition taken up. Except for cases of accidental cancellation of errors, the analytical methods have incured non-negligible errors. It was concluded that the group constants of heavy resonant nuclides should be generated by the accurately numerical calculations.

In Chapter 3, the interference effects between resonances have been studied by using the presently derived multilevel formula. This formula is the same as the Breit-Wigner single-level formula except for the inclusion of the interference parameters (u,v) which represent the contribution of the interference effects in addition to the usual single-level parameters. Using this formula, the interference parameters were calculated for typical resonance regions of ^{235}U, ^{233}U and ^{238}U by using the least sequares fit. In the unresolved resonance region, the present interference parameters can be produced with random sampling method using the average resonance parameters and level-spacings. The contribution of the interference effect to the Doppler effect has been examined from a comparison of the resonance shielding factors. In the generation of the JFS-2 set, the group constants of ^{233}U, ^{235}U, ^{238}U and ^{239}Pu were calculated by the present multilevel formula.

In Chapter 4, a processing code TIMS-1 which calculates the effective cross sections by solving numerically the neutron slowing

down equation using the recurrence formula has been developed to avoid the errors caused from the approximate treatments used in the ETOX and MINX codes as described in Chapter 2. The mutual shielding factors were exactly calculated by using the TIMS-1 code. The mutual shielding effects between ^{239}Pu and ^{238}U on the radial reaction rates of ^{239}Pu were not more than a few percent in the blanket region of a typical fast reactor. For the effective multiplication factor and the Doppler reactivity coefficient, the mutual shielding effect were negligibly small. Furthermore, using the different processing codes TIMS-1 and ETOX, the effects of the difference between the calculational methods for group constants on the integral quantities have been studied and were not much above 0.15 % for effective multiplication factor, -3 % for sodium void effect and -4% for Doppler effect.

In JAERI, at the present day, the TIMS-1 is mainly used for generating the group constants of heavy resonant nuclides for both the thermal and fast reactor calculations.

In Chapter 5, for several important cross sections the evaluations and the adjustment of group cross sections based on the least squares method has been examined to eliminate the systematic dependence of effective multiplication factors on the ^{238}U concentration ratio as seen for the JFS-1. The cross sections, $^{235}\sigma_f$, $^{238}\sigma_c$ and $^{239}\sigma_f$ have been adjusted for the energy range from 3.6 keV to 1.4 MeV, and they evaluated for the range of 1.4 to 10.51 MeV. Moreover, the resonance parameters for ^{235}U, ^{238}U, ^{239}Pu and ^{241}Pu have been evaluated. Especially, the average resonance parameters for ^{235}U, ^{238}U and ^{239}Pu were determined by the least squares fit to the adjusted cross sections. In the resolved regions, the interference parameters (u,v) and the single-level parameters as described in Chapter 3 were used. As a result, the JFS-2 set has been produced by using mainly these evaluated

nuclear data and the ENDF/B-IV data with the use of two processing codes TIMS-1 and PROF·GROUCH·G II. The assessment of JFS-2 has been made through the benchmark tests for many physics mockup benchmark cores. It was shown that the JFS-2 predicted satisfactorily the effective multiplication factor, the reaction rate ratio and the Doppler reactivity coefficient. The mean value and standard deviation for C/E values of k_{eff} was 0.9993 and 0.4 % for the 14 plutonium cores except for the ZPR-3-54 core, and 0.9983 and 1.2 % for all the 21 plutonium and uranium cores, respectively. The prediction of JFS-2 to k_{eff} was very satisfactory as being compared with that of ENDF/B-IV which underestimated by 1% as a whole. The statistical average of C/E for the central reaction rate ratios were 0.997 for ^{238}U capture to ^{239}Pu fission, 0.980 for ^{238}U capture to ^{235}U fission, 0.980 for ^{239}Pu fission to ^{235}U fission and 1.03 for ^{238}U fission to ^{235}U fission, respectively. Furthermore the Doppler reactivity coefficient was accurately predicted with the average of 0.98 and the standard deviation of 4.4 %. Moreover, the applicability of JFS-2 to the sodium void effect, reaction rate distribution and control rod worth has been studied in detail by several researches[27),(177),(178),(203); and satisfactory predictions were shown except for several special cases. However, there existed several problems on the JFS-2 such as the discrepancy for k_{eff} between the underestimate in the pultonium cores and the overestimate in the uranium cores, the underestimate in the ratio of ^{239}Pu fission to ^{235}U fission in the pultonium cores and the apparent dependence of ^{238}U capture to ^{235}U or ^{239}Pu fission on the core volume. The reasons for these problems were not always clear.

In Chapter 6, the accuracy of the group constants calculated by the conventional standard weighting spectrum of 1/E has been examined by being compared with those produced with a fine-group collision

density spectrum for the core composition in a prototype fast reactor MONJU. The 1/E-spectrum method overestimated the elastic removal cross sections for low energy region below 1 keV, because neutron spectrum was steeply reduced in this energy region in fast reactors. Hence, the nuclear characteristics such as the Doppler reactivity coefficient, central sample worths of ^{10}B and M_0 and reaction rate in blanket region which are very sensitive to the neutron flux shape in the low energy region were considerably affected by the softened spectrum due to the overestimate of elastic removal cross sections. Especially, it caused the overestimates of ∿10 % for the Doppler reactivity and ∿5 % for the central sample worths ^{10}B and M_0. However, the systematic dependence of C/E values on the core volume as for the central reaction rate ratios of ^{238}U capture to ^{235}U fission or ^{239}Pu fission and the overestimate for the ratio of ^{238}U fission to ^{235}U fission were not removed by correcting the removal cross sections.

In Chapter 7, the JFS-3-J2 set has been generated as an advanced set for the JFS-2 and JENDL-2B-70 on the basis of the resutls studied mainly in Chapter 6 and Appendix A, using the recently produced nuclear data file JENDL-2B. The benchmark tests of JFS-3-J2 have been performed with the one- and two-dimensional benchmark models. The mean value for the C/E values of k_{eff} was 0.9988 for all the twenty-one cores, and 0.9996 for the fourteen pultonium fuel cores. These results were more satisfactory than those for ENDF/B-IV, JENDL-2B-70 and JFS-2. The predictions of JFS-3-J2 to various central reaction rate ratios were better than them of JENDL-2B-70, and were comparable with them of JFS-2. The Doppler reactivity coefficient was little underestimated, while the sodium void reactivity was remarkable overestimated by about 30%. The JFS-3-J2 predicted various

nuclear characteristics more satisfactory than the prediction of JENDL-2B-70 as a whole. Hence, the JFS-3-J2 is now used for the analyses in JUPITER (Japanese United States Program of Integral Test and Experimental Researches) project. However, several problems which the causes were not always clear were proposed also for JFS-3-J2.

To elevate moreover the applicability of JFS-3-J2 to fast reactor calculations, hence, further study will be required on evaluations and measurements for the fission spectrum and important cross sections of fuel and structural materials. Especially, several problems such as the overestimate for sodium void reactivity, the underestimate for Doppler reactivity and the dependence of the reaction rate ratios of ^{238}U capture and ^{239}Pu fission to ^{235}U fission on core volume, will require the reevaluations for the important cross sections of ^{235}U, ^{238}U and ^{239}Pu. The remarkable overestimate for the sodium void reactivity may be caused by the underestimate of ^{239}Pu fission cross sections, because the adjoint flux is very sensitive to this cross sections. Hence, the reevaluations may be examined on the basis of sensitivity and/or the adjustment studies with simultaneous evaluation as be examined in the production of the JFS-2 set. Moreover, the capture cross sections for structural materials should be reevaluated as seen from the analysis of the structural material Doppler effect in the FCA assemblies.

The discrepancies between the calculations and the experiments for sample worths for scattering materials should be studied from both the calculational method and cross section evaluation. In the calculation, bilinear weighting method may be examined by considering finer group structure than seventy one.

As for the reaction rate distribution, the discrepancies between the calculations and the experiments in the blanket region might be

caused by some reasons other than nuclear data. Further study for this problem will be required on proper treatment for gross region heterogeneity due to different compositions between core and blanket and on proper weighting spectrum to be used for group constant calculations in the blanket region.

Acknowledgments

The author wishes to express his appreciation to Dr. Y Ishiguro for his helpful suggestions and discussions during the course of this work. The author also would like to thank Mr. A. Hasegawa for his aid and cooperation in the production of the JAERI-Fast set version II. The author also is indebted to Drs. S. Katsuragi and T. Asaoka for their encouragement and useful suggestions. The author also wishes to acknowledge the assitances of Mr. Y. Matsui, Mr. K. Kaneko, Mr. H. Inoue and Mr. W. Sato in programming and running several computer codes.

The author also would like to express his sincere thanks to Professor H. Nishihara, Professor I. Kimura, Professor K. Kobayashi and Dr. N. Morishima of Kyoto University for their valuable comments and criticism. Finally, the author wish to acknowledge Drs. M. Nakagawa, Y. Kikuchi and T. Suzuki for their valuable suggestions.

caused by some reasons other than nuclear data. Further study for this problem will be required on proper treatment for gross region heterogeneity due to different compositions between core and blanket and on proper weighting spectrum to be used for group constant calculations in the blanket region.

Acknowledgments

The author wishes to express his appreciation to Dr. Y Ishiguro for his helpful suggestions and discussions during the course of this work. The author also would like to thank Mr. A. Hasegawa for his aid and cooperation in the production of the JAERI-Fast set version II. The author also is indebted to Drs. S. Katsuragi and T. Asaoka for their encouragement and useful suggestions. The author also wishes to acknowledge the assitances of Mr. Y. Matsui, Mr. K. Kaneko, Mr. H. Inoue and Mr. W. Sato in programming and running several computer codes.

The author also would like to express his sincere thanks to Professor H. Nishihara, Professor I. Kimura, Professor K. Kobayashi and Dr. N. Morishima of Kyoto University for their valuable comments and criticism. Finally, the author wish to acknowledge Drs. M. Nakagawa, Y. Kikuchi and T. Suzuki for their valuable suggestions.

Appendix A. Some Remarks on Calculations of Effective Cross Sections and Nuclear Characteristics

1. Accuracy of Interpolation Methods for Resonance Self-Shielding Factors

1.1 Introduction

Multigroup transport and diffusion calculations are often based on the concept of multigroup constants sets such as the ABBN[8] or JFS-1[9] compilations. The principal advantage of the multigroup constant method is that reactor calculation can be made by using the same group constant set for the various reactors with different compositions and sizes. The multigroup constant set prepared for this purpose has the tables, $f(\sigma_0,T)$, of resonance self-shielding factors which are given as function of temperature T and effective background cross section σ_0 of Boundarenko scheme[8]. In reactor calculation, the effective microscopic cross sections for each material zone are calculated from the infinitely dilute cross sections and the self-shielding factors interpolated for the effective temperature and background cross sections from $f(\sigma_0,T)$-tables.

As for the interpolation schemes of $f(\sigma_0,T)$-tables, many methods have been studied. For example, in one-dimensional diffusion code EXPANDA-4[191] a rational function is used for both the σ_0- and T-interpolations, and the Kidman's schemes[192] used in one-dimensional diffusion code 1DX[193] are a Lagrange three-point interpolation on the (ℓn T, f) tabular points and the four-parameter interpolation formula for the $f(\sigma_0)$-table. Furthermore, there are several methods described in the next section. Among these schemes, however, the superiority or inferiority of the accuracy and computing cost is not compared. At the present time, the f-tables can numerically be calculated with high accuracy by the use of a processing

code such as TIMS-1[35]. Hence the erros caused by interpolating the f-tables should be as small as possible.

In this chapter, various interpolation methods are compared in connection with computing cost and accuracy. Moreover, the effects of the difference among various interpolations on integral quantities in fast reactor are studied.

1.2 Accuracy of Various Interpolation Methods

In order to study the accuracy of various interpolation methods, the $f(\sigma_0,T)$-tables for ^{238}U and ^{239}Pu were calculated for $\sigma_0 = 0$, 0.1, 0.31, 1.0, 2.15, 4.65, 10, 21.5, 46.5, 10^2, 215, 465, 10^3, 2150, 4650, 10^4, 2.15×10^4, 4.65×10^4, 10^5, 2.15×10^5, 4.65×10^5 and 10^6 barns and T = 300, 743, 900, 1500, 2100, 2800 and 3500 °K using the TIMS-1[35] code from the nuclear data file of ENDF/B-IV. These f-tables were calculated with the seventy-group structure of JFS-2 in the resonance energy region below 46.5 KeV for ^{238}U and 21.5 KeV for ^{239}Pu.

As for the σ_0-interpolation, the presently examined interpolation formulas are as follows:

(a) $f(X) = \dfrac{C}{X-A} - B, \quad X = \ell n\ \sigma_0$: Ref.(191)

(b) $f(X) = \sqrt{\dfrac{\lambda+X}{\lambda+\eta+X}}, \quad X = \sigma_0$: Ref.(194)

(c) $f(X) = A \tanh (B(X+C)) + D, \quad X = \ell n\ \sigma_0$: Ref.(192)

(d) Natural cubic spline function[195]

(e) Akima method[196]

and for the T-interpolation,

(f) $f(T) = \dfrac{C}{T-A} - B$: Ref.(197)

(g) Three-point Lagrange interpolation formula:

$$f(X) = \frac{f_1(X-X_2)(X-X_3)}{(X_1-X_2)(X_1-X_3)} + \frac{f_2(X-X_3)(X-X_1)}{(X_2-X_1)(X_2-X_3)}$$

$$+ \frac{f_3(X-X_1)(X-X_2)}{(X_3-X_1)(X_3-X_2)} \quad , \qquad X = \ell n\, T$$

(h) $f(T) = \{A + B\,\ell n\, T + C(\ell n\, T)^2\}^{-1}$: Ref.(197)

(d) Natural cubic spline function[195]

(e) Akima method[196]

where the interpolation coefficients in each formula, and the spline and Akima formulas are calculated with the expressions described as follows:

1). Formulas (a) and (f) (EXPAN-method): These formulas are used in the one-dimensional diffusion code EXPANDA-4[191] and the modified versions[99),(173]. The interpolation coefficients are written by

$$A = \frac{f_1x_1(x_2-x_3) + f_2x_2(x_3-x_1) + f_3x_3(x_1-x_2)}{f_1(x_2-x_3) + f_2(x_3-x_1) + f_3(x_1-x_2)} \quad ,$$

$$B = \frac{f_1f_2(x_1-x_2) + f_2f_3(x_2-x_3) + f_3f_1(x_3-x_1)}{f_1(x_2-x_3) + f_2(x_3-x_1) + f_3(x_1-x_2)} \quad ,$$

$$C = -\frac{(x_1-x_2)(x_2-x_3)(x_3-x_1)(f_1-f_2)(f_2-f_3)(f_3-f_1)}{\{f_1(x_2-x_3) + f_2(x_3-x_1) + f_3(x_1-x_2)\}^2} \quad .$$

2). Formulas (b) and (g) (COSMOS-method): These formulas are adopted in the COSMOS-2[198] code for the production of cross section library. The formula (b) is a theoretical expression derived by Segev[194] on the basis of the assumptions in which resonances are well separated and resonance structure in the mixed-macroscopic cross section is small. The coefficients of the formula (b) are expressed by

$$\lambda = \frac{x_1f_2^2(1-f_1^2) - x_2f_1^2(1-f_2^2)}{f_1^2 - f_2^2} \quad ,$$

$$\eta = \frac{(f_1^2 - 1)(f_2^2 - 1)(x_1 - x_2)}{f_1^2 - f_2^2} \quad .$$

3). Formula (c): The coefficients are written by

$$A = \frac{1}{2}\,(f_{+\infty} - f_{-\infty}) \quad , \qquad B = \frac{y_1 - y_2}{x_1 - x_2} \quad ,$$

$$C = \frac{x_1 y_2 - x_2 y_1}{x_1 - x_2} \quad , \qquad D = \frac{1}{2}\,(f_{-\infty} + f_{+\infty}) \quad ,$$

where

$$f_{-\infty}(\sigma_0 = 0) = D - A \quad , \qquad f_{+\infty}(\sigma_0 = 10^6) = A + D \quad ,$$

$$y = \tanh^{-1}\,(\frac{f(x) - D}{A}) \quad .$$

The formulas (c) and (h) are adopted in one-dimensional diffusion code 1DX[193] and are called the TANH method.

4). Formula (h): The coefficients are written by

$$A = -\frac{f_1 f_2 x_1 x_2 (x_1 - x_2) + f_2 f_3 x_2 x_3 (x_2 - x_3) + f_3 f_1 x_3 x_1 (x_3 - x_1)}{f_1 f_2 f_3\ (x_1 - x_2)(x_2 - x_3)(x_3 - x_1)} \quad ,$$

$$B = \frac{f_1 f_3 (x_3^2 - x_1^2) + f_2 f_3 (x_2^2 - x_3^2) + f_1 f_2 (x_1^2 - x_2^2)}{f_1 f_2 f_3 (x_1 - x_2)(x_2 - x_3)(x_3 - x_1)} \quad ,$$

$$C = -\frac{f_1 f_2 (x_1 - x_2) + f_2 f_3 (x_2 - x_3) + f_3 f_1 (x_3 - x_1)}{f_1 f_2 f_3 (x_1 - x_2)(x_2 - x_3)(x_3 - x_1)} \quad .$$

5). Natural cubic spline method[195] (SPLINE-method): This is well-known method which interpolates smoothly among the sample points. The natural cubic spline function is written by

$$f(x) = \begin{cases} f_1 + B_1(x-x_1) + C_1(x-x_1)^2 , & \text{for } x < x_1 \\ f_i + B_i(x-x_i) + C_i(x-x_i)^2 + D_i(x-x_i)^3 , & \\ \qquad \text{for } x_i \leqq x < x_{i+1} , \quad i = 1, ---, n-1 & \\ f_n + B_n(x-x_n) + C_n(x-x_n)^2 , & \text{for } x > x_n \end{cases}$$

where $f(x)$ and its derivatives of orders 1 and 2 are continuous everywhere. If $f''(x) = 0$ in each of the two intervals $(-\infty, x_1)$ and (x_n, ∞), the coefficients are expressed as follows:

$$B_i = \frac{f_{i+1} - f_i}{h_i} - \frac{h_i}{6}(f''_{i+1} + 2f''_i) , \quad i = 1, ---, n-1$$

$$C_i = f''_i / 2 , \quad i = 1, ---, n-1$$

$$D_i = (f''_{i+1} - f''_i) / 6h_i , \quad i = 1, ---, n-1$$

$$B_n = \frac{f_n - f_{n-1}}{h_{n-1}} + \frac{h_{n-1}}{6}(2f''_n + f''_{n-1}) ,$$

$$C_n = f''_n / 2 ,$$

$$h_i = x_{i+1} - x_i ,$$

where $f''_i (i = 1, ---, n)$ are calculated by solving the following simultaneous equations:

$$f''_1 = 0 ,$$

$$h_{i-1}f''_{i-1} + 2(h_{i-1} + h_i)f''_i + h_i f''_{i+1} = 6\left(\frac{f_{i+1} - f_i}{h_i} - \frac{f_i - f_{i-1}}{h_{i-1}}\right) ,$$

$$i = 2, ---, n-1$$

$$f''_n = 0 .$$

6). Akima method[196]: This is a modified method for the cubic spline interpolation, and produces much better results as to an interpolation problem of uneven intervals among the sample points. This method has been prepared[199] as the JAERI Scientific Subroutine Library in the computer of FACOM-230/75 and M-200. The obtained description of Akima method will be seen in Ref.(196) or (199).

The self-shielding factors for σ_0 = 0.31, 2.15, 5.65, 21.5 46.5, 215, 465, 2150, 4650, 21500, 46500 and 215000 barns were calculated by using these interpolation formulas (a) ∿ (e), with some of eight points, 0.0, 1, 10, 10^2, 10^3, 10^4, 10^5 and 10^6 barns. The accuracies of the methods were studied by comparing the deviation of the interpolated value from the exact value calculated by TIMS-1.

Figure A.1.1 shows the dependence of the self-shielding factors on the σ_0-values for typical energy groups. The deviations of the interpolated values from the exact ones are shown in Figs.A.1.2~5. The relation between the interpolation methods and the symbols drawn in these figures is indicated in Table A.1.1. It is seen from these figures as follows: The values interpolated are overestimated or underestimated, depending on the σ_0-range. For example, the errors for the formula (a) with the symbol E are larger and the larger errors are observed for the ranges of σ_0 which the self-shielding factors varies steeply as seen from Fig.A.1.1. The cubic spline formula (symbol S) is seen to give the most excellent and stable accuracies.

The dependence of the self-shielding factors on the temperature shows a similar tendency to the dependence on σ_0 in Fig.A.1.1. As for the T-interpolation, the self-shielding factors for T = 743, 1500 and 2800 °K were calculated by using the formulas (d) ~ (h). The points used were 300, 900, 2100 and 3500 °K. Figures A.1.6 and 7 show the relative errors of the

interpolated values for the capture self-shielding factors of ^{238}U to the exact ones calculated by TIMS-1. Though the errors are small below one percent, the spline method is better also as to the T-interpolation.

On the other hand, the computing cost for these interpolations for σ_0 and T are compared in Table A.1.1. The computing times for σ_0 and T-interpolations are the total times consumed for the calculations in the two cases of 48 groups, 4 reactions and 12 σ_0-values and of 48 groups, 4 reactions and 3 temperatures, respectively. These calculations were performed by using the computer of FACOM-230/75. There may be little difference among the computing times, for example, as compared with the times consumed for two-dimensional diffusion calculation.

1.3 Effects of Differences Among Various Interpolation Methods on Integral Quantities

The self-shielding factors of ^{238}U and ^{239}Pu were calculated for eight σ_0-values and four temperatures as described in Section A.1.2. The effects of the differences among the various interpolations for the f-tables of two nuclides on integral quantities were studied by using the one-dimensional diffusion code EXPANDA-70D[99] and the multi-group cross sections library JFS-2[15]. The integral quantities calculated were the effective multiplication factor (k_{eff}), Doppler effect, Na-void effect, control rod reactivity worth and reaction rate distribution in the several fast reactors, ZPPR-2, SEFOR, MZB and a typical prototype LMFBR.

Table A.1.2 shows the comparison of ratios of the results calculated from various interpolation methods to those calculated by the cubic SPLINE method. The calculational results for the AKIMA, COSMOS and TANH methods are in very good agreement with the SPLINE-results. However, the results of the

EXPANDA-method are underestimated by about 0.2 % for k_{eff} and 1.5 % for the control rod reactivity worth (C.R.W), respectively, as compared with the other results. The underestimated values are comparable to the goal accuracies[18] (±0.2 % for k_{eff} and ±2 % for C.R.W) requested from design study for a large fast breeder reactor.

The calculational results for the Doppler effects are shown in Tables A.1.3~6. In the SEFOR assembly, the isothermal Doppler coefficient of the whole core was calculated with the benchmark model of one-dimensional spherical geometry[100]. In the ZPPR-2 assembly, the ^{238}U Doppler effects were calculated for the natural UO_2 sample Doppler experiments performed with the normal and sodium voided cores.

Tables A.1.3 and 4 show the comparisons of the results calculated by the following procedure: As for σ_0-interpolation, only the SPLINE-method was used and as for T-interpolation, the methods, EXPAN, COSMOS, TANH, SPLINE and AKIMA were used. The differences among the Doppler reactivity effects obtained by the methods, COSMOS, TANH, SPLINE and AKIMA are very small and below about one percent while the EXPAN-method produces larger differences than the another method.

Tables A.1.5 and 6 show the comparisons of the Doppler effects calculated by interpolating the f-tables with the methods indicated in Table A.1.1. As seen from these tables, the accuracy of the interpolation methods for both σ_0 and T affects on the Doppler effects. The difference between COSMOS and EXPAN is about 13 percent for the fission reactivity change $(\Delta K/k)_{\delta\Sigma f}$ in the case of SEFOR, and about 8 ~ 12 percent for the ^{238}U Doppler reactivity change in ZPPR-2 (T = 300 - 500 °K). The difference is larger than the goal accuracy (±7 %) for Doppler effect in Ref.(18). On the other hand, the differences among the SPLINE, TANH and AKIMA methods are very small.

The reaction rate distributions were calculated by using both the

SPLINE- and EXPAN-methods for the Japanese prototype fast reactor "MONJU" mock-up assembly MZB. For the radial distributions of fission reaction rates for ^{235}U, ^{238}U and ^{239}Pu, the deviations of the reaction rates calculated with the SPLINE-method from those for the EXPAN-method are shown in Fig.A.1.8. The reaction rates calculated with SPLINE become smaller by about 2.5 percent for ^{239}Pu and 1.5 percent for ^{235}U at the boundary between the radial blanket and settel reflector.

1.4 Concluding Remarks

Various methods have used to interpolate the resonance shielding factors, mainly because they have the simplest mathematical properties. However, there is now considerable evidence that the cubic spline function is a more adaptable interpolating function than several functions involving a comparable number of parameters. The spline function offers a very practical means with good accuracy and short computing times, as to the interpolation for the resonance shielding factors. This conclusion is based in part on actual numerical experience.

It was shown that the errors for the self-shielding factors calculated with the various interpolation methods produce non-negligible effects on effective multiplication factor, control rod reactivity worth and Doppler effect, because the effects are comparable to the goal accuracy requested from design study for a large fast breeder reactor. Furthermore, the errors produces a slightly anxious effect on reaction rate distribution in blanket region.

The cubic spline interpolation is adopted in the one-dimensional diffusion code SLAROM which is a subprogram in the JAERI fast reactor analysis code system.

Table A.1.1 Computing times for various interpolation methods and relation between the method and the symbol in Figs. A.1.2∿5.

Formula		Name of method	Symbol in Figs. 2∿5	Computing time, CPU* (msec)	
$f(\sigma_0)$	f(T)			$f(\sigma_0)$	f(T)
(a)	(f)	EXPAN	E	432	140
(b)	(g)	COSMOS	C	420	143
(c)	(h)	TANH	T	526	151
(d)	(d)	SPLINE	S	444	155
(e)	(e)	AKIMA	A	429	148

* FACOM-230/75 computer

Table A.1.2 Comparison of the ratios of k_{eff}, control rod worth and Na-void effect calculated by several interpolation methods to those by the cubic spline method

Integral quanitity	Assembly	AKIMA / SPLINE	COSMOS / SPLINE	TANH / SPLINE	EXPAN / SPLINE
k_{eff}	ZPPR-2 (Normal)	0.9995	1.0005	1.000	0.9983
	ZPPR-2 (Na-void)	0.9995	1.0005	1.000	0.9983
	SEFOR	0.9994	1.0004	1.0002	0.9994
	LMFBR*	0.9992	1.0004	1.0000	0.9978
C.R.** Worth	LMFBR*	0.996	1.003	1.001	0.985
Na-void***	ZPPR-2	0.9991	1.0005	1.001	0.9983

* Proto-type NEACRP benchmark core

** Radius of cylindrical control rod zone is 7.716 cm at the core center. The value of C.R.W. calculated by SPLINE-method is 0.00278.

*** Cylindrical voided zone is 30.5 cm at the core center Sodium void reactivity ($k_{voided}-k_{ref.}$) calculated by SPLINE-method is 0.00628.

Table A.1.3 Comparison of Doppler effects calculated for SEFOR benchmark test assembly. The interpolating calculations for σ_0 were performed with SPLINE.

Method	Doppler effect ($\Delta K/K \times 10^3$), T=677∿1365°K		
	by $\delta(\Sigma_f)$	by $\delta(\Sigma_c)$	Total
SPLINE	2.307 (1.00)	-7.998 (1.00)	-5.639 (1.00)
AKIMA	2.297 (0.995)	-7.912 (0.989)	-5.572 (0.988)
COSMOS	2.290 (0.993)	-7.908 (0.989)	-5.568 (0.987)
EXPAN	2.212 (0.958)	-7.753 (0.969)	-5.473 (0.971)
TANH	2.280 (0.988)	-7.903 (0.988)	-5.578 (0.989)

The ratios of the values for various methods to the SPLINE-results are presented in the parentheses.

Table A.1.4 Comparison of Doppler effects calculated for ZPPR-2 assemblies with the normal and sodium voided cores. The interpolating calculations for σ_0 were performed with SPLINE.

Method	Doppler effect ($\Delta K/K \times 10^6$)			
	Normal core		Na-voided core	
	T=300∿500°K	T=300∿1100°K	T=300∿500°K	T=300∿1100°K
SPLINE	-2.633 (1.00)	-7.086 (1.00)	-1.737 (1.00)	-4.568 (1.00)
AKIMA	-2.646 (1.005)	-7.078 (0.999)	-1.759 (1.013)	-4.556 (0.997)
COSMOS	-2.648 (1.006)	-7.073 (0.998)	-1.757 (1.011)	-4.558 (0.998)
EXPAN	-2.681 (1.018)	-7.055 (0.996)	-1.778 (1.024)	-4.547 (0.996)
TANH	-2.642 (1.003)	-7.074 (0.998)	-1.751 (1.008)	-4.560 (0.998)

The ratios of the values for various methods to the SPLINE-results are presented in the parentheses.

Table A.1.5 Comparison of Doppler effects calculated for SEFOR benchmark test assembly. The interpolating calculations for σ_0 and T were performed with each formula indicated in Table 7.1.

Method	Doppler effect ($\Delta K/K \times 10^3$), T=677∿1365°K		
	by $\delta(\Sigma_f)$	by $\delta(\Sigma_c)$	Total
SPLINE	2.307 (1.00)	-7.998 (1.00)	-5.639 (1.00)
AKIMA	2.312 (1.002)	-7.866 (0.983)	-5.510 (0.977)
COSMOS	2.480 (1.075)	-8.190 (1.024)	-5.649 (1.002)
EXPAN	2.197 (0.952)	-8.186 (1.023)	-5.989 (1.062)
TANH	2.291 (0.993)	-7.919 (0.990)	-5.579 (0.989)

The ratios of the values for various methods to SPLINE are presented in the parentheses.

Table A.1.6 Comparison of Doppler effects calculated for ZPPR-2 assemblies with the normal and/or sodium voided cores. The interpolating calculations for σ_0 were performed with each formula indicated in Table A.1.1.

Method	Doppler effect ($\Delta K/K \times 10^6$)			
	Normal core		Na-voided core	
	T=300∿500°K	T=300∿1100°K	T=300∿500°K	T=300∿1100°K
SPLINE	-2.633 (1.00)	-7.086 (1.00)	-1.737 (1.00)	-4.568 (1.00)
AKIMA	-2.600 (0.987)	-6.981 (0.985)	-1.731 (0.997)	-4.491 (0.983)
COSMOS	-2.687 (1.021)	-7.275 (1.027)	-1.798 (1.035)	-4.700 (1.029)
EXPAN	-2.462 (0.935)	-7.149 (1.009)	-1.604 (0.923)	-4.514 (0.988)
TANH	-2.664 (1.012)	-7.138 (1.007)	-1.767 (1.017)	-4.601 (1.007)

The ratios of the values for various methods to SPLINE are presented in the parentheses.

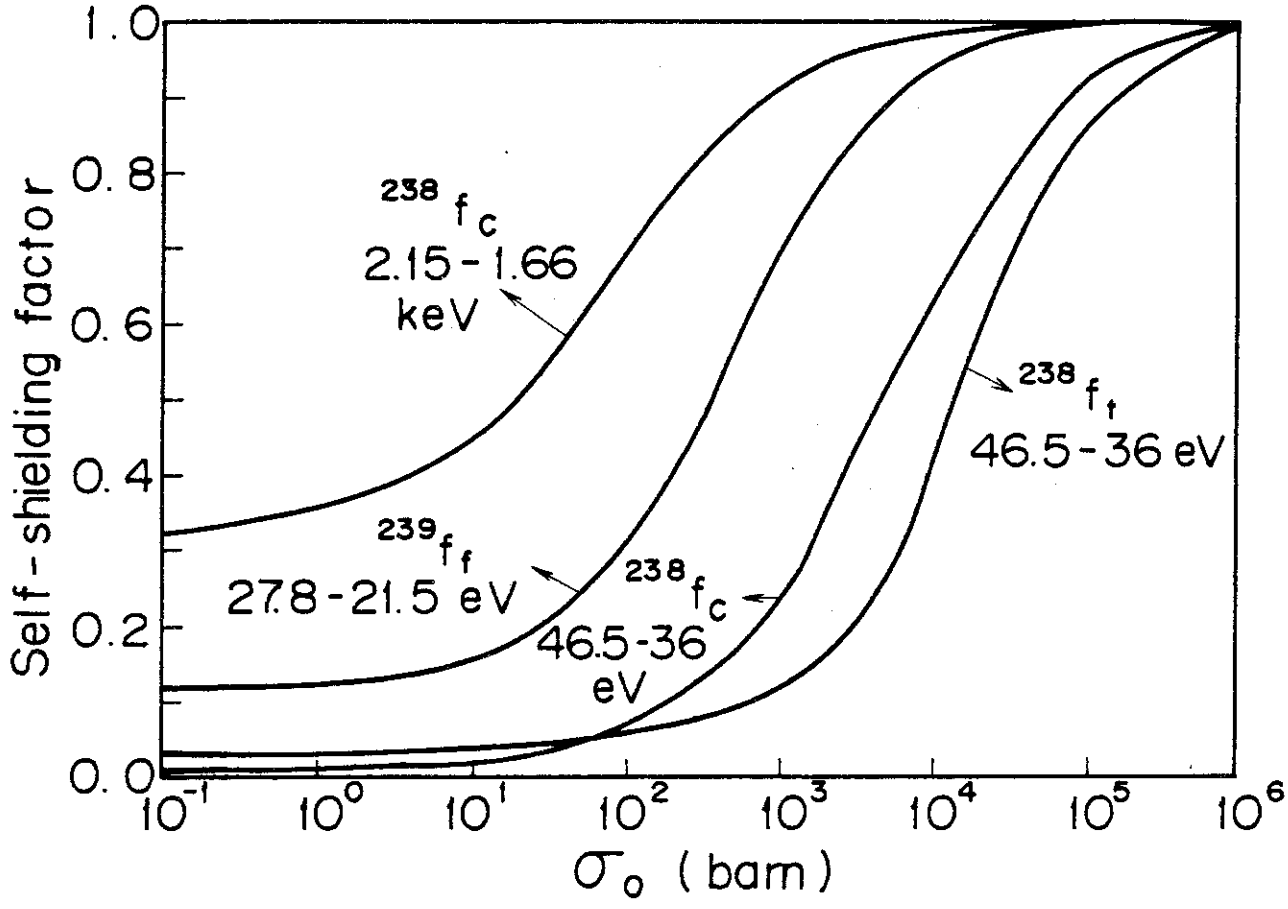

Fig.A.1.1 Dependence of self-shielding factors on σ_0, $^{238}f_c$ and $^{238}f_t$:
capture and total self-shielding factors of ^{238}U
$^{239}f_f$: fission self-shielding factors of ^{239}Pu

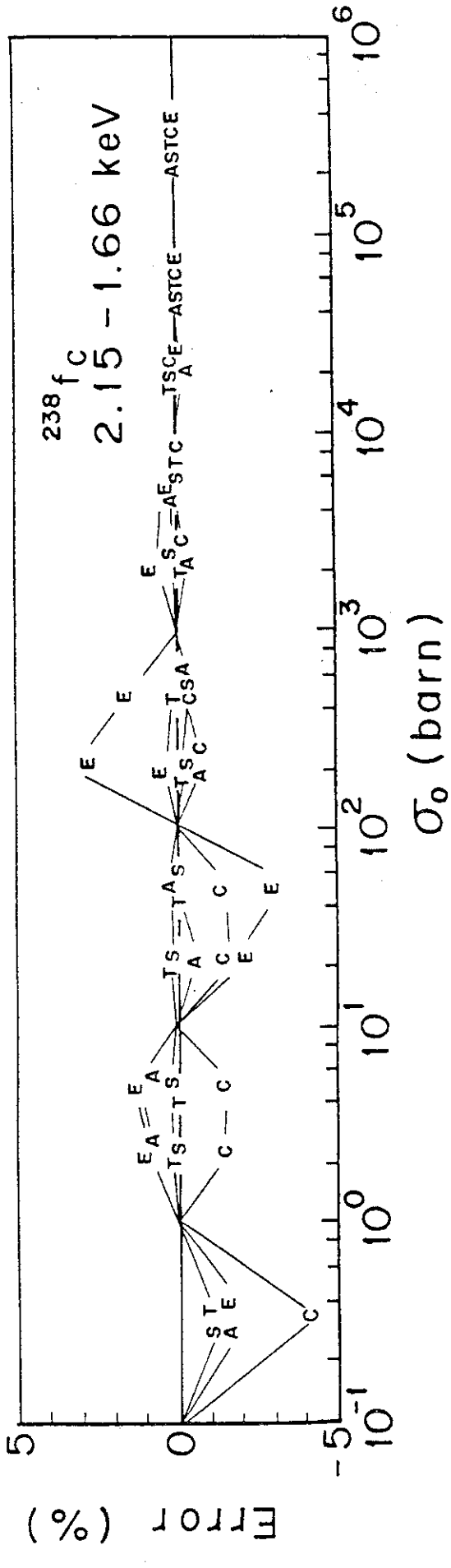

Fig.A.1.2 Deviation of the ^{238}U capture self-shielding factors interpolated by the methods (a)∿(e) from the exact values in the energy range from 2.15 to 1.66 KeV

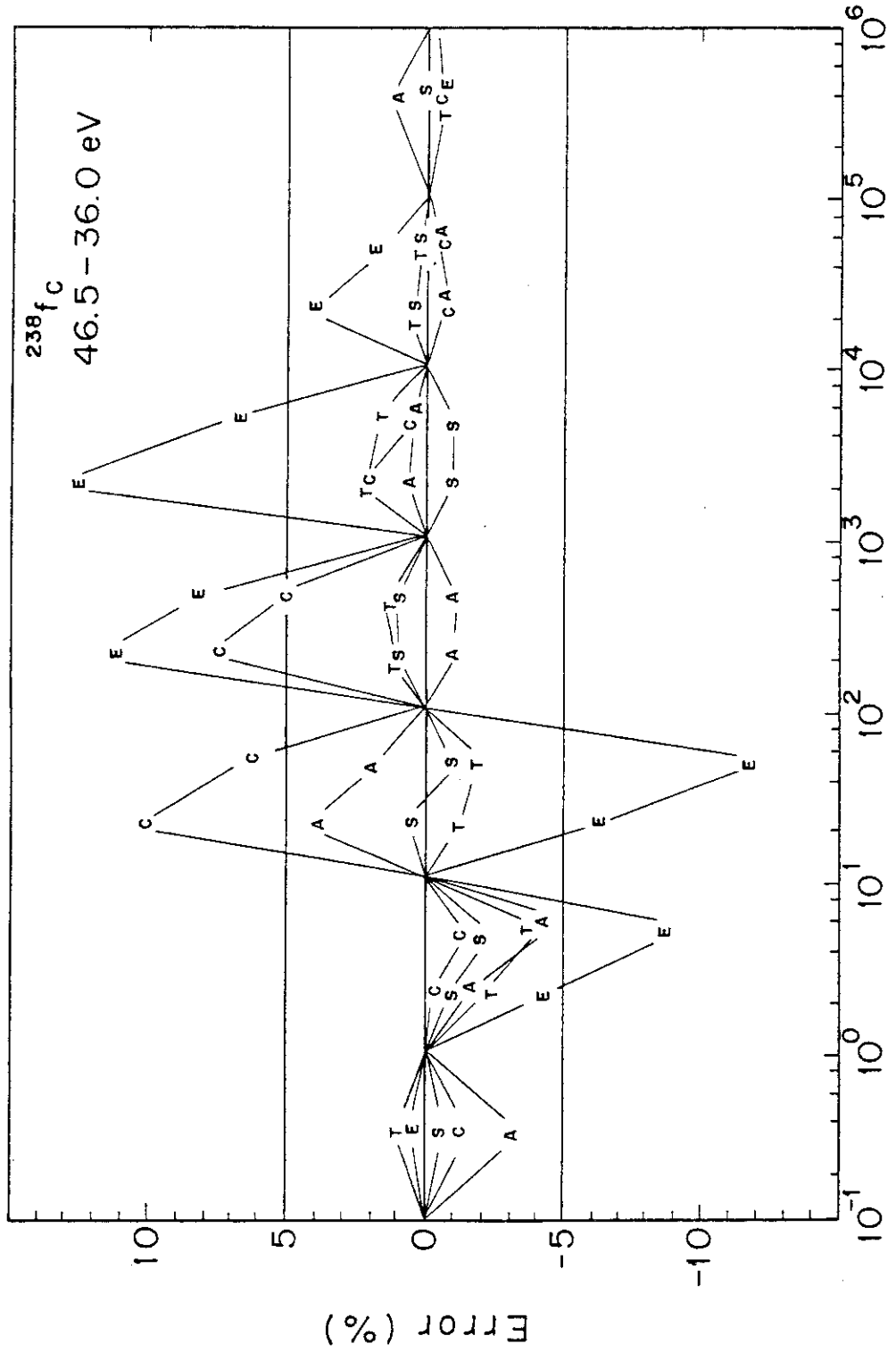

Fig.A.1.3 Deviation of the ^{238}U capture self-shielding factors interpolated by the methods (a)~(e) from the exact values in the energy range from 46.5 to 36 eV

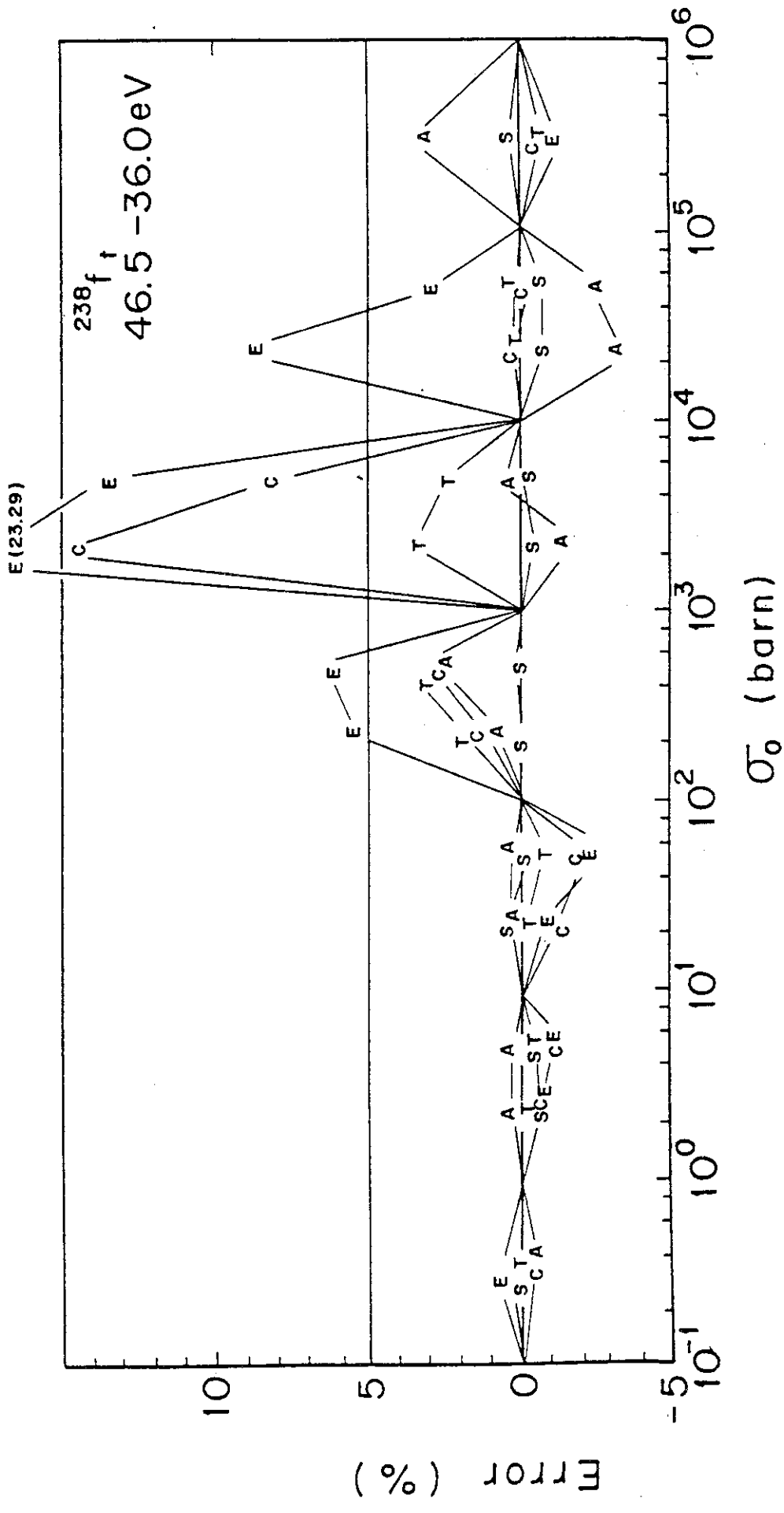

Fig.A.1.4 Deviation of the ^{238}U total self-shielding factors interpolated by the methods (a)~(e) from the exact values in the energy range from 46.5 to 36 eV

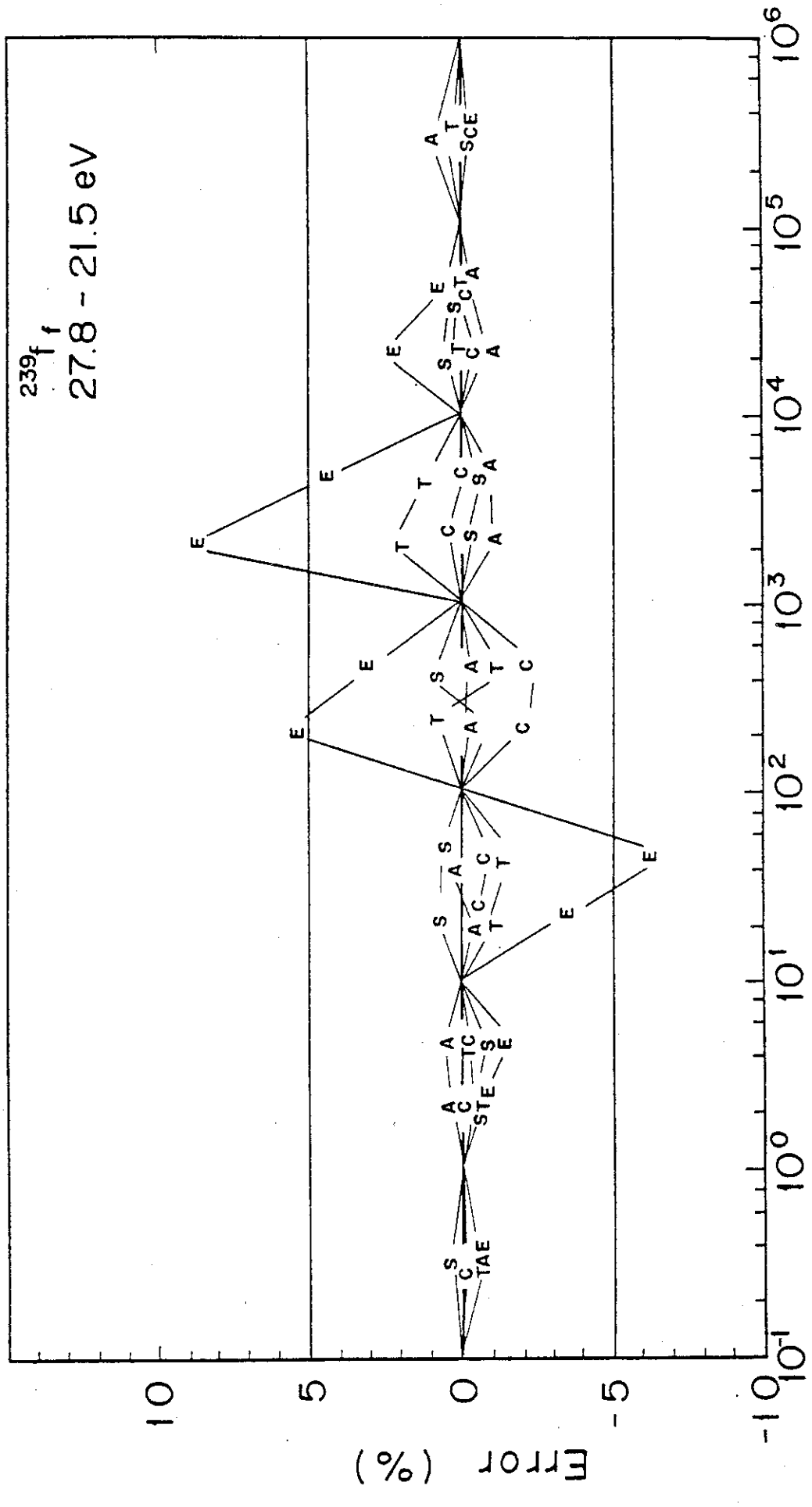

Fig.A.1.5 Deviation of the ^{239}Pu fission self-shielding factors interpolated by the methods (a)ν(e) from the exact values in the energy range from 27.8 to 21.5 eV

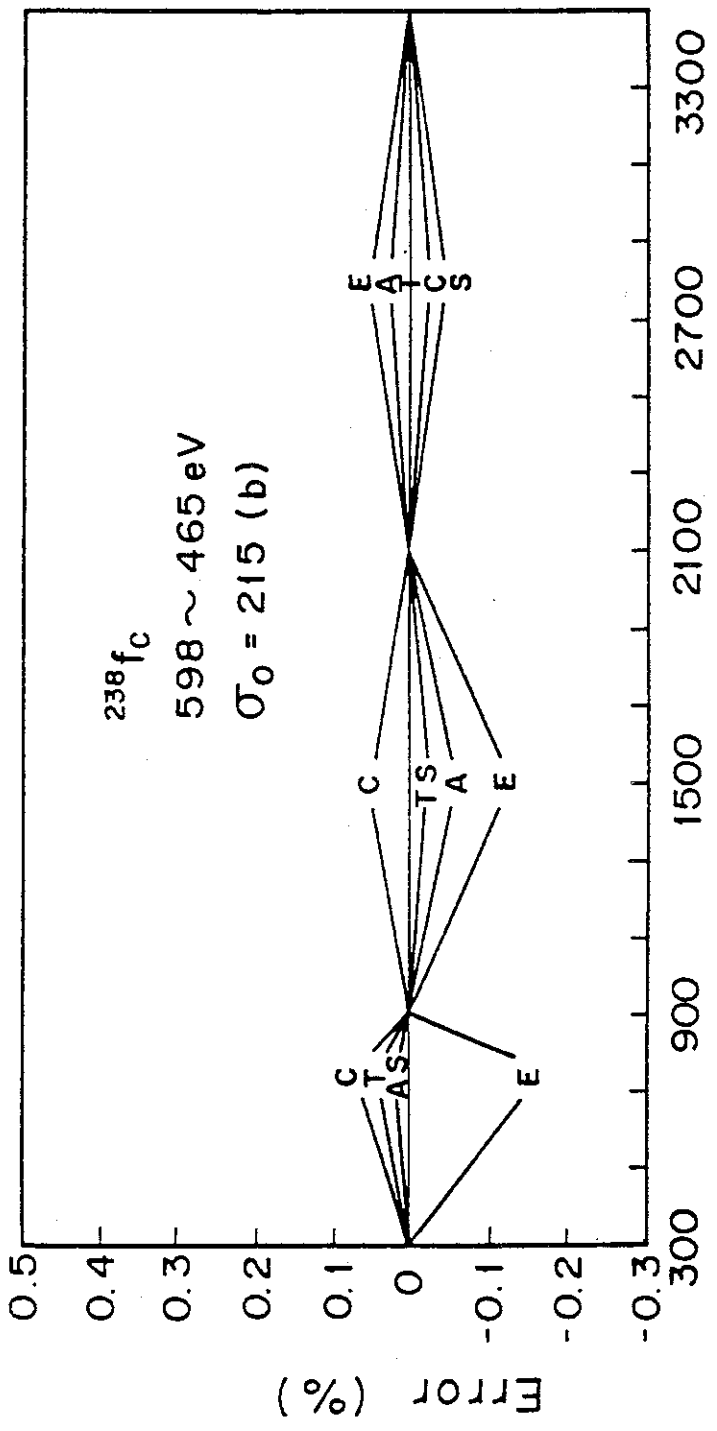

Fig.A.1.6 Deviation of the ^{238}U capture self-shielding factors interpolated by the methods (d)～(h) from the exact values in the energy range from 598 to 465 eV

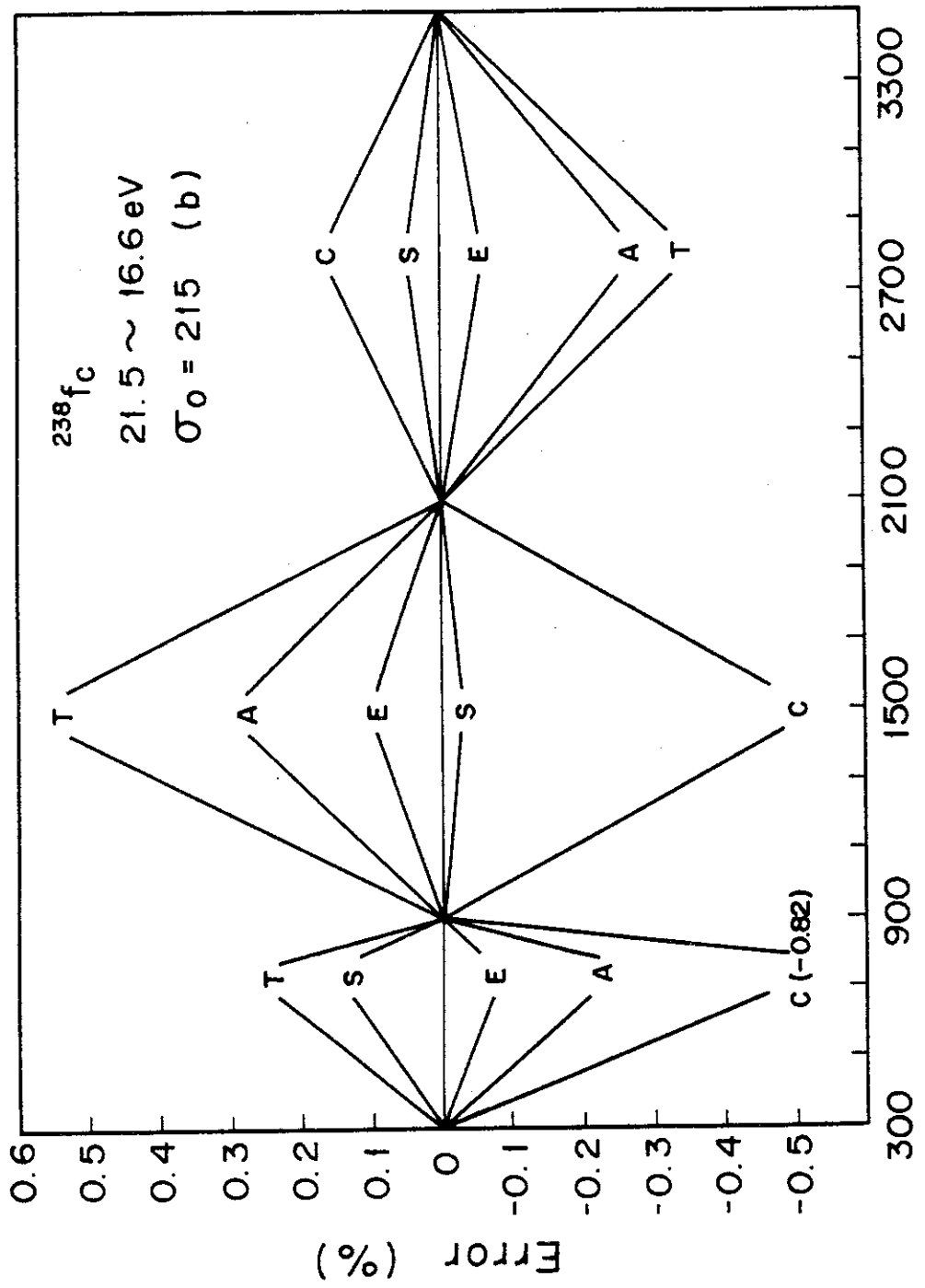

Fig.A.1.7 Deviation of the ^{238}U capture self-shielding factors interpolated by the methods (d)~(h) from the exact values in the energy range from 21.5 to 16.6 eV

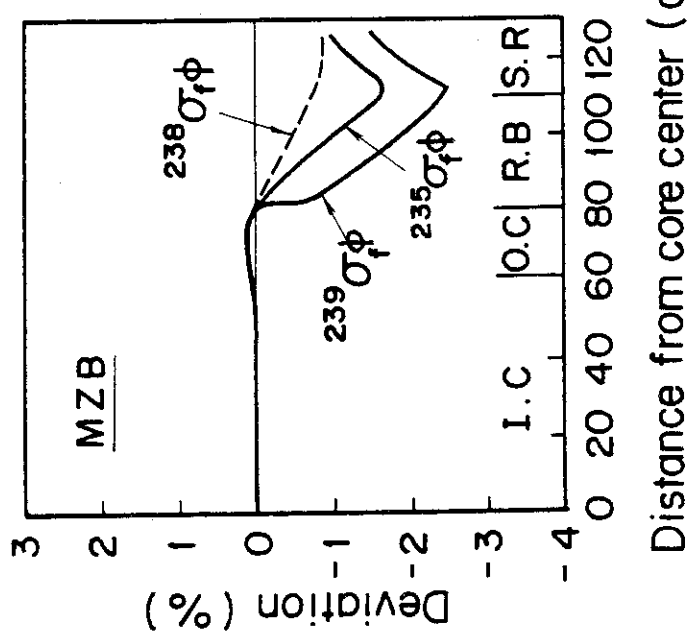

Fig.A.1.8 Deviation of the reaction rate distributions calculated with the SPLINE method from those for the EXPANDA method

2. Doppler Effect of Structural Materials in Fast Reactors

2.1. Introduction

In a fast reactor, a large quantities of iron, chromium and nickel are contained as cladding or structural materials in the core, blanket and reflector. The experiments and analyses for the structural material Doppler effect have been performed and a strong Doppler effect has been observed in stainless steel[200)-(202)]. However, the calculated Doppler effects showed a considerable underestimate to the experimental results[(201),(202)].

The temperature dependence of capture cross sections for the structural materials is mainly due to p-wave neutron resonances and seen in the energy range from 1 to 300 keV, where lies the important range of neutron spectrum in fast reactor. However, the temperature dependence of the cross sections has not been considered in the group constants library such as JFS-2[(15)], LIB-IV[(13)] and/or JENDL-2B[(39)], that is, the cross sections at the zero temperature ($T = 0°K$) are used in fast reactor calculations. Benchmark tests of the group constants libraries have been performed[(15),(39)] by using the cross sections of the structural materials for $T = 0°K$.

In this section, the structural material Doppler effects for the temperature rise from 0 to 300°K are calculated for 23 fast critical assemblies. The correction factors for the k_{eff}-values in the benchmark calculations are evaluated from the calculated Doppler effects. As for a practical temperature rise of the structural materials, the Doppler effect is studied by analysing the whole core Doppler experiment in SEFOR assembly. In order to test the temperature dependence of the capture cross sections, furthermore, the sample Doppler experiments in FCA assemblies are analysed by using the nuclear data of JENDL-2 and ENDF/B-IV, which are not used in the calculation of the references (200) ∿ (202). For this purpose, the temperature

dependent self-shielding factors of iron, chromium and nickel are calculated with the assumption of collision density constant by using the PROF GROUCH G-II code[36]. The group constants are produced with the seventy group structure of JFS-3[203], in which the energy range below 10 MeV is divided with an equal lethargy width 0.25.

2.2 Effective Multiplication Factors in Benchmark Calculations

The benchmark calculations for the 23 fast critical assemblies used in the benchmark tests of JFS-2[15] were performed with one-dimensional diffusion theory by using the group constants library generated from the JENDL-2 compilation. The calculated effective multiplication factors (k_{eff}) are shown in Table A.2.1. The k_{eff}-values are corrected by the necessary factors such as heterogeneity and transport effects taken from Ref.(17). Table A.2.1 shows also the structural material Doppler effect for the temperature rise from 0 to 300°K. The magnitude of the Doppler effects varies depending on the assemblies, i.e., the core size, compositions and neutron spectra. Especially, the effects become larger for the assemblies with large core volume such as MZB, ZPPR-2, ZPR-6-7 and ZPR-6-6A in which the concentration of the structural materials is comparatively high. The Doppler effects of k_{eff} are more than 0.2% for these assemblies, and the effects are comparable to the transport correction factors[17].

We also calculated the Doppler effect for the temperature change from 0 to 300°K of the structural materials on k_{eff} using the nuclear data of ENDF/B-IV. The Doppler effects calculated were very similar to the results for JENDL-2 described above. Hence, the results of the benchmark calculations performed by using the JFS-2 and JENDL-2B libraries must be corrected by considering the structural material Doppler effects shown in Table A.2.1.

2.3 Isothermal Doppler Coefficient in the SEFOR Assembly

The Doppler effect of cladding or structural material has been estimated to 15 - 20% of that of uranium metal, which may be of importance, at least in the isothermal case[204]. In the SEFOR experiments, the isothermal Doppler coefficient was measured by determining the reactivity change due to the power increase from zero to 20 MW, while holding the coolant temperature constant[100]. The calculation of Doppler effect was performed by using one-dimensional spherical model in the benchmark specification[100].

Figure A.2.1 shows the fuel and structural material Doppler effects. The structural material Doppler effect calculated from the nuclear data of JENDL-2 is about 8% of the fuel Doppler effect, but the results calculated with ENDF/B-IV data are smaller. However, the accuracy of the structural material Doppler effect can not be clearly estimated, because the temperature variation of cladding or structural materials with rise of the fuel temperature is unknown. For example, if the temperature of cladding and structural material changes from 300 to 500°K with increase of the fuel temperature of 677 to 1365°K, the structural material Doppler effect is about 6% of the fuel Doppler effect in the case of JENDL-2 as seen from Fig.A.2.1. The value of 6% is comparable to the goal accuracy[18] (±7%) required from the design study for a LMFBR target plant. On the other hand, the ratio of the calculated values (T = 677 → 1365°K) to the experiments of the isothermal Doppler coefficient is 1.08. Hence, the calculated value still more overestimates the experimental value when the structural material Doppler effect is accounted for.

Figure A.2.2 shows the groupwise contribution of the total and structural material Doppler reactivity worths calculated by the use of the JENDL-2 data. It is seen from this figure that the structural material Doppler

effect is mainly caused by the p-wave resonance of iron at 1.15 keV. Additionally, there are considerable discrepancies between the groupwise Doppler reactivities calculated with JENDL-2 and ENDF/B-IV.

2.4 Analysis of Sample Doppler Experiments in the FCA Assemblies

The Doppler experiments for natural iron and stainless steel (74% Fe, 18% Cr and 8% Ni) were performed in FCA-V and VI assemblies[204),(205)]. The Doppler reactivity change was measured at the core center by the small-sample oscillation, using the reactivity difference method. The Doppler samples are cylindrical, 25-mm in diameter and 156-mm in length, and contained in a stainless steel capsule of 0.5 mm in thickness. The analyses of these Doppler experiments were performed[(201),(202)] by a first-order perturbation theory using several nuclear data of ENDF/B-II, III and UK[(206)] for iron, chromium and nickel. The calculated results considerably underestimated the Doppler effect of the structural materials.

In order to test the temperature dependence of cross sections of Fe, Cr and Ni in JENDL-2 and ENDF/B-IV, we again performed the analyses of the sample Doppler experiments. The calculated results are shown in Figs.A.2.3∿8 including the experimental results. As seen from these figures, the results calculated with the nuclear data of JENDL-2 overestimate considerably the Doppler coefficients in FCA-V-1 and 2, while they give a good estimate for FCA-VI-1 and 2. On the other hand, the results of ENDF/B-IV are in good agreement with the experimental values in FCA-V-1 and 2, while they underestimate for FCA-VI-1 and 2. Very large discrepancies are seen between the results for JENDL-2 and ENDF/B-IV and especially for the Doppler coefficient of natural iron. The main cause for these discrepancies can be considered as follows: The neutron spectra in cores of small assemblies

FCA-V-1 and 2 are harder than those of FCA-VI-1 and 2. As seen from Fig.A.2.9 furthermore, the capture cross sections for iron of JENDL-2 are larger than those of ENDF/B-IV in the high energy range, and smaller in lower energy side, especially for resonance cross section at 1.15 keV.

2.5 Concluding Remarks

In the class of prototype fast reactors such as MZB, the Doppler effects of the structural materials for the temperature change from 0 to 300°K on the effective multiplication factors were about 0.2%. Furthermore, the structural material Doppler effect may contribute by about 8% to the isothermal Doppler coefficient in SEFOR, though an exact estimate is not possible due to the ambiguity in the temperature of cladding and structural materials. From these results, we can remark that the cross sections of the structural materials should be calculated by considering the Doppler effect, especially when we consider the goal accuracies ($\pm 0.3\%$[19] for k_{eff} and ± 7[18]$\sim 15\%$[19] for Doppler effect) required from LMFBR design study. Hence, the temperature dependent self-shielding factors for the structural materials were taken into account in the JFS-3 group constants library produced recently in JAERI.

From the analyses of the sample-Doppler experiments, in the other hand, it was shown that the effect of the uncertainty in the nuclear data of the structural materials on the Doppler coefficients was very large. This will demand an accurate evaluation of the nuclear data for the structural materials, particularly for resonances of iron in the energy range below 200 keV.

Table A.2.1 Doppler effect of structural materials on effective multiplication factor for temperature change from 0 to 300°K. The calculations were performed with one-dimensional diffusion theory using the group constant library generated from JENDL-2

Assembly	Ratio*	k_{eff}		Doppler effect (%-Δk/k)
		T = 0 °K	T = 300 °K	
VERA-11A	1.1	0.99452	0.99445	0.01
ZEBRA-3	0.2	0.99989	0.99988	0.0
SNEAK-7A	1.1	1.00688	1.00654	0.03
ZPR-3-54	2.3	0.95886	0.95742	0.15
ZPR-3-53	2.3	0.99651	0.99562	0.09
SNEAK-7B	0.8	1.00448	1.00410	0.04
ZPR-3-50	1.1	1.00342	1.00270	0.07
ZPR-3-48	1.5	1.00534	1.00449	0.08
ZPR-3-49	1.5	1.01011	1.00946	0.06
ZPR-3-56B	2.2	0.99174	0.98969	0.21
ZPR-6-7	2.5	0.99741	0.99506	0.24
ZPPR-2	2.5	1.00417	1.00213	0.20
SEFOR	2.3	1.00180	0.99971	0.21
MZA	2.5	0.99930	0.99774	0.16
MZB(1)	2.5	0.99630	0.99400	0.23
FCA-6-2	2.2	0.99872	0.99756	0.12
FCA-5-2	2.3	0.99178	0.99125	0.05
VERA-1B	1.1	1.00162	1.00151	0.01
ZPR-3-6F	0.7	1.01384	1.01379	0.0
ZPR-3-12	0.4	1.00767	1.00759	0.01
ZPR-3-11	0.2	1.00401	1.00402	0.0
ZEBRA-2	0.3	0.99567	0.99559	0.0
ZPR-6-6A	2.5	1.01120	1.00879	0.24

* Atomic number density ratio of structural (Fe + Cr + Ni) to fuel (U + Pu) materials in the core region

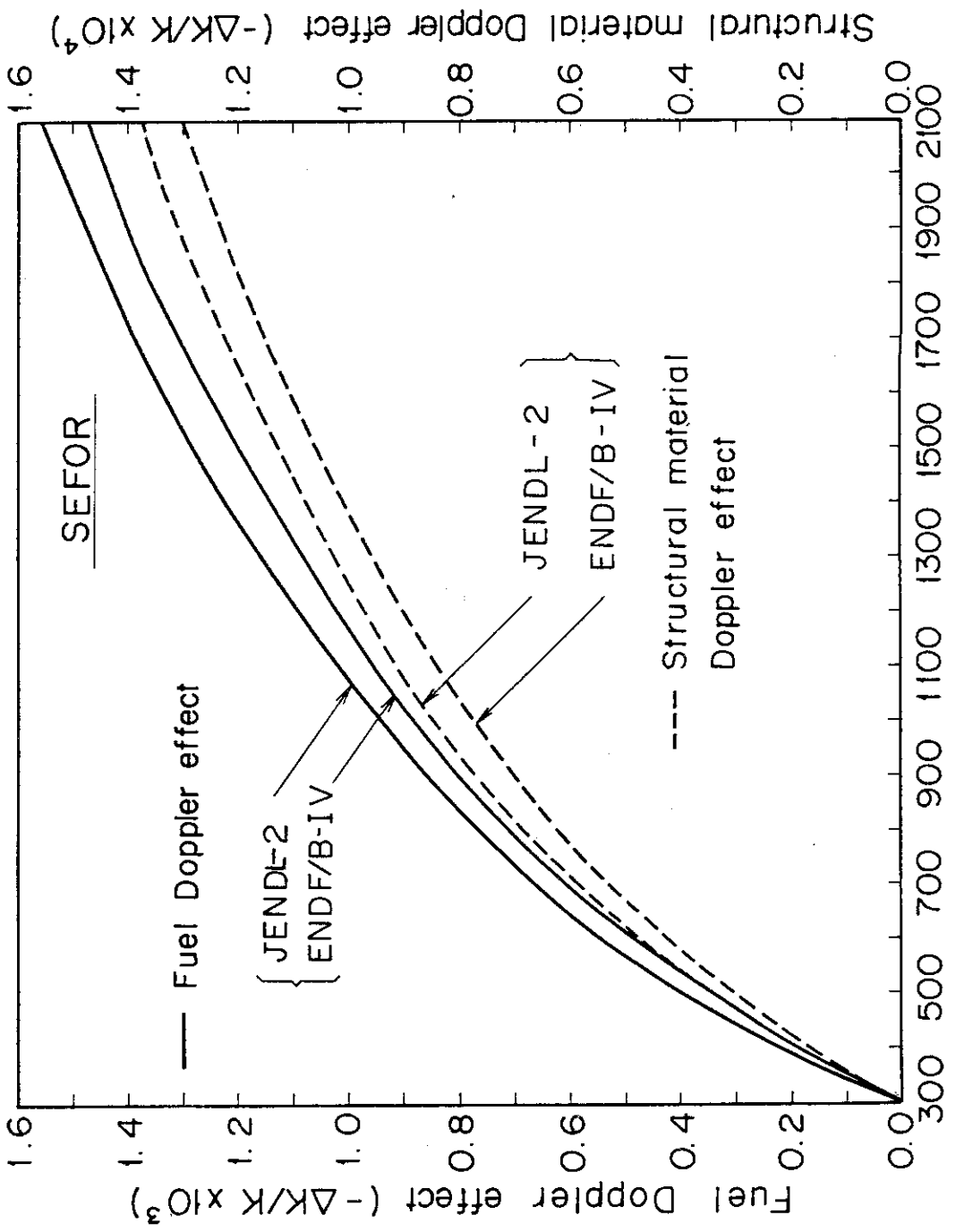

Fig.A.2.1 Comparison of the isothermal Doppler reactivities for fuel and structural materials included in the core region in SEFOR

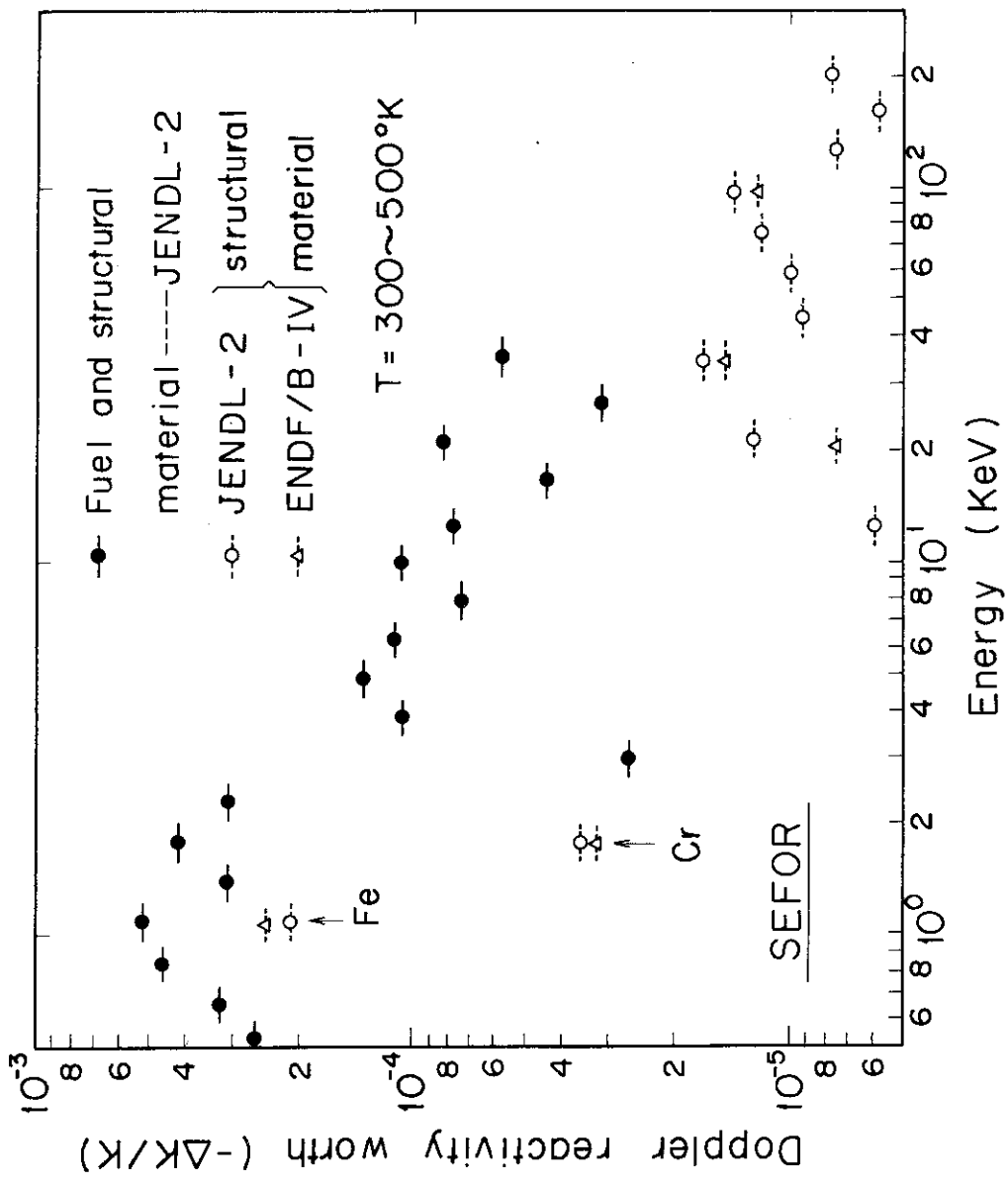

Fig.A.2.2 Groupwise contribution of the fuel and structural material Doppler reactivity works for the temperature change from 300 to 500 °K in SEFOR assembly.

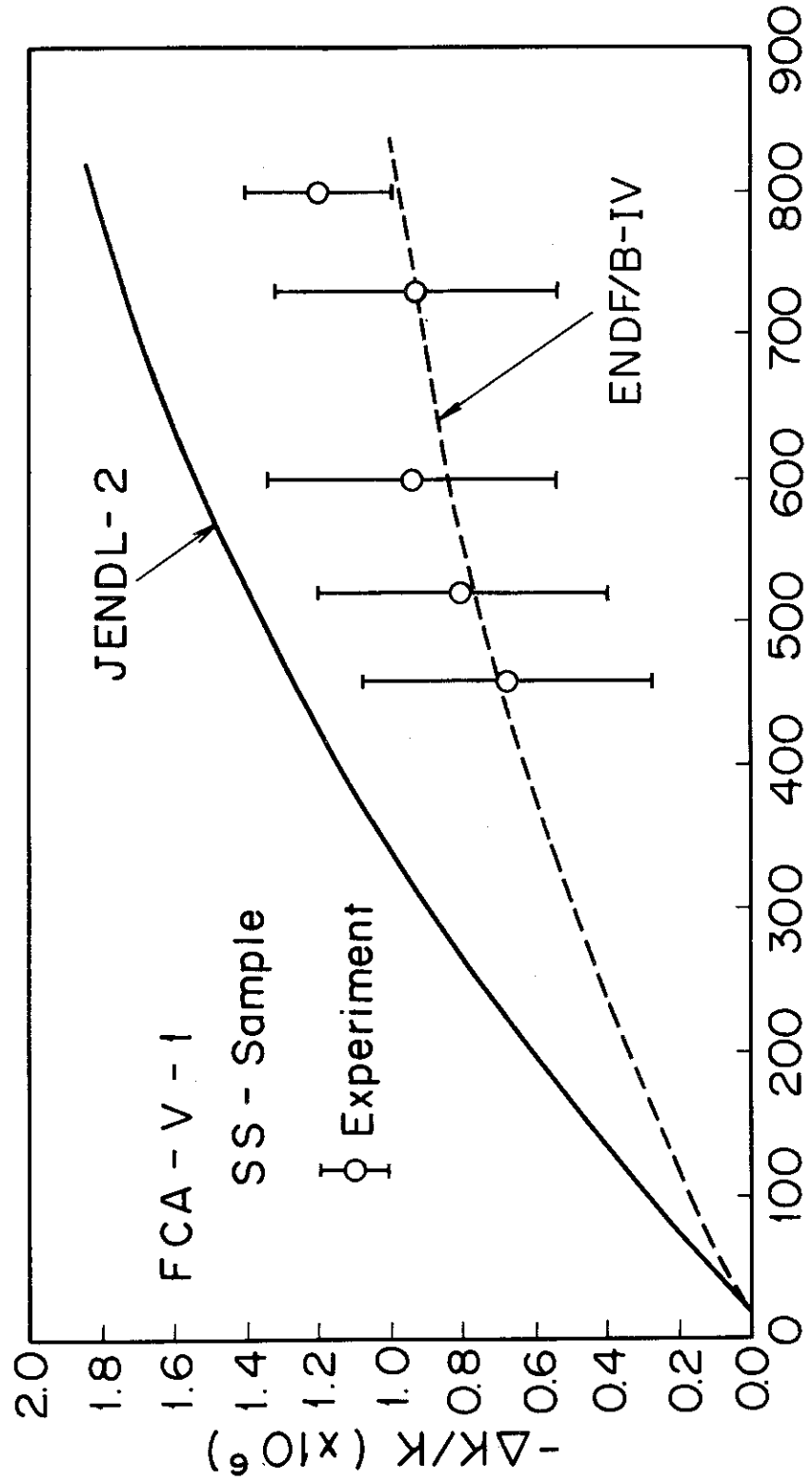

Fig.A.2.3 Comparison of the Doppler reactivity effects of stainless steel calculated and measured in FCA-V-1.

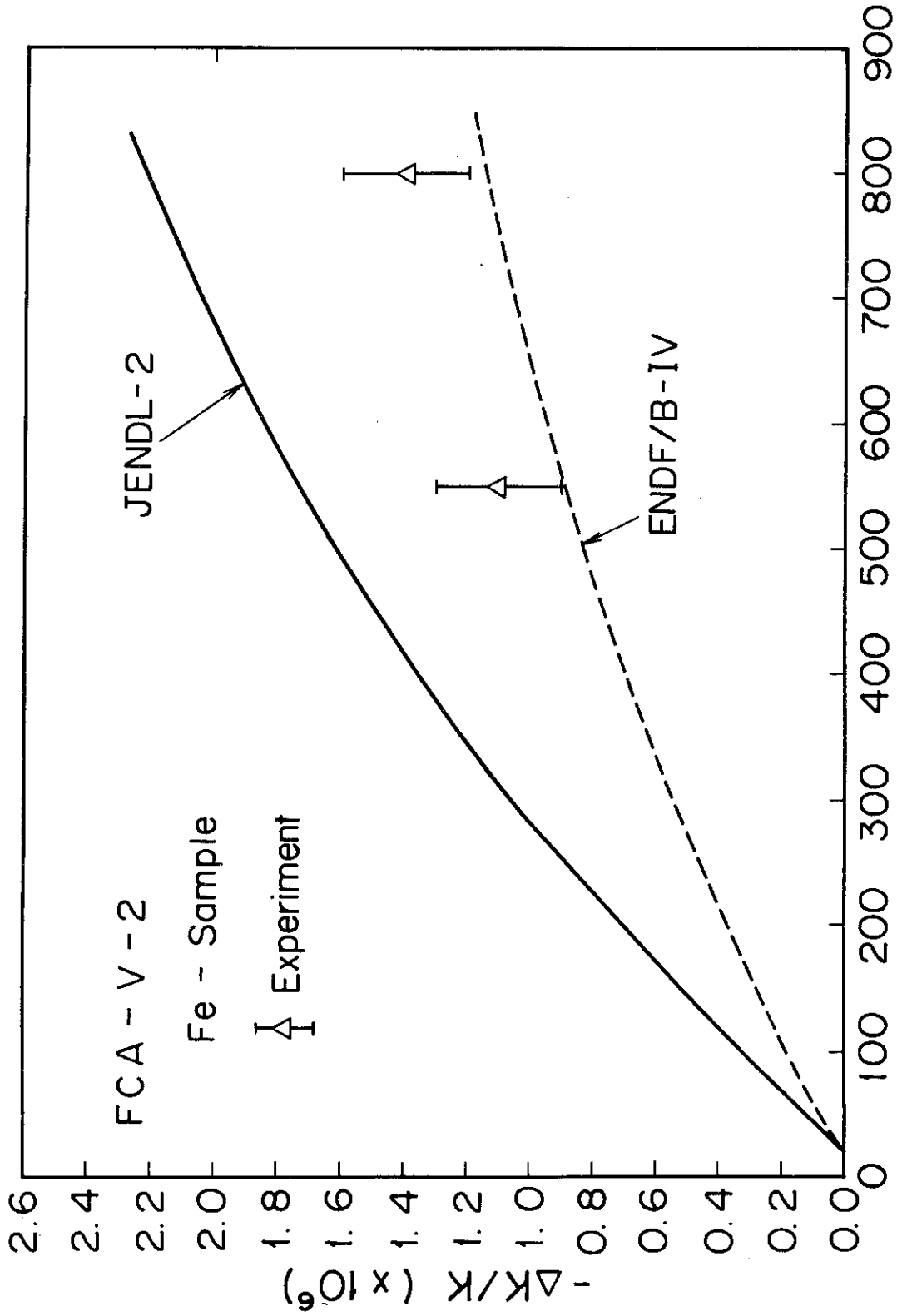

Fig.A.2.4 Comparison of the Doppler reactivity effects of natural iron calculated and measured in FCA-V-2.

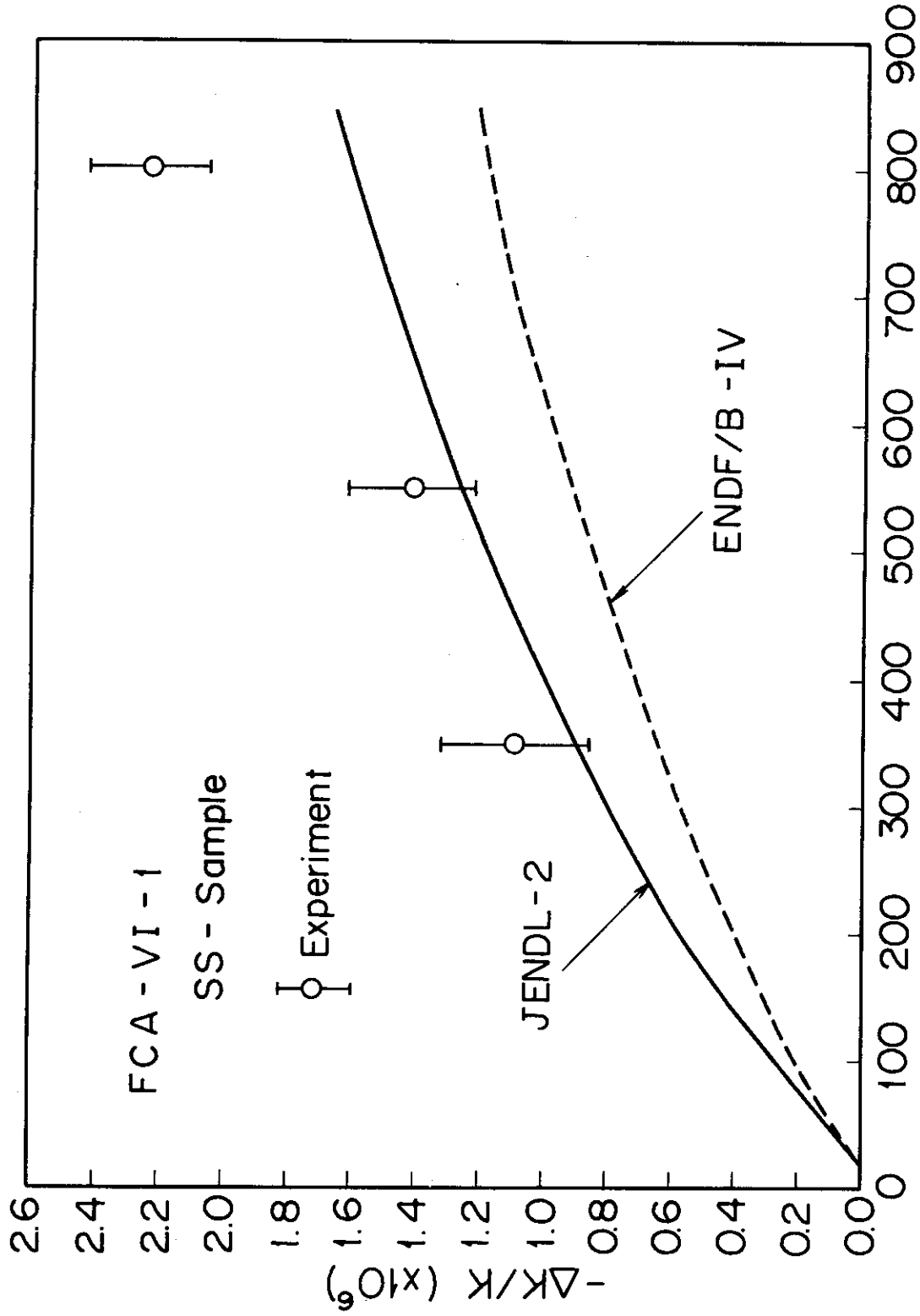

Fig.A.2.5 Comparison of the Doppler reactivity effects of stainless steel calculated and measured in FCA-VI-1.

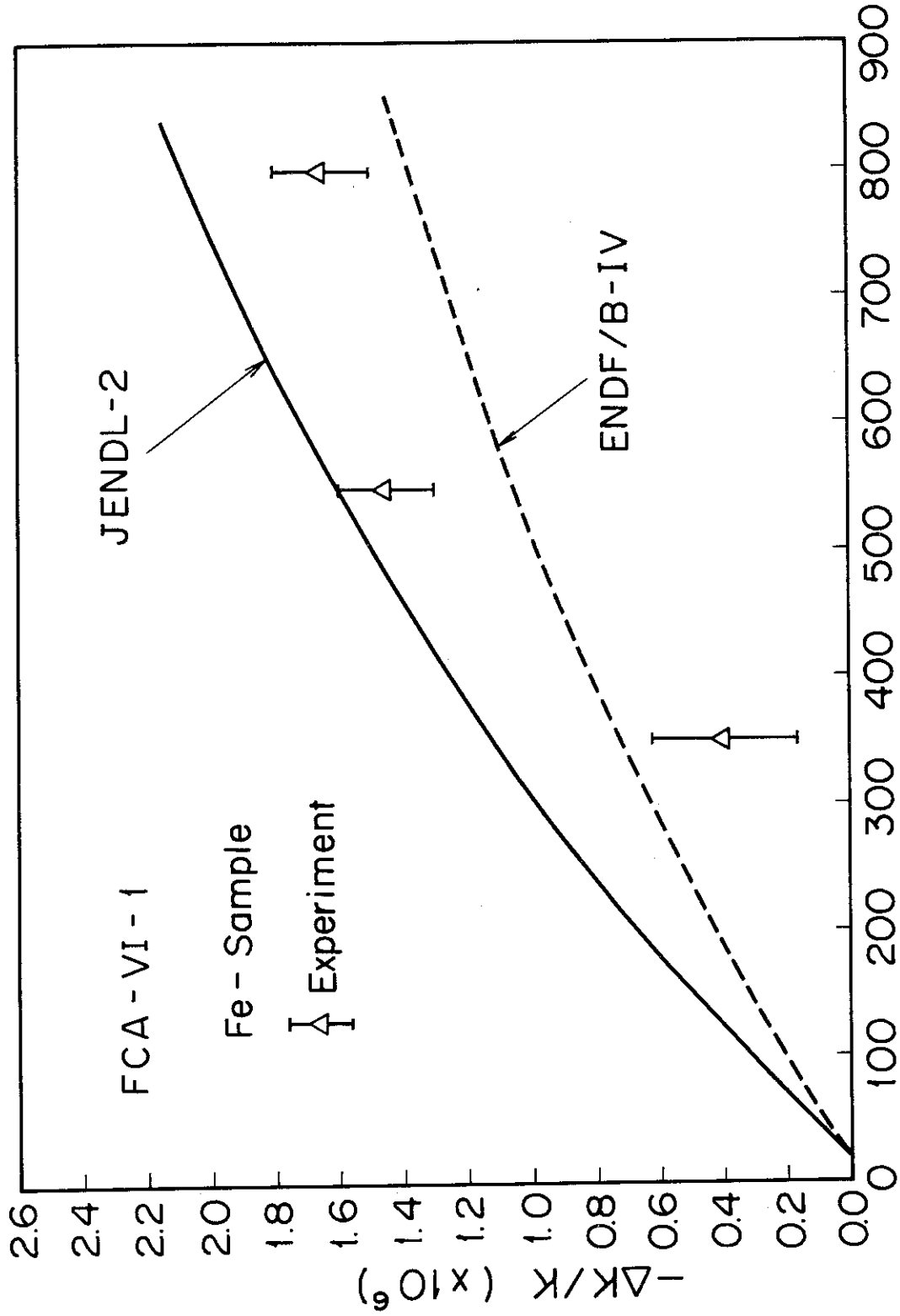

Fig.A.2.6 Comparison of the Doppler reactivity effects of natural iron calculated and measured in FCA-VI-1.

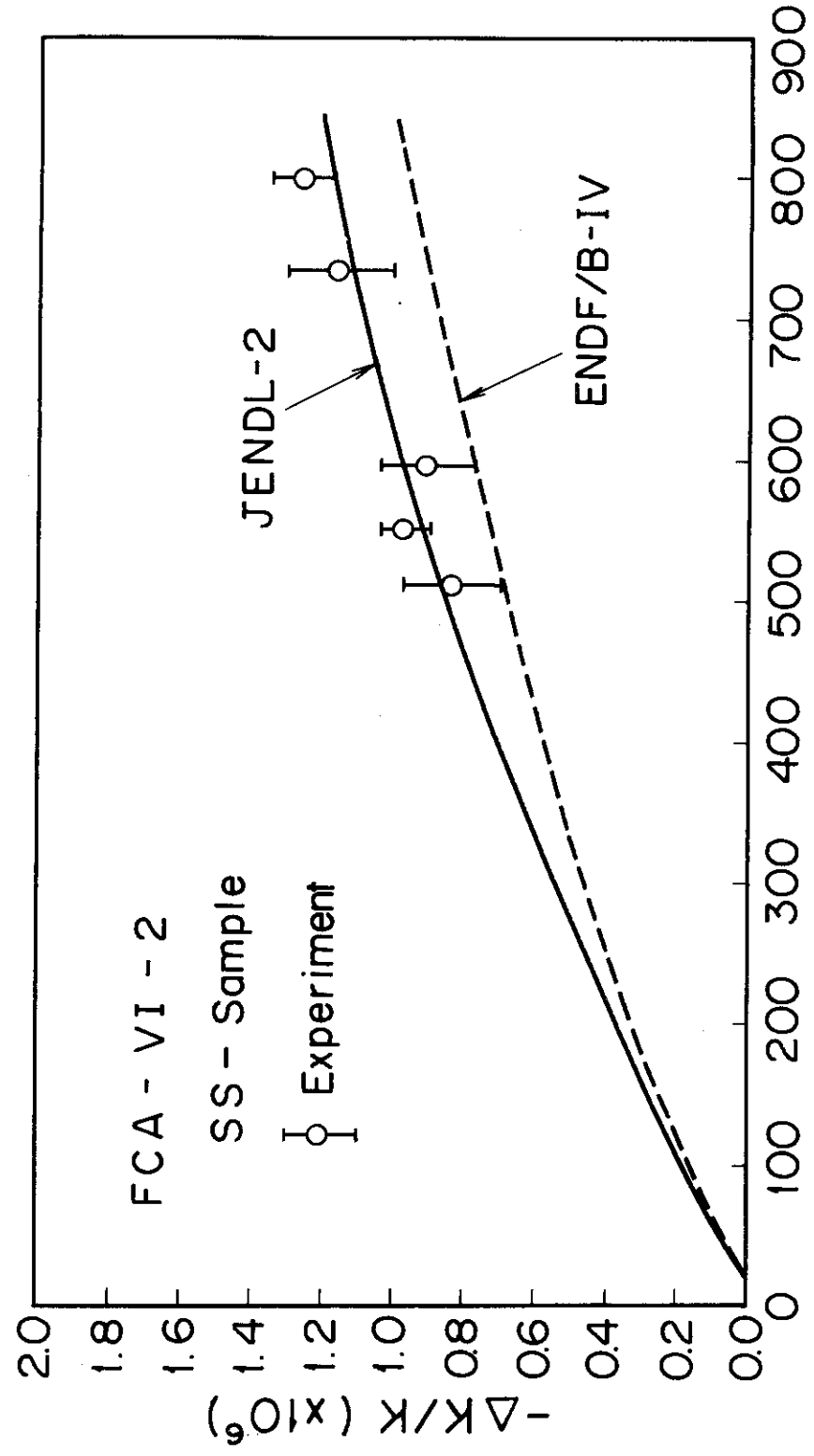

Fig.A.2.7 Comparison of the Doppler reactivity effects of stainless steel calculated and measured in FCA-V1-2.

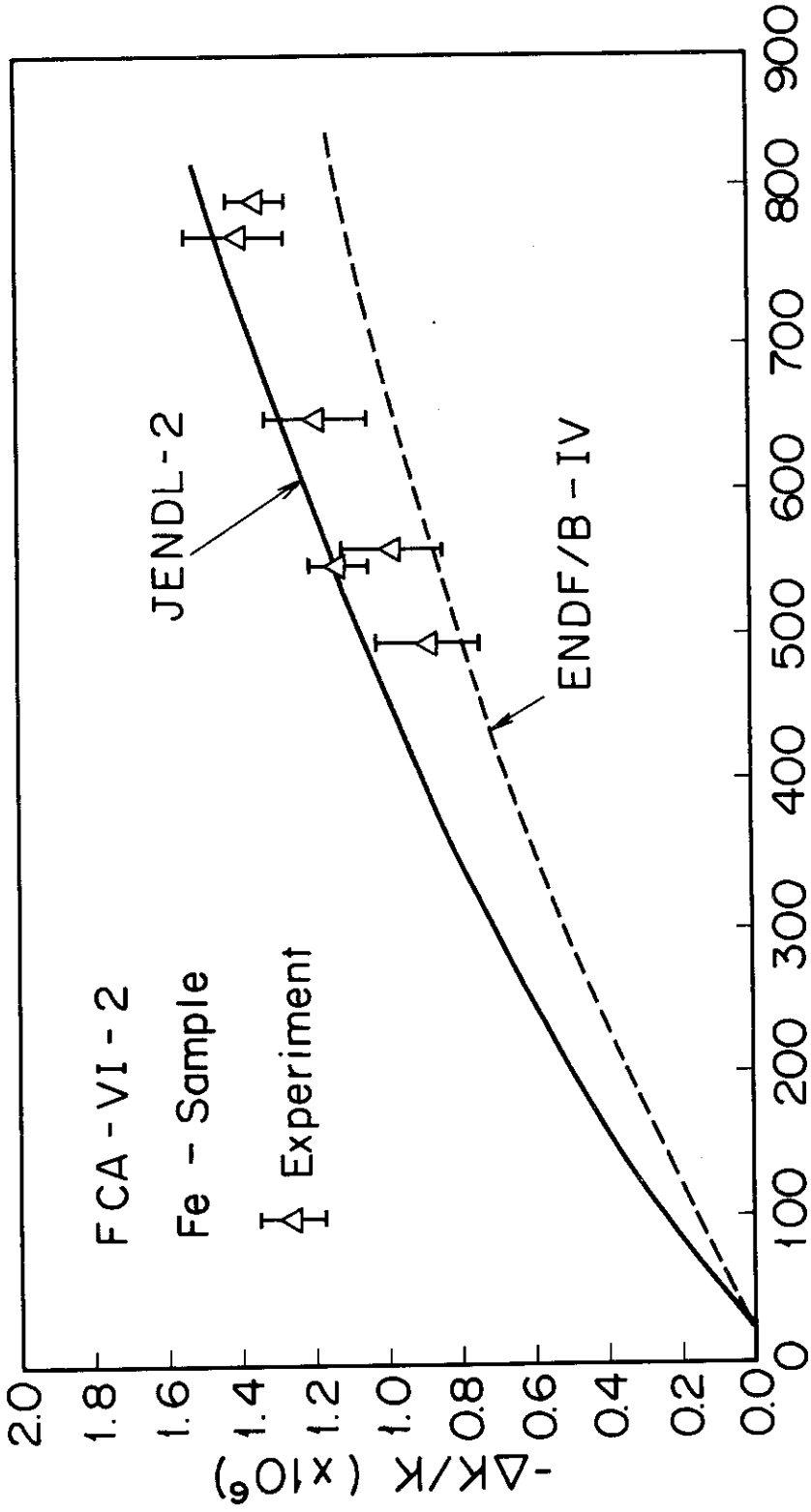

Fig.A.2.8 Comparison of the Doppler reactivity effects of natural iron calculated and measured in FCA-VI-2.

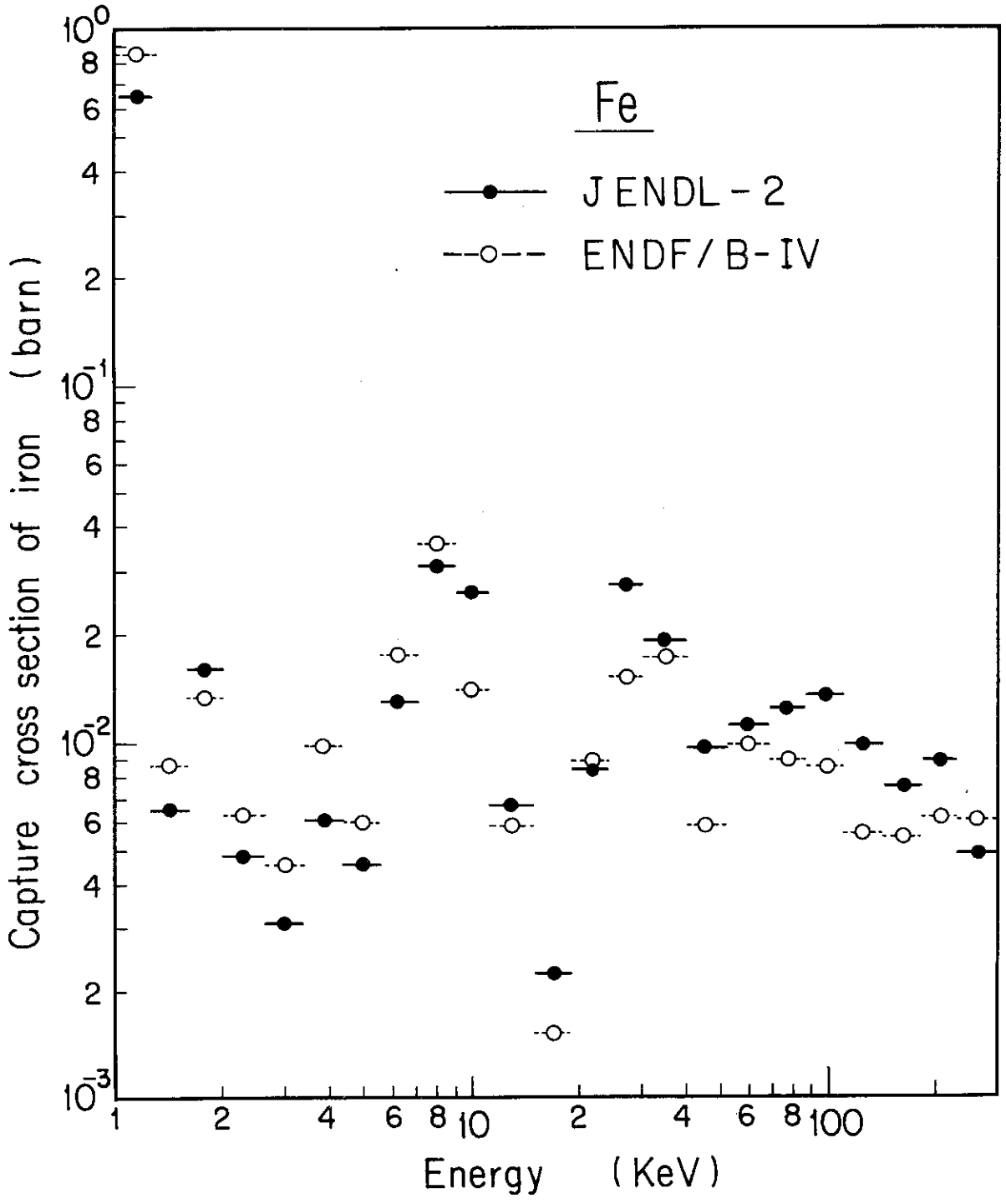

Fig.A.2.9 Comparison of the capture cross sections of iron of JENDL-2 and ENDF/B-IV.

3. The Effect of Self-Shielding of the Iron Inelastic Scattering Cross Section on Neutron Spectra

3.1 Introduction

In reactor calculations, the self-shielding effect on inelastic scattering cross sections was neglected by assuming small energy dependence of the cross sections. This assumption is generally valid. An exception is iron where the energy dependence of both inelastic-scattering and total cross section below ~2 MeV differ from other evaluations, for example, that of Garber and Kinsey[207].

In a fast reactor, the iron is a very important structural and/or reflector material. Further, the principal part of the neutron spectrum in a fast reactor lies below 2 MeV, where the iron inelastic scattering cross sections are strongly energy dependent. In this chapter, we present the inelastic-scattering self-shielding factors of iron and the effect of self-shielding on neutron spectra in fast critical assemblies.

3.2 Self-Shielding Factors

The inelastic-scattering and total cross sections of iron in the JENDL-2 and ENDF/B-IV[208] cross-section files are shown in Fig. A.3.1 and 2, respectively. From these figures, it is seen that the inelastic-scattering and total cross sections fluctuate considerably with energy below 2 MeV. This fact suggests that the inelastic-scattering cross sections may be self-shielded.

The infinitely dilute cross section, σ_{in}^{∞}, and the self-shielding factor, f_{in}, are defined by

$$\sigma_{in}^{\infty} = \int_{\Delta E} \sigma_{in}(E)\phi_0(E)dE \Big/ \int_{\Delta E} \phi_0(E)dE \quad , \tag{A.3-1}$$

$$\tilde{\sigma}_{in} = \int_{\Delta E} \frac{\sigma_{in}(E)\phi_0(E)}{\sigma_t(E)+\sigma_0} dE \Big/ \int_{\Delta E} \frac{\phi_0(E)}{\sigma_t(E)+\sigma_0} dE \quad , \tag{A.3-2}$$

$$f_{in} = \tilde{\sigma}_{in} / \sigma_{in}^{\infty} \tag{A.3-3}$$

with

$$\phi_0 = \begin{cases} \dfrac{1}{E} & (< 1 \text{ MeV}) \quad (A.3\text{-}4) \\ \chi(E) & (\geq 1 \text{ MeV}) \quad , \quad (A.3\text{-}5) \end{cases}$$

where σ_t is the total cross section, σ_0 the effective background total cross section and $\chi(E)$ the fission spectrum. The self-shielding factors were calculated by using the modified version of the PROF-GROUCH·G·II code.

The self-shielding factors calculated by using the nuclear data of the JENDL-2 or ENDF/B-IV compilations are shown as a function of σ_0 in Tables A.3.1 and 2, respectively. When σ_0 is zero, the self-shielding factors differ considerably from unity in several energy groups, while they are nearly equal to unity for $\sigma_0 \geq 10^2$. Hence, the self-shielding of the inelastic-scattering cross section is expected to affect the energy distribution of neutron flux in the fast reactors of high iron content and/or with steel reflectors.

3.3 Effective Multiplication Factor

The multigroup cross-section library was produced with the PROF. GROUCH·G·II and TIMS-1 codes using the JENDL-1[31] and 2 nuclear data files. The energy range below 10 MeV was divided into sections each 0.25 lethargy units wide. This library contains the group constants of twenty-seven nuclides that are necessary for usual reactor calculations. This library is called JFS-3[203].

The effect of the inelastic-scattering self-shielding on central nuclear characteristics (the effective multiplication factor, the central reaction rate ratio, and the central sample worth) was studied by performing benchmark tests[15),(17] for twenty-one fast reactor assemblies using the JFS-3 library. The calculations are based on one-dimensional diffusion theory. The results of benchmark tests are as follows. The effective multiplication factors of the MZB assembly increased by 0.07 %; that of ZPR-6-7, ZPPR-2 and MZA increased ~0.04 % when the inelastic-scattering self-shielding effect was considered. The neutron spectra hardened due to a decrease in slowing down power, but this hardening increases the reactivity of 21 assemblies by only 0.02 % on the average. On the other hand, the effect of self-shielding on the central reaction rate ratios and sample worths is negligibly small.

3.4 Neutron Spectrum and Reaction Rate Distribution

The influence of the inelastic-scattering self-shielding on neutron spectra was studied for assemblies ZPR-3-54 and MZB with steel reflector.

ZPR-3-54: This assembly is composed of a plutonium-fueled core and a steel reflector. The neutron spectra were calculated by using one-dimensional diffusion theory with a spherical model. Figures A.3.3 and 4 show

a comparison of the neutron spectra at the boundary between the core and reflector and at the edge of the reflector, respectively. The effect of the inelastic-scattering self-shielding on the neutron spectrum at the core centre was too small to be observed. In Fig.A.3.3, the self-shielding effect is seen to slightly harden the neutron spectrum. As seen from Fig.A.3.4, however, the neutron spectrum varies considerably in the steel reflector, that is, the spectrum becomes harder because of a decrease of the slowing down power.

The distribution of the radial reaction rate were calculated and the effect of the self-shielding on it was studied. The reaction rates were normalized to the value at the core centre. Figure A.3.5 shows the ratios of the reaction rates calculated with and without considering the self-shielding effect. As seen from this figure, the reaction rate distribution of ^{239}Pu fission becomes smaller by ~1 % in the vicinity of the boundary between the core and reflector and 8 % at the edge of the reflector. On the other hand, the reaction rate of ^{238}U fission becomes large by ~5 % in the reflector as a result of the hardened spectrum.

MZB: The MZB is the fast critical assembly for the Japanese prototype fast reactor "MONJU" mock-up in the MOZART programme. A one-dimensional diffusion calculation was performed with cylindrical geometry composed of the inner core, the outer core, the blanket and the reflector. The neutron spectrum at the edge of the reflector is compared in Fig.A.3.6, with and without considering self-shielding. The spectrum in MZB is softer than that in ZPR-3-54. The inelastic-scattering self-shielding effect produces a hardened spectrum, similar to that of ZPR-3-54. Figure A.3.7 shows the ratios of the fission reaction rates calculated with and without the self-shielding effect. The reaction rate of ^{235}U becomes smaller by ~3 % in the reflector. The same tendency was also seen for the reaction rate distributions of the

fission of ^{239}Pu and the neutron capture by ^{235}U and ^{238}U. The fission reaction rate distribution for ^{238}U became larger due to the spectrum hardening.

3.5 Concluding Remarks

The self-shielding factors of inelastic scattering cross sections of iron were calculated from the evaluated nuclear data files ENDF/B-IV and JENDL-2. The effect of self-shielding by inelastic scattering on the neutron spectra was studied for the fast reactor assemblies ZPR-3-54 and MZB, the fast critical assembly of the Japanese fast reactor program.

The inelastic-scattering self-shielding effect of iron produced a harder neutron spectrum in fast critical assemblies because of a decrease in the neutron slowing down power. Especially the effect on the neutron spectrum was considerably evident in the steel reflector. Hence, the inelastic-scattering self-shielding of iron should be considered in reactor-shield calculations and/or analyses of neutron spectrum experiments in critical assemblies containing iron.

Table A.3.1 Self-Shielding Factors of Inelastic-Scattering Cross Section of Iron Calculated from JENDL-2

Upper Energy	σ_{in}^{∞}(b)	Self-Shielding Factor				
		σ_0=0 (b)	σ_0=1 (b)	σ_0=10 (b)	σ_0=10^2(b)	σ_0=10^3(b)
10.0 (MeV)	1.306	0.9993	0.9995	0.9998	1.0000	1.0000
7.788 (MeV)	1.405	0.9997	0.9998	1.0000	1.0000	1.0000
6.065 (MeV)	1.377	1.0000	1.0000	1.0000	1.0000	1.0000
4.724 (MeV)	1.304	0.9997	0.9998	1.0000	0.9996	1.0000
3.679 (MeV)	1.110	0.9996	0.9997	0.9999	1.0000	1.0001
2.865 (MeV)	0.8902	0.9977	0.9983	0.9996	0.9999	1.0000
2.231 (MeV)	0.7942	0.9753	0.9812	0.9942	0.9994	0.9998
1.738 (MeV)	0.7304	0.9786	0.9840	0.9953	0.9993	0.9999
1.353 (MeV)	0.4965	0.9557	0.9700	0.9913	0.9989	0.9998
1.054 (MeV)	0.2599	0.9162	0.9422	0.9846	0.9981	0.9998
0.8209(MeV)	0.0226	0.9904	0.9939	0.9986	0.9999	1.0000
0.6393(MeV)	0.0208	1.0058	1.0039	1.0009	1.0001	1.0000
0.4979(MeV)	0.0191	1.0067	1.0052	1.0018	1.0003	1.0000
0.3877(MeV)	0.0162	0.9961	0.9971	0.9991	0.9999	1.0000
0.3020(MeV)	0.0162	0.9988	0.9993	0.9999	1.0000	1.0000
0.2352(MeV)	0.0118	1.0610	1.0638	1.0425	1.0077	1.0012
0.1832(MeV)	0.0167	1.3292	1.1602	1.0071	0.9979	0.9998
0.1426(MeV)	0.0505	1.0229	1.0278	1.0191	1.0039	1.0005
0.1111(MeV)	0.0208	1.1015	1.0847	1.0330	1.0050	1.0006
86.52 (KeV)	0.0262	0.7813	0.8790	1.0028	1.0066	1.0007
67.38 (KeV)	0.0197	1.0107	1.0120	1.0076	1.0009	1.0001
52.48 (KeV)	0.0706	0.9275	0.9394	0.9779	0.9976	0.9995
40.87 (KeV)	0.0771	1.0564	1.0488	1.0206	1.0027	1.0003
31.83 (KeV)	0.1723	0.5723	0.6277	0.7923	0.9475	0.9933
24.79 (KeV)	0.0397	1.1359	1.0742	1.0143	1.0015	1.0002
19.31 (KeV)	0.0128	1.0608	1.0471	1.0147	1.0018	1.0002
15.03 (KeV)	0.0001	1.1379	1.1130	1.0402	1.0054	1.0006

Table A.3.2 Self-Shielding Factors of Inelastic Scattering Cross Sections of Iron Calculated from ENDF/B-IV

Upper Energy	σ_{in}^{∞}(b)	Self-Shielding Factor				
		σ_0=0 (b)	σ_0=1 (b)	σ_0=10 (b)	$\sigma_0=10^2$(b)	$\sigma_0=10^3$(b)
10.0 (MeV)	1.418	0.9995	0.9996	0.9998	1.0000	1.0000
7.788 (MeV)	1.485	0.9998	0.9999	1.0003	0.9999	0.9999
6.065 (MeV)	1.549	0.9999	1.0000	1.0001	1.0002	1.0000
4.724 (MeV)	1.446	0.9998	0.9999	1.0000	1.0000	1.0000
3.679 (MeV)	1.175	0.9996	0.9997	0.9999	1.0000	1.0000
2.865 (MeV)	0.9071	0.9979	0.9984	0.9994	0.9999	1.0001
2.231 (MeV)	0.8315	0.9655	0.9744	0.9925	0.9990	0.9998
1.738 (MeV)	0.6957	0.9620	0.9718	0.9917	0.9989	0.9998
1.353 (MeV)	0.4494	0.9326	0.9531	0.9868	0.9983	0.9998
1.054 (MeV)	0.2185	0.8643	0.9034	0.9728	0.9966	0.9996

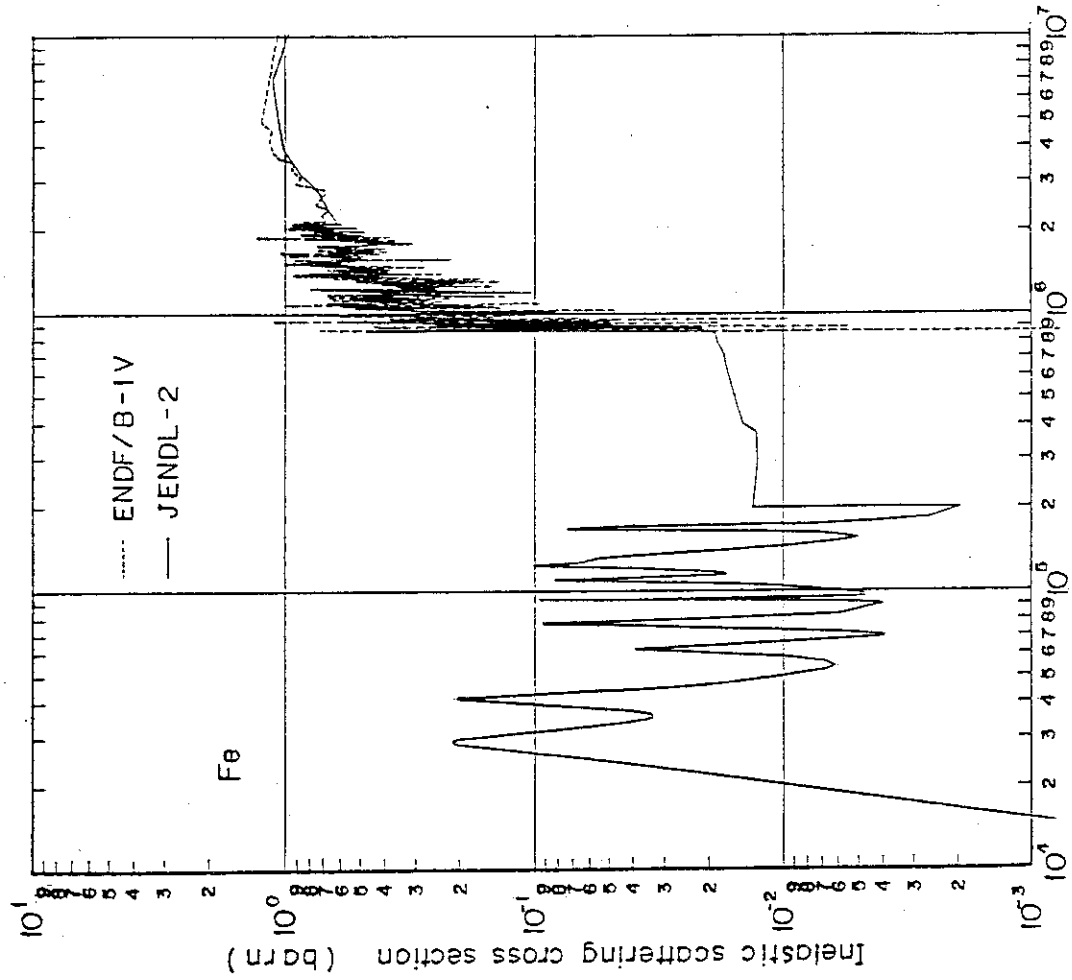

Fig.A.3.1 Energy variation of iron inelastic-scattering cross sections in JENDL-2 and ENDF/B-IV compilations.

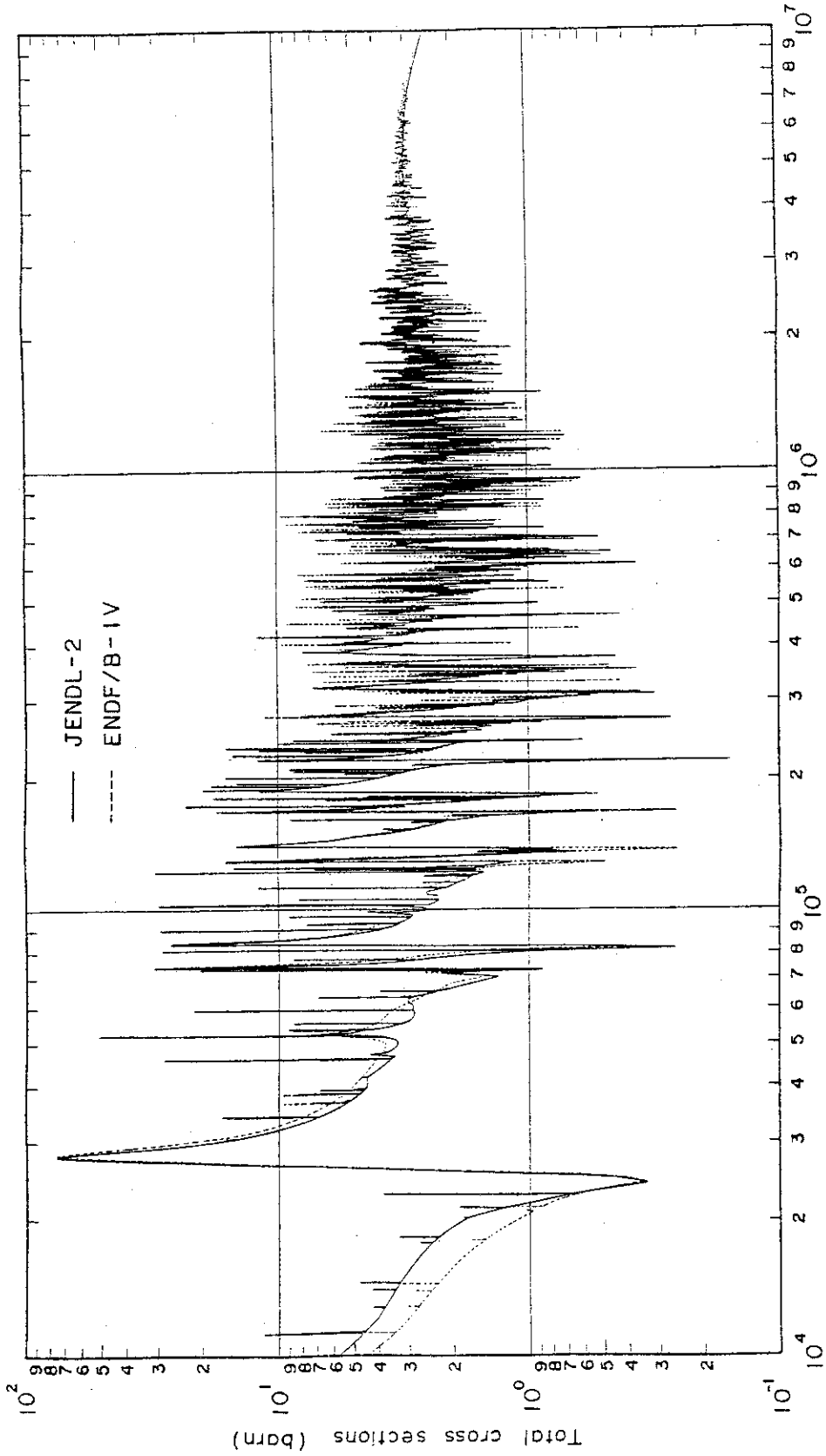

Fig.A.3.2 Energy variation of iron total cross sections in JENDL-2 and ENDF/B-IV compilations.

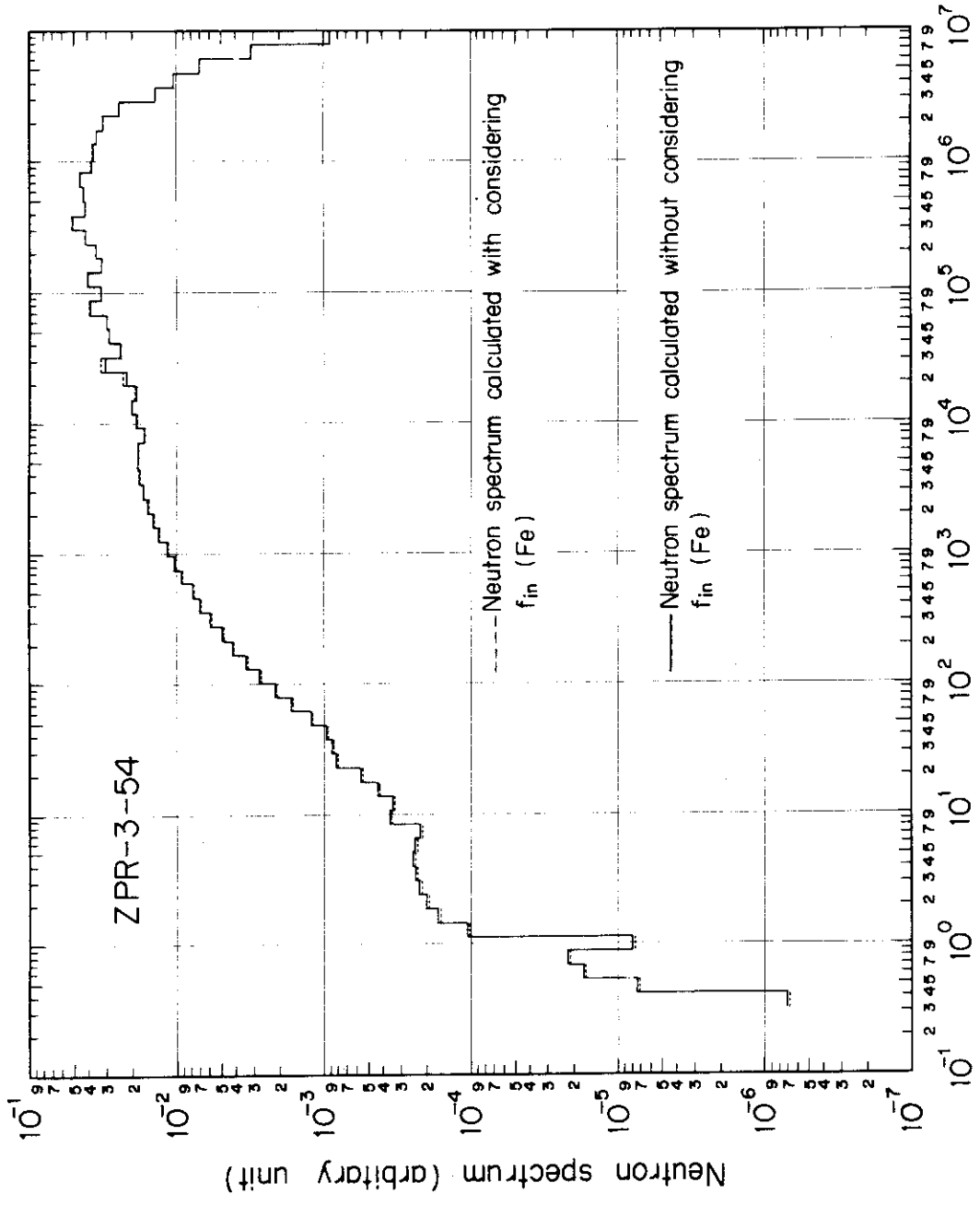

Fig.A.3.3 Effect of inelastic-scattering self-shielding on neutron spectra at the boundary between the core and steel reflector in ZPR-3-54.

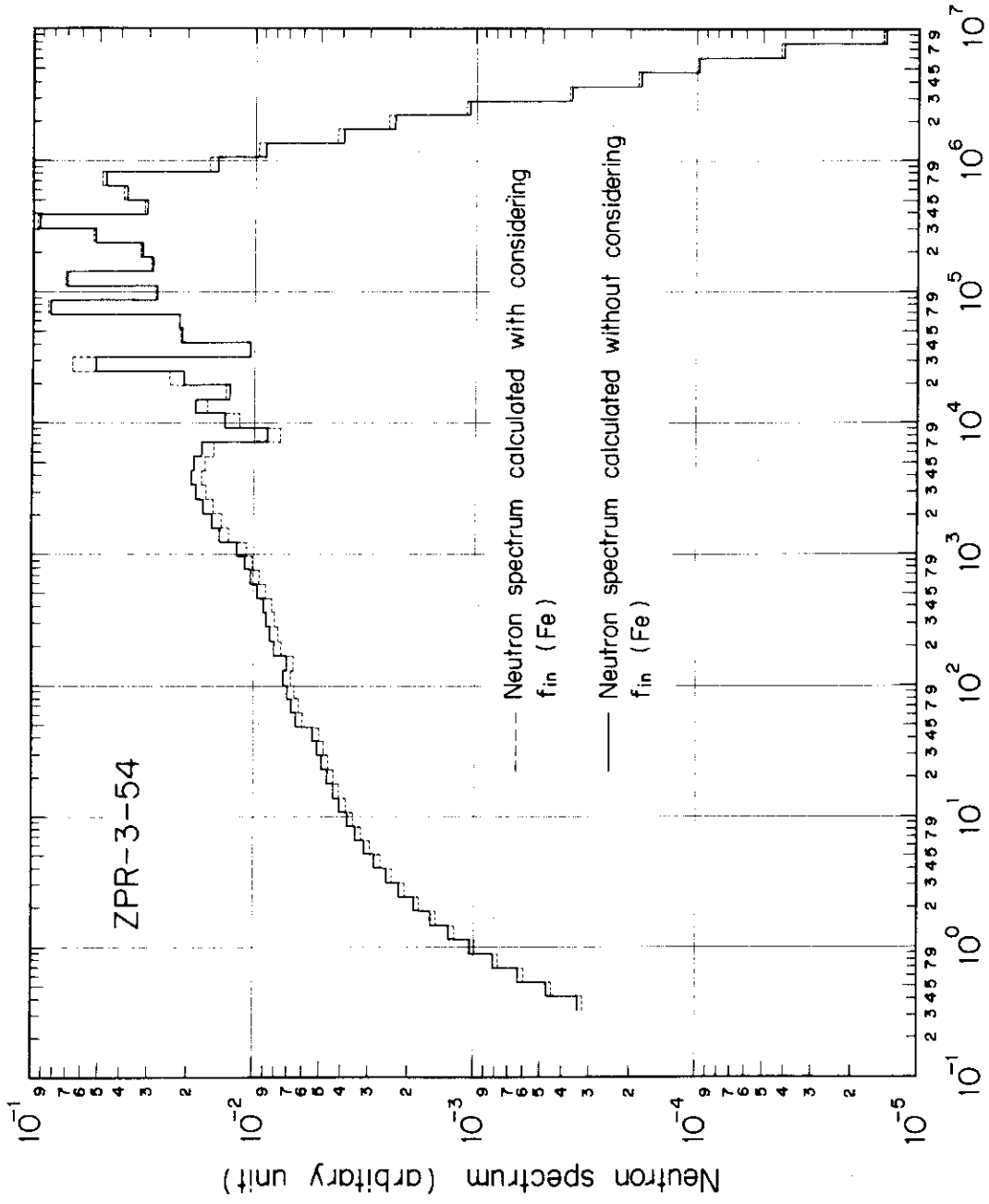

Fig.A.3.4 Effect of inelastic-scattering self-shielding on neutron spectra at the outer edge of the reflector in ZPR-3-54.

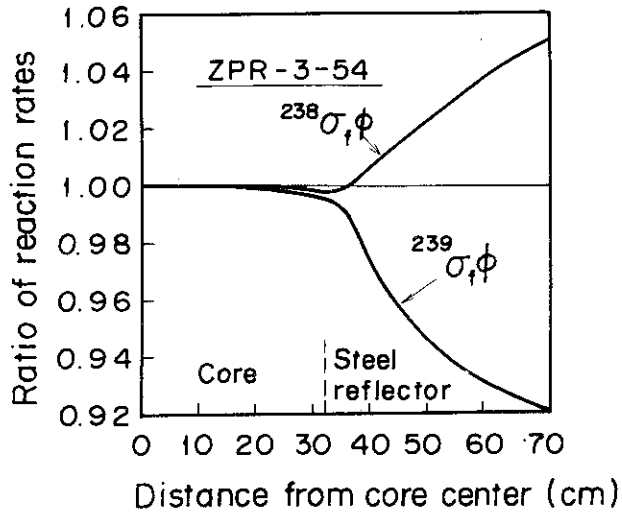

Fig.A.3.5

Ratio of fission reaction rates for ^{239}Pu and ^{238}U calculated with and without considering the self-shielding effect in ZPR-3-54.

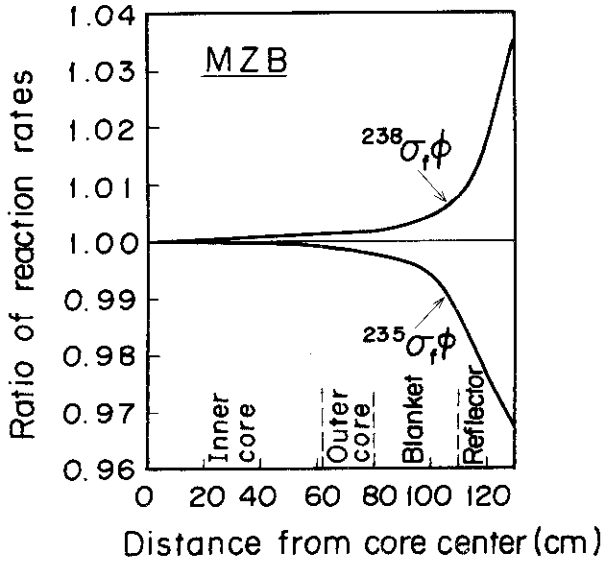

Fig.A.3.7

Ratio of fission reaction rates for ^{235}U and ^{238}U calculated with and without considering the self-shielding effect in the MZB critical assembly.

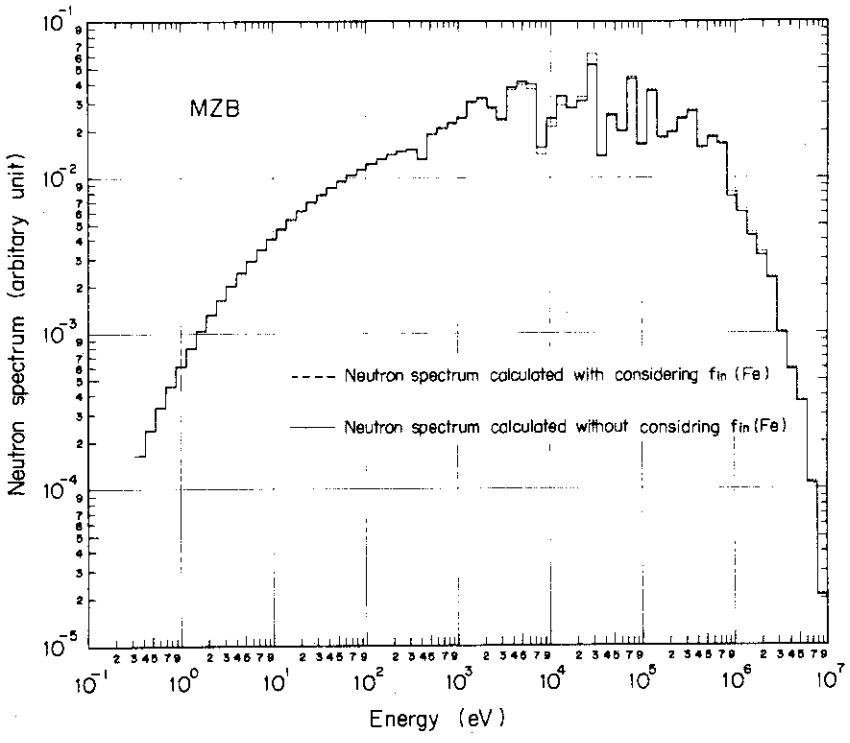

Fig.A.3.6 Effect of inelastic-scattering self-shielding on neutron spectra at the outer edge of the reflector in the MZB critical assembly.

4. Effective Multiplication Factors and Reaction Rates Calculated by Using Fission Spectra of ^{235}U, ^{238}U and ^{239}Pu

4.1 Introduction

In diffusion and/or transport codes for fast reactor calculations, only one fission spectrum is assumed for both fuel core and blanket regions. Generally, the concentration of ^{238}U is higher than that of ^{235}U or ^{239}Pu in core, and especially so in blanket region. Therefore, if the fission energy spectra of $^{235}U(^{235}\chi)$, $^{239}Pu(^{239}\chi)$ and $^{238}U(^{238}\chi)$ differ considerably each other, the effects of the differences among $^{235}\chi$, $^{239}\chi$ and $^{238}\chi$ on the nuclear characteristics in fast reactors should be studied.

Figure A.4.1 shows the comparison of the fission energy spectra of ^{238}U and ^{239}Pu calculated by using the ENDF/B-IV nuclear data. The $^{239}\chi$-spectrum is shifted to higher energy region. These spectra were calculated for the nuclear temperatures at the incident neutron energy 200 KeV for ^{239}Pu and 2 MeV for ^{238}U, respectively. The fission spectrum of ^{235}U at the incident neutron energy 200 KeV was very similar to $^{238}\chi$, though $^{235}\chi$ was not shown in Fig.A.4.1. The incident energy E_i = 200 KeV for ^{235}U and ^{239}Pu was selected so that the fractions of fission events are about the same[15]. i.e.,

$$\frac{\int_{E_i}^{10\ \mathrm{MeV}} \sigma_f(E)\phi(E)dE}{\int_{0}^{E_i} \sigma_f(E)\phi(E)dE} = 1 \qquad \text{(A.4-1)}$$

where $\phi(E)$ is the neutron spectrum in a typical LMFBR core and $\sigma_f(E)$ the fission cross sections.

In this section, the effects of the difference between $^{239}\chi$ and $^{238}\chi$ on effective multiplication factor and radial reaction rate are calculated by using a one-dimensional diffusion code with the group constants library

JFS-3-B4 which was generated by the processing codes PROF·GROUCH·G-II and TIMS-1 from ENDF/B-IV nuclear data. In the calculations, an average fission spectrum for an energy group (g) in the fuel region is defined by

$$\tilde{\chi}_g = \frac{\sum_{i=1}^{3} W_i \chi_{i,g}}{\sum_{i=1}^{3} W_i} \quad , \tag{A.4-2}$$

$$W_i = \sum_g N_i \sigma_{f,i,g} \phi_g \quad , \tag{A.4-3}$$

$$\sum_g \tilde{\chi} = 1 \quad , \tag{A.4-4}$$

where ϕ_g is the neutron spectrum at core center in the prototype fast reactor mockup assembly MZB, the subscript i means the nuclide of ^{235}U, ^{238}U and ^{239}Pu, and N_i the atomic number density in the core region. In the blanket region, only $^{238}\chi$ is used as it is.

4.2 Effective Multiplication Factors

The effective multiplication factors were calculated for the fifteen benchmark critical assemblies with the Pu-fueled cores[15),(17)]. The results calculated are shown in Table A.4.1. The effective multiplication factors calculated with $^{235}\chi$ become smaller by 1.09 % for ZEBRA-3 with the high concentration of ^{238}U and about 0.6 % for MZB, ZPR-3-48 and ZPR-6-7 assemblies, that is the use of $^{235}\chi$ for the Pu-fueled cores produces considerably less reactivities as compared with the results calculated with $^{239}\chi$. In the other hand, the use of only one fission spectrum of $^{239}\chi$ produces larger effective multiplication factors than those calculated with

the average fission spectrum of Eq.(A.4-2).

The difference between the results calculated with the spectra $^{235}\chi$ and $^{239}\chi$ is about 0.5 % in FCA-5-2 which contains both the fuels of ^{239}Pu and ^{235}U. Using the neutron spectrum at the core center in FCA-5-2, the average fission spectrum of Eq.(A.4-2) was calculated. A middle value between the results calculated with $^{235}\chi$ and $^{239}\chi$ is obtained by using the average fission spectrum.

In FCA-6-2 assembly, the inner core is Pu-fueled zone and the outer core is the driver zone with U-fuel. Hence, the average fission spectrum method results in the use of the region dependent spectra, i.e., $^{239}\chi$ for the inner core, $^{235}\chi$ for the outer core and $^{238}\chi$ for the blanket region. The use of this region dependent fission spectra affects the effective multiplication factors by about 0.4 %.

4.3 Radial Reaction Rate

The radial reaction rates were calculated for the MZB assembly. The deviations of the fission reaction rates for ^{238}U calculated with $\tilde{\chi}$ from those calculated with $^{239}\chi$ are shown in Fig.A.4.2. The reaction rate calculated with $\tilde{\chi}$ become smaller by about 3 % in the blanket region, because of a softer neutron spectrum produced with $^{238}\chi$ as seen from Fig.A.4.3. As for the fission reaction rates such as ^{235}U or ^{239}Pu, the differences between the reaction rates calculated with $^{239}\chi$ and $\tilde{\chi}$ were negligibly small, as guessed from Fig.A.4.3.

Figure A.4.4 shows the deviations of the reaction rates calculated with $^{235}\chi$ and $^{239}\chi$ from those calculated with $\tilde{\chi}$ in the FCA-5-2 assembly. In the blanket region, the fission reaction rates calculated with $^{239}\chi$ are larger by about 4 % for ^{238}U and about 2 % for ^{235}U than those calculated with $\tilde{\chi}$,

while the differences between the results calculated with $^{235}\chi$ and $\tilde{\chi}$ are very small.

Figure A.4.5 shows the deviations of the reaction rates calculated with $^{239}\chi$ from those calculated with the region dependent fission spectra in FCA-6-2 assembly. The radial fission reaction rates of ^{238}U calculated with $^{239}\chi$ are overestimated by about 8 % in the blanket region.

4.4 Concluding Remarks

For the cores with the high concentration of ^{238}U such as ZEBRA-3, with the mixed fuels of U and Pu such as FCA-5-2 and with the driver zone such as FCA-6-2, the use of one fission spectrum, for example, only $^{239}\chi$, provides non-negligible errors for the effective multiplication factors and radial fission reaction rates of ^{238}U. In a class of prototype fast reactor, however, the calculations taking account for the average fission spectrum produce only a small correction of about 0.1 percent on the effective multiplication factor and on the reaction rates of $^{238}\sigma_f$ in the blanket by about 3 percent.

Table A.4.1 Effect of different fission spectra on effective multiplication factor (K_{eff}), $\Delta K = \frac{K_{eff} - K_{eff}(^{239}\chi)}{K_{eff}(^{239}\chi)} \times 100$

Assembly	Fertile to Fissile	$K_{eff}(^{239}\chi)$	$\Delta K(^{235}\chi)$	$\Delta K(\tilde{\chi})$
VERA-11A	0.05	0.9852	-0.40	-0.13
ZPR-3-53	1.6	0.9837	-0.31	-0.07
ZPR-3-54	1.6	0.9401	-0.10	-0.01
FCA-5-2	2.3	0.9845	-0.48	-0.31
SNEAK-7A	3.0	0.9940	-0.59	-0.12
MZA	3.9	0.9864	-0.48	-0.08
ZPR-3-48	4.5	0.9922	-0.66	-0.12
ZPR-3-49	4.5	0.9947	-0.71	-0.13
ZPR-3-50	4.5	0.9864	-0.64	-0.11
ZPR-3-56B	4.6	0.9807	-0.44	-0.06
MZB	5.8	0.9836	-0.56	-0.11
ZPR-6-7	6.5	0.9854	-0.59	-0.11
ZPPR-2	6.5	0.9918	-0.52	-0.08
FCA-6-2	6.5	0.9837	-0.53	-0.37
SNEAK-7B	7.0	0.9914	-0.84	-0.25
ZEBRA-3	8.6	0.9922	-1.09	-0.31

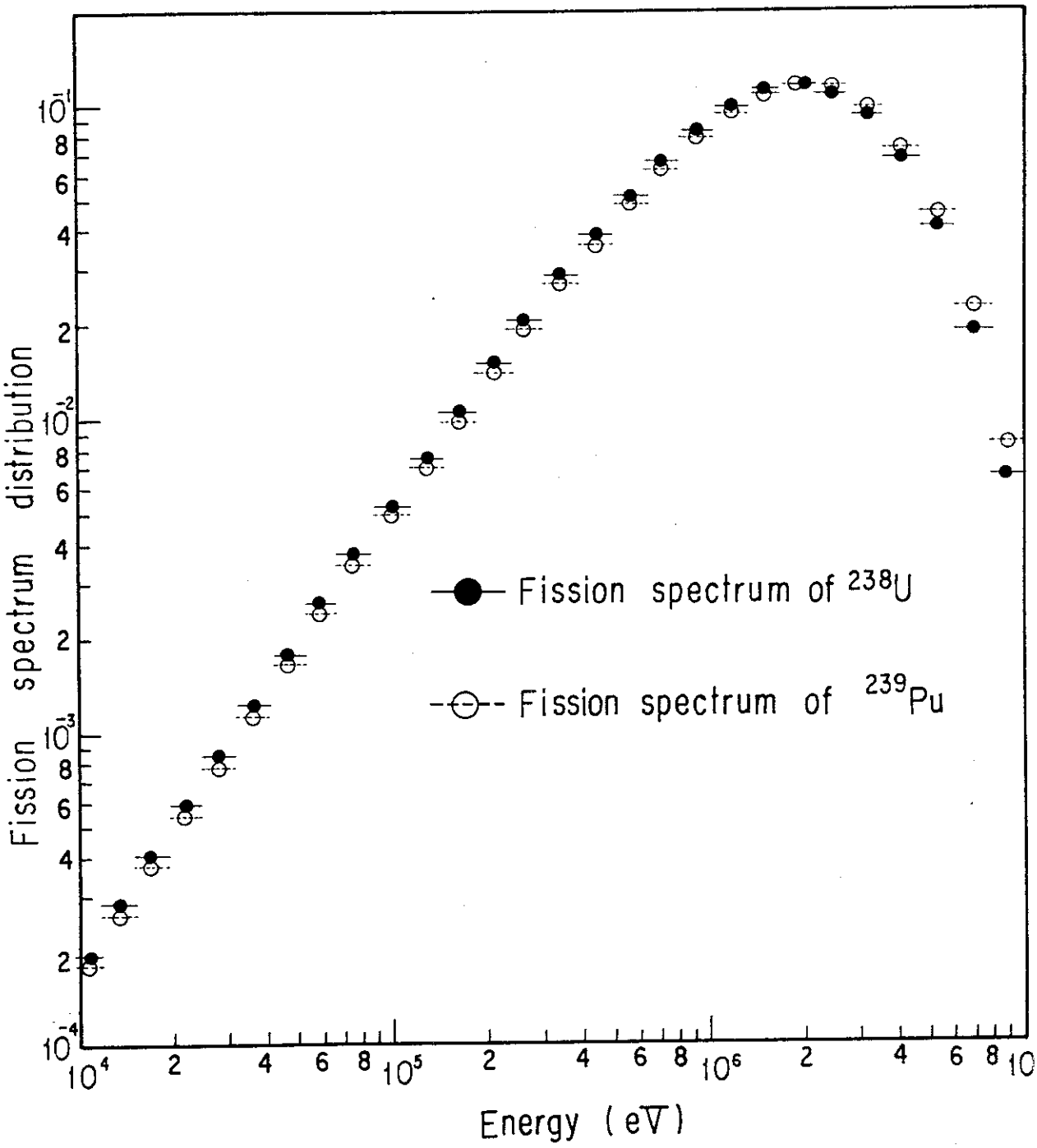

Fig.A.4.1 Comparison of fission spectra of ^{239}Pu and ^{238}U

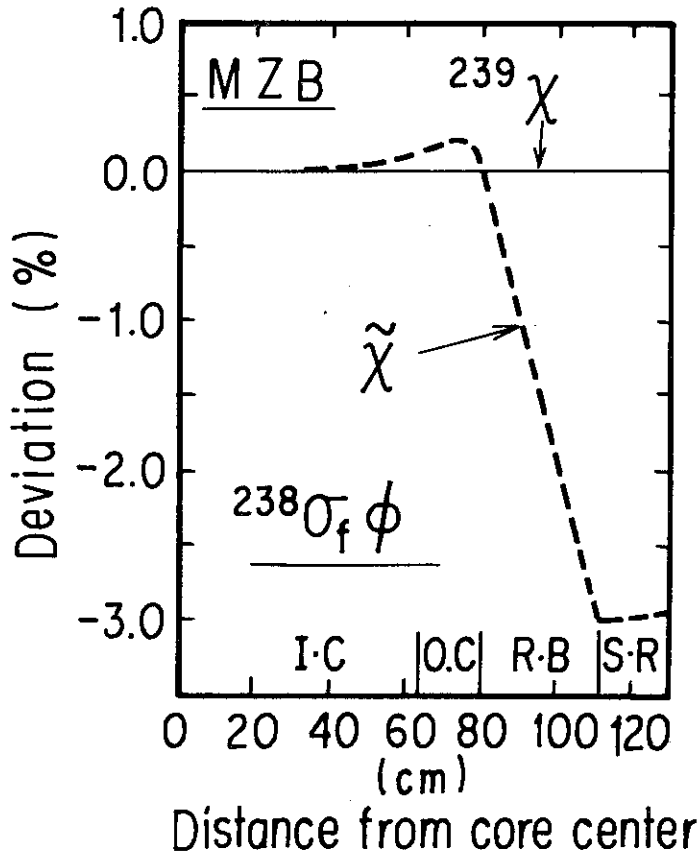

Fig.A.4.2 Deviation of the radial fission reaction rates of ^{238}U calculated with the ^{239}Pu fission spectrum from those calculated with the average fission spectrum in MZB assembly

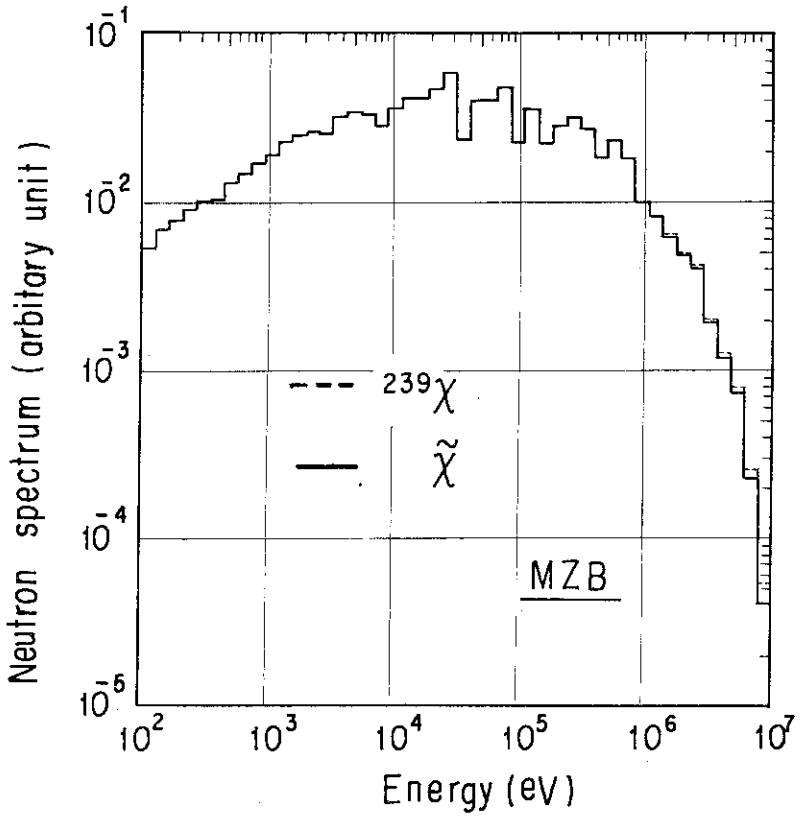

Fig.A.4.3 Comparison of neutron spectra calculated with the ^{239}Pu and average fission spectra at the blanket region in MZB assembly

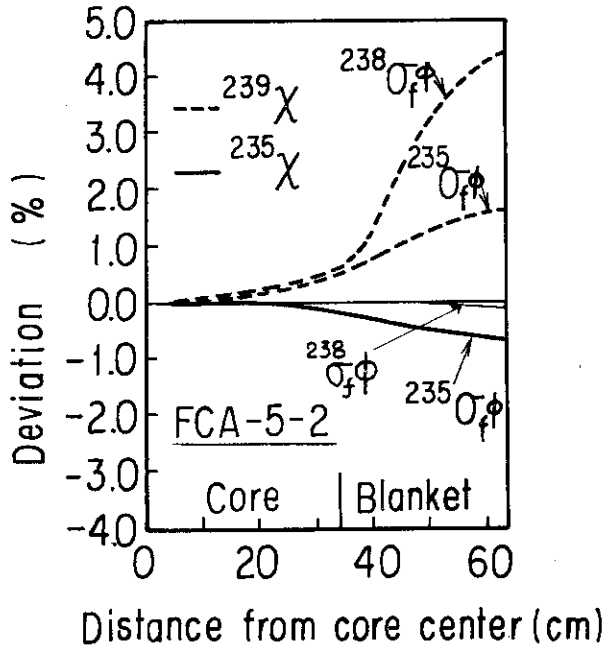

Fig.A.4.4 Deviations of the radial reaction rates calculated with the ^{235}U or ^{239}Pu fission spectrum from those calculated with the average fission spectrum in FCA-5-2 assembly

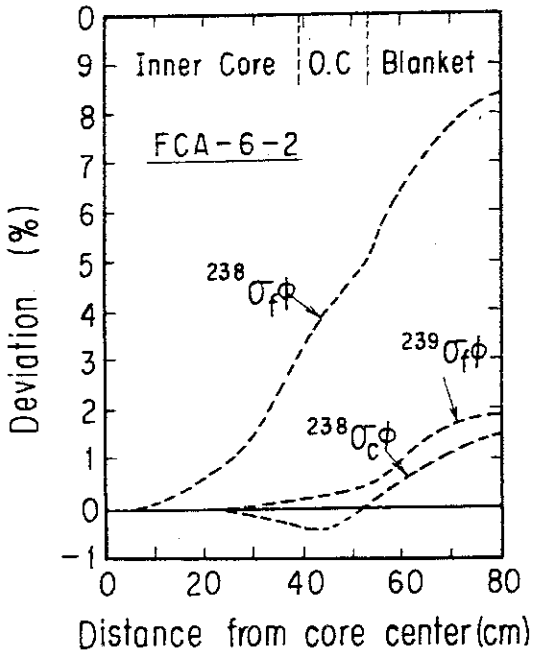

Fig.A.4.5 Deviations of the radial reaction rates calculated with the ^{239}Pu fission spectrum from those calculated with the region dependent fission spectra in FCA-6-2 assembly

Appendix B: Benchmark Calculation Models for the Fast Reactor Critical Assemblies

In this thesis, the benchmark tests of several group constant sets have been performed for the 30 fast benchmark cores, i.e., VERA-11A, VERA-1B, ZPR-3-6F, ZPR-3-11, ZPR-3-12, ZPR-3-47, ZPR-3-53, ZPR-3-54, ZPR-3-48, ZPR-3-49, ZPR-3-50, ZPR-3-56B, ZEBRA-2, ZEBRA-3, SNEAK-7A, SNEAK-7B, ZPR-6-7 (Ref.), ZPR-6-7 (H240), ZPR-6-6A, ZPPR-2, ZPPR-3 Phase 3, ZPPR-9, MZA, MZB, SEFOR, FCA-V-1, FCA-V-2, FCA-VI-1, FCA-VI-2 and NEACRP-LMFBR. The compositions and dimensions for the 18 criticals are described in Refs.(17) and (103). In this appendix. one- and/or two-dimensional specifications for the 12 rest criticals are given in the followings. The atomic number densities for MZA, MZB, ZPPR-3 and ZPPR-9 are not shown, because of the unpublished data.

B.1. FCA-V-1

(1) Two - dimensional R-Z model: Fig. B.1.1

(2) One - dimensional spherical model: Figs.B.1.2 and 3.

(3) Atom densities: Table B.1.1

(4) Plate cell model: Fig.5.27

(5) Doppler sample: Table B.1.2

B.2. FCA-V-2

(1) Two - dimensional R-Z model: Fig.B.2.1

(2) One - dimensional spherical model: Figs.B.2.2 and 3

(3) Atom densities: Table B.2.1

(4) Plate cell model: Fig.5.27

B.3. FCA-VI-1

(1) Two - dimensional R-Z model: Fig.B.3.1

(2) One - dimensional spherical model: Figs.B.3.2 and 3

(3) Atom densities: Table B.3.1

(4) Plate cell model: Fig.5.28

B.4. FCA-VI-2

(1) Two - dimensional R-Z model: Fig.B.4.1

(2) One - dimensional spherical model: Fig.B.4.2

(3) Atom densities: Table B.4.1

(4) Plate cell model: Fig.5.28

B.5. ZPR-6-7 (H240)

(1) Two - dimensional R-Z model: Fig.B.5.1.

(2) One - dimensional spherical model: Figs.B.5.2 and 3

(3) Atom densities: Table B.5.1

(4) Plate cell model: Fig.5.29

B.6. SEFOR

(1) Two - dimensional R-Z model: Fig.B.6.1

(2) One - dimensional spherical model: Fig.B.6.2

(3) Atom densities: Tables B.6.1 and 2

B.7. MZA

(1) Two - dimensional R-Z model: Fig.B.7.1

(2) One - dimensional spherical model: B.7.2

B.8. MZB

(1) Two - dimensional R-Z model: Fig.B.8.1

(2) One - dimensional spherical model: Fig.B.8.2.

B.9. ZPPR-3 Phase 3

(1) Two - dimensional X-Y model: Fig.B.9.1

(2) Two - dimensional R-Z model: Fig.B.9.2

B.10. ZPPR-9

(1) Two - dimensional R-Z model: Fig.B.10.1

B.11. NEACRP-LMFBR

(1) Two - dimensional R-Z model: Fig.B.11.1

(2) Atom densities: Table B.11.1

B.12. ZPR-3-47

(1) Two - dimensional R-Z model: Fig.B.12.1

(2) Atom densities: Table B.12.1

Table B.1.1 Atomic number density (FCA-V-1)

$\times 10^{22}/cm^3$

	Core	Blanket
^{239}Pu	0.10446	0
^{240}Pu	0.009427	0
^{241}Pu	0.001124	0
^{235}U	0.19600	0.02891
^{238}U	0.77810	3.989
O	1.6476	0
Na	0.60431	0
Al	1.1065	0
Cr	0.30535	0.1827
Fe	1.09705	0.6652
Ni	0.14275	0.07964

Table B.1.2 FCA Doppler Sample

$\times 10^{24}/cm^3$

	NUO-2	Iron	SS
diameter	2.5 cm	2.5 cm	2.5 cm
length	15.0 cm	15.6 cm	15.6 cm
U-235	1.503 -4		
U-238	2.0632 -2		
O-16	4.156 -2		
Fe		9.657 -2	6.146 -2
Cr			1.711 -2
Ni			8.0 -3

Table B.2.1 Atomic number density in FCA-V-2 ($\times 10^{22}$/cc)

	Core	Blanket
Pu-239	0.10458	0
Pu-240	0.009325	0
Pu-241	0.001069	0
U-235	0.14700	0.02891
U-238	0.58359	3.989
O	1.3101	0
Na	0.81341	0
Al	0.88295	0
Cr	0.32734	0.1827
Fe	1.1950	0.6652
Ni	0.15345	0.07964

Table B.3.1 Atomic number density in FCA-VI-1 (10^{22}/cc)

Material	Test Region	Driver	Blanket	
			Radial(NU)	Axial(DU)
Pu-239	0.15687			
Pu-240	0.01400			
Pu-241	0.00160			
U-235	0.00152	0.21310	0.0289	0.0086
U-238	0.69057	0.64152	3.9885	4.0070
O	1.5598	1.5306		
Na	0.7656	0.7656		
Al	0.1354	1.0204		
Cr	0.3552	0.3134	0.1827	0.1827
Fe	1.3004	1.1504	0.6652	0.6652
Ni	0.1639	0.1420	0.0796	0.0796

Table B.4.1 Atomic number density in FCA-VI-2 (10^{22}/cc)

Material	Test Region	Driver	Blanket	
			Radial	Axial
Pu-239	0.10458			
Pu-240	0.00933			
Pu-241	0.00092			
U-235	0.00152	0.28483	0.0289	0.0086
U-238	0.69057	0.68915	3.9885	4.0070
O	1.7286	1.3619		
Na	0.7656	0.7656		
Al	0.2403	0.9079		
Cr	0.3413	0.3134	0.1827	0.1827
Fe	1.2504	1.1504	0.6652	0.6652
Ni	0.1566	0.1402	0.0796	0.0796

Table B.5.1 **Homogeneous** atomic number densities for reference core and H240 core of ZPR-6 assembly 7 (10^{21} atoms/cc.)

	Reference Core				H240 Core				
	I.C	O.C	A.B	R.B	H240	O.C	Pu/Al	A.B	R.B
Pu 238	0.00033	0.00049			0.00114	0.00049	<0.0001		
Pu 239	0.8867	0.8879			0.8370	0.8879	1.063		
Pu 240	0.1177	0.1178			0.3212	0.1178	0.0499		
Pu 241	0.0133	0.0152			0.0593	0.0146	0.0049		
Pu 242	0.00141	0.00177			0.0174	0.00177	0.00005		
U 234	0.00006	0.00006	0.0004	0.0004	0.00006	0.00006	0.00006	0.0004	0.0004
U 235	0.0126	0.0126	0.0834	0.0866	0.0122	0.0126	0.0126	0.0834	0.0866
U 236	0.00030	0.00030	0.0020	0.0020	0.00029	0.00030	0.00030	0.0020	0.0020
U 238	5.777	5.802	38.59	40.06	5.585	5.802	5.717	38.59	40.06
Am 241	0.0030	0.0028			0.0067	0.0034	<0.001		
Mo	0.2357	0.2382	0.0046	0.0034	0.2297	0.2382	0.242	0.0046	0.0034
Na	9.2904	9.132			9.288	9.132	9.132		
O	13.98	14.82	0.030	0.021	13.84	14.82	14.82	0.030	0.021
Fe	12.97	13.53	5.652	4.197	12.91	13.53	13.15	5.652	4.197
Ni	1.240	1.212	0.6910	0.5082	1.235	1.212	1.481	0.6910	0.5082
Cr	2.709	2.697	1.579	1.17	2.701	2.697	2.675	1.579	1.172
Mn	0.212	0.213	0.123	0.0897	0.221	0.213	0.210	0.123	0.0897

Table B.6.1 Isotope or number density (x 10^{24}at/cc) for 1-dimensional spherical model of SEFOR assembly

Region / Isotope	1	2	3	4
Fe	1.3574-2	1.3886-2	5.8932-3	7.8587-3
Cr	3.9574-3	3.9511-3	2.8911-3	2.8913-3
Ni	2.0292-3	2.358 -3	3.0178-2	1.3315-3
Na	1.6615-2	6.8099-3	5.4493-3	1.307 -3
Be		3.6011-3	1.8327-5	
O		2.0991-2	1.2597-4	
Mo		1.1999-4	1.5605-5	
B-10		6.11 -5		5.7684-3
B-11		2.64 -4		2.31 -2
U-235		1.5374-5	1.1724-7	
U-238		6.9808-3	5.3438-5	
Pu-239		1.5901-3		
Pu-240		1.4355-4		
Al			2.233 -3	6.58 -3
C		7.677 -5		7.22 -3

Table B.6.2 Atomic number densities (10^{24} at/cc) for 2-dimensional model of SEFOR assembly

Composition No.	1	2	3	4	5	6	7	8	9
Material									
U-235					1.78 E-6	1.585 E-5	1.585 E-5	7.482 E-6	1.78 E-6
U-238					8.1126E-4	7.197 E-3	7.197 E-3	3.3938E-3	8.1126E-4
Pu-239						1.6895E-3	1.6895E-3		
Pu-240						1.522 E-4	1.522 E-4		
Pu-241									
Fe	1.0894E-2	7.0745E-3	1.8373E-2	1.4172E-2	1.2837E-2	1.4151E-2	1.3567E-2	1.7529E-2	1.3748E-2
Cr	3.176 E-3	2.0624E-3	5.3564E-3	4.4759E-3	3.6373E-3	4.0151E-3	3.8493E-3	5.1711E-3	3.9047E-3
Ni	1.6285E-3	1.0575E-3	2.7465E-3	2.3799E-3	3.9552E-2	2.3604E-3	2.2629E-3	3.6597E-3	3.8953E-2
Be					2.3175E-4	2.684 E-3	3.7769E-3	3.7769E-3	3.247 E-4
O					1.866 E-3	2.070 E-2	2.1795E-2	1.0742E-2	1.9589E-3
Na	1.6615E-2	1.6615E-2	1.6615E-2	1.690 E-2	6.9576E-3	6.8099E-3	6.8099E-3	6.8099E-3	6.8702E-3
Mo					1.2014E-4	1.2436E-4	1.1915E-4	1.1916E-4	1.1797E-4
B-10						6.111 E-5	6.111 E-5	6.111 E-5	
B-11						2.46 E-4	2.46 E-4	2.46 E-4	
C						7.677 E-5	7.677 E-5	7.677 E-5	

Table B.6.2 (Continued)

Composition No.	10	11	12	13	14	15
Material						
U-235						
U-238						
Pu-239						
Pu-240						
Pu-241						
Fe	1.8825E-2	1.7345E-2	9.474E-3	2.0489E-3	9.093E-3	7.0523E-3
Cr	5.9192E-3	5.314 E-3	2.762E-3	5.973 E-4	2.659E-3	2.2274E-3
Ni	3.1419E-3	3.8328E-3	1.416E-3	6.240 E-2	8.324E-3	1.1843E-3
Be						
O						
Na	1.3526E-2	1.4842E-2				
Mo	1.2872E-4					
B-10						6.804 E-3
B-11						2.7216E-2
C						8.5149E-3
Al			1.179E-2	2.1303E-3		

Table B.11.1 Atomic number density for NEACRP benchmark core (x $10^{24}/cm^3$)

Nuclide	Inner Core	Outer Core	Axial Blanket	Radial Blanket	Refl.
Na	9.6673-3	9.6673-3	9.6673-3	6.1299-3	9.6673-3
ϕ-16	17.3293-3	17.3293-3	17.8922-3	27.1562-3	---
Fe	11.2693-3	11.2693-3	11.2693-3	8.7384-3	13.9943-3
Ni	2.2435-3	2.2435-3	2.2435-3	1.7397-3	29.5122-3
Cr	3.2840-3	3.2840-3	3.2840-3	2.5464-3	9.6621-3
Mo	0.2339-3	0.2339-3	0.2339-3	0.1814-3	0.2239-3
Mn	0.2842-3	0.2842-3	0.2842-3	0.2203-3	0.3607-3
^{235}U	0.0155-3	0.0149-3	0.0184-3	0.0279-3	---
^{238}U	7.6440-3	7.3256-3	9.0634-3	13.7561-3	---
^{239}Pu	0.7704-3	0.9868-3	---	---	---
^{240}Pu	0.2208-3	0.2828-3	---	---	---
^{241}Pu	0.1165-3	0.1497-3	---	---	---
^{242}Pu	0.0279-3	0.0358-3	---	---	---
^{10}B	---	---	---	---	---
^{12}C	---	---	---	---	---
^{11}B	---	---	---	---	---

Table B.12.1 Compositions of ZPR-3 assembly 47 (10^{22} atoms/cc)

	Inner core	Outer core	Radial Na-Steel	Radial Ni-reflector	Axial Ni-reflector	Axial Steel
$^{239+241}Pu$	0.1430	0.1513				
^{240}Pu	0.0132	0.0072				
^{235}U	0.0015	0.0015				
^{238}U	0.7742	0.7893				
Be	0.5680	0.5413				
C	0.3359	0.3359			0.1755	0.3761
O	1.5663	1.5287				
Na	0.6628	0.6601	0.6156			
Al	0.6986	0.7723	0.0491	0.6160	0.5335	1.0758
Cr	0.2579	0.2816	0.4253	0.1181	0.3190	0.7049
Mn	0.0158	0.0172	0.0260	0.0072	0.0195	0.0432
Fe	0.9847	1.0748	1.6235	0.4510	1.2177	2.6909
Ni	0.1398	0.1526	0.2304	6.5881	4.5325	0.3819
Mo	0.0515					

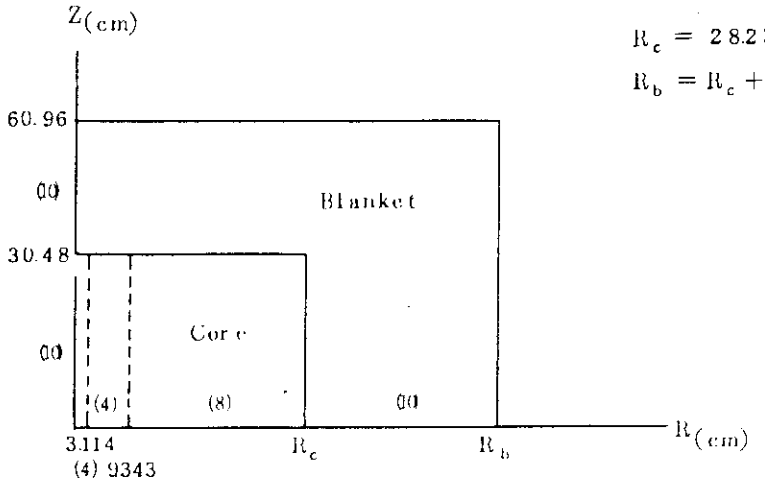

Fig.B.1.1 2－D RZ Model For FCA－V－1 (Ref.)

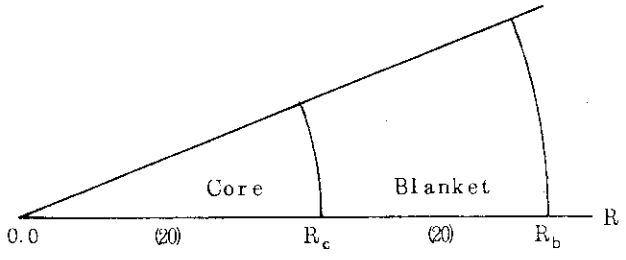

Fig.B.1.2 1－D Spherical Model For FCA－V－1 (Ref.)

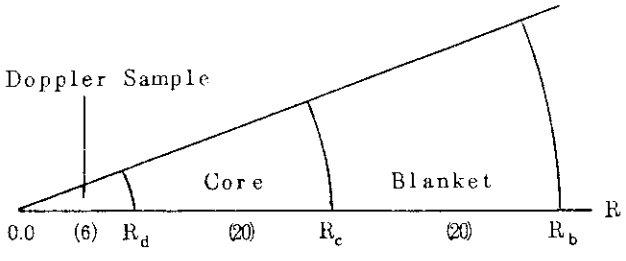

Fig.B.1.3 1－D Spherical Model For FCA－V－1 (Doppler)

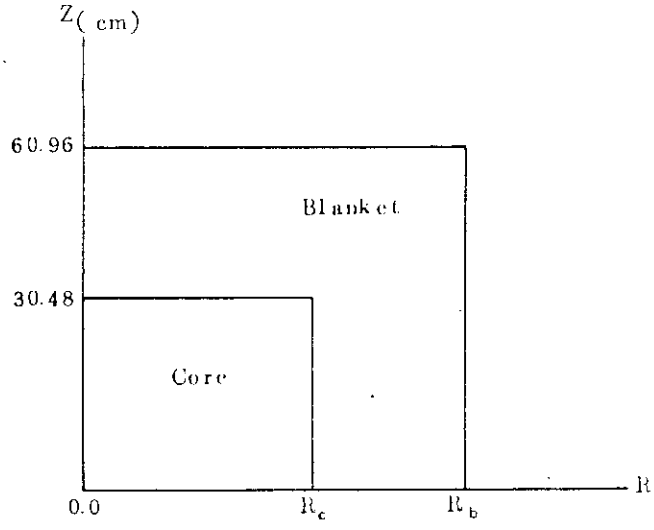

Fig.B.2.1 2－D RZ Model For FCA－V－2 (Ref.)

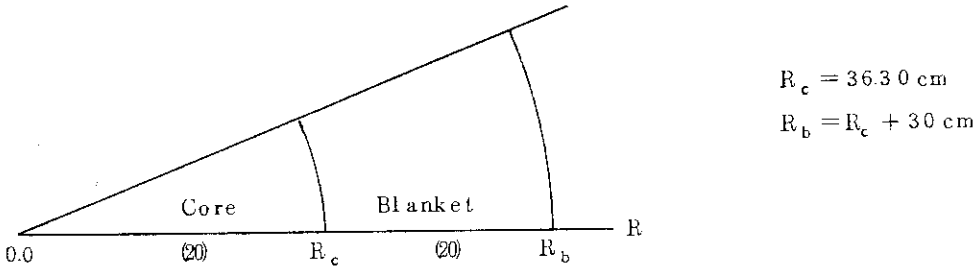

Fig.B.2.2 1－D Spherical Model For FCA－V－2 (Ref.)

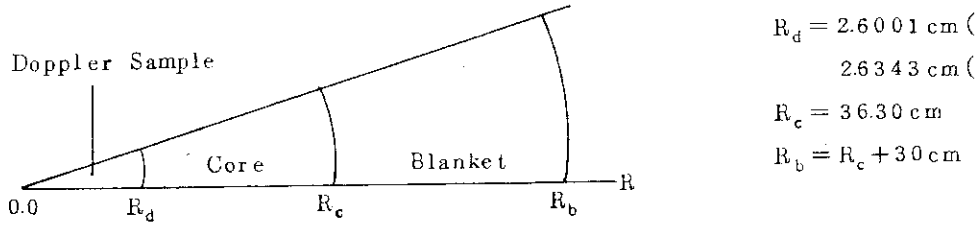

Fig.B.2.3 1－D Spherical Model For FCA－V－2 (Doppler)

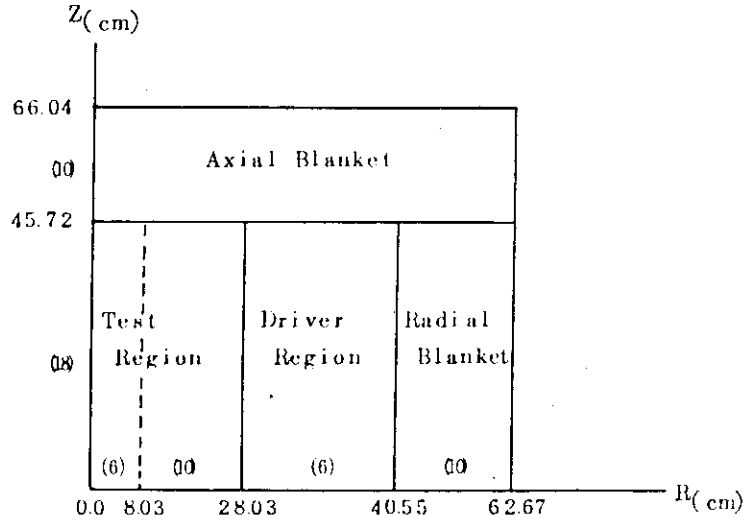

Fig.B.3.1　2－D RZ Model For FCA－Ⅵ－1 (Ref.)

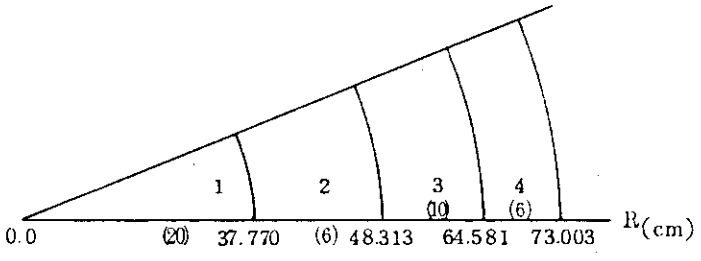

1. Test Region
2. Driver Region
3. Radial Blanket
4. Axial Blanket

Fig.B.3.2　1－D Spherical Model For FCA－Ⅵ－1 (Ref.)

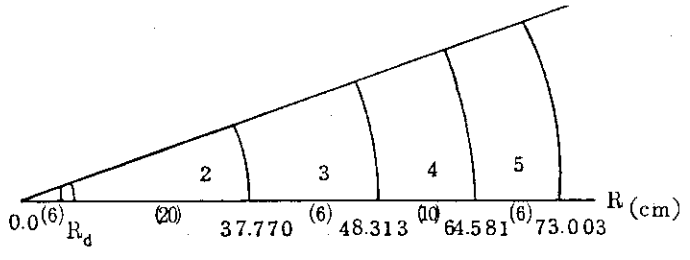

R_d = 2.6001 cm (NUO_2)
2.6343 cm (Iron.SS)

1. Doppler Sample
2. Test Region
3. Driver Region
4. Radial Blanket
5. Axial Blanket

Fig.B.3.3　1－D Spherical Model For FCA－Ⅵ－1 (Doppler)

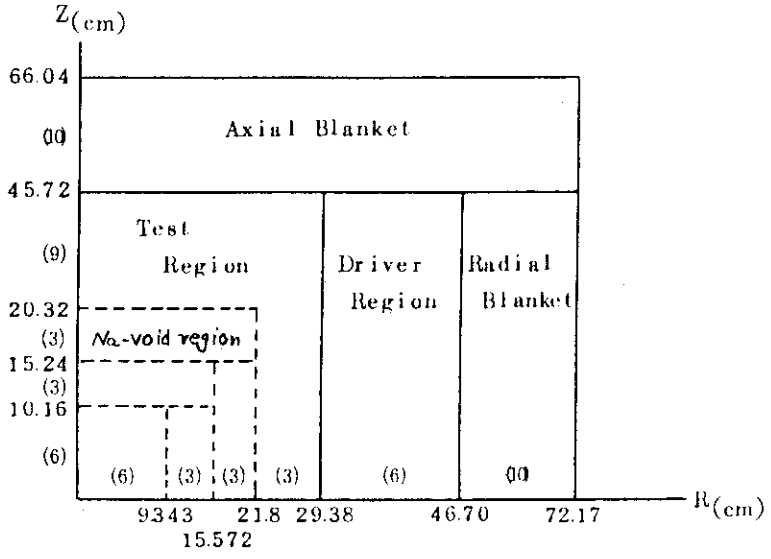

Fig.B.4.1 2－D RZ Model For FCA－Ⅵ－2 (Ref.)

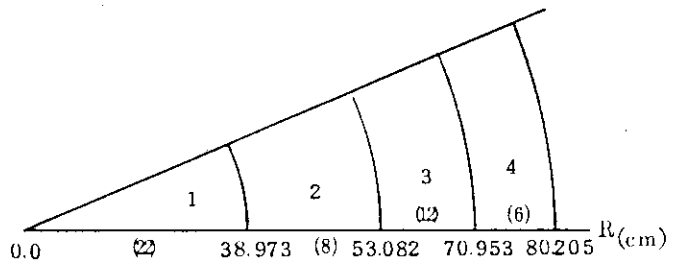

1. Test Region
2. Driver Region
3. Radial Blanket
4. Axial Blanket

Fig.B.4.2 1－D Spherical Model For FCA－Ⅵ－2 (Ref.)

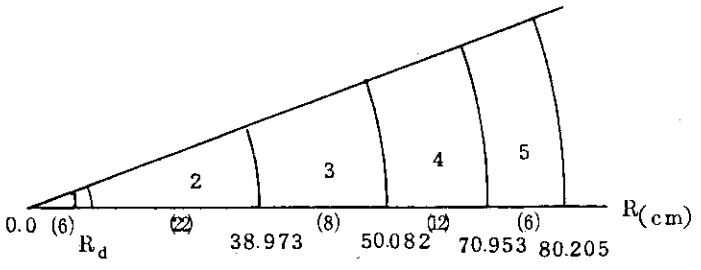

R_d = 2.6001 cm (NUO_2)
2.6343 cm (Irom, SS)

1. Doppler Sample
2. Test Region
3. Driver Region
4. Radial Blanket
5. Axial Blanket

Fig.B.4.3 1－D Spherical Model For FCA－Ⅵ－2 (Doppler)

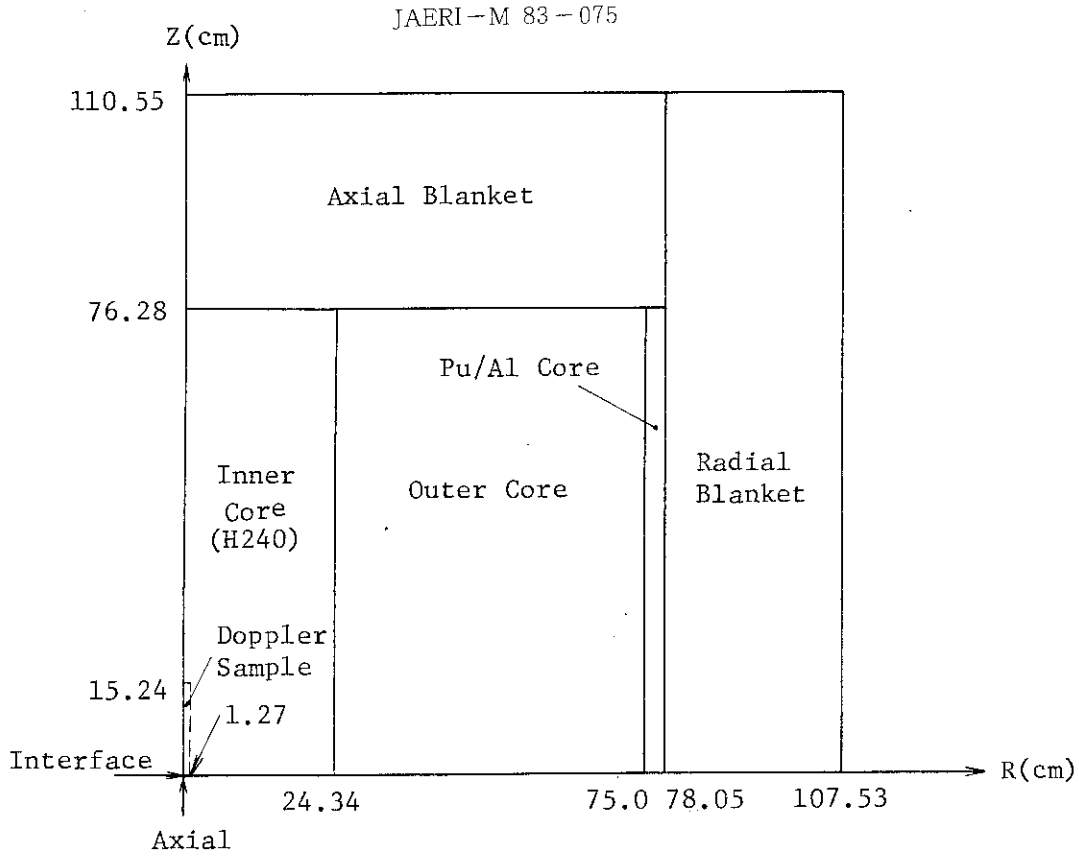

Fig.B.5.1 2-D RZ Calculational Model for ZPR-6-7 (H240)

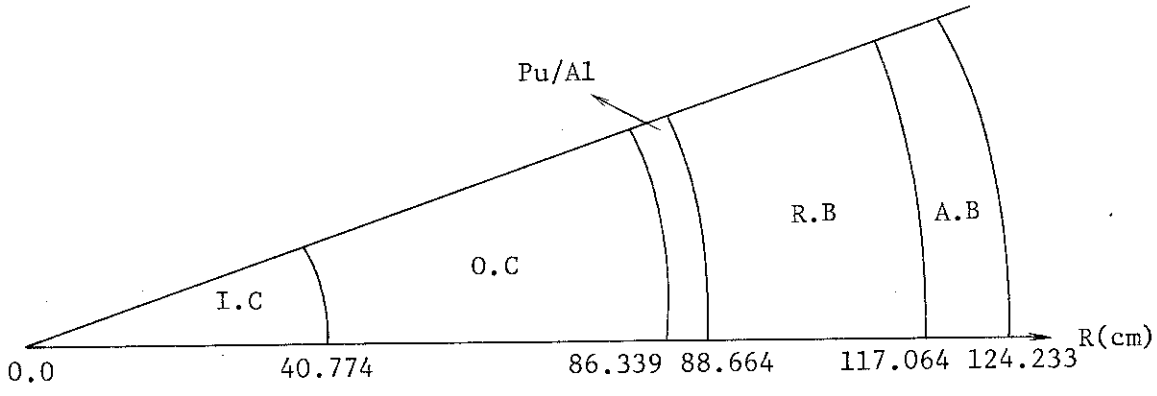

Fig.B.5.2 One-dimensional spherical model for ZPR-6-7 (H240)

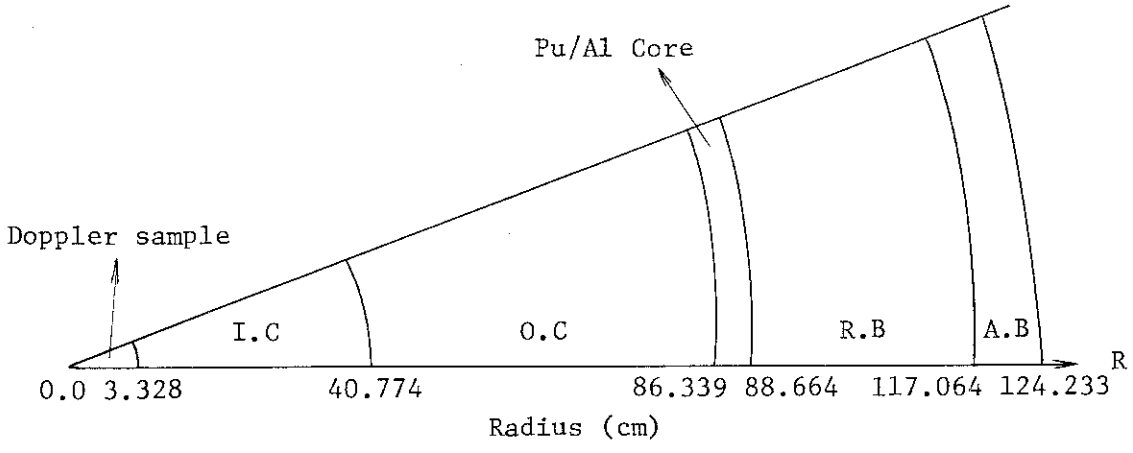

Fig.B.5.3 One-dimensional spherical model for calculation of sample Doppler effect in ZPR-6-7 (H240)

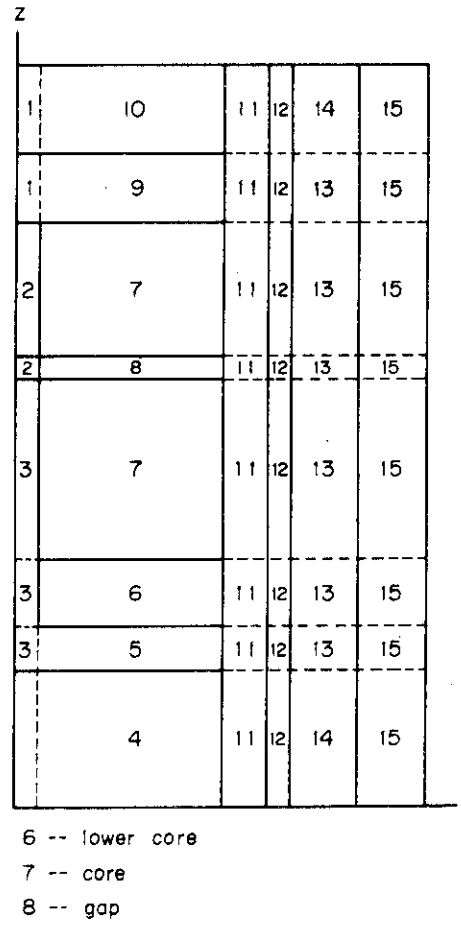

Fig.B.6.1 Two-dimensional R-Z geometry for SEFOR assembly

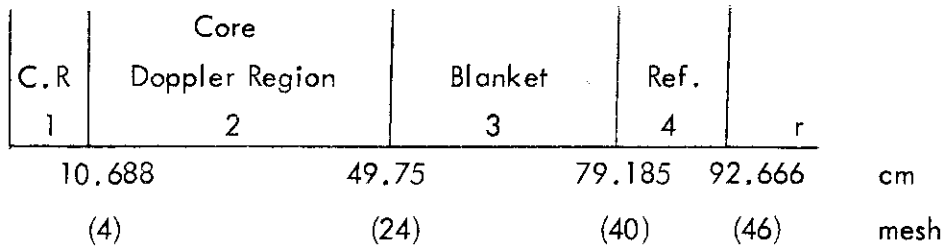

Fig.B.6.2 One-dimensional spherical geometry for SEFOR assembly

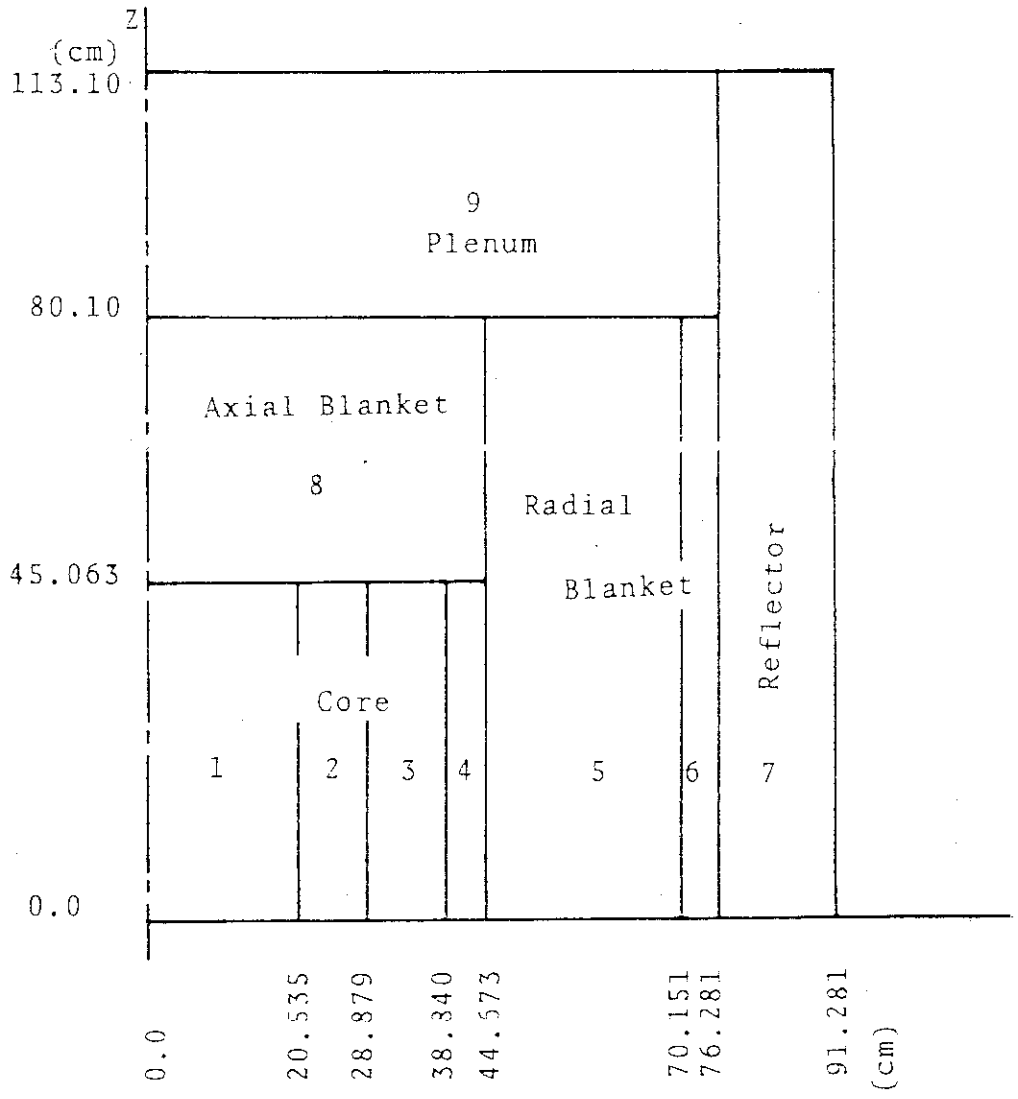

Fig.B.7.1 2-D R-Z calculational model for MZA assembly

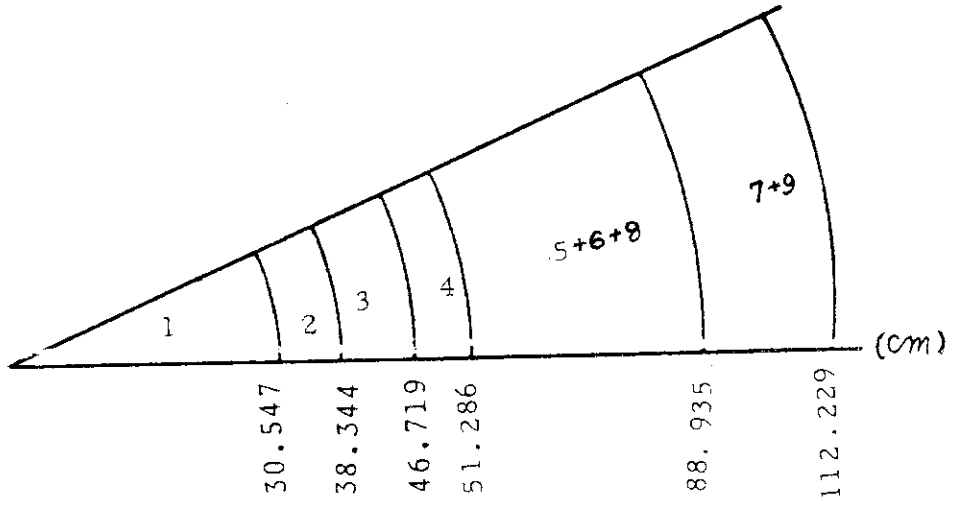

Fig.B.7.2 . 1-D spherical model for MZA assembly.

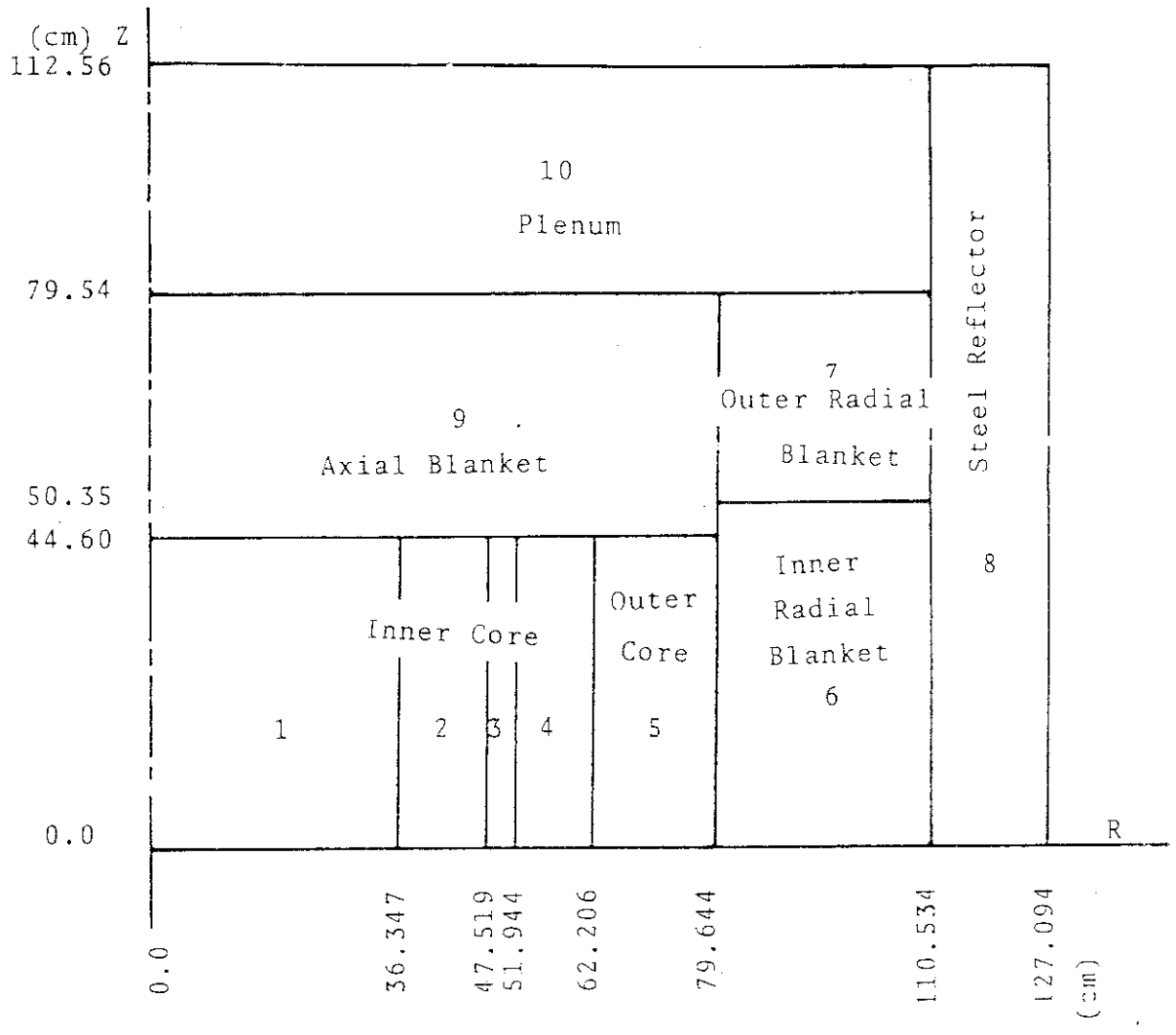

Fig.B.8.1 2-D R-Z calculational model for MZB assembly

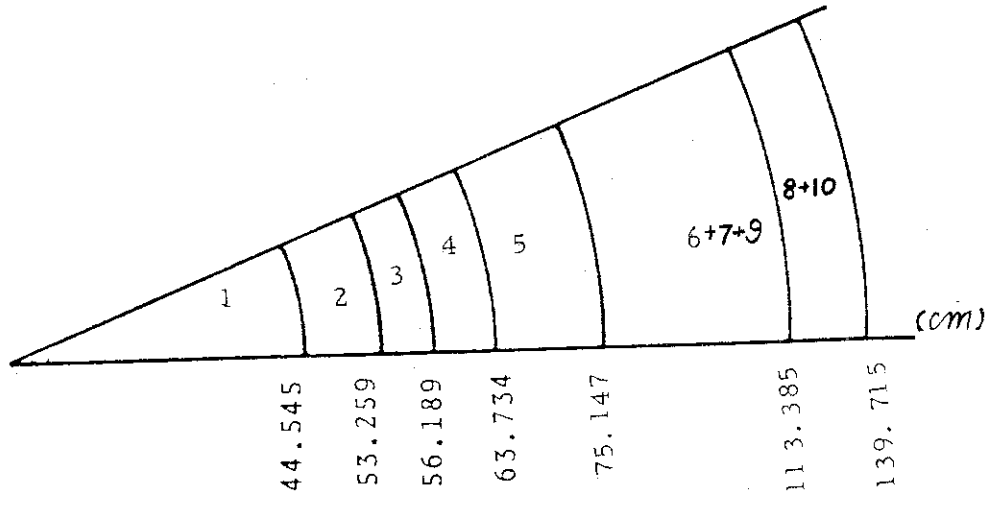

Fig.B.8.2 1-D spherical model for MZB assembly.

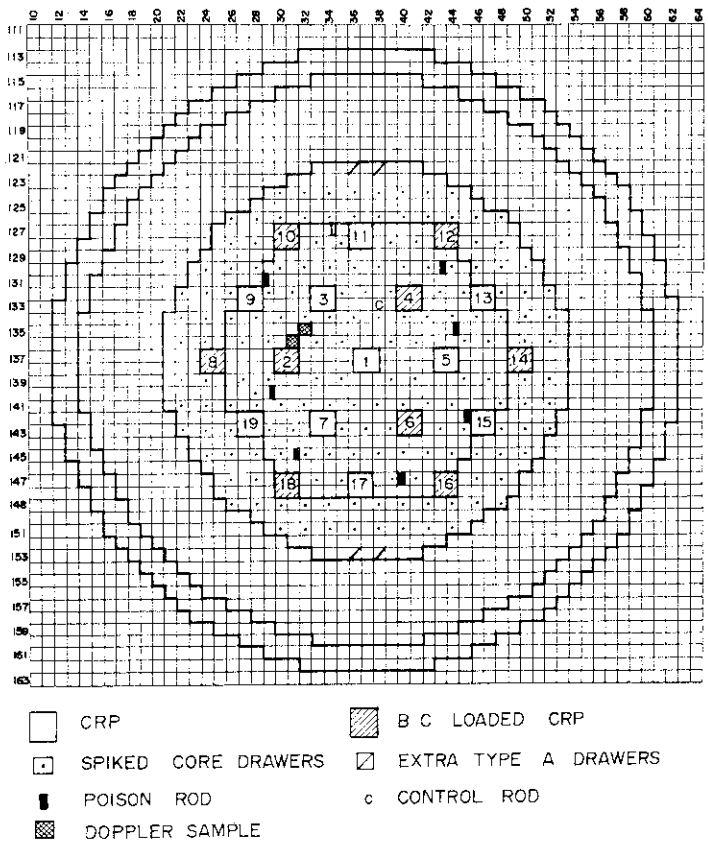

Fig.B.9.1 Configuration of ZPPR-3 (phase 3)

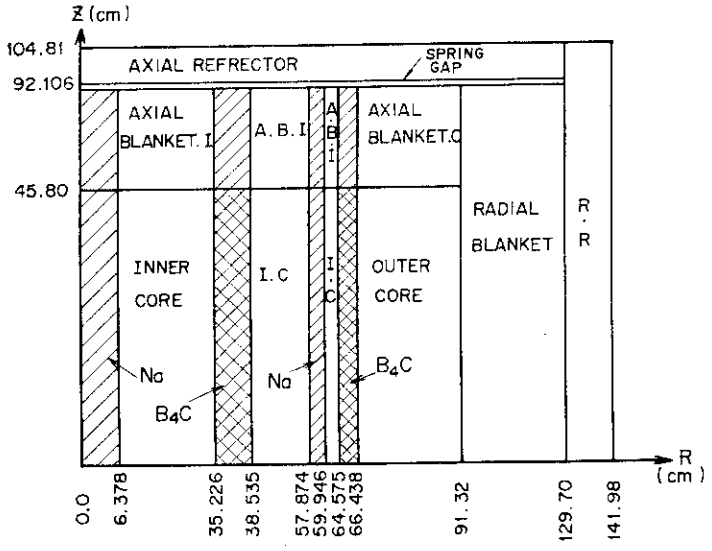

Fig.B.9.2 R-Z model of ZPPR-3 (phase 3)

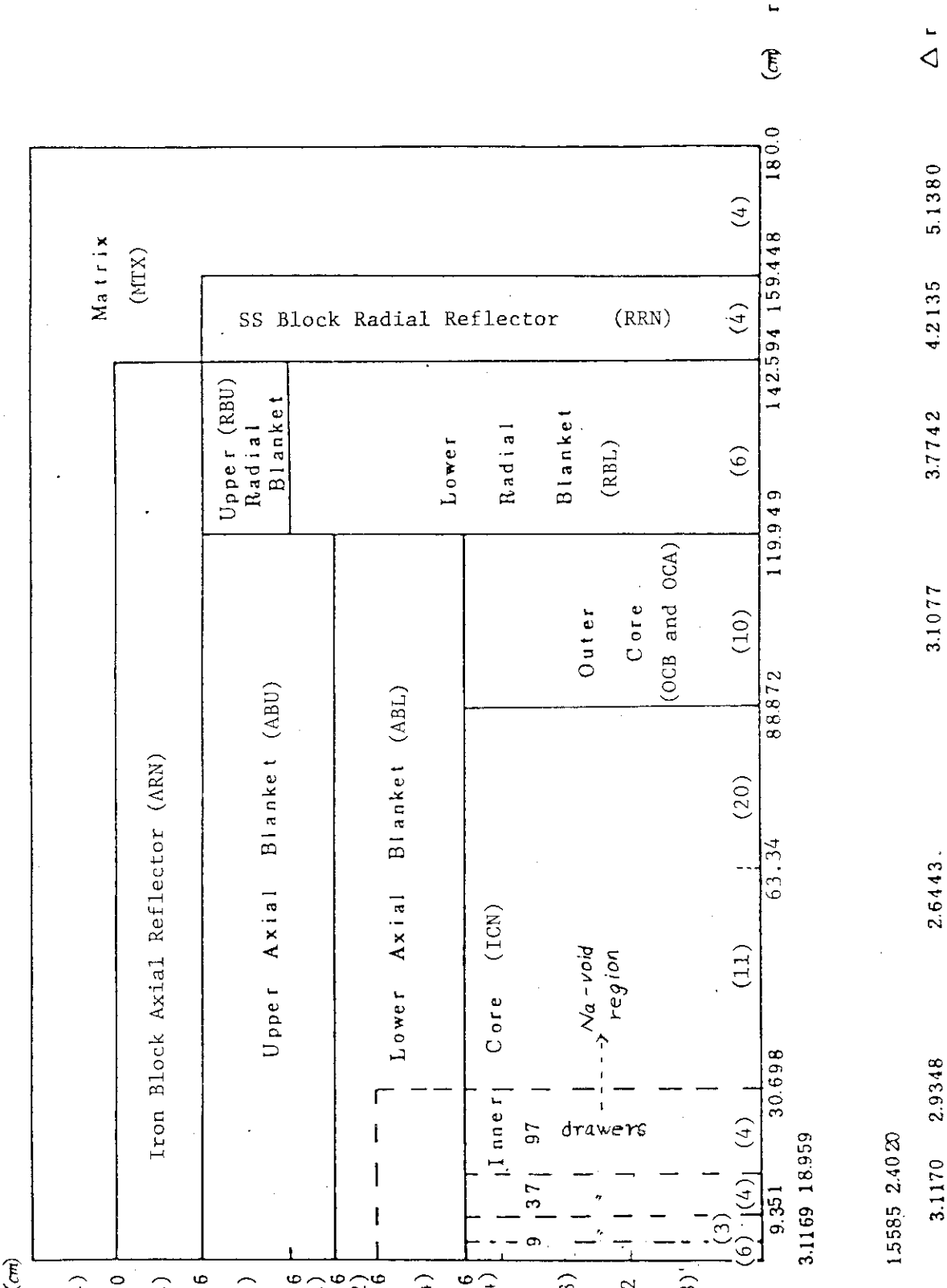

Fig.B.10.1 R-Z Geometry for ZPPR-9

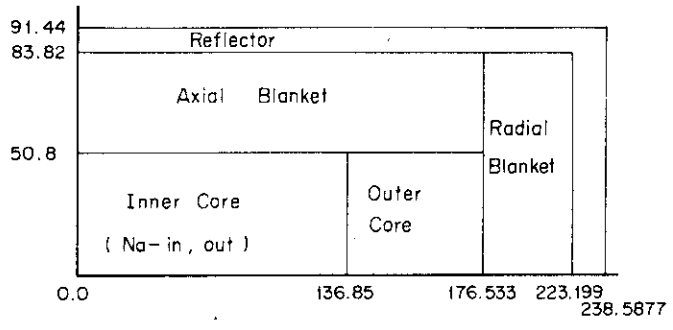

Fig.B.11.1 Configuration of large fast breeder reactor

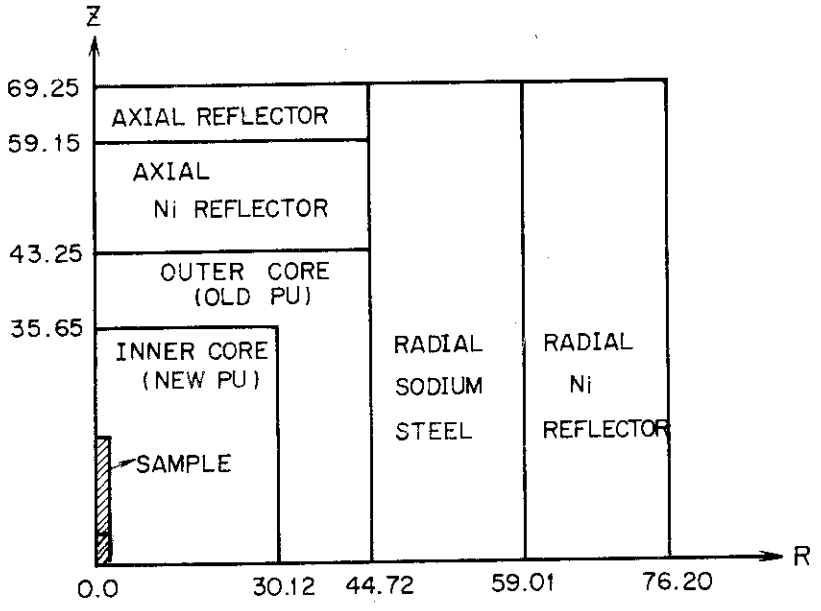

Fig.B.12.1 R-Z calculation model of ZPR-3 assembly 47

References

(1) Marchuk, G.I.: "Numerical Methods for Nuclear Reactor Calculations", (translated from russian), (1959), Consaltants Bureau, Inc., New York.

(2) Katsuragi, S., Ishiguro, Y., Kato, O.: "Group Constants for a Fast Reactor and Sodium Void Effects", JAERI 1109 (1966).

(3) Rago, A.L. Hummel, H.H.: "ELMOE: An IBM-704 Program Treating Elastic Scattering Resonance in Fast Reactors", ANL-6805 (1964).

(4) Toppel, B.J., et al.: "MC^2, A Code to Calculate Multigroup Cross Sections", ANL-7318 (1967).

(5) Nakagawa, M., Katsuragi, S.: "ESELEM 4, A Code for Calculating Fine Neutron Spectrum and Multigroup Cross Sections in Plate Lattice", JAERI 1245 (1976).

(6) Yiftah, S., Okrent, D., Molduer, P.A.: "Fast Neutron Cross Section", (1960), Pergamon Press, London.

(7) Hansen, G.E., Roach, W.H.: "Six and Sixteen Group Cross Sections for Fast and Intermediate Critical Assemblies", LA-MS-2543, (1961).

(8) Abagyan, L.P., et al.: "Group Constants for Nuclear Reactor Calculation", (1964), Consultants Bureau, Inc., New York.

(9) Katsuragi, S., Tone, T., Hasegawa, A.: "JAERI Fast Reactor Group Constants Systems Part I", JAERI 1195 (1970).

(10) Katsuragi, S., Ishiguro, Y., Takano, H., et al.: "JAERI Fast Reactor Group Constants Systems Part II-1", JAERI 1199 (1970).

(11) Chaudat, J.P., et al.: "Improvements of the Predicted Characteristics for Fast Power Reactor from Integral Experiments: CADARACHE Version III Multigroup Cross Section Set", Inter. Symp. Physics of Fast Reactors, Paper A34, 1973, Tokyo.

(12) Rowland, J.L., et al.: "The Production and Performance of the Adjusted Cross-Section Set FGL5", Inter. Symp. Physics of Fast Reactors, Paper A30, 1973, Tokyo.

(13) Kidman, R.B., MacFarlane, R.E.: "LIB-IV, A Library of Group Constants for Nuclear Reactor Calculations", LA-6260-MS, (1976).

(14) Kiefhaber, E.: "The KFKINR-Set of Group Constants", KFK-1572 (1972).

(15) Takano, H., Hasegawa, A., Nakagawa, M., et al.: "JAERI Fast Reactor Group Constants Set, Version II", JAERI 1255 (1978).

(16) Davey, W.G., Hess, S.L.: "Additional Fast Reactor Benchmarks for Phase II Data Testing of ENDF/B", CSEWG Newsletter 18, Cross Section Working Groups (1969).

(17) Hardie, R.W., et al.: Nucl Sci. Eng., 57, 222 (1975).

(18) Vieider, G., et al.: Fast Breeder Reactors Status 1977, STUDSVIK/RA-78/1 (1978).

(19) Hammmer, P.: "Nuclear Data Needs for Plutonium Breeders", Proc. Inter. Conf. on Nuclear Cross Sections for Technol., Knoxiville, Oct.22-16 (1979).

(20) Mitani, H., Kuroi, H.: J. Nucl. Sci. Technol., 9(7), 383 and 9(11), 642 (1972).

(21) Tone, T.: "A Study of Group Constants for Design Calculations of Fast Reactors", JAERI-M 4826 (1972).

(22) Kamei, T., et al.: "Effect of Mock-up Size on Extrapolation Accuracy in Predicting Neutronics Parameters of Large LMFBRs", IAEA-SM-244/5, Proc. Fast Reactor Physics, Aix-en-Provence (1979).

(23) Feshbach, H., et al.: "Estimation of Doppler Effect in Fast Reactors", Nucl. Sci. Eng., 1, 4 (1956).

(24) Nicholson, R.B.: "The Doppler Effects in Fast Neutron Reactors", APDA-139 (1960).

(25) Takano, H., Nakagawa, M., Ishiguro, Y., et al.: "Accuracy of Analytical Treatments for Resonance Absorption in Doppler Resonance Region", J. Nucl. Sci. Technol., 7(10), 500 (1979).

(26) Takano, H., Hasegawa, A., Katsuragi, S.: "An Analysis of Fast Critical Experiments and A Revision of the JAERI Fast Set", JAERI-M 4215 (1971).

(27) Nakagawa, M.: "A Study of Analytical Method for Sodium Void Reactivity in Fast Critical Assemblies", JAERI-M 8138, (1979).

(28) Yoshida, H., et al.: "Analysis of Control Rod Reactivity Worth and Reaction Rate Distribution Measurements Made in the ZPPR Assembly", Unpublished work.

(29) Nakagawa, M., Hirota, M.: "1980 Annual Meeting of the Atomic Energy Society of Japan", C26, 1980.

(30) "ENDF/B Summary Documentation, BNL-NCS-17541 (ENDF-201), 2nd. Edition (ENDF/B-IV), edited by D. Garber, available from the National Nuclear Data Center, Brookhaven National Laboratory, Upton, N.Y. (1975)".

(31) Igarashi, S., et al.: "Japanese Evaluated Nuclear Data Library, Version-1, JENDL-1", JAERI 1261 (1979).

(32) Schenter, R.E., et al.: BNWL-1002, 1969.

(33) Weisbin, C.R., et al.: LA-6486-MS, 1976.

(34) Tone, T., et al.: "PROF-GROUCH-G.: A Processing Code for Group Constants for a Fast Reactor", JAERI 1192, 1970.

(35) Takano, H., Ishiguro, Y., Matsui, Y.: "TIMS-1: A Processing Code for Production of Group Constants of Heavy Resonant nuclei", JAERI 1967, (1980).

(36) Hasegawa, A., et al.: Private communication.

(37) Kikuchi, Y., Hasegawa, A., Takano, H., et al.: "Benchmark Tests of JENDL-1", JAERI 1275 (1982).

(38) Kikuchi, Y., et al.: Private communication.

(39) Kikuchi, Y., Narita, T., Takano, H.: J. Nucl. Sci. Technol.; 17(7), 567 (1980).

(40) Takano, H., Ishiguro, Y.: "Multi-Level Correction to Breit-Wigner Single-Level Formula", J. Nucl. Sci. Technol.; 14(9), 627 (1977).

(41) Kuster, H.: KFK-1632 (1973).

(42) Ishiguro, Y.: Nucl. Sci. Eng., 29, 228 (1972).

(43) Takano, H., Ishiguro, Y.: "The Group Constants for the keV Capture of Structural Materials Cr, Fe and Ni", JAERI-M 5714 (1974).

(44) Takano, H., Inoue, H.: "Doppler Effect of Structural Materials in Fast Reactors", J. Nucl. Sci. Technol., 18 (4); 314 (1981).

(45) Takano, H., Matsui, Y.: "Accuracy of Interpolation Methods for Resonance Self-Shielding Factors", J. Nucl. Sci. Technol.; 18(2), 152 (1980).

(46) Takano, H., Kaneko, K.: "Self-Shielding Effect of Inelastic Scattering Cross Sections of Iron on Neutron Spectrum", Nucl. Sci. Eng., 77, 250 (1981).

(47) Takano, H., Kaneko,K.: J. Nucl. Sci. Technol.; 18(3), 236, (1981).

(48) Dresner, L.: "Resonance Absorption in Nuclear Reactor", (1960), Pergamon Press, N.Y.

(49) Nordheim, L.W.: "The Technology of Nuclear Reactor Safety", Vol.1, Chap.4, (1964), M.I.T. Press, Cambridge.

(50) Ishiguro, Y.: "Improvements to the Intermediate Treatment of Resonance Absorption in Nuclear Reactor Theory", JAERI-memo (published) 3700, (1969).

(51) Goldstein, R., Cohen, E.R.: "Theory of Resonance Absorption of Nuutrons", Nucl. Sci. Eng., 13, 132 (1962).

(52) Ishituro, Y., Takano, H.: "Intermediate Neutron Resonance Absorption with Interference Scattering in Heterogeneous Systems", J. Nucl. Sci. Technol., 6 [7], 380 (1969).

(53) Codd, J., Collins, P.F.: "Some Calculations Concerning the Influence of Resonance Overlapping on the Doppler Effect in a Dilute Fast Reactor", ANL-6792, (1963).

(54) Froelich, R., Ott, K., Schemidt, J.J.: "Calculation of Doppler Coefficients of Dilute Fast Reactors", ANL-6792, (1963).

(55) Hwang, R.N.: "Doppler Effect Calculations with Interference Corrections", Nucl. Sci. Eng., 21. 523 (1965) and 52, 157 (1973).

(56) Fischer, E.A.: "The Overlap Effect of Resonances of Different Fuel Isotopes in Doppler-Coefficient Calculations for Fast Reactors," Nucleonik, 8, 146 (1966).

(57) Haggblom, H.: "A study of the Resonance Interaction Effect between ^{238}U and ^{239}Pu in the Lower Energy Region", ibid., 5, 189 (1969).

(58) Gwin, R., et al.: "Measurement of the Neutron fission and Absorption Cross Sections of ^{239}Pu over the Energy Range 0.01 to 30 keV", p.13 in "Neutron Physics Division Report", ORNL-4280, (1980).

(59) Hwang, R.N.: "Effect of the Fluctuations in Collission Density on Fast-Reactor Doppler Effect Calculations", ANL-7120, (1965).

(60) Kier, P.H.: "RIFF-RAFF, A Program for Computation of Resonance Integral in a Two Region Cell", ANL-7033, (1965).

(61) Brissenden, R.J., Durston, C.: "The Calculation of Neutron Spectra in the Doppler Region", ANL-7050, (1965).

(62) Kier, P.H., Robba, A.A.: "RABBLE, A Program for Computation of Resonance Absorption in Multiregion Reactor Cells", ANL-7326, (1967).

(63) Nakagawa, M., Katsuragi, S.: "ERSE, A Code to Calculation Fine Spectrum and Effective Cross Section", Unpublished work (1970).

(64) Dyos, M.W., Stevens, C.A.: Nucl. Sci. Eng., 25, 294 (1966).

(65) Kelber, C.N., Kier, P.H.: ibid., 24, 383 (1966).

(66) Kelber, C.N., Kier, P.H.: ibid., 25, 67 (1966).

(67) Dyos, M.W.: ibid., 34, 181 (1968).

(68) Ishiguro, Y., Katsuragi, S., Nakagawa, M., Takano, H.: "The Construction of Neutron Cross Sections in the Unresolved Resonance Region", ibid., 40, 25 (1970).

(69) Takano, H.: "MCROSS-2: A Code for Calculation of Microscopic and Effective Cross Sections", JAERI-M 4721 (1972).

(70) Nakagawa, M., Takano, H., Ishiguro, Y., et al.: J. Nucl. Sci. Technol., 6 [7], 408 (1969).

(71) Sumer, H.M.: "ERIC2, A Fortran Program to Calculate Resonance Integrals and from Them Effective Capture and Fission Cross-Sections", AEEW-R 323, (1964).

(72) Greebler, P., Hutchings, B.A.: "Proc. Sem. Physics Fast Intermediate Reactors", Vienna, Vol.3, 121, (1961).

(73) Hwang, R.N.: "An Improved Method for Doppler Effect Calculations for Fissile Materials in the Intermediate Energy Region", ANL-6792, (1963).

(74) Vogt, E.: "Resonance Theory of Neutron Cross Sections of Fissionable Nuclei", Phys. Rev., 112, 1, 203 (1958).

(75) Breit, G., Wigner, E.P.: Phys. Rev., 49, 519 (1936).

(76) Shore, F.J., Sailor, V.L.: Phys. Rev., 112, 191 (1958).

(77) Reich, C.W., Moore, M.S.: Phys. Rev., 111, 929 (1958) and Phys. Rev., 118, 718 (1960).

(78) Vogt, E.: Phys. Rev., 112, 203 (1958) and Phys. Rev. 118, 724 (1960).

(79) Wigner, E.P., Eisenbud. L.: Phys. Rev., 72, 29 (1947).

(80) Adler, D.B., Adler, F.T.: Trans. Am. Nucl. Soc., 5, 53 (1962), Trans. Am. Nucl. Soc., 7, 86 (1964) and "Neutron Cross Sections in Fissile Element", Proc. Conf. Breeding Economics and Safety in Large Fast Reactors, Argonne, ANL-6792, p.695 (1963) and CONF-660303, p.837 (1966).

(81) Hwang, R.N.: Nucl. Sci. Eng., 39, 32 (1970).

(82) For example: Sthen, J.R., et al.: "Neutron Cross Sections", BNL 325 2nd ed. (1964) and Mughabghab, S.G., et al.: BNL 325 3rd ed. (1973).

(83) Porter, C.E., Thomas, R.G.: Phys. Rev., 104 493 (1956).

(84) Wigner, E.P.: Proc. conf. on Neutron Physics by Time-of-flight, Gatlinburg, 1956, p.59 Oak Ridge National Laboratory, ORNL-2309.

(85) Lane, A.M., Thomas, R.G.: Rev. Mod. Phys., 30, 257 (1958).

(86) Buckler, MRS. P.A.C., Pull, I.C.: "Doppler Broadening of Cross Sections", AEEW-R226 (1962).

(87) Takano, H., Kobayashi, K.: "MXSFIT, A Code for Fitting the Resonance Cross Section", JAERI-M 4999, (in Japanese) (1972).

(88) Michauden, A.: "Contribution A L'Etude par des Methodses du Temps de Vol de L'Interaction des Neutrons Lents Avec L' U^{235}, "CEA-R 2552 (1964).

(89) Bergen, D.W., et al.: "Fission Cross Sections from Patrel," p.16, LA-3386 (1966) and CONF-660303, p.895 (1966).

(90) Bergen, D.W.: "The ^{233}U Fission and Capture Cross Sections and Their Analysis at Low Energies," LA-3676-MS (1967).

(91) Grag, J.B., et al.: Phys. Reg., 134, B985 (1964).

(92) Takano, H.: "Interference Effects between Resonance Levels in the Unresolved Resonance Regions," Annual Meeting of the Atomic Energy Society of Japan, B17, 1973.

(93) Takano, H., Ogawa, S.: "Codes for Revision of Group Constants for Heavy Nuclei of JAERI-Fast Set.", JAERI-M 6372 (in Japanese) (1975).

(94) Lynn, J.E.: Proc. Int. Conf. on the Study of Nuclear Structure with Neutrons, Antwerp 1965. North Holland Publishing Co.

(95) Garrison, J.D.: "Two-Level Interference Effects in Neutron Cross Sections", Proc. of the National Topical Meeting of the American Nuclear Society, San Diego 1966. The M.I.T. PRESS.

(96) Drake M.K.: "Data Formats and Procedures for the ENDF Neutron Cross Section Library", BNL-50274, 1970.

(97) Ishiguro, Y. and Takano, H.: "PEACO: A Code for Calculation of Group Constants of Resonance Energy Region in Heterogeneous Systems", JAERI 1219 (1971).

(98) Kamei, T. and Mizuta, H.: J. Nucl. Sci. Technol. 9[5], 312 (1972).

(99) Hasegawa, A., et al.: "EXPANDA-70D: A One-Dimensional Diffusion Code for Multigroup Criticality and Perturbation Calculations with JAERI-Fast set of 70 Group Structure", JAERI-M 4953 (1972).

(100) Freeman, D.D.: "SEFOR Experimental Results and Applications to LMFBR", GEAP-13929 (1973).

(101) Harris, R.A. and Nelson, J.V.: "SEFOR-Core I Doppler Constant Analysis", HEDL-TME, 72-78 (1972).

(102) Kallfeltz, J.M., et al.: "Modifications to Fissile Element Cross Sections and Their Influence on Calculated Fast Reactor Parameters," EACRP Meeting Report (1969).

(103) Alter, H., Kidman, R.B., LaBauve, R., Protsik, R. and Zolotar, B.A., "Cross Section Evaluation Working Group Benchmark Specifications", ENDF-202 (1974).

(104) Hasegawa, A. and Katsuragi, S.: "An Estimate of Uncertainties in the Experimental Data of $^{235}U(n,f)$, $^{239}Pu(n,f)$ and $^{238}U(n,\gamma)$ Cross Sections", JAERI-M 5536 (1974) (in Japanese).

(105) Mcknight, R.D., et al.: "Conf. on Advanced Reactors Physics Design and Economics", 260 (1975).

(106) Cecchini, G., et al.: ANL-7320, 107 (1977).

(107) Hemment, C.E., Pendlebury, E.D.: ibid., 88.

(108) Pazy, A., et al.: ibid., 270.

(109) Rowlands, J.L., Macdougall, J.D.: "Proc. Int. Conf. Phys. Fast Reactor Operation Design, London, P/1, 16 (1969).

(110) Barre, J.Y., et al.: ibid., P/1, 15.

(111) Campbell, C.G., Rowlands, J.L.: IAEA-CN-26/116 (1970).

(112) Haggblom, H.: AE-422 (1971).

(113) Kuroi, H., et al.: "Proc. Int. Symp. Phys. Fast Reactor, Tokyo", A33, (1973).

(114) Kuroi, H., and Mitani, H.: J. Nucl. Sci. Technol., 12 [11], 663, (1975).

(115) Takano, H., et al.: "1973 Topical Meeting on Fast Reactor Physics", A9, (1973).

(116) Takano, H., et al.: "Number of Resonances to be Adopted for Obtaining Practically Reliable Cross Section Curves", J. Nucl. Sci. Technol., 7 [11], 592 (1970).

(117) CCDN.: NEUDADA System DESCRIPTION, CCDN/SYS-2 (1969).

(118) Pfletschinger, E., et al.: Nucl. Sci. Eng., 40, 375 (1970).

(119) Davey, W.G.: Nucl. Sci. Eng., 39, 3 (1970).

(120) Leroy, J.L.: "Nuclear Data for Reactors, Conf. Proc., Helsinki, 1970", Vol.1, 227, IAEA, Vienna.

(121) Smirekin, G.N., et al.: AE, 13, 366 (1962).

(122) Moxon, M.C.: AERE-R-6074 (1969).

(123) Fricke, M.P., et al.: "Nuclear Data for Reactors, Conf. Proc., Helsinki, 1970", Vol.2, 265, IAEA, Vienna.

(124) Szabo, I.: Proc. Conf. Neut. Cross Sections and Technol., Knoxville, 1971", Vol.2, 573.

(125) Szabo, I., et al.: "Symp. on Neutron Standards and Flux Normalization", Argonne, 257 (1970).

(126) Prince, A.: "Conf. Proc. Nuclear Data for Reactors, Helsinki, 1970", CN-26/91, IAEA, Vienna.

(127) Poenitz, W.P.: Nucl. Sci. Eng., 40, 383 (1970).

(128) Kikuchi, Y., Nakagawa, T., Matsunobu, H., et al.: "Neutron Nuclear Data of ^{235}U, ^{238}U, ^{239}Pu, ^{240}Pu and ^{241}Pu Adopted in JENDL-1, JAERI-M 6996 (1977).

(129) Pitterle, T.A.: "Nuclear Data for Reactors, Conf. Proc., Helsinki, 1970", CN-26/83, IAEA, Vienna.

(130) Glass, N.W., et al.: "^{238}U Neutron Capture Results from Bomb Source Neutron", Neutron Cross Section Technol. Conf., Washington, D.C. (1968).

(131) Asghar, M., et al.: Nucl. Phy., 85, 305 (1966).

(132) Rahn, F.J., et al.: "Proc. the Third Conf. Neut. Cross Section Technol.", Vol.2, 658 (1971).

(133) Abagyan, L.P., et al.: INDC (CCP)-11 (1971).

(134) Seth, K.K., et al.: "Proc. Conf. Paris, 1964", Vol.2, 916.

(135) Mughabghab, S.F., et al.: BNL-325, 3rd (1973).

(136) Hughes, D.J., et al.: Phys. Rev. Letters, 1, 461 (1958).

(137) Pattenden, N.T., et al.: AERE-PR/NP6, (1964).

(138) Craig, D.S., Westcott, C.H.: CRRP-1186, (1964).

(139) Watanabe, T., et al.: Phys. Rev., 135, B945 (1964).

(140) Simpson, O.D., et al.: IDO-16679, (1961).

(141) Reich, C.W., Moore, M.S.: Phys. Rev., 111, 929 (1958).

(142) James, G.D.: AERE-R 4597, (1964).

(143) Stehn, J.R., et al.: Neutron cross sections, Vols.III, BNL-325, 2nd ed. Suppl. No.2 (1965).

(144) Doherty, G.: AEEW-M 714, (1967).

(145) Hennies, H.H.: Cross-Sections and resonance parameters for ^{235}U, ^{233}U, ^{239}Pu and ^{241}Pu between cadminum cut off and 10 keV, Proc. Conf. Nucl. Data for Fast Reactors, Paris, Oct. 1966, 333 (1967), IAEA.

(146) Prince, A., Analysis of height energy neutron cross section for fissile and fertile isotopes, Proc. Conf. Nucl. Data for Reactors, Helsinki, June 1970, IAEA-CN-26/91, (1970), IAEA.

(147) Uttley, G.A.: AERE-PR/NP-6, (1963).

(148) Yiftah, S., et al.: Israel At. Energy Comm. Rep. LA-1152, (1967).

(149) Simpson, O.D., Fluharty, R.G., Moore, M.S., et al.: Fission cross section from petrel, LA-3586, p.72 (1966); CONF0660303, p.190 (1966).

(150) Kikuchi, Y.: Analysis of intermediate structure in fission cross section of ^{241}Pu, ANL-7710, (1971).

(151) Wheeler, J.A.: Channel Analysis of fission, Fast neutron physics Part II, (J.B. Marison, J.L. Fowler, Eds.) p.2052 (1963), Intersci. Publ., New York.

(152) Lynn, J.E.: Interpretation of Neutron-induced fission cross sections and related data, Proc. Conf. Data for Fast Reactor, Paris, Oct. 1966, Vienna, 1. 89 (1967), IAEA.

(153) Perkin, J.L., et al.: J. Nucl. Energy. A/B, 19, 423 (1965).

(154) Hardy, J.D., et al.: Nucl. Sci. Eng., 9, 341 (1961).

(155) Schmidt, J.J.: KFK-120, Part I, Karlsruhe (1967).

(156) Drawbaugh, D.W. and Gibson, G.: "Conf. Proc., Nuclear Data for Fast Reactor Paris, Oct. 1966", IAEA, Vol.II, 251 (1967).

(157) Takano, H., "Evaluation of Neutron Cross Section of ^{241}Pu in Unresolved Resonance Region",: J. Nucl. Sci. Technol., 8[11], 656, (1971).

(158) Pattenden, N.T., et al.: AERE-PR/NP6 (1974).

(159) Cote, L.M., et al.: Bull. Am. Phys. Soc., 1, 187 (1956).

(160) Czirr, J.B., et al.: Nucl. Sci. Eng., 58, 371 (1975) and ibid, 57, 18 (1975).

(161) Sowerby, M.G., et al.: AERE-R 7273 (1973).

(162) Meadows, J.W.: Nucl. Sci. Eng., 49, 310 (1972).

(163) Grundl, J.A.: Nucl. Sci. Eng., 39, 39 (1967).

(164) Hansen, G., et al.: private communication.

(165) Wright, R.Q., et al.: "A Program to generate five group constants and P_n scattering matrices from ENDF/B", ORNL-TM-2679 (1969).

(166) Ingram, G., et al.: Proc. Int. Symp. Physics of Fast Reactors, Tokyo, Oct. 16-19, 1973, Vol.I, p.269 (1973).

(167) LeSage, L.G., Mcknight, R.D.: "Nuclear Cross Sections for Technology", Proc. Int. Conf., Knoxville, Oct. 22-26, 1979, p.297 (1980).

(168) Iijima, T., et al.: "Doppler Experiment in FCA", paper submitted for presentation at the 14th EACRP Meeting Stockholm, June 1971.

(169) Ishiguro, Y., et al.: "Proc. Int. Symp. Phys. Fast Reactors, Tokyo", 1133 (1973).

(170) Till, C.E., et al.: ANL-7910, (1972).

(171) Bohn, E.M., et al.: ibid, 102 (1972).

(172) Davey, W.G., et al.: Nucl. Sci. Eng., 51, 415 (1973).

(173) Nakagawa, M., et al.: "SLAROM: A Code for Calculation of a Heterogeenous Core in Fast Reactors", JAERI-M 5916 (1974) (in Japanese).

(174) Fowller, T.B., et al.: ORNL-TM-2496 (1971).

(175) Nakagawa, M., et al.: "CIPER: A Two- and Three-Dimensional Perturbation Code Based on Diffusion Theory", JAERI-M 6722 (1976) (in Japanese).

(176) Hutchins, B.A., et al.: "SEFOR Doppler Benchmark Problem", private communication.

(177) Nakagawa, M.: "Analysis of Reaction Rate Distribution in Assemblies ZPPR-2, ZPPR-3 phase 2, MZB(2) and MZB(3)", unpublished work (1980).

(178) Yoshida, H. et al.: "AN Evaluation of Control Reactivity Worth of the Prototype Fast Breeder Reactor "MONJU"", unpublished work (1977).

(179) Howerton, R.J. and Perkins: "Evaluators for ^{9}Be (MAT 1289)", BNL-NCS-17541 (ENDF-201), 2nd ed. ENDF/B-1V, (1975).

(180) Perey, F.G. and Fu, C.Y.: "Evaluators for ^{12}C (MAT 1274)", ibid. (1975).

(181) Young, P., Foster, D.G., Hale, G.: "Evaluators for ^{16}O (MAT 1276)", ibid. (1975).

(182) Paik, N.C. and Pitterle: "Evaluators for ^{23}Na (MAT 1156)", ibid. (1975).

(183) Young, P.G., Foster, D.G.: "Evaluators for ^{27}Al (MAT 1193)", ibid. (1975).

(184) Prince, A.: "Evaluator for Cr (MAT 1191)", ibid. (1975).

(185) Takahashi, H.: "Evaluator for Mn (MAT 1197)", ibid. (1975).

(186) Bhat, M.R.: "Evaluator for Ni (MAT 1190)", ibid. (1975).

(187) Drake, M.K. and Fricke, F.P.: "Evaluators for Cu (MAT 1295)", ibid. (1975).

(188) Howerton, R.J.: "Evaluator for Mo (MAT 1287)", ibid. (1975).

(189) Cowan, C.: "Evaluator for ^{11}B (MAT 1160)", ibid. (1975).

(190) Stewart, L., Labauve, R.J., Young, P.G.: "Evaluators for H (MAT 1269)", ibid. (1975).

(191) Suzuki, T.: "EXPANDA-4: One-Dimensional Diffusion Equation Code for Fast Reactors Using the JAERI-Fast Set", JAERI-M 3660 (1969).

(192) Kidman, R.B. et al.: Nucl. Sci. Eng., 48, 189 (1972).

(193) Hardie, R.W., LITTLE, W.W.: BNWL-954, Battelle Northwest Laboratory (1959).

(194) Segev, M.: Nucl. Sci. Eng., 56, 72 (1975).

(195) Grevilie, T.N.E.: "Theory and Applications of Spline Function", Academic Press, New York (1965).

(196) Akima, M.: "New Method of Interpolation and Smooth Curve Fitting Based on Local Procedures", J. ACM, 17, 589 (1972).

(197) Semi, Y.: Private Communication.

(198) Kamei, T.: Private communication.

(199) Ise, T., Tsutsui, T.: "Computer Programs for Interpolations", JAERI-M 7419 (1977) (in Japanese).

(200) Ishiguro, Y.: Nucl. Sci. Eng., 49, 228 (1972).

(201) Ishiguro, Y., et al.: "Measurements and analyses of the Doppler Effect of Structural Material", Proc. Int. Symp. Physics of Fast Reactors, Tokyo (1973).

(202) Takano, H., Ishiguro, Y.: "Group Constants for the keV Capture of Structural Materials Cr, Fe and Ni", JAERI-M 5714 (1974).

(203) Takano, H., Ishiguro, Y.: "Production and Benchmark Tests of Group Constant Set JFS-3-J2", JAERI-M 82-135 (1982).

(204) Iijima, T., et al.: Doppler Experiments in FCA, paper submitted to the 14th EACRP Meeting, Stockholm, June (1971).

(205) Iijima, T., et al.: Unpublished work (1971).

(206) Story, J.S.: Private communication (1973).

(207) Garber, D.T. and Kinsey, R.R., "Neutron Cross Sections Volume II, Curves", BNL 325, 3rd ed., Vol.II, 1976.

(208) Perey, F.G., FU, C.Y., Penny, S.K., "Evaluators, ENDF/B data file for Iron (MAT 1192)", BNL-NCS-17541 (ENDF-201), 2nd ed. (ENDF/B-IV), edited by D. Garber, available from the National Nuclear Data Center, Brookhaven National Laboratory (1975).

(209) Huschke, H.: "Grouppenkonstanten für dampf- und natriumgekühlte schnelle Reaktoren in einer 26-Gruppendarstellung", KFK 770 (1968).

(210) Stacey, W.M.: Nucl. Sci. Eng., 47, 29 (1972).

(211) Nakagawa, M., et al.: J. Nucl. Sci. Technol., 15 [4], 302, 1978.

(212) Küsters, H., Ed.: KFK-1632 (1973).

(213) Ishiguro, Y., et al.: 1977 Fall Meeting of the Atomic Energy Society of Japan, F16, p.304, 1977.

(214) Nakagawa, M., et al.: 1977 Fall Meeting of the Atomic Energy Society of Japan, F15, p.303, 1977.

(215) Takano, H., Hasegawa, A., Kaneko, K.: "TIMS-PGG: A Code System for Producing Group Constants in Fast Neutron Energy Region", JAERI-M 82-072 (1982).

(216) Nakagawa, T.: Private communication. The RESEND code is a modified version of RESEND which is a processing code for ENDF/B-IV.

(217) This code is a modified version of PROF-GROUCH-G Ⅱ for producing the group constants of JFS-3-J2 type.

(218) Seki, Y., et al.: Private communication.

(219) Tuchihashi, K., Takano, H., Horikami, K., et al.: "SRAC: JAERI Thermal Reactor Standard Code System for Reactor Design and Analysis", JAERI-1285 (1982).